Pareto Optimal Solutions in Process Design Decisions using Evolutionary Multi-objective Optimization

THESIS

Submitted in partial fulfillment

of the requirements for the degree of

DOCTOR OF PHILOSOPHY

By

ASHISH MADHUKAR GUJRATHI

Under the supervision of

Prof. B. V. Babu

BIRLA INSTITUTE OF TECHNOLOGY AND SCIENCE

PILANI (RAJASTHAN) INDIA

2010

BIRLA INSTITUTE OF TECHNOLOGY AND SCIENCE
PILANI, RAJASTHAN, INDIA

CERTIFICATE

This is to certify that the thesis entitled **"Pareto Optimal Solutions in Process Design Decisions using Evolutionary Multi-objective Optimization"** and submitted by **Ashish Madhukar Gujrathi** ID. No. **2004PHXF415P** for the award of PhD Degree of the Institute embodies the original work done by him under my supervision.

Signature in full of the Supervisor _____

Name in capital block letters **Prof B V BABU**

Designation Dean-Educational Hardware Division
Professor-Chemical Engineering Group
BITS-Pilani, India

Date:

DEDICATED

TO

The sweet memories of my son
(late) Aarav

ACKNOWLEDGEMENTS

It gives me a deep sense of gratitude and an immense pleasure to sincerely thank my guide **Prof (Dr) B V Babu**, Dean-Educational Hardware Division and Professor- Chemical Engineering Group for his constant encouragement, constructive & valuable suggestions, and moral support throughout the period of this research work. It has been a privilege for me to work under his valuable guidance.

I thank the members of Doctoral Advisory Committee, Dr Arvind Kumar Sharma, Assistant Professor and Dr Suresh Gupta, Assistant Professor, Chemical Engineering Group for their support and suggestions to carry out this work effectively.

My sincere thanks go to Prof L K Maheshwari, Vice-Chancellor, BITS Pilani for giving me the opportunity to carry out the PhD work in BITS. I am thankful to Prof V S Rao, Director (Hyderabad Campus), Prof K E Raman, Acting Director (Goa Campus), Prof G Raghurama, Deputy Director (Academics), Prof R K Mittal, Deputy Director (Administration) and Prof Ravi Prakash, Dean-Research and Consultancy Division for providing the necessary facility and infrastructure to carry out this work.

I am extremely thankful to Prof Suman Kapur (Chief, CWIRU) for providing her kind support and motivation throughout the phase of this study.

I extend my sincere thanks to Prof J P Mishra [Chief, Information Processing Center (IPC), BITS] for his constant help in providing me high speed computers, as and when required throughout the phase of this work. I also wish to acknowledge Mr Bhulichand, Mr Banwarilalji, Mr Sushil, Mr Surendra (and entire IPC staff) for their help and cooperation they extended in running the optimization programs of this study (24X7 basis) in the IPC.

I extend my special thanks to Prof B R Natarajan, Dr Bharat Bhushan Gulyani, Dr Harekrishna Mohanta, Mr Pratik N. Sheth, Mr Sushil Kumar, Mr Nikhil Prakash, Mrs. Smita Raghuvanshi, Mr Amit Jain, Mr Dipaloy Dutta, Mr Deepesh Patle, Mr Utkarsh Maheshwari, and other members of chemical engineering group for their valuable advice and moral support throughout the work. My sincere thanks to Prof R P Vaid and Prof H S Moondra for their constant support and encouragement during my PhD work. I also thank Dr S D Manjare, Dr Rakesh Angira, Dr Basudeb Munshi, and Dr Kailash Wasewar for providing me all the support during the start of my PhD work. I would also like to thank Mr Amit Gaikwad, Mr Pankaj Kandalkar, for their help in getting scientific literature and support throughout the work. I also thank my other colleagues having created a good environment to carry out the work. I am also helpful to my faculty colleagues Dr Biju, Dr Keskar, Dr Chadrashekhar for helping me during the course of this study. I am thankful to Dr Wang and Dr Li Xi for communicating important literature and update on purified terephthalic acid (PTA). I am also

thankful to Prof Suganthan (NTU, Singapore) for providing necessary true Pareto fronts data that have been used in the present study. I am also thankful to Prof G P Rangaiah (NUS, Singapore) for having discussion with me on optimization of industrial studies and optimization opportunities in the field of Chemical Engineering.

Besides all the faculty members and other friends, I would also take this opportunity to thank Mr Ashok Saini and Mr Jeevan Verma for their extended help. Thanks are also due to Mr Babu Lal Saini and Shri Jangvirji for their cooperation during my PhD. I am indebted to all my students at BITS, Pilani (especially, Digvijay, Saket, Divya, Ramesh, Kshitij, Manasi, Abhishek) for their keen interest that they have shown in working under my guidance.

This work could not have been completed without the moral support I got from my loving parents – Shri Madhukar P Gujrathi and Smt Mandakini Gujarathi. I am unable to put my feelings in words to express the support that I received from my loving wife – Jaya. Her patience, support, confidence, immense encouragement helped me in devoting late night hours for this study and made this work possible.

Last but not the least, I pray and thank to ALMIGHTY GOD for showering HIS divine blessings and giving me an inner strength and patience.

ASHISH M GUJRATHI

ABSTRACT

An optimization problem involving more than one objective to be optimized simultaneously is referred as multi-objective optimization (MOO) problem. Unlike single objective optimization problems, multi-objective optimization problems deal with two kinds of search spaces. These are the decision variable search space and the objective search space. Thus, while searching for the optimum in MOO problems, (1) the perturbation of variables takes place in the decision variable space, (2) the cost corresponding to the objective space is evaluated, and (3) the selection from the objective space is based on the value of objective function. The objective space for complex problems is often nonlinear and they have multi-dimensional decision variable space. The objective functions also conflict with each other. Thus, combining these basic aspects, the multi-objective optimization problems are more complex to solve than the single objective optimization problems. In case of multi-objective optimization problems, due to the conflicting nature of objectives, the decision maker is often interested in obtaining a set of non-dominated solutions (Pareto front) instead of a single solution. Therefore evolutionary multi-objective optimization algorithms (as they result in set of solutions in a single run) are preferred for solving multi-objective optimization problems over the deterministic search methods which yield a single solution in a run. Due to the nonlinear nature of objective functions and multi-dimensional decision variable space with nonlinear constraints, there is a need for developing new and efficient algorithms.

In the present study, an existing evolutionary multi-objective optimization algorithm, i.e., multi-objective differential evolution (MODE) is improved for better performance in terms of convergence to the Pareto front and the diversity of solutions on the obtained Pareto front. Strategies of MODE, namely, MODE II and MODE III are developed. MODE II algorithm is further improved by incorporating the concepts of elitism and the crowding distance sorting approach. MODE III algorithm is hybridized with deterministic search method, i.e., sequential simplex method. The trigonometric mutation strategy of MODE algorithm is also proposed in this study.

The performance of newly developed strategies of MODE algorithm (namely, MODE III, elitist MODE, hybrid MODE, and trigonometric MODE) is compared with respect to the convergence and divergence with other evolutionary multi-objective optimization algorithms from the literature [NSGA II (real- and binary –coded variants), SPEA and PAES]. The Pareto fronts obtained using newly developed algorithms for benchmark test problems (SCH, FON, KUR, ZDT1, ZDT2, ZDT3, ZDT4) are also compared with the true Pareto front and that obtained using another evolutionary MOO algorithm (i.e., NSGA-II). The robustness of original MODE algorithm is checked with respect to its control parameters [crossover constant (CR), number of population points (*NP*), and scaling factor (*F*)]. Subsequently MOO of industrial case studies involving process design decisions [namely, styrene reactor (both adiabatic and steam injected configurations), polyethylene terephthalate (PET) reactor, oxidation of *p*-xylene to purified terephthalic acid (PTA), low density polyethylene (LDPE) tubular reactor, and supply chain & planning] is carried out using the newly developed algorithms. The performance of newly developed algorithms is checked with respect to the

effects of dominant decision variables on the Pareto front. The Pareto fronts obtained using the algorithms developed in this study are compared among themselves, with the industrial data, and the data reported in the literature. The results obtained in this study show that the developed algorithms are able to converge to the true Pareto front for majority of the test problems. However the diversity of solutions obtained using newly developed algorithms is comparable with those obtained using other evolutionary MOO algorithms reported in the literature. The newly developed strategies of MODE algorithm are able to converge to a better Pareto front as compared to the Pareto fronts obtained using MODE and NSGA for styrene reactor. For PET reactor, where NSGA algorithm gave a single point solution, the strategies of MODE algorithm resulted in a Pareto front (consisting of setoff solutions). For oxidation of *p*-xylene problem, the Pareto front obtained using elitist MODE and MODE algorithms is better than that obtained using other strategies of MODE. For LDPE tubular reactor, the results obtained in this study show that MODE III algorithm is able to give a wide range of solutions on the Pareto front as compared to those obtained using other strategies of MODE. MODE algorithm gave a good distribution of solutions when applied on MOO of supply chain and planning problem. The points on the Pareto front are of interest to the decision makers (plant engineers) involved in process design decisions.

Keywords: *Multi-objective Optimization; Optimization; Evolutionary Algorithms; Multi-objective Differential Evolution; Differential Evolution; Pareto Front; Industrial Problems; Modeling and Simulation; Styrene; PET; PTA; Supply Chain & Planning; Test Problems; Process Design Decisions.*

TABLE OF CONTENTS

LIST OF FIGURES

LIST OF TABLES

NOMENCLATURE

Symbol	Description
[*C*o]	catalyst concentration (ppm) (by mass)
[*i*]	concentration of i^{th} species per 1000 C atoms
[Z]	di-ester groups (-)
A	acetaldehyde (-)
A	frequency factor (1/s; m^3/kmol.s; $m^{3.3}$/kmol.s);
A	cross-sectional area of reactor (m^2)
A_1	Cross-sectional area of the melt in the reactor, m^2
a_v	parameter used in the viscosity estimation (-)
C	molar concentration (kmol/m^3)
C_i	molar concentration of the i^{th} component (kmol/m^3)
C_j	exit concentration of j^{th} species (mol/kg $_{HOAc}$.)
$C_{j,0}$	initial concentration of j^{th} species (mol/kg $_{HOAc}$.)
*C*p	molar heat capacity (kJ/kmol.K)
C_{Pi}	specific heat of reaction mixture in the i^{th} zone (kJ/kg.K)
CR	cross over constant (-)
D	diameter (m)
d[*i*][*j*]	crowding distance vector for j^{th} objective and for i^{th} solution (-)
d_i	model parameter (Table C2)
*D*i	inside diameter of the reactor (m)
D_{JI}	inner diameter of out jacket (m)
D_o	outer diameter of out jacket (m)
DP	degree of polymerization or the number average chain length of the polymer (-)
E	activation energy (kJ/kmol)
E_a	acid end groups (mol/m^3)
E_{DEG}	DEG end groups (excluding those on pure DEG) (mol/m^3)
E_g	hydroxyl end groups (excluding those on pure EG) (mol/m^3)
E_j	actiavtion energy for the j^{th} reaction (kJ/mol)
E_v	vinyl end groups (mol/m^3)
F	molar flow rate (kmol/h)
F	scaling factor used in differential evolution
f	friction factor (-)
F_{Feed}	total feed to reactor (kg/h)
F_i	mass flow rate for i^{th} component (kg/s)
f_m	initiator efficiency of the m^{th} initiator
F_{PX}	*p*-xylene feed to reactor (kg/h)
G	mass velocity of the gas mixture (kg/m^2.h)
H_w	wall heat transfer coefficient (W/m^2.^{0}C)
H_x	cost factor of component *x* ($/kmol)

I_i	i^{th} initiator
K	equilibrium rate constant (bar)
$k_i^{'}$,	equilibrium rate constants for reactions A1, A5, A7, A8
k_j^0	oxidation reaction rate constants (min^{-1})
k	reaction rate constant (kmol/kg.h .bar^n /1/s; m^3/kmol.s; $m^{3.3}$/kmol.s/min^{-1})
$k_{j,0}$	frequency factor for j^{th} reaction (min^{-1})
L	total length of the reactor (m)
L_a	reactor length at the maximum temperature (m)
M	monomer (-)
M_e	methyl end group (SCB)
N	speed of the agitator (rpm)
N^*	dimensionless value ($\equiv N / N_{ref}$)
NP	number of population used in differential evolution (-)
p	partial pressure (bar);
P	total pressure (bar/mm hg)/ pressure of the reactor (mm Hg)
P_{in}	inlet pressure (MPa)
r	reaction rate (kmol/kg per h)
R	universal gas constant (8.314 kJ/kmol K)
$R_{i(x)}$	growing macroradical with x monomeric units and i long chain branches
r_j	rate of j^{th} step reaction (mol/kg $_{HOAc.}$min)
S	selectivity (%)
S	solvent (telogen)
SOR	steam over reactant (ethyl benzene) molar ratio (-)
T	temperature (K)
t	wall thickness (m)
T_C	temperature of first crystallizer (K)
T_i	inlet temperature (K)
$T_{J,i}$	jacket fluid temperature on jacket side (K)
T_{MAX}	maximum temperature attained in the reactor (K)
T_R	temperature of reactor (K)
u	**v**ector of parameters (-)
v	velocity of the reaction mixture (m/s)
V_i	vinyl end group (per 1000 C atoms)
V_{id}	vinylidene end group (per 1000 C atoms)
$V_{J,i}$	volumetric flow rate of jacket side fluid (m^3/h)
V_{OC}	vent oxygen from the crystallizer (%)
V_{OR}	vent oxygen from the reactor (%)
V_{O_2}	total vent O_2 content from the reactor (vol. %)
W_{H_2O}	water content in the solvent (vol. %)
WWD	water withdrawal rate
x	conversion (%)
X_M	monomer conversion at any axial position (-)
Y	yield (%)
Z	length of the reactor (m)
z	dimensionless axial location (≡ axial position/L)

Abbreviations

4-CBA	4-carboxybenzoic acid
DE	differential evolution
DEG	di-ethylene glycol
EG	ethylene glycol
HOAc	acetic acid
LDPE	low density polyethylene
PE	poly ethylene
PTA	purified terephthalic acid
PX	*p*-xylene
p-T	*p*-toluic acid
SCB	short chain branching
TA	crude terephthalic acid
TALD	tolualdehyde
W	water

Greek symbols

α,	reflection factor used in hybrid MODE (Table 5.1)
β	contraction factor used in hybrid MODE (Table 5.1)
λ	fraction of reactor bed where steam is injected (-)
λ_{np}	n,p order moments for the chain length distribution of macro radicals (kmol/m^3); n=0,1; p=0,1,2
δ	fraction of steam distributed (-)
Δ	divergence metric (Eq. 5.2)
ΔH	heat of reaction (kJ/kmol)
ε	void fraction (-)
γ	convergence metric (Eq. 5.1)
γ	expansion factor used in hybrid MODE (Table 5.1)
γ	constants used in water content correlation (Eq. C13).
ρ	density (kg/m^3)
μ	viscosity (kg/m s)
μ_{np}	n,p order moments for the chain length distribution of dead polymer molecules (kmol/m^3); n=0,1; p=0,1,2
θ^*	dimensionless value ($\equiv\theta/\theta_{ref}$)
θ	cocrystallization factor as defined in Eq. 4.44
τ	residence time (min^{-1})

Subscripts/superscripts

b	bulk
BZ	benzene
C	catalyst
CO	carbon monoxide
CO_2	carbon dioxide

d	desired value
d_i	desired weight on i^{th} objective in case of overall objective
EB	ethyl benzene
ETH	ethylene
f	feed-end of reactor
G	gas
gen	generation
H_2	hydrogen
H_2O	steam
i	reaction i
ind	industrial
j	component j
m	model
MET	methane
mix1	mixture of fresh steam and feed ethyl benzene fed at reactor inlet
mix2	mixture of fresh steam and reactor effluent from first reactor
o	initial
out	at the reactor outlet
p	particle
ref	reference value
ST	styrene
t	total
TOL	toluene

CHAPTER – 1

INTRODUCTION

1.1 Motivation

An optimization problem involving more than one objective to be optimized is referred as multi-objective optimization problem (MOOP). The optimum solution corresponding to a single objective optimization problem refers to the optimal basic feasible solution (satisfying bounds of variables and the constraints). However, in case of multi-objective optimization, the optimum solution refers to a compromised (not necessarily the optimum with respect to any objective) set of multiple feasible solutions. In the most general form, the multi-objective optimization problem (with m objectives, n variables, p inequality constraints and q equality constraints) can be expressed as given by Eq. (1.1):

$$\left.\begin{aligned} &Min \quad f(x_i) = [f_1(x_i), f_2(x_i), ..., f_m(x_i)]^T \\ &\text{subject to} \\ &u_j(x_i) \geq 0, \quad j = 1,2,..., p \\ &v_k(x_i) = 0, \quad k = 1,2,..., q \\ &x_i^{(L)} \leq x_i \leq x_i^{(U)}, \quad i = 1,2,...n \end{aligned}\right\} \tag{1.1}$$

The optimization algorithms can be broadly classified into two categories, i.e., traditional or classical methods and the non-traditional or population based search algorithms. The traditional algorithms often start with a single point (guess value) and end up with a single point solution. The ideal outcome of a single objective optimization problem is a single global solution. However, the outcome of gradient based traditional algorithms largely depends on its control parameters such as the step size and the

direction of search that are being used. In a complex and non-linear search space (as shown in Fig. 1.1), which may involve multiple local and a single global solutions, an inefficient local search algorithm may get trapped at local optimal solution. In contrast, evolutionary algorithms which mimic nature's principle of survival of the fittest, start with multiple population points (Goldberg, 1989; Deb, 2001, 2005; Babu, 2004; Onwubolu and Babu, 2004). Due to the strong genetic operators, evolutionary algorithms are found to achieve the global optimum in majority of industrial applications for single objective optimization (Angira, 2005).

In case of MOO problems, the decision maker is always interested in obtaining a solution suitable to his/her design requirements, i.e., a single solution. But due to the multi-objective nature of the problem and the associated trade-off, the desired solution may vary as per the decision makers need and the choice. Thus providing multiple solutions rather than a single optimum solution (traditional multi-objective optimization algorithms give single optimum solution) would be an advantage to the decision maker, so that one can have a choice of selecting one from the several equally good solutions from the Pareto front. The specialty of such solutions is that as we move from one solution to the other we gain in terms of one objective at the cost of loss in another objective involved in the study. Such a set of solutions are referred as the Pareto optimal set and the solutions in this set are non-dominated with respect to each other.

1.1.1 Definition of dominance

A solution $x^{(1)}$ is said to dominate the other solution $x^{(2)}$, if both the following conditions 1 and 2 are true.

1. The solution $x^{(1)}$ is no worse than $x^{(2)}$ in all objectives, or $f_j\left(x^{(1)}\right) \not\triangleleft f_j\left(x^{(2)}\right)$ for all j=1,2,…M
2. The solution $x^{(1)}$ is strictly better than $x^{(2)}$ in at least one objective, or $f_j\left(x^{(1)}\right) \triangleleft f_j\left(x^{(2)}\right)$ for at least one ($j \in 1,2,...M$)

If any of the two conditions is violated, the solution $x^{(1)}$ does not dominate the solution $x^{(2)}$ (Deb, 2001). As multi-objective optimization algorithm results in a set of solutions, the following two goals are associated with each multi-objective optimization algorithm.

1. The algorithm should converge to the true Pareto front
2. The algorithm should maintain a diverse set of solutions on the Pareto front.

In pursuit of achieving the convergence, the algorithm may loose diversity of solutions in the Pareto front. But it is worth to mention here that though both convergence and divergence issues are equally important in MOO study, the diverse set of solutions is meaningless if the algorithm did not converge to the true Pareto front. Thus, any efficient multi-objective optimization algorithm should first focus on achieving the convergence to the true Pareto front and then new solutions in the neighborhood of solutions on Pareto front may be searched to enhance the divergence. Though both the goals of achieving convergence and maintaining diverse set of solutions are important, focus should first be given in algorithm to attain the convergence.

Unlike single objective optimization, the MOO problems deal with two kinds of search space. Fig. 1.2 shows the decision variable space and objective space with global

and local Pareto fronts. The decision variables space is obtained by plotting decision variables and constraints within bounds. On evaluation, each point in the decision variable space generates an additional point in the objective space. Thus a given algorithm proceeds based on the comparison of objective function values from the objective space but perturbation of variables occurs in the decision variable space. Thus multi-objective optimization problems are more difficult to solve as compared to single objective optimization problems.

In case of simple test problems (where there exists a direct relationship between the objective function and the decision variables), the cost of the objective function can easily be evaluated and then used in evolutionary algorithm. However, in case of industrial problems, the mathematical model needs to be evaluated first. Once the model is formulated, it needs to be integrated and simulated using suitable numerical technique. Judicious choice of numerical technique is made to solve the mathematical model.

Fig. 1.3 shows the solution methodology for model based evaluation of Pareto front. The decision variables are initialized randomly within the bounds. These decision variables are then converted to the specific input form of model. These input parameters are passed to the model. The model is integrated and simulated along the space coordinate and/or time domain. The objectives are evaluated from the output of the model.

The termination criteria are checked, and if not terminated, the offspring is generated after applying the corresponding genetic operators. Selection is performed based on the objective function values of the parent and the offspring. The algorithm continues until the termination criteria are met.

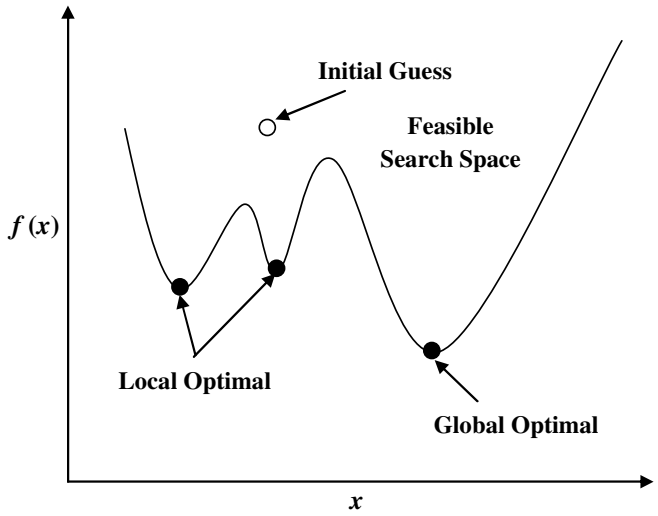

Fig. 1.1 Local and global optimal solutions of a complex search space

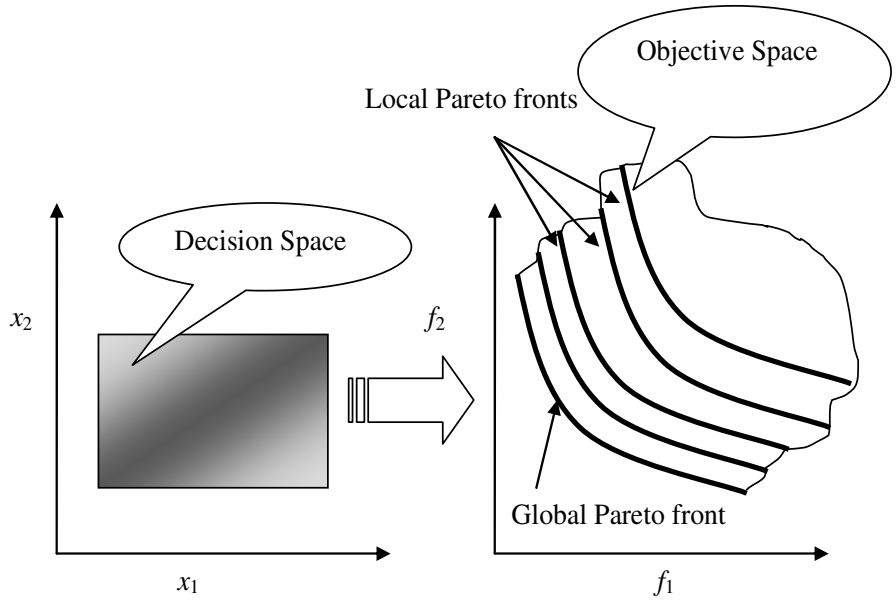

Fig. 1.2 Decision space, objective space, local and global Pareto fronts involved in multi-objective optimization study

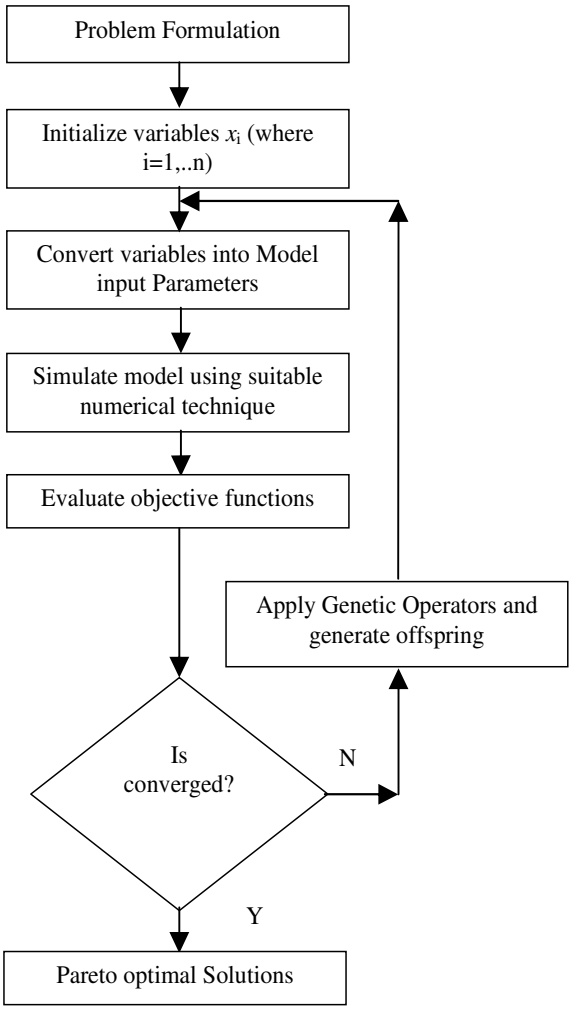

Fig. 1.3 Solution methodology for model based evaluation of Pareto front

While achieving these two goals of MOO and dealing with two search spaces, the search for the true Pareto front in case of MOO study depends upon the following key issues:

- Number and type of decision variables (continuous, discontinuous) and nature of decision variable space
- Type of objective functions (minimization, maximization) and nature of objective space
- Nonlinearity and stiffness of model equations
- Type of constraints (equality, inequality)
- Ability of algorithms to handle the search spaces of objectives and decision variables

Out of 5 aspects as mentioned above, first four are problem specific. However, Pareto front output also largely depends on the algorithm's ability to converge towards the true Pareto front and then produces a well diverse set of solutions. An inefficient algorithm may get trapped at local optimal nondominated set of solutions (Fig. 1.2) or may result in a single point solution. Few of the reasons by which algorithm may result in local Pareto front or a single point solutions are:

- Algorithms may not produce a superior offspring which is nondominated with respect to other solutions in the current population
- An inefficient selection scheme of algorithm may restrict a new solution to enter in the current population
- In case of binary coded algorithms, accuracy of newly obtained solutions depends on the number of bits used in defining string
- Of its inability to handle the complexity of a problem (i.e., multi-dimensional decision variable space)

Thus it is necessary to have an algorithm, which not only overcome above limitations but also results in a well diverse Pareto front and close to true Pareto front. The literature survey on several evolutionary algorithms shows a large demand towards developing new algorithms. The algorithm output also depends on the complexity of MOO problems. The industrial engineering problems and some of the test problems involve multi-dimensional decision variable space, multi-modal objective space with equality and inequality constraints. Some of the commonly observed trade-offs associated with process design decisions involved in industrial problems are described below.

1.1.2 Industrial styrene reactor

Styrene is commercially produced from ethyl benzene [Sheel and Crowe (1969); Yee et al. (2003); Babu et al. (2005a)]. The main reaction producing styrene is a reversible endothermic reaction. As per the Li-Chatelier's principle, for a reversible endothermic reaction, high temperature and low pressure favors the rate of forward reaction. But as the temperature is increased, other side products (due to thermal cracking) such as toluene, benzene, etc. are formed. Thus, at low temperature the yield and productivity are low, while selectivity is high. If the temperature of reactor is increased, the selectivity decreases (due to the formation of byproducts) but the yield increases. But the objectives of the process are to increase simultaneously the yield, selectivity and the productivity. If the decision variables such as temperature of ethyl benzene (feed), steam over reactant (SOR), operating pressure and initial ethyl benzene flow rate are used subject to a constraint on temperature, the optimization problem would become more complex and trade-off among the objectives would clearly be observed. The decision maker has to

sacrifice for one of the objectives, while achieving the better value of another objective. Thus, in case of industrial styrene reactor there exits potential trade-off among the said objectives of simultaneous maximization of yield, productivity and the selectivity.

1.1.3 Wiped film polyethylene terephthalate reactor (PET) reactor

The production process of PET [Ravindranath and Mashelkar (1982, 1986a, 1986b); Laubriet et al. (1991); Bhaskar et al. (2000, 2001); Babu et al. (2007)] involves four stages, (1) trans-esterification or direct esterification, (2) prepolymerization, (3) melt condensation, and (4) solid state polycondensation. In trans-esterification process dimethyl terephthalate (DMT) is reacted with ethylene glycol (EG). Methanol is continuously removed and bis (hydroxyethyl) terephthalate (BHET) is recovered. In direct esterification process, terephthalic acid (TPA) is reacted with EG and side product (water) is removed. In second stage, prepolymerization of BHET and some oligomers from stage-1 is carried out to produce a polymer having degree of polymerization (DP) value of 30. In stage-3, DP value is increased to approximately 100 using high vacuum and a special agitator system. Solid state polycondensation process is employed to produce PET having a value of DP >150. The two major and important objectives for this process are the minimization of the concentrations of the acid and vinyl end group, E_a and E_v, respectively, in the product of the finisher. During the downstream separation operation, the acid end group makes the polymer susceptible to hydrolysis and leads to the breakage of the filaments during spinning (where the humidity is very high). The vinyl end groups are responsible for the unfavourable coloration of PET. The reduction of E_a simultaneously increases the rate of polymerization of the acid end group catalysed

poly-condensation reaction and thus the throughput is maximized. Thus the simultaneous minimization of acid and vinyl end groups can be formulated as a multi-objective optimization problem.

1.1.4 Low density Polyethylene (LPPE) tubular reactor

Polyethylene is commercially produced by both high pressure (free-radical) and low pressure (ionic) addition ethylene polymerization processes. Two types of reactors (tubular and stirred autoclave) are essentially applied in the free-radical high-pressure polymerization processes. Ethylene free-radical polymerization is conducted in the presence of free-radical initiators such as azo compounds, peroxides, or oxygen at very high pressures (1300-3400 bars) and high temperatures (225-610 K). Under the reaction conditions employed in high-pressure processes, LDPE is produced as a result of short-chain branching formation. A commercial reactor consists of 3-5 reaction zones and several cooling zones (Brandoline et al., 1998; Agarwal et al., 2003). The reactor includes a number of initiator side-feed points. The temperature and flow rate of each coolant stream entering a reaction/cooling zone is used to control the temperature profile in the reactor. A mixture of ethylene, a free-radical initiator system, and a solvent are injected at the entrance of reactor. Maximization of monomer conversion is one of the objectives to be considered during MOO of LDPE. While maximizing the conversion, the undesirable side chain concentration (sum of methyl, vinyl, and vinylidene) also increases. Thus, minimization of unwanted side products and maximization of monomer conversion gives rise to conflicting set of objectives. More meaningful and industrially important results

can be generated if these sets of objectives are coupled with equality constraints on number average molecular weight.

1.1.5 Liquid phase oxidation of p-xylene

Liquid phase oxidation of hydrocarbons, using air or oxygen has gained popularity in industrial applications due to its ability of converting petroleum hydrocarbon feed stocks such as olefins, aromatics and alkanes, into industrial organic chemicals which are important in many polymer and petrochemical industries. One of the important chemicals produced from *p*-xylene is purified terephthalic acid (PTA). Liquid phase oxidation of *p*-xylene to PTA is a complex process which involves series of multiple oxidation steps. In liquid phase *p*-xylene oxidation process, the quality of product, is decided by the amount of 4-carboxybenzoic acid (4-CBA) present in it. Several properties of PTA such as optical density and 4-carboxy-*p*-terphenyl (4-CTr) concentration of crude terephthalic acid (CTA) are related to the amount of 4-CBA present in the final product. 4-CBA can also contaminate CTA as it is prone to co-crystallization with crude TA (Mu et al., 2004). Thus minimization of the concentration of 4-CBA in the final product is one of the major objective in the production of PTA. The operating profit of the industry depends on the production rate, and the production rate is directly related to the flow rate of the feed entering the reactor. Thus maximization of feed flow rate can be considered as one the objectives of the study. But with an increase in the production rate, the level of impurity (concentration of 4-CBA) also increases. A set of decision variables may exist, which may favor the objective of increasing the productivity, but may not favor the objective of

minimization of 4-CBA concentration. Thus there exists a clear conflict in both the objectives and they can be modeled as a multi-objective optimization problem.

1.1.6 Supply chain and planning

The supply chain is basically the integrated network (Chopra and Meindl, 2004) among retailers, distributors, transporters, storage facilities and suppliers that participate in the sale, delivery and production of a particular product for the following purposes:

1. Maximizing the overall profit generated
2. Increasing the competitiveness of the whole chain
3. Minimizing the systemwide costs while satisfying the service level requirements
4. Matching the supply and demand profitably for products and services

It is due to the above reasons that the supply chain optimization problem is considered as a multi-objective optimization problem (MOOP). The supply chain problem therefore has to be considered as a whole (system optimization) without placing the individual preferences of the individual objectives. The built up supply chain model should be capable of integrating all the entities so that the flow of information happens among the entities in order to meet the highly fluctuating demand of the market. The important issues that drive the supply chain models and subsequently govern its design are:

1. Inventory planning and management
2. Transportation and logistics management
3. Facilities location and layout design
4. Flow of information among the entities

These four drivers represent the major flows associated with supply chain problem. In order to maximize overall profitability, it is not possible to get a unique solution that satisfies either all the criteria or the objectives. If all the objectives are satisfied then the solution obtained could be a non-Pareto optimal point. Hence in multi-objective optimization problem, we are interested in set of solutions (rather than a single solution) which are non-inferior with respect to each other and are part of Pareto optimal front. Simultaneous optimization of individual objectives is necessary without giving weightage to individual objectives. A goal programming approach to optimization would not result in a set of solutions and a compromised, but a single solution, would result in a single run. Evolutionary algorithms have shown a good potential to generate multiple equally good solutions for many engineering and test problems both for single and multi-objective optimization problems. Hence an attempt to solve such problems using newly developed evolutionary algorithms may result in a possibly better set of solutions.

Thus, to deal with above mentioned problems there is a need towards development of new and efficient algorithms. To judge the robustness of newly developed algorithms, it needs to be tested on several benchmark test problems and then applied on industrial applications. This motivated us to design following objectives of the present study research.

1.2 Objectives of research

The following objectives of the present research-based study are formulated based on the background on this subject:

1. To identify some process design decision problems involving multi-objectives to be optimized
2. To apply evolutionary multi-objective optimization approach for finding Pareto optimal set of solutions
3. To improve the existing population based search algorithms by using hybrid concept and to develop new strategies for evolutionary computation
4. To validate by the performance of various existing evolutionary strategies applied to selected multi-objective optimization problems (benchmark test problems and real world industrial engineering problems)

1.3 Organization of thesis

The above mentioned objectives are achieved in this study and an exhaustive literature survey on evolutionary algorithms and modeling, simulation aspects & process design decisions involved in several industrial applications is given in chapter 2. Detailed working principles of newly developed strategies of MODE algorithms, i.e., multi-objective differential evolution-III, elitist-multi-objective differential evolution (E-MODE), hybrid multi-objective differential evolution (H-MODE), and trigonometric mutation multi-objective differential evolution (T-MODE) are discussed in chapter 3. Multi-objective optimization problem formulation is given in Chapter 4. In section 4.1, various test problems (both constrained and unconstrained) considered in this study are

defined. In Section 4.2, formulation of various process design decisions based multiple objectives involved in several industrial applications (such as styrene reactor, polyethylene terephthalate reactor, liquid phase oxidation of *p*-xylene, low density polyethylene tubular reactor, and supply chain management) is given. Detailed parametric estimation and simulation analysis of LDPE tubular reactor is given in section 4.3. The obtained simulated results are discussed in detail in chapter 5. In section 5.1, Pareto fronts obtained using various proposed strategies of MODE are compared with NSGA-II and parametric estimation of selected test problems is carried out using MODE algorithm. In section 5.2, Pareto optimal fronts obtained using proposed strategies of MODE are compared with the Pareto front reported in the literature for several cases of the industrial case studies as mentioned above. Performance evaluation of proposed strategies of MODE is carried out by comparing the performance metric values obtained in this study with other well known algorithms from the literature. Chapter-6 deals with the summary of the work and important conclusions drawn from the present study.

CHAPTER – 2

LITERATURE REVIEW

Various studies reported in literature on development of multi-objective optimization algorithms and industrial applications on multi-objective optimization are discussed in detail in section 2.1 and 2.2 respectively.

2.1 Multi-objective optimization algorithms

The multi-objective optimization algorithms can be broadly classified into classical or traditional methods (deterministic) and nontraditional or population based search algorithms. Since last two decades, evolutionary population based search algorithms have captured more attention due to their ability of giving number of population points in a single simulation run. Classical methods also have their own place in the research of multi-objective optimization due to their simple transition rules as compared to evolutionary algorithms. In the following sections, a brief survey on classical and nontraditional methods used for solving multi-objective optimization problems is given.

2.1.1 Classical methods

The classical methods for solving multi-objective optimization (MOO) problems have been in use for more than five decades. The classical methods transform the multi-objective optimization problem into a single objective optimization problem. Thus classical methods avoid the complexities involved in a true MOO problem. As multi-

objective optimization problem is solved using a single objective optimization problem, such methods result in a single point solution in a single run. In this section some of the classical methods used for solving MOO problems are discussed in brief.

2.1.1.1 Weighted sum method

The weighted sum method (Deb, 2001) transforms MOO problem into a single objective optimization problem by pre-multiplying each of the objective functions with user defined weights. As MOO problem is converted into a single objective problem, this method is considered to be simplest one to solve MOO problems. In the weighted sum method the optimization problem is formulated as follows:

$$\begin{aligned}
&\text{Minimize}: F(x) = \sum_{i=1}^{k} \lambda_i f_i(x) \\
&\text{subject to}: g_j(x) \geq 0 \qquad \text{where j} = 1,...,\text{n} \\
&\qquad\qquad h_k(x) = 0 \qquad \text{where k} = 1,...\text{p} \\
&\qquad\qquad x \in S \\
&\qquad\qquad \lambda_i \in \Lambda \\
&\qquad\qquad \Lambda \equiv \left\{ \lambda_i \geq 0 \;\&\; \sum_{i-1}^{k} \lambda_i = 1 \right\}
\end{aligned} \tag{2.1}$$

The value of weights to be used during optimization runs is based on the importance of given objectives to a decision maker. These may also be obtained from the previous experience of decision maker. The extreme solutions of each objective can be obtained by solving the problem as a single objective optimization problem by setting $\lambda_i = 1$ for the desired objective and $\lambda_i = 0$ for the remaining objectives. However, in case of nonlinear and multimodal search space, set of weights may not give uniformly distributed solutions of the Pareto front. It is usual practice to set the weights such that the sum of weights

equals to 1. As only a single solution is obtained during each run, in order to obtain the solutions of the Pareto front using weighed sum method, several runs may be simulated (by varying λ_i value during each run). A Weighted sum method may not find certain solutions on the Pareto set in case of non-covex search space (Deb, 2001). However, bi-objective adaptive weighted sum method (Kim and Weck, 2004), determines uniformly-spaced Pareto optimal solutions and finds solutions on non-convex regions. This method can only solve the problems with two objective functions. The major drawbacks associated with weighted sum method include:

1. They cannot provide all points of the Pareto front
2. They cannot provide a good control over location of the optimal point on the Pareto optimal front
3. They result in a single point solution in a single simulation run
4. They cannot handle non-convex search space efficiently

2.1.1.2 ε-Constraint method

Haimes et al. (1971) used ε-constraint method to solve problems having non-convex objective space. ε-constraint method consists of reformulating the MOOP by considering only one of the objectives and forcing the remaining objectives within user specified bounds as constraints.

$$\left.\begin{array}{lll} \textit{Minimize} & f_m(x), & \\ \textit{subject to} & f_p(x) \le \varepsilon_p, & \mathrm{p} = 1,2,...,\mathrm{M} \text{ and } \mathrm{p} \ne \mathrm{m} \\ & g_j(x) \ge 0, & \mathrm{j} = 1,2...,\mathrm{J} \\ & \mathrm{h_k(x)} = 0, & \mathrm{k} = 1,2,.....,\mathrm{K} \\ & x_i^{(L)} \le x_i \le x_i^{(U)} & \end{array}\right\} \qquad (2.2)$$

This method is especially applicable, where the decision maker is interested in optimum value of only one of the objectives with slight relaxation in other objectives involved in the studies. A value of ε is considered in such a way that it marks the upper bound as permissible limit of the objectives. The range of feasible solution is increased in such a way that it lies in the domain of the ε values.

2.1.1.3 Goal programming method

Charnes et al. (1955) introduced goal programming to solve single objective linear programming problem. Later, goal programming gained much popularity due to its simplicity in converting MOO problems in goals as per the priorities set by the decision maker. Goal programming attempts to find solutions which attain a predefined target (goal) for one or more objectives. If no solutions exists which achieves the specific goal, then the objectives are relaxed by certain deviation from the original goal. Each inequality is converted into a flexible goal in which the corresponding constraints may be violated. This goal is then achieved by minimizing the deviation considered in the study. Consider the following problem, where two goals need to be achieved as given by Eqs. 2.3a and 2.3b:

$$x_1 + x_2 \geq 16 \tag{2.3a}$$

$$x_3 \leq 2 \tag{2.3b}$$

$$x_1, x_2, x_3 \geq 0$$

The flexible goals may be written as Eqs. 2.4a and 2.4b:

$$x_1 + x_2 + s_1^- - s_1^+ = 16 \tag{2.4a}$$

$x_3 + s_2^- - s_2^+ = 2$

(2.4b) $x_1, x_2, x_3 \geq 0$

$s_i^-, s_i^+ \geq 0, \quad i = 1,2$

The nonnegative variables s_i^- and s_i^+ are called deviational variables as they represent the deviations below and above the R.H.S. of constraint *i*. These deviation variables are dependent and at most one of the two deviation variables can assume a positive value. If the i^{th} inequality is of the ≤ type, and its s_i^- >0, then the i^{th} goal is satisfied; otherwise if s_i^+ >0, the goal *i* is not satisfied (Taha, 2007). Thus the reformulated goals of problem become Eq. 2.5a and 2.5b:

Minimize $G_1 = s_1^-$ (2.5a)

Minimize $G_2 = s_2^+$ (2.5b)

A good review on goal programming applications is reported by Trzaskalik and Michnik (2002). One of the drawbacks of goal programming is that each goal needs to be addressed separately. Evolutionary algorithms have shown a good potential in handling MOO problems in the recent past.

2.1.2 Population based search algorithms

The population based search algorithms have specific characteristics that they start with multiple population points and all points usually converge towards the Pareto optimal front after required number of simulation runs. The detailed survey on some of the evolutionary algorithms (population based search algorithms) is given in the literature (Back, 1996; Miettinen, 1999; Deb, 2001; Abbas et al., 2001; Onwubolu and Babu, 2004;

Eiben and Smith, 2003; Coello and Lamont, 2004; Tan et al., 2005; Biswas, et al., 2009a, 2009b). Following sections give the working principles of some of the widely accepted MOO algorithms in brief.

2.1.2.1 Nondominated sorting genetic algorithm-II (NSGA-II) and its jumping gene variants

NSGA-II was proposed by Deb et al. (2002a) as an improved and modified version of NSGA (Srinivas and Deb, 1994). NSGA is an extension of genetic algorithm (Goldberg, 1989) to solve the multi-objective optimization problems. NSGA has major disadvantages like high computational complexity of nondominated sorting, lack of elitism and a need for specifying the sharing parameter. Considering those drawbacks of NSGA, two major changes were proposed in NSGA-II namely fast non-dominated sorting based on the concept of dominance and the crowding distance assignment as a measure of density.

Fast nondominated sorting

A rank value is assigned to each individual of the population using fast nondominated sorting. All individuals are compared with each other and the number of solutions dominating the individual i is referred as n_i. S_i is a set of individuals dominated by individual i. For each level of nondominated front on which the nondominated individual i posses n_i=0, a repeated search is performed untill no further individual for the next level is found.

Crowding distance sorting

The sharing function was used in NSGA to maintain diversity of solutions. The sharing function approach was replaced by crowding distance sorting approach in NSGA-II. Following pseudo-code describes the crowding distance assignment applied on a population of size NP.

Function (Crdst) = CROWDING(pop)

Fun (i, j)=the normalized jth objective function of individual I in population pop

$f_j^{\max} = \max\left(\left(F(i,j)\forall i = 1,2,...NP\right)\right)$

$f_j^{\min} = \min\left(\left(F(i,j)\forall i = 1,2,...NP\right)\right)$

for i=1:size of pop

Crdst(i)=0

end for

for m=1:number of objectives

I^m *= Sort population in worse order of* f_m *and store it in index vector I*

Crdst(1)=Crdst(Np)=∞ *%Extreme points*

for i=1: size of pop-1

$$Crdst(I(i)) = Crdst\left(I\left(i\right)\right) + \frac{\left[F\left(I\left(i+1\right),m\right) - F\left(I\left(i-1\right),m\right)\right]}{f_m^{\max} - f_m^{\min}}$$

End for

End for

End function

The function CROWIDNG describes the working of crowding distance assignment operation. A crowding distance measure of each element of population is returned by CROWDING function which represents the average distance of two

individuals on either side of the population member with respect to each of the objectives. First, the population is sorted in an ascending order of the objective function values with respect to each of the objectives. To give preference to the extreme solution, a sufficiently high value of crowding distance is assigned to the extreme points of population. For the remaining population members the crowding distance is calculated as the normalized absolute distance of the objective function between the two neighboring population members. The crowding distance is calculated for each of the objective functions. The sum of the individual crowding distance with respect to each objective function is called the crowding distance of the particular population member. The larger the value of crowding distance of a population member, the less crowded is the population member. The following pseudo-code shows the working principle of NSGA-II.

Set value of maximum number of generation

Set upper and lower bounds of variables

Initialize population pop of size NP

Initialize offspring population Off_pop as NULL

gen=0

While (the stopping criterion is not met)

Combo_pop= pop ∪ offspring_pop

rank_pop=NONDSORT(Combo_pop)

pop=NULL

rank_NP=rank value of NPth member in Combo_pop sorted in ascending order of rank

pop=members from Combo_pop with rank_pop<rank_NP

popsize= size of (pop)

Top_pop=members from Combo_pop with rand value of rank_NP

Crdst=CROWDING(Top_pop)

pop=pop ∪[(NP-popsize) members with largest value of Crdist]

Off_pop=genetic_algorithm_operators(pop)

gen=gen+1

end while

Return set of non-dominated set and decisions variable

NSGA-II-JG and NSGA-II-aJG: Two types of jumping genes (JGs) (namely replacement and reversion) were applied on NSGA-II after mutation operation (Kasat and Gupta, 2003). A probabilistic approach is used where a fraction, p_{jump}, of randomly selected strings in population are modified by the jumping gene operator. In both the replacement and reversion operations, two sites (between which replacement or reversion occurs) are selected randomly. In replacement, a part of binary string in the offspring population is replaced with a randomly generated binary string of same length. In reversion, the string in the offspring population is reversed. In case of binary coded NSGA-II-aJG, the second site in the chromosome is selected by the predefined string length of JGs (Agarwal et al., 2006).

2.1.2.2 Strength Pareto evolutionary algorithms (SPEA)

Zitzler and Thiele (1999) proposed strength Pareto evolutionary algorithm, an elitist multi-criterion evolutionary algorithm with the concept of non-dominance. An external

population archive (P') at every generation is maintained. All nondominated solutions identified from Parent population (P) are stored in this archive and any dominated individuals in the archive are removed. This external population participates in evolutionary operations. At each generation, a combined population with the external and the current population is first constructed. All non-dominated solutions in the combined population are assigned a fitness based on the number of solutions they dominate. Thus a higher fitness value (also called as strength) is assigned to a nondominated solution having more dominated solutions in the combined population. To avoid overcrowding of nondominated individuals, if the number of population members in archive exceeds a predefined threshold, the archive is shortened by means of clustering, i.e., elites which are less crowded in the non-dominated front are kept. The individuals in the population are evaluated with reference to the members of archive, while the individuals in the external population archive are ranked with reference to the members of population. SPEA algorithm includes fitness sharing where niches are not allowed in terms of distances but are based on Pareto dominance.

In SPEA2 (an improved version of SPEA) (Zitzler et al., 2001), changes are included related to fitness assignment strategy, archive size and replacement of clustering. The changes are given below:

i) A fitness assignment strategy was included which consists of density information and considers for each individual regarding how many other individuals it dominates or dominated by.

ii) A fixed archive size (where as in SPEA, the size of archive was floating), i.e., archive may also contain dominated individuals whenever the number of nondominated individuals are less than the predefined threshold value.

iii) The clustering was replaced with an alternate truncation method which does not loose boundary points.

An empty archive (NewPop) is created in the beginning and at each generation, fitness values are assigned to individuals in population (NPop) and the archive.

$$Z(i) = \left| \left(i \middle| i \in NewPop \cup NPop \;\&\&\; j \text{ dominates } i \right) \right|$$

Where, $|..|$ denotes the cardinality of a set. Based on the value of Z, the raw fitness R(i) of an individual i is defined by the strength of its dominators as given by

$$R(i) = \sum_{Z(i)} Z(j)$$

Nondominated population members from NPop and NewPop are stored in a temporary population (TmpPop). If the size of TmpPop exceeds the predefined threshold (NP), TmpPop is truncated. If the size of TmpPop is less than NP, then the nondominated individuals having higher fitness value from NPop and NewPop are copied into TmpPop. All new individuals in TmpPop are copied into NewPop. Genetic operators are applied on NewPop and to generate the offspring in NPop. This process continues till the stopping criterion is met. When the stopping criterion is met, the latest individuals in NewPop are returned.

The density estimation (as given by Eq. 2.6) is applied to those individuals which have identical raw fitness value.

$$D(i) = \frac{1}{d_i^k + 2} \tag{2.6}$$

Where d_i^k is the distance of individual *i* to its k^{th} nearest neighbor. The summation of D(i) and R(i) gives the overall fitness *F*(i), which is used in the process of removing any extra individuals from the archive (NewPop) or filling up the archive with other individuals. The pseudo-code for SPEA2 is given as below.

Initialize population of size NP

Initialize generation, g=0;

Set Gmax value,

While (Stopping criterion is not met)

Evaluate Fitness of individuals in NPop and NewPop.

TmpPop={Nondominated solutions from NewPop and NPop}

If size of Tempop > NP

Truncate TmpPop to size NP based on fitness value

Else

Add individuals from NewPop and NPop (based on their fitness values) to the empty space in TmpPop

End

NewPop=TmpPop

Apply genetic operators on NewPop and store the offspring in NPop

g=g+1

End while loop

Return (NewPop,…)

2.1.2.3 Pareto archived evolution strategy (PAES)

The PAES algorithm was proposed by Knowles and Corne (1999) to serve two main objectives. The first objective is that the algorithm should strictly be restricted to local search. It is expected to move from a current solution to a nearby neighbour using a local search operator (mutation) only. The second objective is that the algorithm should converge to a true Pareto front. An archive of previously found nondominated solutions is maintained and used as a means of estimating the true dominance ranking of a pair of solutions. Considering these two-objectives, the algorithm is called a (1 + l)- evolution strategy. The algorithm is composed of three main parts, i.e., the candidate solution generator (*pop*), the candidate solution acceptance function, and the Non-dominated solutions (*NDS*) archive. The candidate solution generator function is similar to simple mutation or hill climbing for the current individual where it maintains a single current solution, and at each iteration produces a single new candidate via random mutation. Archive NDS is applied to a set of solutions to explicitly store nondominated individuals so as to maintain the spread of solutions on Pareto front. The (1+1) PAES algorithm was modified to a better version, i.e., $(\mu+\lambda)$, where μ and λ include current individuals of population and mutants respectively (Knowles and Corne, 2000). This approach was used to solve a wide range of problems. The working principle of PAES is given by the following pseudo-code.

Generate an initial current population, pop

Initialize generation, g=0;

Set Gmax value,

NDS=NDS $\cup$ *{pop}*

While (stopping criterion is not met)

Use local search (mutation) to product offspring M from pop

If pop dominates M

Discard M

Else if M dominates pop

pop=M

NDS= NDS ∪{M}

Else

If M is dominated by any individual in NDS

Discard M

Else if size(NDS)<NP

NDS= NDS ∪{M}

If M is in a less crowded region of NDS than pop

pop=M

End

Else

If M is in a less crowded region of NDS than X for some members in NDS

NDS=NDS/{a member of NDS from the most crowded region}

NDS= NDS ∪{M}

If M is in a less crowded region of NDS than pop

Pop=M

End

Else if M is in a less crowded region of NDS than pop

Pop=M

End if

End if

End if

End

g=g+1

End (while)

Return (NDS,..)

2.1.2.4 Multi-objective simulated annealing (MOSA)

Multi-objective simulated annealing (Nam and Park, 2000) is an extension of simulated annealing algorithm (of single objective optimization) to solve multi-objective optimization problems. However, as multi-objective evolutionary algorithms are expected to give a set of solutions on the Pareto front, the major problem with MOSA is that it cannot find multiple solutions in a single run. In order to obtain a set of solutions on the Pareto front, multiple runs are taken by repeating the trials.

The following three major objectives are considered in the SA based multi-objective optimization algorithm (MOSA):

1. The objective function corresponding to the energy function to be identified.
2. To select a proper annealing scheme of decreasing temperatures with an increase in number of iterations.
3. A need for a method of generating a neighbour near the current search position.

Psuedo-code for MOSA is given below:

$S = S_0$

$T = T_0$

While ((the stopping criterion is not met)

Generate a neighbour S'=N(s)

If C(S') dominates C(S)

move current solution to S'

else if C(S) dominates C(S')

move to current solution to S' with transition probability $P_t(C(S), C(S'), T)$

else if C(S) and C(S') are nondominated with respect to each other

move to S'

end if

T=annealing (T)

End while

Parameters S and T are the current search position (or current state) and temperature respectively. The temperature is gradually decreased as time goes on. A new search position S' is generated in the neighbourhood by the N(s) function, its cost is evaluated and compared with the previous cost. The domination based test is carried out and a new state corresponding to a better solution is accepted. Even though the new position is dominated by the current state, it is accepted with some acceptance probability. When there is no superiority between the current state and the next state (i.e., they are equally good), the new state is accepted instead of the current one. Moving in the nondominated situation helps increase the spread and avoid convergence to the local optima. When it is determined either to move or stay, the algorithm repeats its loop with lower temperature until the termination conditions are satisfied. Like deterministic methods, MOSA also has the same disadvantage that of not being able to produce a set of data in a single run.

2.1.2.5 Non-dominated sorting differential evolution (NSDE)

NSDE algorithm (Angira, 2005; Angira and Babu, 2005) is a simple extension of DE for solving multi-objective optimization problems. The working of NSDE and DE is similar except the selection operation that is modified in order to solve the multi-objective optimization problems. The detail of the NSDE algorithm is as follows: First of all set the key parameters, i.e., *CR*- crossover constant, *F* - scaling factor, *NP* - population size, *Max_gen* - maximum number of generations of NSDE algorithm. And then randomly initialize the population points within the bounds of decision variables. After initialization of population, randomly choose three mutually different vectors for mutation and crossover operation (as is done in DE algorithm) to generate trial vector. Evaluate the trial and target vector and perform a dominance check. If trial vector dominates the target vector, the trial vector is copied into the population for next generation otherwise target vector is copied into population for next generation. This process of mutation crossover, and dominance check is repeated for specified number of generations. Evaluate and then sort this final population to obtain the non-dominated solutions. Sorting can be done using naïve and slow approach or any of the standard approaches reported in Deb (2001). If no solution is found to dominate solution *i*, it is member of the non-dominated set otherwise it does not belong the non-dominated set. The stopping criteria for the algorithm can be any one of the following conditions:

(a) There is no new solution added to the non-dominated front for a specified number of generations.

(b) Till the specified number of generations.

Pseudo-code for NSDE algorithm can be given as below:

***Pseudo-code for NSDE algorithm*

Set the values of NSDE parameters *D, NP,* CR and *Max_gen* (maximum generations).

Initialize all the vectors of the population randomly within the bounds.

for i = 1 to NP

for j = 1 to D

$\mathbf{X}_{i,j}$ *=Lower bound+ random number *(upper bound - lower bound);*

End for

End for

Perform mutation, crossover, selection and evaluation of the objective function for trial and target vector for a specified number of generations.

While (gen < Max_gen)

*{ for i = 1 to NP /** first for loop***/*

{_ For each vector $\mathbf{X}_i$ *(target vector), select three distinct vectors* $\mathbf{X}_a$, $\mathbf{X}_b$ *and* $\mathbf{X}_c$ *randomly from the current population other than the vector* $\mathbf{X}_i$

do

*{ r1 = random number * NP*

*r2 = random number * NP*

*r3 = random number * NP*

} While (r1=i) OR (r2=i) OR (r3=i) OR (r1=r2) OR (r2=r3) OR (r1=r3)

Perform mutation and crossover for each target vector $\mathbf{X}_i$ and create a trial vector, $\mathbf{X}_{t,i}$.

For binomial crossover:

{ p = random number

j_{rand} *= int (rand[0,1]* D)+1*

for n = 1 to D

{ if (p<CR or n = j_{rand} *)*

$\mathbf{X}_{t,i} = \mathbf{X}_{a,i} + F (\mathbf{X}_{b,i} - \mathbf{X}_{c,i})$

} else $\mathbf{X}_{t,i} = \mathbf{X}_{i,j}$ *}*

2.1.2.6 Multi-objective differential evolution (MODE)

MODE is an extension of DE to handle multi-objective optimization problems (Babu et al., 2005a). The flow chart for MODE is given in Fig. 2.1. The specific characteristic of MODE algorithm is that in each generation, the dominated solutions are removed from the list and only the non-dominated solutions are allowed to undergo DE operations. The scaling factor *F* is generated from a random number generator between 0 and 1.2. The off-springs are placed into the population if they dominate the main parent. The algorithm works as follows: An initial population is generated at random. All dominated solutions are removed from the population. The remaining non-dominated solutions are retained for recombination. Three parents are selected at random. A child is generated from the three parents and is placed into the population if it dominates the first selected parent; otherwise a new selection process takes place. The stopping criteria may be of two kinds: (1) There is no new solution added to the non-dominated front for a specified number of generations, or (2) Assign an upper bound on the number of generations. The stopping criteria may be a combination of the two as well. In this study, the second criterion is applied.

Fig. 2.1 Working principle of MODE algorithm

2.2 Industrial applications on multi-objective optimization

One of the major uses of optimization techniques is to find optimum design and operating variables of the process that give an optimum value of the desired objective. However, most of the industrial processes are rich in terms of objectives which may show conflict among the objectives. That is, if the decision maker attempts to minimize the cost of one of the objectives, he/she has to sacrifice for the other (out of two objectives). Thus the decision makers are interested in obtaining a set of solutions (called Pareto optimal set) rather than a single point solution. Out of several solutions obtained in the Pareto set, the decision maker can then judiciously choose one of the solutions suitable to his/her design requirements. A brief account on literature survey of several processes which involve multiple process design decisions to be optimized simultaneously is given below.

2.2.1 Industrial Styrene reactor

Styrene, $C_6H_5CH=CH_2$, (a synthetic chemical) is used extensively in the manufacture of plastics, rubber, and resins. Manufacturers across the globe use styrene-based resins to produce a wide variety of everyday goods ranging from cups and utensils to furniture, bathroom, and kitchen appliances, hospital and school supplies, boats, sports and recreational equipment, consumer electronics, automobile parts, and durable lightweight packaging (Styreneforum, 2009). In terms of monomer production rate, styrene ranks fourth with an annual turnover of 60 billion USD in the United States behind ethylene, vinyl chloride and propylene. The styrene monomer is largely used for crystalline and

rubber-modified polystyrene. Styrene is also copolymerized with other monomers for use in a variety of products. Industrially important and easily recognizable products obtained from styrene include polystyrene, acrylonitrile-butadiene styrene (ABS), styrene-acrylonitrile (SAN) plastic, styrene-butadiene rubber (SBR), and unsaturated polyester resins, commonly known as fibreglass and two types of foams - extruded polystyrene foam (XPS) and expanded polystyrene foam (EPS). With such a large demand, even a slight improvement in the multiple process design decisions related to yield, selectivity and product flow rate of the process may improve the operating profit of an organization.

Sheel and Crowe (1969) proposed a model for the dehydrogenation of ethyl benzene to produce styrene by a reversible reaction. Actual plant data was used to tune the pseudo-homogeneous model (with axial dispersion neglected and diffusional resistance or mass and heat transfer related limitations were lumped into rate constants). The model predicted the profiles of temperature and other major products along the length of reactor within acceptable accuracy. Rosenbrock's multivariable search technique was used to seek optimum operating conditions for the reactor using a set of decision variables (namely, steam temperature, steam rate and bed depth). From the results observed in their study, they concluded that the plant was running under suboptimal conditions. The mathematical model of steam injected reactor was proposed by Clough and Ramirez (1976). They emphasized on location of steam injection port in their study. Later, Abdalla et al. (1994) and Elnashaie et al. (1993) included an account of diffusion in the catalyst pellet and used the pseudo-homogeneous model (Sheel and Crowe, 1969) as well as the more detailed heterogeneous model. The kinetic data was extracted from the industrial data using this model. The intrinsic kinetics for three

promoted iron oxide catalysts using the pseudo-homogeneous and heterogeneous models was compared to check the performance of catalysts by Abdalla et al. (1994). Considering the valuable outcome of pseudo-homogeneous mathematical model, conflicting set of objectives namely productivity, yield and selectivity of styrene were identified by Yee et al. (2003). Yee et al. (2003) used NSG algorithm to carry out the multi-objective optimization study of styrene reactor for the adiabatic and steam injected reactor configurations. However, in their study, they mainly emphasized on the adiabatic operation. The results on the steam injected configuration, though reported in their study, were not discussed extensively. Four decision variables (namely temperature of feed (ethylbenzene), pressure of reactor, steam over reactant and initial flow rate of ethyl benzene) were used for adiabatic configuration where as two additional decision variables (namely location of steam injection port and fraction of steam injected) were employed in steam injected configuration. Two constraints (namely flow rate of steam and temperature of ethylbenzene and steam mixture entering the reactor inlet) were used.

Babu et al. (2005a) applied MODE algorithm to solve adiabatic configuration of styrene reactor. As DE was found to give better results than GA for single objective optimization problems (Babu and Sastry, 1999; Babu and Munawar, 2000, 2001; Babu and Angira, 2005; Babu et al, 2005b), the application of DE was extended to solve MOO problems. Another study showed (Babu and Jehan, 2003) that MODE algorithm showed promising results when compared with the NSGA results for the test problems. Babu et al. (2005a) considered same set of objectives and decision variables as those used by Yee et al. (2003) to test the performance of MODE algorithm. It was observed that MODE algorithm resulted in a better Pareto front when compared to the Pareto front obtained

using NSGA. It was found that the decision variables those were responsible for producing Pareto front were feed temperature of ethyl benzene and initial molar flow rate of ethyl benzene. Though same set of decision variables and constraints are used, two algorithms may result in different non-dominated set of variables. Thus, due to the complexity associated with industrial multi-objective optimization problems, the algorithm may need to be tuned for its performance before it is used to find the Pareto front for an industrial application. Though NSGA and MODE algorithms resulted in a set of solutions (said to be Pareto front) for industrial styrene reactor problem, there exist a need to explore the search space associated with the problem using a better algorithm to obtain the possibly the true Pareto front.

2.2.2 Polyethylene terephthalate reactor

Polyethylene terephthalate is a major polymer made into a resin, fibre or film and exists both as an amorphous (transparent) and a semi-crystalline (opaque and white) thermoplastic. World polyester fiber demand is expected to continue growing at 6% year (ICIS, 2009a). PET has captured market share in the bottled water market due to its good transparent look and not leaving any taste in the water. It is also used by majority of food grade industries in the packing of soft drinks, fruit juices, cooking and salad oils, sauces and dressings, etc. It is predicted that by 2011 the carbonated soft drinks will represent 36% of total PET packaging. From 2007-2011 in United States, PET solid state resins, polyster fibres and PET engineering resins are expected to grow by 7% , 5% and 4% per year respectively (ICIS, 2009b). With such a demand and growth, a slight improvement

in the process parameters due to simulation based research may prove to be beneficial to the industry.

Ravindranath and Mashelkar (1982) reported modeling of final stage polycondensation process. Higbie's penetration theory was applied to a film phase where the mass transfer of ethylene glycol was assumed to be the rate controlling process. Following approximation (as given by Eq. 2.7) for the rate of change in hydroxyl group concentration in the film was derived assuming concentration of ester linkages [*Z*]:

$$\frac{d[E_g]}{dt} = -2a_i (Dk)^{1/2} ([EG]_0 - [EG]_i) \tag{2.7}$$

in which, $k = 4k`[Z]$, where $k`$ is the polycondensation of EG in the film; and $[EG]_0$, $[EG]_i$, are the initial concentration of EG in the film and the interfacial concentration of EG respectively. This rate expression was used in the reactor modeling, where both plug flow and axial dispersion were examined. Only the main polycondensation reaction was considered and the side reactions leading to other end groups and byproductss were not considered in their modeling.

Ravindranath and Mashelkar (1986a, 1986b) presented extensive review on polyethylene terepthalate. In their first review article, they focused on chemistry, thermodynamics and transport properties related issues on PET. Historical perspective of synthesis of PET was given in their review article. Detailed production process and chemistry pertaining to PET synthesis was discussed. A detailed mechanism of catalysis related to tran-esterification catalysis and polycondensation catalysis was explored. The catalysts used in the trans-esterification reaction include salts, or mixed salts of sodium, potassium, lithium, calcium, manganese, magnesium, lead, zinc, aluminium and cadmium. However, acetates of zinc, manganese, calcium and sodium gained commercial

acceptance due to their good solubility and catalytic effect in the trans-esterification reaction. Antimony trioxide or antimony triacetate catalysts are commonly used during the polycondensation stage. They presented kinetics of trans-esterification, esterification and polycondensation reactions. A detailed review related mechanism and kinetics of degradation reactions (which occur during all the stages of PET synthesis and during PET processing) were also given. Thermodynamic and transport data pertinent to PET formation mainly focusing on phase equilibria, molecular diffusion in PET, diffusion in molten polymers, diffusion experiments in molten PET and diffusion of volatile products in solid PET were reported.

In their second review article, Ravindranath and Mashelkar, (1986b) presented a detailed engineering analysis of PET. In their work, they extended their earlier modelling (Ravindranath and Mashelkar, 1982) by including various reactions. However it was limited to the analysis of polycondensation in the thin film. In their study, the literature based review related to design of PET reactor system pertaining to stirred polymerization reactors for batch processes, interfacial surface generators for continuous processes, rotating disc contactors, wiped film devices and partially filled screw extruders were reported. Models of PET reactors (e.g. semibatch and continuous trans-esterification, continuous direct esterification, semibatch and continuous polymerization and polycondensation reactors) were also discussed in their review article. In addition, brief review on molecular weight distribution (MWD) related to reversible reactions, interchange reactions, practical implications of MWD equilibration were also given.

Laubriet et al. (1991) presented a steady state analysis of two-phase model for continuous final stage melt polycondensation of PET. The drawbacks of the work of

Ravindranath and Mashelkar (1986b) were identified in their study and an improved mathematical model was proposed. It was proposed that the flow pattern of the melt phase was of the plug flow type and that the vapour phase was well mixed. No distinction between the film phase and the bulk pool was made. No reaction was assumed to occur in the vapour phase. Also it was assumed that mass transfer resistances reside in melt phase only. The major difference in the models proposed by Ravindranath and Mashelkar (1986b), and Laubriet et al. (1991), was that later viewed both the film and the bulk phases as a single reacting phase with mass transfer to a vapour phase through vapour-liquid interface. Thus specific interfacial area (a) represents both the reactor geometry and melt flow distribution pattern in the reactor (Laubriet et al., 1991).

The steady state model proposed by Laubriet et al. (1991) was improved by Saint et al. (1991). They proposed a transient state model for continuous final stage melt polycondensation of PET. The effects of various reactor parameters, such as polymerization pressure, temperature, residence time, feed polymer molecular weight, and the mass transfer parameters, on polymer molecular weight and ethylene glycol rate were examined through numerical simulation of the reactor model. The sensitivity analysis related to the effect of heat-, and mass-transfer coefficients on the reactor performance was also reported.

Bhaskar et al. (2000) used NSGA to carry out the multi-objective optimization of reactor producing fiber-grade PET. In their study, they modified the model of Laubriet et al. (1991) and simulated an industrial wiped film reactor. The model parameters were tuned using three sets of industrial data. Multi-objective optimization study results showed that they obtained a unique optimum solution (no Pareto set of several equally

good, non-dominating points was obtained). They also found several minima in the decision-variable space, where the values of both the objective functions were almost identical. This result, though interesting, was somewhat unexpected and so they attempted to explore this problem further to develop more insight in their subsequent study (Bhaskar et al., 2001). It was found that for the wiped film PET reactor, Pareto set of solutions was obtained whenever temperature was kept constant and was not used as a decision variable. In contrast, a unique point was obtained when the temperature was taken as one of the decision variables. This was due to the conflicting effect of dominant decision variable, i.e., temperature of reactor, on the objective function's value. Thus, NSGA results were dependant on the choice of decision variables. These results also prove the need for a robust algorithm, which caters towards both the convergence to the true Pareto front and the diversity of solution to give maximum spread. They concluded that there is a need to improve NSG algorithm as it failed to give a set of solutions.

Babu et al. (2007) carried out multi-objective optimization of wiped film PET reactor using MODE algorithm. In their study, using same problem formulation, MODE algorithm resulted in a set of solutions, as against single solution obtained using NSGA. The Pareto front obtained using MODE algorithm was due to the conflicting effect of decision variables θ^* and N^*, temperature was found to be at its lower bound at 564.02K and pressure was found to be scattered when plotted against one of the objectives. Though MODE resulted in a set of non-dominated solutions against a single point solutions obtained using NSGA, MODE algorithm needs further improvement. Therefore there exists a need for improving the existing MODE algorithm and test the performance of newly developed strategies of MODE on industrial applications.

2.2.3 Low density polyethylene tubular reactor

Low-density polyethylene (LDPE) is a thermoplastic made from ethylene with a density ranging from 0.915-0.935 g/cm^3. It was the first grade of polyethylene, produced in 1933 by Imperial Chemical Industries (ICI) using a high pressure process via free radical polymerization. Since the inception of production technology of LDPE, there have been a lot of changes in its process due to high demand of the quality finished product. It can be produced using a continuous process either in tubular or autoclave reactors at very high pressure (1300-3400 bars) and high temperatures (225-610 K). The high pressure polymerization using tubular reactors has gained popularity due to its better heat removal capacity, which helps in controlling the properties of the finished product. Some of the desirable properties of LDPE include low crystallinity, low density (0.915-0.935 g/cm^3), and resistance to solvents, chemicals and oxidating agents, apart from the acceptable rheological behaviour (Kalyon et al., 1994). LDPE is widely used for manufacturing various high demand products such as containers, dispensing bottles, wash bottles, tubing, plastic bags for computer components, and various molded laboratory equipment. Due to these varied uses, there has been an increase in demand of LDPE.

Agarwal and Han (1975) reported the effect of various operating parameters such as the axial mixing parameter (the Peclet number), change of feed conditions, the chain transfer to the dead polymers, etc. on the performance of reactor. Axial mixing analysis of tubular reactor was carried out by incorporating the Peclet number in the model. However, Chen et al. (1976), in their study, observed the condition of excessive turbulence and concluded that the axial mixing must not be included due to a high value of Peclet number. Shirodkar and Taien (1986) presented a mathematical model for

tubular reactor and compared the performance of the model with the actual plant data. Their predicted conversion and temperature profiles matched well with actual plant data within 10% accuracy. Brandoline et al. (1988) presented a mathematical model for high pressure tubular reactor for ethylene polymerization. The rate law parameters were evaluated using a set of experimental data available with them. They also reported the order of reaction to be 1.1 for the reaction of oxygen initiation. Dhib and Al-Nidawy (2002) carried out the modeling of free radical polymerization of ethylene using di-functional initiators in an autoclave reactor. The mechanism of di-functional initiation was investigated and the proposed model was tested with the conversion data of ethylene collected from the literature for one mono-functional initiator and two di-functional initiators. Goto et al. (1981) investigated the reaction mechanism of LDPE tubular reaction. They discussed the important experimental and modeling based aspects of polymerization describing the correlations of molecular structure, overall rate of polymerization, termination and propagation, chain transfer to solvent, backbiting, chain transfer to polymer, formation of unsaturated structure, etc. The values of rate law parameters corresponding to the above mentioned mechanism and the calculation method for molecular weight were reported. A simulation based study of the single initiator feed tubular reactor showing the effect of several parameters such as change in initiator concentration, initial temperature, jacket temperature, reactor diameter, wall heat transfer coefficient, etc. on reactor performance was reported by Gupta et al. (1985). They showed the importance of such simulation based study and concluded by emphasizing the need for a detailed stability analysis considering that the inherent reactor instability can pose a considerable problem. Very few researchers (Lacunza et al., 1998) discussed the

heat transfer aspects involved in the high pressure tubular reactor. They showed that the assumption of constant overall heat transfer coefficient (U) lead to a certain degree of error in conversion and the polymer property when compared with the experimental values. Lee et al. (2000) investigated the effects of change in initiator flow rate, and monomer flow rate, initiator concentration using a mathematical model for industrial high pressure autoclave polyethylene reactor including the decomposition phenomena. Brandoline et al. (1991) presented an optimization study and discussed the technical feasibility of each set of objectives with respect to the weight based multi-objective optimization scenario. Issues related to the effect of multiple feeds on temperature profile, and the trade-off between the conversion and the polydispersity index were discussed. The optimal control of the industrial reactor with and without initiator injections was carried out to maximize the final monomer conversion using the reactor jacket temperature as the control variable. Kalyon et al. (1994) presented a mathematical model and the rheological characterization of LDPE. Data from a commercial reactor having a reactor length of 720 (m) was used. They presented the results of their model predictions and the experimentally determined LDPE properties for long- and the short-chain branching for three different polyethylene resins. Rheological behavior of these different resins was studied with respect to apparent viscosity, shear stress, modulus of elasticity, etc. Recently, Kim and Iedema (2008) carried out the modeling of branching density and branching distribution in LDPE polymerization. They concluded that the concentration of long chain branching (LCB) is close to those of first branching moment in both the CSTR and the tubular reactor systems.

Table 2.1a Rate constant parameters and bounds used in some of the studies reported in the literature

Reaction	Parameter	Bounds of variables considered in this study	Values reported by Goto et al. (1981)*		Values reported by Chen et al. (1976)**		Values reported by Agarwal and Han (1997)*		Values reported by Shirodkar and Tsien (1986)*	
			A_0 (L/mol.s)	E (cal/mol)	A_0 (L/mol,s)	E (cal/mol)	A_0 (L/mol. s)	E (cal/mol)	A_0 (L/mol.s)	E (cal/mol)
Initiation	E_o	$125604<E_o<138164$	$2.39x10^{19}$	37300 + 0.06P	$1.6x10^{16}$	38400	$0.75k_{d0}$	E_d+0.17P	--	--
Peroxide Initiation 1	E_{d1}	$117230<E_{d1}<136071$	--	--	--	--	--	--	--	--
Peroxide Initiation 2	E_{d2}	$117230<E_{d2}<133977$	--	--	--	--	--	--	--	--
Propagation	E_p	$14653<E_p<18003$	$5.63x10^{11}$	10520-0.477P	$2.95x10^{7}$	7091	$1.25x10^{8}$	7800+0.5P	$5.8x10^{7}$	7,769-0.259P
Chain transfer to solvent/ modifier	E_{trs}	$14653<E_{trs}<20934$	$1.23x10^{19}$	12820-0.4722P	--	--	$k^0_{trs}\exp(12000/RT^0)$	12000	--	--
Backbitting (Intramolecular chain transfer)	E_{bb}	$56521<E_{bb}<66988$	$5.63x10^{12}$	13030-0.569P	--	--	--	--	--	--
β-Scisson of seco. radical	E_{b1}	$71175<E_{b1}<87922$	$8.51x10^{10}$	14530-0.477P	$2.72x10^{11}$	20000	--	--	--	--
β-Scisson of tert. radical	E_b	$62802<E_b<87922$	$5.82x10^{11}$	15760 –0.547P	--	--	--	--	--	--
Termination by combination	E_{bc}	--	$3.00x10^{11}$	3000 +0.3418P	$1.6x10^{9}$	2400	$2.2x10^{10}$	1000+0.244P	$2.8x10^{8}$	298+0.012P
By thermal degradation	E_{tdt}	--	--	--	--	--	--	--	--	--
By chain transf. to polymer	E_{trp}	--	$1.75x10^{12}$	14080+0.1065P	$9.0x10^{5}$	9000	$k^0_{trp}\exp(12000/RT^0)$	12000	$7.5x10^{6}$	8942+0.019P

*E in cal/mol, P in atm, $k=A_0 \exp(-E/RT)$, **E at 2000 atm

Table 2.1b Rate constant parameters and bounds used in the remaining studies (continued from Table 2.1a)

Reaction	Parameter	Values reported by Brandoline et al. (1991)*		Values reported by Lee et al. (2000)*		Values reported by Kim and Iedema(2008)*		Values reported by Brandoline et al (1996)#		Values reported by Agrawal et al. (2006)#
		A_0 (L/mol.s)	E (cal/mol)	A_0	E (cal/mol)	A_0	E (cal/mol)	A_0	E (kJ/kmol)	E (kJ/kmol)
Initiation	E_o	$3.0x10^{10}$	27,941	--	--	--	--	$^{\$}1.6x10^{16}$	135945	132168
Peroxide Initiation 1	E_{d1}	--	--	$^{@}1.309x10^{19}$	33,872	$^{\&}1.35x10^{13}$	14130+0.033P	$^{\theta}1.0x10^{14}$	94621-133140	119929
Peroxide Initiation 2	E_{d2}	--	--	$^{@}1.396x10^{13}$	30,103	$^{\&}2.89x10^{14}$	16627+0.1217P	$^{\theta}1.0x10^{12}$	94621-132721	123117
Propagation	E_p	$1.0x10^{6}$	5,245	$^{\Delta}4.16x10^{6}$	6477-0.56P	$^{\theta}1.88x10^{7}$	4125-0.324P	$^{\theta}1.6x10^{16}$	17626	17431
Chain transfer to solvent/ modifier	E_{trs}	$1.7x10^{6}$	9,443	$^{\Delta}1.309x10^{19}$	33,872	$^{\theta}1.99x10^{7}$	5499-0.3253P	$^{\theta}4.0x10^{5}$	17253	18406
Backbitting (Intramolecular chain transfer)	E_{bb}	--	--	--	--	--	--	$^{\theta}1.6x10^{16}$	61964	60537
β-Scisson of seco. Radical	E_{b1}	--	--	--	--	--	--	$^{\theta}1.6x10^{16}$	79967	84747
β-Scisson of tert. radical	E_b	--	--	--	--	--	--	$^{\theta}1.6x10^{16}$	79967	70205
Termination by combination	E_{bc}	$3.0x10^{8}$	3,950	$^{\Delta}3.0x10^{8}$	3.950	$^{\theta}8.11x10^{8}$	553.26+0.19P	$^{\theta}1.6x10^{16}$	15282	15282
By thermal degradation	E_{tdt}	$7.3x10^{6}$	11,315	$^{\Delta}3.0x10^{8}$	3.950	--	--	$^{\theta}1.6x10^{16}$	79968	79968
By chain transf. to polymer	E_{trp}	$4.4x10^{6}$	9,500	$^{\Delta}3.0x10^{4}$	9375-0.48P	$^{\theta}2.15x10^{5}$	5921-0.04059P	$^{\theta}1.6x10^{16}$	36844	36844

*E in cal/mol, P in atm, $k=A_0 \exp(-E/RT)$, **E at 2000 atm; $^{\theta}A_0$ in m^3/kmol.s; $^{\&}A_0$ in m^3/s; $^{@}A_0$ in L/mol.s; $^{\Delta}A_0$ in s^{-1}

#$k=A_0 \exp(-(E+10^3 P\Delta V)/RT)$, where, P in Mpa, E in kJ/kmol, ΔV in m^3/mol, $A_0=m^3kmol^{-1}s^{-1}$; $^{\$}$ $m^{3.3}kmol^{-1}s^{-1}$

[a] Asteasuain et al. (2001)

Large variation in the rate law parameters is observed from the literature survey and the data observed in those studies is reported in Table 2.1a and Table 2.1b. The large variation in the values of rate law parameters is attributed to the complexity of the process and also to the variation in the geometry (length, number of initiator injections and their positions) of the reactor considered by the individual workers. Agarwal et al. (2006) used NSGA-IIaJG to solve LDPE tubular reactor under multi-objective optimization scenario. They maximized the monomer conversion and minimized the sum of the normalized concentrations of the three important side products (methyl, vinyl, and vinylidene groups). There exists a scope to reconsider the same problem for parametric estimation using different solver (if required) and reattempt to solve the problem for MOO, as true Pareto front for industrial problems is not known. It is possible that a new algorithm may or may not give a better Pareto front, but in search of true Pareto front, there exists a need to reconsider the problem with improved newly obtained parameters and using a new evolutionary MOO algorithm.

2.2.4 Supply chain and planning

The supply chain is an integrated network of retailers, distributors, transporters, storage facilities and suppliers that participate in the sale, delivery and production of a particular product. The purpose of supply chain is to enhance the profit of an organization by availing of raw materials, transforming raw materials into finished products, enhancing distribution system of products and facilitating the flow of raw materials, finished products, information and liquidity among suppliers, manufactures, retailers, distributors and the logistic providers. Lasschuit and Thijssen (2004) had emphasized the importance

of supply chain planning and scheduling decisions in the oil and chemical industry. The decisions taken at various stages within the supply chain (i.e., supply, manufacturing and distribution) and at various levels in the management hierarchy (i.e., planning, scheduling and operation) differ in business scope, time horizon adn resolution, data certainty and accuracy. They recommended the need for integrated planning of these entities. The mathematical model resulting at strategic and global planning level is a mixed-integer non-linear programming (MINLP). They mentioned that inclusions of such mathematical models during the strategic decision-making process yields substantial benefits in economic terms and also provide an improved understanding of the interactions among various components of business.

Masini et al. (2009) presented the optimization of supply chain planning in fruit industry. They developed a mixed integer linear programming model for apple and pears concentrated juice plant. The net profit was maximized considering the cost of each variety of raw material, selling prices of each product in different markets, fruit production for each farm and fruit variety, distances (among farms, processing plants and markets), packaging and juice plant capacities, demands for each product and market, etc., as model parameters. The whole model comprised of 14,335, continuous variables, 3,372 binary variables, 4,421 equality and 7,524 inequality constraints. The open solver licensing (OSL) within GAMS package was used to solve the MILP optimization model and generate the optimum solutions. Ferrio and Wassick (2008) presented a MILP which is capable of optimizing a multi-product supply chain network made up of production sites, an arbitrary number of echelons of distribution centres, and customer sites. The model results were processed to assign cost components to individual customer records.

Silva et al. (2009) used ant colony optimization to optimize the distributed supply chain management. Based on the modeling of a generic supply with suppliers, logistics and distributers as a distributed optimization problem, they presented a supply chain management technique. Considering the importance of supply chain planning in academics and industry, several books are published (Simchi-Levi et al., 2008; Shah, 2009; Silver et al., 1998, etc.).

Researchers used models based on multi-objective optimization functions (Melachrinoudis and Min, 2000; Nozick and Turnquist, 2001) but they solved these problems using classical method converting the problem into a single objective optimization problem. Considering the potential of evolutionary algorithms, Pinto (2007) used NSGA-II to optimize supply chain planning model for multiple objectives. Objectives such as minimization of total operating cost, minimization of the ratio of manufacturing costs to total operating cost, maximization of profit, minimization of manufacturing cost, minimization of total cost, and maximization of revenue were considered under 4-cases of two-objective optimization study. This MOO problem involved 36 variables and 6 constraints in the study.

2.2.5 Liquid phase oxidation of *p*-xylene

Liquid phase oxidation of hydrocarbons, using air or oxygen has gained popularity in industrial applications due to its ability of converting petroleum hydrocarbon feed stocks such as olefins, aromatics and alkanes, into industrial organic chemicals which are important in many polymer and petrochemical industries. One of the important chemicals produced from *p*-xylene is purified terephthalic acid (PTA).

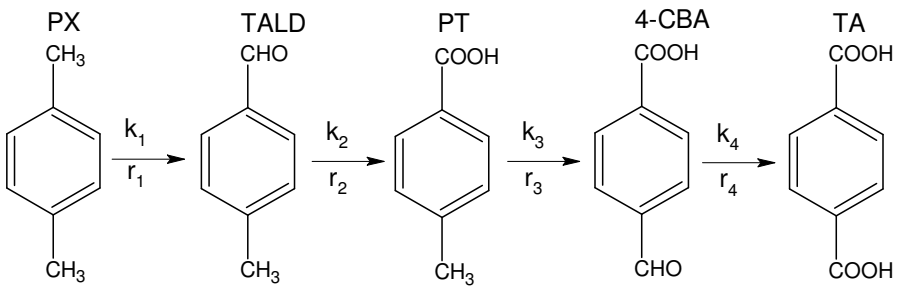

(2.8)

PTA is mainly consumed worldwide in the production of polyester fiber (65%). Other uses of PTA include the production of polyethylene terephthalate bottle resin (27%) and the remaining (8%) is used in the production of plastic end products such as cyclohexane dimethanol, terephthaloyl chloride, copolyester-ether elastomers, plasticizers and liquid crystal polymers (ICIS, 2007). Considering the demand of this product, it is mandatory to either develop new plants or to improve the efficiency of existing plant by means of proper scale up and modeling, simulation and optimization of the existing process. Even a slight improvement in yield/quality of the desired product can be of immense importance in the production of PTA. Liquid phase oxidation of *p*-xylene to PTA is a complex process which involves series of multiple oxidation steps. The reaction scheme for catalytic oxidation of *p*-xylene is shown by Eq. 2.8. The process is called Amoco Mid-Century (MC) process which is named after the discovery of Mid-Century catalyst (Partenheimer, 1995). The reaction takes place in a continuously stirred tank reactor (CSTR) with Ti/hastelloy lining. Liquid phase mixture of *p*-xylene (PX), acetic acid (solvent), water, and catalyst are added into the reactor. The temperature is allowed to increase to a desired value. The gas, i.e., air is then continuously fed through the liquid. The reaction takes place in a typical temperature range of 190-205 ^{0}C and at a pressure in the range of 15-30 bar. The initial water content in the solvent plays an important role in the reaction mechanism. For oxidation of first methyl group, the

oxidation rate decreases monotonically with an increase in water content, thus inhibiting the oxidation rate. But for the oxidation of second methyl group, the oxidation rate increases with an increase in the water content. There also exists an optimal water content for the reaction. When water content is less than this optimum value, the overall oxidation rate increases with an increase in water content, and when the water content is greater than the optimal value, overall oxidation rate decreases with the increase in water content (Wang et al., 2005a). The catalyst concentration also has a strong influence on the main reaction step. At low concentration of the catalyst, the reaction rates are more sensitive to catalyst concentration than at high catalyst concentration. The variation of catalyst concentration affects the rate constants k_1 and k_2 much more significantly than k_3 and k_4 (Wang et al., 2005b). Therefore, reaction rates k_1 and k_2 only are correlated with the catalyst concentration in the present study. Vent oxygen content also has a significant effect on the reaction performance. Wang et al. (2005b) have shown that partial pressure of oxygen in the range of 10-20 kPa influences the reaction significantly. The temperature dependence of each of the reaction is given by Arrheneous rate law. Thus the outcome of complex series reaction mechanism depends on several parameters.

Several studies related to kinetics of *p*-xylene are reported in the literature. Suresh et al. (2000) have given elaborated engineering aspects of industrial oxidation of several hydrocarbons, such as *p*-xylene, cyclohexane, cumene, isobutane, cycloalkenes, vinyl cyclohexene etc. Their study includes survey, mechanism, chemistry, kinetics and other processing aspects of industrial hydrocarbons oxidation. The *p*-toluic acid is 10 times less reactive than *p*-xylene and high yields of *p*-toluic acid can be obtained before oxidation of second methyl group commences (refer Eq. 2.8 for reaction sequence). Milan et al.

(1985) presented the kinetics and the mechanism for cobalt catalyzed oxidation of *p*-xylene in the presence of water. They mentioned that with an increase in conversion, the concentration of 4-carboxybenzoic acid (4-CBA) increases in the final product. Raghavendrachar and Ramchandran (1992) reviewed the technological aspects of *p*-xylene oxidation highlighting several industrial processes for manufacturing of PTA. They discussed several processes for technical grade PTA such as HNO_3 oxidation of *p*-xylene, catalytic liquid phase air oxidation, Mid-Century process, Eastman-Kodak process, Maruzen process, Toray process, Teijin process, etc. Cao et al. (1994a) presented a lumped kinetic scheme for catalytic oxidation of *p*-xylene to terephthalic acid. They concluded that all lumped reactions were of first order with respect to the liquid reactant and of zero order with respect to oxygen. In another study, Cao et al. (1994b) presented a model for simulation of gas liquid semi-batch reactor for oxidation of *p*-xylene. Their model accounts for zero-order kinetics by checking at each time whether the oxygen flux entering the liquid bulk is sufficient enough to sustain the reaction. The studies related to the development of kinetic scheme in the field of catalytic liquid phase oxidation of *p*-xylene are well documented in the literature (Cheng et al., 2005, 2006; Yan et al., 2004; Milan et al., 1982). Mu et al. (2004) carried out multi-objective optimization study of industrial purified terephthalic acid (PTA) oxidation process using Neighborhood and Archived Genetic Algorithm (NAGA). Their study included 7 decision variables, namely, total feed rate (F_{FEED}), catalyst concentration (C_0), water withdrawal rate from the reactor (WWD), vent oxygen content of reactor (V_{OR}), vent oxygen content of crystallizer (V_{OC}), temperatures of reactor (T_R) and crystallizer (T_C). Out of these 7 decision variables which Mu et al. (2004) considered, the data and the correlations for some of them are either

unavailable in the literature or proprietary with the industry and hence inaccessible, as mentioned by the authors (Mu, 2007). Taking this practical problem into account we made an attempt to simplify the above problem by reformulating and incorporating the readily available and easily measurable decision variables. There also exists a scope for reconsidering the same problem to be solved using an improved multi-objective optimization algorithm and compare the performance of new algorithm.

2.3 Existing gaps of research

The existing literature on evolutionary multi-objective optimization algorithms suggests that great strides have been made in developing new algorithms based on natural phenomena in the last two decades. However, due to the complexity involved in the industrial processes and benchmark test problems, the attainment of global Pareto front with good diverse set of solutions is scarce. Various algorithms such as NSGA, NSGA-II and their improved variants, SOMA, SPEA, PAES are applied successfully to find the Pareto optimal set of solutions. Though these algorithms have been successfully applied to some problems, they failed to give global Pareto fronts with diverse set of solutions for many other problems. MODE algorithm has been successful even for those problems which the popular EMO algorithms (NSGA) failed to give multiple solutions on Pareto front. Differential evolution which is an improved version of GA is found to give optimal solutions at a faster rate for single objective optimization (Angira, 2005; Angira and Babu, 2006a, 2006b, 2006c). Therefore there exists a scope to extend DE to solve multi-objective optimization problems. Though MODE algorithm was developed earlier, it has specific problems such as removal of dominated solutions in each generation and

non-preservation of solutions. MODE algorithm gave comparable Pareto fronts for few industrial problems. However, there is a great scope and potential to improve the existing MODE algorithm. There is also a need to test the performance and robustness of MODE algorithm with the help of benchmark test problems.

Various industrial applications as discussed in section 2.2 involving multiple objectives to be optimized are studied and gaps have been identified as mentioned against each of process in section 2.2. These problems are solved using different algorithms. But as true Pareto optimal front for industrial applications is not known, there is a need to revisit such industrial applications and then apply the newly developed and validated (for their performance) algorithms to find the Pareto optimal fronts and the optimal set of decision variables.

Taking some of the limitations of MODE algorithm into account, there exists a need to develop new strategies of MODE. Hybrid algorithms involve a combination of traditional deterministic methods and the evolutionary algorithms to improve the performance of a standalone evolutionary algorithm. Hybrid algorithms have shown good potential in terms of achieving the optimal solutions at a faster rate in case of single objective optimization (Chiou and Wang, 1999). Hybrid methods have been developed for solving both single- and multi-objective optimization problems. But MODE algorithm or its strategies are not yet been hybridized with the local search methods. Therefore there is a great potential and need to develop a hybrid strategy of MODE algorithm and test its performance on identified processes and benchmark test problems. NSGA-II algorithm involves combination of elite population preservation and a crowding distance approach for solving MOO problems. There is a scope towards developing an elitist

strategy of MODE. Along with Elitist and hybrid strategy of MODE, there also exists a need towards improving the performance of MODE by perturbing its mutation strategy using trigonometric mutation approach.

It is necessary to test the performance of newly developed algorithms (especially in terms of Pareto front and convergence and divergence) with other well known algorithms. Many evolutionary algorithms, though give good visual view of the Pareto front, its comparison with true Pareto front using benchmark test function is important. Therefore, there exists a need towards testing the performance metrics of newly developed strategies of MODE algorithm and compare them with those obtained using other popular algorithms.

2.4 Scope of Work

Industrial applications reported in the literature which involve multiple process design decisions are studied and the gaps of the research have been identified (as mentioned in section 2.2 and 2.3). These processes are simulated using suitable numerical techniques and multi-objective differential evolution algorithm is used to obtain the Pareto optimal set of solutions and the decision variables. The industrial applications include Styrene reactor, PET reactor, LDPE tubular reactor, oxidation of p-xylene to PTA and supply chain and planning. New strategies of MODE namely MODE III, Elitist MODE, hybrid MODE and trigonometric MODE are developed. The Pareto optimal set of solutions is obtained for benchmark test problems using new strategies of MODE and are compared with the results obtained using NSGA-II. The Pareto optimal set for industrial applications (case studies) is also obtained using strategies of MODE and is compared

with Pareto front obtained using other evolutionary algorithms. Important performance metrics such as convergence metric and divergence metrics are computed for newly developed strategies and their performance is compared with other well known algorithms from the literature [such as NSGA-II (both real- and binary- versions), SPEA, PAES].

Summary of chapter: In this chapter a detailed literature survey on MOO algorithms and few of the industrial applications on multi-objective optimization is given. MOO algorithms are classified into two categories, namely, classical methods and the evolutionary population based search algorithms. The industrial applications include MOO of styrene reactor, MOO of PET reactor, MOO of oxidation of *p*-xylene, MOO of LDPE tubular reactor and MOO of supply chain and planning. Existing gaps of the research are identified and are reported. The chapter ends with scope of the present work.

Next chapter deals with detailed description of various strategies of MODE algorithms developed in this work.

CHAPTER – 3

DEVELOPED ALGORITHMS AND DETAILED WORKING PRINCIPLES

Inspiring from the outcome of MODE algorithm, a need towards developing new and innovative strategies of MODE was felt. Therefore, few improved strategies were

developed. This chapter presents various multi-objective differential evolution strategies developed in this study.

Strategies of MODE Algorithm

MODE algorithm proposed by Babu et al. (2005) has been successfully used for multi-objective optimization of industrial styrene reactor. Differential evolution (DE) (Price and Storn, 1997; Babu, 2004; Onwubolu and Babu, 2004; Babu and Angira, 2005; Babu and Angira, 2005, 2006; Angira and Babu, 2006a, 2006b, 2006c; Babu et al, 2005b; Babu, 2007) is an improved version of Genetic Algorithms (GA) (Goldberg, 1989). MODE is an extension of differential evolution for multi-objective optimization study.

3.1 MODE -I algorithm

The simplified flowchart of the original MODE algorithm (MODE-1) is presented in Fig 3.1. The detailed flowchart of MODE algorithm is given in chapter 2. In MODE-1 algorithm, in each generation, the dominated solutions are removed from the list and only

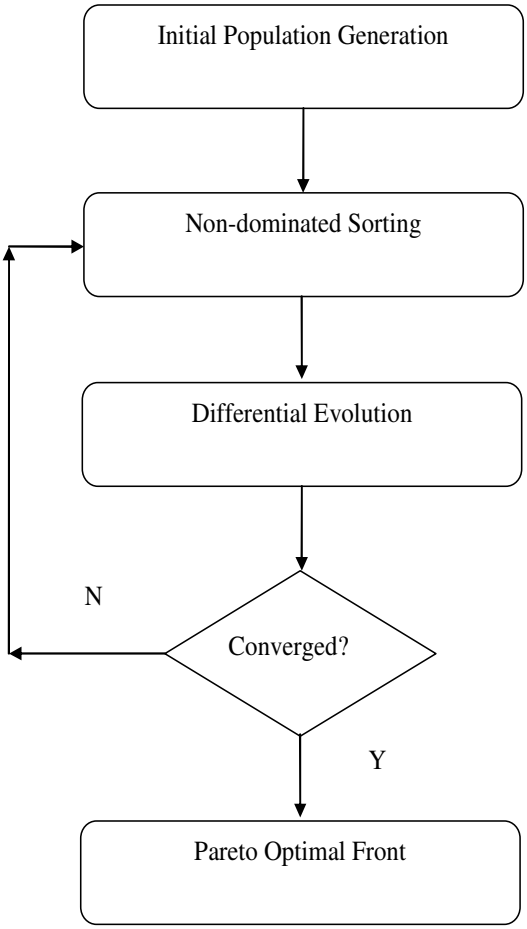

Fig. 3.1 Simplified flowchart of MODE-I algorithm

the non-dominated solutions are allowed to undergo DE operations. The scaling factor is generated from a random number generator between 0 and 1. The off springs are placed into population if they are better than the the main parent. The pseudo-code of MODE-I algorithm is given below:

***Pseudo-code for MODE - I*

• *Choose a seed for the random number generator.*

• *Initialize the values of D, NP, CR and MAXGEN.*

• *Initialize all the vectors of the population randomly. The*

variables are normalized within the bounds.

for i = 1 *to NP*

{ *for j* = 1 *to D*

$\boldsymbol{X}i,j$ = *Lower bound* + *random number* ∗ *(upper bound*

−lower bound)}

• *All the vectors generated should satisfy the constraints* (*if present*). *Penalty function approach, i.e., penalizing the vector by giving it a large value, is followed only for those vectors, which do not satisfy the constraints.*

• *Evaluate the functions of each vector.*

for i = 1 *to NP*

$\boldsymbol{C}i,j$ = *functj ( ) j* = 1, . . . , *no of objectives*

• *Remove all the dominated solutions using naïve and slow approach.*

• *Perform mutation, crossover, selection and evaluation of the objective function for non-dominated solutions for a specified number of generations.*

While (*gen* < *MAXGEN*)

{ *for i* = 1 *to number of Non-dominated solutions*

{

• *For each vector* $\mathbf{X}i$ (*target vector*), *select three distinct*

vectors $\mathbf{X}a$, $\mathbf{X}b$ *and* $\mathbf{X}c$ *randomly from the current population*

other than the vector $\mathbf{X}i$

do

{*r*1= *random number* ∗ *NP*

*r*2= *random number* ∗ *NP*

*r*3= *random number* ∗ *NP*

}*while*(*r*1 = *i*)*OR*(*r*2 = *i*)*OR*(*r*3 = *i*)*OR*(*r*1 = *r*2)*OR*

(*r*2 = *r*3)*OR*(*r*1 = *r*3)

• *Perform crossover for each target vector* $\mathbf{X}i$ *with its noisy vector* $\mathbf{X}n,i$ *and create a trial*

vector, $\mathbf{X}t,i$. *The noisy vector is created by performing mutation*.

• *for binomial crossover*

{*p*= *random number*

*j*rand = *int*(*rand*[0, 1] ∗ *D*) + 1

for n = 1 *to D*

{*if* (*p* <*CR or n* = *j*rand)

$\mathbf{X}n,i = \mathbf{X}a,i + F(\mathbf{X}b,i - \mathbf{X}c,i)$

$\mathbf{X}t,i = \mathbf{X}n,i$

} *else* $\mathbf{X}t,i = \mathbf{X}i,j$

Again, the NP noisy random vectors that are generated should satisfy the constraints (if present). Penalty function approach is applied to those vectors which do not satisfy the constraints.

• Perform selection for each target vector, ***X****i by comparing*

its function value with that of the trial vector, ***X****t,i . If* ***X****t,i*

dominates completely ***X****i then replace* ***X****i by* ***X****t,i*

*if (****C****t,i dominates* ***C****i)*

new ***X****i =* ***X****t,i*

else new ***X****i =* ***X****i* }

/∗ return the set of non-dominated solutions ∗/

}

Print the results (*after the stopping criterion is met*).

3.2 MODE -II algorithm

In MODE-I algorithm, we apply non-dominated sorting procedure in each generation. Due to this, the size of population decreases in every generation. In order to perform differential evolution operations, we need at least four chromosomes (one target vector and three other vectors for mutation operation). In any generation, if the population size becomes less than four after non-dominated sorting, then it will not be possible to run DE algorithm and Pareto optimal front will not be obtained. This problem can be overcome by increasing the initial population size. But even then we cannot guarantee that more than minimum required (four) non-dominated solutions will be obtained. Other way is to keep the population size constant in every generation by adding randomly generated

chromosomes to the non-dominated chromosomes after non-dominated sorting. As the number of generation increases, the non-dominated individuals will increase and finally all the individuals will converge to the Pareto optimal front. The Simplified flow chart of MODE-II is presented in Fig. 3.2.

The pseudo-code of MODE-II algorithm is given below:

***Pseudo-code for MODE - II*

• *Choose a seed for the random number generator.*

• *Initialize the values of D, NP, CR and MAXGEN.*

• *Initialize all the vectors of the population randomly. The variables are normalized within the bounds.*

for i = 1 *to NP*

{ *for j* = 1 *to D*

X*i,j = Lower bound + random number ∗ (upper bound*

−lower bound)}

• *All the vectors generated should satisfy the constraints* (*if present*). *Penalty function approach, i.e., penalizing the vector by giving it a large value, is followed only for those vectors, which do not satisfy the constraints.*

• *Evaluate the functions of each vector.*

for i = 1 *to NP*

C*i,j = functj ( ) j* = 1, . . . , *no of objectives*

• *Remove all the dominated solutions using naïve and slow approach.*

• *Perform mutation, crossover, selection and evaluation of the objective function for non-dominated solutions for a specified number of generations.*

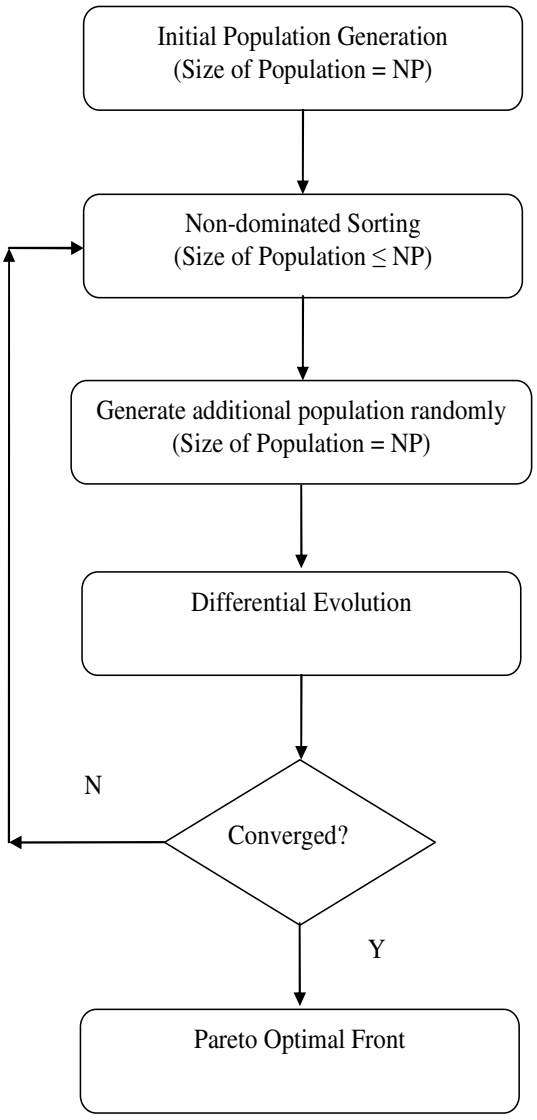

Fig. 3.2 Simplified flowchart of MODE-II algorithm

While (*gen* < *MAXGEN*)

• Remove dominated points from the population and g*enerate additional population points randomly using the mapping rule till total population size is NP.*

{ *for i* = 1 *to number of Non-dominated solutions*

{

• *For each vector* ***X****i* (*target vector*), *select three distinct*

vectors ***X****a*, ***X****b and* ***X****c randomly from the current population other than the vector* ***X****i*

do

{*r*1= *random number* ∗ *NP*

*r*2= *random number* ∗ *NP*

*r*3= *random number* ∗ *NP*

}*while*(*r*1 = *i*)*OR*(*r*2 = *i*)*OR*(*r*3 = *i*)*OR*(*r*1 = *r*2)*OR*

(*r*2 = *r*3)*OR*(*r*1 = *r*3)

• *Perform crossover for each target vector* ***X****i with its noisy*

vector ***X****n,i and create a trial vector*, ***X****t,i . The noisy vector*

is created by performing mutation.

• *for binomial crossover*

{*p*= *random number*

*j*rand = *int*(*rand*[0, 1] ∗ *D*) + 1

for n = 1 *to D*

{*if* (*p* <*CR or n* = *j*rand)

$\boldsymbol{Xn,i} = \boldsymbol{Xa,i} + F(\boldsymbol{Xb,i} - \boldsymbol{Xc,i})$

$\boldsymbol{Xt,i} = \boldsymbol{Xn,i}$

} *else* $\boldsymbol{Xt,i} = \boldsymbol{Xi,j}$

Again, the NP noisy random vectors that are generated should satisfy the constraints (if present). Penalty function approach is applied to those vectors which do not satisfy the constraints.

• *Perform selection for each target vector,* $\boldsymbol{Xi}$ *by comparing its function value with that of the trial vector,* $\boldsymbol{Xt,i}$ *. If* $\boldsymbol{Xt,i}$ *dominates completely* $\boldsymbol{Xi}$ *then replace* $\boldsymbol{Xi}$ *by* $\boldsymbol{Xt,i}$

if ($\boldsymbol{Ct,i}$ *dominates* $\boldsymbol{Ci}$ *)*

new $\boldsymbol{Xi} = \boldsymbol{Xt,i}$

else new $\boldsymbol{Xi} = \boldsymbol{Xi}$ }

/ return the set of non-dominated solutions */*

}

Print the results (*after the stopping criterion is met*).

The algorithm works as follows: An initial population is generated at random. In every generation all dominated solutions are removed from the population. And same number of random solutions is added to the non-dominated population to maintain the population size constant. DE operations, recombination and selection, are performed on this population to obtain the next generation individuals. This process continues till stopping criterion is met or Pareto optimal front is obtained.

3.3 MODE -III algorithm

The recombination operation in DE is proved to be a powerful technique. In recombination, a competition is made between trial and target vectors. It means that there is a competition between the child (offspring) and Parent vector. The non-dominated vector between the trial and target vectors is sent to the next generations (Survival of the fittest). This domination check alone can give the Pareto optimal front. So the non-dominated sorting before the DE loop can be removed (from original MODE algorithm). At the end of the maximum generations, a non-dominated sorting check is kept to remove the individuals which are not on the Pareto optimal front. Simplified flow chart of MODE-III algorithm is presented in Fig 3.3.

The algorithm works as follows: An initial population is generated at random. In every generation the DE operations, recombination and selection, are performed on the individuals of the population to obtain the next generation of individuals. This process continues till stopping criterion is met or Pareto optimal front is obtained. After the last generation non-dominated sorting is performed to remove the dominated solutions, if any. The pseudo-code of MODE III algorithm may be represented as below:

***Pseudo-code for MODE - III*

Initialize the Crossover Constant (CR), Maxgen, Size of Population (NP), Number of Dimensions (D)

for i=1:NP

for j=1:D

X_{ij}= *Lower (j) + (Upper (j) –Lower (j)) *rand (0,1);*

End for

Evaluate Cost(i)

End for

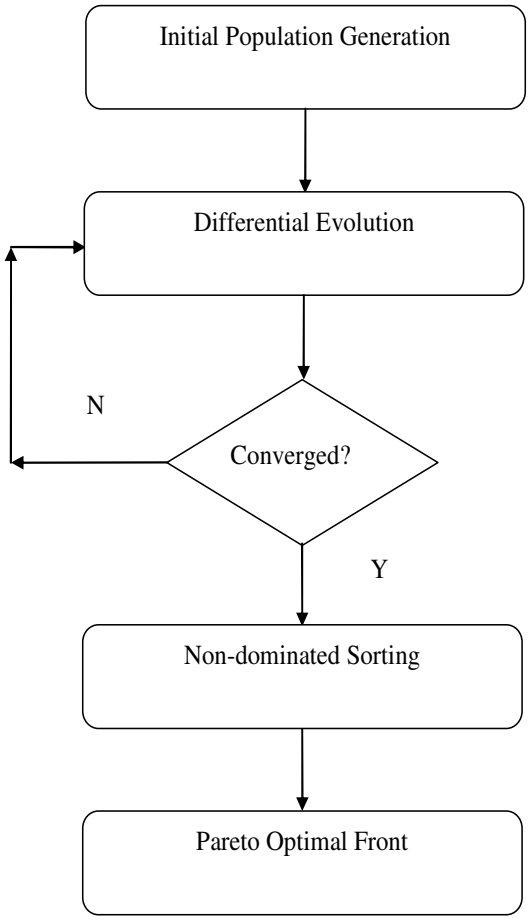

Fig. 3.3 Simplified flowchart of MODE-III algorithm

%Perform mutation, crossover, selection and evaluation of the objective function for %trial and target vector for a specified number of generations.

*For gen=1:Maxgen **Generation Loop***

For i:1:NP ***Population Loop***

Select Target vector X_i

Select three distinct vectors X_a, X_b *and* X_c *other than* X_i

do

{

r_1*=round (rand*NP)*

r_2*=round (rand*NP)*

r_3*=round (rand*NP)*

}

while $[(r_2 == i) \| (r_1 == i) \| (r_3 == i) \| (r_1 == r_2) \| (r_1 == r_3) \| (r_2 == r_3)]$

J_{rand}*=int[rand(0,1)*D] + 1*

for q=1:D

{

if $(p<CR \| q == j_{rand})$

$X_{t,i} = Xr_1 + F(Xr_2 - Xr_3)$ *%Trial vector*

else

$X_{t,i} = X_{i,,j}$ *%Trial vector*

}

Evaluate Trial vector

%Perform selection for each target vector, $\mathbf{X}_i$ *by comparing its function value with %that of the trial vector,* $\mathbf{X}_{t,i}$ *. If* $\mathbf{X}_{t,i}$ *dominates* $\mathbf{X}_i$ *then select* $\mathbf{X}_{t,i}$ *otherwise select* $\mathbf{X}_i$ *%for the %next generation population.*

If ($\mathbf{X}_{t,i}$ *dominates* $\mathbf{X}_i$)

Replace Target with current $\mathbf{X}_{t,i}$

else Retain current $\mathbf{X}_i$ *as a Target vector*

*end for **population loop end***

*end for **generation loop end***

/ return the set of non-dominated solutions */*

Print the results (*after the stopping criterion is met*).

Although MODE is a powerful algorithm which captures a global search space and generates the trial vector by its efficient recombination operation (crossover and mutation), it needs a sufficient minimum number of population points for converging to the global Pareto front. However, non-dominated sorting technique reduces the number of population points and thus limiting the number of non-dominated solutions obtained in MODE algorithm. This problem of reduction of number of non-dominated solutions was identified and two additional strategies of MODE algorithm namely MODE II and MODE III are proposed. Further improvements of MODE algorithm could be realized, (1) by incorporating the concept of elitism in MODE-II, (2) by using trigonometric mutation operator in MODE-III, and (3) by hybridizing MODE-III with selected deterministic method for local search.

3.4 Elitist-multi-objective differential evolution

The schematic diagram of elitist MODE is shown in Fig. 3.4. There are three major steps in elitist MODE algorithm: (1) Processing of initial population of size *NP* using differential evolution, (2) Combining the solutions obtained from DE (*NP*) and those obtained from non-dominated sorting (*Q*) to get a total of (*NP*+*Q*) solutions ensuring elitism, and (3) Maintaining *NP* number of population points in the next generation by using a crowding distance sorting.

Step 1: Processing of initial population using DE

An initial population of size *NP* (parent population) is created using the mapping rule (Price and Storn, 1997). A target vector is chosen from the population points. Three different vectors X_a, X_b and X_c are also chosen randomly from the initial population. The weighted difference of X_a and X_b vectors is then added into the third vector, X_c. This vector is termed as noisy random vector. Cross over is carried out between target and noisy random vectors to generate the trial vector (X_c'). Competition is then made between the trial and target vectors and the vector giving better cost values is replaced into the population for the next generation.

Step 2: Combining the solutions obtained from DE (NP) and those obtained from non-dominated sorting (Q) to get a total of (NP+Q) solutions ensuring elitism

In a parallel operation, the initial population (parent population) is also sorted for getting the non-dominated solutions. Naïve and Slow sorting algorithm (Deb, 2001) is used for non-dominated sorting of solutions. Say, the number of these non-dominated solutions is *Q*.

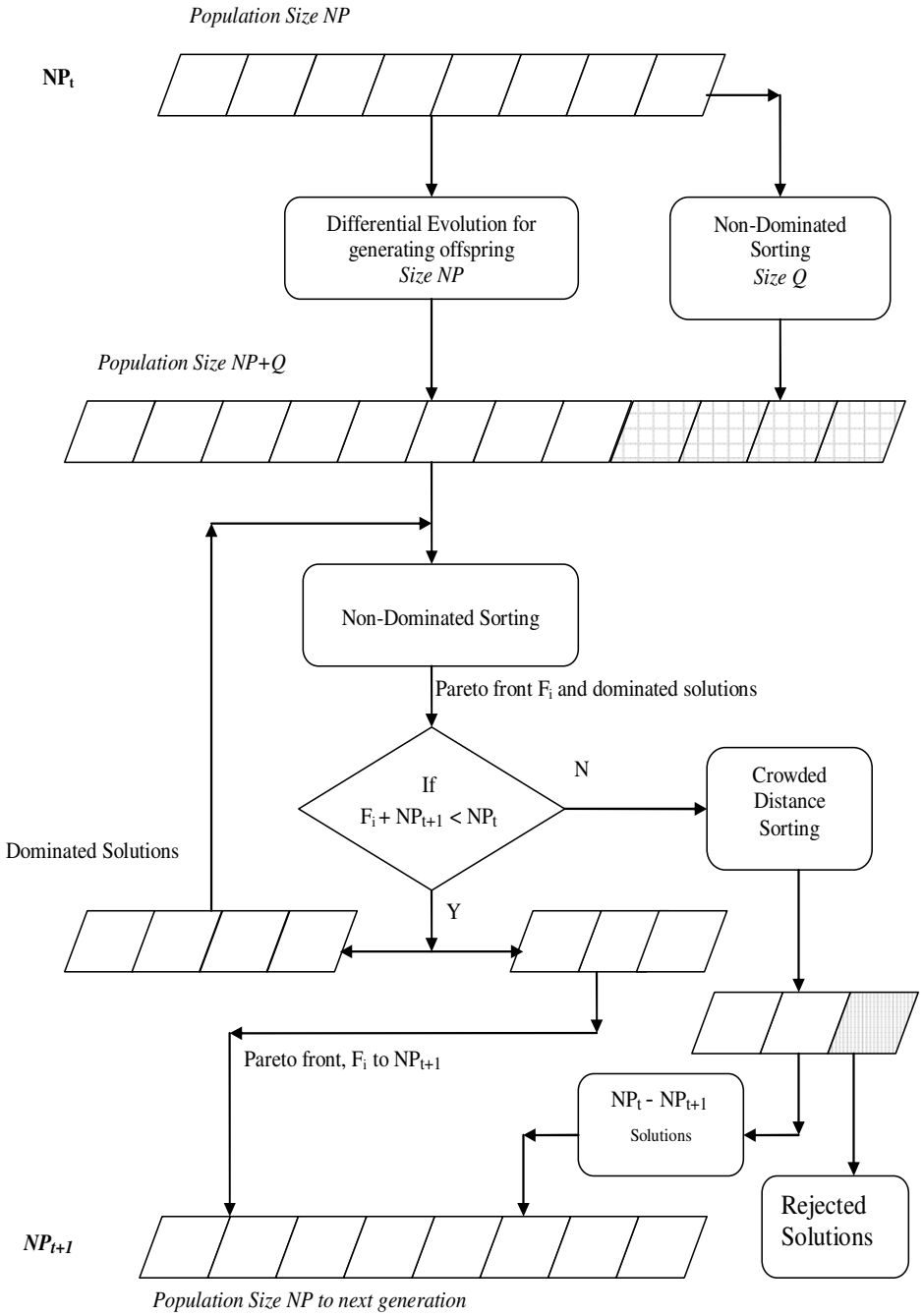

Fig. 3.4 Working principle of elitist MODE algorithm

This Q number of non-dominated population points is then mixed with NP number of offspring population points (as obtained in step-1 above) to generate a total mixed population of size $NP+Q$.

Step 3: Maintaining NP population points in the next generation by using crowding distance sorting:

The $NP+Q$ number of population points is sorted for non-dominance to classify the solutions in different fronts. The first non-dominated solution is referred as front 1.This front is copied into NP_{t+1} population of next generation. The non-dominated sorting is recursively carried out on remaining number of population points and fronts 2, front 3, front 4, upto front N are copied into the population. Since the overall size of intermediate population is $NP+Q$ ($>NP$), not all the fronts may be accommodated into NP_{t+1} (of size NP). Out of $NP+Q$ population points (as generated in steps 1 and 2 above), only NP number of solutions are to be passed through to the next generation. For ensuring this, a crowded tournament selection operator is used. According to the crowded tournament selection operator, a solution i wins the tournament with another solution j if any of the following conditions are true (Deb, 2001):

1. If solution i has a better rank, i.e. $r_i < r_j$.

2. If they have the same rank but solution i has a better crowding distance than solution j, i.e. $r_i = r_j$ and $d_i > d_j$.

This procedure is illustrated in Fig. 3.4. When the previously considered front is not allowed into NP_{t+1}, it may be containing more number of solutions than the vacant space in NP_{t+1}. Crowded distance sorting is then carried out, and the solution containing higher crowding distance value is copied into NP_{t+1} in vacant space.

This operation is continued till the convergence criterion is met. The convergence criteria may be of the following three types: (1) There is no new solution added to the non-dominated front for a specified number of generations, or (2) An upper bound on the number of generations is met, or (3) Combination (1) and (2) mentioned above. In this study, the second criterion is applied.

The pseudo-code of elitist MODE algorithm is given below:

***Pseudo-code for elitist MODE*

• *Choose a seed for the random number generator.*

• *Initialize the values of D, NP, CR and MAXGEN.*

• *Initialize all the vectors of the population randomly. The variables are normalized within the bounds.*

for i = 1 *to NP*

{ *for j* = 1 *to D*

$\boldsymbol{X}i,j$ = *Lower bound* + *random number* ∗ *(upper bound*

–lower bound)}

• *All the vectors generated should satisfy the constraints* (*if present*). *Penalty function approach, i.e., penalizing the vector by giving it a large value, is followed only for those vectors, which do not satisfy the constraints.*

• *Evaluate the functions of each vector.*

for i = 1 *to NP*

$\boldsymbol{C}i,j$ = *functj ( ) j* = 1, . . . , *no of objectives*

• *Remove all the dominated solutions using naïve and slow approach.*

• *Perform mutation*, *crossover*, *selection and evaluation of the objective function for non-dominated solutions for a specified number of generations*.

While (*gen* < *MAXGEN*)

• Remove dominated points from the population and g*enerate additional population points randomly using the mapping rule till total population size is NP.*

{ *for i* = 1 *to number of Non-dominated solutions*

{

• *For each vector* ***X****i* (*target vector*), *select three distinct*

vectors ***X****a*, ***X****b and* ***X****c randomly from the current population other than the vector* ***X****i*

do

{*r*1= *random number* ∗ *NP*

*r*2= *random number* ∗ *NP*

*r*3= *random number* ∗ *NP*

}*while*(*r*1 = *i*)*OR*(*r*2 = *i*)*OR*(*r*3 = *i*)*OR*(*r*1 = *r*2)*OR*

(*r*2 = *r*3)*OR*(*r*1 = *r*3)

• *Perform crossover for each target vector* ***X****i with its noisy*

vector ***X****n,i and create a trial vector*, ***X****t,i . The noisy vector is created by performing mutation*.

• *for binomial crossover*

{*p*= *random number*

*j*rand = *int*(*rand*[0, 1] ∗ *D*) + 1

for n = 1 *to D*

{*if* (*p* <*CR or n* = *j*rand)

$\boldsymbol{Xn,i} = \boldsymbol{Xa,i} + F(\boldsymbol{Xb,i} - \boldsymbol{Xc,i})$

$\boldsymbol{Xt,i} = \boldsymbol{Xn,i}$

} *else* $\boldsymbol{Xt,i} = \boldsymbol{Xi,j}$

Again, the NP noisy random vectors that are generated should satisfy the constraints (if present). Penalty function approach is applied to those vectors which do not satisfy the constraints.

• *Perform non-dominated sorting of parent population. Say the number of non-dominated solution is Q.*

• *Merge NP number of noisy random vectors and Q number of non-dominated vectors to get a total size of population of (NP + Q)*

• *Carry out nondominated sorting of NP+Q number of population points recursively*

• *Append the obtained non-dominated solutions in an array of next generation, if size of current population array + nondominated solutions < NP*

• *If size of current population array + nondominated solutions > NP, Use crowding distance sorting. Calculate the crowding distance for each population points. Assign a high value of crowding distance to the corner points (to give them more priority to enter in next generation population). Sort the population in descending order of crowding distance. Append the required number nondominated solutions in the current population and discard the remaining points.*

/∗ return the set of non-dominated solutions ∗/

}/* End of generation loop */

Print the results (*after the stopping criterion is met*).

3.5 Trigonometric mutation multi-objective differential evolution algorithm

The mutation operation is carried out in MODE and MODE-III algorithms by using three distinct vectors. These vectors are perturbed by applying a scale factor so that a new and hopefully efficient vector (noisy random vector) is created (Price and Storn, 1997). However, the noisy random vector thus created does not get any direction towards the better function value. This is achieved by applying trigonometric mutation operation to the selected vectors. Earlier trigonometric mutation operation was applied to differential evolution algorithm to solve single objective optimization problems (Fan and Lampinen, 2003, Angira and Alladwar, 2007)). In this work we apply trigonometric mutation operation to MODE III algorithm to solve multi-objective optimization problems. The simplified flowchart of trigonometric mutation multi-objective differential evolution algorithm is given in Fig. 3.5. The pseudo-code of trigonometric MODE algorithm may be represented as below:

***Pseudo-code for trigonometric mutation operation for MOO*

Select three distinct vectors X_a, X_b and X_c other than X_i

do

{

r_1=round (rand*NP)

r_2=round (rand*NP)

r_3=round (rand*NP)

} while [(r_2== i) || (r_1==i) ||(r_3== i) ||(r_1== r_2) ||(r_1== r_3) ||(r_2== r_3)]

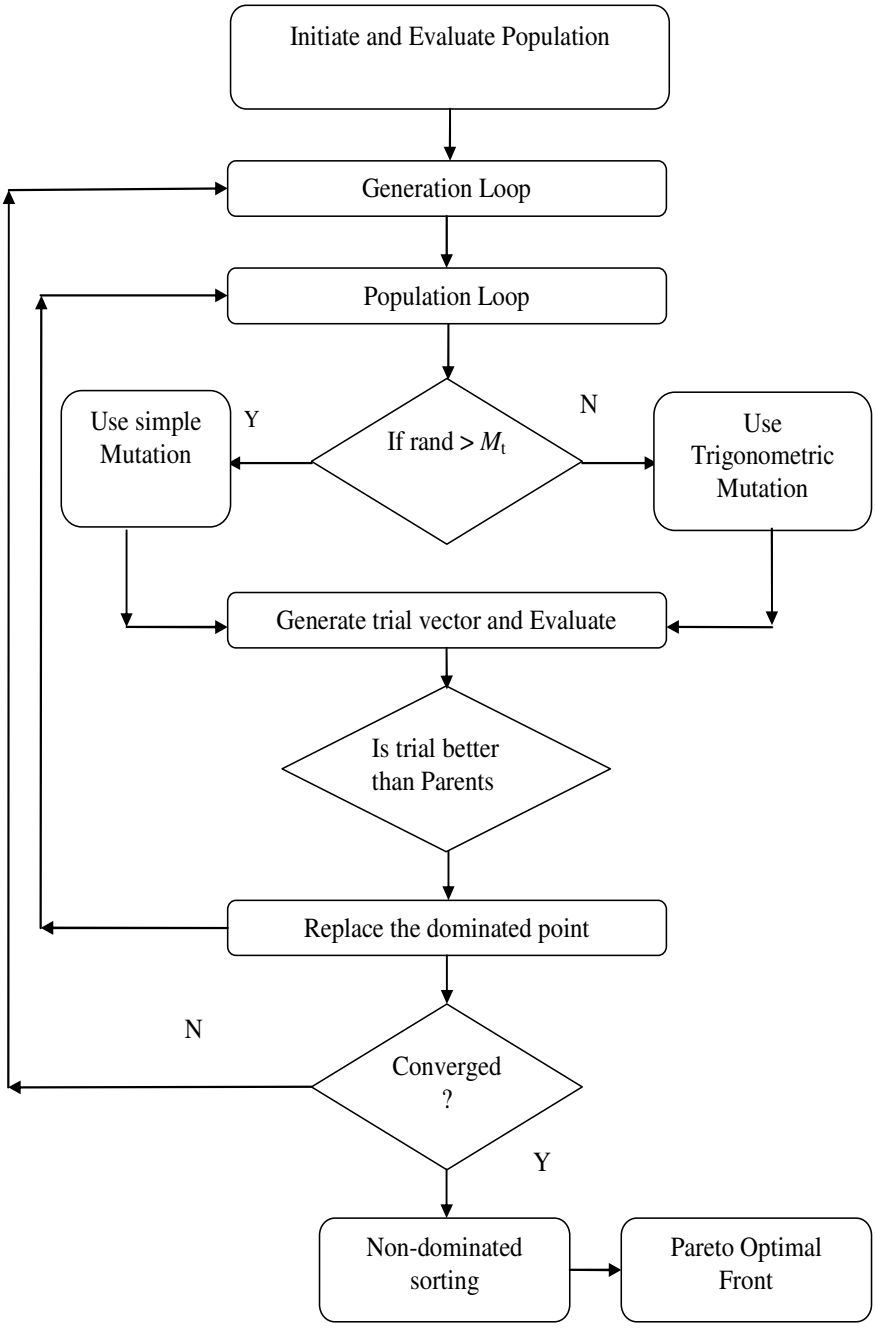

Fig. 3.5 Simplified flowchart of trigonometric MODE algorithm

If (rand(0,1) >Mt)

$Tempp_1$=f(Xr_1);

$Tempp_2$=f(Xr_2);;

$Tempp_3$=f(Xr_3);

Sum= |$Tempp_1$|+| $Tempp_1$|+| $Tempp_1$|

p_1= |$Tempp_1$|/sum;

p_2= |$Tempp_2$|/sum;

p_3= |$Tempp_3$|/sum;

for j=1:D

Xt,i,j = (Xr_1(1,j)+X r_2(1,j) + X r_3(1,j))/3 + abs(p_2-p_1)(X r_1 (1,j) - X r_2 (1,j)) + abs(p_3-p_2)*(X r_2(1,j) - Xr_3(j)) + abs(p_1-p_3)*(X r_3 (1,j)-X r_1(1,j));*

end for

else

$X_{t,i}$=Xr_1 + F (Xr_2-Xr_3) %Trial vector

End

Simple mutation operation involves the random selection of first individual vector out of the randomly selected three vectors. The weighted difference of the two vectors is added to the third randomly selected individual. In case of trigonometric mutation operation, the center point of the hyper geometric point is taken as the vector to be perturbed. As seen from the pseudo-code of trigonometric mutation operation for MOO, the perturbation in the trigonometric mutation operation is contributed together by three vertices of the triangle defined by three randomly selected vectors. The weights applied to the vectors differentials i.e. (p_2-p_1), (p_3-p_2), and (p_1-p_3) ensures that the new point

moves in the direction of improved objective function value. In case of single objective optimization, $Tempp_1$, $Tempp_2$ and $Tempp_3$ (as given in pseudo-code above) are the variables which contain a single objective function value.

However, in case of multi-objective optimization $Tempp_1$, $Tempp_2$ and $Tempp_3$ are the vectors which contain the values of evaluated multiple objective functions. The sum is also a vector which contains the sum of individual objective functions. The mean value of all the objectives is calculated as shown by p_1, p_2 and p_3 variables. The noisy random vector is now created by using the p_1, p_2 and p_3 variables as weight as given in above pseudo-code. It is ensured that the noisy random vector moves towards a better direction where there is an improvement in the objective function value. The mutation probability used in this algorithm is 0.5%, i.e., if the random number generated is greater than 0.5 then trigonometric mutation operation is carried out otherwise simple mutation operation as given in MODE III algorithm is used.

3.6 Hybrid multi-objective differential evolution

Both the methods of optimization (deterministic and evolutionary) in isolation have their own limitations and advantages over the other. For example, the evolutionary optimization algorithms starts with multiple population points and all the population points usually converge to a single point (in case of single objective optimization) or non-dominated optimal set (in case of multi-objective optimization) after the specified number of generations are met. However, the deterministic methods often start with a single initial guess. The new point is created either by the method of gradient or by certain perturbation law (in case of direct search methods) and the new point is compared

with the existing point. If the new point is found to be better than the current point, then it replaces the current point. The outcome of these methods is often dependent on initial guess and the method of perturbation or the step size of the gradient. It may be possible in the deterministic methods that it may get converged to local minima, if the initial guess is selected wrongly. But at the same time it has the advantage of faster convergence. The evolutionary based optimization methods, due to multiple function evaluations in a single run, are more accurate at the cost of slower convergence. In this work, we propose the hybrid strategy of multi-objective differential evolution algorithm taking the advantage of both the deterministic local search method and the evolutionary approach based optimization method. The deterministic sequential simplex method is used for local search, whereas one of the evolutionary multi-objective differential evolution strategy (MODE-III) is used for global search. The deterministic method is used as an accelerator, which finds new superior points to converge to the Pareto front at a faster rate. Chiou and Wang (1999) applied hybrid strategy of differential evolution algorithm to solve the static and dynamic single objective problems with application to fed-batch fermentation process. Gradient based descent local search method was used to accelerate the algorithm while evolutionary algorithm (DE) was used for migration to a wider domain. Multi-objective genetic algorithm (MOGA) was hybridized with a neural network (NN) and a gradient-based optimizer to solve complex design problem in fluid dynamics (Poloni et al., 2000). Recently NSGA-II was hybridized with simplex method which is named as nonlinear simplex search genetic algorithm (NSS-GA) (Martinez and Coello, 2008). A detailed working principle and application of random-weight based generic local search (RWGA) and multi-objective genetic local search (MOGLS) methods is available in the

literature (Deb, 2001). Thus, though this concept of hybrid algorithms in general is not new (Fonesca and Flemming, 1995), this is the first attempt to hybridize MODE algorithm with a local search method for solving MOOPs.

Sequential Simplex method (Nelder and Mead, 1965; Rao, 1995; Babu, 2004) is used as a local search algorithm in the hybrid MODE strategy. Fig. 3.6 shows the working principle of hybrid multi-objective differential evolution algorithm. The population set is initialized randomly within the specified bounds of the variables and the corresponding costs (objective function value) are evaluated. Entire population points are preserved for recombination operation. Three vectors from the initial population are selected at random in order to create a noisy random vector. Then the trial (child) vector is generated by cross over between the target and noisy random vectors (parents). The cost of the trial vector is compared with that of the target vector for dominance. The winner vector is then used for local search to obtain a better population point in the neighbourhood using sequential simplex algorithm. The local search deterministic methods cannot handle multiple objectives directly. They require a single objective function to evaluate. Therefore, in order to handle multiple objectives using a deterministic sequential simplex method, the *Overall objective* (*D*) is calculated. The *Overall objective* (*D*) of a population point for a min-min type of problem; is defined as given by Eq. 3.1.

$$Overall\ Objective\,(D) \quad = abs\left(\frac{1}{\sum_{n=1}^{n} d_i f_i}\right)^{1/n} \tag{3.1}$$

Where $0 \le d_i \le 1$ and $\sum_{i=1}^{n} d_i = 1$ (n = number of objective functions)

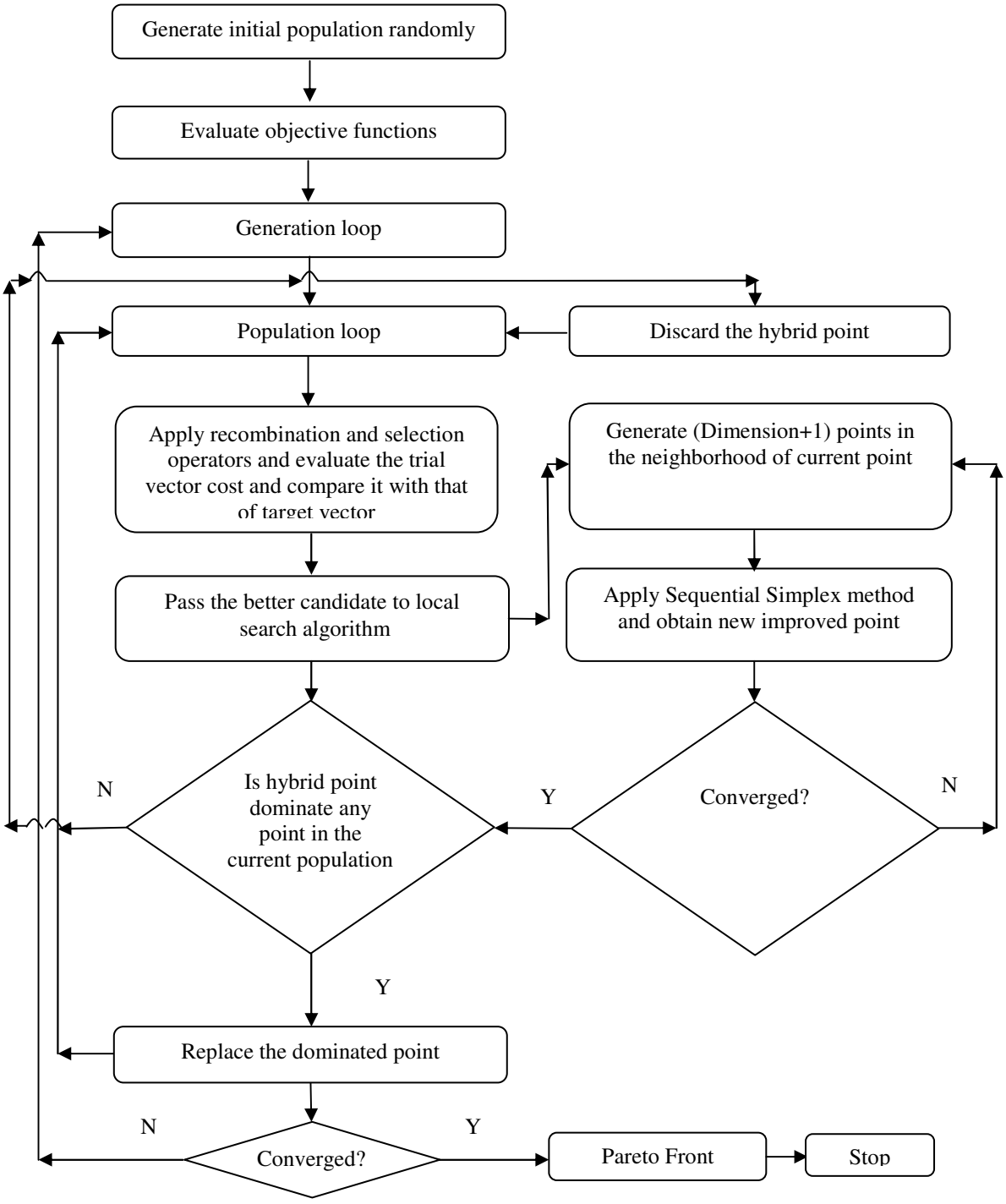

Fig. 3.6 Working principle of hybrid MODE algorithm

For a two-objective min-min type of problem, the overall objective is given by Eq. 3.1a:

$$Overall\ Objective\ (D) \quad = abs\left(\frac{1}{d_1 f_1 + d_2 f_2}\right)^{1/2} \tag{3.1a}$$

Here, to avoid the priority based weightage, values of both the weights are assumed to be the same, i.e., $d_1 = d_2 = 0.5$. This formulation is applicable provided that both f_1 and f_2 function values are in the same range. If the range of function values is different, say $f_1 \in (0,1)$ and $f_2 \in (1e^4, 1e^6)$, then normalized function value may be used, as given by Eq. 3.2.

$$f_i = \frac{f_i - f_{i,\min}}{f_{i,\max} - f_{i,\min}} \tag{3.2}$$

Where, f_i, $f_{i,\min}$ and $f_{i,\max}$ are the actual, minimum and maximum value of i^{th} function respectively. In case of an industrial problem, where the minimum and maximum values of individual functions are not known, then current population is sorted with respect to an individual function to obtain the minimum and maximum value of individual function. All function values are evaluated corresponding to the best point obtained in the sequential simplex method. Though a single objective based overall objective function is used in the sequential simplex method, the best point obtained in the sequential simplex method is checked for non-dominance before it is accepted in the current population. If the point obtained using sequential simplex method dominates any point in the current population, the dominated point gets replaced by the new point, and otherwise a new selection procedure takes place. As a local search method is applied on each point, not

only convergence becomes faster, but diversity of solutions is also maintained. The value of the overall objective function acts as a guideline for determining new simplex value. (n+1) number of vertices (where n is the number of dimensions of the problem) are used in the local search sequential simplex algorithm. The overall objective function value (*D*) is evaluated at each of these vertices. In every-iteration of the sequential simplex method, the simplex is changed to enhance the function values. Several possible transformations are considered, namely reflection, contraction and expansion. The reflection is the simplest one, where the vertex at which the function value is worst, is reflected in the hyper plane formed by the other *n* vertices. The function value at the new vertex is then evaluated and the process is repeated. However, it may be possible that the function value may be worst at the new vertex, in which case, if it is reflected, we will get back to the old simplex and no progress can be made. It is also possible that the reflection operation leads to a cyclic process i.e. after some iteration it gets back to the original simplex. Under these circumstances, the simplex is extended or contracted in some direction. The iteration proceeds in such a manner that the volume of simplex keeps on decreasing once appropriate conditions are satisfied, and ultimately the volume may shrink to the required accuracy. The process is repeated till the termination criterion is met. Following selection strategy is used in hybrid MODE algorithm.

If the newly obtained point using hybrid mode dominates any point in the population

{

If newly obtained point further improves the divergence metric or convergence metric

{

Replace the dominated point and its cost with the new point and cost

}

}

The newly obtained point replaces the dominated point in the population; otherwise a new selection procedure takes place.

This operation is continued till the convergence criterion is met. The convergence criteria may be of the following three types: (1) there is no new solution added to the non-dominated front for a specified number of generations, or (2) an upper bound on the number of generations is met, or (3) combination of (1) and (2) mentioned above. In this study, the second criterion is applied.

Summary of chapter: In this chapter the detailed working principles of newly developed strategies of multi-objective differential evolution in terms of flowchart, pseudocode, and detailed description of algorithm are given. Strategies of MODE algorithm include MODE-II, MODE-III, elitist-MODE, trigonometric mutation MODE and hybrid MODE.

In the next chapter, MOO problem formulation of benchmark test problems and selected industrial case studies considered in the present work are given.

CHAPTER – 4

PROBLEM FORMULATION OF CASE STUDIES ON MULTI-OBJECTIVE OPTIMIZATION

This chapter is divided into two major sections. Section 4.1 includes the benchmark test problems of MOO (both constrained and unconstrained) considered in this study. Section 4.2 gives the problem formulation of various industrial case studies of MOO considered in this study.

4.1 Bench Mark Test Problems

Table 4.1 and 4.2 show 12-unconstrained and 5-constrained test problems of MOO considered in this study taken from various literature sources respectively. The objective function, its type (minimization/maximization, convex/non-convex and continuous/discontinuous), number of variables and bounds of each of the MOO problem considered are also shown in these tables. The 12-uncosntrained test problems (Table 4.1) consists of three categories: (1) SCH-1, SCH-2 (Schaffer, 1984), ZDT-1, ZDT-4, (Zitzler, 2000), Max-Max (Deb, 2001), and B&C (Belegundu and Chandragupta, 2002) test problems have a convex search space and a convex Pareto front, (2) FON (Fonesca and Fleming, 1995) and ZDT-2 (Zitzler, 2000) test problem have a non-convex search space and a non-convex Pareto front.

Table 4.1 Unconstrained MOO test functions, problem type and number & bounds of variables

Sr. No.	Test problem	Problem type	Objective functions	Number of variables and bounds
1	SCH-1 (Schaffer, 1984)	Min-Min Convex	$f_1(x) = x^2$ $f_2(x) = (x-2)^2$	$n = 1$ $10^{-3} \le x \le 10^3$
2	SCH-2 (Schaffer, 1984)	Min-Min Non-convex Disconnected	$f_1(x) = \begin{cases} -x & if\ x \le 1 \\ x-2 & if\ 1 < x \le 3 \\ 4-x & if\ 3 < x \le 4 \\ x-4 & if\ x > 4 \end{cases}$ $f_2(x) = (x-5)^2$	$n = 1$ $-5 \le x_1 \le 10$
3	FON (Fonseca and Fleming, 1995)	Min-Min Non-convex	$f_1(x) = 1 - \exp\left(- \sum_{i=1}^{n} \left(x_i - \frac{1}{\sqrt{n}} \right)^2 \right)$ $f_2(x) = 1 - \exp\left(- \sum_{i=1}^{n} \left(x_i + \frac{1}{\sqrt{n}} \right)^2 \right)$	$n = 3$ $-4 \le x_i \le 4$

Table 4.1 Unconstrained MOO test functions, problem type and number & bounds of variables (Contd..)

Sr. No.	Test problem	Problem type	Objective functions	Number of variables and bounds
4	KUR (Kursawe, 1990)	Min-Min Non-convex Disconnected	$f_1(x) = \sum_{i=1}^{n-1}\left(-10\exp\left(0.2\sqrt{x_i^2 + x_{i+1}^2}\right)\right)$ $f_2(x) = \sum_{i=1}^{n}\left(\lvert x_i\rvert^{0.8} + 5\sin x_i^3\right)$	$n = 3$ $-5 \le x_i \le 5$
5	ZDT1 (Zitzler et al., 2000)	Min-Min Convex	$f_1(x) = x_1$ $f_2(x) = g(x)\left[1 - \sqrt{x_1 / g(x)}\right]$ $g(x) \equiv 1 + \frac{9}{n-1}\sum_{i=2}^{n} x_i$	$n = 30$ $0 \le x_i \le 1$
6	ZDT2 (Zitzler et al., 2000)	Min-Min Non-convex	$f_1(x) = x_1$ $f_2(x) = g(x)\left[1 - \left(\frac{x_1}{g(x)}\right)^2\right]$ $g(x) \equiv 1 + \frac{9}{n-1}\sum_{i=2}^{n} x_i$	$n = 30$ $0 \le x_i \le 1$

Table 4.1 Unconstrained MOO test functions, problem type and number & bounds of variables (Contd..)

Sr. No.	Test problem	Problem type	Objective functions	Number of variables and bounds
7	ZDT3 (Zitzler et al., 2000)	Min-Min Non-convex Disconnected	$f_1(x) = x_1$ $f_2(x) = g(x)\left[1 - \sqrt{\frac{x_1}{g(x)}} - \left(\frac{x_1}{g(x)}\right)\sin\left(10\pi x_1\right)\right]$ $g(x) \equiv 1 + \frac{9}{n-1}\sum_{i=2}^{n} x_i$	$n = 30$ $0 \le x_i \le 1$
8	ZDT4 (Zitzler et al., 2000)	Min-Min Convex	$f_1(x) = x_1$ $f_2(x) = g(x)\left[1 - \sqrt{\frac{x_1}{g(x)}}\right]$ $g(x) \equiv 1 + 10(n-1) + \sum_{i=2}^{n}\left(x_i^2 - 10\cos\left(4\pi x_i\right)\right)$	$n = 10$ $0 \le x_i \le 1$
9	POL (Poloni et al., 2000)	Min-Min Non-convex Disconnected	$f_1(x) = \left[1 + (A_1 - B_1)^2 + (A_2 - B_2)^2\right]$ $f_2(x) = \left[(x_1 + 3)^2 + (x_2 + 1)^2\right]$ $A_1 = 0.5\sin 1 - 2\cos 1 + \sin 2 - 1.5\cos 2,$ $A_2 = 1.5\sin 1 - \cos 1 + 2\sin 2 - 0.5\cos 2$ $B_1 = 0.5\sin x_1 - 2\cos x_1 + \sin x_2 - 1.5\cos x_2$ $B_2 = 1.5\sin x_1 - \cos x_1 + 2\sin x_2 - 0.5\cos x_2$	$n = 2$ $-\pi \le x_i \le \pi$

Table 4.1 Unconstrained MOO test functions, problem type and number & bounds of variables (Contd..)

Sr. No.	Test problem	Problem type	Objective functions	Number of variables and bounds
10	B&C (Belegundu and Chandragupta, 2002)	Max-Max Convex	$f_1(x) = 3x_1 + x_2 + 1$, $f_2(x) = -x_1 + 2x_2$	$n = 2$ $0 \le x_1 \le 3$ $0 \le x_2 \le 3$
11	Max-Max (Deb, 2001)	Max-Max Convex	$f_1(x) = 1.1 - x_1$, $f_2(x) = 60 - \frac{(1 + x_2)}{x_1}$	$n = 2$ $0.1 \le x_1 \le 1.0$ $0 \le x_2 \le 5$

Table 4.2 Constrained MOO test functions, constraints, problem type and number & bounds of variables

Sr. No.	Test problem	Problem type	Objective functions and constraints	Number of variables and bounds
1	CONSTR-Ex (Deb, 2001)	Min-Min Non-convex Continuous	$f_1(x) = x_1$ $f_2(x) = \frac{1+x_2}{x_1}$ Subject to $g_1(x) \equiv x_2 + 9x_1 \geq 6$ $g_2(x) \equiv -x_2 + 9x_1 \geq 1A$	$n = 2$ $0.1 \leq x_1 \leq 1$ $0 \leq x_2 \leq 5$
2	TNK (Tanaka, 1995)	Min-Min Non-convex Discontinuous	$f_1(x) = x_1$ $f_2(x) = x_2$ Subject to $g_1(x) \equiv x_1^2 + x_2^2 - 1 - 0.1\cos\left(16\arctan\frac{x_1}{x_2}\right) \geq 0$ $g_2(x) \equiv (x_1 - 0.5)^2 + (x_2 - 0.5)^2 \leq 0.5$	$n = 2$ $0 \leq x_1 \leq \pi$ $0 \leq x_2 \leq \pi$

Table 4.2 Constrained MOO test functions, constraints, problem type and number & bounds of variables (Contd..)

Sr. No.	Test problem	Problem type	Objective functions and constraints	Number of variables and bounds
3	BNH (Binh and Corn, 1997)	Min-Min Convex Continuous	$f_1(x) = 4x_1^2 + 4x_2^2$ $f_2(x) = (x_1 - 5)^2 + (x_2 - 5)^2$ Subject to $g_1(x) \equiv (x_1 - 5)^2 + x_2^2 \le 25$ $g_2(x) \equiv (x_1 - 8)^2 + (x_2 + 3)^2 \ge 7.7$	$n = 2$ $0 \le x_1 \le 5$ $0 \le x_2 \le 3$
4	SRN (Chankong and Haimes, 1983)	Min-Min Convex Continuous	$f_1(x) = 2 + (x_1 - 2)^2 + (x_2 - 1)^2,$ $f_2(x) = 9x_1 - (x_2 - 1)^2,$ Subject to $g_1(x) \equiv x_1^2 + x_2^2 \le 225,$ $g_2(x) \equiv x_1 - 3x_2 + 10 \le 0,$	$n = 2$ $-20 \le x_1 \le 20$ $-20 \le x_2 \le 20.$
5	Min-Min (Deb, 2001)	Min-Min Convex Continuous	$f_1(x) = (x_1),$ $f_2(x) = \frac{1 + x_2}{x_1},$ Subject to $g_1(x) \equiv x_2 + 9x_1 \ge 6,$ $g_2(x) \equiv -x_2 + 9x_1 \ge 1$	$n = 2$ $0.1 \le x_1 \le 1$ $0 \le x_2 \le 5$

(3) SCH-2 (Schaffer, 1984), KUR (Kursawe, 1990), ZDT-3 (Deb, 2001) and POL (Poloni et al., 2000) have non-convex search space and a non-convex and discontinuous (or disconnected) Pareto front.

Table 4.2 shows the constrained MOO problems considered in this study. The 5-constrained test problems consist of three categories: (1) BNH (Binh and Corn, 1997), SRN (Chankong and Haimes, 1983) and Min-Min (Deb, 2001) test problems are constrained MOO problems having convex search space and the convex Pareto front, (2) CONSTR-Ex (Deb, 2001) is a constrained MOO problem with non-convex search space and the convex Pareto front, (3) TNK (Tanaka, 1995) involves non-convex search space and disconnected and non-convex Pareto front.

4.2 Industrial case studies

Five industrial case studies, taken from various literature sources, are considered for carrying out MOO study. These are: industrial styrene reactor, polyethylene terephthalate reactor, liquid phase oxidation of *p*-xylene, low density polyethylene tubular reactor and supply chain planning involving various process design decisions. Detailed process description and objective function formulations of these studies are given in the following subsections.

4.2.1 Industrial styrene reactor

4.2.1.1 Process description and modeling aspects

Adiabatic dehydrogenation is the most widely used technology for the production of commercial grade styrene (Li and Hubbell, 1982; Chen, 1992; Denis and Castor, 1992).

The process flow diagram for the production of styrene by dehydrogenation of ethyl benzene is shown in Fig. 4.1. The pressure of the reactor varies from 8-15 psig during an industrial operation. Fresh and recycled ethyl benzene streams are mixed with steam which are subsequently vaporized and heated in the heat exchangers. The ethyl benzene and steam vapor mixture is further heated to desired reaction temperature of over 875 K by mixing it with steam (superheated) in a direct-fired heater and sent to the first reactor. The temperature of ethyl benzene and steam mixture decreases along the length of the reactor as the reaction is endothermic. Superheated steam provides the necessary heat of reaction and lowers the partial pressure of styrene and hydrogen to shift the thermodynamic equilibrium in favor of the dehydrogenation of ethyl benzene to styrene. In addition, it not only inhibits the coke formation by reaction, but also flushes away the traces of coke deposited on the catalyst surface by sudden sparging of steam with the coke deposited on the catalyst surface. Usually the molar ratio of steam to ethyl benzene in the feed is fixed to 15:1. In case of steam injected reactor, the reaction effluent from the first reactor is mixed with the fresh superheated steam before it enters the next reactor. Six main reactions occurring in the styrene reactor are:

$$C_6H_5CH_2CH_3 \quad \Leftrightarrow \quad C_6H_5CHCH_2 + H_2 \tag{4.1}$$

$$C_6H_5CH_2CH_3 \quad \Rightarrow \quad C_6H_6 + C_2H_4 \tag{4.2}$$

$$C_6H_5CH_2CH_3 + H_2 \Rightarrow \quad C_6H_5CH_3 + CH_4 \tag{4.3}$$

$$2H_2O + C_2H_4 \quad \Rightarrow \quad 2CO + 4H_2 \tag{4.4}$$

$$H_2O + CH_4 \quad \Rightarrow \quad CO + 3H_2 \tag{4.5}$$

$$H_2O + CO \quad \Rightarrow \quad CO_2 + H_2 \tag{4.6}$$

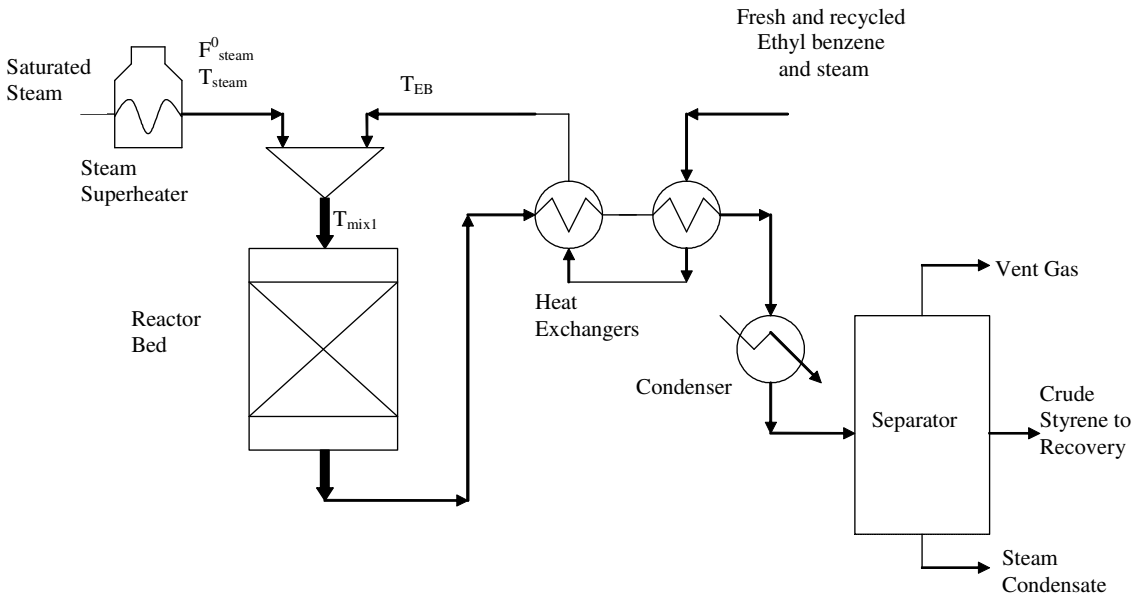

Fig. 4.1 Simplified process flow sheet for production of styrene

The major aromatic byproducts from the dehydrogenation of ethyl benzene are benzene and toluene. The light gases produced from the reaction include hydrogen, carbon dioxide, carbon monoxide, methane and ethylene. The main reaction in the styrene reactor is the reversible endothermic conversion of ethyl benzene to styrene and hydrogen (Eq. 4.1). A high temperature lowers the yield, while the catalytic reaction increases the yield. As per Le Chatelier's principle, a reversible reaction producing two moles of products to one mole of reactant, low pressure and high temperature favor the forward reaction. Some preliminary calculations based on the energy balance have been carried out to get the data on equilibrium conversion profile for styrene (Eq. 4.1) as a function of temperature, and plotted in Fig. 4.2.

At equilibrium, the reversible reaction results in 80-85 % conversion of ethyl benzene in the given temperature range. Although the dehydrogenation of ethyl benzene is both kinetically and thermodynamically favored by high temperature, more byproducts [benzene and toluene (see Eq. 4.2 and Eq. 4.3)] are produced by thermal cracking at high temperatures, thus reducing the styrene yield. High temperature favors the styrene productivity but it also affects adversely by the formation of byproducts. Therefore, an optimum inlet temperature needs to be used.

The flow in the reactor is considered to be plug flow for simulation of both adiabatic and pseudo-isothermal configurations. Axial dispersion is neglected in pseudo-homogeneous model and any limitation of mass or heat transfer to the catalyst pellet or diffusion within the pellet is lumped into the rate constants.

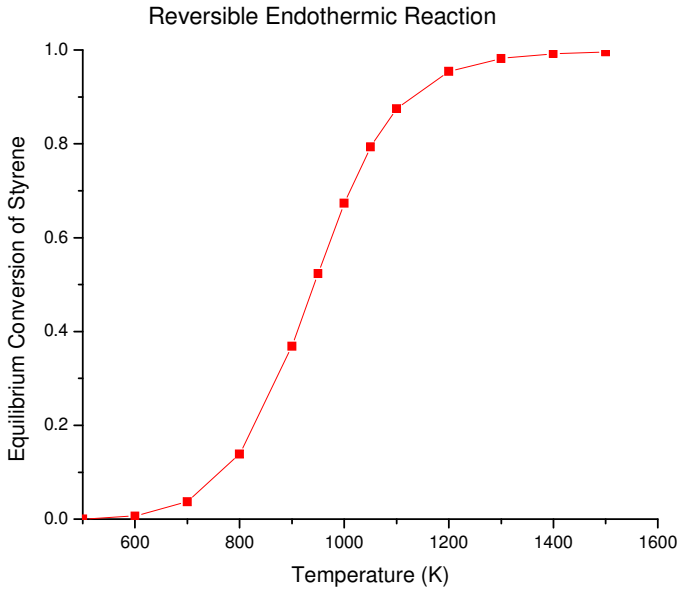

Fig. 4.2 Equilibrium conversion profile for styrene

Sheel and Crowe (1969) reported the design and operating conditions of this pseudo-homogeneous model. Abdalla et al. (1994) and Elnashaie et al. (1993) used this model as well as the more detailed heterogeneous model, which takes into account of diffusion in the catalyst pellet. This model was used by them to extract the kinetic data from the industrial data. Abdalla et al. (1994) reported intrinsic kinetics for three promoted iron oxide catalysts using the pseudo-homogeneous and heterogeneous models, and compared the performance of these catalysts. Among these models, the kinetic model proposed by Sheel and Crowe (1969) has been widely used (Clough and Ramirez, 1976; Elnashaie et al., 1993; Abdalla et al., 1994; Savoretti et al., 1999 and Sheppard et al., 1986). In their studies, Babu et al. (2005) and Yee et al. (2003) observed that the predictions by both pseudo-homogeneous and heterogeneous models are comparable, but pseudo-homogeneous model took significantly less time than the heterogeneous model. Hence the pseudo-homogeneous model is considered for multi-objective optimization of styrene reactor in this study. The operating conditions and design parameters for the industrial reactor are given in Appendix A (Table A1). The differential equations employed in the current study are also given in Appendix A (Eq. A1 - A15).

4.2.1.2 Formulation of objective functions

Simultaneous maximization of three-objectives namely styrene productivity (F_{ST}), selectivity (S_{ST}), and yield of styrene (Y_{ST}) are considered in this study. The three-objectives are given by Eqs. 4.7 - 4.9.

Maximize: (4.7)

Maximize: (4.8)

Maximize: (4.9)

Styrene is widely used as a raw material for several polymer products. Styrene is also known in the market place as one of the costly products. Therefore maximization of productivity and yield are considered as the objectives. Minimization of the unwanted byproducts such as toluene and benzene is also important as it causes the raw material loss and also increases the cost of separation. In order to minimize the production of toluene and benzene (byproducts) in the reactor, the selectivity of styrene should be increased and hence maximization of selectivity is considered as another objective function in this study. F^0_{EB} is one of the decision variables and as it appears in Eq. 4.9 (independently) and along with unconverted ethyl benzene (F^0_{EB-} F_{EB}) in Eq. 4.8, the trade-off associated with all the three objectives is apparent. The multi-objective optimization problem of Styrene production is well-documented in the literature [Yee et al., 2003; Babu et al., 2005]. Two reactor configurations are considered for the multi-objective optimization study. Fig. 4.3a shows a single bed adiabatic reactor in which entire amount of steam is mixed with ethyl benzene and enters the reactor at the inlet

In case of steam injected operation (Fig. 4.3b), the total amount of steam is bifurcated into two fractions. A fraction (δ) of steam is mixed with ethyl benzene at the reactor inlet while the remaining steam is injected at λ fraction of total reactor length, where λ and δ are considered as decision variables that are to be optimized. For the optimization of styrene reactor, the decision variables were chosen from the operating variables of existing plants and from the key decision variables of the reactor (Sheel and Crowe, 1969; Elnashaie and Elshishini, 1994; Yee et al., 2003 and Babu et al., 2005).

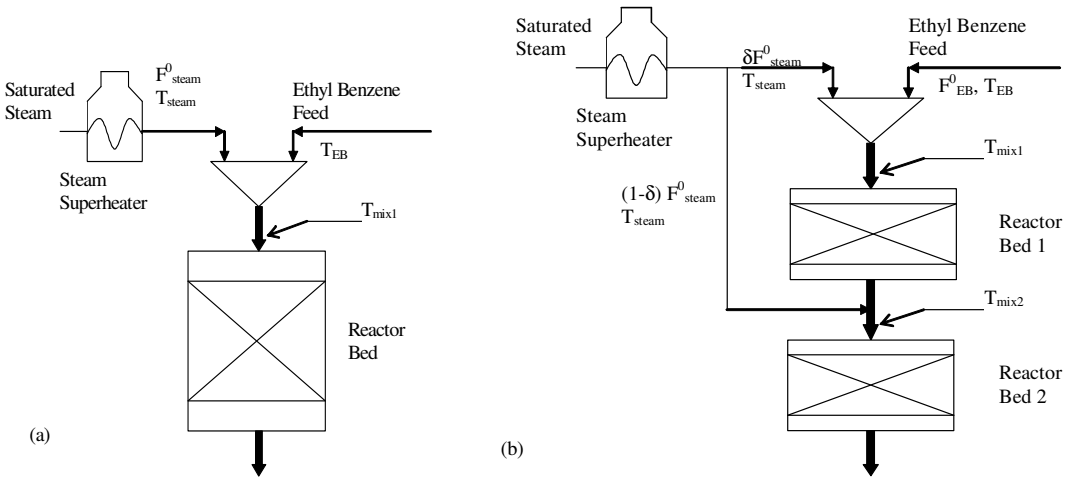

Fig. 4.3 Schematic diagram of (a) Single bed adiabatic (b) Steam injected styrene reactor with steam injection partway of the reactor length

In earlier studies, the inlet temperature of the superheated steam was fixed at 1025 K. But practically in any process plant, it is nearly impossible to get the steam at one constant temperature. Therefore one additional variable i.e., the temperature of steam is included in this study. So, for adiabatic operation, five decision variables namely, feed temperature (T_{EB}), pressure (P), steam over reactant ratio (SOR), initial ethyl benzene flow rate ( ) and temperature of steam (T_{STEAM}) are considered for optimization. The bounds of decision variables are given by Eq. 4.10 through Eq. 4.14.

K (4.10)

bar (4.11)

(4.12)

kmol/h (4.13)

K (4.14)

The lower and upper limits of the inlet pressure are taken as 1 and 2.63 bar, respectively, following the industrial practice. In Fig. 4.3a, T_{mix1} is the temperature of the mixture of ethyl benzene and steam. The lower bound on the temperature of ethyl benzene (T_{EB}) is fixed at 550 K, in order to ensure that T_{mix1} is not too low for the reaction to occur. The upper bound on T_{EB} is set at 800 K to prevent undesirable side reactions before ethyl benzene enters the reactor (Claugh and Ramirez, 1976). The lower bound on the steam to ethyl benzene molar ratio, SOR (steam over reactant) is chosen as 7 to prevent the coke formation on the catalyst surface and to regenerate the catalyst by removing the traces of coke already deposited on the catalyst surface. The upper limit of SOR is chosen as 20 as too high a value of SOR would be uneconomical due to the

higher energy needed for heating the excess steam to the required reaction temperature. Also, the downstream reactor units such as condenser and heat exchangers have to be considered for capacity limitations. F^0_{EB} refers the total pure ethyl benzene feed and the bounds on this variable individually lie between -25% and +10% of the industrial value of 36.87 kmol/h (Claugh and Ramirez, 1976). The temperature of the superheated steam varies between 1000 K and 1050 K.

Two additional decision variables are considered for steam injected reactor configuration, (δ, the fraction of steam used at the reactor inlet, and λ, the fraction of reactor length and location of injection port for the remaining fraction of steam).

(4.15)

$$0.1 < \lambda < 1 \tag{4.16}$$

Normally 10 % of the superheated steam (F^0_{EB}) is mixed with the feed (ethyl benzene) to prevent the side reactions before ethyl benzene feed is injected into the reactor. Hence, the steam fraction, δ, has been given a range of 0.1 to 1.0. Because minimum 10% of the total steam enters at the inlet of the reactor, we set the lower limit of λ as 0.1 for the steam injected reactor considering linear drop in temperature in a shorter (initial 10%) length of reactor. Three constraints as shown by Eqs. 4.17 – 4.19 are also considered for the optimization study.

kmol/h (4.17)

K (4.18)

K (Valid for the steam injected reactor only) (4.19)

Although the furnace in Fig. 4.3(a) and 4.3(b) can produce more steam, may be at a lower temperature, the downstream condenser may not be able to handle the increased

throughput (Sheel and Crowe, 1969). The first constraint (Eq. 4.17) is based on the size limitation of the condenser. T_{mix1} [see Fig. 4.3(a)] of Eq. 4.18 is the temperature of the mixture of ethyl benzene and steam entering the reactor. T_{mix2} [see Fig. 4.3(b)] of Eq. 4.19 is the temperature of the same at a reactor length of $z = \lambda L$. For the adiabatic reactor configuration only two constraints (Eq. 4.17 and Eq. 4.18) are applicable, whereas for the steam injected case all three constraints (Eqs. 4.17-4.19) are applicable. The constraint on both T_{mix1} and T_{mix2} is based on the minimum temperature required for the reaction to take place, and the temperature at which the catalyst starts to deactivate (Claugh and Ramirez, 1976). Constraints are incorporated into each of the objective functions mentioned above and handled using the penalty approach (Deb, 2001). As discussed subsequently in sections 5.1 and 5.2 of chapter 5, where rigorous simulations on parametric estimation of MODE on several test problems are included, it was found that the penalty weights are highly problem specific, especially during the initial generation runs. MODE algorithm (due to its strong recombination operation) is found to approach to the same front at higher value of generations for certain test problems. And hence, the present industrial case study problem is also tested with several penalty weights along with the dominant MODE parameters. It is ensured that a high value of penalty parameter is used. It assigns a very low value to the infeasible objective function (in case of maximization type of problems). Thus the infeasible solutions are removed from the competition. The modified objective functions are shown in Eq. 4.20 through Eq. 4.27.

Maximize: $$I_1 = F_{ST} - 10^6 \sum_{i=1}^{5} f_i \tag{4.20}$$

Maximize: $$I_2 = S_{ST} - 10^4 \sum_{i=1}^{5} f_i \tag{4.21}$$

Maximize: $I_1 = Y_{ST} - 10^6 \sum_{i=1}^{5} f_i$ (4.22)

where i = 1 to 5 and

(4.23)

(4.24)

(4.25)

(4.26)

(4.27)

Three cases of two-objective optimization (Eqs. 4.28 - 4.30) and one case of three-objective optimization (Eq. 4.31) are possible for the three-objectives, namely, maximization of F_{ST}, S_{ST} and Y_{ST} (Eqs. 4.28 - 4.31).

Case-1: Maximization of F_{ST} and S_{ST} (4.28)

Case-2: Maximization of S_{ST} and Y_{ST} (4.29)

Case-3: Maximization of F_{ST} and Y_{ST} (4.30)

Case-4: Maximization of F_{ST}, S_{ST} and Y_{ST} (4.31)

4.2.2 Polyethylene terephthalate (PET) reactor

4.2.2.1 Process description and modeling aspects

Commercially, PET is manufactured in three stages (namely, esterification, pre-polymerization and the poly-condensation in the finishing reactor), using continuous reactors. PET is manufactured in three continuous reactors using ethylene glycol (EG) and purified terphthalic acid (PTA). Usually EG is taken in excess. In the first stage, esterification is carried out in continuous stirred tank reactor (CSTR) or plug flow reactor (PFR) at 270–280 ^{0}C and at atmospheric pressure. A poly-condensation catalyst,

antimony trioxide, is injected in small concentrations (0.03 – 0.05 wt.%) into the oligomer stream leaving this reactor. In the second stage, pre-polymerization is carried out to get a degree of polymerization (DP) of 30 – 40. Agitated vessel is used and maintained at a pressure in the range of 15 – 30 mm Hg and at a temperature range of 270–280 ^{0}C. In the third stage (wiped-film reactor), final condensation occurs at a pressure of 1 – 2 mm Hg and at a temperature of 280 – 295 ^{0}C. Optimization of third stage (wiped film reactor stage) is more important as it controls the final properties of the product. Due to a high value of viscosity of the reaction mass, the finishing reactor has a special construction (a jacketed cylindrical vessel with a horizontal agitator, with large screens mounted on the latter) in order to enhance the mass transfer and the removal of by-product (ethylene glycol).

The continuous removal of ethylene glycol, drives the reaction in the forward direction and gives a product having a high value of degree of polymerization (DP) (Bhaskar et al., 2001). The reaction mass in the third-stage reactor is usually heated by condensing vapor in the jacket of the reactor. A horizontal vessel equipped with a screw-type or rotating disk agitator is used as a reactor for continuous finishing poly-condensation (Fig. 4.4). Such agitators create polymer films on the screw or disk surfaces continuously. These films, after exposure to a bulk vapor phase, are mixed with a bulk polymer melt (Laubriet et al., 1991). Low molecular weight PET pre-polymer from pre-polymerization reactor is fed to the wiped-film reactor. Various volatiles such as ethylene glycol, di-ethylene glycol (*DEG*), water, and acetaldehyde are removed from the bulk melt phase by applying high vacuum (e.g., 0.1 –1.0 mm Hg) and high temperature (e.g., 270 – 300 ^{0}C).

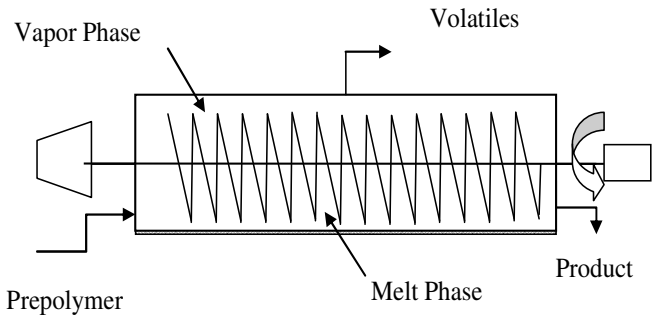

Fig. 4.4 Simplified schematic diagram of horizontal wiped film PET reactor

Bhaskar et al. (2000) proposed the model for continuous finishing stage melt poly condensation of PET. The assumptions considered by Bhaskar et al. (2000) for proposing a two-phase model are: (1) flow pattern of melt phase is of plug flow type and that of vapor phase is of well mixed, (2) no distinction between the film and bulk part in melt phase, (3) no reaction in vapor phase, and (4) mass transfer resistance resides in only melt phase. The set of equations in the melt polymerization of PET is given in Appendix B. In the present study, a two-phase reactor model originally proposed by of Laubriet et al. (1991), and as described by Bhaskar et al. (2001) is used. The simplified model equations are given by Eqs. 4.32 - 4.33.

$$\frac{dx}{dz} = f(x,u);\ x(z=0) = x_0 \tag{4.32}$$

where x is the vector of state variables, defined by

$$x = \left(\left[E_g\right], [E_a], [Z], [E_v], [E_{DEG}], [EG], [W], [DEG]\right) \tag{4.33}$$

and u is the vector of decision variables. In Eq. 4.32, z represents the (dimensionless) axial position in the wiped-film reactor. Table B1 (In Appendix B) shows the values of initial conditions corresponding to the given ordinary differential equations (ODEs). Values of the parameters / properties for the reference case are listed in Table B2 (In Appendix B). The ODE 23s subroutine with adaptive step size of MATLAB (Ver. 7.0) is used to integrate these equations. Upon integration, the model provides the values of *DP* and the concentrations of the hydroxyl end groups (E_g), acid end groups (E_a), di-ester end groups (Z), vinyl end groups (E_v), DEG end groups (E_{DEG}), EG, W and DEG, as a function of the axial position in the reactor.

4.2.2.2 Formulation of objective functions

In this study simultaneous minimization of two objectives, namely, acid end group concentration and vinyl end group concentration is considered. The multi-objective optimization problem is described mathematically as given by Eqs. 4.34 - 4.42:

Minimize

$$I(P,T,\ \theta^*,\ N^*) \equiv \left[I_1, I_2\right]^T = \left(\left[E_a\right]_{out}, \left[E_v\right]_{out} \right)^T \tag{4.34}$$

Subject to

$$DP_{out} = DP_d \tag{4.35}$$

$$\left[E_a\right]_{out} \leq 1.038\times10^{-3}\ kmol/m^3 \tag{4.36}$$

$$0.1660 \leq \left[E_{DEG}\right]_{out} \leq 0.17\ kmol/m^3 \tag{4.37}$$

$$\frac{dx}{dz} = f(x,u); \qquad x(z=0) = x_0 \tag{4.38}$$

$$(0.4 \leq P \leq 2.0\ mmHg) \tag{4.39}$$

$$564 \leq T \leq 570\ K \tag{4.40}$$

$$0.9 \leq \theta^* \leq 1.06 \tag{4.41}$$

$$0.93 \leq N^* \leq 1.05 \tag{4.42}$$

The acid end group makes the polymer susceptible to hydrolysis during the downstream operations and leads to breakage of the filaments during spinning, where the humidity is very high. The vinyl end groups have been shown to be responsible for the unfavourable coloration of PET (Bhaskar et al., 2000). Hence the minimization of these two end groups are considered as the main objectives as used in the earlier study (Babu et al., 2007b). The reduction of E_a simultaneously increases the rate of polymerization of the acid end

group catalyzed poly-condensation reaction and helps maximize the throughput. One equality constraint on degree of polymerization (DP) (Eq. 4.35) and two inequality constraints on the concentration of acid (Eq. 4.36) and DEG end groups (Eq. 4.37) are also considered in the present study. The constraints are handled using the penalty approach (Deb, 2001). The DEG end groups affect the crystallinity and hence the melting point of the polymer unfavourably, they also improve the dye ability of the fiber. The inequality constraint on DEG is imposed to ensure the melting point and dye ability in an allowable range. A further inequality constraint on the maximum allowable limit for the acid end group concentration is imposed to ensure that it is not only minimized but also lies below an upper limit.

Decision variables namely, the reactor pressure (P), temperature (T), residence time of the polymeric reaction mass inside the reactor (θ), and the speed of the wiped-film agitator (N) are used in the present study (Eqs. 4.39 - 4.42). The variables, θ^* and N^*, represent dimensionless values, θ / θ_{ref} and N / N_{ref}, where θ_{ref} and N_{ref} are values being used currently in the industrial reactor being studied. These two values are kept confidential in the literature and hence the value of $\theta_{ref} = 99$ was found by trial and error method in our earlier study (Babu et al., 2007b). All of these decision variables can easily be changed in any industrial, wiped-film reactor for PET manufacture, including the one being studied, and are therefore used to obtain the best optimal operating conditions in the present study.

4.2.3 Liquid phase oxidation of *p*-xylene

4.2.3.1 *Process description and modeling aspects*

Fig. 4.5 is the simplified schematic flowsheet for the manufacturing of TA from liquid phase oxidation of *p*-xylene. In order to simulate the entire process, it is necessary to build up a mathematical model which takes into account of the reaction mechanism in the reactor and crystallizer, the separation, and the heat and mass transfer aspects in distillation column and absorbers. The raw materials of the process such as *p*-xylene, catalyst, air, and mother liquor are fed into the reactor. Oxidation takes place in the reactor through a series of reactions (see Eq. 2.8). After a stipulated residence time, the effluent from the reactor is further passed through a series of three crude terephthalic acid (CTA) crystallizers. The reactor effluent undergoes secondary oxidation and crystal aging in these crystallizers. The slurry from these crystallizers is then pumped into a pressure filter and a vacuum dryer to get the CTA Powder. The obtained CTA powder can be treated by hydrogenation procedure to obtain the purified terephthalic acid (PEP, 2007). The off-gas from the reactor passes through a series of heat exchangers from which steam is generated. The off-gas stream after getting cooled in the heat exchangers passes through the absorbers and the purifiers. The separation of acetic acid and other combustion byproducts (such as carbon dioxide and carbon monoxide) occur in the absorber and the subsequent distillation column. The stream finally passes through the expanders for the recovery of pressure energy. Part of the condensate is refluxed to the reactor and the remaining is fed to the distillation column (Wang, 2007). The model equations of the process and the objective function formulation that are being used in the simulation of this study are discussed in the following section.

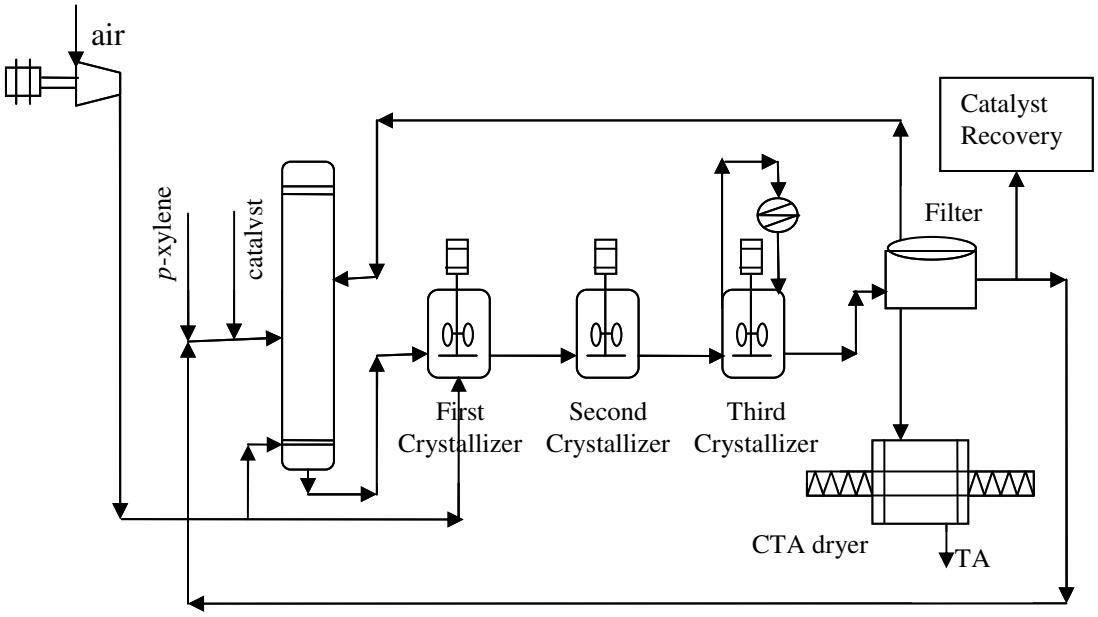

Fig. 4.5 Simplified process flow sheet for liquid phase oxidation of *p*-xylene for CTA production

4.2.3.2 Formulation of objective functions

For CSTR, the design equations are expressed in terms of a set of algebraic equations given by Eq. 4.43:

$$C_{j,0} - C_j = -(r_j - r_{j-1})\tau \qquad \text{for } j = 2 \text{ to } 4$$

$$C_{1,0} - C_1 = -(r_1)\tau \quad \text{and} \qquad C_5 - C_{5,0} = (r_4)\tau \tag{4.43}$$

$C_{j,0}$ *and* C_j are the feed and exit concentrations of *p*-xylene, tolualdehyde, *p*-toluic acid, 4-carboxy benzaldehyde for j = 1 to 5 respectively.

The reactor model considered in this study includes the reaction process in the reactor and the first crystallizer (Mu et al., 2004). The rate law is given by Eq. 4.44 (Wang, 2005a).

$$r_j = k_j \frac{C_j f_j}{\left(\sum_{i=1}^{4} d_i C_i + \theta\right)^{\beta_j}} \qquad j = 1 \text{ to } 4 \tag{4.44}$$

The mathematical model of the process is based on two sequential ideal CSTRs and a crystallizer. The outlet stream from the second reactor consisting of unconverted reactant (PX), the three intermediate products (TALD, P-T, and 4-CBA), and the product (TA) goes to the crystallizer. In the liquid phase *p*-xylene oxidation process, the quality of product is decided by the amount of 4-CBA present in it. Several properties of PTA such as the optical density and the concentration of 4- carboxy-*p*-terphenyl (4-CTr) in CTA are related to the amount of 4-CBA present in the final product. 4-CBA can also contaminate CTA as it is prone to co-crystallization with crude TA (Mu et al., 2004). Thus minimizing the concentration of 4-CBA in the final product is one of the major objectives in the production of PTA. The profit of an industry depends on the production

rate. The production rate is directly related to the flow rate of the feed entering the reactor. Thus the maximization of feed flow rate can be considered as one the objectives of the present study. But with an increase in the production rate, the % of impurity (concentration of 4-CBA) also increases. A set of decision variables may exist, which may favor the objective of increasing the productivity, but may not favor the objective of minimizing the 4-CBA concentration. Thus there exists a clear conflict in both these objectives and they can be modeled as a multi-objective optimization problem. Minimization of the concentration of 4-CBA in the crude TA and the maximization of feed flow rate of reactor are the main objectives of this study. Mu et al. (2004) carried out the multi-objective optimization study of industrial purified terephthalic acid. Their study included 7 decision variables, namely, total feed rate (F_{FEED}), catalyst concentration (C_0), water withdrawal rate from the reactor (WWD), vent oxygen content of reactor (V_{OR}), vent oxygen content of crystallizer (V_{OC}), temperatures of reactor (T_R) and crystallizer (T_C). Out of these 7 decision variables Mu et al. (2004) considered, the data and the correlations for some of them are either unavailable in the literature or proprietary with the industry and hence inaccessible, as mentioned by the authors (Mu, 2007). Taking this practical problem into account we made an attempt to simplify the above problem by reformulating and incorporating the readily available and easily measurable decision variables as explained below.

Oxidation (about 2-3%) also takes place in the first crystallizer. The low value of vent oxygen content in the crystallizer may not affect the product quality to a great extent because the air flow rate to the first crystallizer is only 2% of the whole requirement of air flow rate of the PTA oxidation reaction. Eq. 4.44 represents the kinetic model based

on radical chain reaction mechanism (Wang, 2005b). It contains important parameters, such as the co-crystallization factor (θ) and the kinetic parameters (d_i and β_j). These kinetic parameters are designed to consider the reaction in both the crystallizer and the reactor. Therefore, in this study we incorporated this kinetic model. The vent oxygen from the reactor (V_{OR}) and crystallizer (V_{OC}) are merged and denoted as V_{O_2}. The difference in the temperature of reactor (T_R) and crystallizer (T_C) is insignificant, and hence the temperature of reactor only is considered in this study. The rate constant is directly related to the total water content in the solvent (W_{H_2O}) (Wang, 2005a). The correlations for rate constants in terms of water content are well documented in the literature. Industrially it is easy to control the water content in solvent than controlling the water withdrawal rate from the reactor. Therefore, in this study the decision variable WWD (total water withdrawal) is replaced with W_{H_2O}, to study its effect in the presence of other decision variables. The detailed mathematical model (Eqs. C1 - C5) and the correlations used (Eqs. C6 - C14) in the present study are given in Appendix C. The flow rate of *p*-xylene in the feed determines the mole fraction of xylene in the feed stream. The mole fraction of *p*-xylene is an important term in rate law. Therefore considering its importance, we included the flow rate of *p*-xylene as an extra decision variable in the present study. The correlations related to the new decision variables added in this study are easily available in the open literature. They are easily measurable quantities and it is also more feasible to control these variables. By incorporating these changes, the objective function has been simplified and reformulated in the present study as given by Eqs. 4.45 - 4.47:

$$Maximize \quad F_{FEED} \tag{4.45}$$

$$Minimize \quad c_{4-CBA}(F_{PX}, F_{FEED}, [Co], W_{H_20}, V_{O_2}, T) \tag{4.46}$$

Subject to $F_{Feed} \geq 130000$ kg/h

$$c_{4-CBA} \leq 3500 \quad \text{ppm} \tag{4.47}$$

The second objective function (minimization of 4-CBA concentration) is a function of 6 process decision variables, namely F_{PX}, F_{FEED}, $[C_0]$, W_{H_2O}, V_{O_2} and T. However, during a normal operation of the plant, it is difficult to control/manipulate all the decision variables (mentioned above) together due to practical limitations. Usually the industrial plant is operated by controlling only one or two decision variables mentioned above by keeping the rest of the decision variables constant during a normal operation. We considered a total of 6 variables in order to study the effect of those decision variables on the objective functions. Four combinations of decision variables (as given by Eqs. 4.48 - 4.51) are considered for multi-objective optimization in this study.

1. $[C_0], F_{FEED}$ (4.48)
2. $[C_0], F_{FEED}, W_{H_2O}$ (4.49)
3. $[C_0], F_{FEED}, W_{H_20}, F_{PX}, V_{O_2}$ (4.50)
4. $[C_0], F_{FEED}, W_{H_20}, F_{PX}, V_{O_2}, T$ (4.51)

Case-1

$$Maximize \quad F_{FEED}$$

$$Minimize \quad c_{4-CBA}(F_{FEED}, [C_0]) \tag{4.52}$$

In this case study, the first objective function (F_{FEED}) appears as one of the decision variables in the second objective function. The most widely used tunable decision variable in PTA oxidation process industry is $[C_0]$. The operating value of $[C_0]$ is 341.1

ppm, however in this study we have selected the range of $[C_0]$ as 300-800 ppm to see the effect of increased catalyst feed concentration. Other decision variables such as F_{PX}, W_{H_2O}, V_{O_2}, and T are kept constant during the simulation runs for this case.

Case-2

$$Maximize \quad F_{FEED}$$

$$Minimize \quad c_{4-CBA}(F_{FEED}, [C_0], W_{H_2O}) \tag{4.53}$$

Earlier studies showed the effect of water content on the reaction kinetics (Wang, 2005b; Suresh, et al., 2000). The water content in the reactor also regulates the reactor temperature. Wang et al. (2005b) showed the importance of the optimal water content while operating the PTA reactor. It is suggested to have the water content less than the optimal water content value so that the overall rate of oxidation increases with an increase in the water content. The optimal water content in the reactor also ensures the decreased concentration of 4-CBA. The amount of water present in the reactor is in saturated state in the given range of temperature and pressure, having the degrees of freedom value of 1. In this state, the pressure of the reactor automatically gets fixed with a change in the temperature. Therefore both the temperature and pressure of the reactor depend on the percentage water content in the reactor. The reactor pressure in turn determines the percent vent oxygen content. As the percentage water is indirectly related to several operating parameters of PTA oxidation process, it has been included as one of the decision variables in this study.

Case-3

$$Maximize \quad F_{FEED}$$

$$Minimize \quad c_{4-CBA}(F_{FEED}, [C_0], W_{H_20}, F_{PX}, V_{O_2}) \tag{4.54}$$

The amount of excess oxygen in the feed air determines the values of vent oxygen from the reactor and the first crystallizer. Due to the saturated state of process mixture, pressure is also related to the temperature as discussed earlier. Optimum vent oxygen content is necessary in the PTA oxidation reaction. If the vent oxygen content value is less than the optimum value, then an excess amount of 4-CBA gets formed, thus degrading the quality of final product. The flow of *p*-xylene fixes the mole fraction of *p*-xylene in the process stream. It is necessary to have an optimum amount of *p*-xylene in the inlet stream; otherwise undesired excessive byproduct formation may take place. Decision variable, V_{O_2} also plays an important role in the reactor operation, as the amount of vent oxygen from the reactor is directly related to the pressure in the reactor.

Case-4

$$Maximize \quad F_{FEED}$$

$$Minimize \quad c_{4-CBA}(F_{FEED}, [C_0], W_{H_20}, F_{PX}, V_{O_2}, T) \tag{4.55}$$

The catalyst concentration affects the 4-CBA concentration at the exit of reactor. We considered the bound on catalyst concentration as 300 - 800 ppm. The lower bound is set considering the minimum catalyst concentration necessary for the reactor while the upper bound is fixed to a relatively higher value in order to consider the effect of an increased concentration of the catalyst on the process. The mole fraction of *p*-xylene in the feed stream affects the rate of forward reactions greatly. Therefore the lower and upper bounds of flow rate of *p*-xylene are fixed at 20 % of the total feed rate at both the ends. The total feed rate (one of the decision variables) is directly related to the production capacity, which ranges between 1,30,000 to 1,70,000 kg/h (Mu et al., 2004). The amount of water present in the reactor plays an important role in deciding the conversion value in the

reactor as it is directly related to the rate constant. Wang et al. (2005a) concluded that the overall oxidation rate of *p*-xylene to TA reaches a certain maximum (optimum) amount of water content in the solvent. Therefore, in this study, we considered the water content in the solvent as a decision variable and its bounds are selected between 0 - 8 % of the total reactor volume. The amount of vent oxygen from the reactor is varied between 0 - 6 % as per the industrial practice. All the other decision variables are directly or indirectly linked with the reactor operating temperature. Due to this reason, even a small change in the reactor temperature may cause a large operational instability in the process. Therefore, controlling the temperature of reactor is chosen as a last choice when all the other decision variables fail to regulate the optimal operation. The ranges of various decision variables considered in this study are given by Eq. 4.56 through Eq. 4.61.

$$453 \le T \le 461 \quad \text{K} \tag{4.56}$$

$$300 \le [\text{C}_0] \le 800 \ \text{ppm} \tag{4.57}$$

$$26000 \le F_{PX} \le 34000 \ \ \text{kg/h} \tag{4.58}$$

$$130000 \le F_{FEED} \le 170000 \ \ \text{kg/h} \tag{4.59}$$

$$0 \le W_{H_2O} \le 8 \ \% \tag{4.60}$$

$$2 \le V_{O_2} \le 6 \ \% \tag{4.61}$$

Values of various constants and parameters involved in the study are reported in Tables C1 - C3.

4.2.4 Low density polyethylene (LDPE) tubular reactor

4.2.4.1 Process description and modeling aspects

Fig. 4.6 shows the schematic of 5 zone LDPE tubular reactor. The reactor being tubular in nature has a specific characteristic of high value of length to diameter ratio. Depending upon the requirement of degree of reaction occurring in the reaction, the total length of 1390 m is divided into five different zones. Zone 1 is considered to be a heating zone, in which no reaction occurs.

The feed [consisting of ethylene monomer, telogen solvent, oxygen, peroxide, and inert (*n*-butane)] is fed at the inlet of the reactor. Initiator I_1 (tert-butyl peroxypivalate) is injected at the entrance of 3rd zone while initiator I_2 (tert-butyl, 3,5,5 trimethyl peroxyhexaonate) is injected at the entrance of 5th zone. The reactor model includes mass, energy and momentum balances for tubular reactor (Agrawal et al., 2006). Ideal plug flow conditions are assumed both in the reactor and in the jacket. The reaction mixture is assumed to be homogeneous. The characteristic growing and dead polymer concentrations are expressed in terms of bi-variate moments (Katz and Saidel, 1967). An average constant temperature of jacket fluid is used for each zone. The physical properties of the reaction mixture such as density, viscosity and thermal conductivity are assumed to vary along the length of the reactor in axial direction. The temperature and pressure dependence of specific reaction rate is given by Arrhenius rate law (Eq. D28). The reaction scheme, model equations, the kinetic rate constants and correlations (Eqs. D1 – D29c) related to LDPE tubular reactor considered in this study are given in Appendix D.

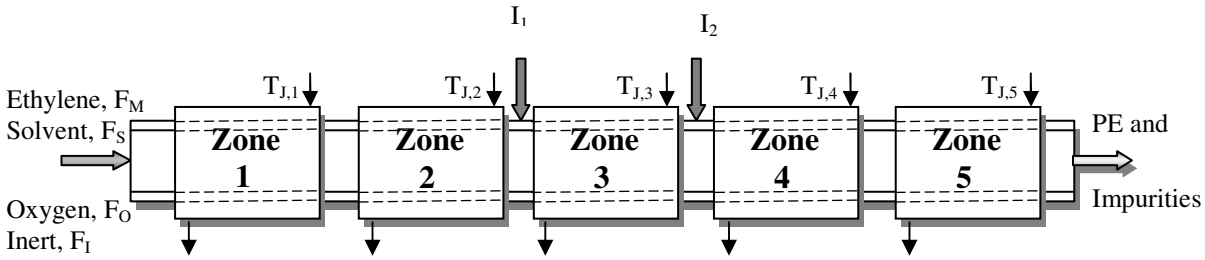

Fig. 4.6 Schematic diagram of 5-zone tubular LDPE reactor

4.2.4.2 Formulation of objective functions

Two objective functions namely, maximization of the monomer conversion ($X_{M,f}$) and minimization of the (weighted average value of the) undesirable side product contents ($[M_e]_f$, $[V_i]_f$, and $[V_{id}]_f$) are considered. The undesired side products are minimized to improve the final product quality and strength. The economics of an organisation is largely related to optimum conversion, therefore maximization of conversion is considered as the second objective. The problem formulation considered in this study is same as that considered by Agarwal et al. (2006). Following two case studies are considered for MOO of LDPE tubular reactor.

Case-1: Two-objective optimization (maximization of conversion and minimization of the weighted average value of the undesirable side products)

Case-2: Four-objective optimization (maximization of conversion and minimization of side products (namely, methyl, vinyl and vinylidene side chians content) is considered independently)

Case-1: Maximization of Conversion and Minimization of the weighted average value of the undesirable side products (Eqs. 4.62 - 4.63) subject to constraint on temperature and number average molecular weight (Eqs. 4.64 and 4.65) and variable bounds (Eqs. 4.66 - 4.76). Three additional variations are considered in case study 1 by varying the bounds of second constraint (Eq. 4.65) by ± 20 kg/kmol, ± 200 kg/kmol, ± 1100 kg/kmol and keeping the objectives, rest of the constraints and bounds of variables as same.

$$Maximize\ f_1 \equiv X_{M,f} \tag{4.62}$$

$$Minimize\ \ f_2 \equiv \frac{[M_e]_f}{30} + \frac{[V_i]_f}{0.1} + \frac{[V_{id}]_f}{0.7} \tag{4.63}$$

Subject to

$$T_{\max}(z) \leq 610.15 \text{ K} \tag{4.64}$$

$$M_{\text{n,f}} = 21{,}900 \text{ kg/kmol} \tag{4.65}$$

$$323.15 \text{ K} \leq T_{in} \leq 423.15 \text{ K} \tag{4.66}$$

$$182.30 \text{ MPa} \leq P_{in} \leq 248.25 \text{ MPa} \tag{4.67}$$

$$5\times10^{-5} \text{ kg/s} \leq F_0 \leq 10\times10^{-5} \text{ kg/s} \tag{4.68}$$

$$2\times10^{-2} \text{ kg/s} \leq F_s \leq 0.5 \text{ kg/s} \tag{4.69}$$

$$5\times10^{-5} \text{ kg/s} \leq F_{I,1} \leq 10\times10^{-3} \text{ kg/s} \tag{4.70}$$

$$5\times10^{-5} \text{ kg/s} \leq F_{I,2} \leq 10\times10^{-3} \text{ kg/s} \tag{4.71}$$

$$\text{s}\,413.15 \text{ K} \leq T_{J,1} \leq 543.15 \text{ K} \tag{4.72}$$

$$473.15 \text{ K} \leq T_{J,2} \leq 543.15 \text{ K} \tag{4.73}$$

$$473.15 \text{ K} \leq T_{J,3} \leq 543.15 \text{ K} \tag{4.74}$$

$$413.15 \text{ K} \leq T_{J,4} \leq 543.15 \text{ K} \tag{4.75}$$

$$413.15 \text{ K} \leq T_{J,5} \leq 543.15 \text{ K} \tag{4.76}$$

Case-2: Maximization of conversion and minimization of side products (namely, methyl, vinyl and vinylidene side chians content) is considered independently as given by Eqs. 4.77 - 4.80): subject to constraint on temperature and number average molecular weight (Eqs. 4.81 and 4.82) and variable bounds (Eqs. 4.66 – 4.76).

$$Maximize\, f_1 \equiv X_{M,f} \tag{4.77}$$

$$Minimize\ f_2 \equiv \frac{[M_e]_f}{30} \tag{4.78}$$

$$Minimize\ f_3 \equiv \frac{[V_i]_f}{0.1} \tag{4.79}$$

$$Minimize\ f_4 \equiv \frac{[V_{id}]_f}{0.7} \tag{4.80}$$

Subject to

$$T_{\max}(z) \leq 610.15 \ \text{K} \tag{4.81}$$

$$M_{\text{n,f}} = 21{,}900 \pm 200 \ \text{kg/kmol} \tag{4.82}$$

Two constraints on maximum temperature in the reactor [$T_{\max}(z)$] and on number average molecular weight (M_n) are imposed in both the case studies. Due to the injection of initiator in the reactor and due to exothermic nature of reaction, the temperature of the reaction mixture shoots up suddenly. The high temperature gives rise to undesirable side reactions and is also not suitable from the safety considerations. Therefore maximum temperature of the reactor is restricted to 610.15 K. The number-average molecular weight is constrained to lie at 21900 kg/kmol. Penalty method (Deb, 2001) is used to handle constraints. 11 decision variables namely, inlet temperature (T_{in}), the feed flow rates (F_o, F_S, $F_{I,1}$, and $F_{I,2}$) of oxygen, solvent and the two additional initiators added, the five average temperatures, $T_{J,1}$ - $T_{J,5}$, of the jacket fluids and the inlet pressure (P_{in}) are considered.

4.2.5 Supply chain and planning

4.2.5.1 Supply chain viewed as a network model

As a part of the planning process, the structure of the supply chain needs to be represented. This is usually done using a network model. A network model is used in this study to graphically represent a supply chain model. Fig. 4.7 represents the flow of material and entities involved in the supply chain. Each node represents existing facilities (e.g., supplier, plant and customer). The arks and link are used to connect the nodes in the supply chain model. These arks represent the flow of material from one node to another, e.g., the raw material supply from the supplier to the plant and then from the plant to the customer zone. Supplier also represents the most upstream entity whereas customer zone represents the most downstream entity. Thus, the flow of material occurs from supplier to customer zone and the flow of financials occurs from customer zone to the supplier. The direction of these flows can change only in the case of reimbursement or rebate. In this problem only one way flow of material and the financials is considered. Present study also considers that a single product is manufactured from three different components (raw materials). The nomenclature used in the present problem is as follows (Fig. 4.7): S1 - S5 denote the five suppliers; P1-P3 denotes the three Manufacturing establishments (plants), and C1 - C4 denote the four customer zones. The flow of goods and finance are also shown in Fig. 4.7. It is considered that all five suppliers can supply three different components to all three plants. These components can be transported by road/rail or shipped to any of the three plants where the product is manufactured. The cost of transportation is also taken into account.

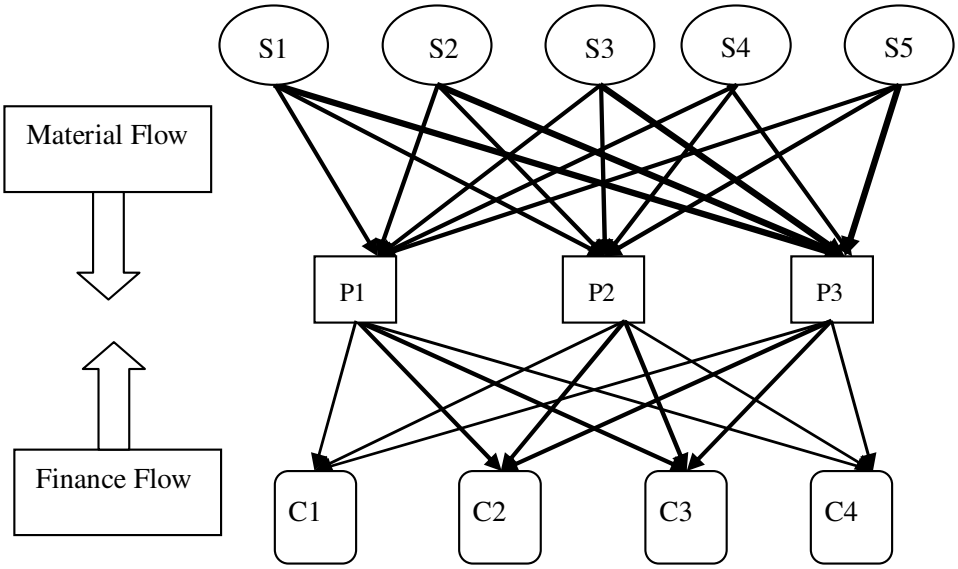

Fig. 4.7 Flow of financials, materials and the entities involved in supply chain problem

The finished product from the plant is then shipped to the customer zones based on demand. In actual practice, few suppliers are preferred over others depending on their previous performance, quality, and timeliness of goods delivered. Thus the most preferred supplier has a lowest cost for a particular component. Different indices describe the interactions between different entities in supply chain model. The set of those indices are:

(i, j): Component-Supplier

(i, j, k): Component-Supplier-Plant

(k, l): Plant-Customer Zone

4.2.5.2 Formulation of optimization functions

In this study, five objective functions are considered which are divided into three sets of two objective problems. The objective functions reported in this study are taken from literature (Pinto, 2007). The objectives are minimization of Total operating cost (TOC), Total cost (TC) and Machinery cost (MC) and maximization of profit and revenue. Three sets of objective functions used in this formulation are as follows:

1) Objective Functions Set 1

Objective Function 1: *Minimize TOC*

Objective Function 2: *Minimize MC/TOC*

Total operating cost plays an important role in statistics of manufacturing of product. Therefore, minimization of *TOC* has been given greater importance in supply chain optimization problems. The second objective function is the ratio of manufacturing cost to total operating cost. This objective function also holds importance since it is very

important to ensure that manufacturing cost falls within a certain permissible bound as a percentage of the total operating cost. Those two objectives clearly show the trade-off between each other, as the value of first objective (*TOC*) is appearing in the denominator of second objective function.

2) Objective Functions Set 2

Objective Function 1: *Maximize Profit*

Objective Function 2: *Minimize MC*

In this problem, the conflict is not easily seen. The results are analyzed in the subsequent section, which show the conflict among the objectives.

3) Objective Functions Set 3

Objective Function 1: *Maximize Revenue*

Objective Function 2: *Minimize TC*

This multi-objective optimization problem consists of maximization of revenue and minimization of transportation cost. The transportation cost is an important component in the total operating cost and it also acts as an interacting medium between different entities of the supply chain model. Therefore it needs to be considered in every supply chain optimization problem. Total 36 variables are involved in this study. The summary of these variables is as follows: 15 variables for 3 components transported from 5 suppliers to three plants; 12 variables for amount of product from 3 plants to 4 customer zones, and 9 variables for inventory of each component (3) at each plant (3). The constraints are also imposed on plant capacities, supplier capacities, inventory balancing and total operating cost of the supply chain model. Penalty function method (Deb, 2005) is used to handle constraints. The constraints involved in the study include:

$$\sum_{l} Y_{k,l} \le U_k \forall k \tag{4.83}$$

$$\sum_{k} S_{i,j} X_{i,j,k} = L(i,j) \forall i,j \tag{4.84}$$

$$\sum_{j} S_{1,j} X_{1,j,k} = \sum_{l} Y_{k,l} + I_{1,k} \forall k \tag{4.85}$$

$$\sum_{j} S_{2,j} X_{2,j,k} = \sum_{l} Y_{k,l} + I_{2,k} \forall k \tag{4.86}$$

$$\sum_{j} S_{3,j} X_{3,j,k} = \sum_{l} Y_{k,l} + I_{3,k} \forall k \tag{4.87}$$

$$TC = \sum_{i}\sum_{j}\sum_{k}\left(X_{i,j,k} S_{i,j} STC(i,j,k)\right) + \sum_{k}\sum_{l} Y_{k,l} PTC(k,l)$$

$$TMC = \sum_{k}\left(LC(k) + MC(k) + IC(k)\right) \tag{4.88}$$

(4.89)

$$SC = \sum_{i}\sum_{j}\left(CS(i,j) S_{i,j} X_{i,j,k}\right) \tag{4.90}$$

$$TOC = TC + TMC + SC \tag{4.91}$$

Eqs. 4.86 - 4.87 represent the constraints used in the present study. Eqs. 4.86 - 4.87 represent the constraints on plant and supplier capacity respectively. Constraints are imposed on inventory balance of component 1, 2 and 3, which are represented by set of Eqs. 4.88, - 4.90. A variable *S(i, j)* in the above constraints is a binary variable which denotes whether component *i* is supplied by supplier *j* or not. In this study, the *S*(*i, j*) values are fixed as 0 and 1 randomly. Eqs. 4.88, 4.89 and 4.90 are expressions for transportation cost (TC), total manufacturing costs [TMC; which include the plant labor, inventory (IC) and manufacturing costs (MC)] and supplier costs (SC). Eq. 4.91

represents the total operating cost (TOC), which a sum of transportation cost, total manufacturing costs and supplier costs.

Summary of chapter: In this chapter MOO problem formulation, for benchmark test problems (both constrained and unconstrained) and industrial case studies considered in this study, is discussed. The problem formulation for test problems include detailed description of the test problems. In case of industrial case studies, process and mathematical model pertaining to specific process is discussed followed by formulation of MOO problem (which includes optimization functions, constraints & variables and their bounds).

Next chapter deals with results and discussion of MOO test problems and MOO process design decisions pertaining to specific process considered in this study.

CHAPTER – 5

RESULTS AND DISCUSSION

In this chapter the results obtained on benchmark test problems and industrial processes using newly developed strategies of MODE algorithms are discussed. In section 5.1 the performances of newly developed algorithms are tested with other algorithms reported in the literature on bench mark test problems using widely accepted performance measures. The Pareto fronts are obtained and compared for each of the test problems. In section 5.2 newly developed algorithms are used to obtain Pareto fronts for industrial processes considered in this study.

5.1 Bench Mark Test Problems

5.1.1 Parametric performance evaluation of MODE algorithm

Differential Evolution (DE) algorithm is considered to be robust algorithm for parametric setting, i.e. it does not depend upon its control parameters, [i.e. Crossover constant (CR), Number of population points (*NP*), Scaling factor (*F*), Number of generations (*N*g) and Penalty parameter (*R*)] (Angira, 2005). To check this, we tried to test the performance of MODE algorithm by varying its control parameters, such as CR, *F*, and *NP*, *N*g and *R*. Four benchmark MOO problems are used in the investigation of effect of key control parameters of MODE on the resulting Pareto front. These results are obtained during the preliminary stage of this thesis. Each Test problem consists of two objective functions

with/without constraints. The following Test problems namely, B & C, Max-Max, BNH, SRN and Min-Min (Tables 4.1 and 4.2) are considered in this study.

Fig. 5.1a shows the objective space and Pareto optimal front at various generations, with CR = 0.9, R = 0.1 and NP = 1000. It is observed that MODE approaches to the true Pareto front at lower value of generation. Once converged, with increase in the number of generations, the solutions on Pareto front remain unchanged. In Fig. 5.1b, Pareto optimal front is plotted at various values of CR and NP combinations. Irrespective of CR values, with lesser values of NP (in the range of 100) the performance of MODE is very poor. With low value of initial population size, the possibility of getting diversified and well – distributed solutions in the feasible region is very less, as MODE algorithm involves removal of dominated solutions at each generations. Fig. 5.1b also shows that with CR value of 0.9 and NP value of 1000 the Pareto optimal front is well spread as compared to non-dominated solutions obtained when NP value of 100, 500 were used. Fig. 5.1c shows that a small penalty parameter results in an infeasible set of non-dominated solutions. Since penalty terms are added to each objective function, the resulting penalized objective functions may form a Pareto optimal front, i.e., different from the true Pareto-optimal front, particularly if the chosen penalty parameter values are not adequate. However, higher values of penalty parameters are recommended, and used throughout the present study. It also reveals from Figs. 5.1b - 5.1c that local Pareto fronts seem to approach to the true front with increasing value of R but the population with a large R (R = 100) shows a poor spread of solutions.

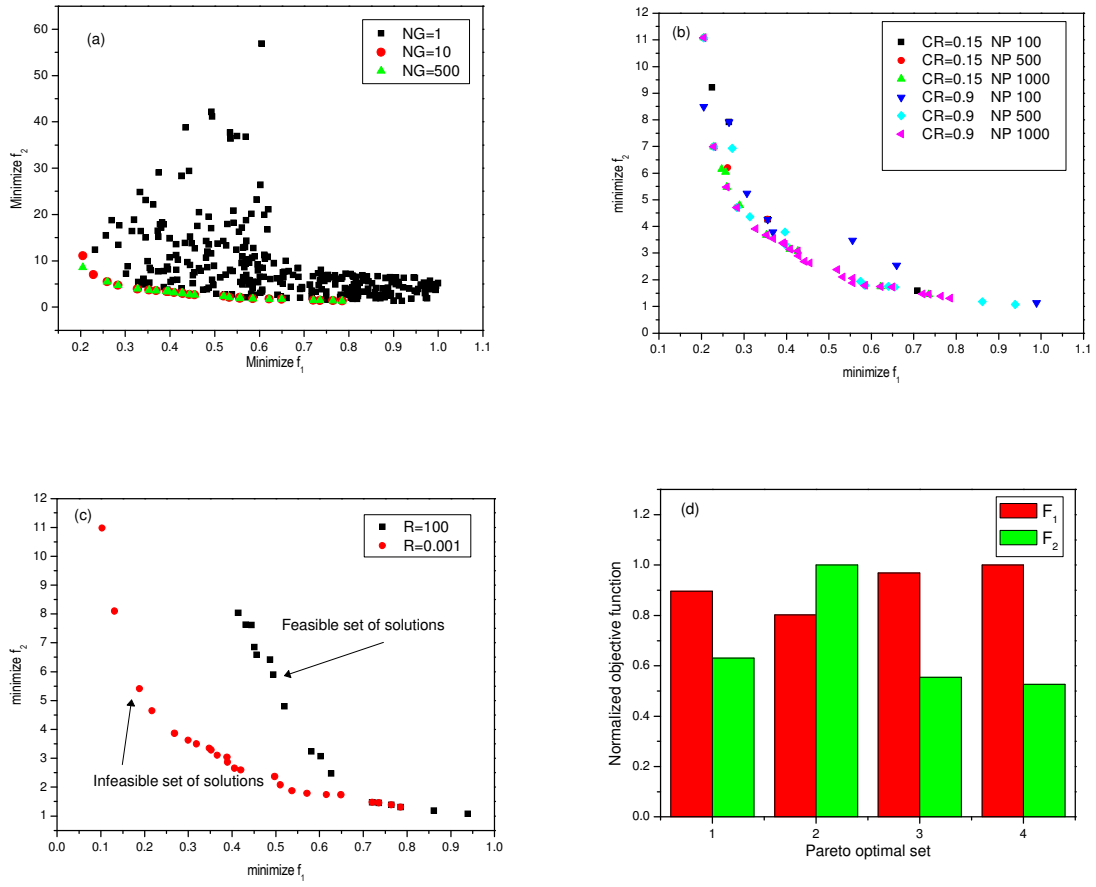

Fig. 5.1 Objective space at various generations [Fig. (a)]; Effect of CR at various values of *NP* [Fig. (b)]; Feasible and infeasible solutions at various values of Penalty parameter [Fig. (c)]; Bar chart representation of Pareto solution [Fig. (d)] for Constr-Ex test problem

Fig. 5.1d shows the bar chart representation of the objective functions, which is one of the ways of representing normalized values of Pareto solutions. This representation is especially suitable for lower number of Pareto solutions.

In Fig. 5.2a all the solutions obtained for B & C unconstrained test problem are plotted at various values of generations using MODE algorithm. In the objective space, the distribution of solutions is nearly uniform during the initial generations. In Fig 5.2b, the Pareto front is plotted at various values of CR. MODE converges to the same Pareto Optimal front with all CR values considered in this study. Fig. 5.3a shows the Pareto front obtained using different values of CR (i.e., CR = 0.15, 0.5, 0.9 and 1.0) for Max-Max test problem. The algorithm converges to the same Pareto front, however, the distribution of solutions is poor at lower value of CR. Fig. 5.3b shows the obtained Pareto front at various generations, (i.e., Ng = 1, 10, 100, and 10000) with CR = 0.9 and NP = 1000. The points shown at generation 1 show the feasible objective space for the Max-Max test problem. The numbers of non-dominated solutions (for B & C test problem) in generations 1, 10, 100 and 1000 are 298, 10, 8 and 2 respectively. The results obtained in present study had expected a tremendous improvement in the working of MODE algorithm, which motivated us to find new strategies of MODE. Binh and Korn (1997) introduced the two variable constrained problem (BNH) as given in table 4.2. Figs. 5.4a - 540f show the Pareto front obtained using MODE algorithm for two variable constrained test problem of minimize-minimize type. Fig. 5.4a shows the effect of CR on the Pareto front. MODE is found to converge to the same front at various values of CR. But the number of non-dominated solutions is found to be increasing with increasing the value of CR.

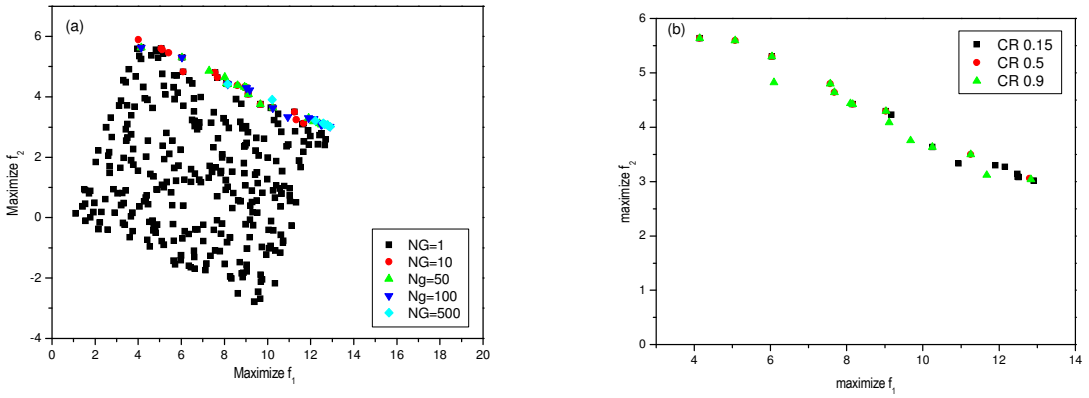

Fig. 5.2 Objective space at various generations [Fig. (a)]; Effect of CR on the Pareto optimal solutions [Fig. (b)] for B & C test problem

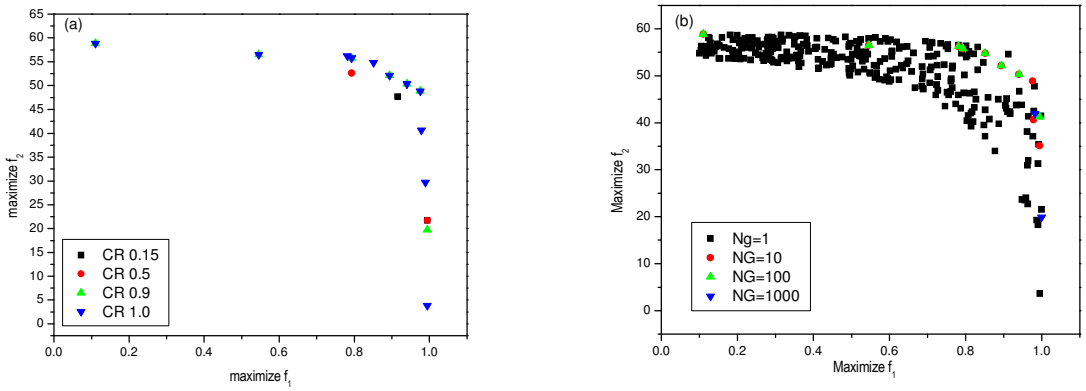

Fig. 5.3 Effect of CR on the Pareto optimal solutions [Fig. (a)]; Objective space and the Pareto solutions[Fig. (b)] for Max-Max test problem

The non-dominated solutions at the CR value of 0.15, 0.5 and 0.9 for BNH problem are 101, 136 and 149 respectively after 500 generations. Pareto front is plotted with various *NP* values after 500 generations in Fig. 5.4b. MODE algorithm is tested with various *NP* values and results with *NP* 100, 500 and 1000 are shown in Fig. 5.4b. MODE is found to converge to the same front at any value of *NP*. However the number of non-dominated solutions in the Pareto set is found to vary with *NP* values. Number of non-dominated solutions for *NP* 100, 500 and 1000 is 107, 98 and 147 respectively. The objective space and the Pareto Optimal front for BNH problem at various generations is shown in Fig. 5.4c. MODE is found to converge to true Pareto Optimal front within 10 generations. After 500 generations although Pareto front remains same as that at generation 10, it contains 2 non-dominated solutions less than that at generation 10. Effect of scaling factor *F* on Pareto Optimal front is shown in Fig. 5.4d. MODE algorithm converges to the true Pareto front irrespective of the value of *F* in the range. The number of non-dominated solutions is found to be same at all values of *F* including the random generation of *F*. The results obtained in this study showed that MODE algorithm requires high value of initial population size. But with increase in initial population size, the complexity of algorithm increases, thus making the algorithm more complex. A high value of CR is recommended, which is used consistently in the rest of the study. Focusing on these issues, MODE is developed further and additional strategies of MODE are developed, which caters towards the need of achieving both the convergence and divergence of Pareto solutions in case of MOO study.

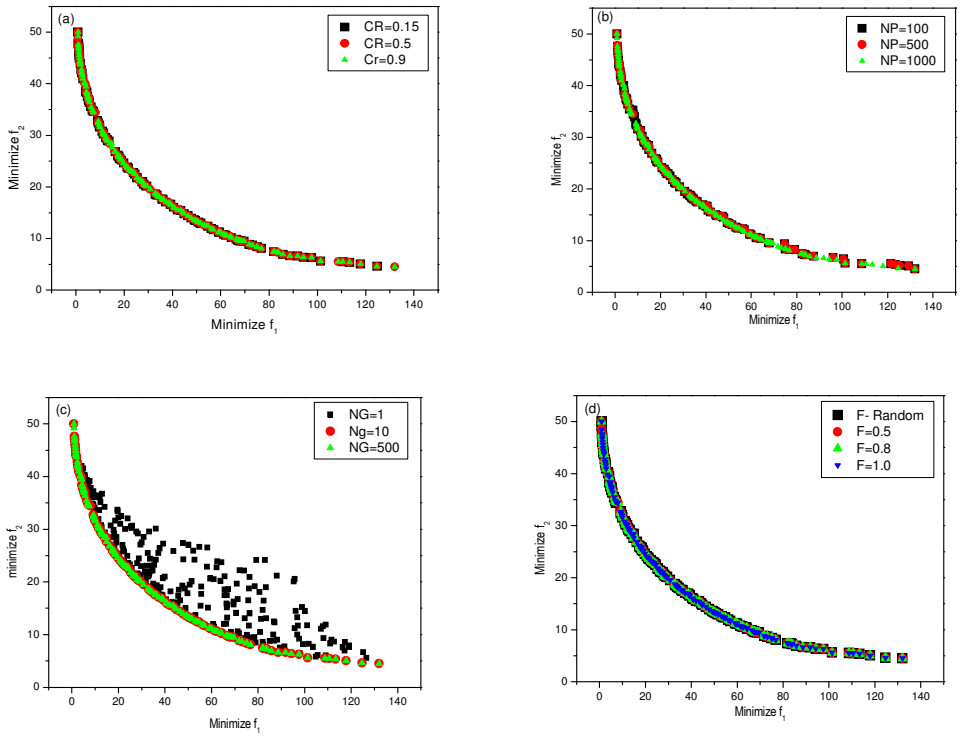

Fig. 5.4 Effect of CR on the Pareto optimal solutions [Fig. (a)]; Effect of *NP* on the Pareto front [Fig. (b)]; Objective space and the Pareto solutions at various generations [Fig. (c)]; Effect of scaling factor on Pareto solutions obtained [Fig. (d)] using MODE for BNH test problem

5.1.2 Performance assessment using benchmark test problems

Some of the most difficult test problems are selected from the literature for evaluating and comparing the performance of the proposed strategies of MODE algorithm with other well known algorithms such as NSGA (both real- and binary-coded versions), SPEA and PAES. 7 test problems are used to judge the performance of algorithms, which include SCH, FON, KUR, ZDT1, ZDT2, ZDT3, and ZDT4 (refer Table 4.1).

5.1.2.1 Measures for performance assessment of the obtained Pareto front

The decision maker is always interested in selecting a single point from the set of points available in the Pareto front. Therefore, it is better to obtain a Pareto front that is as close as possible to the true or global Pareto front and also the points are as diverse as possible from each other. Mere visual observation cannot provide the idea of efficiency of any multi-objective optimization algorithm. The two possible criteria for the evaluation of Pareto front comprise the measurement of the obtained non-dominated solutions closeness with the true Pareto front and avoidance of crowding (among the solutions), thereby maintaining a uniform diversity of non-dominated population points. Therefore, the widely accepted performance measures [such as convergence metric (γ) and divergence metric (Δ)] (Deb, 2001; Knowles and Corne, 2002) are used to calculate the performance measure for strategies of multi-objective differential evolution algorithms and are compared with the existing algorithms from the literature such as binary coded NSGA-II, real coded NSGA-II, SPEA and PAES in this study. The details of the performance measures such as the extreme solutions, Global Pareto front, algorithm output and the Euclidean distance are shown in Fig. 5.5. The global Pareto fronts used in this study are taken from the literature (Huang et al., 2005) and the corresponding actual

data is obtained from the authors through personal communication (Sugandhan, 2008). Various terms associated with performance measures are explained by taking a specific test problem as an example (SCH, refer Table-4.1) and demonstrated in Fig. 5.5. The output (set of non-dominated solutions), obtained for this problem using MODE algorithm shown through the points 1-9, is plotted and compared with the global Pareto front. The global Pareto front is termed as P*. The line joining points 1 and 2 represents the Euclidian distance shown as d_1. d_1^e and d_2^e are the distances between the extreme solutions of global Pareto front and the algorithm output (non-dominated solutions) corresponding to 1st and 2nd objectives respectively.

Convergence Metric (γ)

The convergence metric (γ), which measures the extent of convergence to a known Pareto set of solutions is adapted for measuring the extent of convergence of the obtained set of solutions from the true Pareto front. It is necessary to have a prior knowledge of true Pareto front. The true Pareto front (considered in this study) for each test problem consists of a set of 500 equally spaced points named as P^*. The convergence metric (as given by Eq. 5.1), calculates the average of distance of each solution with the nearest member in the set P^*. The smaller is the value of γ, the better is the convergence toward the true Pareto optimal front. The total number of non-dominated solutions (Pareto front) obtained using current algorithm is stored in set Q.

Table 5.1 Values of control parameters used in reference run of present study

Parameter	MODE	MODE III	Elitist MODE	Trigonometric MODE	Hybrid MODE	NSGA-II real coded
Population size (*NP*)	100	100	100	100	100	100
Number of generations (Genmax)	300	300	300	300	300	300
Scaling factor (*F*)	(0,1) Random	(0,1) Random	(0,1) Random	(0,1) Random	(0,1) Random	--
Crossover rate(CR)	0.8	0.8	0.8	0.8	0.8	0.8
Mutation probability (*M*) / Trigonometric mutation probability (M_t)	--	--	--	0.5	--	0.05
Reflection factor (α)	--	--	--	--	1	--
Contraction factor (β)	--	--	--	--	0.5	--
Expansion factor (γ)	--	--	--	--	2	--

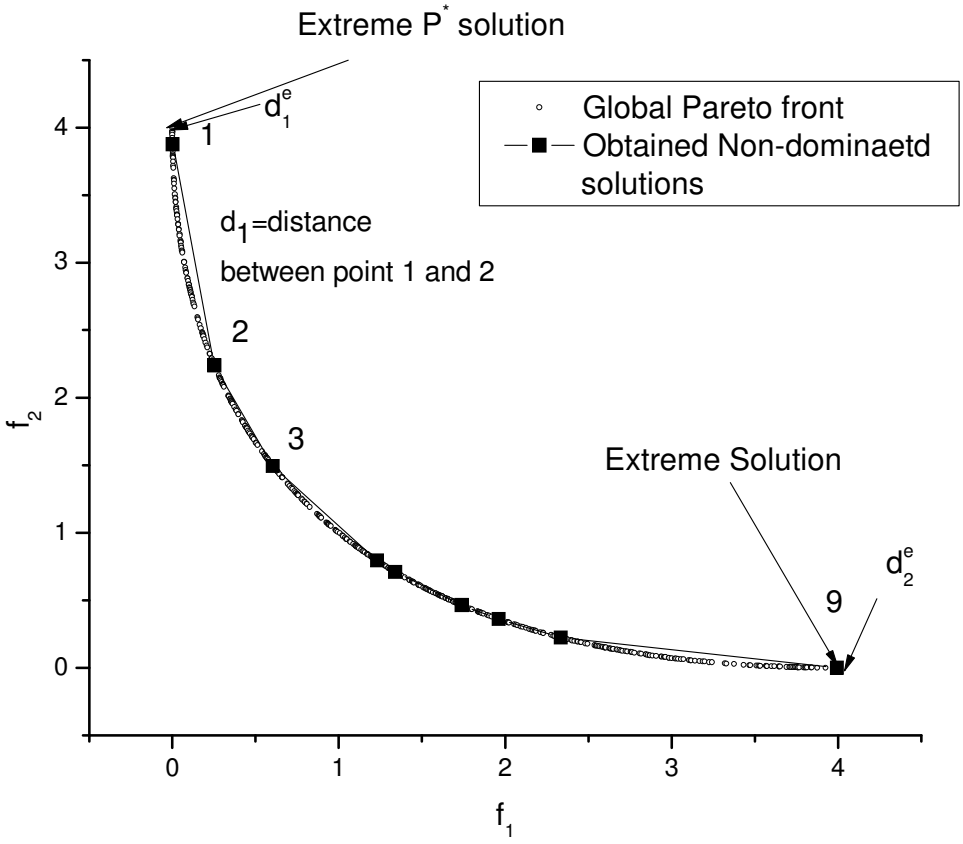

Fig. 5.5 Performance measure details used in MOO

$$\gamma = \frac{\left(\sum_{i=1}^{Q} d_i\right)}{|Q|} \tag{5.1}$$

Where d_i is the Euclidean distance between the solution $i \in Q$ and the nearest member of P^*.

Diversity Metric (Δ)

The distribution of solutions obtained in the Pareto front should be as diverse as possible. The diversity metric is used to measure the spread of solutions lying on the obtained Pareto front. The Euclidean distance d_i (the distance between consecutive solutions on the Pareto front) is calculated, and the average of all such distances is taken. Extreme solutions corresponding to each individual objective is calculated and the divergence metric (Δ) is used to calculate the extent of divergence. The diversity metric, Δ, measures the extent of the spread achieved among the Pareto optimal solutions. The metric Δ is calculated using Eq. 5.2.

$$\Delta = \frac{d_f^e + d_l^e + \sum_{i=1}^{|N-1|} \left| d_i - \bar{d} \right|}{d_f^e + d_l^e + |N-1|\bar{d}} \tag{5.2}$$

Where, $d_f^e + d_l^e$ is the sum of the Euclidean distances between the currently obtained extreme solutions and the extreme solutions of Pareto set, d_i is the Euclidean distance between the consecutive non-dominated solutions. The parameter, $\bar{d}$, is the average of all Euclidean distances d_i, i = 1, 2,. . ., (N−1), assuming that there are N solutions on the final non-dominated front or the obtained Pareto optimal front. The higher value of metric Δ shows a worse distribution of solutions within the extreme Pareto optimal solutions.

Parameter Settings

The simulation runs were performed on several test problems of MOO taken from the literature. All the cases of MODE algorithms developed in this study are written using Matlab (7.0) software, whereas C++ version of NSGA-II code used is taken from open sources of KanGAL (http://www.iitk.ac.in/kangal/codes.shtml). Visual C++ of Visual studio (version 6.1) is used to run NSGA-II codes. Pareto fronts are generated using MODE, MODE III, Elitist MODE, Trigonometric MODE, hybrid MODE, and real-coded NSGA-II in the present study. However, values of performance measures of NSGA-II (both binary- and real-code versions), SPEA and PAES are taken from the literature (Deb, 2001). The comparison of performance measure is entirely based on selected test problems as true Pareto front data for these test problems is known. The outcome of performance measures comparison is also helpful in establishing the performance efficiency of the proposed algorithms, so that it could be confidently applied subsequently to real world industrial problems. Ten experimental runs are performed for each problem so as to have the same basis of comparison for all the algorithms, i.e., NP = 100, CR = 0.8, and Genmax = 300. In order to carry out the comparative study, the control parameters such as maximum number of generations, crossover constant (cross over probability in case of other EMO algorithms), initial population size, etc. are kept same as those reported in the literature (Deb, 2001). The scaling factor (used in DE operation) is obtained randomly in this study. The mutation probability for NSGA is chosen to be 0.05. The trigonometric mutation probability for trigonometric MODE algorithm is set as 0.5. The list of control parameters and their values used in the present study is given in Table 5.1.

5.1.2.2 Performance assessment using selected benchmark test problems

Two important and widely used metrics are employed to calculate the convergence and divergence extents of algorithm to assess the quality of the Pareto front. The results obtained in the present study and their comparison with the results of other algorithms with respect to the convergence is shown in Table 5.2. The values of diversity metric obtained using different algorithms are shown in Table 5.3. The average (γ for convergence and Δ for divergence) and the variance (σ^2_γ for convergence and σ^2_Δ for divergence) of 10 individual runs are used [as given in the literature (Deb, 2001)] to judge the performance of algorithms for both the metrics. For the SCH test function, all the strategies of MODE and NSGA-II algorithms are able to converge to the true Pareto optimal solutions (Fig. 5.6a). However, a smooth and well diverse Pareto front is observed in case of Trigonometric MODE, Hybrid MODE, and NSGA-II (both real- and binary coded versions). The number of non-dominated solutions obtained using hybrid MODE, and Real- coded NSGA-II is 100 against 40 obtained using MODE III algorithm (Table 5.4). The lesser number of non-dominated solutions resulted in a scattered Pareto front using MODE and MODE III. Table 5.2 shows that hybrid MODE, elitist MODE, trigonometric MODE and PAES are equally good in terms of average of convergence metric. However, the variance for all the strategies of MODE algorithm is 0 as against 0.000003 obtained in case of PAES. The variance value of 0 also indicates that the algorithm is able to give consistent results. Real coded NSGA-II algorithm performed better in terms of diversity metric achieving the lowest value of 0.449265.

Table 5.2 Performance metric (convergence) comparison of several algorithms on selected test problems

Algorithm	Metric	SCH	FON	KUR	ZDT1	ZDT2	ZDT3	ZDT4
Real coded NSGA-II˜	γ	0.003391	**0.001931**	0.028964	0.033482	0.072391	0.114500	**0.513053**
	σ^2_γ	**0**	**0**	0.000018	0.004750	0.031689	0.007940	**0.118460**
NSGA-II Binary˜	γ	0.002833	0.002571	0.028951	**0.000894**	**0.000824**	0.043411	3.227636
	σ^2_γ	*0.000001*	**0**	0.000016	**0**	**0**	0.000042	7.307630
SPEA˜	γ	0.003465	0.010611	0.049077	*0.001249*	*0.003043*	0.044212	9.513615
	σ^2_γ	**0**	*0.000005*	0.000081	**0**	*0.000020*	0.000019	11.321067
PAES˜	γ	**0.001313**	0.151263	0.057323	0.082085	0.126276	0.023872	*0.854816*
	σ^2_γ	0.000003	0.000905	0.011989	0.008679	0.036877	**0.00001**	*0.527238*
MODE*	γ	0.0021	0.02554	0.03837	--	--	--	--
	σ^2_γ	**0**	0.00063	0.00057				
MODE III*	γ	0.002236	0.003381	*0.003028*	0.010329	2.7777	**0.01019**	75.67845
	σ^2_γ	**0**	**0**	**0**	*0.000002*	0.0303	*0.00002*	96.38974
Hybrid MODE*	γ	0.001967	0.002807	0.003723	0.033624	0.06813	*0.010681*	7.0635
	σ^2_γ	**0**	**0**	**0**	0.000541	0.001413	0.000013	18.39044
Elitist MODE*	γ	*0.001948*	*0.002119*	**0.002921**	0.389309	0.856404	0.287371	12.58368
	σ^2_γ	**0**	**0**	**0**	0.010519	0.016157	0.002854	13.18463
Trigonometric MODE*	γ	0.002035	0.003151	0.00665	1.752266	3.242328	1.406625	2.244484
	σ^2_γ	**0**	**0**	*0.000009*	0.046958	0.046701	0.066905	0.721678

*Results obtained in the present study; ˜Results reported in Ref (Deb, 2001)

First Best: **Bold** Font; Second Best: *Italic* font

Table 5.3 Performance metric (divergence) comparison of several algorithms on selected test problems

Algorithm	Metric	SCH	FON	KUR	ZDT1	ZDT2	ZDT3	ZDT4
Real coded NSGA-II˜	Δ	*0.477899*	**0.378065**	**0.411477**	**0.390307**	**0.430776**	0.738540	0.702612
	σ^2_Δ	0.003471	**0.000639**	**0.000992**	*0.001876*	*0.004721*	0.019706	0.064648
NSGA-II˜ Binary	Δ	**0.449265**	*0.395131*	*0.442195*	*0.463292*	*0.435112*	**0.575606**	**0.479475**
	σ^2_Δ	0.002062	0.001314	0.001498	0.041622	0.024607	0.005078	0.009841
SPEA˜	Δ	0.818346	0.804113	0.880424	0.730155	0.678127	0.665726	0.732097
	σ^2_Δ	0.004497	0.002961	0.009066	0.009066	0.004483	0.000666	0.011284
PAES˜	Δ	1.063288	1.162528	1.079838	1.229794	1.165942	0.789920	0.870458
	σ^2_Δ	0.002868	0.008945	0.013772	0.004839	0.007682	**0.001653**	0.101399
MODE*	Δ	0.67099	0.70069	0.82097	--	--	--	--
	σ^2_Δ	0.01332	0.03397	0.0053				
MODE III*	Δ	0.59953	0.620052	0.671036	0.732524	0.8022	*0.593596*	0.788153
	σ^2_Δ	0.00155	0.00095	0.00192	0.00582	0.0103	0.00399	0.019711
Hybrid MODE*	Δ	0.597286	0.538185	0.675896	0.614445	0.615554	0.654213	0.631216
	σ^2_Δ	*0.001238*	*0.000891*	0.002681	0.001567	**0.001502**	0.0065652	*0.002158*
Elitist MODE*	Δ	0.571475	0.700227	0.714344	0.62127	0.892956	0.677013	1.073553
	σ^2_Δ	0.006496	0.018964	0.003301	0.00368	0.019759	0.004157	0.02861
Trigonometric MODE*	Δ	0.596636	0.612571	0.661016	0.605579	0.653906	0.670325	*0.612488*
	σ^2_Δ	**0.000926**	0.002878	*0.001459*	**0.00068**	**0.000274**	*0.002343*	**0.001702**

*Results obtained in the present study; ˜Results reported in Ref (Deb, 2001)

First Best: **Bold** Font; Second Best: *Italic* font

Table 5.4 Percent of initial population points converged to the Pareto front for several test problems

Algorithm	SCH	FON	KUR	ZDT1	ZDT2	ZDT3	ZDT4
MODE	9	3	3	--	--	--	--
MODE III	40	49	100	9	9	26	--
Hybrid MODE	100	98	100	100	86	100	94
Elitist MODE	100	100	100	100	100	100	100
Trigonometric MODE	100	99	87	100	100	40	100
Real Coded NSGA-II	100	100	100	100	100	100	--

To increase the clarity of Pareto fronts, the Pareto fronts obtained using individual algorithms is plotted separately along with true Pareto front through Figs. 5.6b - 5.6h. The Pareto front of FON is a non-convex type, as shown in Figs. 5.7a - 5.7h, and therefore it is difficult for any algorithm to converge to the true Pareto front. The Pareto optimal solutions correspond to $x_i^* = -1/\sqrt{3}$. MODE algorithm resulted in only 2 numbers of points on the Pareto front (out of initial population of 100) after a specified numbers of generations. All the algorithms are able to cover the entire range of solutions on the Pareto front except MODE algorithm. Comparison of Pareto fronts show that the non-dominated solutions obtained with MODE III are slightly scattered and are away from the global Pareto front. However, the Pareto fronts obtained using other strategies of MODE and NSGA-II algorithms are converged to the true Pareto fronts. In terms of convergence, both the versions of NSGA (i.e., binary and real coded) and strategies of MODE (i.e., MODE III, Elitist MODE, Trigonometric MODE and hybrid MODE) attained good accuracy as compared to other algorithms such as SPEA and PAES. However, diversity metric of NSGA-II (Binary) is better as compared to other algorithms. Elitist MODE algorithm resulted in second best in terms of convergence metric.

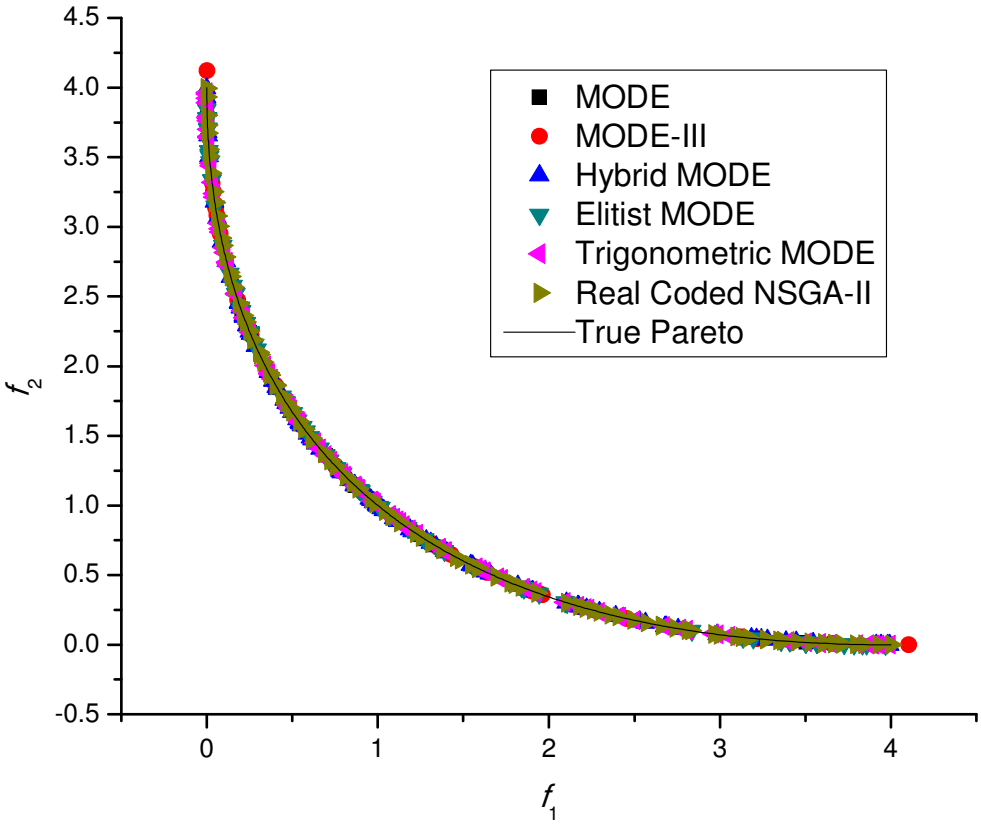
MODE
MODE-III
Hybrid MODE
Elitist MODE
Trigonometric MODE
Real Coded NSGA-II
True Pareto
f_2
f_1

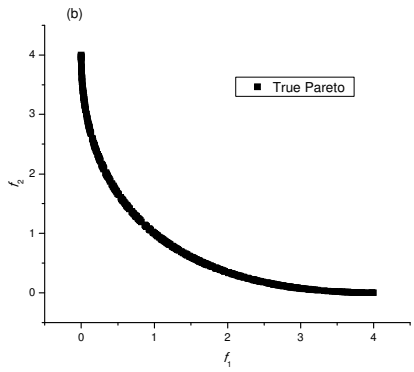
(b)
True Pareto
f_2
f_1

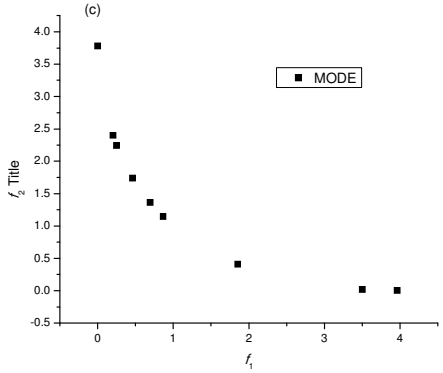
(c)
MODE
f_2 Title
f_1

Fig. 5.6 (Contd…)

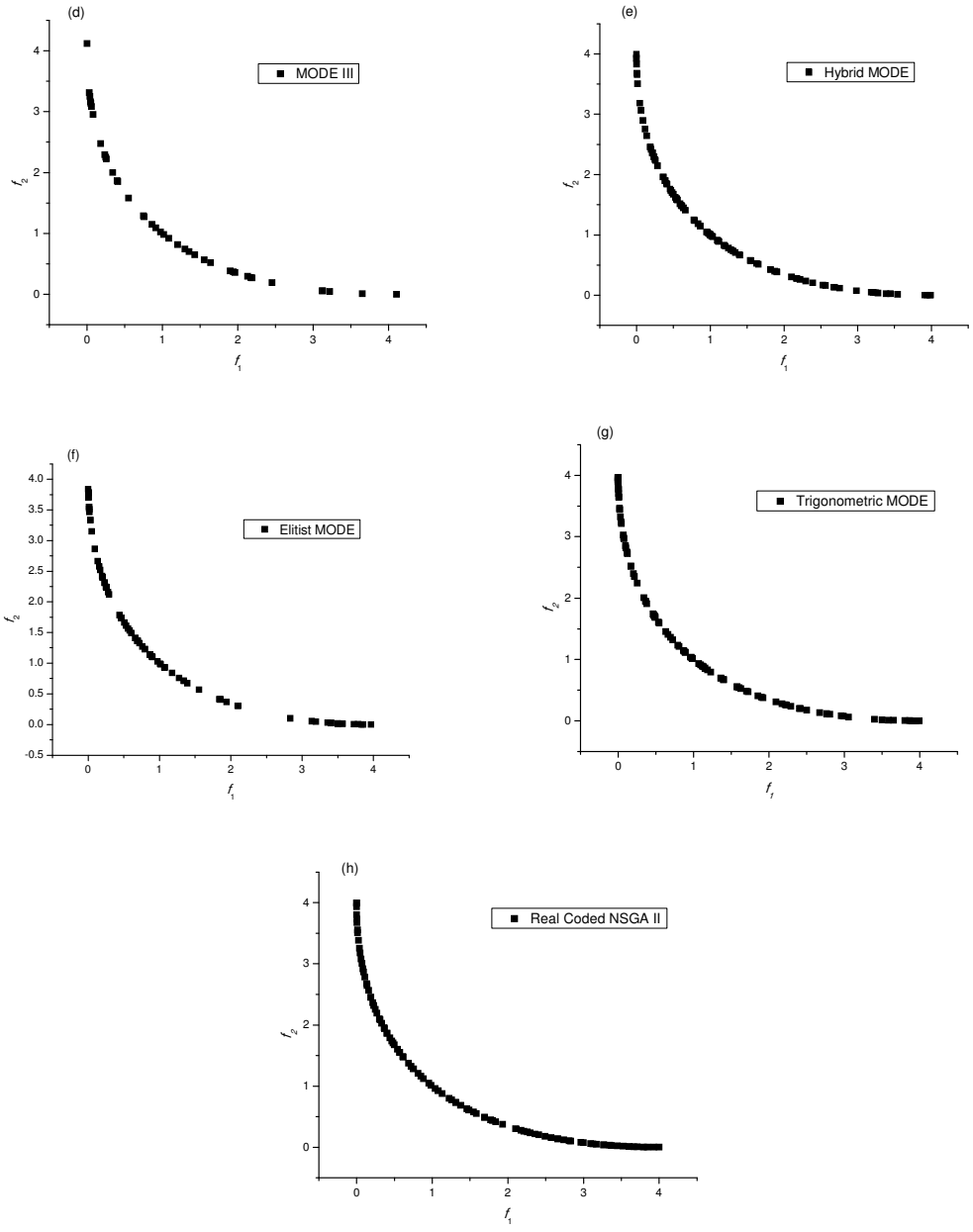

Fig. 5.6 (a) Pareto optimal solutions for SCH test problem using MODE, MODE-III, Elitist MODE, Trigonometric MODE, Hybrid MODE, real-coded NSGA-II, and true Pareto front; (b - h) Pareto fronts plotted independently for SCH test problem

KUR test problem has multiple disconnected non-convex Pareto fronts as shown in Figs. 5.8a - 5.8h. The special feature of KUR test problem is to obtain the unique point (such as point *P*) in Fig. 5.8a. Point *P* is a non-dominated solution with $x_i^* = 0$ for all the variables. Region *y* and region *z* (as shown in Fig 5.8a) have a good distribution of solutions as compared to region *x*. Region *x* and point *P* appear with a value of decision variable (DV) $x_1 = 0$, while region *x* and region *y* correspond to $x_1 < 0$. Hybrid MODE and MODE III algorithms approached the Pareto front to the closest accuracy as compared to other algorithms. However, diversity of solutions corresponding to real coded NSGA-II is better than that obtained with other algorithms.

Zietler, Deb and Thiele (ZDT) test problems (Deb, 2001) are few of the most difficult test problems specially designed to test the ability of newly developed algorithms for convergence to the true Pareto front. NSGA-II (Binary-coded) converged to the best accuracy for ZDT1 test problem. Both real coded NSGA-II, and hybrid MODE algorithms resulted in closely associated (or nearly same) value of convergence metric. MODE algorithm due to its basic feature of removal of dominated solutions in each generation could not produce any result in any of the ZDT series problems. For ZDT1, the diversity of real-coded NSGA-II algorithm is better than other algorithms. Fig. 5.9 shows the Pareto front obtained using strategies of MODE and real-coded NSGA. It is observed that MODE-III, elitist MODE and trigonometric MODE algorithms could not approach the true Pareto front. This is also evident from Table 5.2, where the value of convergence metric for those algorithms is fairly high.

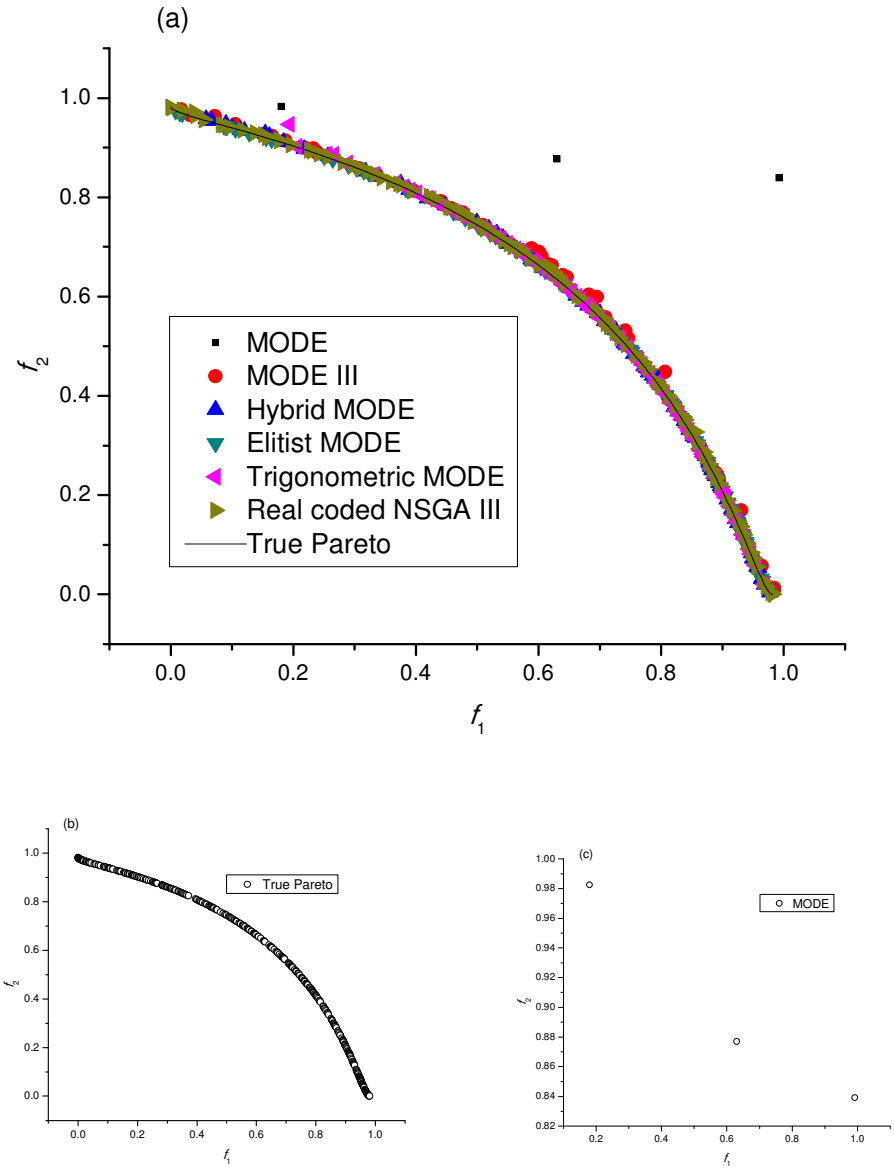
(a)
MODE
MODE III
Hybrid MODE
Elitist MODE
Trigonometric MODE
Real coded NSGA III
True Pareto
f_1
f_2
(b)
True Pareto
(c)
MODE

Fig. 5.7 (Contd…)

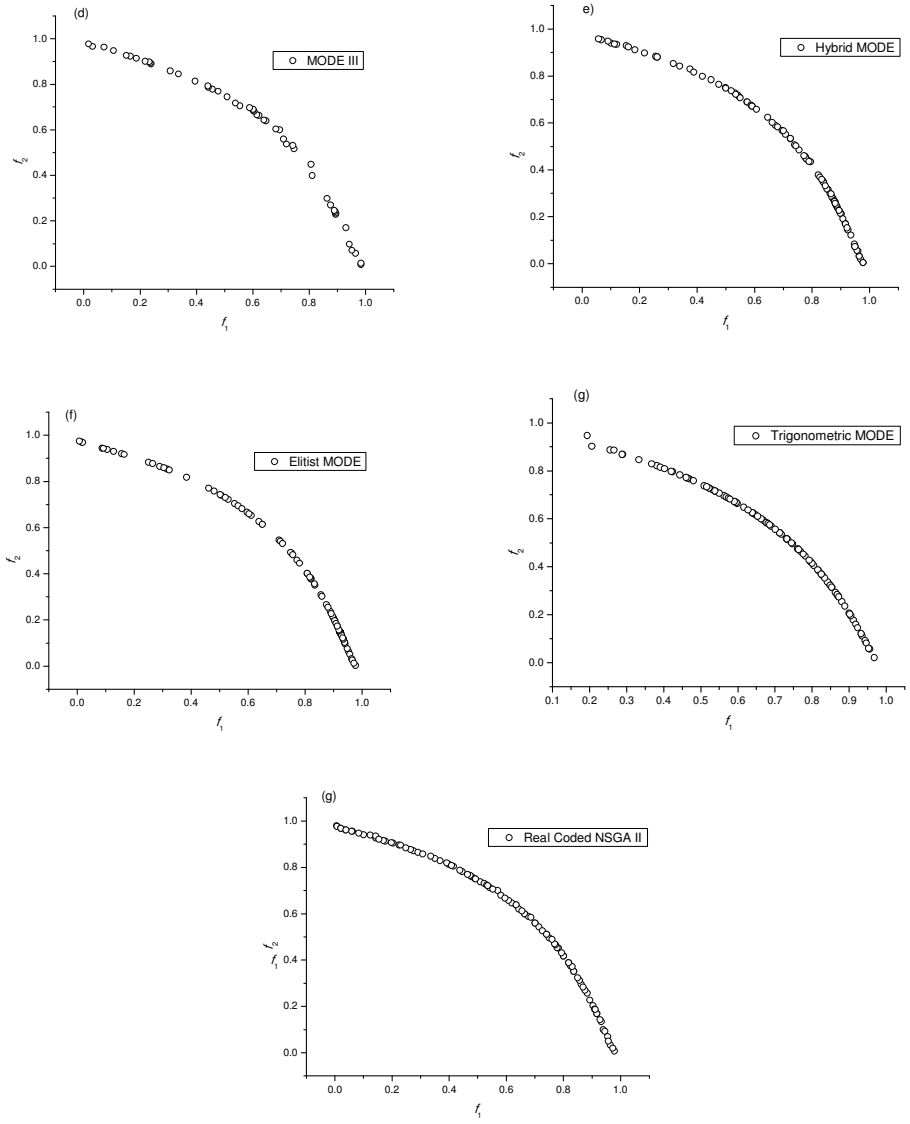

Fig. 5.7 (a) Pareto optimal solutions for FON test problem using MODE, MODE-III, Elitist MODE, Trigonometric MODE, Hybrid MODE, real-coded NSGA-II and true Pareto front; (b-h) Pareto fronts plotted independently for FON test problem

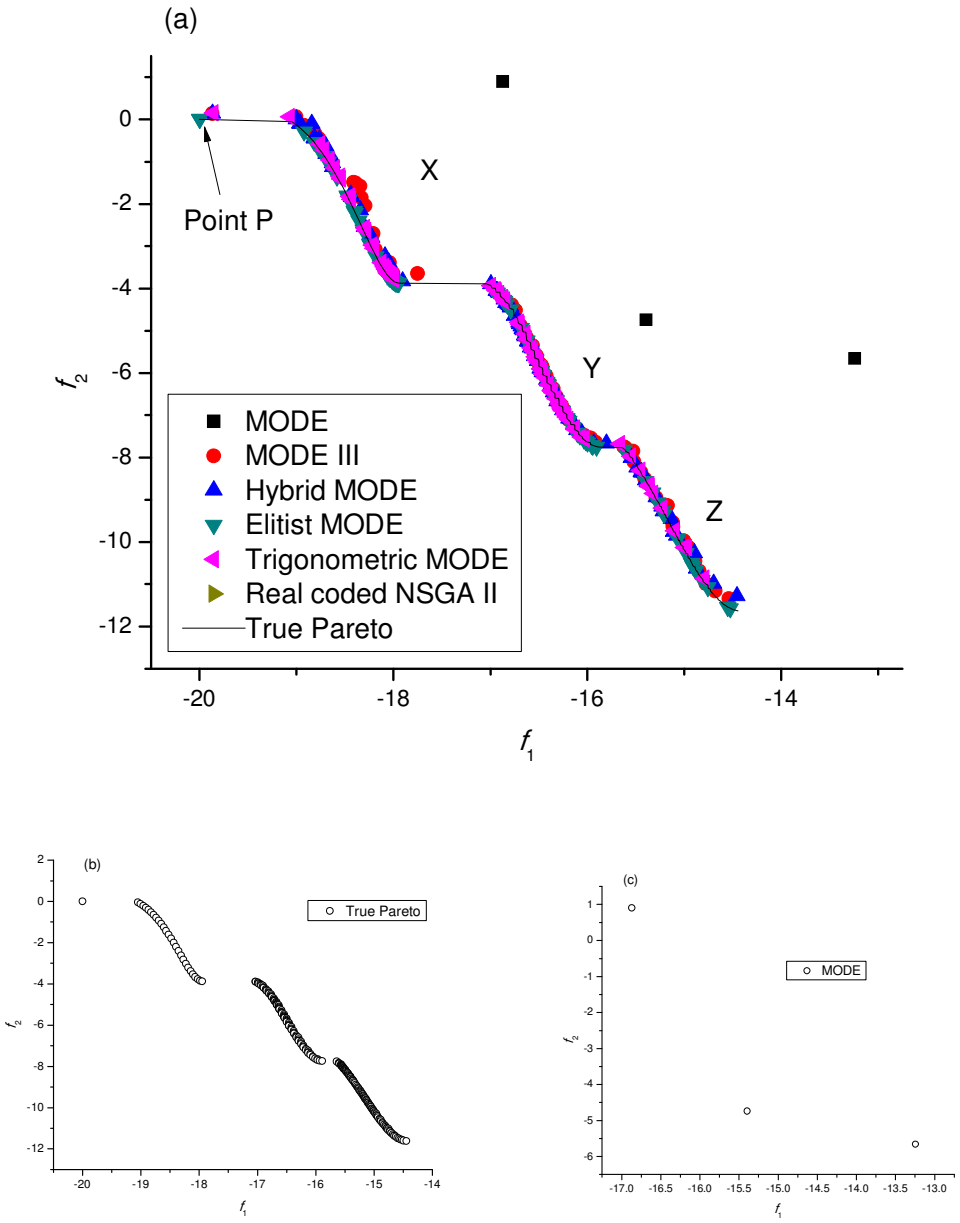
(a)
Point P
X
Y
Z
MODE
MODE III
Hybrid MODE
Elitist MODE
Trigonometric MODE
Real coded NSGA II
True Pareto
f_1
f_2
(b)
True Pareto
(c)
MODE

Fig. 5.8 (Contd…)

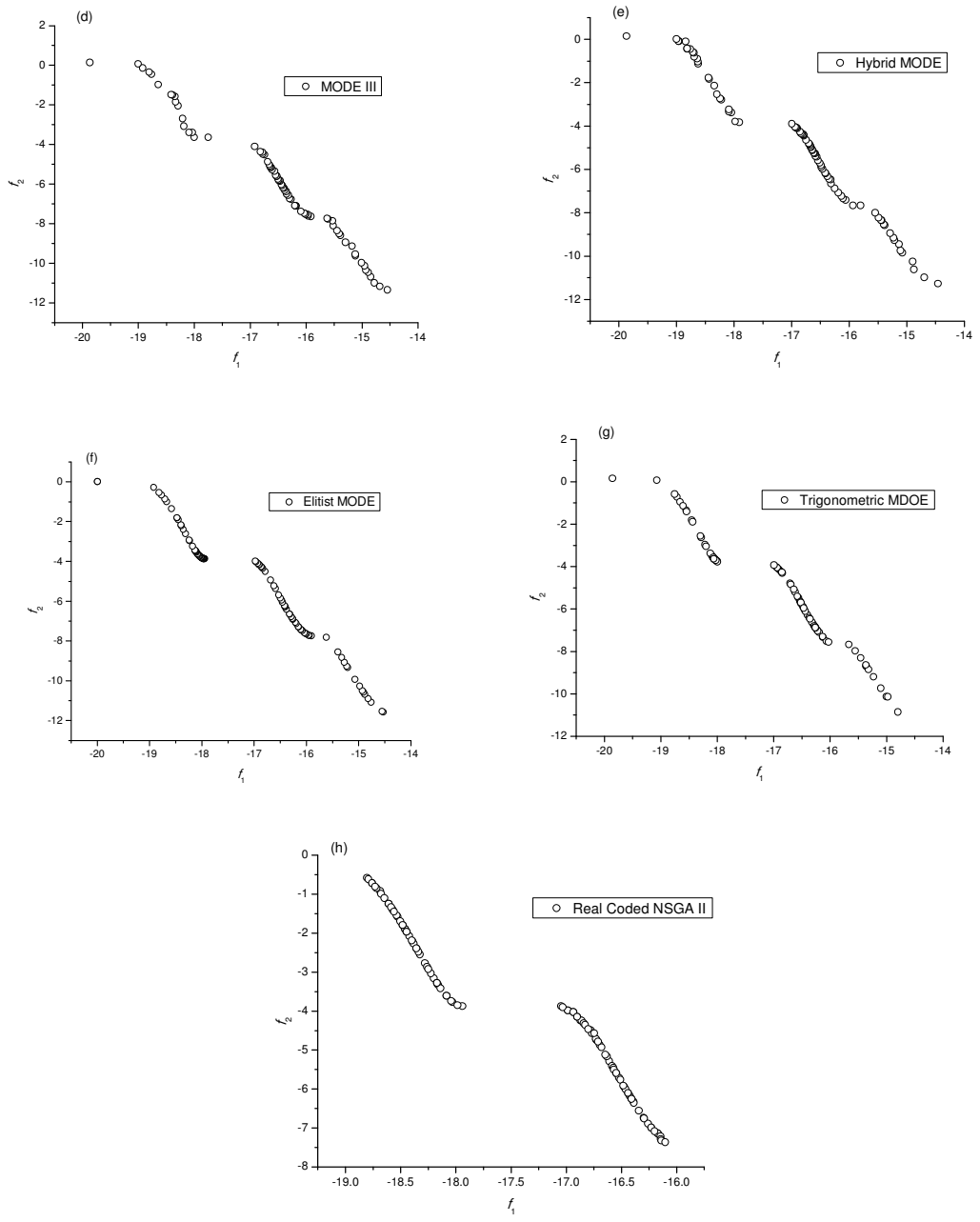

Fig. 5.8 (a) Pareto optimal solutions for KUR test problem using MODE, MODE-III, Elitist MODE, Trigonometric MODE, Hybrid MODE, real-coded NSGA-II and true Pareto front; (b - h) Pareto fronts plotted independently for KUR test problem

The Pareto front obtained for ZDT2 test problem using MODE III and hybrid MODE algorithm is shown in Fig. 5.10. Hybrid MODE and real-coded NSGA-II algorithms are able to converge to the true Pareto front with fairly good distribution of solutions. However, other strategies of MODE algorithm could not approach the true Pareto front as shown in Fig. 5.10, and therefore resulted in a very high value of convergence metric as shown in Table 5.2. The convergence metric of ZDT3 test problem is least for MODE III and Hybrid MODE algorithm as compared to other algorithms as shown in Table 5.11. However, the divergence of NSGA-II (Binary-coded) is good. As discussed in earlier sections, the evolutionary algorithms are relatively slower in terms of convergence. Fig. 5.11 shows that MODE III, Elitist MODE and trigonometric MODE algorithms are not able to converge towards the true Pareto front. However, the hybrid strategy of MODE and real-coded NSGA-II algorithms converged to the true Pareto front covering the entire range of solutions. Fig. 5.11 shows the comparative Pareto front of strategies of MODE, real-coded NSGA-II and the global Pareto front. ZDT4 test problem is one of the most difficult problems in terms of attaining the true Pareto front. None of algorithms is able to converge towards the true Pareto front. In the present study, real-coded NSGA-II also could not converge on the Pareto front. After 300 iterations, real coded NSGA-II algorithm resulted in two points with negative values in it. The NSGA-II code is downloaded from KanGAL (http://www.iitk.ac.in/kangal/codes.shtml) and Visual Studio platform is used to run the codes. In case of MODE III algorithm, the convergence metric value is very high. This is mainly attributed to the lesser number of solutions (7 solutions) obtained on the Pareto front.

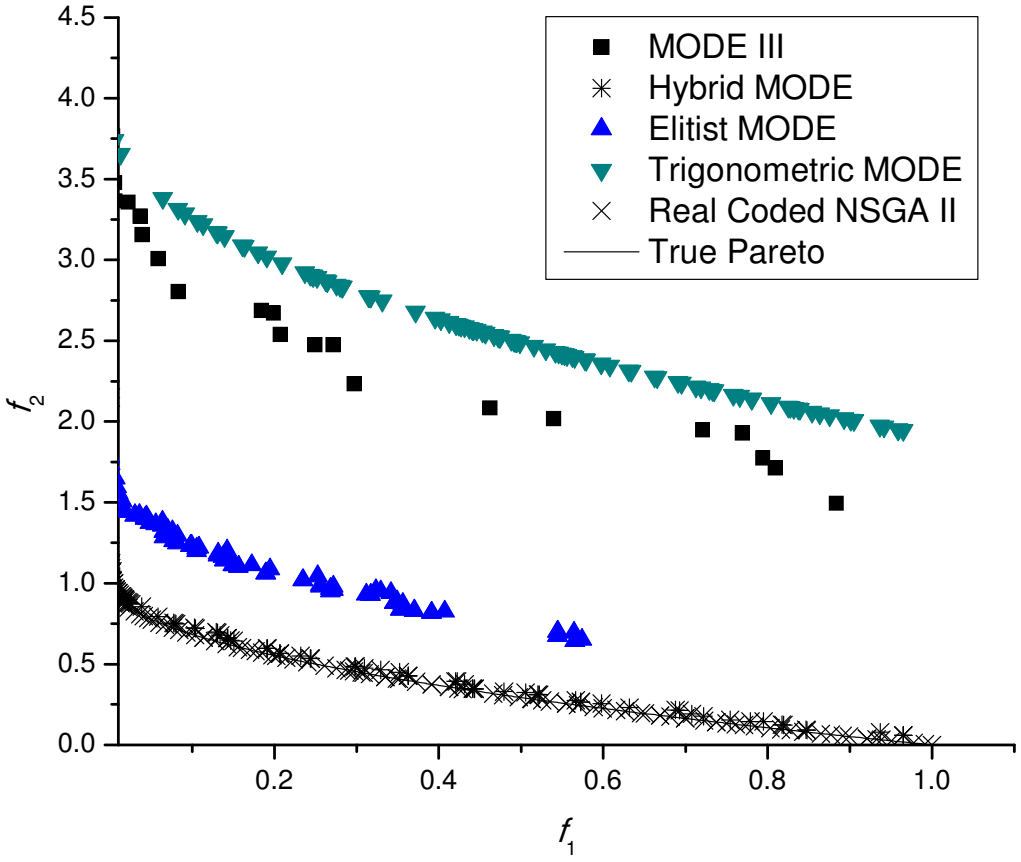

Fig. 5.9 Pareto optimal solutions for ZDT1 test problem using MODE-III, Elitist MODE, Trigonometric MODE, Hybrid MODE, real-coded NSGA-II and true Pareto front

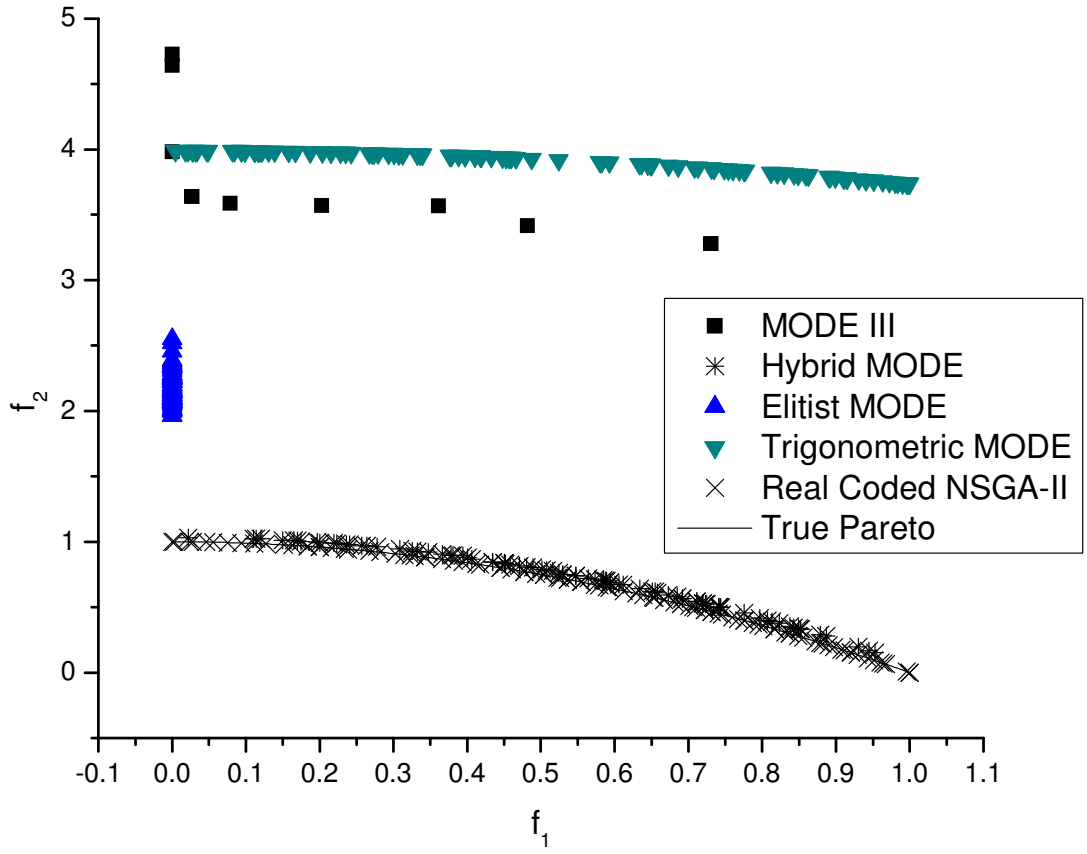

Fig. 5.10 Pareto optimal solutions for ZDT2 test problem using MODE-III, Elitist MODE, Trigonometric MODE, Hybrid MODE, real-coded NSGA-II and true Pareto front

The global Pareto front corresponds to $0 \le x_1^* \le 1$ and $x_i^* = 0$ for x = 2, 3,...10 (Deb, 2001). With these values of variables, the value of $g(x^*)$ (refer Table 4.1) is 1. In case of hybrid MODE algorithm, the values of $g(x)$ at generations 1, 50, 100, 150, 200, and 250 are 164.21, 164.49, 10.51, 10.51, 10.51, 10.51 respectively. As multiple local Pareto fronts are possible [starting with $g(x)$ = 1 to $g(x)$ = 25], the Pareto optimal front obtained in this study is also one of the local Pareto with $g(x)$ = 10.51. As the value of convergence metric is fairly high for all the algorithms (as shown in Table 5.2), it shows that none of the algorithms completely converged to the true Pareto front for ZDT4 test problem.

Figs. 5.13a -5.13c and Figs. 5.14a – 5.14c show the convergence metric plotted against the generations and the number of function evaluations (NFE) for FON and KUR test functions respectively. Both the figures show that the strategies of MODE algorithm (i.e. hybrid and trigonometric) converged to these metrics during the initial generations and remain almost constant thereafter as compared to other strategies of MODE (i.e. MODE-III and elitist MODE). Fig. 5.13a shows that hybrid MODE and trigonometric MODE algorithms converged to the true Pareto front within 12-15 generations. Thereafter, the points of the Pareto front do not change thus keeping a constant value of convergence metric. In case of KUR test function, the convergence is achieved in 25th generation as shown in Fig. 5.14a. Hybrid MODE algorithm involves several function evaluations during the local search, thus the number of function evaluations increases.

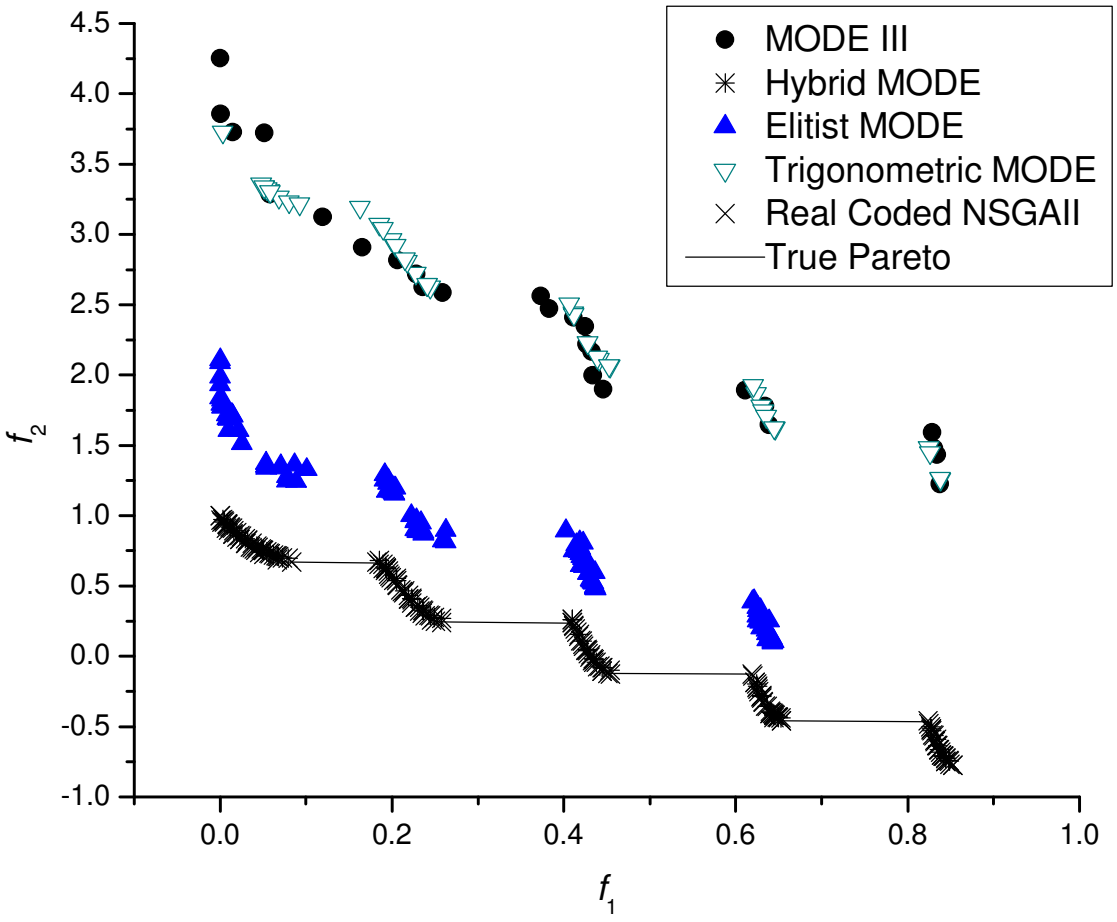

Fig. 5.11 Pareto optimal solutions for ZDT3 test problem using MODE-III, Elitist MODE, Trigonometric MODE, Hybrid MODE, real-coded NSGA-II and true Pareto front

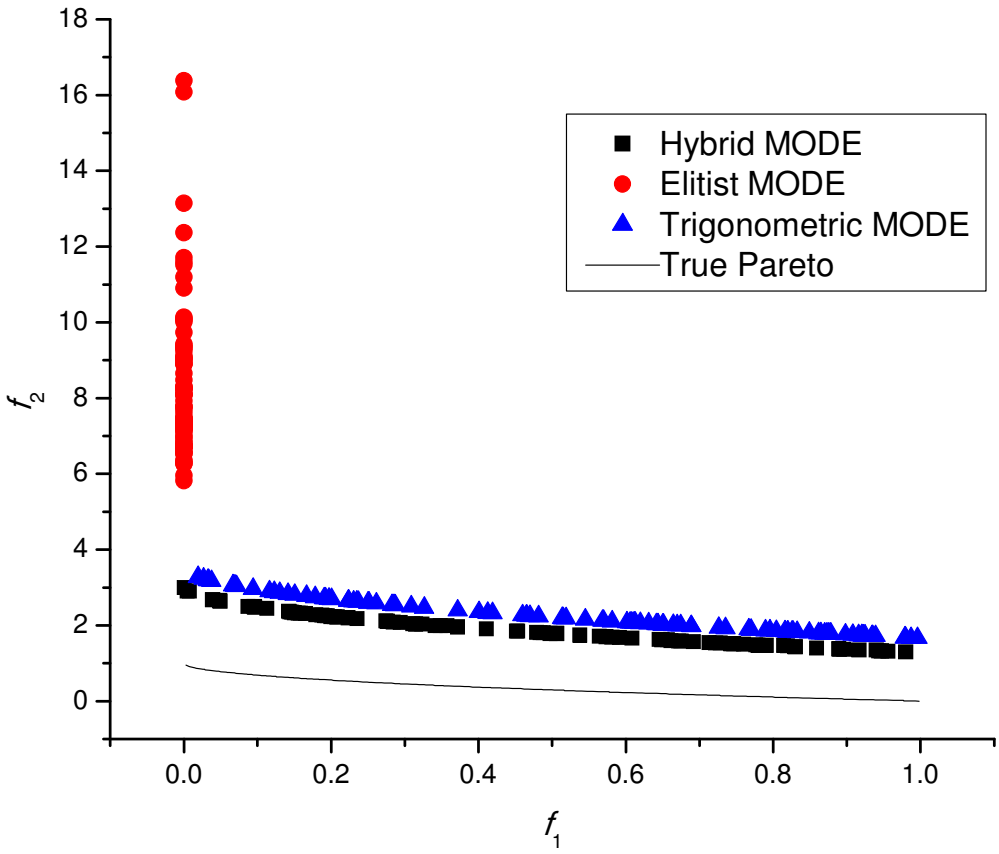

Fig. 5.12 Pareto optimal solutions for ZDT4 test problem using Elitist MODE, Trigonometric MODE, Hybrid MODE, and true Pareto front

It is important to compare the convergence not only with respect to the number of generations but also with NFE. The NFE vs. convergence plots (Figs. 5.13b and 5.14b) show that the trigonometric MODE and hybrid MODE algorithms converged to the true Pareto front in less number of function evaluations for both FON and KUR test problems indicating their speed in convergence. While achieving the convergence at relatively faster rate, the hybrid and trigonometric strategy of MODE are also able to maintain a good diversity of solutions for FON and KUR test problems. In Fig. 5.13c and Fig. 5.14c the divergence metric is plotted against the number of generations for FON and KUR test problems respectively. The diversity metric obtained using hybrid MODE algorithm also remains constant once the convergence is achieved. The diversity of elitist and trigonometric strategy of MODE also remains consistent. However, the diversity metric obtained using MODE III algorithm does not remain constant (this is mainly attributed to non-convergence of MODE III towards the true Pareto front during the initial generations). The speed with which the trigonometric- and hybrid- MODE algorithms converged is clearly evident from Figs. 5.13a - 5.13b & 5.14a- 5.14b. Thus Hybrid MODE is a very capable algorithm for handling the complex engineering problems as it acquires both the speed and accuracy in achieving the true Pareto front for almost all the test problems. The % of initial population points converged to the Pareto optimal front using strategies of MODE and real-coded NSGA-II for various test problems is shown in Table 5.4.

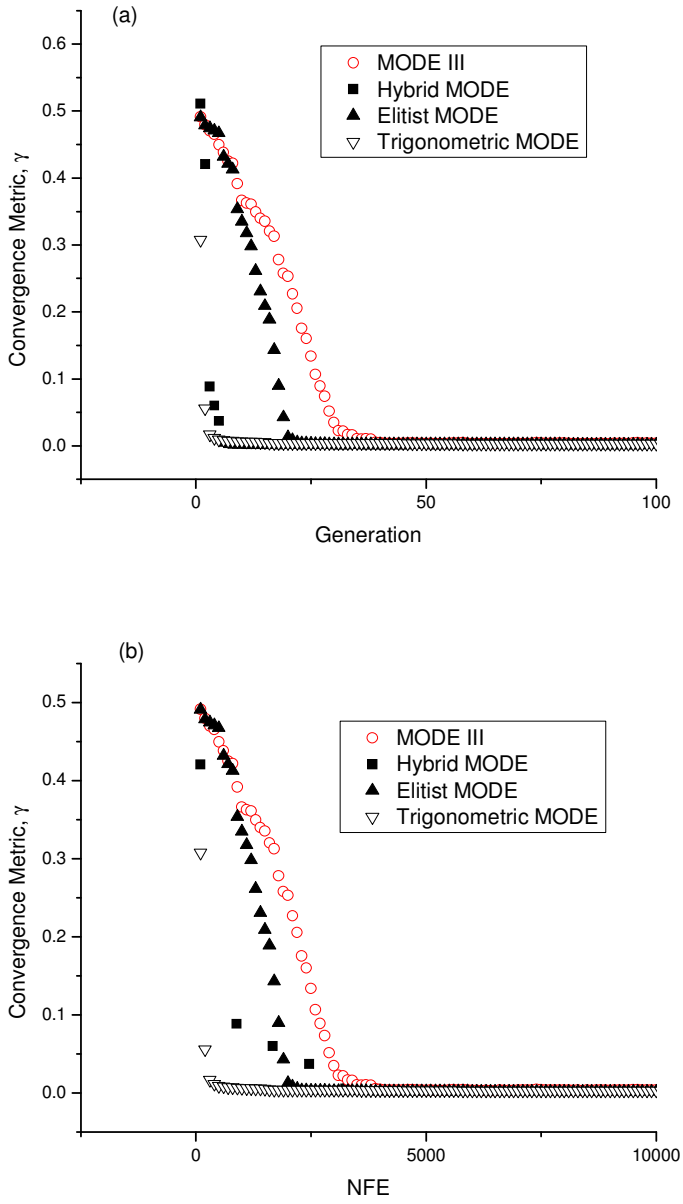

Fig. 5.13 (Contd…)

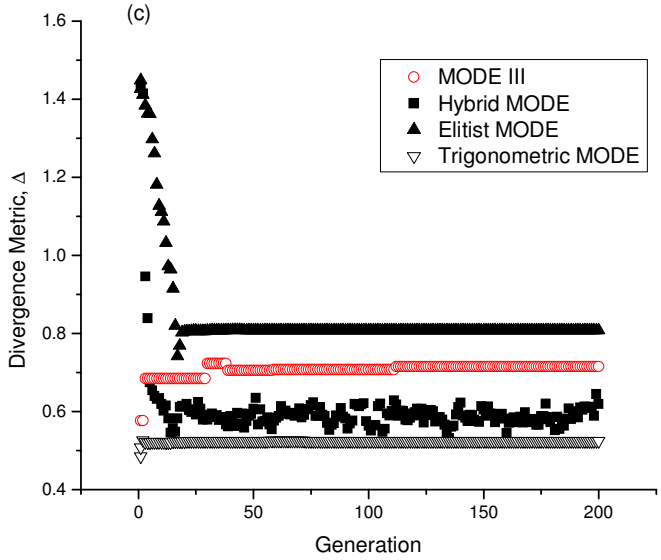

Fig. 5.13 Convergence and divergence metric for FON test problem. Convergence metric plotted against generation number [(Fig. (a)]; Convergence metric plotted against number of function evaluations (NFE) [(Fig. (b)]; Divergence metric as a function of generation number [Fig. (c)]

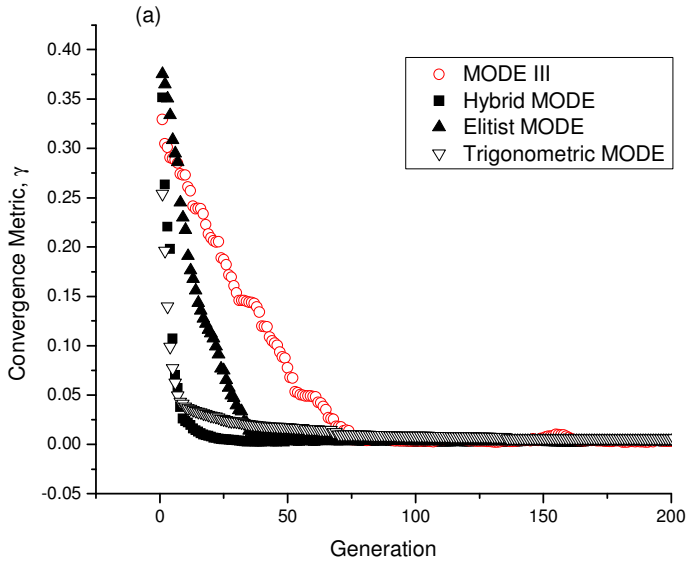

Fig. 5.14 (Contd…)

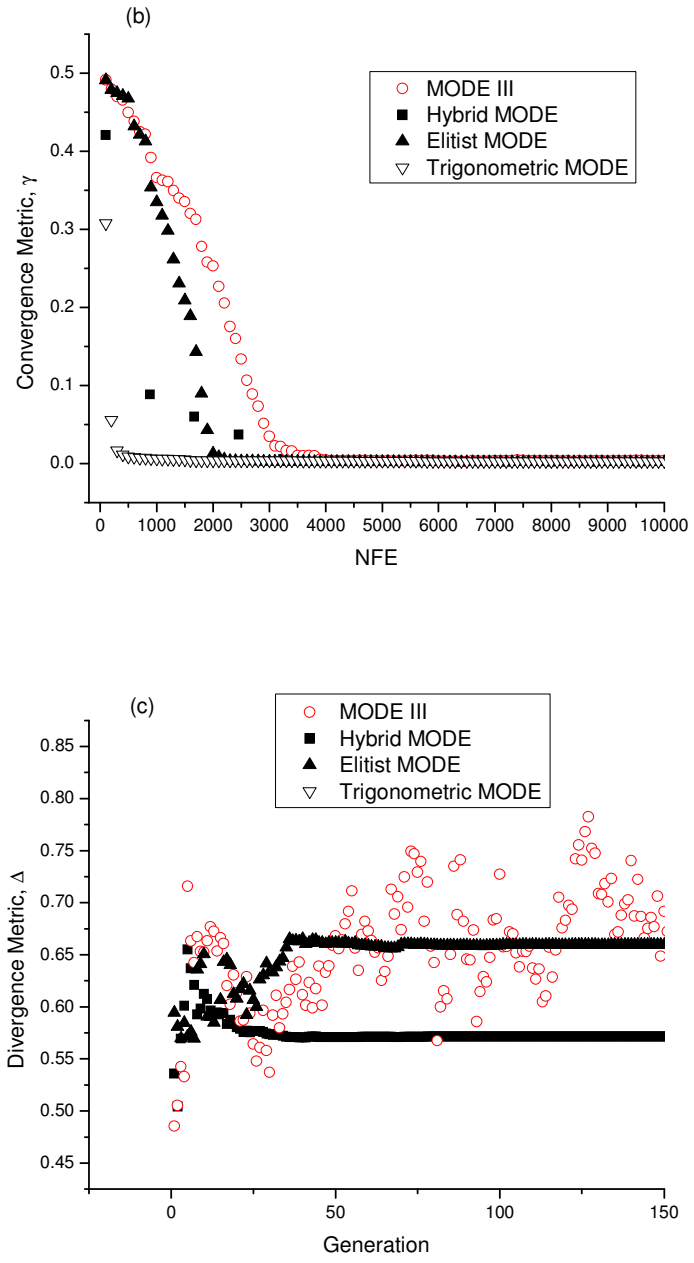

Fig. 5.14 Convergence and divergence metric for KUR test problem. Convergence metric plotted against generation number [(Fig. (a)]; Convergence metric plotted against number of function evaluations (NFE) [(Fig. (b)]; Divergence metric as a function of generation number [Fig. (c)]

5.1.3 Search space analysis of selected constrained and unconstrained test problems

Many test problems may have a continuous objective space but may result in discontinuous/disconnected Pareto front. The disconnected Pareto fronts may render difficulty in search procedure, which may lead to a premature convergence of algorithm to a local region or in one of the disconnected regions. It is therefore, necessary to study such problems separately with respect to objective space and have a critical review of the Pareto solutions. Four test problems [Two unconstrained test problems (SCH2, and POL) and two constrained test problems (Constr-Ex and TNK) (Table 4.1 and Table 4.2)] are considered for study under this section. All simulation runs are taken with the same parameter values as reported in Table 5.4.

5.1.3.1 Unconstrained test problems

SCH2 is a single variable bi-objective optimization problem with two discontinuous regions as shown in Fig. 5.15 and Fig. 5.16. The objective space is nonconvex in nature. The dominated region and the objective space boundary are shown in Fig. 5.15. The Pareto optimal front is shown in the region marked with box. The Pareto front lies in the range of decision variable $x^* \in [1,2] \cup [4,5]$. Region AB (in Fig. 5.15) corresponds to f_1 value in the range of [-1 0] and region CD corresponds to f_1 value in the range of [0 1] satisfying the x^* value as given above. The Pareto fronts obtained using several strategies of MODE algorithm is shown in Fig. 5.16. The percent of initial population points (IIP) converged to the final Pareto front along with the maximum and minimum individual function values attained by algorithm (i.e., f_{1max}, f_{1min}, f_{2max}, f_{1min}) are shown in

Table 5.5 Elitist MODE is able to produce 100% of initial population converged to the Pareto front. This is due to non- removal of solutions, and preserving the elite population members. But this feature of preserving of elite population members, also resulted in premature convergence (as mentioned in section 5.2) for ZDT series problems. Some of the ZDT test problems have a typical characteristic of high number of decision variables (30 decision variables) (refer Table 4.1) and nonconvex Pareto front. They also have a number of local Pareto fronts (Deb, 2001) which restricts the algorithm to search for new solutions. This study also shows the need for improving elitist MODE algorithm by combining a new selection strategy along with the partial preservance of elite members (as complete preservance of elite members with present selection strategy resulted in local Pareto fronts).

The nonconvex objective space and the discontinuous and nonconvex Pareto fronts for POL test problem are shown in Fig. 5.17. Region X and region Y totally depend on the bounds of the decision variables. Region X is obtained when the decision variable x_1 converged to its lower bound. Fig. 5.18 shows that MODE algorithm converged to the local Pareto front in region X. Point A [(f_1, f_2) = (1.00, 28.422)] is the dominated point when the algorithm gets converged to the global Pareto front. Thus the local Pareto optimal front may not only shrunk but also may widen the local Pareto front in the given search space. The value of $f_1 < 2$ is obtained when x_1 approaches its lower bound of $-\pi$.

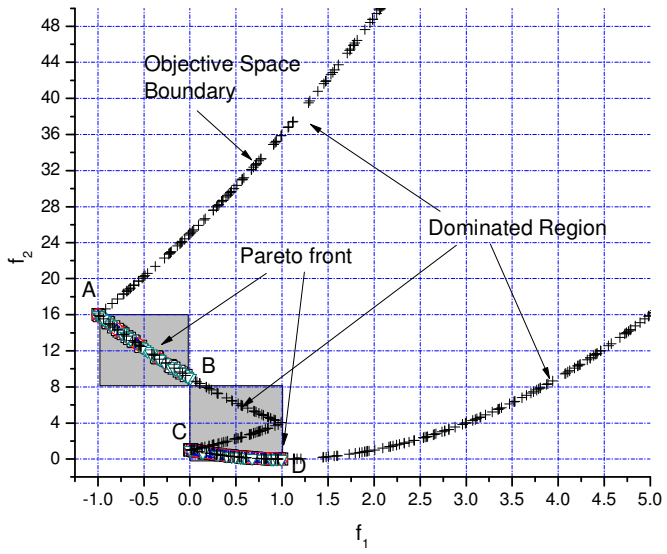

Fig. 5.15 Search space and the disconnected Pareto front for SCH2 test problem

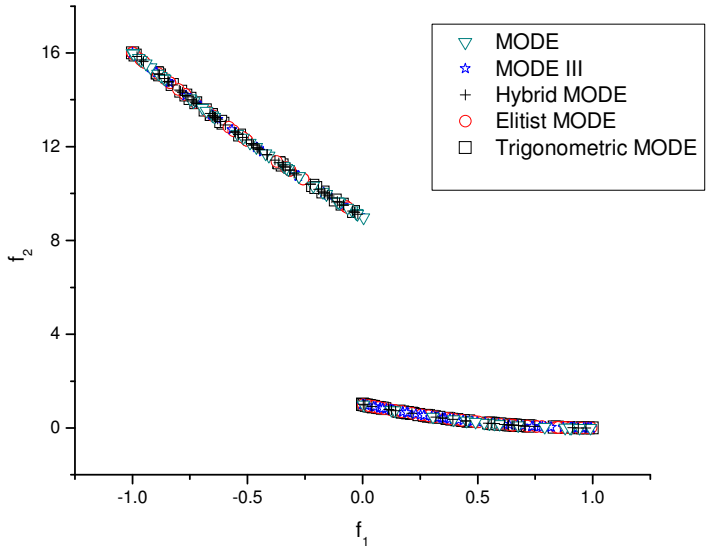

Fig. 5.16 Pareto front using several algorithms for SCH2 test problem

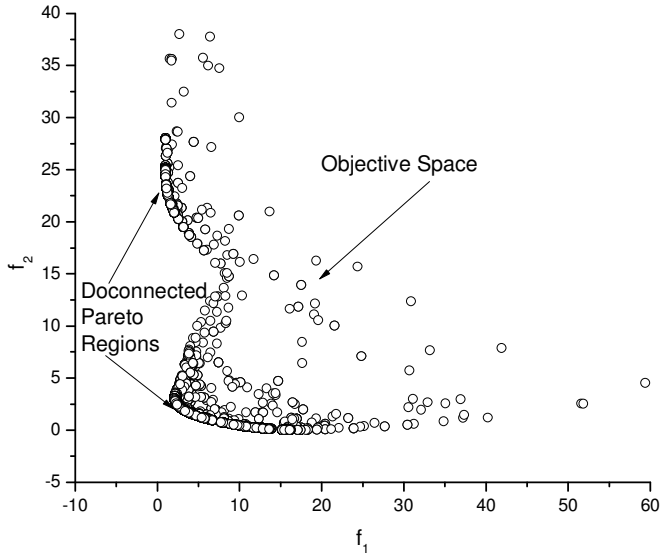

Fig. 5.17 Search space and the disconnected Pareto front for POL test problem

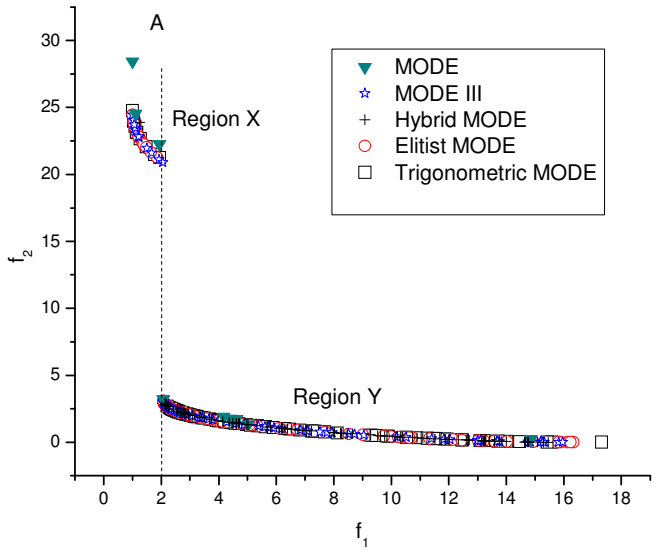

Fig. 5.18 Pareto front for POL test problem

Table 5.5 Percent of initial population points (IPP) converged to the Pareto front and minimum & maximum values of objective functions (OF)

Test Problem	IIP & OF	MODE	MODE-III	Hybrid MODE	Elitist MODE	Trigonometric MODE
SCH 2	NPS	60	100	100	100	100
	f_{1max}	0.99028	0.99407	0.9712	0.99427	0.99916
	f_{1min}	-0.99994	-0.99985	-0.98051	-0.99957	-0.9992
	f_{2max}	15.99948	15.99883	15.84447	15.9966	16.00641
	f_{2min}	0.000094	0.00003521	0.00082972	0.0000328129	0.00000071
POL	NPS	9	100	100	100	98
	f_{1max}	14.85726	15.96278	15.45174	16.33451	17.31232
	f_{1min}	1.00087	1.00954	1.2582	1.00925	1.00181
	f_{2max}	28.42291	24.45336	23.89765	24.46115	24.75925
	f_{2min}	0.23863	0.00352	0.00926	9.55E-04	0.0075
Constr-Ex	NPS	00	76	93	100	98
	f_{1max}	--	1.03589	1.04856	1.02096	1.03333
	f_{1min}	--	0.04929	0.0464	0.07388	0.24835
	f_{2max}	--	1.04233	1.04208	1.01719	1.03848
	f_{2min}	--	0.05505	0.05448	0.0747	0.07286
TNK	NPS	00	74	84	100	92
	f_{1max}	--	0.04929	0.0464	0.07388	0.24835
	f_{1min}	--	1.04233	1.04208	1.01719	1.03848
	f_{2max}	--	0.05505	0.05448	0.0747	0.07286
	f_{2min}	--	1.03589	1.04856	1.02096	1.03333

5.1.3.2 Constrained test problems

Strategies of MODE developed in this work, are also tested on some of the constrained test problems. In this section, two widely used test problems [Constr-Ex (Deb, 2001) and TNK (Tanaka, 1995)] (Table 4.2) having nonconvex search space are studied in terms of the objective space and the obtained Pareto front. Penalty function approach using a high value of penalty weight (= 10,000) is employed to handle the constraints. The selection strategy of MODE III and hybrid MODE algorithm is designed in such a way that even the not so efficient constraint handling technique such as the Penalty approach works well with the strategies of MODE. If a newly obtained solution is infeasible, then the Penalty approach will assign a very high weight to that solution. In this way, as per the selection strategy, this solution will never enter in a current set of solutions. If initial population points are infeasible, then the crossover and recombination operation will diversify the search and the feasible points would replace the current infeasible point. During the initial generations the infeasible points present in the population help in diversifying the search by the recombination operation to produce a diverse noisy random vector. The first problem considered is Constr-Ex test function, which is of minimize-minimize type of bi-objective optimization problem. In this problem, both objective functions and constraints formulate the feasible search space boundary. The second problem under consideration is TNK test problem. TNK test problem has a discontinuous and nonconvex Pareto front. For both the test problems, simulation runs are taken with same parametric settings as reported in Table 5.1.

Fig. 5.19a shows the objective space (both feasible and infeasible) for CONSTR test problem. Both constrained and unconstrained regions of CONSTR test problems have a nonconvex search space. Unconstrained Pareto front, constrained Pareto front, constrained search space and the constraints boundary for CONSTR test problem are shown in Fig. 5.19b. As the Pareto front is a concatenation of both the constraint boundary and the objective functions, it is difficult to obtain a well diverse Pareto front. Specially using the penalty method to solve constrained problems it is difficult to obtain the true Pareto front in both the regions (i.e., region X and region Y) as shown in Fig. 5.19b. This is evident from the results shown in Fig. 5.19c, where the Pareto fronts obtained using developed strategies of MODE are plotted. The convergence of Pareto front obtained using MODE III is restricted to a small portion of the front (region X in Fig. 5.19b). However, the hybrid-, trigonometric- and elitist strategy of -MODE algorithms are able to capture entire region (i.e., regions X and Y in Fig. 5.19b) and thus give a well diverse Pareto front. These results are attributed to its wide spread search benefit (i.e. both local and global search) in case of hybrid MODE, to the strong mutation operation in case of trigonometric MODE, and to an enhanced selection strategy in case of elitist MODE. The region Y is achieved if x_2* achieves the value of 0. For CONSTR test problem it is observed that 93%, 76%, 100% and 98 % of initial population points converged to the final Pareto front using hybrid MODE, MODE III, elitist MODE and trigonometric algorithms respectively.

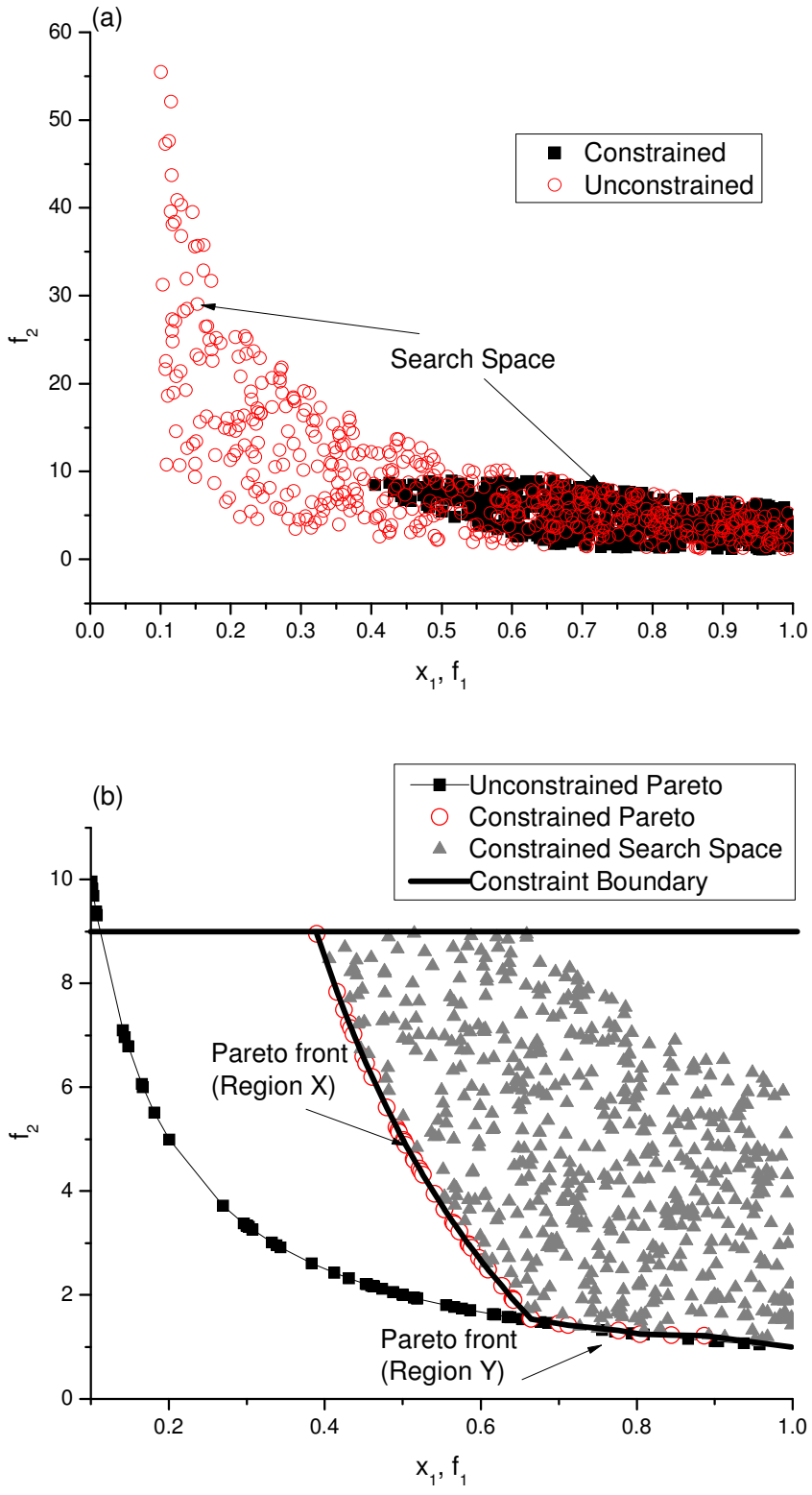

Fig. 5.19 (Contd…)

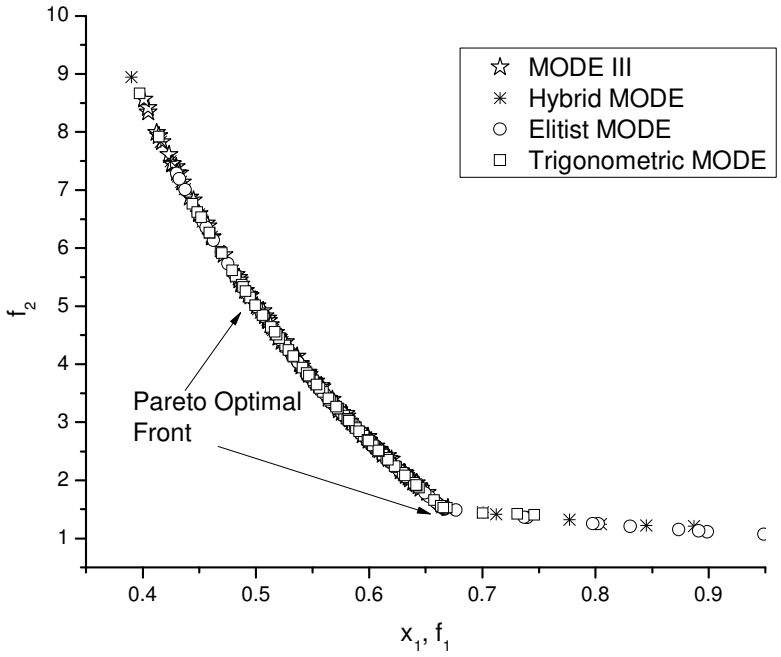

Fig. 5.19 Constrained and unconstrained objective search space [Fig. (a)]; Constrained and unconstrained Pareto front [Fig. (b)]; Pareto optimal front obtained using hybrid MODE and MODE III algorithms [Fig. (c)] for CONSTR test problem

Fig. 5.20a shows the feasible and infeasible objective space for TNK test problem. Both the constraints act in such a way that the feasible space occupies the internal region of total search space. Fig. 5.20a also shows both the decision variable space and the objective space, as the objective functions and the decision variables are same in TNK test problem. Unconstrained problem has a decision space ranging between $0 \le x_1, x_2 \le \pi$. In this way, if unconstrained test problem is optimized simultaneously for both the objectives, it will result in an extreme single (corner point) optimal solution as shown by (0, 0) in Fig. 16a. The Pareto front cannot be obtained for such problems. However, the constraints are responsible for producing the Pareto front as shown in Fig. 5.20b. Fig. 5.20b shows the constrained search space and multiple disconnected Pareto regions, which are responsible for producing a disconnected Pareto front. Fig. 5.20c shows the Pareto optimal fronts obtained using newly developed strategies of MODE algorithm. 84%, 74%, 100% and 92% of initial population points converged to the Pareto front using hybrid MODE, elitist MODE and trigonometric MODE algorithms respectively. Fig. 5.20c also shows that trigonometric MODE algorithm resulted in local solutions especially in the region $f_1 x_1 \in (0.2 - 0.4)$.

In the next subsection, results obtained on multi-objective optimization of selected industrial case studies using the newly developed strategies in this work are discussed.

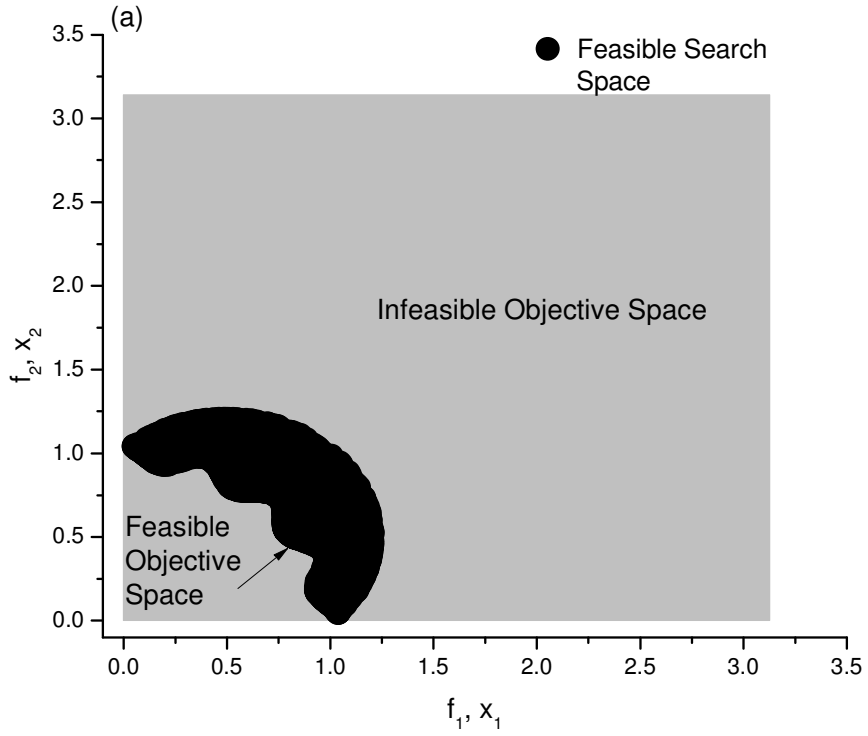

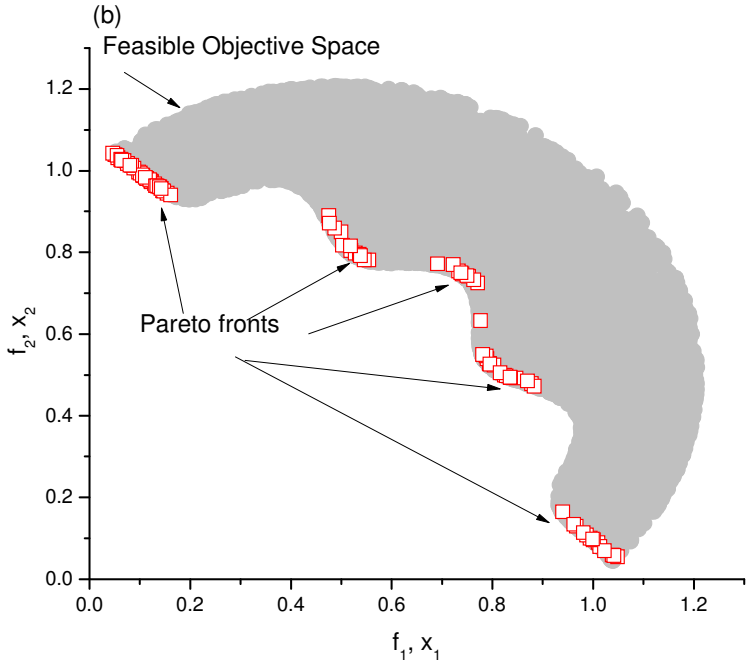

Fig. 5.20 (Contd…)

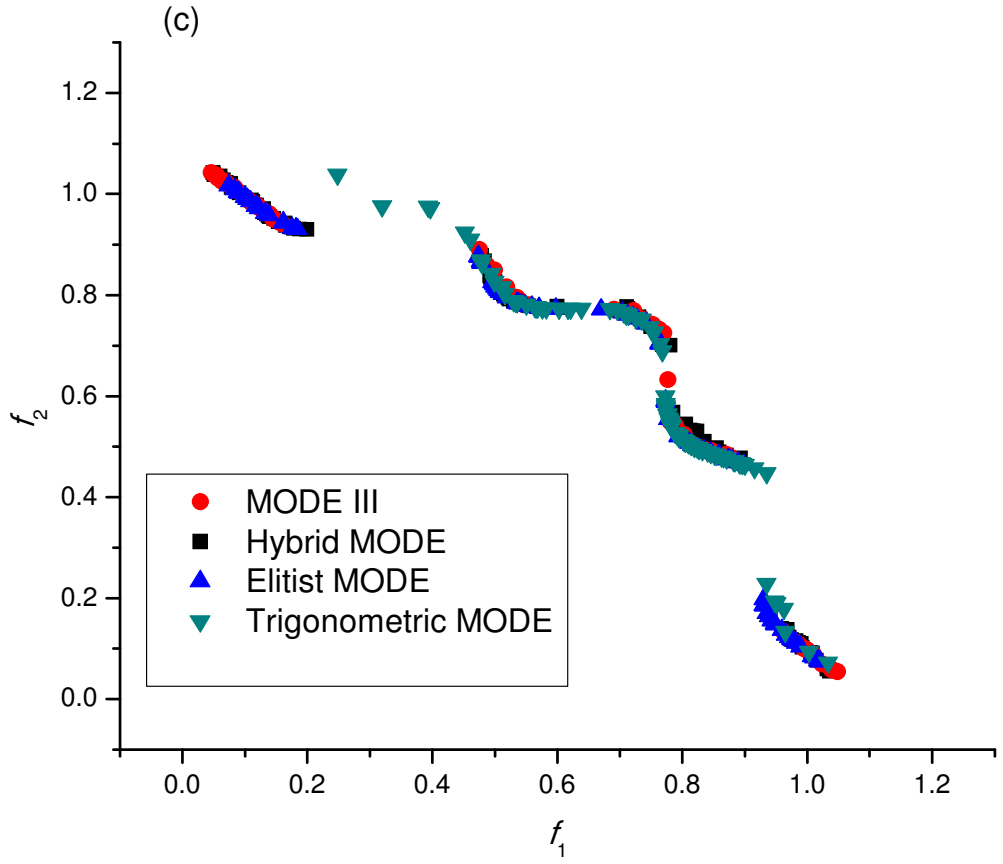

Fig. 5.20 (Contd…)

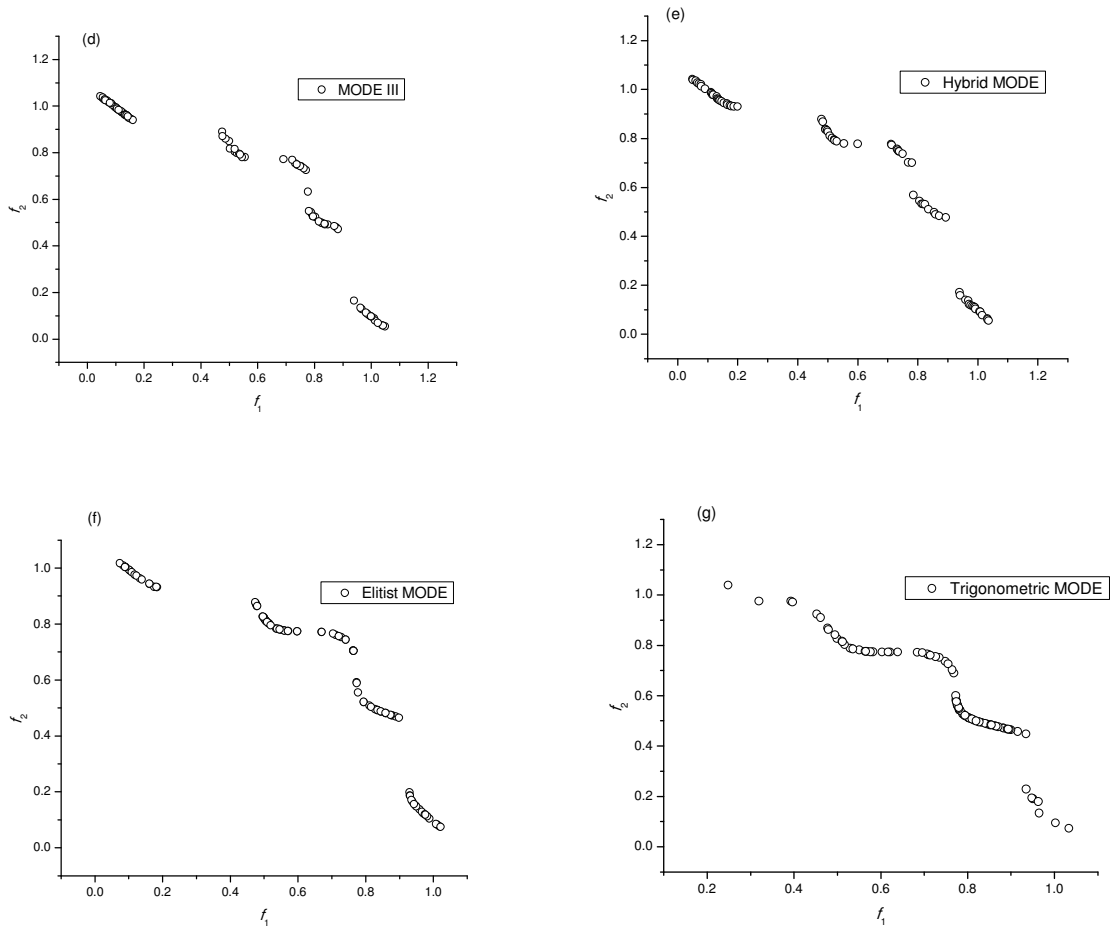

Fig. 5.20 Feasible and infeasible objective search space [Fig. (a)]; Constrained search space and Pareto region [Fig. (b)]; Pareto optimal front obtained using strategies of MODE algorithm [Fig. (c)]; Individual Pareto fronts obtained for using strategies of MODE [Fig. (d-g)] for TNK test problem

5.2 Industrial case studies

This section of thesis deals with the results and discussion of the multi-objective optimization of industrial case studies considered in this study. Several process design decisions based objectives (as formulated in section 4.2) for several industrial processes (such as styrene reactor, Polyethylene terephthalate (PET) reactor, oxidation of *p*-xylene to purified terepthhalic acid (PTA), Low density polyethylene (LDPE) tubular reactor, and supply chain and planning) are solved using newly developed strategies of MODE algorithm.

5.2.1 Multi-objective optimization of styrene reactor

A set of ordinary differential equations (ODEs), as given in Appendix A through Eqs. A8 - A15, describing the reaction scheme were integrated and simulated using the ODE45 subroutine of MATLAB (7.0) library. ODE45 uses a fourth-order Runge-Kutta method to integrate the ODEs. The model equations were solved on Pentium-IV, 2.4 GHz core 2 duo processor. The cpu time for MODE III, hybrid MODE, elitist MODE and trigonometric MODE algorithms for 300 generations is 1576.125, 50,144, 2716.05, and 4730.70 seconds respectively. The design and operating conditions, as well as the thermodynamic and kinetic data, related to the reaction scheme (as given by Eqs. 4.1 – 4.6) of the styrene reactor considered in this study are taken from the literature. (Elnashaie and Elshishini, 1994; Yee et al., 2003). The simulated model output is compared with the industrial data and is shown in Table A6 (Appendix A). The simulated model profiles of (a) Temperature (3 chromosomes and industrial, Adiabatic operation), (b) Flow rate styrene, (c) Yield, and (d) Pressure (comparison of adiabatic and steam

injected operation), and (e) molar concentration of side products along the length of reactor profiles for selected chromosomes for adiabatic and steam injected configurations are shown through Figs. 5.21a - 5.21e.

5.2.1.1 Case-1: Simultaneous maximization of S_{ST} and Y_{ST}

The first case considers simultaneous maximization of selectivity and yield. Four decision variables (namely T_{EB}, *P, SOR* and F_{EB}^{0}) are used. As discussed in section 5.1, the hybrid- MODE algorithm is much faster in terms of convergence for the benchmark test problem. A similar trend is observed in the case of the industrial styrene problem as well. In Fig. 5.22, the conflicting objectives (selectivity and yield) are plotted at various generations, as indicated. The penalty function method was used to handle the constraints with a very high value of weights (10^4) in order to ensure that the constraint-dominated solutions were removed from the Pareto solutions. The effect of the penalty function parameter on the Pareto front was studied and is discussed in section 5.2.1.3.

The numbers of points violating the constraints at several generations as obtained using the strategies of MODE algorithms are reported in Table 5.6. In all algorithms, all the initial population solutions are evaluated first and then sent to the generation loop. The values given in Table 5.6 correspond to the output obtained after the specified number of generations. As the initial population was generated randomly, the number of solutions violating the constraint in the initial population can vary depending on the random population generated.

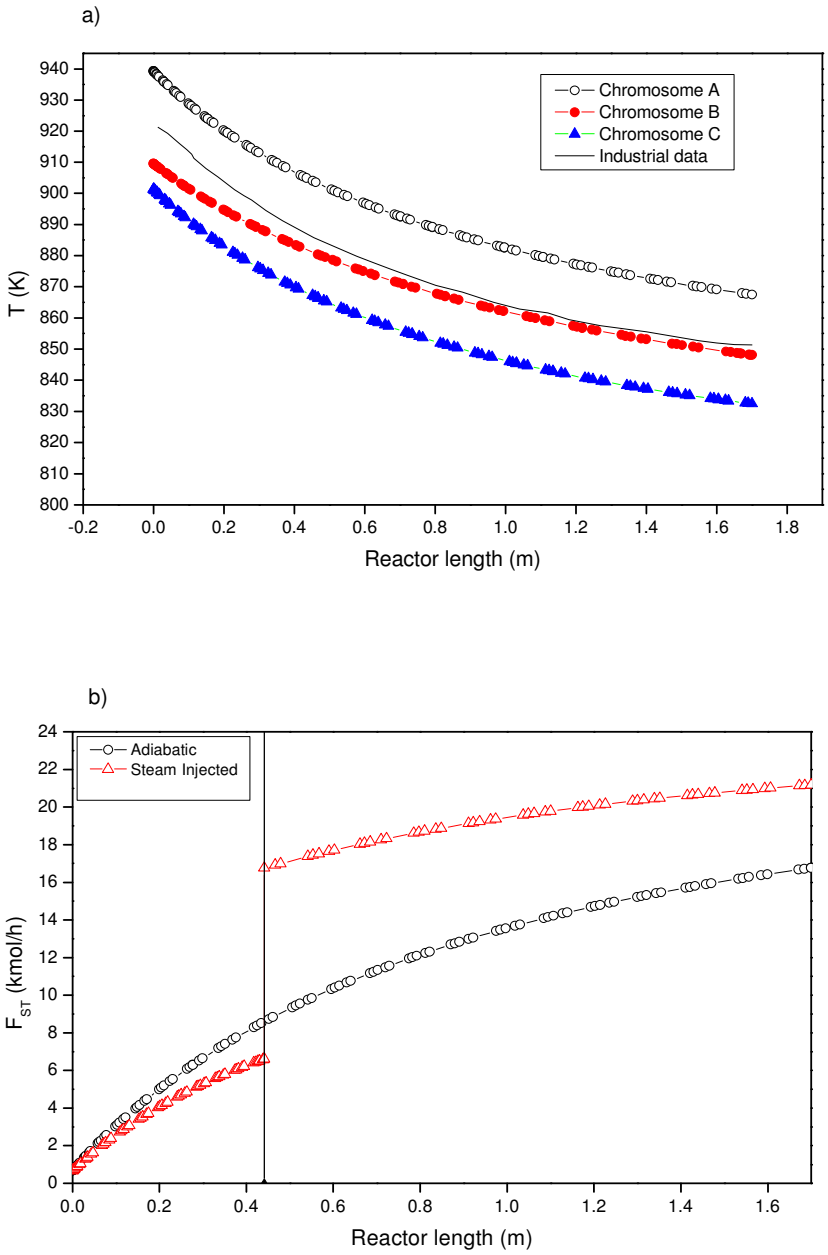

Fig. 5.21 (Contd…)

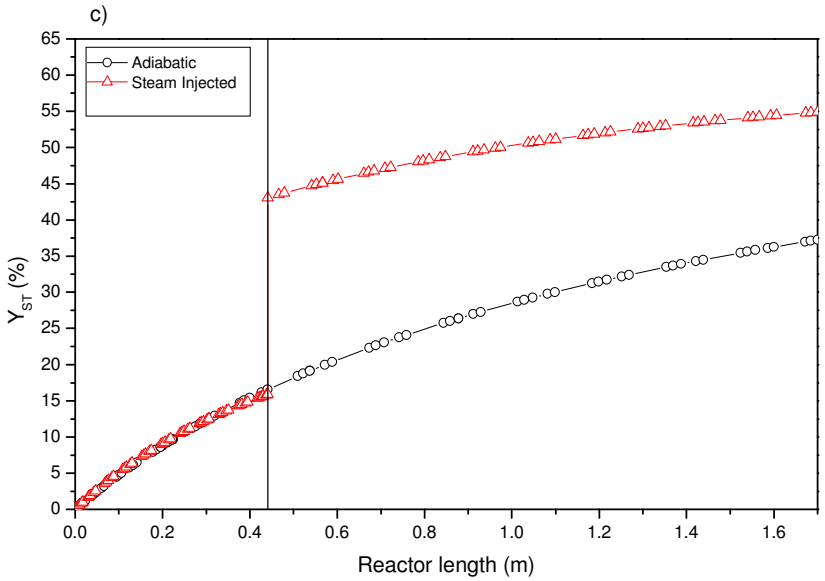

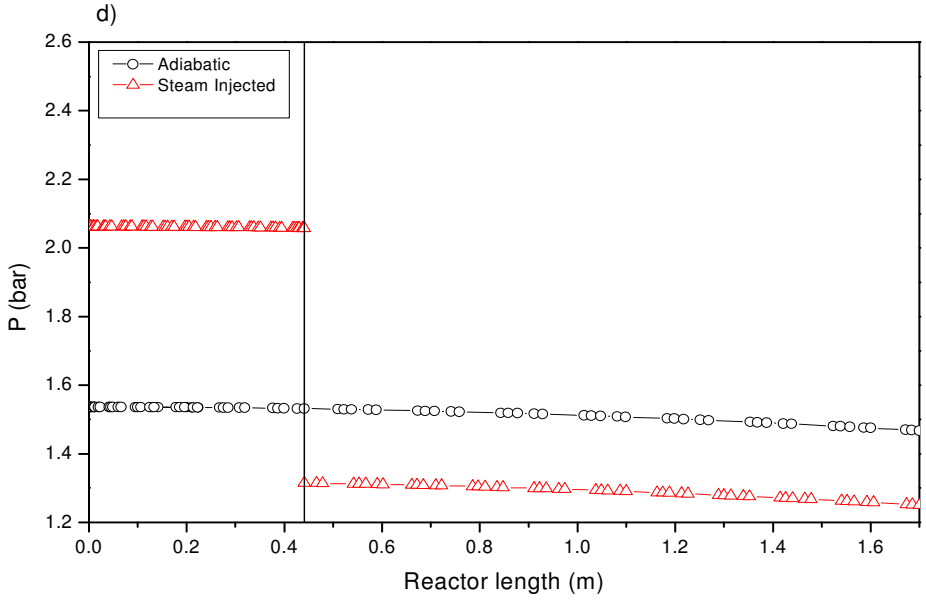

Fig. 5.21 (Contd…)

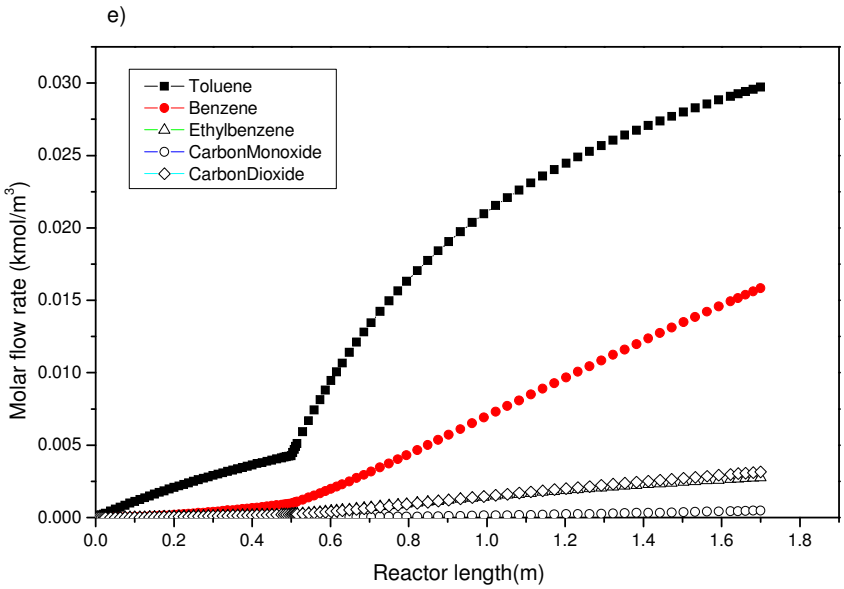

Fig. 5.21 Profiles of (a) Temperature (3 chromosomes and industrial, adiabatic operation), (b) Flow rate of styrene, (c) Yield and (d) Pressure (comparison of adiabatic and steam injected operation) and (e) Molar concentration of side products along the length of reactor

Table 5.6 Number of points violating the constraints (VNP) and number of point satisfying constraints (SNP) at various generations

Generation	MODE	MODE III	Hybrid MODE	Elitist MODE	Trigonometric MODE
	VNP/SNP	VNP/SNP	VNP/SNP	VNP/SNP	VNP/SNP
1	0/18	33/67	15/85	0/100	0/100
3	0/15	3/97	0/100	0/100	0/100
5	0/12	0/100	0/100	0/100	0/100
300	0/10	0/100	0/100	0/100	0/100

The hybrid MODE algorithm, because of its acceleration phase (sequential simplex method coupled with evolutionary MODE algorithm); was able to remove the constraint-dominated solutions more quickly, thus leading towards the true Pareto front. However, trigonometric MODE and Elitist MODE algorithms, due to improved mutation strategy and preserving of elite population members, are able to remove all constraint dominated solutions in first generation. Original MODE algorithm has very limited number of solutions from generation 1 onwards (Table 5.6), thus resulted in a local Pareto front. The MODE III algorithm had zero constraint-violated points in generation 5, whereas the hybrid MODE algorithm achieved this stage during generation 3. It is possible that, during the search process, a new point might be encountered that has a violation of constraints. The selection strategy of MODE algorithms (both MODE III and hybrid MODE) does not allow such solution (point) to enter into the current population list. However, if both the current point and the newly obtained point are constraint-violated points, then the better of the two points gets a place in the population. Thus, the selection strategy of the MODE algorithms is designed in such a way that even a not-very-efficient constraint handling technique such as the penalty approach works very well, ensuring that the constraint dominated solutions are removed from the initial generations and are not allowed to enter during later generations, unless they are better than the current constraint-dominant solutions.

Table 5.6 and Figs. 5.22a and 5.22b clearly show that the hybrid strategy of MODE algorithm is able to converge towards the Pareto front more quickly than MODE III algorithm. Pareto fronts obtained for case-1 using various strategies of MODE algorithms is shown in Fig. 5.23a. The results of Fig. 5.23a are re-plotted (for better

clarity of Pareto fronts) in Fig. 5.23b with vertical shift in value of ordinate by +2 in MODE III, +4 in Hybrid MODE, +6 in Elitist MODE and +8 in Trigonometric MODE data points. The inferences from Figs. 5.21-5.23b can also be drawn with the help of a set of decision variables (i.e., T_{EB}, P, SOR, and F_{EB}^{0}). The decision variables corresponding to the Pareto solutions in Figs. 5.23a - 5.23b are shown against one of the objective functions in Figs. 5.24a - 5.24h. Figs. 5.24a - 5.24b show the effect of the temperature of ethyl benzene on the objective functions (namely, selectivity and yield, respectively). Because the main reaction is reversible and endothermic in nature, a high temperature favors the rate of the forward reaction. This is apparent from the plot of yield versus temperature (Fig. 5.24b). However, at higher temperature, side products such as toluene and benzene are also formed, thus reducing the selectivity value (Fig. 5.24a).

Thus a clear conflicting behavior is observed in both the objectives, which is attributed to the dominance of temperature on the objectives and hence it is termed as a dominant variable. To select a particular value of yield, the user has to sacrifice for the selectivity, and vice versa. If a too high value of yield is selected, then the corresponding value of selectivity would be on lower side, thus increasing the cost of separation incurred on the separation of side products from the main product, i.e., styrene. Operating pressure also affects desired values of objective functions. According to the Li-Chatelier's principle, the low pressure favors the formation of main product. By lowering the value of the operating pressure, the selectivity is increased while the yield is decreased (Figs. 5.24c - 5.24d).

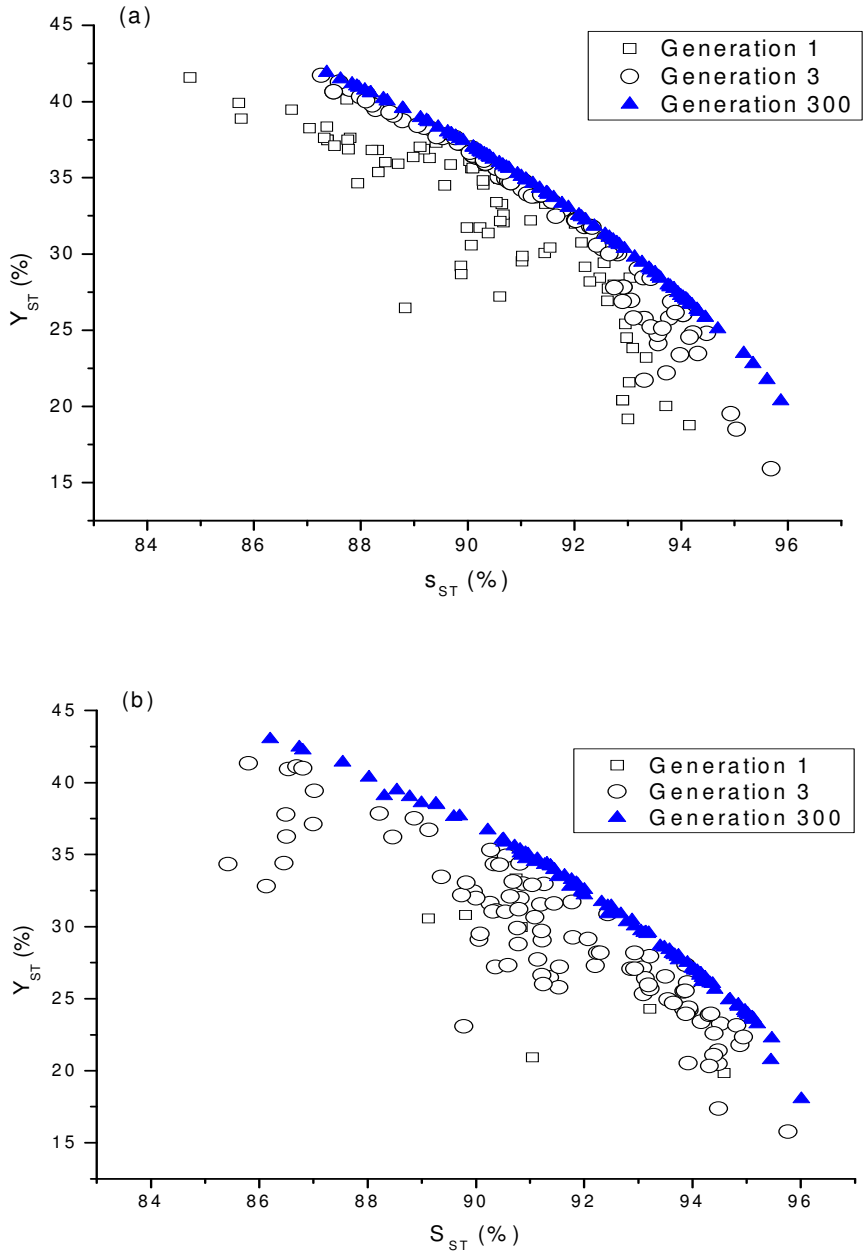

Fig. 5.22 Convergence of algorithm towards Pareto front for case-1 (a) Hybrid MODE; (b) MODE III

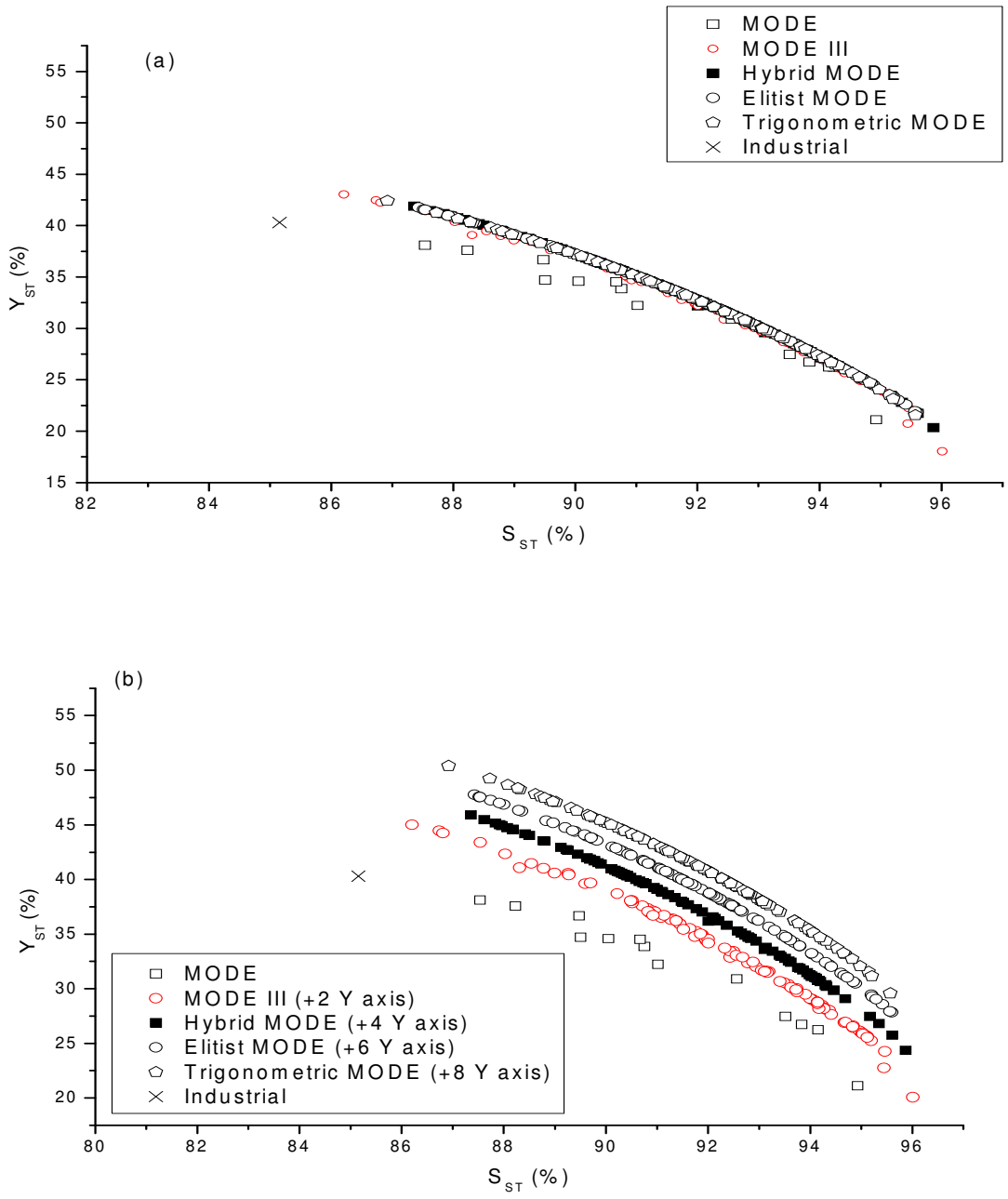

Fig. 5.23 (a) Pareto fronts obtained for case-1 using strategies of MODE algorithms; (b) The results of Fig. 5.23a are re-plotted (for better clarity of Pareto fronts) with vertical shift in value of ordinate by +2 in MODE III, +4 in Hybrid MODE, +6 in Elitist MODE and +8 in Trigonometric MODE data points

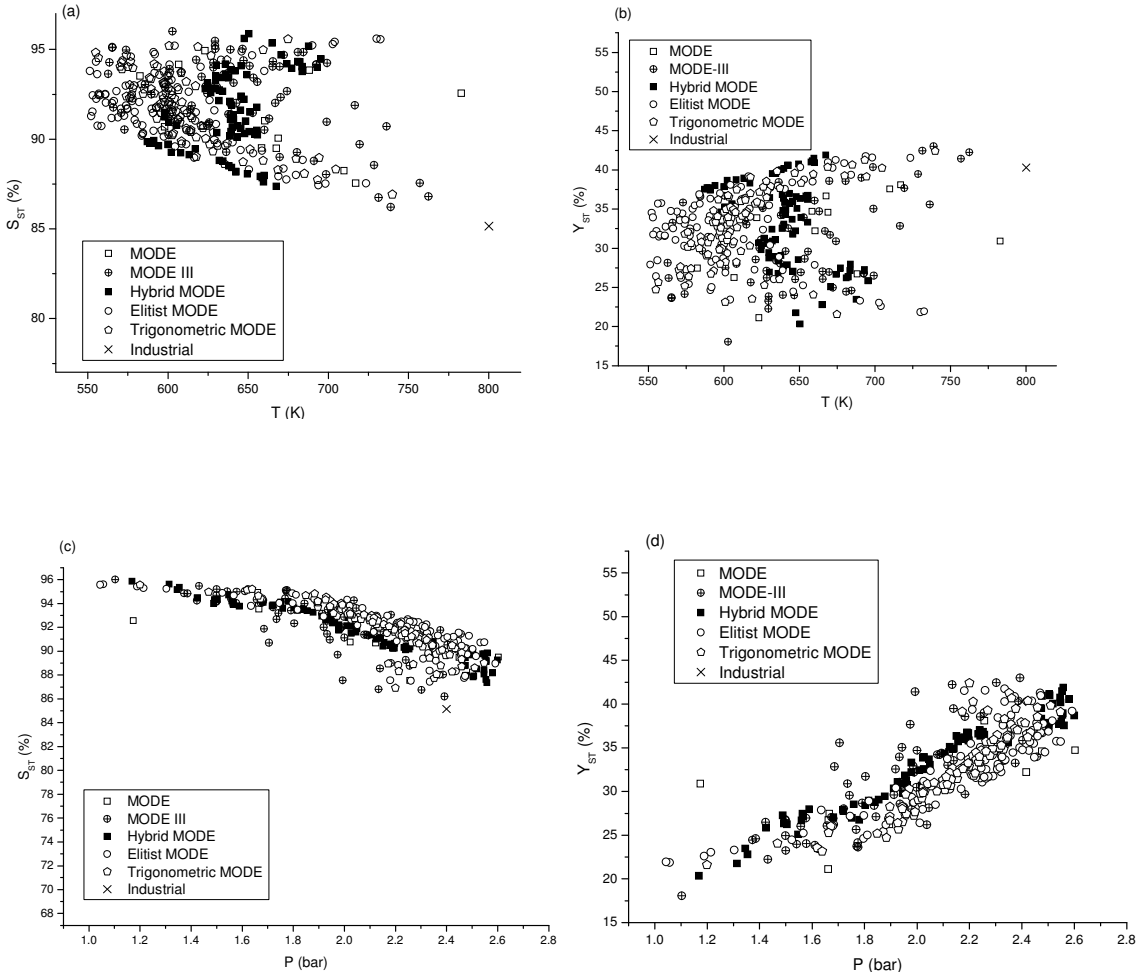

Fig. 5.24 (Contd….)

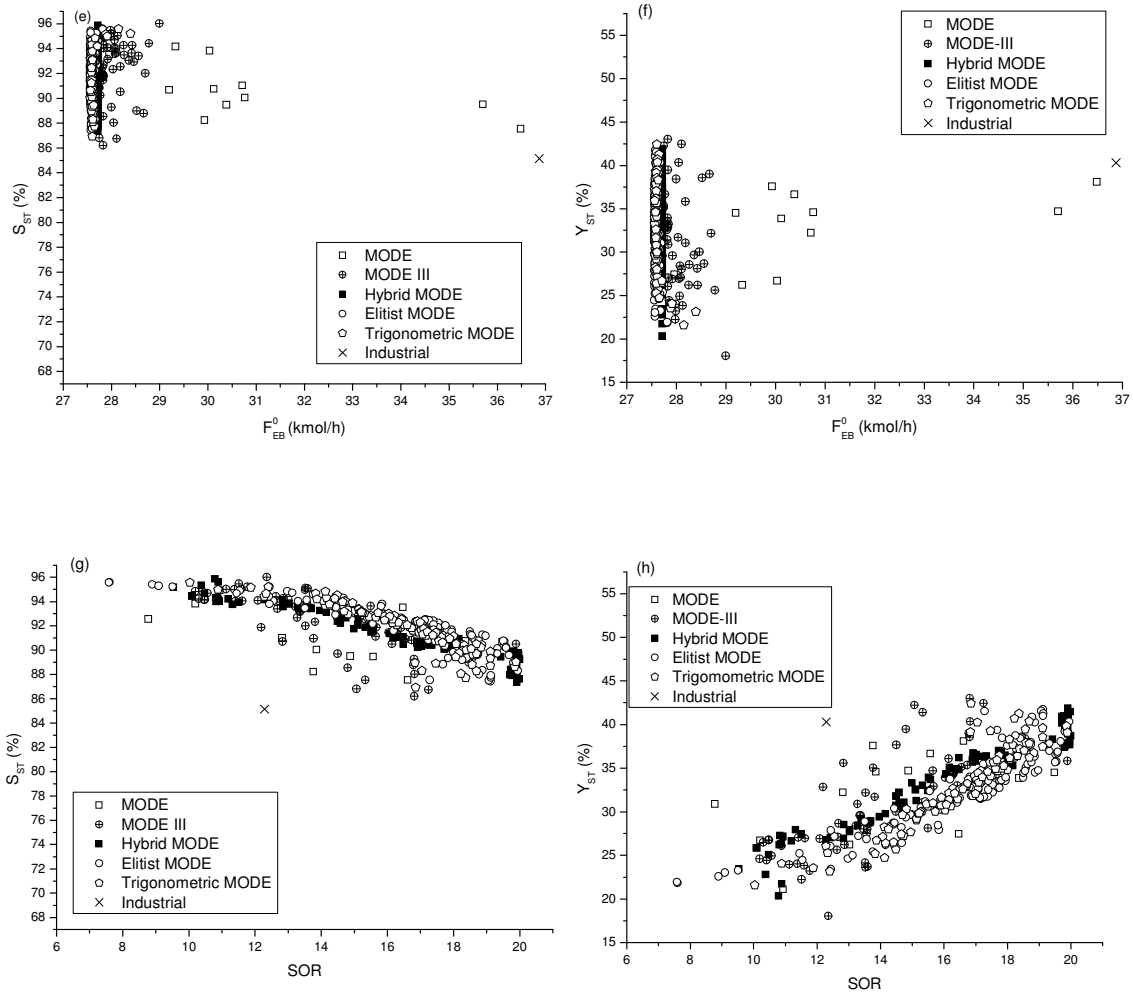

Fig. 5.24 (a-h) Decision variables (*T, P,* F^0_{EB}, and *SOR*) plotted against one of the objective functions

The feed flow rate of ethyl benzene has approached a lower bound because the lower flow rate is also responsible for generating relatively low pressure. If an initial ethyl benzene flow rate is maintained at a lower value, the mixture of ethyl benzene and the steam would produce a relatively higher temperature (as per energy balance of mixing streams). High temperature and low pressure are favored at lower initial flow rate of ethyl benzene and therefore all the points corresponding to the Pareto optimal solutions belong to the lower initial ethyl benzene flow rate (Figs. 5.24e - 5.24f). The steam over reactant ratio (*SOR*) also controls the desired objectives. Higher *SOR* value is favored for high value of yield and vice versa for the selectivity. Figs. 5.24a - 5.24h also show the comparison of decision variables corresponding to the Pareto optimal solutions obtained using MODE III, hybrid MODE, elitist MODE, and trigonometric MODE algorithms. A comparatively better trend of decision variables is observed in case of hybrid MODE, elitist MODE and trigonometric MODE algorithms whereas the decision variables are slightly scattered in case of MODE and MODE III algorithms. Figs. 5.24b and 5.24f show that for few of the points, MODE algorithm approached lower bound of temperature and upper bound of initial flow rate of ethyl benzene. This resulted in a lower combined inlet temperature of the steam and the ethyl benzene mixture. Thus MODE algorithm resulted in local Pareto solutions, as due to high value of initial ethyl benzene flow & lower steam temperature. Thus, in order to reach towards the global Pareto solutions, it is necessary to attain a relatively high temperature of the combined stream of mixture of steam and ethyl benzene to the inlet of reactor.

Effect of initial number of population points on hybrid MODE

The initial number of population points may play an important role in deciding the distribution of solutions on the Pareto front. However, as the number of initial population points increases, the total number of function evaluations also increases. Thus an optimum size of an initial population is very necessary in any MOO algorithm. Fig. 5.25 shows the Pareto front obtained using initial population size of 100 and 200, where the convergence is equally good for both the cases. The Pareto front is able to cover a wider range (with scattered points) when initial population size is kept 200. However, with an initial population size of 100, the convergence of algorithm to the Pareto front is good with nearly uniform diversity. Thus, the population size is chosen as 100 for the rest of the experimental runs in this study.

Effect of Step size used for obtaining a new neighborhood solution in Hybrid MODE algorithm

Hybrid algorithm uses a local search of solutions by creating a neighborhood point near the current point. Following mapping rule is used to generate a new neighborhood point (Eq. 5.3).

New neighborhood solution = current solution ± rand (0, 1)*desired step size (5.3)

The step size used in the above equation also affects the quality of the Pareto front. This aspect is studied by considering various values of step size. Three different step sizes are considered for each of the variables depending upon the number of digits of the variable in the current solution. For e.g., the upper bounds of four decision variables considered in this study, i.e., T_{EB}, P, SOR and F_{EB}^{0} are 800 K, 2.63 bar, 20 and 40.56

kmol/h respectively. Then for these cases, depending upon the number of digits of the variables the three sets of step sizes are 100, 1, 10 & 10 (step size-1); 10, 0.1, 1 & 1 (step size-2) and 1, 0.01, 0.1 & 0.1 (step size-3) respectively. The effect of step size on the Pareto front is studied and is shown in Fig. 5.26a. The percentage of initial population points converged to the final Pareto front for step size-1, step size-2 and step size-3 are 86%, 96% and 93% respectively (Fig. 5.26a). Because all the results with these 3 step sizes converged to the same front and as it is difficult to distinguish the overlapping points on the Pareto front, these results are re-plotted in Fig. 5.26b, using vertical displacements in the values by +2 in the results with step size-2, and by +3 in the results with step size-3. Also the diversity of Pareto front is better when a step size-2 is used. With step size-1, the location of neighborhood solution may be far away from the current solution (as per Eq. 5.3), which may not give a better solution when local search method is used. However, when step size-3 is used, the solutions are crowded on the Pareto front as shown in Fig. 5.26a and Fig. 5.26b. With step size-2, a well-diversified Pareto front is obtained with a maximum number of solutions on the Pareto front. Therefore, in entire simulation runs step size-2 is used for creating a new neighborhood point. Similar results were obtained when hybrid MODE algorithm was tested on several other test problems.

Effect of an additional decision variable (T_{STEAM}) on the Pareto front

Superheated steam is used to preheat the reaction mixture. It is difficult to obtain a uniform temperature of steam. Therefore, in the second set of decision variables, the effect of an extra variable, i.e., temperature of the inlet steam (along with the set-I decision variables) is also considered. The Pareto front obtained using set-II decision variables are compared with the Pareto front obtained using set-I decision variables and is

shown in Fig. 5.27. The inlet steam temperature is responsible for altering the temperature of mixed stream entering the reactor. The temperature of mixed steam largely affects the reaction kinetics and reactor performance as stated above. Thus a variation in inlet steam temperature creates conflicting scenario in the desired objectives (i.e., selectivity and yield). Therefore, the Pareto front obtained using set-II variables is scattered in nature as shown in the Fig. 5.27. Hence, set-I variables are used in the rest of the experimental runs in this study. However, as not much difference is observed in the Pareto front due to addition of a new variable, this variable is omitted from the rest of the study and only 4 regular variables (as defined by Eqs. 4.10 – 4.13) are used.

5.2.1.2 Analysis of profit function

Table 5.7 shows the values of objective functions, decision variables and profit functions obtained in this study using strategies of MODE algorithm for selected data points. A profit function can be used as a further guideline for choosing the appropriate non-dominated point from the Pareto front. The profit function considers the cost of major feed materials (cost of ethyl benzene and steam) and final valued products (such as Styrene, benzene and toluene).

For this purpose, a simplified profit function (Yee et al., 2003) is defined as given by Eq. 5.4a.

$$Profit = Revenue\ generated\ by\ styrene\ and\ byproducts - Raw\ material\ cos\ t \quad (5.4a)$$

Eq. 5.4a in mathematical form can be written as Eq. 5.4b

$$Profit = F_{ST}H_{ST} + F_{BZ}H_{BZ} + F_{TOL}H_{TOL} - \left(F_{EB}^{0} - F_{EB}\right)H_{EB} - F_{H_2O}H_{H_2O} \quad (5.4b)$$

The costs of styrene, ethyl benzene, benzene and toluene are based on the prices published in the on-line purchasing magazine (Purchasing, 2009). However, we considered the older cost values (as on April 2001) in this study in order to have a comparison with the previously obtained results of Yee et al. (2003).

Table 5.7 also shows the profit function values obtained using different algorithms for adiabatic styrene reactor. The objectives namely, F_{ST}, S_{ST} and Y_{ST} (calculated values) are plotted against the profit function in Figs. 5.28a, 5.28b and 5.28c respectively using the strategies of MODE algorithm. Table 5.7 and Figs. 5.28a, 5.5.28b and 28c show that as the value of F_{ST} increases, the profit value increases. Figs. 28a also shows that using MODE III algorithm, the maximum profit obtained is 584 ($/h) which is obtained at F_{ST} value of 11.91 kmol/h. Using hybrid MODE the maximum profit obtained is 728 ($/h). In terms of both the selectivity and yield, nearly same values are obtained using both the algorithms. However, using MODE III and hybrid MODE algorithms, the values of S_{ST} vary in between 87.14 - 95.5 % and 87.22 - 95.41 % whereas the values of Y_{ST} vary in between 21.38 - 42.02 % and 20.41 - 36.90 % respectively. The profit obtained using MODE III and hybrid MODE algorithms ranges in between 344.62 - 584.47 $/h and 383.32 - 728.44 $/h respectively.

The profit obtained using elitist MODE and trigonometric MODE algorithms ranges between the values of 362.5 - 732.5 $/h and 344.6 – 701.5 $/h respectively. The major improvement obtained in profit function value is due to the increased value of F_{ST} obtained using hybrid MODE. The value of F_{ST} ranges from 6.60 - 12.36 kmol/h and from 7.72 - 15.81 kmol/h using MODE III and hybrid MODE algorithms respectively. However, with F_{ST} value of 15.50 kmol/h and 14.48 kmol/h, the trigonometric MODE

and elitist MODE resulted in a profit value of 701 $/h and 738 $/h. The maximum profit obtained among all the algorithms corresponds to that obtained using elitist MODE. The reason for this improvement can be observed from Table 5.7, where the values of decision variables are also shown along with the values of objective functions and the profit function; and from Figs. 5.28d- 5.28g, where the decision variables are plotted against the profit function.

Both Figs. 5.28d and 5.28e show that the enhancement in profit function is obtained because hybrid MODE is able to capture the upper bound of the decision variables, namely T_{EB} and the F_{EB}^{0}. As per the kinetics, for the reversible endothermic reactions, the higher temperature is favored to enhance the rate of forward reaction, thus giving a higher productivity. The higher initial temperature coupled with a higher initial flow rate of ethyl benzene, is responsible for producing higher flow rate of styrene, which in turn is responsible for giving higher profit values. Table 5.7 also shows that as the value of temperature (decision variable) increases, the values of objective function F_{ST} and the profit also increase.

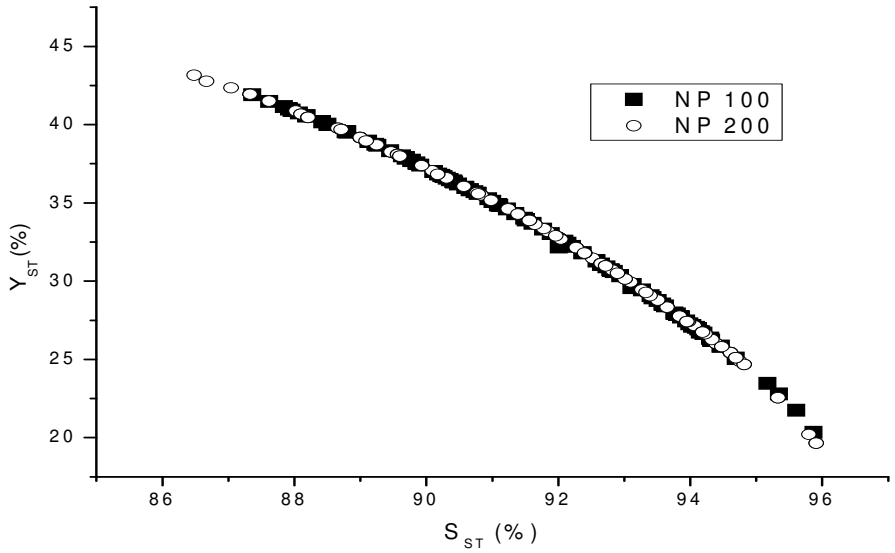

Fig. 5.25 Effect of initial population size (*NP*) on convergence of hybrid MODE after 300 generations

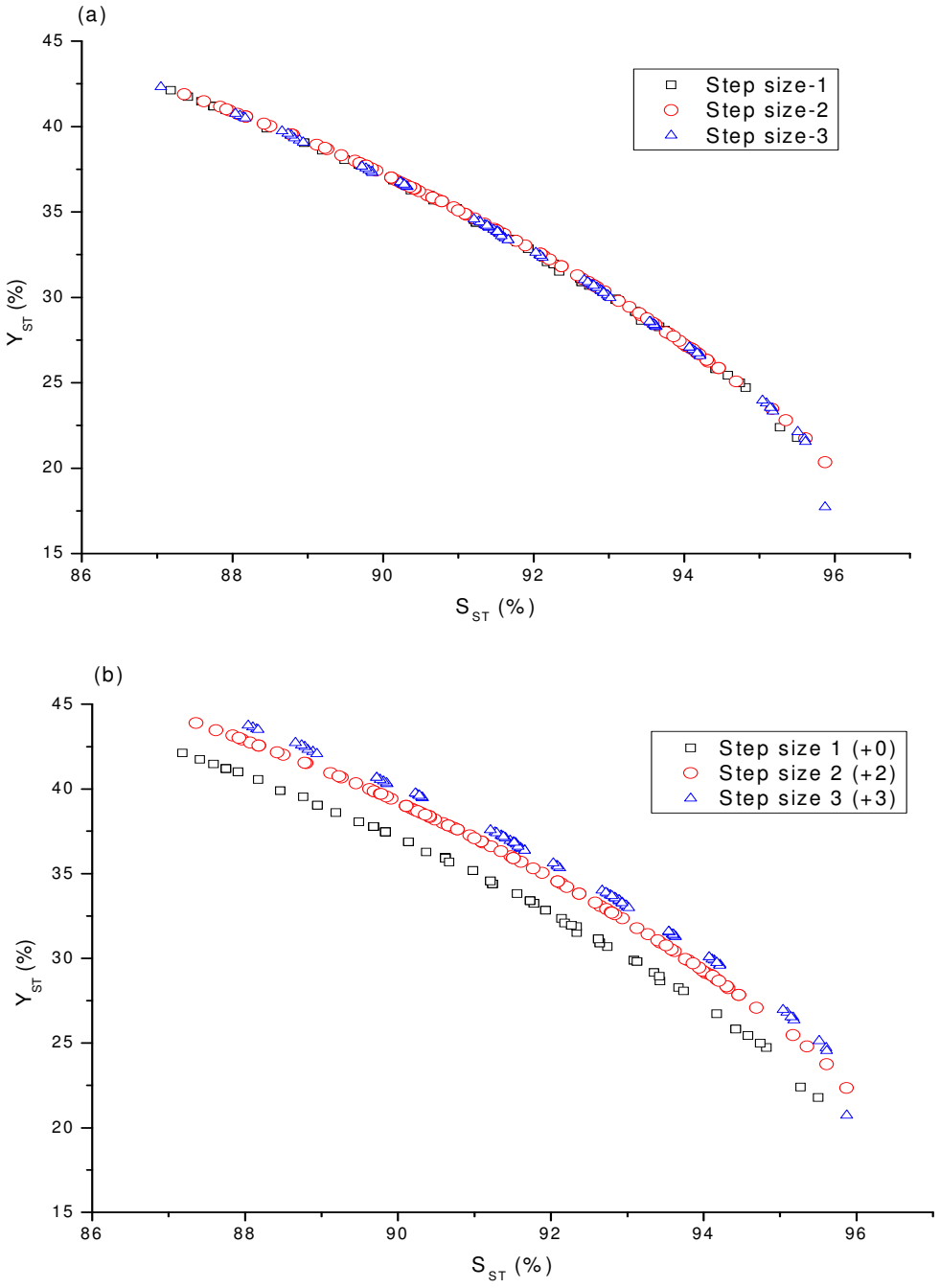

Fig. 5.26 (a) Effect of the step size used in obtaining a neighborhood solution on the Pareto optimal solutions using hybrid MODE algorithm; (b) The results of Fig. 5.26a are re-plotted with vertical shift in value of ordinate by +2 in step size-2, and by +3 in step size-3 data points

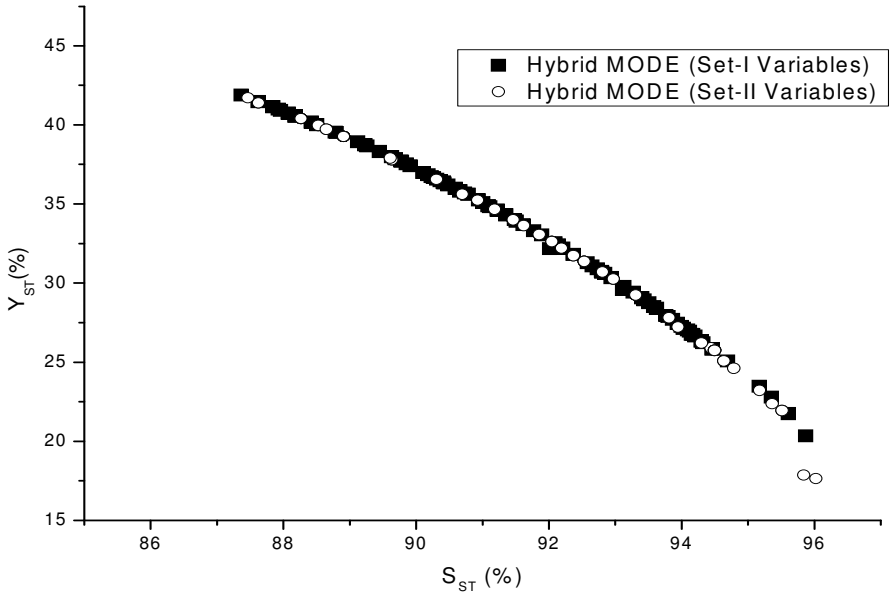

Fig. 5.27 Effect of number of decision variables on the Pareto front after 300 generations using hybrid MODE algorithm

Table 5.7 Values of objective functions, decision variables and profit functions for selected data points using strategies of MODE algorithm

Sr. No.	MODE III								Hybrid MODE							
	F_{ST} (kmol/h)	S_{ST} (%)	Y_{ST}^{*} (%)	T (K)	P (bar)	F_{EB}^{0} (kmol/h)	*SOR*	*Profit* ($/h)	F_{ST} (kmol/h)	S_{ST} (%)	Y_{ST}^{*} (%)	T (K)	P (bar)	F_{EB}^{0} (kmol/h)	*SOR*	*Profit* ($/h)
1	6.60	95.50	21.38	702.13	1.02	27.77	9.470	344.6	7.72	95.41	20.41	692.90	1.201	34.56	8.78	393.3
2	7.52	94.78	24.38	743.52	1.19	28.12	7.416	415.9	8.14	95.20	20.96	613.54	1.571	35.64	11.39	380.0
3	7.80	94.49	25.49	597.88	1.69	27.97	13.79	367.3	9.09	94.73	21.88	694.78	1.415	38.52	8.78	458.1
4	8.39	94.03	26.66	662.48	1.68	28.98	11.38	420.8	9.33	94.67	21.87	646.1	1.665	39.6	10.32	446.0
5	8.50	93.70	28.08	590.35	1.95	27.88	14.62	398.2	9.57	94.50	22.08	596.47	1.821	40.32	12.19	429.5
6	8.72	93.38	29.08	596.11	2.00	27.71	14.81	409.7	10.41	93.76	24.38	650.35	1.860	39.96	10.95	495.5
7	9.10	92.81	30.54	676.66	1.80	27.62	12.44	454.3	10.80	93.29	25.59	629.02	1.921	39.6	12.68	493.8
8	9.29	92.74	30.66	580.08	2.15	28.13	16.09	425.7	11.18	93.05	26.08	695.94	1.793	40.32	9.90	551.9
9	9.37	92.47	31.37	635.9	2.06	27.75	14.21	450.9	11.50	92.68	26.86	735.88	1.651	40.32	8.53	589.0
10	9.57	92.24	32.04	645.45	1.99	27.77	14.53	458.2	11.76	92.42	27.75	646.92	2.064	39.96	12.73	544.0
11	9.65	92.04	32.60	625.49	2.13	27.56	15.33	456.1	12.22	92.07	28.39	639.64	2.157	40.68	13.33	557.1
12	9.71	92.03	32.60	638.46	2.00	27.75	15.29	458.7	12.47	91.72	29.27	675.58	2.099	40.32	12.15	589.6
13	9.93	91.75	33.29	557.29	2.35	27.82	18.28	440.1	12.96	91.14	30.48	592.57	2.449	40.32	16.23	556.7
14	10.10	91.40	34.12	635.89	2.06	27.63	16.44	468.5	13.30	90.76	31.33	601.05	2.565	40.32	15.99	578.8
15	10.17	91.33	34.30	584.44	2.37	27.71	17.78	459.1	13.52	90.50	31.60	639.60	2.573	40.68	14.21	615.0
16	10.31	91.01	34.95	711.99	1.82	27.60	13.43	510.2	14.17	89.71	33.18	746.45	1.979	40.68	11.26	692.3
17	10.61	90.36	35.99	742.34	1.59	27.63	13.62	523.6	14.75	88.81	34.93	744.74	2.035	40.32	12.84	701.3
18	11.17	89.79	37.30	697.68	2.07	28.17	15.40	533.9	15.12	88.17	35.85	742.20	2.270	40.32	12.69	723.0
19	11.67	88.67	39.33	721.25	2.13	27.99	15.29	562.1	15.68	87.56	36.90	739.63	2.278	40.68	14.20	728.4
20	12.36	87.18	42.02	686.97	2.47	27.82	19.21	559.1	15.81	87.22	37.55	705.58	2.556	40.32	16.17	708.2

[*] Calculated value of third objective function during two-objective optimization study

Table 5.7 Values of objective functions, decision variables and profit functions for selected data points using strategies of MODE algorithm (Contd..)

Sr. No.	Trigonometric MODE								Elitist MODE							
	F_{ST} (kmol/h)	S_{ST} (%)	Y_{ST}^{*} (%)	T (K)	P (bar)	F_{EB}^{0} (kmol/h)	SOR	$Profit$ ($/h)	F_{ST} (kmol/h)	S_{ST} (%)	Y_{ST}^{*} (%)	T (K)	P (bar)	F_{EB}^{0} (kmol/h)	SOR	$Profit$ ($/h)
1	7.93	95.59	18.65	612.0	1.44	38.94	10.8	362.5	6.60	95.50	21.38	702.1	1.02	27.77	9.47	344.6
2	9.07	94.98	20.80	577.2	1.89	40.41	11.7	407.9	8.39	95.47	19.20	700.4	1.24	40.24	7.76	428.5
3	9.73	94.44	22.38	602.2	1.95	40.51	11.5	447.2	8.85	95.16	20.21	710.5	1.32	40.51	7.38	459.1
4	10.5	93.74	24.32	626.2	1.96	40.52	11.7	488.5	9.12	94.94	20.85	718.4	1.34	40.52	7.25	475.8
5	10.87	93.41	25.18	636.3	1.97	40.53	11.8	506.7	9.17	94.89	21.04	645.2	1.63	40.40	10.04	438.1
6	11.05	93.24	25.61	642.7	1.98	40.53	11.7	517.0	9.47	94.65	21.78	607.6	1.89	40.43	11.15	439.0
7	11.31	92.98	26.26	650.1	1.99	40.52	11.8	530.4	9.59	94.55	22.07	610.1	1.89	40.44	11.24	444.2
8	11.69	92.60	27.19	662.9	1.98	40.54	11.8	550.8	9.71	94.46	22.31	579.3	2.08	40.52	11.92	440.6
9	11.89	92.39	27.68	676.6	1.95	40.53	11.5	565.5	10.00	94.20	23.07	565.9	2.10	40.47	12.86	443.5
10	12.25	92.01	28.56	678.3	1.99	40.55	11.9	579.7	10.04	94.16	23.16	616.3	1.99	40.46	11.26	468.6
11	12.51	91.71	29.23	688.3	1.99	40.52	11.8	595.1	10.70	93.57	24.76	609.4	2.07	40.54	12.37	489.0
12	12.74	91.45	29.80	695.0	2.00	40.52	11.8	607.8	11.05	93.23	25.63	562.0	2.35	40.52	13.87	486.4
13	13.29	90.80	31.16	714.4	1.97	40.52	11.8	637.5	11.80	92.48	27.47	627.1	2.22	40.54	12.91	541.5
14	13.64	90.38	32.01	719.9	2.01	40.52	12.0	653.6	11.93	92.34	27.82	584.5	2.37	40.48	14.55	524.8
15	14.30	89.50	33.66	741.9	1.98	40.50	12.0	688.5	12.55	91.68	29.31	633.8	2.30	40.55	13.70	570.9
16	14.53	89.19	34.22	746.8	2.01	40.52	12.0	701.2	13.03	91.12	30.50	684.9	2.08	40.53	12.74	610.5
17	14.79	88.82	34.87	742.8	2.05	40.49	12.8	702.7	13.84	90.13	32.53	669.3	2.34	40.50	14.32	631.4
18	14.89	88.67	35.11	764.8	1.95	40.51	11.7	723.3	13.99	89.94	32.89	671.1	2.35	40.51	14.51	636.4
19	15.20	88.19	35.93	766.9	2.00	40.44	12.1	733.6	14.63	89.07	34.50	681.1	2.43	40.48	15.08	662.2
20	15.48	87.71	36.61	764.8	2.01	40.46	13.2	732.2	15.50	87.80	36.61	706.6	2.46	40.51	15.45	701.7

*Calculated value of third objective function during two-objective optimization study

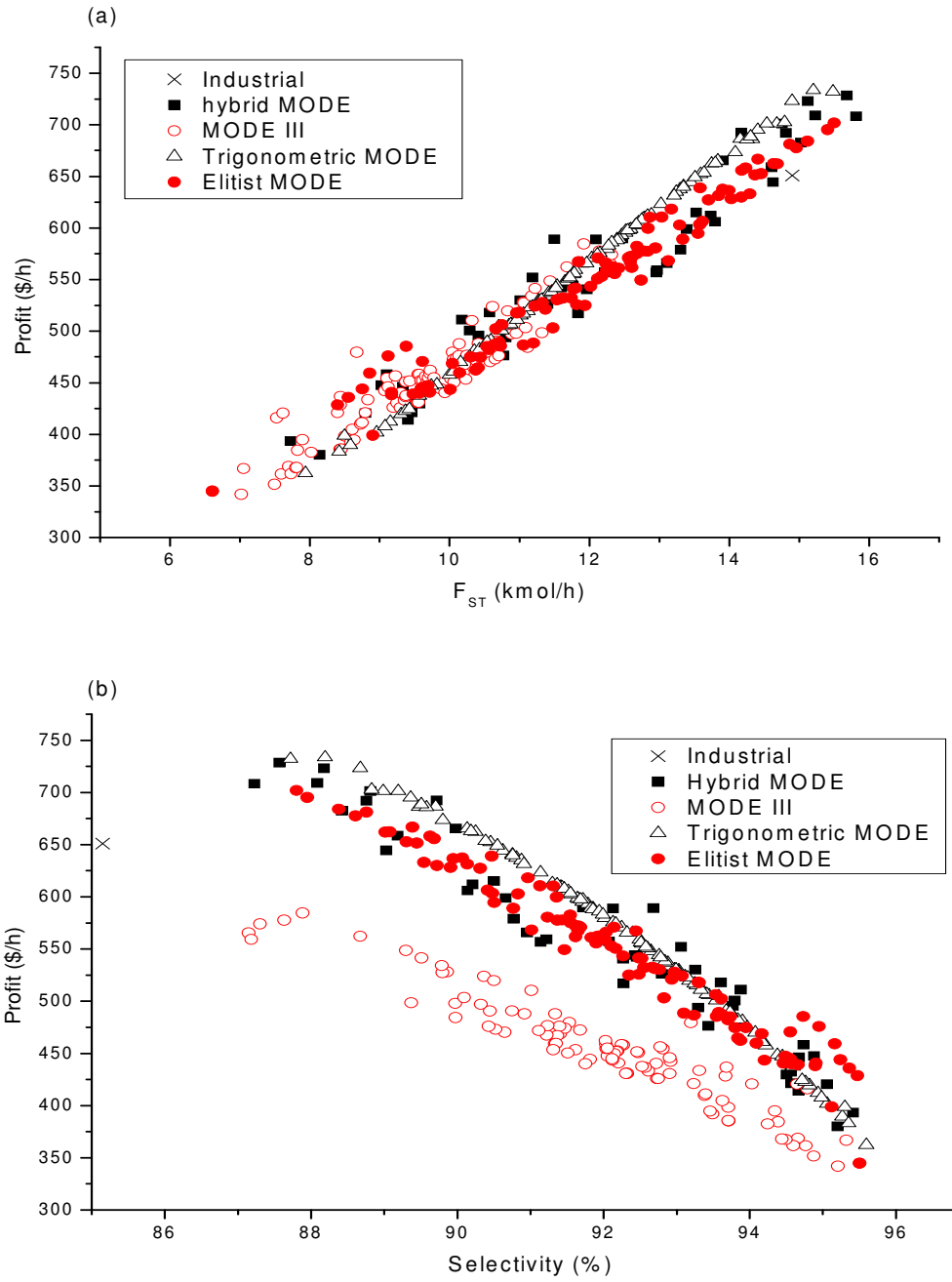

Fig. 5. 28 (Contd…)

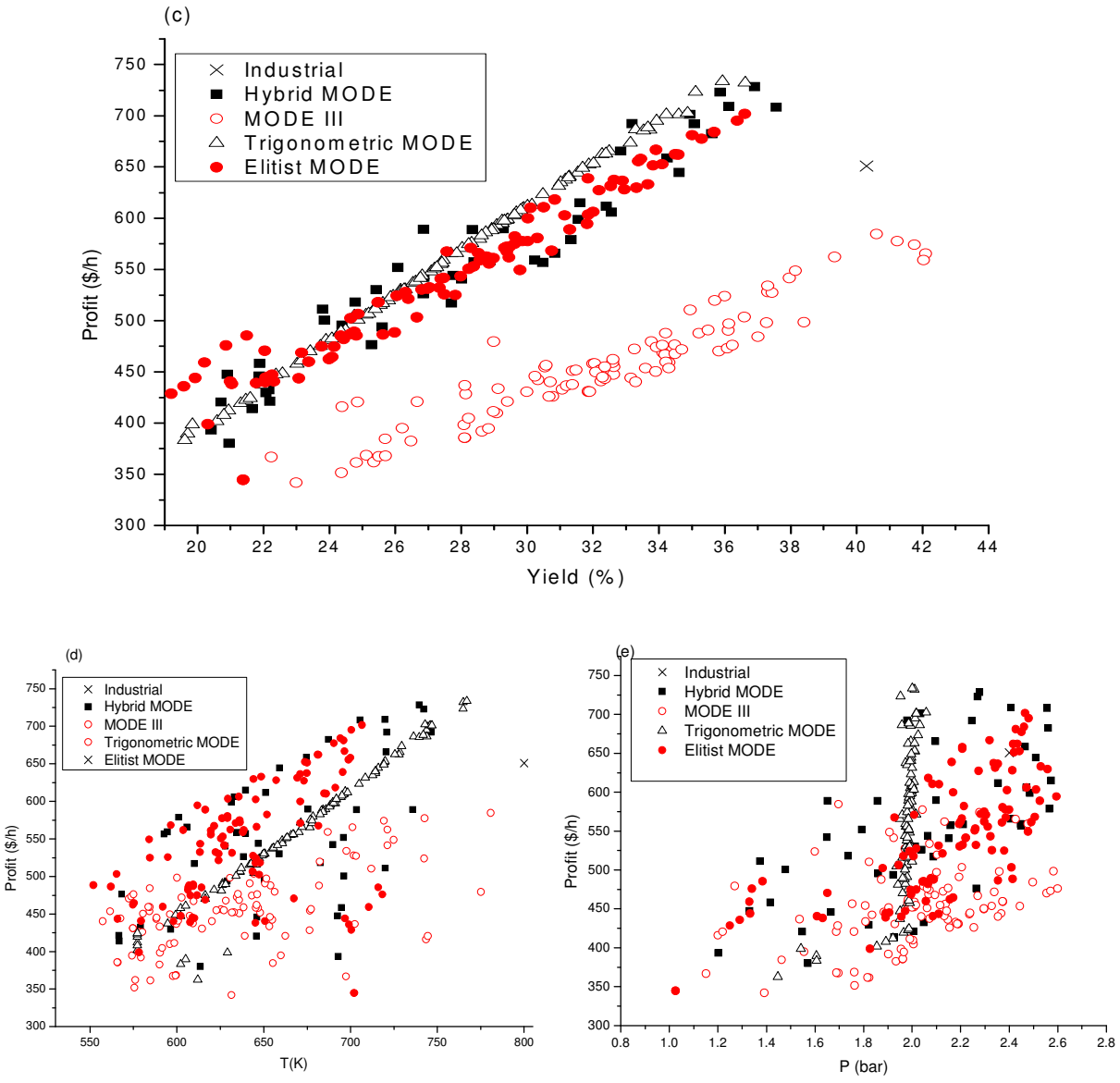

Fig. 5. 28 (Contd…)

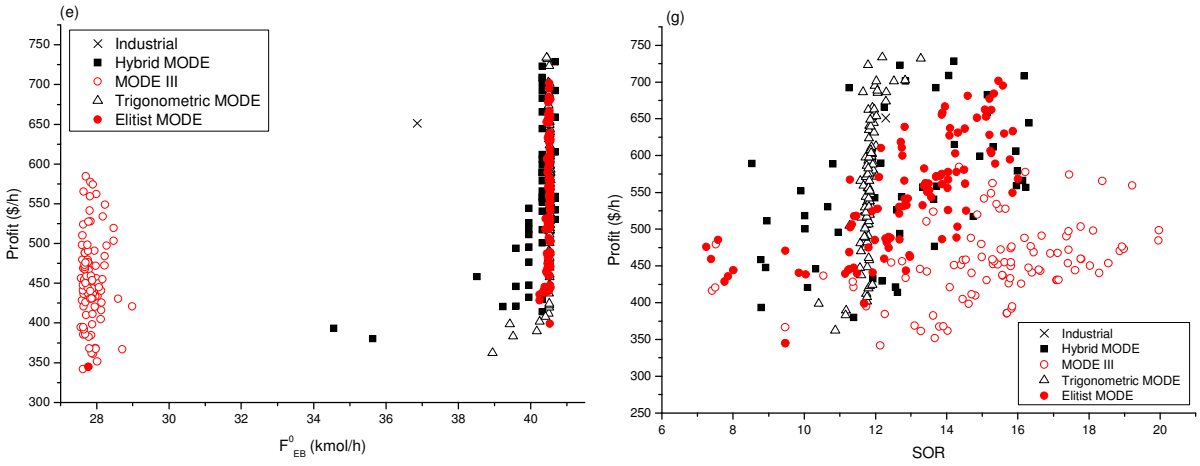

Fig. 5. 28 Analysis of the profit-function with respect to objective functions and the decision variables. Profit function plotted against F_{ST} (Fig. [a]), S_{ST} (Fig. [b]) and Y_{ST} (calculated objective) (Fig. [c]). Profit function plotted against decision variables *T* [Fig. (d)], *P* [Fig. (e)], F_{EB}^{0} [Fig. (f)] and *SOR* [Fig. (g)]

5.2.1.3 Case-2: Simultaneous maximization of F_{ST} and S_{ST}

Simultaneous maximization of F_{ST} and S_{ST} objectives is carried out using MODE, MODE III, hybrid MODE, elitist MODE and trigonometric MODE algorithms. However, to compare the performance of hybrid MODE algorithm with MODE III, the comparative results of MODE III and hybrid MODE are presented first. Fig. 5.29 shows the Pareto optimal solutions obtained after 300 generations using the hybrid MODE and MODE III algorithms. 20 points are selected at random from Fig. 5.29 and are shown along with their respective decision variables in Table 5.7. Table 5.7 shows that the range covered by MODE III and hybrid algorithms in terms of objective-1 (i.e., F_{ST}) is 6.60 - 12.36 kmol/h and 7.56 - 15.84 kmol/h and in terms of objective-2 (i.e., S_{ST}) is 87.18 - 95.5 % and 87.22 - 95.41 % respectively. Hybrid MODE algorithm produced a wider range in terms of both the objectives when compared to the range of objectives obtained using MODE III and the industrial operating point (Sheel & Crowe, 1969; Elnashaie and Elshishini, 1994). MODE III algorithm resulted in lower values of F_{ST} as compared to the hybrid MODE because MODE III approached the lower bound of decision variable F_{EB}^{0}. If F_{EB}^{0} (decision variable) values are compared for both MODE III and hybrid MODE, then it is observed that the hybrid MODE approached the upper bound (i.e. 40.56 kmol/h) whereas MODE III approached the lower bound (i.e. 27.56 kmol/h).

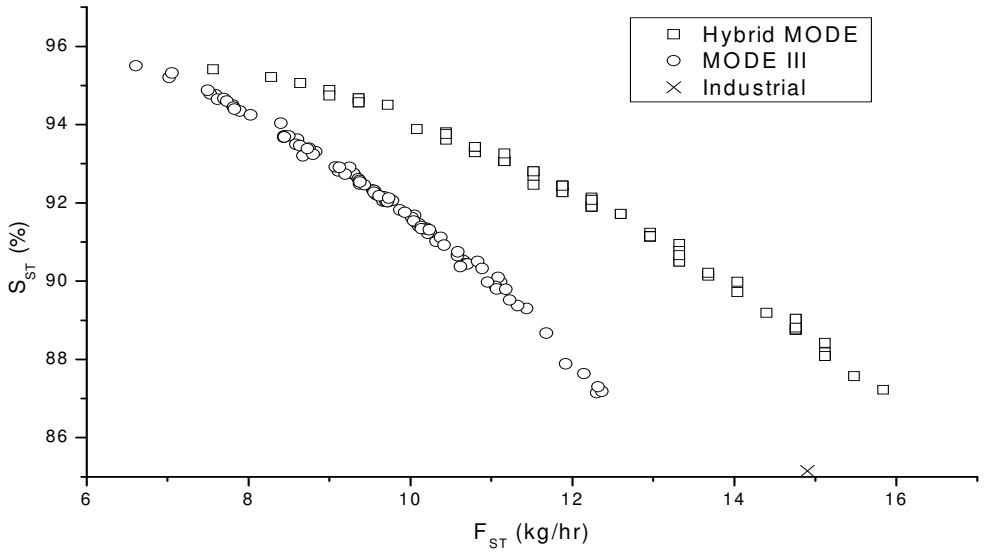

Fig. 5.29 Pareto optimal solutions obtained after 300 generations using hybrid MODE and MODE III algorithms

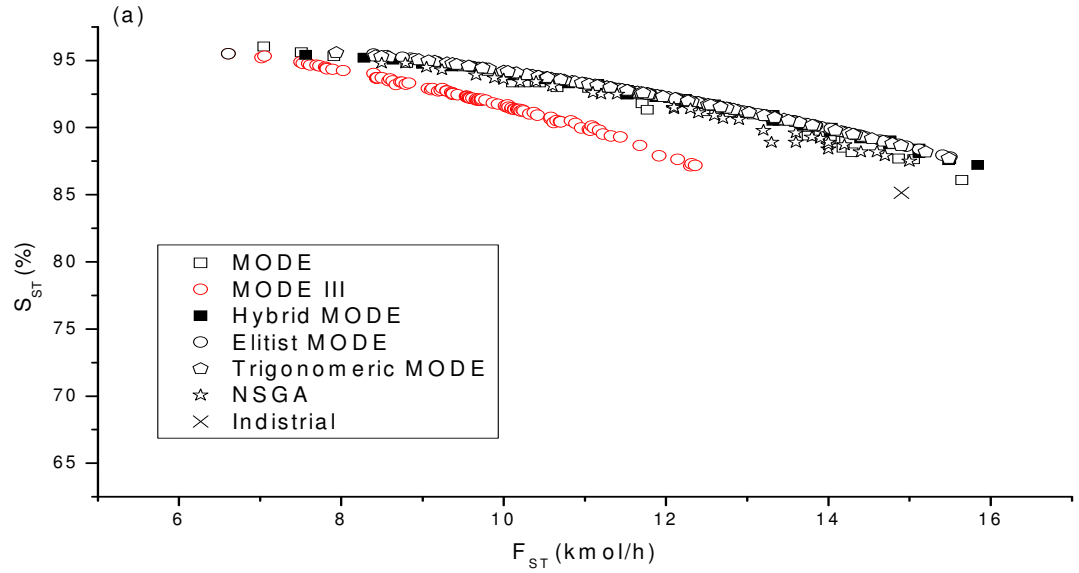

Fig. 5.30 (Contd..)

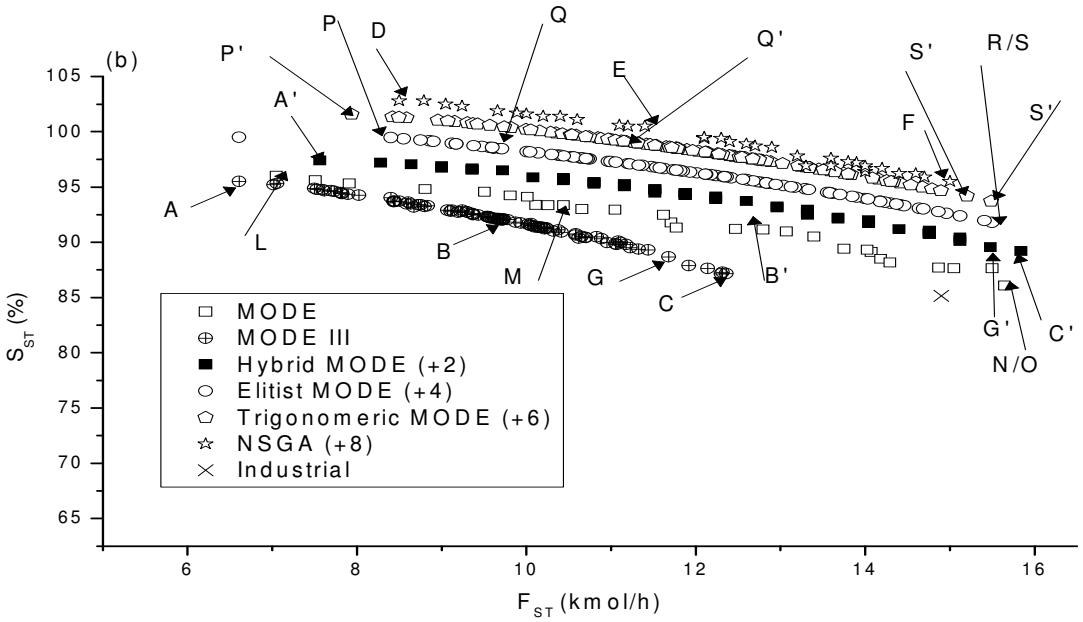

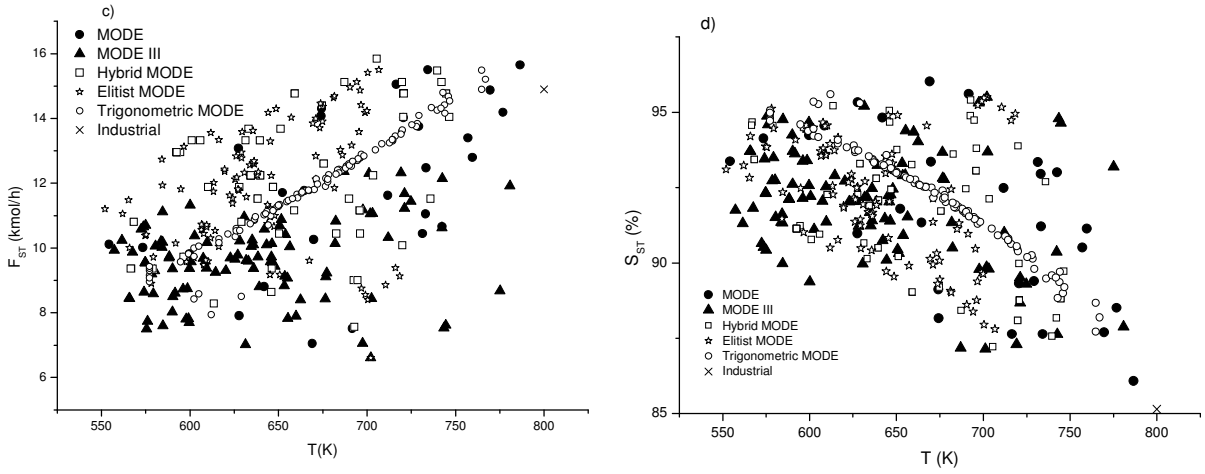

Fig. 5.30 (Contd...)

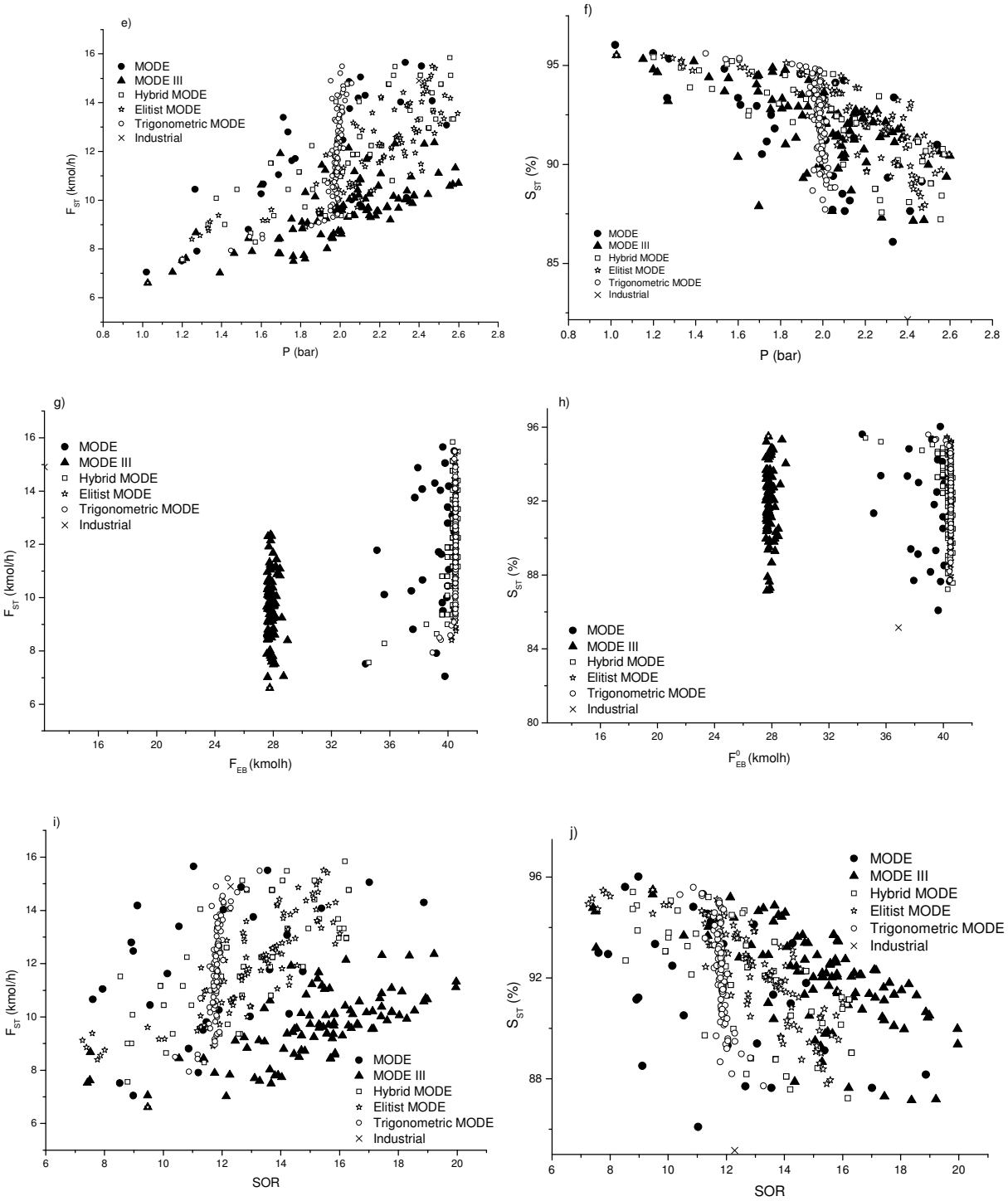

Fig. 5.30 (a) Comparison of Pareto fronts obtained using MODE, MODE III, hybrid MODE, elitist MODE, trigonometric MODE and NSGA. (b)The results of Fig. 5.30a are re-plotted with vertical shift in value of ordinate by +2 in hybrid MODE, +4 in Elitist MODE, +6 in Trigonometric MODE and +8 in NSGA results data points; (c-j) Decision variables plotted against corresponding objectives

In earlier studies of Yee et al. (2003) and Babu et al. (2005), it was observed that the multi-objective optimization study of maximization of F_{ST} and S_{ST} was independent of this decision variable (F_{EB}^{0}) because the lower bound of F_{EB}^{0} was captured in these studies. But in this study, it is seen that only a robust algorithm can search entire search space and gives a possibly-true Pareto optimal front for an industrial problem. A compromise (corresponding to the set of optimum non-dominated solutions) with other conflicting variables (such as *T, P,* and *SOR*) is required to get the suitable Pareto front with higher values of initial ethyl benzene flow rate. If such compromise is not met along with the initial ethyl benzene flow rate (one of the decision variables), then it may produce a non-optimal or a set of non-dominated solutions away from the true Pareto optimal front. Hence, the algorithm may result in a local Pareto front. When higher initial ethyl benzene flow rate is obtained (in case of hybrid algorithm), the values of corresponding decision variables such as *T* and *SOR* are also high.

This is because higher temperature of mixed stream (steam and initial ethyl benzene) is responsible for higher productivity. It is important for any efficient algorithm to explore the entire corner of multi-dimensional search space so that a true Pareto front is obtained. MODE III algorithm in this study (see Fig. 5.29), and MODE and NSGA algorithms in earlier studies (Yee et al., 2003; Babu et al., 2005) converged to the lower bound of initial ethyl benzene flow rate, hence resulted in local Pareto front. Table 5.7 also shows the conflicting scenario, wherein the value of S_{ST} decreases while the value of calculated Y_{ST} increases as the value of F_{ST} increases. The range covered by MODE III and hybrid MODE algorithm in terms of calculated value of Y_{ST} is 21.38 - 42.02 % and 20.41 - 37.51 % respectively. The results of current study are compared with those

obtained with NSGA algorithm published in the literature (Yee et al., 2003). Fig. 5.30 shows the comparison of Pareto fronts obtained using MODE, MODE III, hybrid MODE, elitist MODE, trigonometric MODE and NSGA algorithms along with an industrial operating point.

From the results obtained with each of the algorithms, some data points are selected from Fig. 5.30b and are marked as L-M-N-O for MODE, A-B-C-D for MODE III, A`-B`-C`-D` for Hybrid MODE, P-Q-R-S for elitist MODE, P`-Q`-R`-S` for trigonometric MODE, and D-E-F for NSGA. These selected data points are analyzed further and are shown in Table 5.8. Table 5.8 shows the selected data points from the Pareto front of Fig. 5.30b (points as L-M-N-O for MODE, points A-B-C-D for MODE III, points A`-B`-C`-D` for Hybrid MODE, points P-Q-R-S for elitist MODE, points P`-Q`-R`-S` for trigonometric MODE, and points D-E-F for NSGA.). Figs. 5.30a - 5.30b show that the hybrid MODE, elitist MODE and trigonometric MODE algorithms resulted in better non-dominated solutions (Pareto fronts) as compared to those obtained using MODE III and NSGA when the same set of decision variables is used. Pareto solutions obtained using hybrid-, elitist- and trigonometric- strategy of -MODE algorithms covered a wider range on Pareto front as compared to non-dominated solutions obtained when NSGA was used. Fig. 5.30b also shows that both MODE III and NSGA algorithms converged to a local Pareto front compared to the Pareto front obtained using hybrid MODE. Hybrid MODE algorithm is able to give better results in terms of both the objectives. The variation of objective space with respect to key decision variables obtained using individual runs and industrial data can be seen through Figs. 5.30c – 5.30j. Table 5.8 also gives the comparison of industrial operating point with the selected points

obtained using different algorithms using various parameters. As we move from point A to C (similarly from point A` to C`; from points D to F; from L to N; from P to R and from P` to R`), both the values of F_{ST} and profit increase. The value of F_{ST} and profit increases in case of MODE III algorithm output, primarily due to the increase in *SOR* (from 9.47 to 19.21). MODE III algorithm resulted in local Pareto solutions because a point (now onwards we refer it as 'chromosome' as per the evolutionary terminology) which has a higher value of T_{EB} (chromosome A) and a lower value of *SOR* and vice versa (chromosome C). As per the energy balance, this combination of decision variables (T_{EB} and *SOR*) is responsible for generating the temperature of the mixed stream entering the reactor (T_{mix1}). In case of hybrid MODE algorithm, a high value of either T_{EB} or *SOR* resulted in a higher value of T_{mix1} [e.g. chromosome A` against D: $T_{EB}$=692.9 K & *SOR*=8.78 by hybrid MODE against $T_{EB}$=651.5 K & *SOR*=10.74 by NSGA; and chromosome C` against F: T_{EB}=705.5 K & *SOR*=16.71 by hybrid MODE against T_{EB}=799.9 K & *SOR*=10.94 by NSGA]. T_{mix1} has a strong opposing effect on F_{ST} and S_{ST}. High T_{mix1} maximizes the flow rate of styrene (point C`) while low $T_{mix1}$ maximizes the selectivity (point A`). This is due to the reversible endothermic nature of the main reaction (Eq. 4.1). The NSGA algorithm resulted in local Pareto front because *SOR* approached a lower bound. Thus it is necessary for an efficient algorithm to have a wide spread search of population points in all the dimensions. As hybrid MODE algorithm approached the Pareto optimum values of all the decision variables, it resulted in a wider and a better Pareto front as compared to NSGA and MODE III. Point G (profit = 584 $/h) and G' (profit = 728 $/h) (in Fig. 5.30 and Table 5.8) are the points having maximum profit values obtained using MODE III and hybrid MODE algorithm respectively.

Table 5.8 Comparison of MODE, MODE III, hybrid MODE, elitist MODE, trigonometric MODE and NSGA algorithms for selected data points

Parameter	Industrial value	MODE (present study)				MODE III (present study)					Hybrid MODE (present study)		
		L	M	N	O	A	B	C	G	A`	B`	C`	G'
F_{ST} (kmol/h)	14.9	7.04	11.62	15.54	15.54	6.608	9.93	12.36	11.91	7.72	12.47	15.81	15.68
S_{ST} (%)	85.15	96.02	92.48	86.08	86.08	95.50	91.75	87.18	87.88	95.41	91.72	87.22	87.56
Y_{ST} (%)	40.30	16.01	27.68	37.77	37.77	21.38	33.29	42.02	40.60	20.41	29.27	37.55	37.55
T_{EB}	800.00	669.15	711.80	786.52	786.52	702.1	557.29	686.9	780.7	692.9	675.5	705.5	739.5
P (bar)	2.4	1.01	1.75	2.32	2.32	1.02	2.35	2.47	1.69	1.20	2.09	2.55	2.55
SOR (-)	12.29	8.98	10.14	11.02	11.02	9.47	18.28	19.21	14.35	8.78	12.15	16.17	14.20
F_{EB}^{0}	36.87	39.80	39.55	39.65	39.65	27.77	27.82	27.82	27.7	34.56	40.32	40.32	40.68
F_{BZ}	1.37	0.302	0.613	1.34	1.34	0.30	0.60	1.18	1.18	0.32	0.70	1.47	1.43
F_{TOL}(kmol/h)	1.20	0.95	1.26	2.06	2.06	0.96	1.21	1.52	1.36	1.00	1.34	1.73	1.68
Profit ($/h)	651	335.91	574.97	774.05	774.05	344	440	559	584	393	589	708	728

Table 5.8 Comparison of MODE, MODE III, hybrid MODE, elitist MODE, trigonometric MODE and NSGA algorithms for selected data points (Contd..)

Parameter	Industrial value	Elitist MODE (present study)				Trigonometric MODE (present study)				NSGA (Yee et al.)		
		P	Q	R	S	P`	Q`	R`	S`	D	E	F
F_{ST} (kmol/h)	14.9	6.608	9.13	15.501	15.501	7.93	11.02	15.48	15.20	8.45	11.04	15.01
S_{ST} (%)	85.15	95.50	94.46	87.80	87.80	95.59	93.27	87.71	88.19	94.86	92.69	87.51
Y_{ST} (%)	40.30	21.38	22.31	36.61	36.61	18.65	25.53	36.61	35.93	21.88	27.38	35.26
T_{EB}	800.00	702.1	557.29	706.66	706.66	612.01	641.84	764.83	766.98	651.5	713.5	799.9
P (bar)	2.4	1.02	2.08	2.46	2.46	1.44	1.98	2.01	2.00	1.84	1.84	2.03
SOR (-)	12.29	9.47	11.92	15.45	15.45	10.87	11.752	13.28	12.19	10.74	10.69	10.94
F_{EB}^{0}	36.87	27.77	40.52	40.51	40.51	38.94	40.52	40.46	40.44	38.63	40.31	40.47
F_{BZ}	1.37	0.301	0.385	1.36	1.36	0.325	0.527	1.46	1.317	0.24	0.50	1.25
F_{TOL}(kmol/h)	1.20	0.968	1.13	1.68	1.68	0.999	1.20	1.59	1.617	0.22	0.37	0.90
Profit ($/h)	651	344.62	440.67	701.73	701.73	362.50	515.27	732.27	733.66	330	467	673

The point O` has the maximum value of profit among the non-dominated solutions obtained using different algorithms (i.e., MODE III, hybrid MODE, elitist MODE, trigonometric MODE and NSGA) and an industrial operating point as shown in Table 5.8. A high value of profit is also mainly due to the high value of side products that are being formed (such as benzene and toluene). This also shows a drawback of the profit functions, as it does not consider the cost of separation of these byproducts. But this profit can give some preliminary idea of the profit, provided that the separation systems followed by reactors (i.e., train of distillation columns) are efficient.

Effect of a penalty parameter on the Pareto front

The Penalty function approach is used to handle the constraints. Three different weights of penalty parameters (i.e., 10^4, 10^8 and 10^{12}) are used in the present work to study the effect of the penalty parameter on MOO of adiabatic styrene reactor and the Pareto fronts obtained are shown in Fig. 5.31.

The algorithm converged to the same Pareto front but the diversity of solutions is different for each of the penalty parameter value. However, the diversity of solutions is found to be independent of the penalty parameter for most of the range, excepting that there is no specific trend is observed towards the extreme ends of the Pareto front. Considering the same convergence rate, the penalty parameter value of 10^4 is used in this study. It may be noted that a population size of 100 is used for these simulations consistently throughout this study. However, with a population size of 200 and with a penalty parameter value of 10^4, the Pareto front covers the entire range as is with population size of 100 and with a penalty parameter value of 10^{12}. The diversity of the

obtained solutions is one area of the hybrid MODE algorithm, which needs to be further improved. Considering the same convergence rate and computational complexity (with high value of NP), the penalty parameter value of 10^4 and population size of 100 are used in this study.

5.2.1.4 Case-3: Simultaneous maximization of F_{ST} and Y_{ST}

The Pareto front obtained for case-3 (simultaneous maximization of F_{ST} and Y_{ST}) and corresponding decision variables are shown in Figs. 5.32a–5.32i. Unlike the results obtained for case-1 and case-2 (where the decision variable F_{EB}^0 either approached lower or upper bound), for case-3 the decision variable F_{EB}^0 is also equally important in producing the Pareto solutions. While maximizing F_{ST} and Y_{ST} simultaneously, the decision variable *P*, remains practically constant and acquires the upper bound. The conflicting variables observed in this study (which are responsible for producing the Pareto solutions) are *T, SOR* and F_{EB}^0. These results show the ability of existing algorithm to produce more valuable and practical results which are important to the plant engineer. Fig. 5.32a shows that the industrial point lies below the Pareto front and the non-dominated solutions are present on either side of the industrial point, thus offering a wide range and choice to the decision maker. However, in the study of Yee et al.(2003), the industrial point (for maximization of F_{ST} and Y_{ST}) lies at one extreme (left) end of the obtained non-dominated solutions (Pareto front in their work) giving a limited choice for the decision maker. Figs. 5.32b–5.32c and Figs. 5.32f–5.32i show that the temperature of industrial operating point is higher than optimum Pareto temperatures, and *SOR* of industrial point is lower than the optimum Pareto *SOR* obtained in this study.

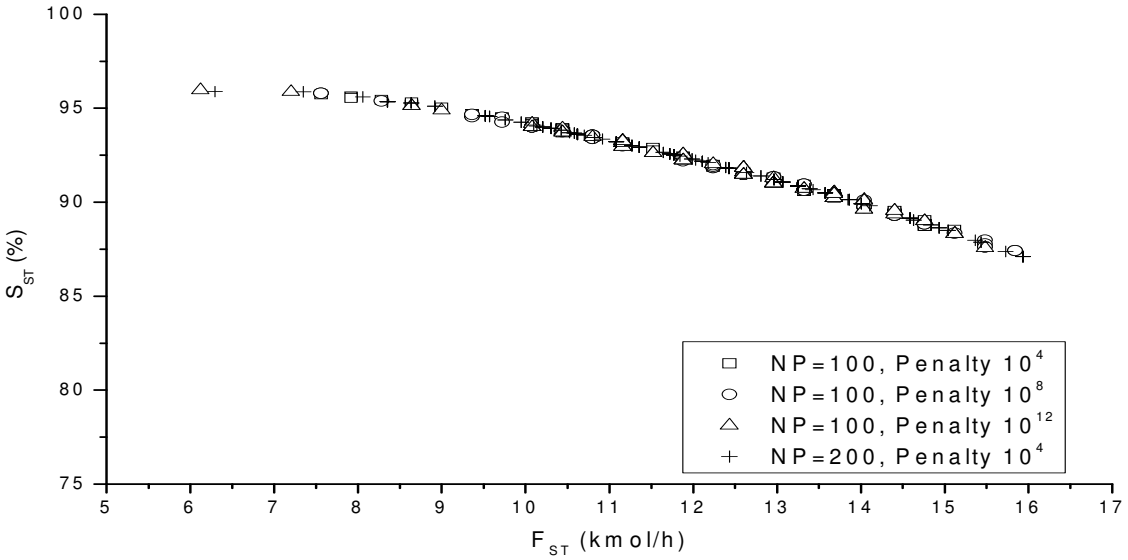

Fig. 5.31 Effect of Penalty parameter and population size on the Pareto optimal solutions obtained using hybrid MODE algorithm

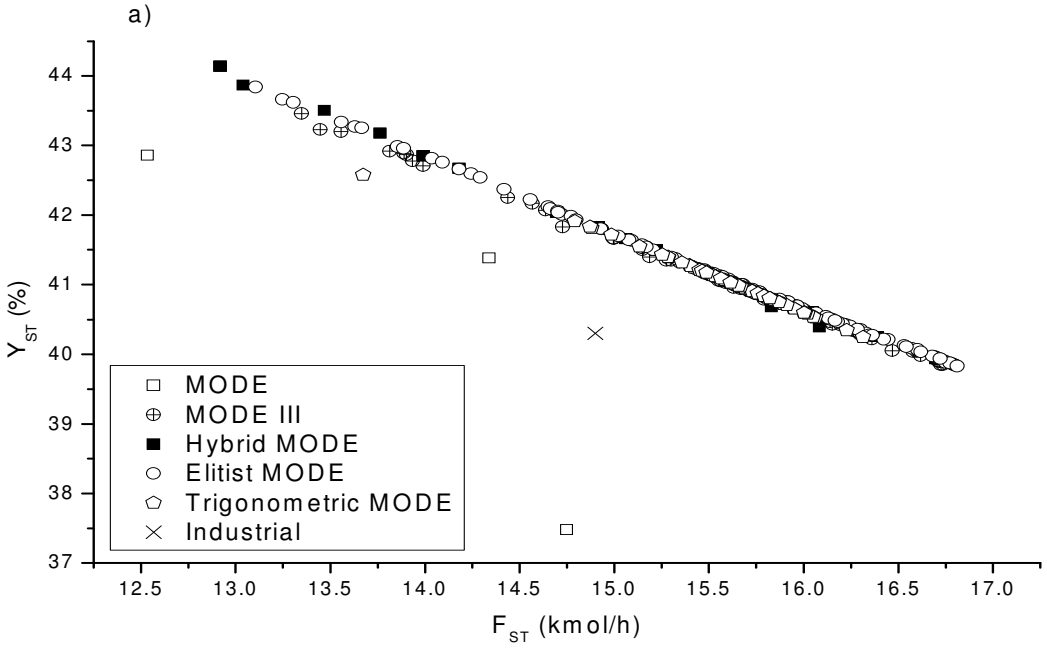

Fig. 5.32 (Contd….)

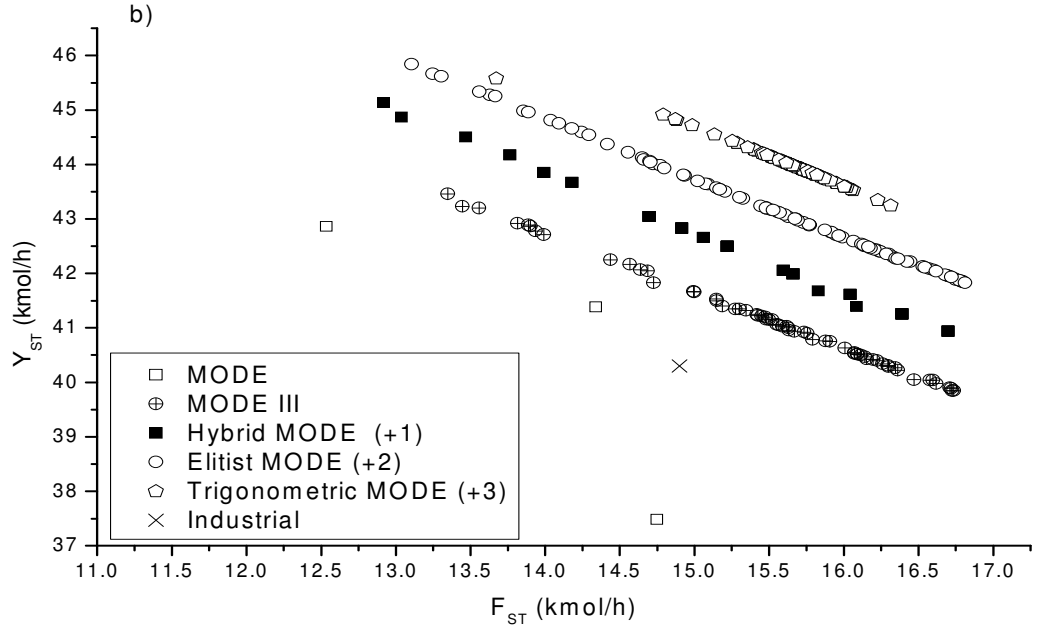

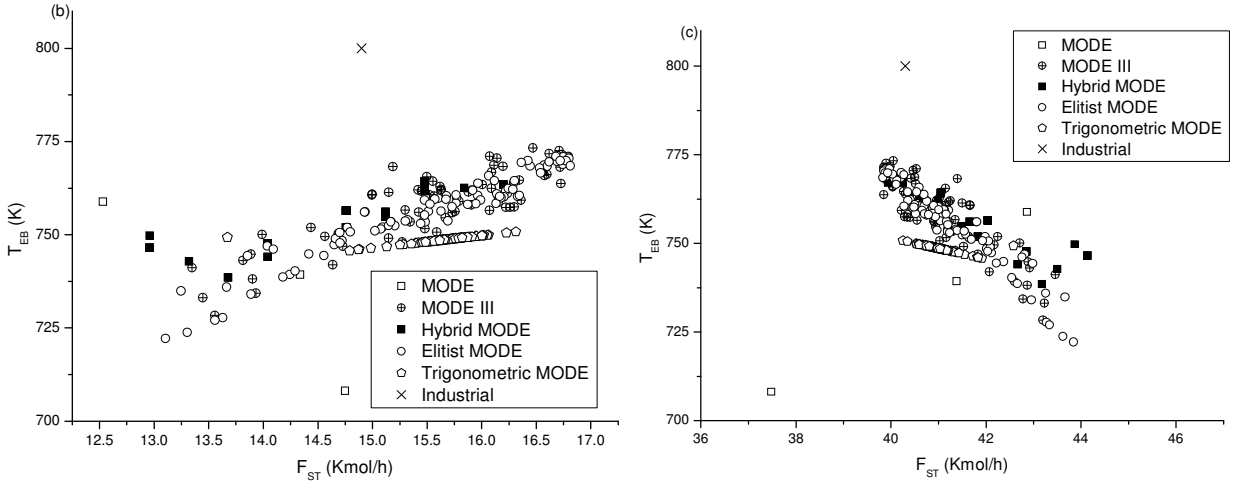

Fig. 5.32 (Contd….)

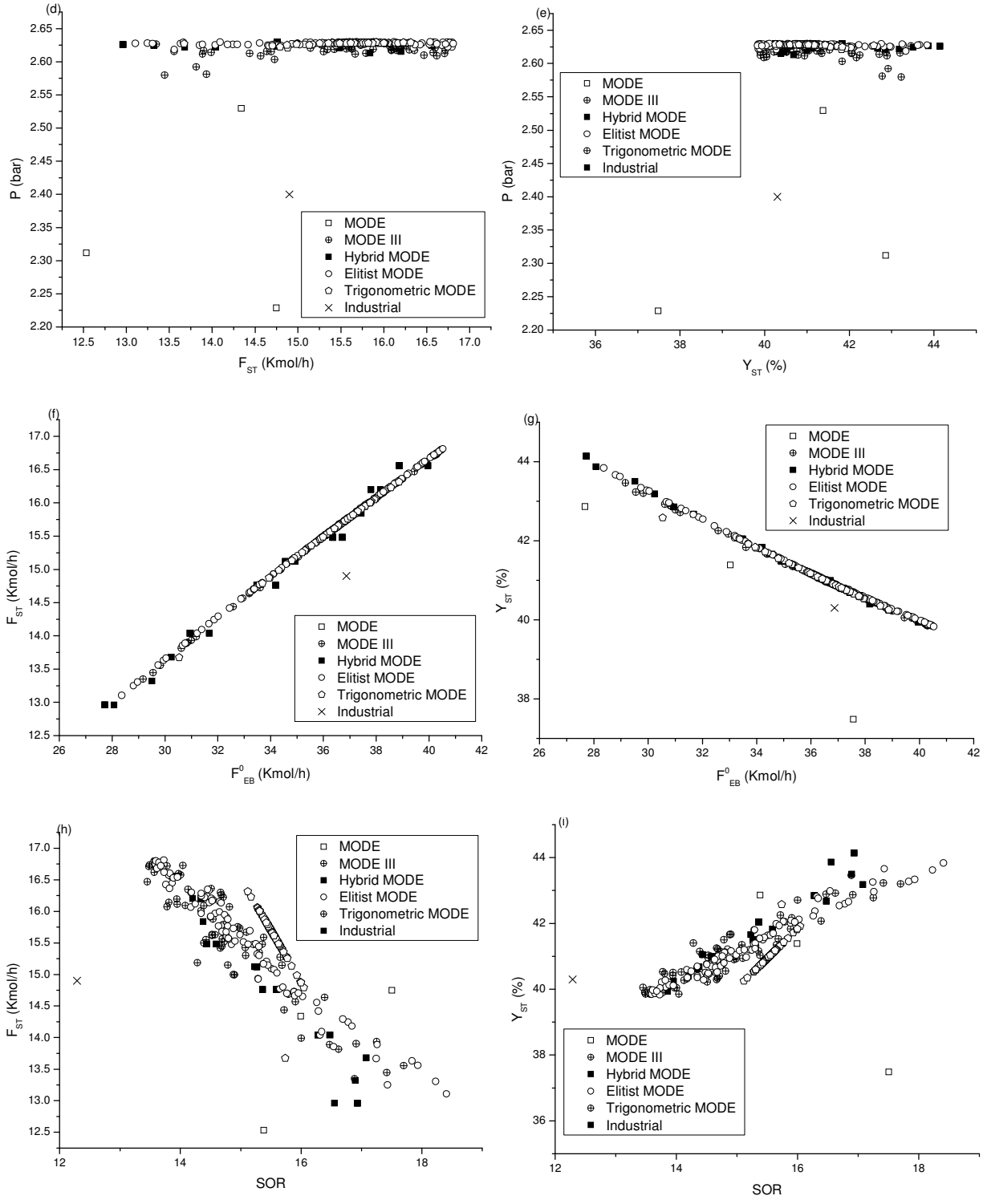

Fig. 5.32 (a) Pareto optimal solutions obtained after 300 generations using the strategies of MODE (b-i) corresponding decision variables plotted against one of the objectives

However, though the value of F_{EB}^{0} (decision variable) is same as that of the Pareto values, the Pareto front is away from the industrial point due to the effect of conflicting effect of temperature and *SOR* on the said objectives. Therefore an optimum and judicious compromise of all the conflicting decision variables is important in such industrial multi-objective optimization studies.

5.2.1.5 Case-4: Simultaneous maximization of F_{ST}, S_{ST} and Y_{ST}

Three-objective optimization study is carried out by simultaneously maximizing F_{ST}, S_{ST} and Y_{ST}. The point corresponding to the best profit is taken from each of the case studies. The decision variables, objectives, concentration of unwanted byproducts and profit corresponding to these selected points along with those for the industrial point are shown in Table 5.9. The profit obtained for S_{ST} vs. Y_{ST} objectives (case-2) (using MODE III, hybrid MODE and NSGA) is lower than the profit of industrial operating point. The profit strongly depends on the amount of styrene produced. As the productivity of styrene is not one of the objectives in S_{ST} vs. Y_{ST} studies, the obtained best profit is lower than that of the industrial operating point. However, for the remaining cases (case-1, case-3 and case-4) (both two-objective and three-objective optimization studies), hybrid MODE resulted in a higher profit than that obtained with the industrial operating point using MODE III & NSGA algorithms. Unlike hybrid MODE and MODE III algorithms results, NSGA algorithm results show that the profit obtained during a three-objective optimization study is less than the industrial operating profit. An evolutionary multi-objective optimization algorithm usually results in a set of solutions (probably Pareto

front) in a single simulation run. The set of decision variables corresponding to these sets of solutions are also known. The decision maker can select any one particular solution from the Pareto front suitable to his/her requirements. Once the decision maker selects a point suitable to his/her need from the objective space, the corresponding decision variables may be obtained from the decision variable space. It is expected that if the mathematical model output matches with industrial data (along with satisfaction of constraints), the selected set of decision variables if adopted, may result in the desired values of objectives as selected by the decision maker.

5.2.1.6 Adiabatic and steam injected configurations

In this section, MOO of simultaneous optimization of three objectives namely, productivity, selectivity, and yield are considered using adiabatic and steam injected reactor configuration. In case of steam injected configuration, a part of steam is injected at the entrance of the reactor and the remaining half is added to a partway of reactor at a desired length. The schematic and discussion related to steam injected configuration is given in section 4.2.1. In this section MOO problem results obtained using elitist strategy of MODE algorithm are used to compare the adiabatic and steam injected reactor configuration.

Figs. 5.33a - 5.33c show the Pareto fronts obtained for case-1, case-2 and case-3 respectively using elitist MODE algorithm. As the steam is injected partway along the reactor length, two additional variables are involved in the steam injected reactor configuration. Due to proper utilization of the steam, this reactor configuration is supposed to give a better result as compared to an adiabatic reactor configuration.

Table 5.9 Summary of optimization case studies using MODE III, hybrid MODE and NSGA algorithms

Parameter	Industrial	MODE III (present study)				Hybrid MODE (present study)				NSGA (Yee et al., 2003)			
		F_{ST} vs. S_{ST}	S_{ST} vs. Y_{ST}	F_{ST} vs. Y_{ST}	3-Obj. Opt. Study	F_{ST} vs. S_{ST}	S_{ST} vs. Y_{ST}	F_{ST} vs. Y_{ST}	3-Obj. Opt. Study	F_{ST} vs. S_{ST}	S_{ST} vs. Y_{ST}	F_{ST} vs. Y_{ST}	3-Obj. Opt. Study
F_{ST} (kmol/h)	14.9	11.91	12.38	16.73	14.47	15.68	12.26	16.64	16.41	15.01	10.89	14.48	13.09
S_{ST} (%)	85.15	87.88	86.80	84.75	88.24	87.56	87.35	84.89	86.14	87.51	88.83	84.70	88.18
Y_{ST} (%)	40.30	40.60	42.23	39.84	36.52	37.55	41.83	39.97	39.10	35.26	39.47	40.80	38.23
T_{EB}	800.00	780.7	762.4	771.51	791.61	739.5	667.53	767.15	732.60	799.98	787.25	800.00	776.13
P (bar)	2.4	1.69	2.13	2.62	1.75	2.55	2.55	2.62	2.54	2.03	1.76	2.45	1.99
SOR (-)	12.29	14.35	15.07	13.49	11.35	14.20	19.91	13.86	16.03	10.94	12.54	12.47	13.16
F_{EB}^{0}	36.87	27.7	27.74	40.31	37.81	40.68	27.72	39.96	40.25	40.47	27.58	35.49	34.24
F_{BZ}	1.37	1.18	1.18	1.67	1.29	1.43	1.15	1.67	1.67	1.25	0.85	1.36	1.10
F_{TOL}(kmol/h)	1.20	1.36	1.58	2.20	1.53	1.68	1.51	2.16	1.84	0.90	0.82	1.25	0.66
Profit ($/h)	651	584	601	792	716	728	547	783	741	673	482	637	565

Figs. 5.33a - 5.33c show that an enhanced value of the selectivity (in case-1 and case-2 results), and enhanced values of the yield and the productivity (in case-3 results) are obtained using the steam injected reactor configuration as compared to an adiabatic rector configuration. Decision variables involved in the steam injected reactor configuration are plotted against Case-1 objectives and are shown through Figs. 5.33d - 5.33o. Figs. 5.33d - 5.33e show that the majority of the variables (temperature of ethyl benzene) approached an upper bound as compared to adiabatic configuration decision variables for (T_{EB}). Figs. 5.33f - 5.33g show that a lower pressure value is preferred for the steam injected reactor configuration. The major reaction being a reversible endothermic reaction, high temperature and low pressure are preferred for forward reaction, which resulted in higher selectivity values for some of the variables of the steam injected reactor configuration. As productivity is directly related to the feed flow rate, an upper bound on the initial flow rate of ethyl benzene is approached for both the reactor configurations (Figs. 5.33h - 5.33i). SOR variable range varies between 9.47 - 15.45 and 12.59 - 19.73 for the adiabatic and the steam injected reactor configuration respectively (Figs. 5.33j - 5.33k). These ranges of variables resulted in the productivity values varying between 9.47 & 15.45 kmol/h and 6.26 & 14.413 kmol/h for the adiabatic and the steam injected reactor configuration respectively. The selectivity values vary between 87.8 & 95.5 % and 89.28 & 96.15 % respectively for the adiabatic and the steam injected reactor configurations. Thus an upper bound of selectivity is achieved in case of steam injected configuration, while an upper bound of productivity is achieved in case of the adiabatic configuration. Figs. 5.33l - 5.33m and Figs. 5.33n - 5.33o show the variation of objectives, namely F_{ST} and the S_{ST}, with respect to the variation in the decision variable, δ (fraction of steam fed at the entrance), and λ (the location of steam

injection partway the reactor length) respectively, for the steam injected reactor configuration. All the decision variables approached the lower bound of δ. The remainder of the fraction is fed at λ fraction of the length of the reactor. The values of location of the second steam injection port vary in the ranges of 27 to 80% of the reactor length.

In the next sub-section the results obtained using several strategies of MODE algorithm on PET reactor are discussed.

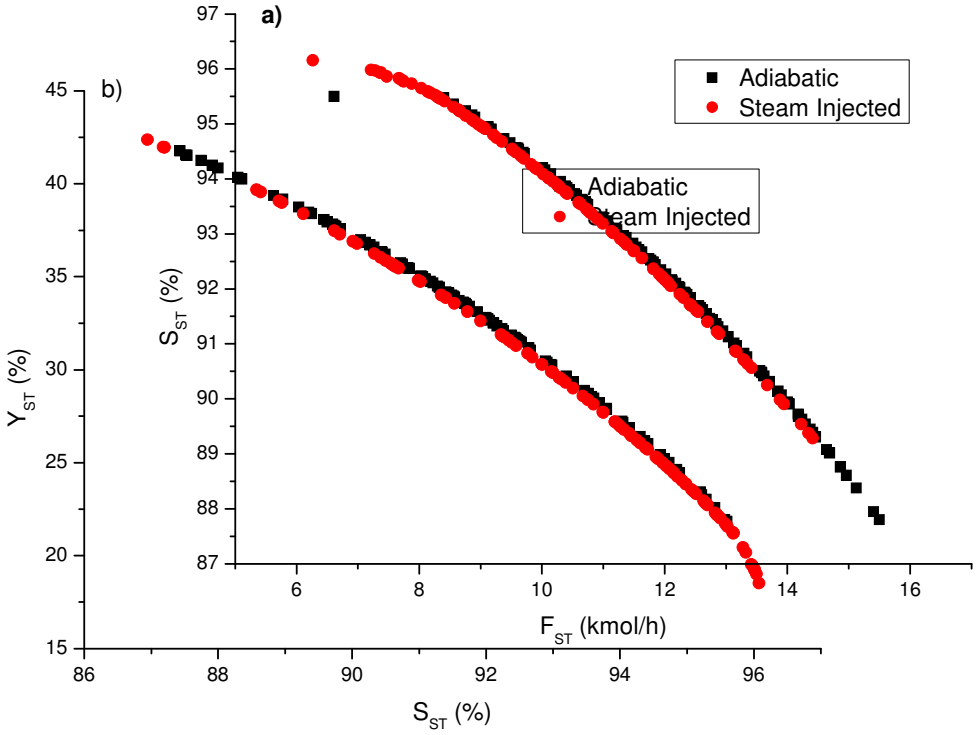

Fig. 5.33 (Contd…)

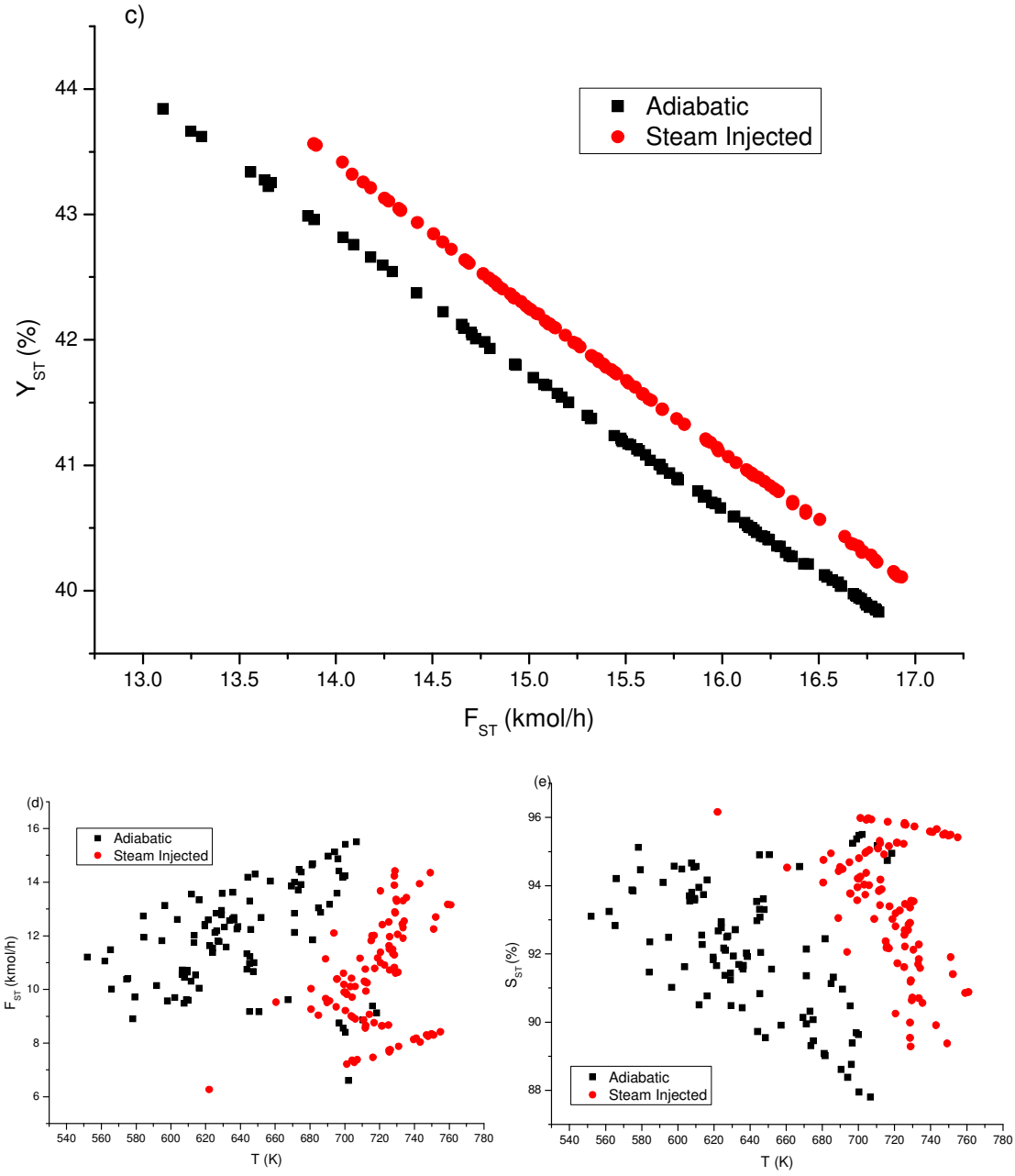

Fig. 5.33 (Contd…)

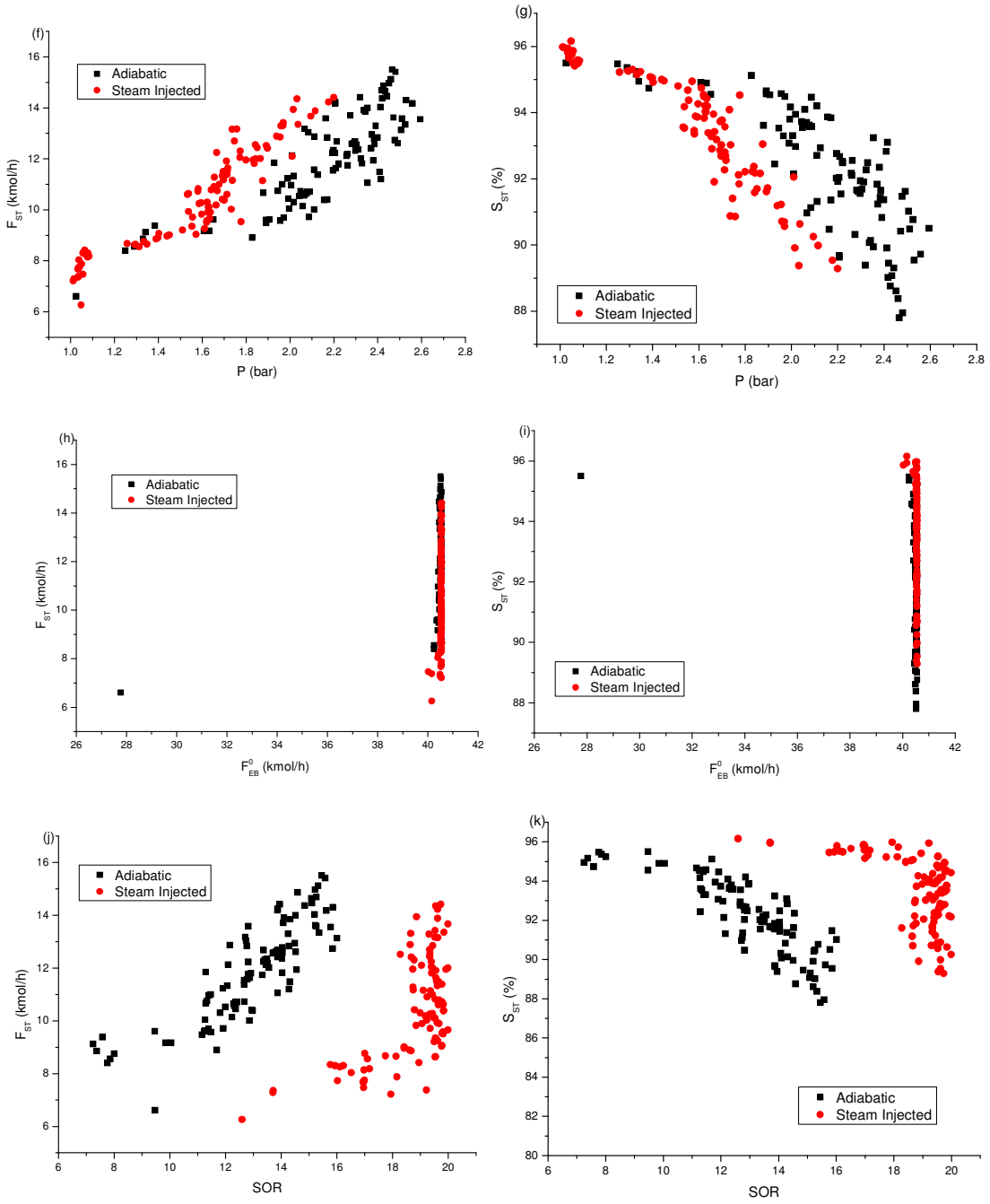

Fig. 5.33 (Contd…)

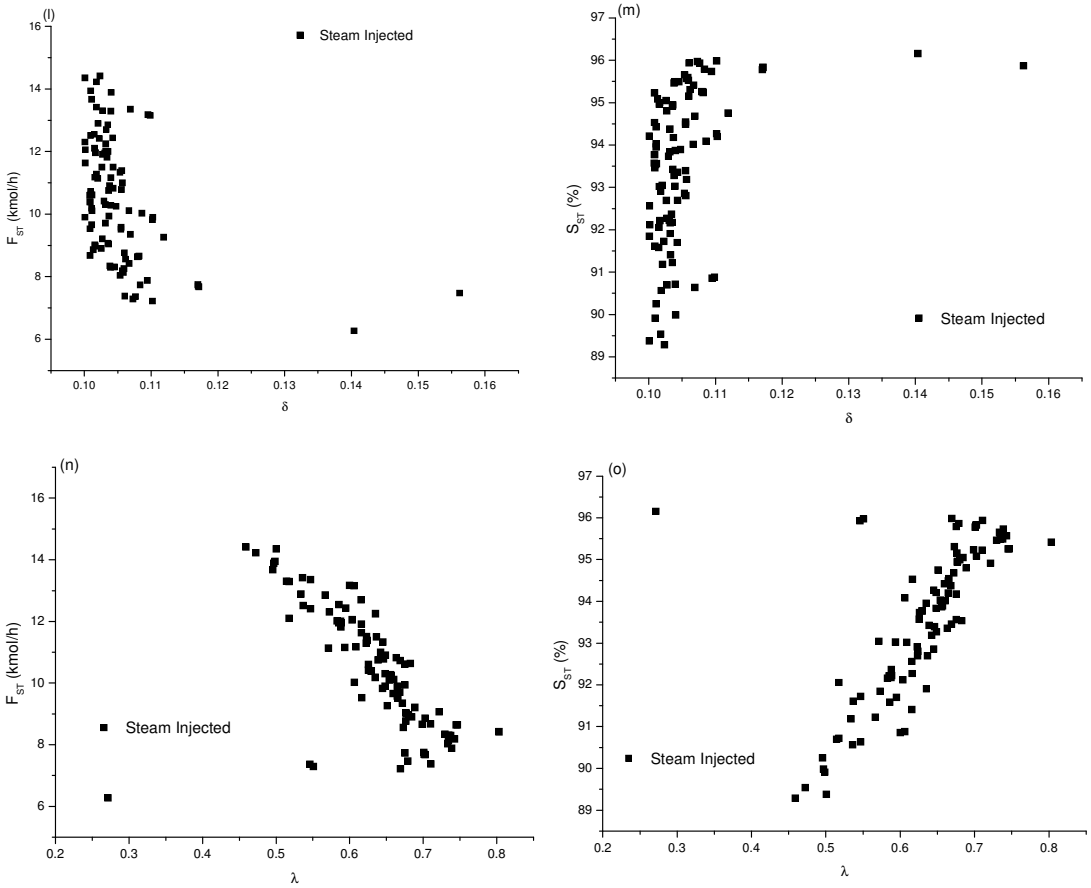

Fig. 5.33 Steam injected reactor configuration. Pareto fronts obtained for (a) case-1, (b) case-2, (c) case-3, (d-o) variation of case-1 objectives with respect to key decision variables using elitist MODE algorithm

5.2.2 Multi-objective optimization of polyethylene terephthalate (PET) reactor

The set of reaction schemes (Eqs. B1-B9 in Appendix B), the objective functions (Eq. 4.34), the constraints and the variables (as defined by Eqs. 4-35 – 4.42) are solved using ODE23s routine of Matlab (version 7.0) library. The model equations were solved on Pentium-IV, 2.4 GHz core 2 duo processor. The cpu time for MODE III, hybrid MODE, elitist MODE and trigonometric MODE algorithms for 300 generations is 1884.92, 59,973, 3553.34, and 5658.64 seconds respectively. Table B1 (Appendix B) shows the initial values of model parameters used in the present study. The values of parameters & properties, and the mathematical model output compared with industrial data are given in Tables B2-B3 (Appendix B) respectively. Simulation results obtained in the present study, such as concentration profiles along the length of the reactor of, the hydroxyl end group ($[E_g]$), the acid end group ($[E_a]$), ester linkages ([Z]), the vinyl end group ($[E_v]$), the diethylene glycol end group ($[E_{DEG}]$), the ethylene glycol ([EG]), water ([W]), and free DEG ([*DEG*]) are shown in Figs. 5.34a-5.34g. In simulation, the following values of parameters are used for multi-objective optimization: NP = 200, CR = 0.9, F = random (0, 1), and GenMax=200.

Five cases of two-objectives namely, simultaneous minimization of concentrations of acid end groups and the vinyl end groups are considered by varying the set of decision variables. The results obtained using MODE, MODE III, hybrid MODE, elitist MODE and the trigonometric MODE algorithms (developed in this study) are discussed by emphasizing on the ability of algorithms to produce the Pareto fronts and the effects of dominant decision variables on the conflicting set of objectives.

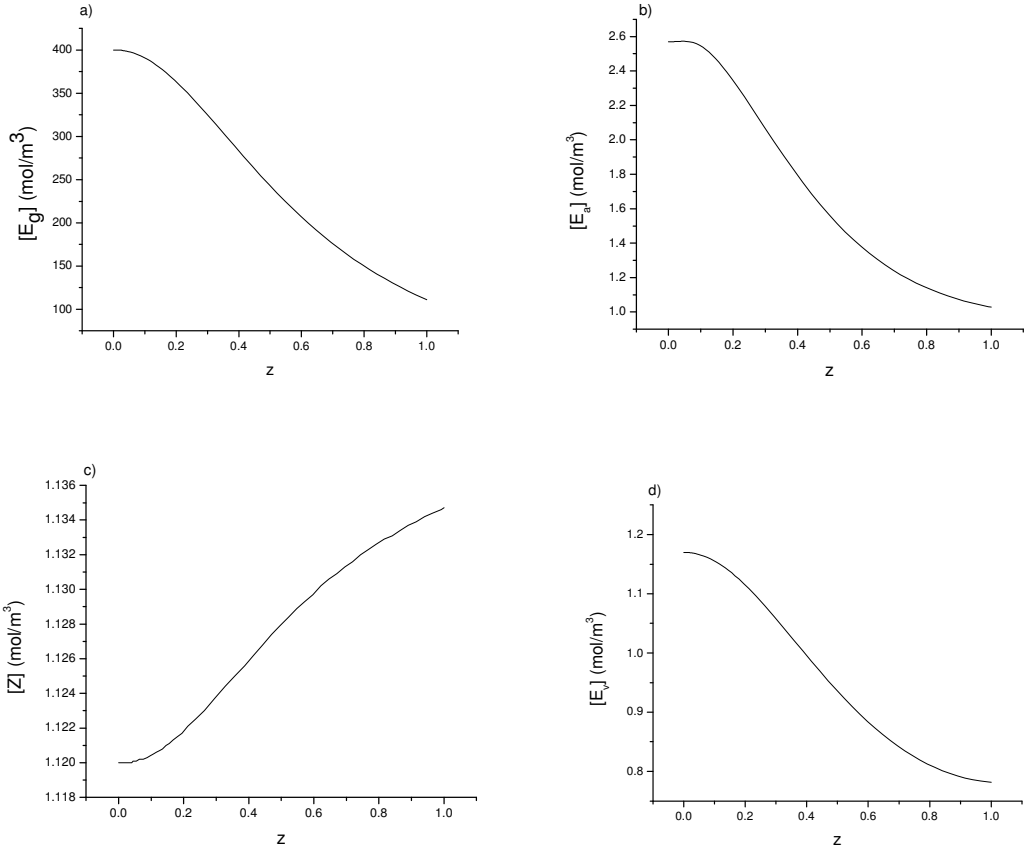

Fig. 5.34 (Contd….)

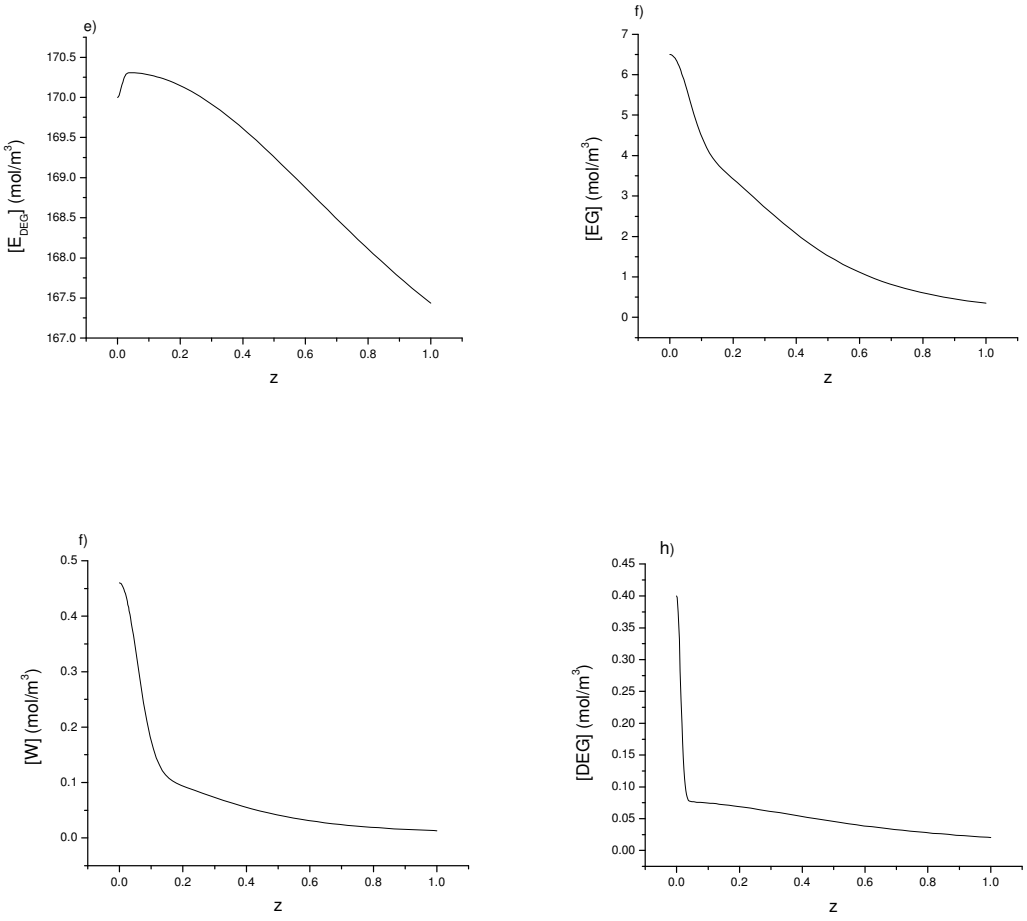

Fig. 5.34 Concentration profiles along the length of reactor: (a) Hydroxyl end group ([E_g]); (b) Acid end group ([E_a]); (c) Ester Linkages ([Z]); (d) Vinyl end group ([E_v]); (e) Diethylene glycol end group ([E_{DEG}]); (f) Ethylene glycol ([EG]); (g) Water ([W]) (h) Free DEG ([*DEG*])

5.2.2.1 Case-1: With T, P, θ^* and N^* as decision variables

Fig. 5.35 shows the Pareto optimal fronts obtained using the strategies of MODE algorithm for case-1. In this case, the optimization problem of simultaneous minimization of acid and vinyl end groups is solved using four decision variables namely, temperature, pressure, dimensionless time and the dimensionless agitator speed. In the earlier studies, Bhaskar et al. (2001) and Babu et al., (2007b), it was observed that the NSGA algorithm converged to a single optimal point. But MODE algorithm was able to give sufficient number of Pareto optimal points (9 points in this case) against the single point obtained using NSGA code. In this study, newly developed strategies are used to obtain the set of non-dominated solutions for PET reactor. Fig. 5.35 shows the quality of Pareto fronts obtained using these strategies of MODE algorithm. MODE algorithm resulted in local Pareto fronts as compared to the Pareto fronts obtained using MODE II, hybrid MODE, elitist MODE and the trigonometric MODE. The solutions obtained using MODE III, hybrid MODE, elitist MODE and trigonometric MODE algorithms lie on the same front. However the diversity and range of solutions vary. The Pareto fronts obtained using MODE III, hybrid MODE and elitist MODE algorithms are well spread with uniform diversity which covers a wide range of objective function values against that obtained using trigonometric MODE algorithm. It is interesting to note that NSGA study resulted in a single optimum point for the same problem, when same set of decision variables and constraints were used. However, for a min-min type of problem, through it seems that NSGA resulted in a better point, but it is more important in any MOO study to generate large number of wide spread points, which can serve the purpose of decision making. NSGA algorithm resulted in the lowest value in terms of vinyl end group objective function as compared to the solutions obtained using strategies of MODE.

However, NSGA algorithm could not capture the range of solutions in terms of another objective, i.e., the minimization of acid end group. Each point on Fig. 5.35a corresponds to a set of decision variables as given in Figs. 5.35b - 5.35i. Figs. 5.35a - 5.35b show that hybrid MODE and MODE III algorithms approached the lower bound of pressure (P = 0.4 mm Hg), whereas the objective function values obtained using elitist strategy of MODE algorithm varies with pressure. The scattered solutions (values of decision variable, P) are obtained when trigonometric MODE algorithm is used. A lower bound of decision variable, T is approached. As both the reactions (B2 & B9 in Appendix B) are degradation reactions, an increase in the temperature increases the production of $E_{a,out}$ and $E_{v,out}$, and hence a lower bound of temperature is approached. The decision variable θ^* nearly attains a constant value of 1.06. However slight scattered set of values are obtained using MODE III algorithms (as shown in Figs. 5.35f - 5.35g). The trend of solutions obtained using elitist and MODE II strategy of MODE show that the concentration of acid end group decreases with an increase in the speed of agitation, while the concentration of vinyl end groups increases with increasing the speed of agitation (Figs. 5.35h -5.35i).

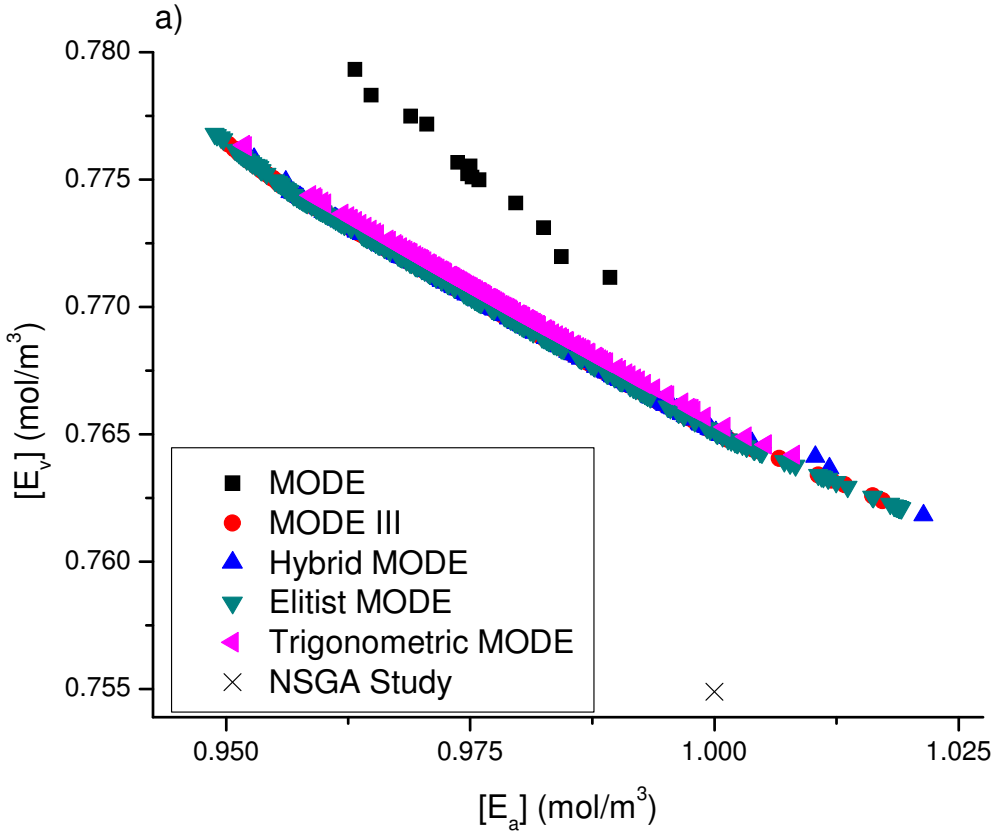

Fig. 5.35 (Contd…)

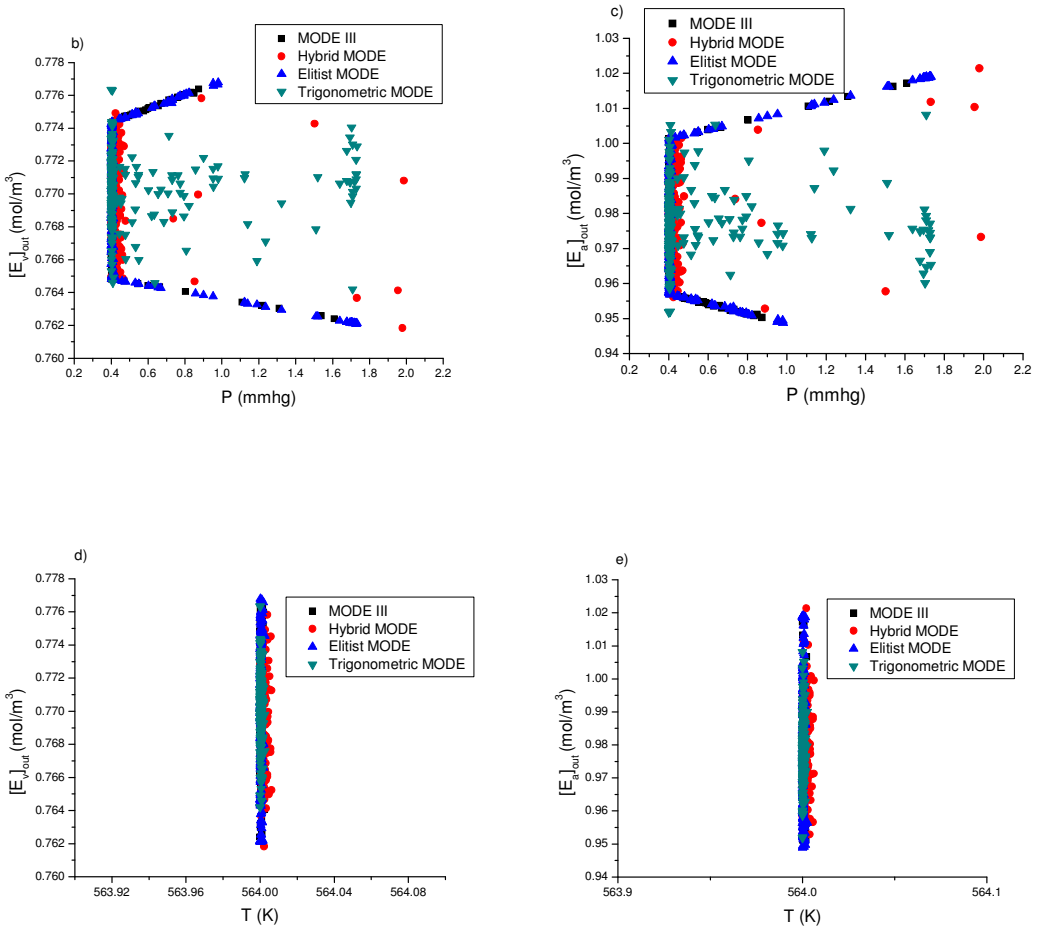

Fig. 5.35 (Contd…)

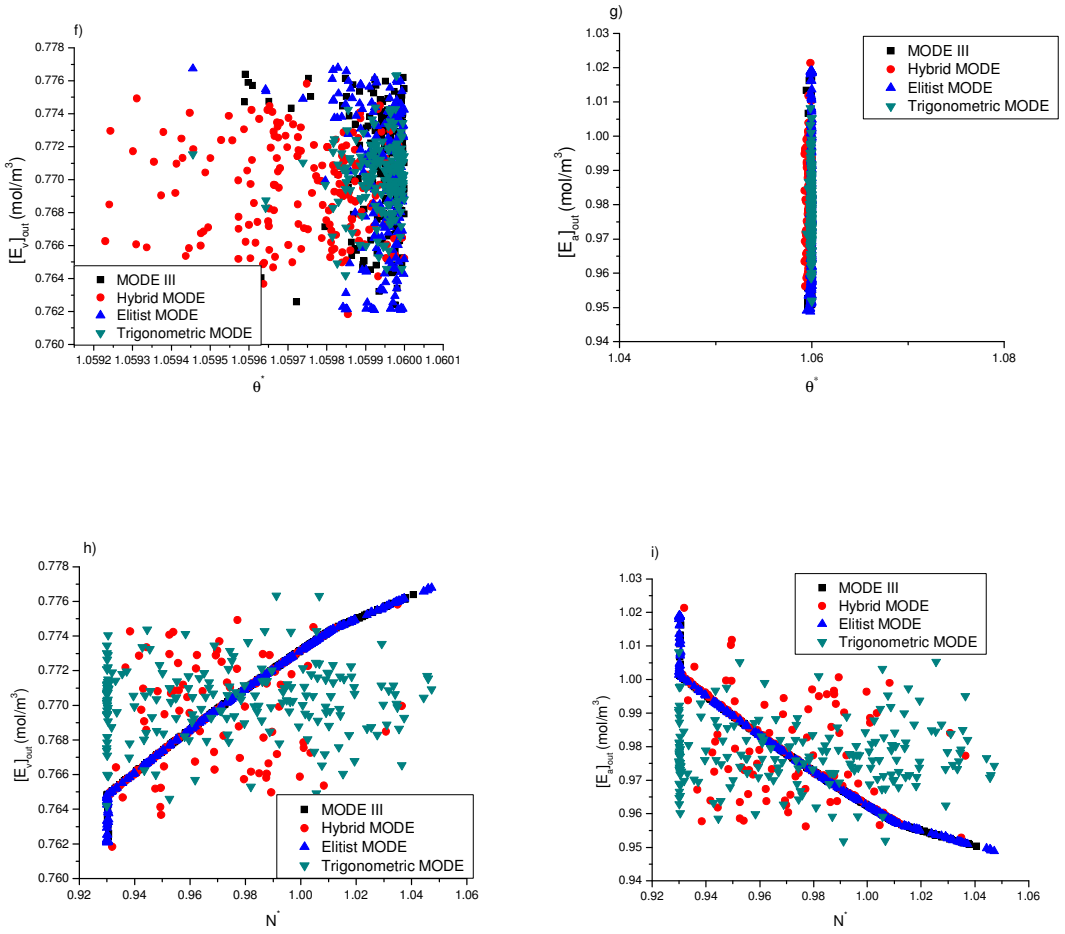

Fig. 5.35 (a) Pareto front obtained for Case-1 using the strategies of MODE, (b-i) decision variables plotted against the respective objectives

5.2.2.2 Case-2: With P, θ and N^* as the decision variables*

It is interesting to note that the value of the decision variable temperature, *T*, remains constant and it is at its lower bound (value of 564.02 K) (Figs. 5.35d and 5.35e). As temperature does not cause any conflict among the objectives, the decision variable temperature, *T*, is removed from the multi-objective optimization problem.

Fig. 5.36a shows the Pareto front obtained using the strategies of MODE algorithm developed in the present study. Fig. 5.36a shows the Pareto front obtained using a constant value of decision variable *T* as 568 K. From the results obtained in case-1, it is observed that a lower value of *T* is approached for meeting both the objectives simultaneously. However, in the industrial practice, it is possible that the temperature may shoot up by few degrees. Under these circumstances, in order to achieve both the objectives values, it becomes important to control the process by controlling other decision variables. Simulations are carried out by increasing the value of temperature to a value of 568 K. MODE algorithm could not result in any feasible solution when *T* was set to 568 K. However, other strategies of MODE resulted in a set of solutions as shown in Fig. 5.36a. The Pareto fronts obtained using the strategies of MODE with two different values of temperatures (i.e., *T* = 564 and *T* = 568) are shown on the same Fig. (i.e., Fig. 5.36b). It shows that by increasing the temperature, the decision maker has to sacrifice for both the objectives under consideration. This is because the degradation reactions (B2 and B9) are more favourable at high temperatures, and thus tend to increase the concentrations of acid and vinyl end groups, which is evident from Fig. 5.36b.

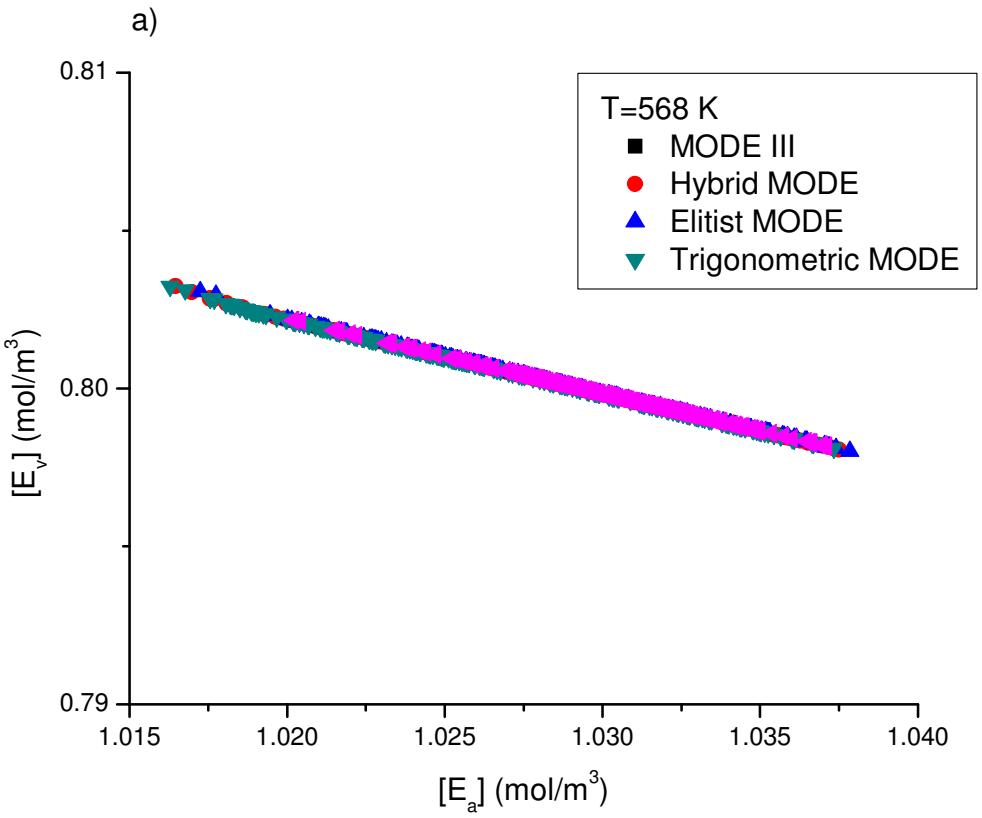

Fig. 5.36 (Contd…)

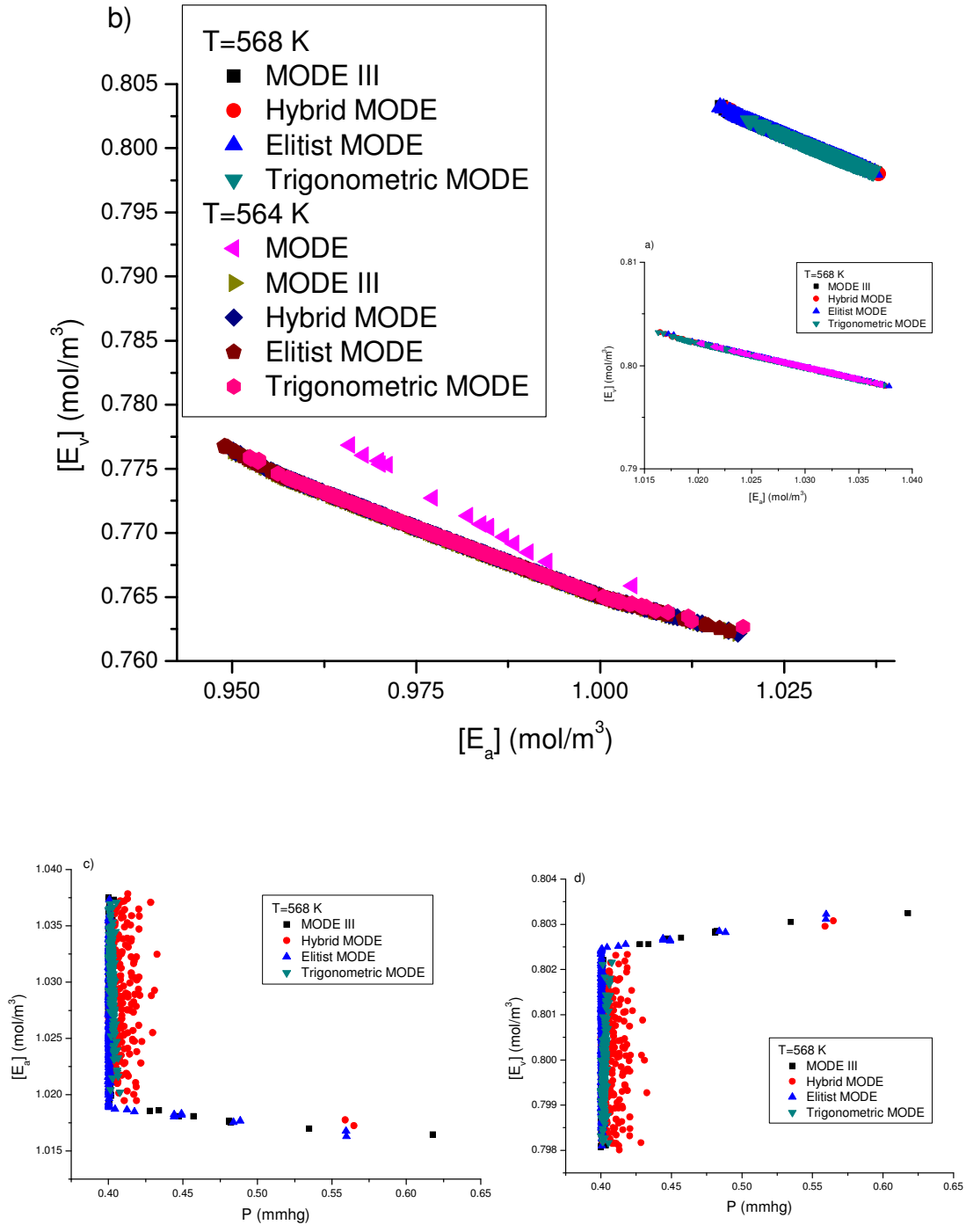

Fig. 5.36 (Contd…)

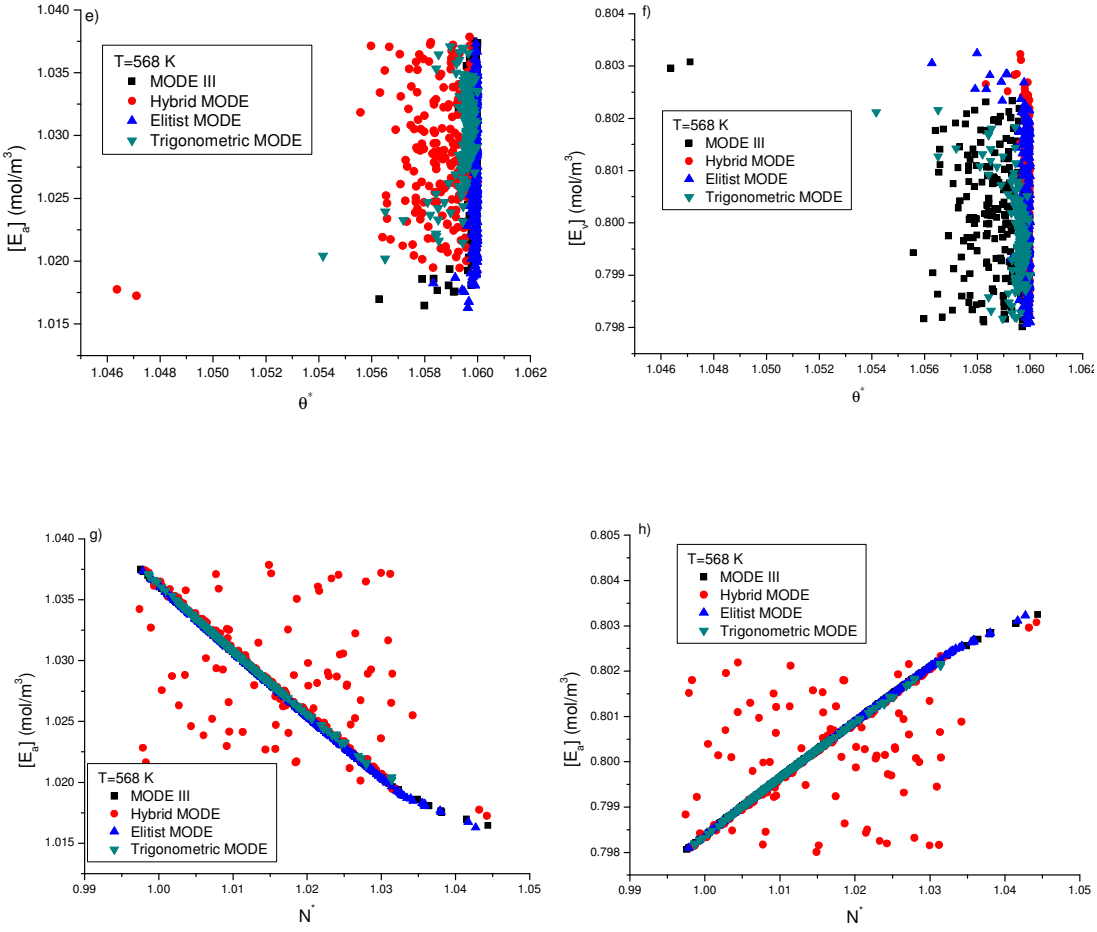

Fig. 5.36 Pareto fronts obtained for Case-2 results using the strategies of MODE, (a) Pareto fronts obtained using T=568 K, (b) Pareto fronts obtained using *T* = 564 K and *T* = 568 K, (c-h) decision variables plotted against the respective objectives

When the temperature of reactor is kept constant at a higher value, the acid and vinyl end groups are independent of pressure of the reactor and the time of operation (as nearly constant values are approached). However, in an earlier study using MODE algorithm by Babu et al., 2007b, the objectives were dependent on the value of variable, dimensionless time. Thus, if the temperature of reactor is increased, the dimensionless time turns out to be a independent variable. Thus, the decision variable, temperature has more dominant effect than the variable dimensionless time, on the set of objectives considered in this study. In case-1, all the strategies of MODE algorithm resulted in a lower bound of temperature, i.e., T = 564. This is equivalent to the problem considered in Case-1, with T = 564. Hence, to avoid the repetition, the results obtained using T=564 are not discussed here. Unlike the results obtained using NSGA (where a single point solution was obtained), and the results obtained using MODE [with T = 564] (Babu et al., 2007b), the results obtained in this study show that, at higher temperature, the values of the objective function depend upon the speed of agitation.

*5.2.2.3 Case-3: With θ^* and N*as the decision variables*

In order to a gain further understanding of the problem and to check the robustness of the code developed, the modified multi-objective optimization is used in case-3. As θ^* and N^* are the main decision variables that are responsible for producing Pareto optimal front, we tried to simplify the formulation with only these two as the decision variables. For pressure, a reference value of 2.0 mm Hg is used during the simulations, and for the temperature the optimal value of 564.02 K from case-1 is chosen.

Since both the variables θ^* and N^*, which are responsible for producing the Pareto front, are considered, the algorithm should give Pareto set of solutions. However, at a higher value of temperature, MODE and MODE III strategies could not produce even a single feasible solution. This is because; a lower bound of pressure is approached when a high value of temperature is used (from Case-2 results). Thus at a high temperature, i.e., T = 568 K, if high pressure value is used, the set of equally good solutions or the Pareto set cannot be obtained. However, if the value of temperature is lowered to T = 564 K (or if the pressure is lowered [at high temperatures (i.e., T = 568) as discussed in case-2 results], the Pareto front is obtained. However, hybrid MODE, elitist MODE and the trigonometric MODE algorithms are able to produce the Pareto set of solutions even when a high value of temperature is selected for case-3 study. The reasons, for obtaining a smooth and well diverse Pareto front, are (1) improved local and global search in case of hybrid MODE algorithm, (2) improved selection strategy and preserving the elite population members in case of elitist MODE, and (3) an improved local search mutation approach in case of trigonometric MODE algorithm. The Pareto front obtained for case-3 using T = 564 K, using the strategies of MODE algorithm after 200 generations is shown in Fig. 5.37a. As a reference value of pressure (2 mm Hg) is considered in this case, the Pareto front is slightly above than, that reported in case-1 and -2. This also underlines the fact that the reference value of pressure is not the optimal value for an operation of a PET reactor. The trend followed by the two decision variables considered, is same as seen in the previous cases (case-1 and -2) (Figs. 5.37b - 5.37e). However, the elitist MODE algorithm approached an upper bound of decision variable, N^*, as shown in Figs. 5.37d - 5.37e.

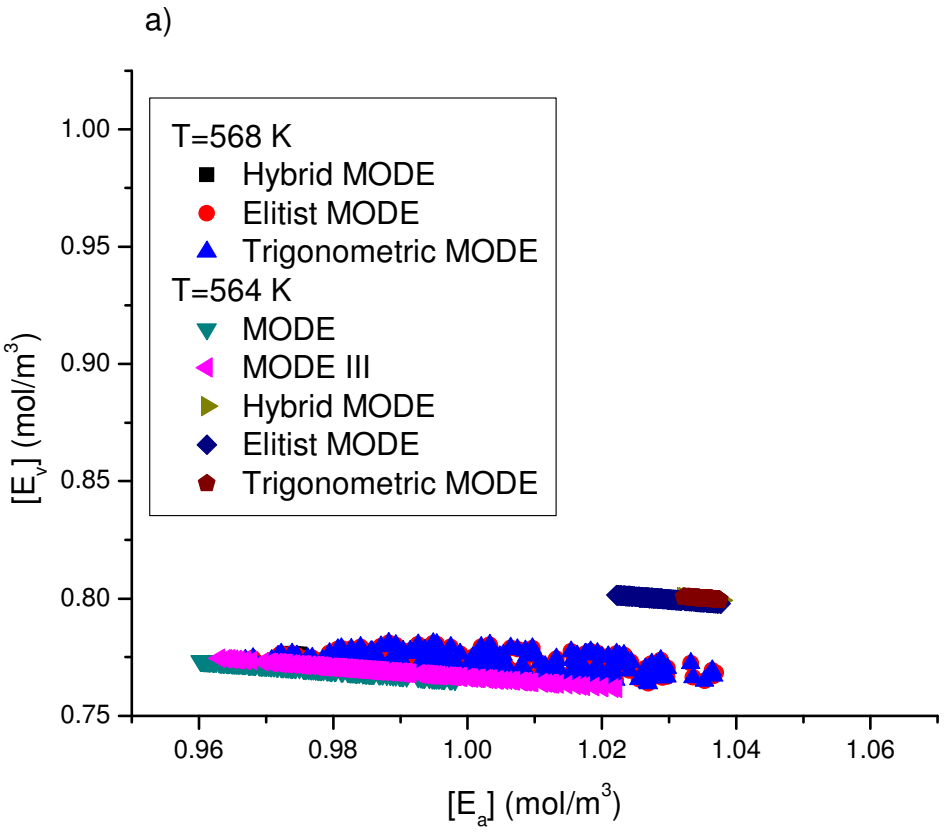

Fig. 5.37 (Contd….)

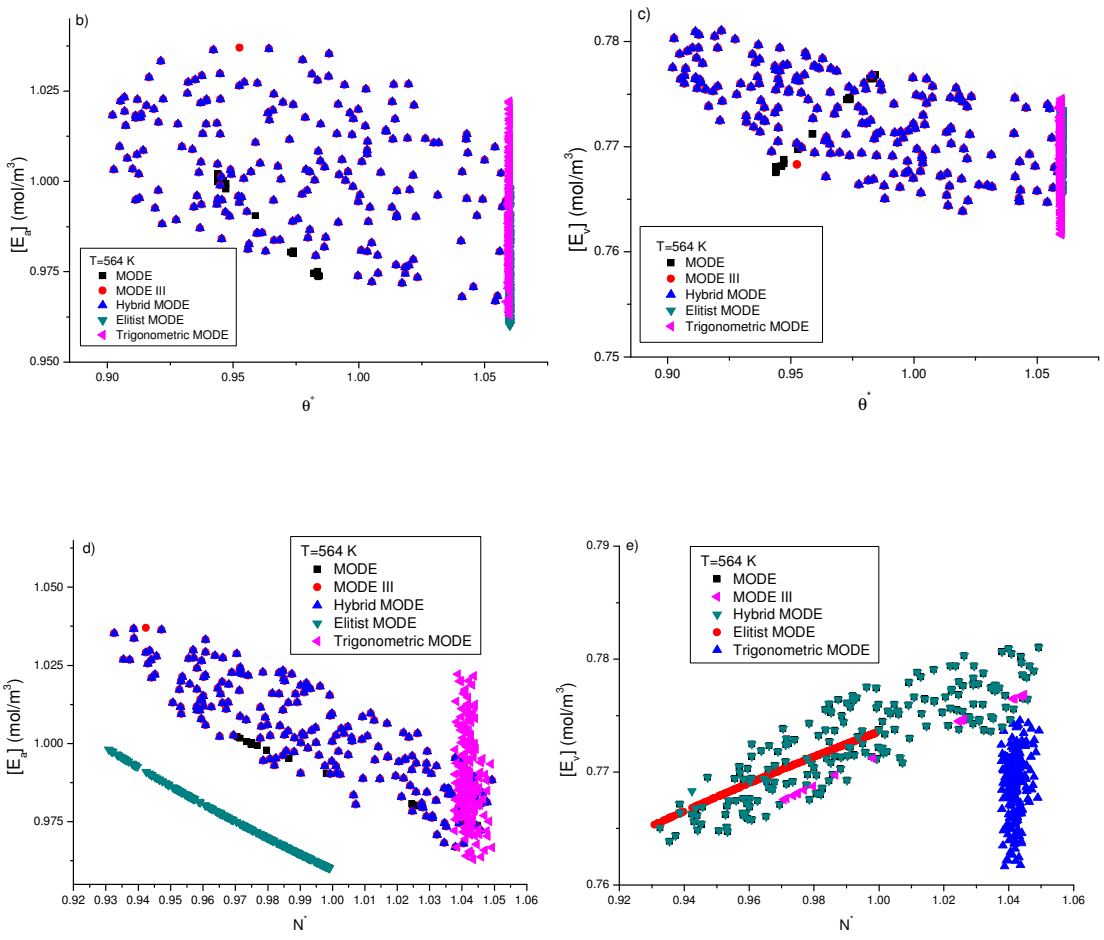

Fig. 5.37 Pareto fronts obtained for Case-3 results using the strategies of MODE, (a) Pareto fronts obtained using T = 568 K, and T = 564 K, (b-e) decision variables plotted against the respective objectives

5.2.2.4 Case-4: Only with P as the decision variable

The importance of θ^* and N^* in producing a Pareto set of solutions is highlighted in this case. Here, all the values except pressure, are taken to be constant. The bounds on the pressure are kept same, while an optimal value of temperature is taken (564.02 K), and reference values are taken for θ^* and N^* (See Table B3 in Appendix B). The reason for considering only pressure as the decision variable is to study, how it affects the operation of PET reactor when other variables are considered constant. From cases -1 and -2, it is evident that pressure plays an important role in the optimization as its effect on the objective function is scattered and not the constant one. In the present MOO case, only P is allowed to vary.

Fig. 5.38a shows the Pareto fronts obtained using the strategies of MODE. None of the algorithms resulted in any feasible set of solutions, when T is held constant to a value of 568 K. However, a smooth Pareto front is obtained when T is allowed to reduce to a lower value and kept constant at a value of T = 564 K. The results are found to be interesting. Fig 5.38a shows that when θ^* and N^* are considered constant, there is no Pareto front, but a unique solution is obtained, when MODE algorithm is used. However, a smooth Pareto front is obtained using MODE II, hybrid MODE, elitist MODE and the trigonometric MODE. Also in case of results obtained when MODE algorithm is used, the values of pressure are found to be almost same, i.e., around 0.6 mm Hg and not scattered (Fig 5.38b). However, a uniform variation of pressure against the objectives is observed when, the improved strategies of MODE (developed in this study) are used (Figs. 5.38b - 5.38c). These results show that the effect of pressure is dependent on the speed of rotation of agitator. However, if the agitator speed is kept constant at a reference value, a single optimum value of pressure is obtained and not a scattered one, when MODE algorithm is used. Thus the

effect of pressure on producing Pareto front depends on the agitator speed, and there is no Pareto front produced using MODE algorithm when θ^* and N^* are constant. However, the values of the decision variable, P, corresponding to the solution on the Pareto front (Fig. 5.38a), varied between its range (0.4 – 2.0 mm Hg), when improved strategies of MODE algorithm is used. These results also show that the improvements made in the MODE algorithm resulted in a better set of solutions when industrial problem of MOO of PET reactor is reattempted to solve in this study.

5.2.2.5 Case-5: With T and P as the decision variables

The importance of reference time and reference speed values in producing a Pareto set of solutions is further stressed by considering only T and P as decision variables, and assuming a constant value for the decision variables θ^* and N^*. The results, as expected, produced a single optimal solution when MODE algorithm is used. There are no trade-off solutions seen, and a unique solution obtained using MODE algorithm as shown in Fig. 5.39a. The solution obtained in this case is slightly different from the one obtained in case-4. In addition, a constant temperature value of 565 K is obtained, and not 564.02 K, when MODE algorithm is used (Figs. 5.39b-5.39c). This discrepancy in the value of temperature is due to the inability of MODE algorithm to effectively search the equally good global optimum points. Fig. 5.39a, though, shows a single point solution in case of hybrid MODE algorithm, yet it is a set of solutions not visible due to the increased scale used on both the axes.

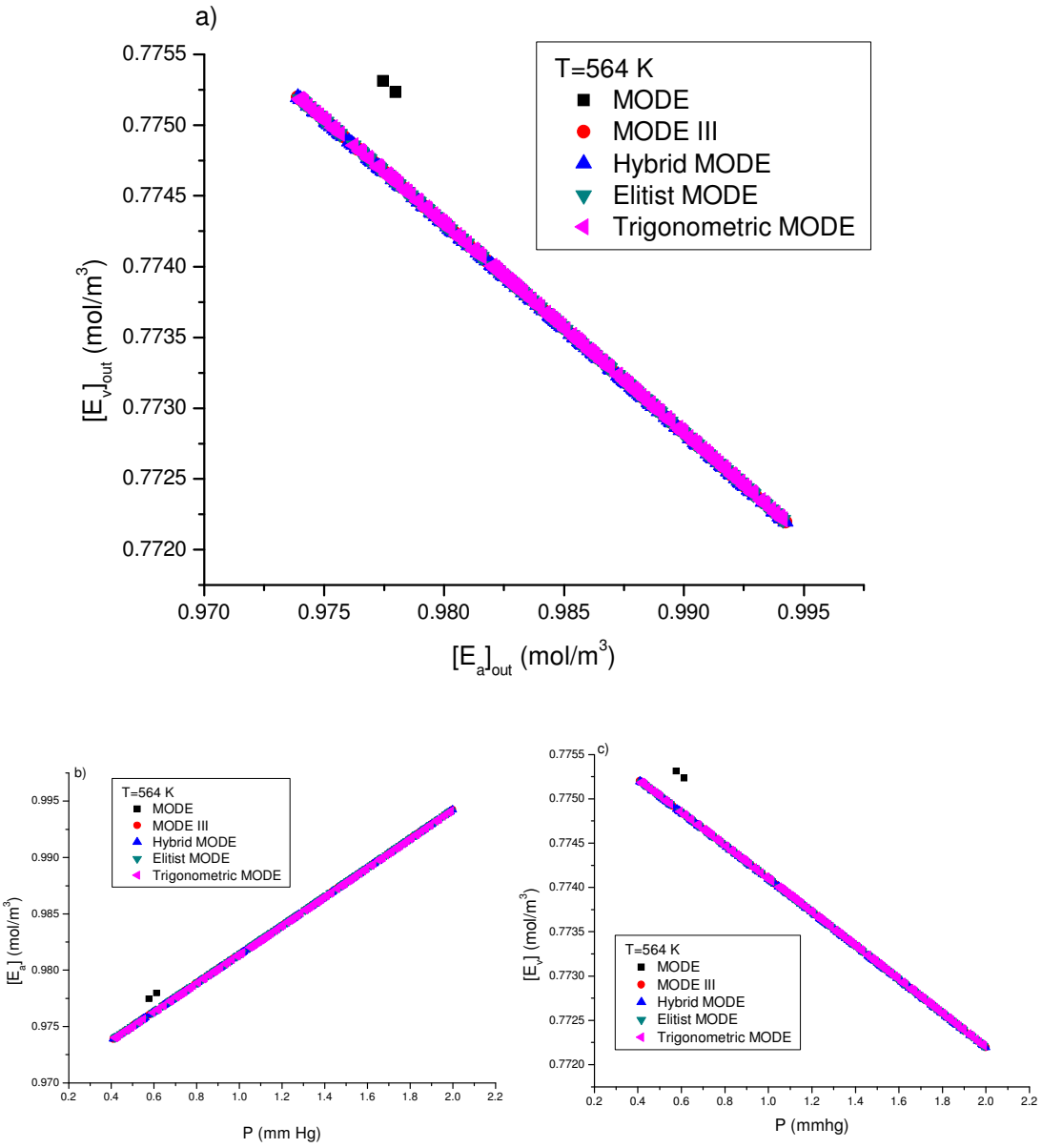

Fig. 5.38 (a) Pareto fronts obtained for Case-4 results using the strategies of MODE, (b-c) decision variable *P* plotted against the respective objectives

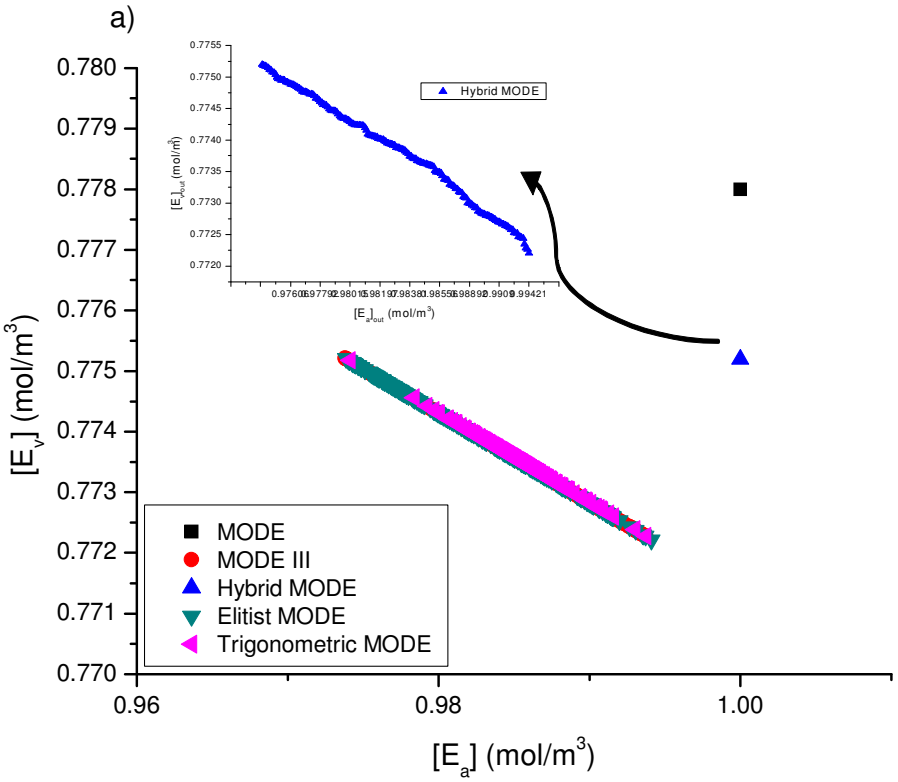

Fig. 5.39 (Contd…)

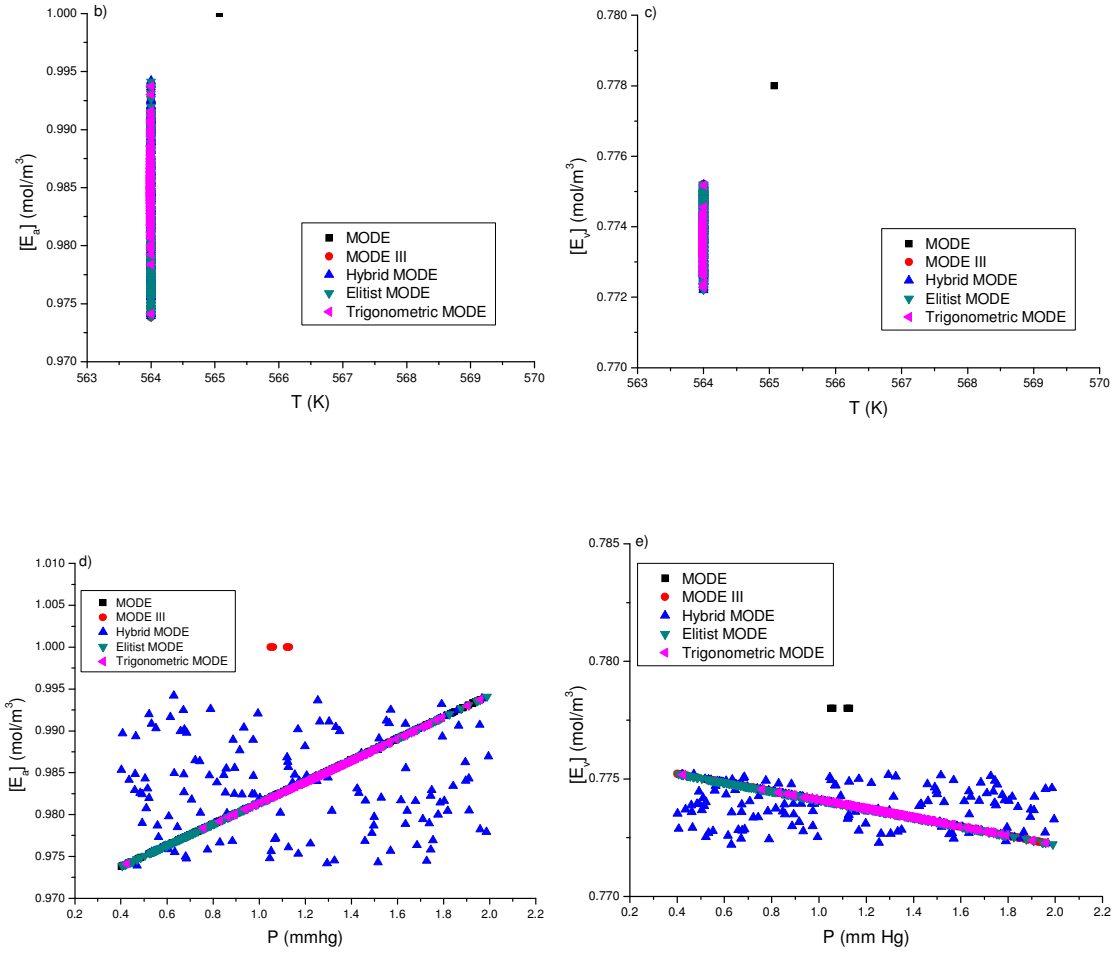

Fig. 5.39 (a) Pareto fronts obtained for Case-5 results using the strategies of MODE, (b-e) decision variables plotted against the respective objectives

The Pareto front obtained using hybrid MODE algorithm is shown as a snapshot in Fig. 5.39a itself. However, the Pareto front obtained using hybrid MODE, (though superior to that obtained when MODE algorithm is used), is a local Pareto front as compared to the other Pareto fronts obtained when MODE III, elitist and trigonometric strategy of MODE are used. Among the Pareto fronts obtained using MODE III, elitist and trigonometric MODE algorithms, the MODE III and elitist Pareto fronts are well diverse, as compared to the Pareto fronts obtained using the trigonometric MODE algorithm.

Figs. 5.39b -5.39c show the effect of temperature on the objective functions $E_{a,out}$ and $E_{v,out}$. The values are again found to be constant as in cases -3 and -4. Scattered points of decision variable, *P,* are obtained when MODE or hybrid MODE algorithms are used. This is because both the algorithms converged to a local region leading to a local Pareto front. However, a linear dependency of pressure on the values of objectives is obtained using MODE III, elitist- and the trigonometric-MODE algorithms. The results obtained in this section, prove that an improvement (MODE III, hybrid MODE, elitist MODE and trigonometric MODE algorithms) in an existing algorithm (MODE), resulted in providing a (perhaps) global Pareto front for the said industrial case study.

In the next sub-section (Sec. 5.2.3) results obtained in the present study on MOO of oxidation of *p*-xylene to produce purified terephthalic acid are discussed.

5.2.3 Multi-objective optimization of oxidation of *p*-xylene to purified terephthalic acid (PTA)

Fourth order Runge-Kutta method is used to solve the coupled differential equations of the model using ODE23 subroutine of Matlab (7.0). The model equations were solved on Pentium-IV, 2.4 GHz core 2 duo processor. The cpu time for MODE III, hybrid MODE, and trigonometric MODE algorithms for 50 generations is 684.09, 2629.063, and 332.90 seconds respectively.The values of key parameters of different MODE strategies used in this study are reported in Table 5.10. The trigonometric mutation probability is set to 0.5. As discussed in section 5.1.1, MODE algorithm requires a high number of initial population points. Also, as MODE algorithm could not produce any feasible solution with a population size of 600 for case-4, an initial population size of 1000 is used in the present study. The reference values of several variables considered in the study are shown in Table C4 (Appendix C). Fig. 5.40 shows the output of simulated results and typical concentration profiles for the liquid phase oxidation of *p*-xylene. Differential equations (Eqs. C1-C14) corresponding to series of oxidation reactions (see Eq. 2.8) are given in Appendix C. All the concentration terms of various species in terms of kinetic parameters for each step are obtained by solving the series of step reactions analytically. As the final product of interest is terephthalic acid (TA), its maximum yield can be obtained if 4-CBA concentration is optimum (minimum). Thus, *p*-toluic acid (intermediate) product concentration increases along with the final product (TA). This is evident from Fig. 5.40, where the TA concentration increases monotonically while 4-CBA concentration decreases with respect to time. It can also be inferred from, Fig. 5.40, that the formation of TA commences only after the formation of *p*-toluic acid. The oxidation process takes place in the reactor and crystallizer as well.

Table 5.10 Key parameter values of MODE and elitist MODE used in the present study

Algorithm	**NP**	**CR**	**F**	**MaxGen**
MODE	1000	0.9	Random (0,1)	50
MODE III	600	0.9	Random (0,1)	50
Hybrid MODE	600	0.9	Random (0,1)	50
Elitist MODE	600	0.9	Random (0,1)	50
Trigonometric MODE	600	0.9	Random (0,1)	50

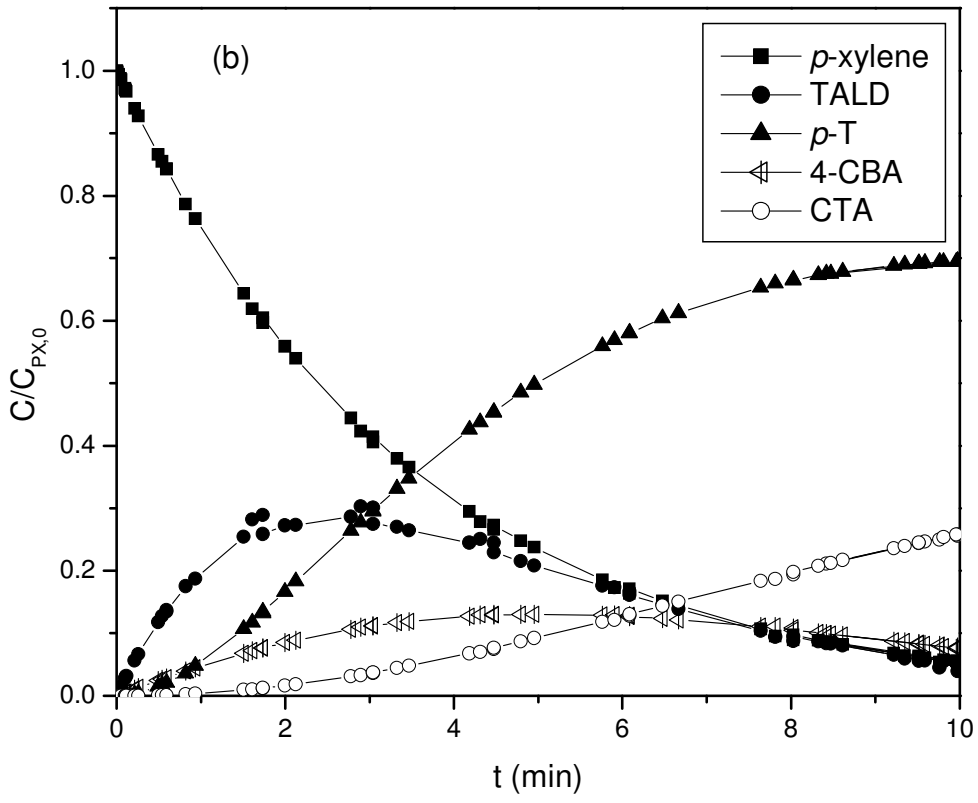

Fig. 5.40 Concentration profiles for liquid phase oxidation of *p*-xylene

Therefore, apart from the initial concentration of *p*-xylene, another factor which determines the conversion in the reactor is the residence time. The residence times of reactor and crystallizer are combined to get a total residence time of the process (Mu et al., 2004). In the following sections, different cases, (case-1- case-4 as defined in section 4.2.3) are discussed with respect to the industrial process parameters and corresponding objective function values.

5.2.3.1 Case-1: [C_0], and F_{FEED} as decision variables

Fig. 5.41a shows the Pareto optimal solutions obtained using MODE, MODE III, hybrid MODE and elitist MODE algorithms for case-1. Pareto solutions obtained from all the strategies of MODE algorithms lie on the same Pareto front (Fig. 5.41a). The results of Fig. 5.41a are re-plotted (for better clarity of Pareto fronts) in Fig. 5.41b with horizontal shift in value of abscissa by +100 in MODE III, +200 in Hybrid MODE, +300 in Elitist MODE and +400 in Trigonometric MODE data points. Though, the inference obtained from Fig. 5.41a and Fig. 5.41b show that all the algorithms converged to the same level, the distribution of solutions, the range of solutions and the number of final solution converged on the Pareto front are different. Table 5.11 gives the lower and upper bounds of objective functions for each individual case attained by the strategies of MODE algorithm developed in this study. Table 5.12 shows the number of points converged to the Pareto fronts (NOS) and percent of points converged (% CON) on the Pareto front using the individual strategy of MODE. Both MODE and elitist MODE algorithms are found to cover same range on the Pareto front. The value of all other decision variables is kept constant as shown in Table C4 (Appendix C) except for [C_0] and F_{FEED}. The plot of decision variable [C_0] against 4-CBA concentration is shown in Fig. 5.41c. Majority of the points lie on the upper bound of the decision variable in case of elitist MODE. However, a scattered set of variables are observed in the results obtained using all the strategies of MODE. The MODE and trigonometric MODE algorithms resulted in 173 and 170

numbers of points (NPS) converged on the Pareto front (17.3% and 28.3% of initial points) respectively. Fig. 5.41b shows that majority of the points obtained using MODE algorithms lie on the upper bound of [C_0]. In case of trigonometric MODE algorithm, most of the points of decision variable, [C_0], converged towards the middle portion of the bounds (i.e., 500-600 ppm). Hybrid MODE and Elitist MODE algorithms resulted in higher percent of initial points converged on the Pareto front as shown in Table 5.12.

5.2.3.2 Case-2: [C_0], $F_{FEED,}$ and W_{H_2O} as decision variables

In case-2, an additional decision variable, namely, water content, W_{H_2O}, is considered along with the set of decision variables considered in case-1. Fig. 5.42a shows the Pareto optimal front and the objective space. For a max-min type of problem, the Pareto front should lie on top left corner region. Fig. 5.42b shows the Pareto fronts obtained using the strategies of MODE and NSGA-II. All the algorithms captured the boundary of the feasible search space. Elitist MODE algorithm performs better than the other strategies of MODE in terms of distribution of solutions on the Pareto front. In order to check, whether the strategies of MODE algorithms converged to the global Pareto front or not, NSGA-II algorithm is also used for case-2. Fig. 5.42b shows that the Pareto solutions obtained in this study using MODE, MODE III, hybrid MODE, elitist MODE, trigonometric MODE and NSGA-II algorithms lie on same Pareto front.

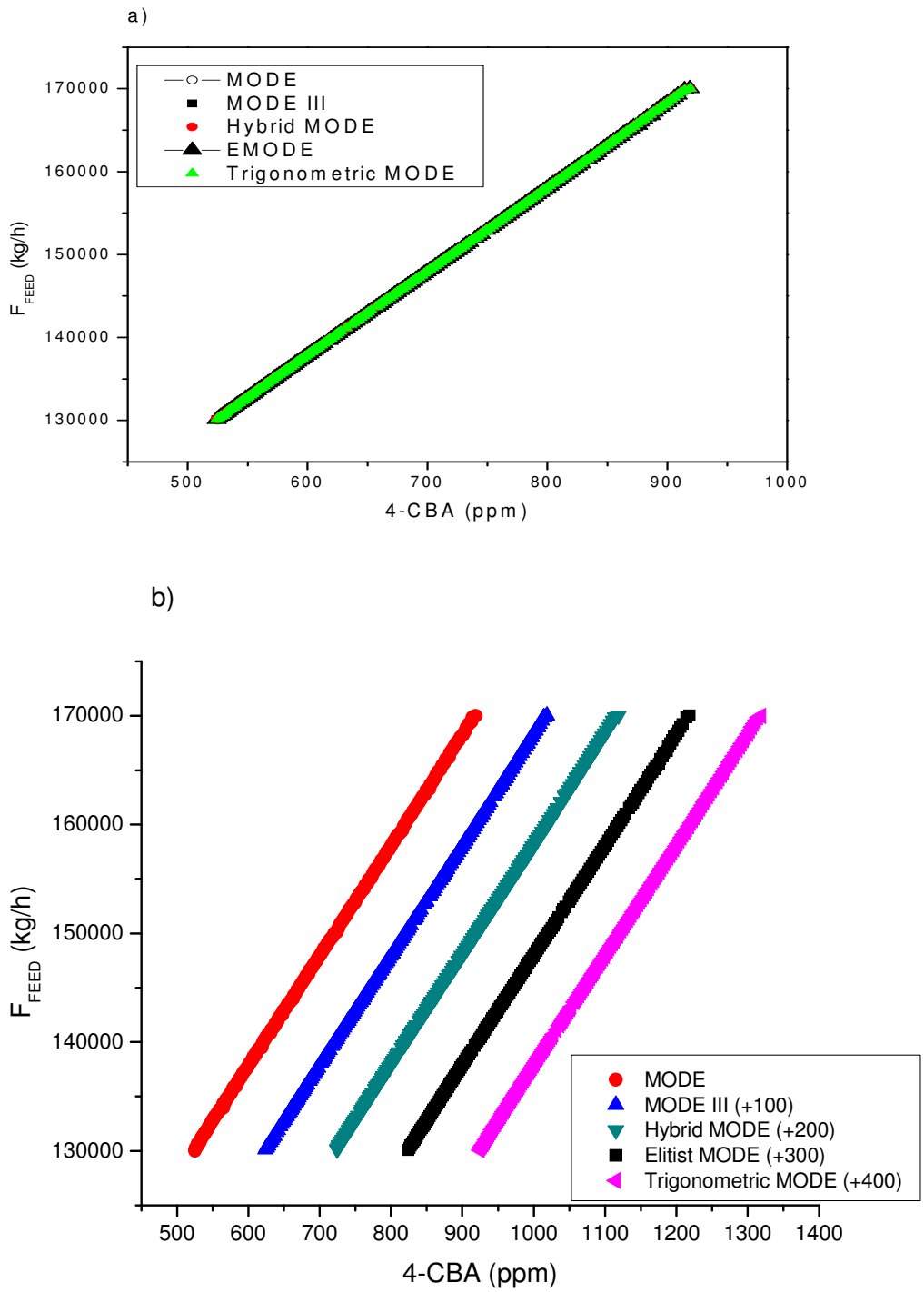

Fig. 5.41 (Contd….)

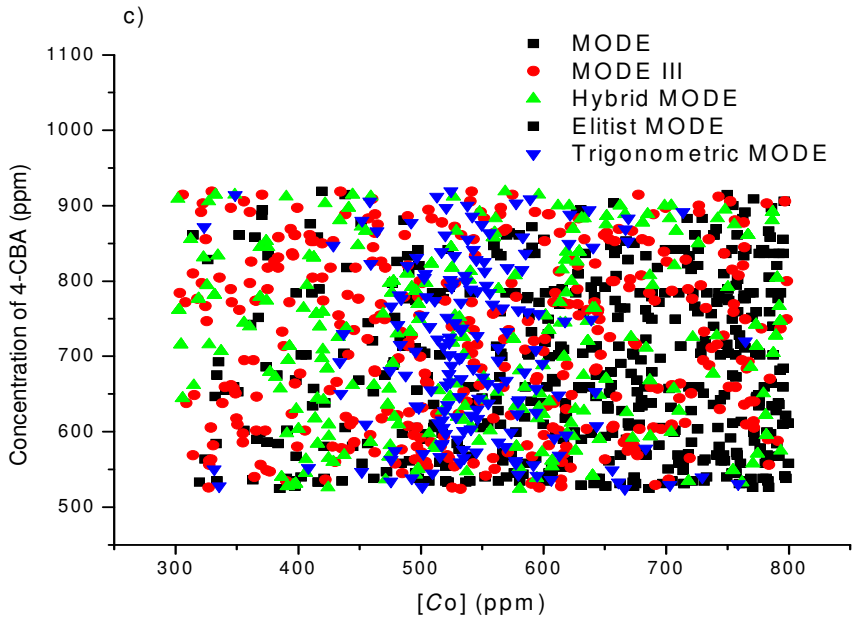

Fig. 5.41 Case-1: (a) Pareto optimal solutions using the strategies of MODE algorithm; (b) The results of Fig. 5.41a are re-plotted (for better clarity of Pareto fronts) in Fig. 5.41b with horizontal shift in value of abscissa by +100 in MODE III, +200 in Hybrid MODE, +3000 in Elitist MODE and +400 in Trigonometric MODE data points, (c) Effect of catalyst concentration [C_0] (decision variable) on the concentration of 4-CBA

Table 5.11 Lower and upper bound attained by objective functions in each individual case

Algorithm	Case	F_{FEED} (kg/h)		$c_{4\text{-}CBA}$ (ppm)	
		Bounds attained		Bounds attained	
		Lower	Upper	Lower	Upper
MODE	Case-1	130013.00	169991.00	524.99	918.76
	Case-2	130380.93	169991.19	527.60	1076.18
	Case-3	130102.96	169991.19	101.55	1037.61
	Case-4	139445.55	169955.82	171.18	2450.69
MODE III	Case-1	130122.02	169999.18	524.08	918.69
	Case-2	130122.65	169999.18	524.08	918.69
	Case-3	130122.57	169996.56	524.08	918.00
	Case-4	130122.99	169855.53	524.77	914.36
Hybrid MODE	Case-1	130123.38	169996.55	524.07	918.71
	Case-2	130298.66	169998.20	524.07	918.70
	Case-3	130122.39	169857.22	524.08	914.5
	Case-4	130170.78	169999.31	524.20	918.69
Elitist MODE	Case-1	130091.00	169998.00	524.34	918.70
	Case-2	130101.49	169999.60	522.67	907.06
	Case-3	137394.50	169957.80	122.01	1132.90
	Case-4	133248.43	169406.10	148.99	1953.26
Trigonometric MODE	Case-1	130088.45	169970.63	524.36	918.95
	Case-2	130298.66	169990.54	525.81	918.77
	Case-3	130105.14	169998.07	524.22	918.07
	Case-4	130123.36	169975.42	524.07	918.90

Table 5.12 Number of points converged on the Pareto front (NPS) and the percent of initial points converged (% CON) on the Pareto front in each case

Algorithm	Case-1		Case-2		Case-3		Case-4	
	NPS	%Con	NPS	%Con	NPS	%Con	NPS	%Con
MODE	173	17.3	231	23.1	20	2.0	10	1.0
MODE III	369	61.5	368	61.3	433	72.16	438	73
Hybrid MODE	555	92.5	557	92.8	488	81.33	491	81.83
Elitist MODE	600	100	600	100	600	100	600	100
Trigonometric MODE	170	28.3	372	62.0	398	66.33	482	80.33

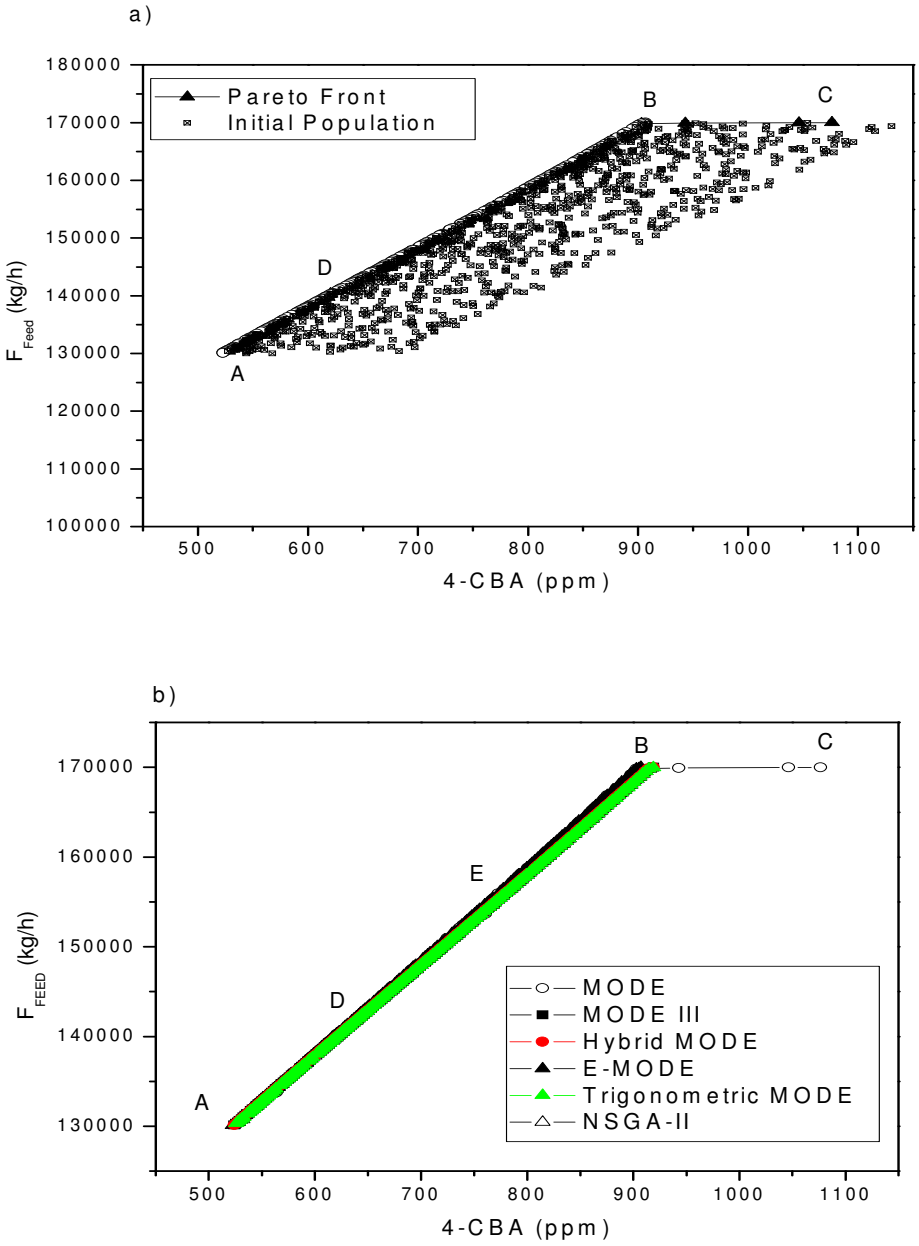

Fig. 5.42 (Contd…)

c)

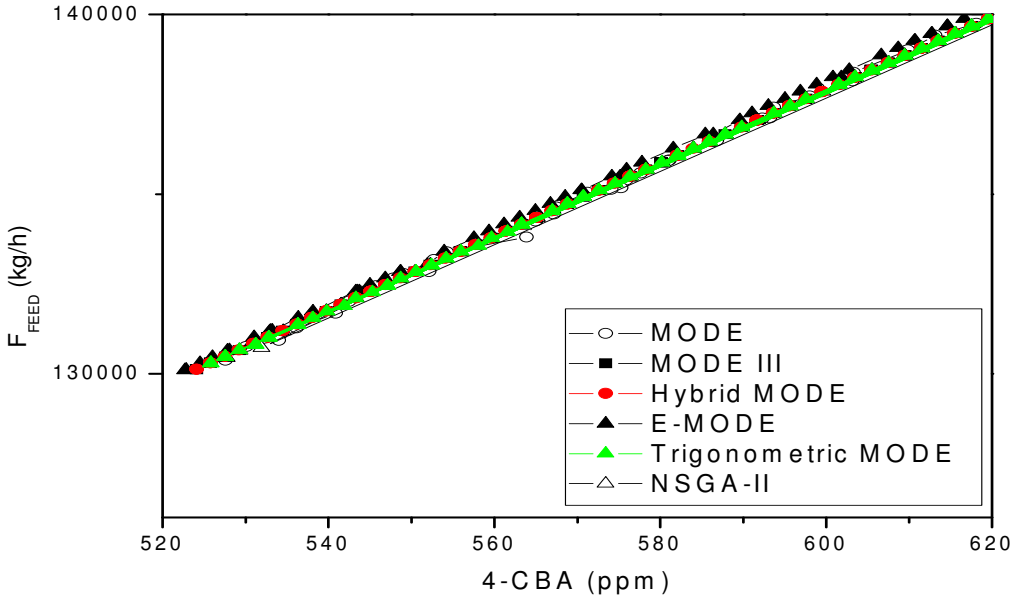

d)

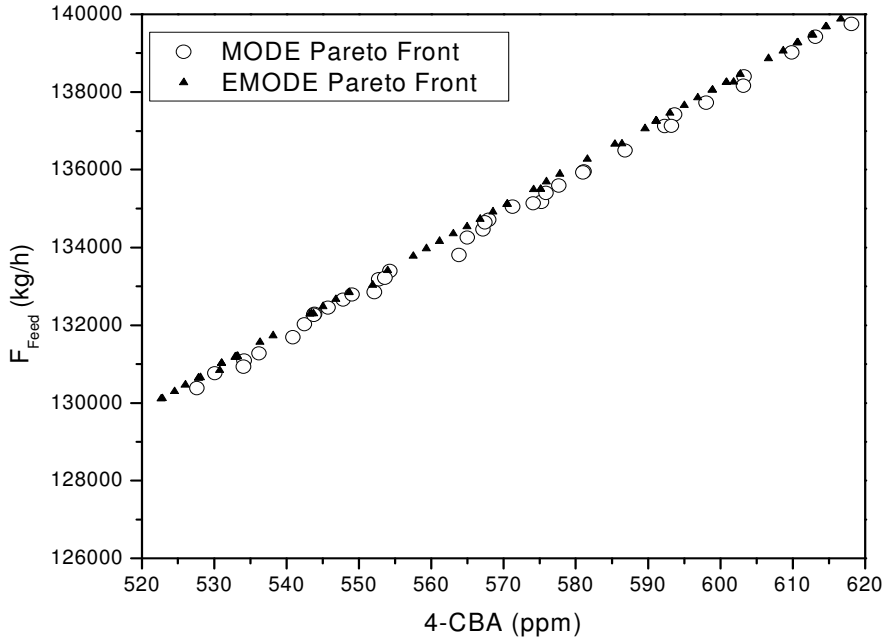

Fig. 5.42 (Contd…)

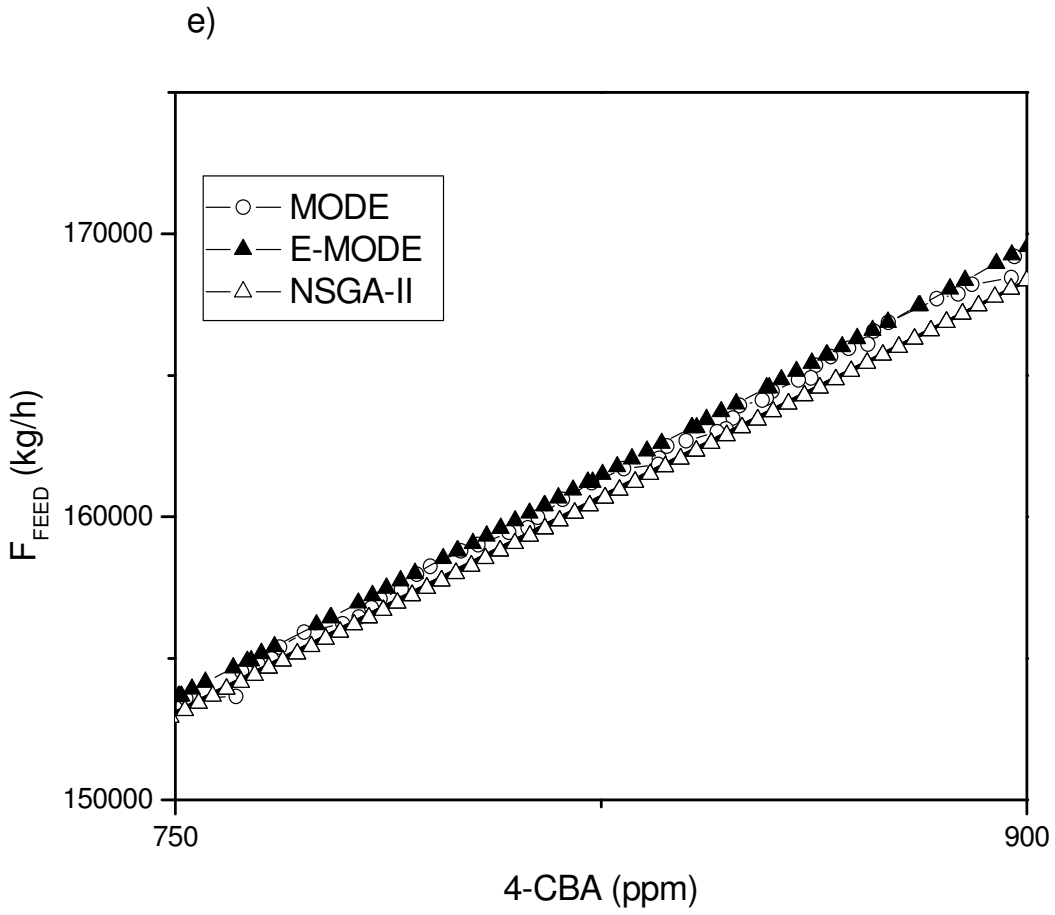

Fig. 5.42 Case-2:(a) The objective space and the Pareto front; (b) Pareto optimal solutions and objective space using MODE and Elitist MODE; (c) Comparison of Pareto front with actual range of values; (d) Magnified view with small range of values (A to D); (e) Magnified view with small range of values (E to B)

As all algorithms converged to the same front, the Pareto front resulted in present study may be termed as a global Pareto front. However, MODE is able to cover a better range than other strategies of MODE and NSGA-II as shown in Fig. 5.42c. For clarity, a portion of Fig. 5.42b (4-CBA concentration ranging 520 - 620 ppm, between A and D) is magnified and shown in Fig. 5.42c. Fig. 5.42c shows that the solutions obtained using the strategies of MODE are spread uniformly and almost at equidistance from each other. The Pareto fronts obtained using MODE and elitist MODE algorithm are shown with same range (as Fig. 5.42c) and is shown in Fig. 5.42d.

Fig. 5.42d shows that the elitist MODE algorithm gave a better distribution of solutions compared to the MODE algorithm. Thus an improvement proposed in terms of preserving the elite population members resulted in a better set of solutions with equal distribution on the Pareto front. Again, a portion of Fig. 5.42b (4-CBA concentration ranging 750 - 900 ppm between E and B) is magnified and shown in Fig. 5.42e. The elitist MODE algorithm is found to give a well converged Pareto front when compared to Pareto fronts obtained using MODE and NSGA-II (Region E to B in Fig. 5.42e). Table 5.11 shows that all the strategies of MODE are able to capture the upper bound of the total feed rate (first objective function). Only MODE algorithm could capture the lower bound of first objective function. However, in case of second objective function, i.e., concentration of 4-CBA, MODE algorithm alone could capture the region BC as shown in Fig. 5.42b. This is the region of interest to those industries, which focus more on profit rather than the quality of product. Only three points are observed in region B-C using MODE algorithm. In elitist MODE algorithm the decision variables corresponding to point A are 688.96 ppm and 7.82 % ([C_0] and water % respectively) and corresponding variables for point B are 798.418 ppm and 6.74 % respectively. This clearly indicates that in the presence of high concentration of catalyst, 4-CBA concentration increases with a slight decrease in % water content. Fig. 5.43a shows 4-CBA concentration as a function of catalyst

concentration. Fig. 5.43b shows the variation of 4-CBA concentration with % water. Catalyst concentration plays an important role in controlling 4-CBA concentration at the exit of the reactor, but in the presence of another decision variable, i.e., % of water in the solvent, catalyst concentration becomes almost independent of the 4-CBA concentration as shown in Fig. 5.43a. The values of other decision variables are kept constant as shown in Table C4 in Appendix C. Fig. 5.43c shows a 3-dimensional view of the decision variables plotted against 4-CBA concentration (objective function). The XZ plane shows the projection of Water % and 4-CBA concentration and the projection of $[C_0]$ and 4-CBA concentration is shown on YZ plane. Such projection plots are in general very useful for predicting the effect of individual decision variable on the objective function in a 3-dimensional plot. From this 3-D plot, it is clear that the 3D surface formed is due to the effect of decision variable (water %) on 4-CBA concentration. Fig. 5.43b and 5.43c show that 4-CBA concentration increases with an increase in % water content.

5.2.3.3 Case-3: $[C_0]$, F_{FEED}, W_{H_2O}, F_{PX} and V_{O2} as decision variables

Fig. 5.44a shows the Pareto optimal solutions for case-3. In Figs. 5.44b- 5.44e the corresponding decision variables are plotted against one of the objective functions, (concentration of 4-CBA).

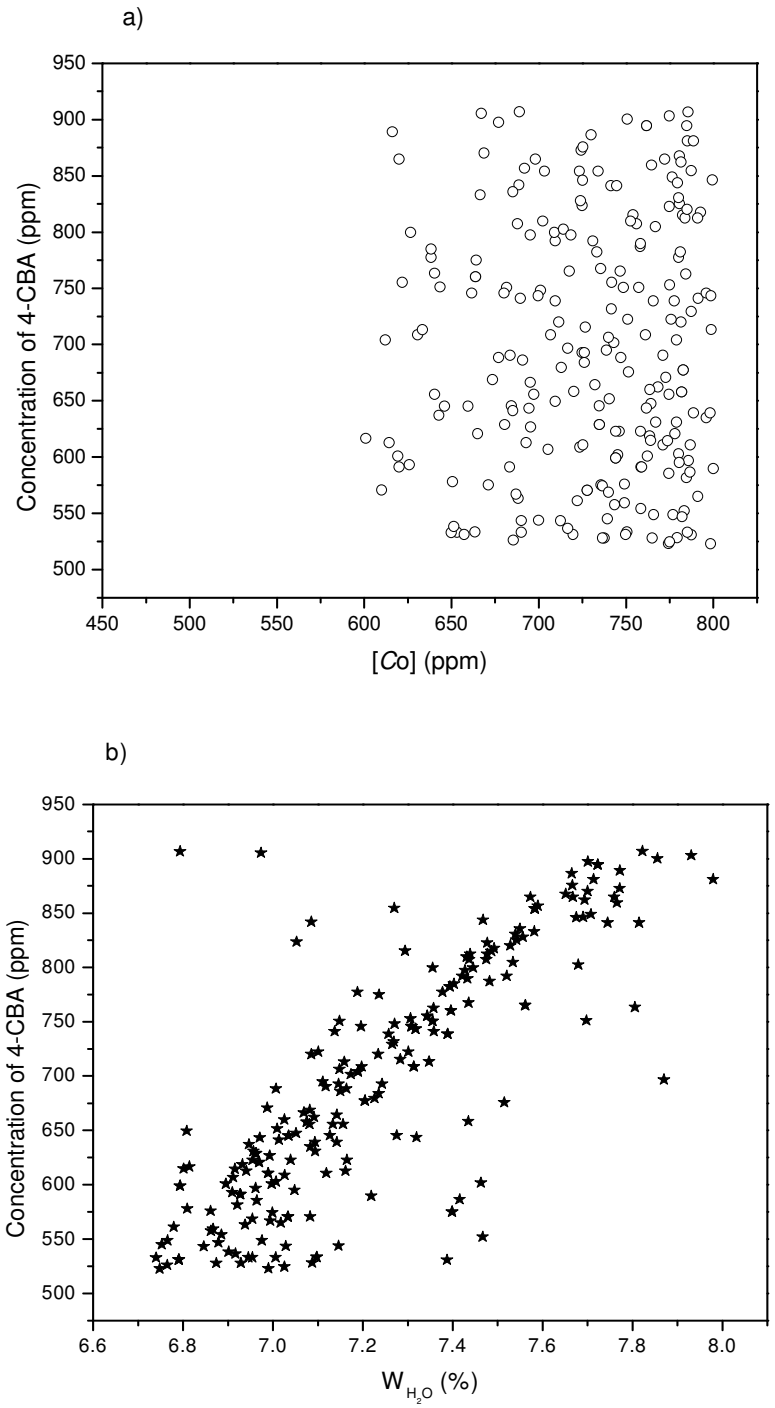

Fig. 5.43 (Contd….)

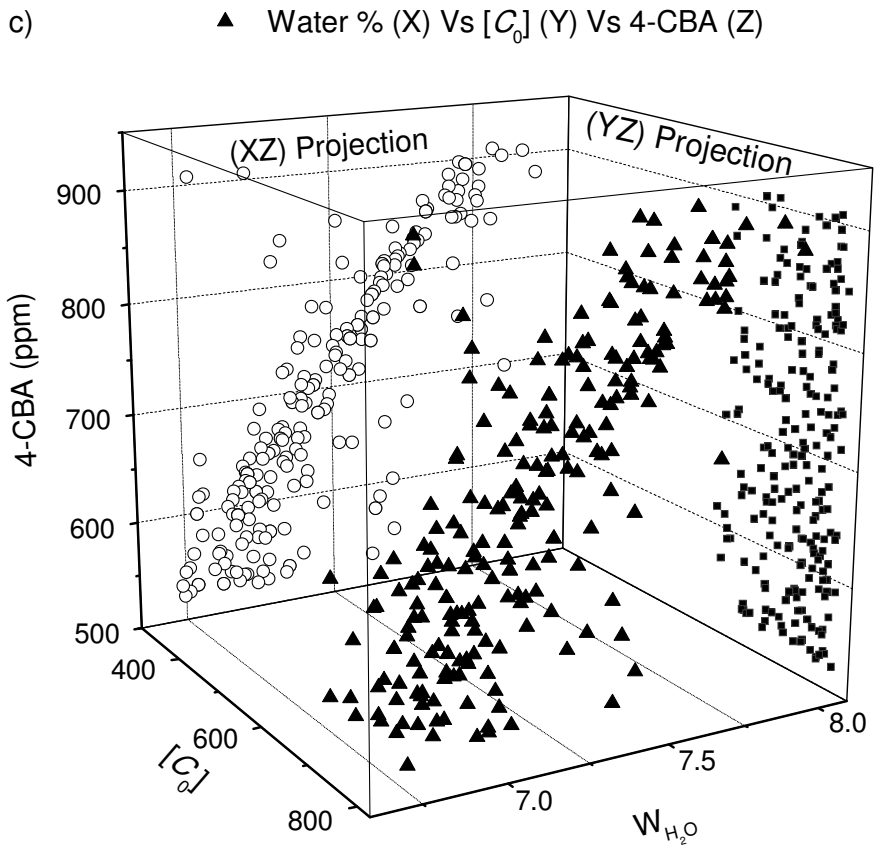

Fig. 5.43 Case-2: (a) Effect of catalyst concentration [C_0] on concentration of 4-CBA; (b) Effect of water content W_{H_2O} on concentration of 4-CBA; (c) 3-dimensional view of 4-CBA concentration vs. decision variables

The decision variables considered in this study are feed (xylene) flow rate, total feed rate, % water in the solvent, catalyst concentration and vent oxygen content. The value of the sixth decision variable, i.e., temperature of the reactor is kept constant at 461 K during the entire simulation run (optimum value obtained in results of case-4). From the result of case-4, it is observed that most of the decision variables approach the value of 461 K as a higher temperature favors the rate of forward reaction. The number of non-dominated solutions after 50 generations in case of MODE algorithm is 20 with an initial population size of 1000. However, in elitist MODE algorithm after 100 generations, the number of non-dominated solutions is same as that of the initial population and multiple copies of a few solutions are formed. But both the MODE and elitist MODE algorithms converged to the same front. Other strategies of MODE, which include MODE III, hybrid MODE, and the trigonometric MODE algorithms converged to the same but local Pareto front as against the global Pareto front obtained using MODE and elitist MODE algorithms.

The MODE and elitist MODE captured the entire range of second objective, i.e., concentration of 4-CBA (Fig. 5.44a & Table 5.11). MODE III, hybrid MODE and the trigonometric MODE converged to a local front and could not cover a complete range of second objective, i.e., concentration of 4-CBA, below a value of 500 ppm. In Fig. 5.44b, the outcome of MODE and elitist MODE are shown together, as these algorithms give a better Pareto front as compared to the Pareto fronts obtained using other strategies of MODE. As we move from point A towards D (In Fig. 5.44b and Table 5.11), we observe that the values of $c_{4\text{-}CBA}$ and F_{FEED} increase. If we compare points A, B and C with point D, we observe that point D has a very high value of 4-CBA content as compared to point A, B and C (in Fig. 5.44b). However, the total feed rate value (value of first objective function) is almost same for point B and D. The decrease of value of decision variable, % water content, from 3.33 % to 1.84 % and increase in value of another decision variable F_{PX} from 31,610 kg/h to 33,165 kg/h has

increased the value of objective function $c_{4\text{-CBA}}$ from 302.03 ppm to 1037.6 ppm. Also, the comparison of points A, B and C reveals that the increase in 4-CBA impurity is mainly due to the decrease in % water content in the solvent and increase in the feed xylene rate. As we move from points A' to D' (in Fig 5.44b and Table 5.11), we observe an increase in 4-CBA impurity concentration. We find a sharp peak in the value of 4-CBA from point B and D. But in this case, unlike the result obtained using MODE, this peak in the value of 4-CBA concentration is due to a decrease in water content and a decrease in vent oxygen. Fig. 5.44c shows the effect of value of F_{PX} on the objective function $c_{4\text{-CBA}}$. Lower flow rate of xylene is desirable for low value of 4-CBA concentration at the exit of reactor. Fig. 5.44d shows that the decrease in vent oxygen content increases the 4-CBA concentration at the exit of reactor.

Unlike the results of case-2, in the presence of other decision variables (V_{O_2}, $[C_0]$, and F_{PX}), the effect of value of W_{H_20} is negligible. Fig. 5.44e shows that the concentration of 4-CBA is almost independent of % water content (unlike the results of case-2). Thus in the presence of oxygen content, the water content does not affect the 4-CBA concentration at the exit of reactor. The concentration of 4-CBA depends more on oxygen content irrespective of the presence of % water content. This consolidates the dominance of vent oxygen content over water content.

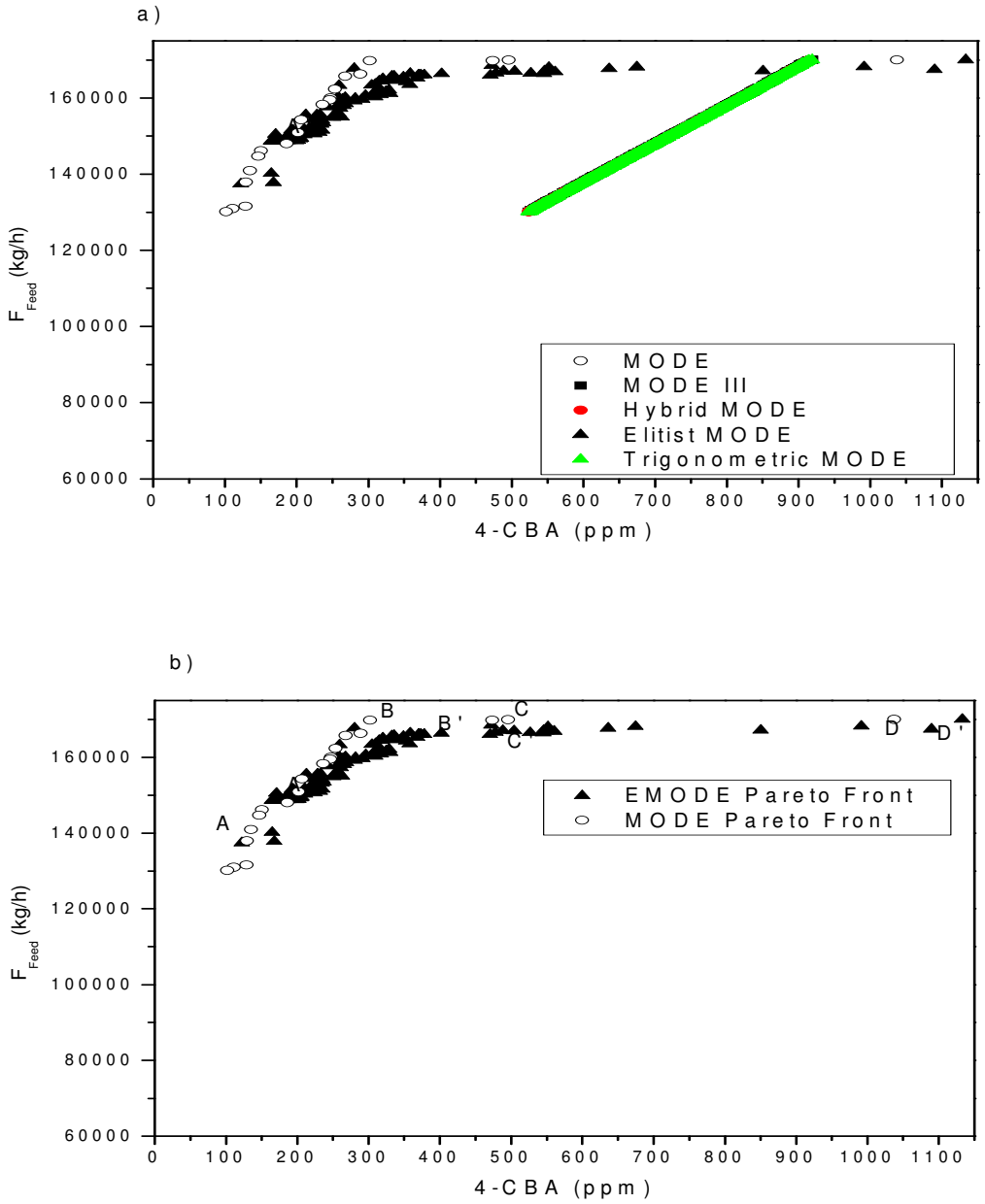

Fig. 5.44 (Contd….)

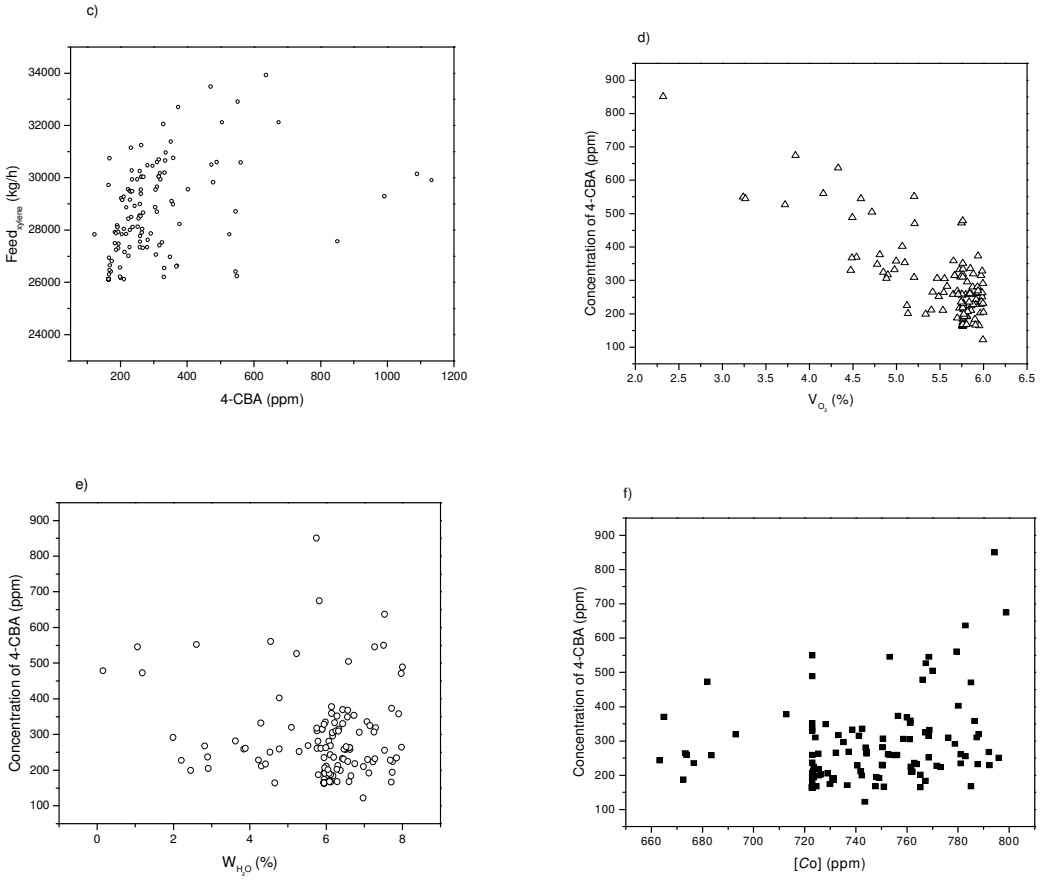

Fig. 5.44 Case-3: (a) Pareto fronts obtained using the strategies of MODE algorithm; (b) MODE and elitist MODE Pareto fronts; (c-f) Effect of different decision variables on concentration of 4-CBA

However, in the absence of vent oxygen content (or when vent oxygen content value is fixed), the W_{H_20} parameter plays an important role in deciding the exit concentration of 4-CBA. The catalyst concentration is found to lie on the upper bound of its range as shown in Fig. 5.44f. High catalyst concentration is preferred for the reduction in 4-CBA concentration at the exit of reactor. From Fig. 5.44f, it is evident that the majority of the points have a value of $[C_0]$ greater than 720 ppm. Hence, we may conclude at this juncture that it is not a single variable that controls the output (4-CBA concentration) at the exit. But, the output depends on several variables, which is the typical feature of dependence of objective functions on the values of decision variables that are responsible for generating a trade-off in multi-objective optimization problems.

5.2.3.4 Case-4: $[C_0]$, F_{FEED}, W_{H_2O}, F_{PX} V_{O2}, and T as decision

The Pareto fronts for strategies of MODE and elitist MODE algorithms for case-4 are shown in Fig. 5.45a. Similar to the results obtained in case-3 the Pareto fronts obtained using MODE III, hybrid MODE and the trigonometric MODE algorithms lie on the same, but, a local Pareto front for case-4 also. The smoothness of Pareto fronts obtained using MODE and elitist MODE algorithms is missing mainly due to the complexity of search space, which limits the algorithms to find improved and uniformly spread solutions on the Pareto front. This difficulty is also observed because the number of solutions converged on the Pareto front are less. The total number of solutions obtained using MODE algorithm with an initial population size of 1000 is 10. All population points are found to converge towards the Pareto front in case of elitist MODE algorithm. A summary of number of solutions and the percent of initial points converged to the Pareto front for all the cases (case-1 – case-4), using the strategies of MODE algorithms are given in Table 5.12.

Fig. 5.45b shows the effect of vent oxygen content on 4-CBA concentration. As observed in case-3, the concentration of 4-CBA increases with a decrease in vent oxygen content. For the favored region of the Pareto front (lower value of 4-CBA), the vent oxygen content occupies the upper region. Liquid phase *p*-xylene oxidation is a zero-order reaction with respect to the oxygen content and first-order reaction with respect to *p*-xylene concentration. Lowest value of the 4-CBA concentration is achieved at the exit of reactor, if the first oxidation step occurs at a faster rate. This is possible by means of higher temperature (according to Arrheneous law) or at a higher oxygen concentration. If the first-stage oxidation is restricted, due to lack of oxygen concentration or reduced temperature, then the unconverted *p*-xylene may compete for reaction with the remaining oxidation products. In this way, it is possible to have an unconverted 4-CBA in the final product as an impurity. This is evident from Fig. 5.44b. It shows that at lower concentration of vent oxygen, the concentration of 4-CBA in the reactor effluent increases.

Fig. 5.44c shows the effect of water present in the solvent on the concentration of 4-CBA at the reactor exit. A higher amount of % water content is required to reduce the concentration of 4-CBA. But this high amount of water has another practical difficulty in the separation step. The excess water and the water generated during oxidation reactions, form an azeotrope with solvent acetic acid, causing difficulty in separation of solvent from the process liquor for possible recycle of the solvent. Therefore in order to ensure a maximum possible rate of reaction, an optimum water content in the reactor is very necessary (considering the formation of water during the reaction also). In industrial PTA process, this excess water is usually removed by means of condensers connected to the reactor. Low pressure steam is generated from the heat recovered in condensing the vapors of water and solvent. This condensed stream is then sent to an azeotropic distillation column for further purification (Wang et al., 2007).

A higher catalyst concentration is preferred in liquid phase oxidation of *p*-xylene as shown in Fig. 5.44d. Catalyst plays an important role in enhancing the rate of reaction. However, there are a few points on the Pareto front, which lead to high 4-CBA concentration despite having high catalyst concentration. A careful observation of those points reveals that those points either belong to a low water content or to a low temperature. In the same way, there are a few points which have low catalyst concentration values but also have a low value of 4-CBA concentration as they possess high temperature values. The effect of temperature of reactor on the reaction is evident from Fig. 5.44e. A high temperature is favored for oxidation reactions. Thus, most of the points approach the upper bound as shown in Fig. 5.44e. The value of temperature was fixed to a reference value in case-3 (a high temperature favors the rate of forward oxidation reactions). Therefore, the Pareto front for case-3 is better than that obtained for case-4.

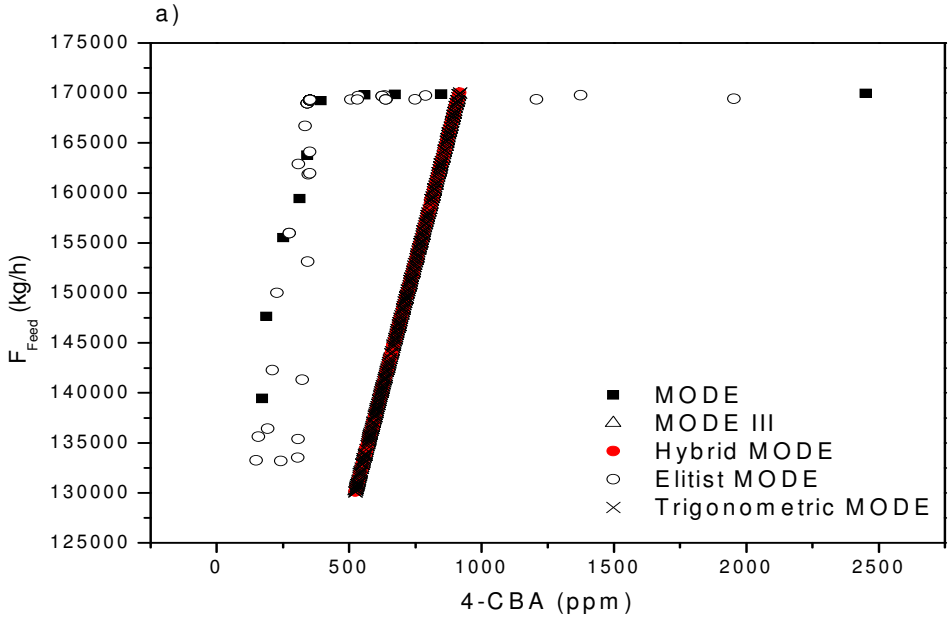

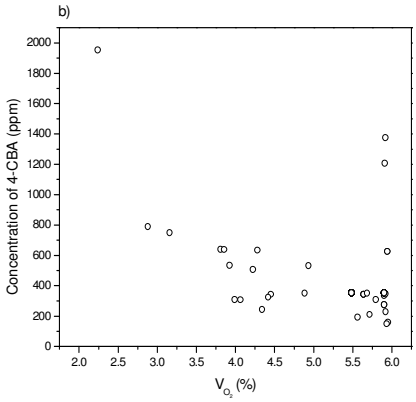

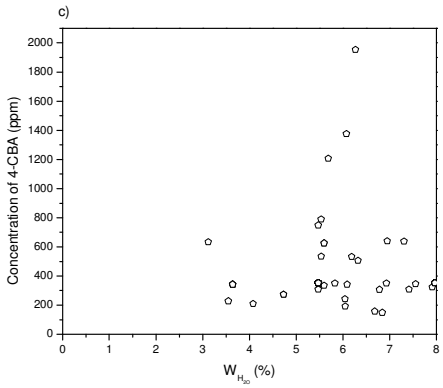

Fig. 5.45 (Contd….)

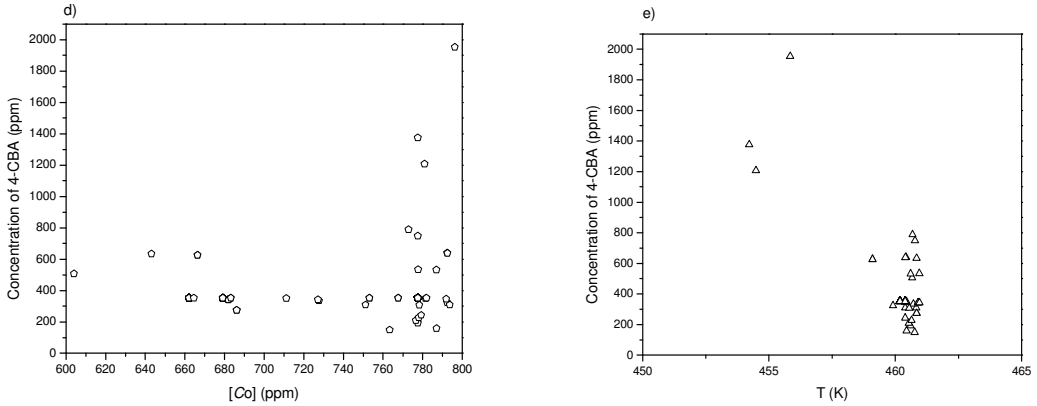

Fig. 5.45 Case-4: (a) Pareto optimal solutions using the strategies of MODE; (b-e) Effect of different decision variables on concentration of 4-CBA

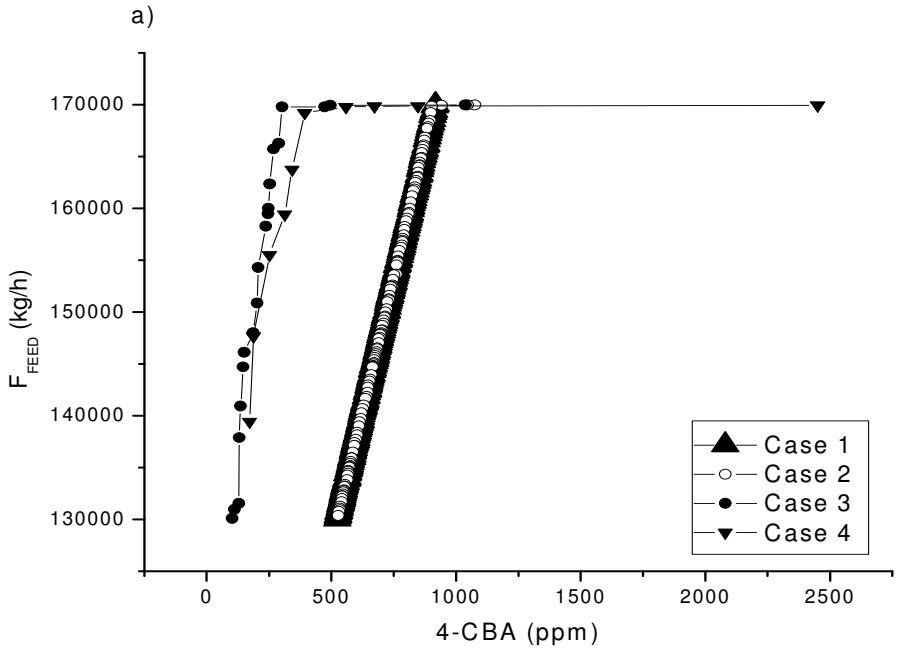

Fig. 5.46 (Contd…..)

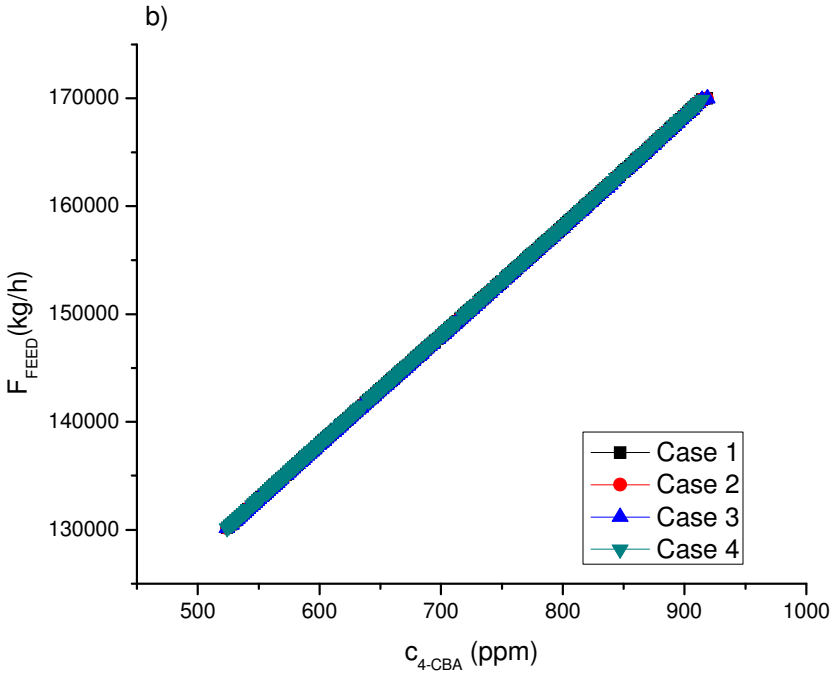

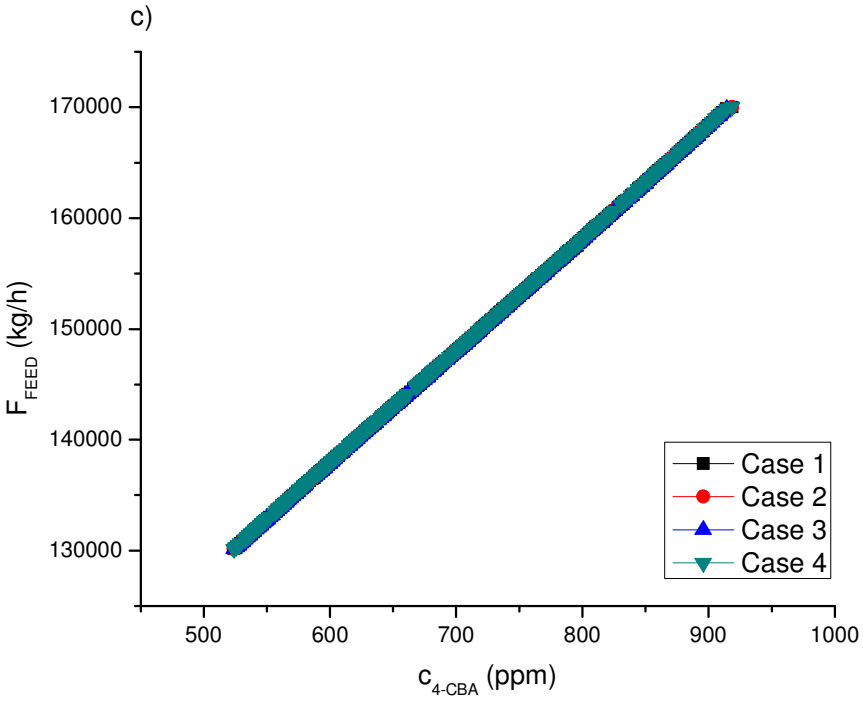

Fig. 5.46 (Contd…..)

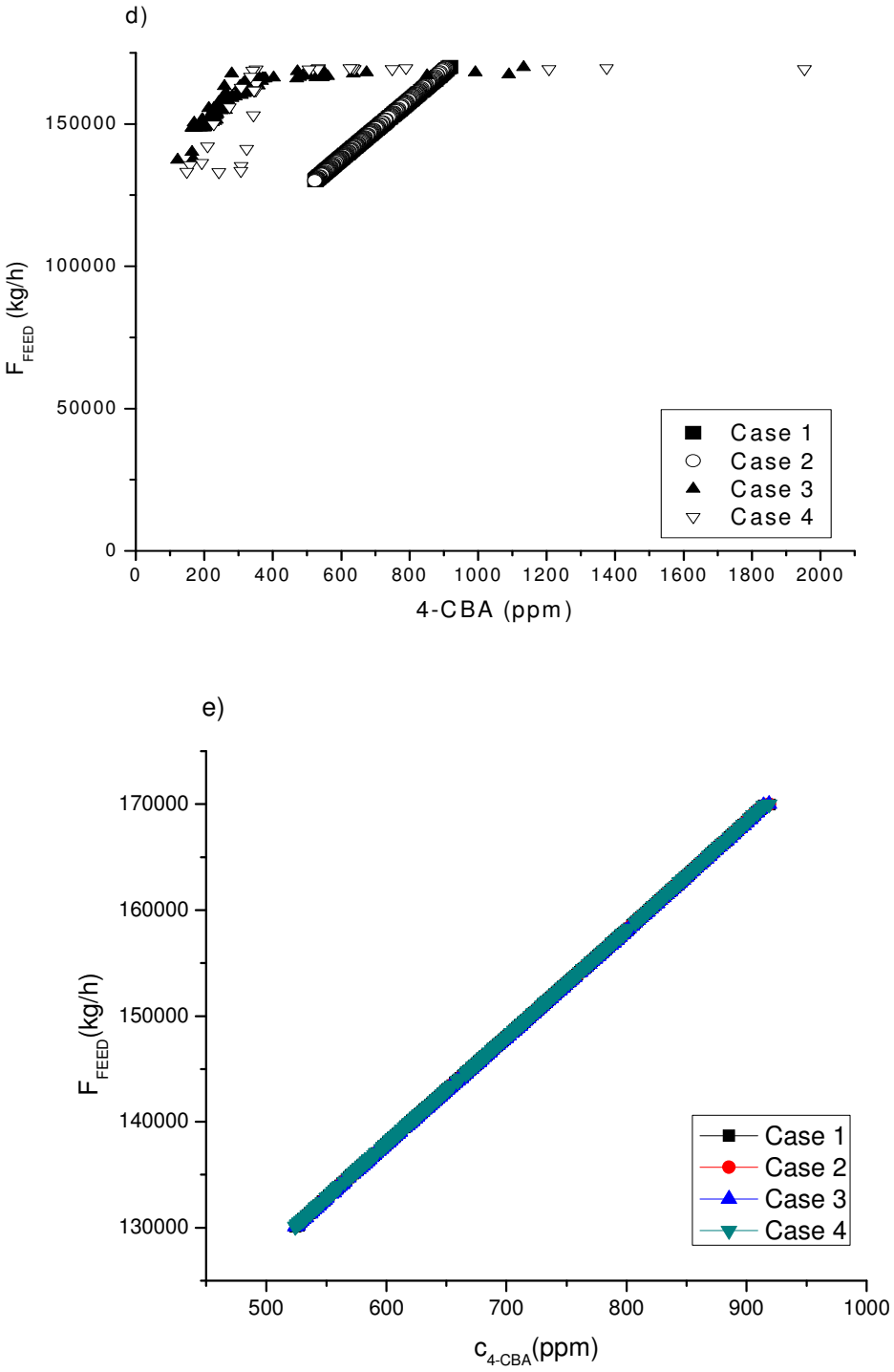

Fig. 5.46 Comparison of Pareto front for all 4 cases; (a) MODE; (b) MODE III; (c) Hybrid MODE; (d) Elitist MODE; (f) Trigonometric MODE

5.2.3.5 Comparison of cases 1-4

Figs. 5.46a- 5.46e show the comparison of Pareto front obtained for case-1- case-4, using, MODE, MODE III, hybrid MODE, elitist MODE and trigonometric MODE algorithms respectively. MODE algorithm as expected from the results obtained in section 5.1.1, resulted in a very little number of points, though started with a high number of initial points. Elitist MODE algorithm gave maximum number of Pareto solutions, resulting in 100 % convergence to the Pareto front with respect to the initial number of points for all the cases. However, MODE algorithm gave fairly good number of solutions, lying on the same front as that of elitist MODE. MODE III, hybrid MODE and trigonometric MODE algorithms resulted in local Pareto fronts for case-3 and case-4, as compared to the Pareto fronts obtained using Elitist MODE and the MODE algorithms. The reason for this is that hybrid MODE and trigonometric MODE algorithms are the extension of MODE III algorithm, whereas elitist strategy of MODE is an extension of MODE II algorithm (where new points are created and preserved). MODE II and elitist MODE algorithm work on the principle of adding new population points and preserving the best among them, However, in the strategies of MODE III algorithm, new points are created by perturbation and are added to the existing population, if and only if, the new points dominate any of the member of current population. Thus, both the extensions of MODE II and MODE III algorithms have their own advantages and disadvantages. The summary of the number of non-dominated solutions obtained in each case using the strategies of MODE algorithm is shown in Table 5.12.

In the next subsection, results obtained for MOO of low density polyethylene tubular reactor are discussed.

5.2.4 Multi-objective optimization of Low Density Polyethylene (LDPE) Tubular Reactor

The reaction scheme (Eqs. D1 - D10), model equations (Eqs. D11 - D18), and the kinetic rate constants and equations related to LDPE tubular reactor (Eqs. D19 - D29c) considered in this

study are given in Appendix D. Open literature contains several studies which incorporated several aspects related to modeling of continuous LDPE reactor. But due to the complexity of reaction mechanism, large number of kinetic parameters and a wide range of experimental conditions over which the kinetic parameters are to be determined, the consistent set of rate constants has not been established. Table 2.1a shows the rate constant parameters in some of the studies reported in the literature. Table 2.1b shows the rate constant parameters used in the remaining studies (continued from Table 2.1a) and in the present study. Kiparissides et al. (1993) reported that under normal operating (experimental) conditions the values of propagation and termination (by combination) rate constants cannot be obtained. The reported values of rate constants by various authors (Tables 2.1a and 2.1b) also show a large deviation. Differential Evolution (DE), an evolutionary, population based search algorithm is found to be successful in handling many complex and non-linear engineering problems both in the field of single and multi-objective optimization (Price and Storn, 1997; Lee et al., 1999; Stumberger et al., 2000; Chakraborty et al., 2003; Babu, 2004; Babu et al., 2005; Babu and Munawar, 2007). To bring down the deviation in the rate constant parameters and operating parameters, the differential evolution algorithm is used in the present study to obtain the optimum values of the parameters. The industrial values of temperature are read from the plot (Asteasuain et al., 2001), using a computer oriented 'scanit' software which can read the data with high accuracy. The data is read at 28 discrete points from the plot and are shown in Table 5.13a along with the model predicted data at a specified length. Apart from the temperature at 28 discrete points, the exit values of monomer conversion, the side product concentration and the number-average molecular weight are used for minimizing function, *I*. Brandoline et al. (1996) presented a comprehensive model that proved to be a well known model which included several mechanisms of termination reactions. Agarwal et al. (2006) made use of a model proposed by Brandoline et al. (1996). They carried out the tuning of important rate parameters involved in

the model. When we tried to use the model predicted parameters reported by Agarwal et al. (2006) in the present study simulation runs using Matlab, we observed an average deviation of 0% in X_m, 14.36 % in [*SCB*] and 12.58 % in M_n respectively at the exit of reactor. However, the trends obtained for each species in our study remain the same, as reported in the literature (Brandoline et al., 1996; and Agarwal et al., 2006). The important equations (such as friction factor) related to the heat transfer operations were not reported in the literature (Agarwal et al., 2006). Therefore we considered two different cases of heat transfer in this study. In Case A, Eq. D29a, which represents the explicit form of friction factor (Brandoline et al., 1991) is used. In case B, an implicit form of friction factor (Eqs. D29b and D29c), as reported by Kiparissides et al. (1993) is considered. The comparison of industrial data and the model predictions (for both case A and case B) is given in Table 5.13b. In terms of monomer conversion, model predictions are exactly matching with industrial data in both the cases (i.e., case A & case B). Case B model predicted the exact value of number-average molecular weight, whereas case A model predicted the value of M_n with a relative error of 0.48%.

Both Tables 5.13a and 5.13b show that with an efficient numerical solution procedure (NDFs), the model predicted values of present study match well with the industrial data. The difference in parameter values obtained in the present study and in the previous study (Agarwal et al., 2006) may be attributed to the two different solution procedures used in these studies. Considering the much accurate estimation of model output, case B is used for simulation in this study.

5.2.4.1 Simulation, parametric estimation using differential evolution and parametric analysis

Simulation and parametric estimation using differential evolution

ODE15s subroutine of Matlab (7.0) library is used in the present study. Agarwal et al. (2006) used the Gears Routine (D02EJF of NAG library) in their simulation runs. ODE15s (in

MATLAB 7.0 library) is a variable order solver based on the numerical differentiation formula. ODE15s has an option to use backward differentiation formula (BDFs, also known as Gears method) that is usually less efficient. NDF can achieve the same accuracy as BDF with step size about 26% bigger (Shampine and Reichelt, 1997). This clearly highlights the inefficiency of BDF (Gears routine) in comparison with NDF. The slight deviation in the exit concentration of various species [obtained using the reported values of parameters in literature (Agarwal et al., 2006)] encouraged us to fine tune the model in order to find the rate law parameters associated with the eight reactions of initiation, propagation and termination. Differential Evolution (DE) algorithm is used to minimize the sum of square of the normalized error, *I*, between the model-predicted values and the industrial values (Eq. 5.5).

$$Minimize \quad I(u) = \sum_{i,j} \left(1 - \frac{N_i^{ind}\left(z_j\right)}{N_i^{model}\left(z_j\right)_{exit}} \right)^2 \tag{5.5}$$

where, N_i is the value of i^{th} property, and the superscripts *m* and "ind" represent the values predicted by the model and the industrial values, respectively. Properties used in the estimation of function *I* in this study are temperature of reactor, number-average molecular weight, monomer conversion, and methyl, vinyl and vinylidene end groups per 1000 carbon atoms in the chain. The decision variables involved in this study are given by Eq. 5.6.

$$I(u) \cong f\left(E_o, E_{d1}, E_{d2}, E_p, E_{trs}, E_{bb}, E_{b1}, E_b, V_{j2}, V_{j3}, V_{j4}, a_v\right) \tag{5.6}$$

The internal heat transfer coefficient also affects the reaction kinetics and therefore the jacket fluid flow rates and parameter involved in viscosity estimation were also incorporated in the list of decision variables as shown in Eq (5.5). The final iteration of DE algorithm resulted in several near global solutions with an accuracy of the order of 10^{-4}. Out of those near global solutions, the set of optimal decision variables is randomly selected and the variables are reported (for both case A and case B) in Table 5.14 along with the optimum values reported by Agarwal et al. (2006), operating plant values reported by Brandoline et al. (1996) and the

bounds of the parameters used for optimization study. Brandoline et al. (1996) provided the values of initiator concentration in the form of ranges due to certain proprietary reasons. Initial initiator concentration plays an important role in controlling the performance of reaction scheme (especially in the presence of varied set of input conditions). Table 5.14 shows that most of the optimum parameters obtained in this study are close to those obtained by Brandoline et al. (1996). As the model predictions are matching well with the industrial data (Table 5.13b), a detailed parametric study is carried out through extensive simulations by varying different variables and design parameters. In the next sub-sections, the results of simulation of LDPE tubular reactor are discussed by considering the effect of various feed conditions and the operating design parameters.

Effect of feed and jacket temperature on the reactor performance

The effect of feed and jacket temperature is analyzed by plotting the axial variation of temperature, short chain branching (SCB), vinyl and vinylidene end group per 1000 C atoms along the length of the reactor as shown in Figs. 5.47-5.50. The data is analyzed by varying one variable, while fixing the values of other variables constant at reference values (Table D1 in appendix D). Table 5.15 shows the effect of change in feed and jacket temperature on various aspects [such as, $T_{MAX,}$ L_a, M_w, M_n, PDI, X_m and the exit concentrations of side groups (i.e. SCB, vinyl and vinylidene groups per 1000 C atoms as given by Eqs. D23-D29)].

Table 5.13a Comparison of model predictions with the industrial data on temperature profile along the axial length of the reactor

Axial length (m)	**Temperature, T (K)**		**Axial length (m)**	**Temperature, T (K)**	
	Industrial data (Asteasuain et al., 2001)	**Model predicted** [present study]		**Industrial data** (Asteasuain et al., 2001)	**Model predicted** [present study]
0	350.0	350.00	603	529.2	528.27
80	390.1	386.89	640	520.1	522.02
113	407.8	402.99	677	514.4	516.38
139	421.3	414.09	720	507	510.32
173	439.9	431.14	762	499.2	504.89
180	450.9	437.56	810	492.6	499.20
209	516.4	531.68	857	503.7	497.42
273	588.8	610.97	904	543.3	533.35
307	592.7	600.36	940	562.3	555.54
350	584.9	586.58	980	568.8	570.19
388	575.4	576.03	1034	563.9	566.00
430	563.8	565.27	1110	560.4	557.00
463	553.5	555.63	1176	556	550.00
510	546.1	545.51	1254	547.5	541.00
549	539.1	537.81	1329	542.7	533.86

Table 5.13b Comparison of model predictions of present study with the reported industrial data (Agarwal et al., 2006) **of various properties at the exit of the reactor**

Specific property at the exit of reactor	**Industrial**	**Model Predicted values**		
		Using gears routine (Nag library) and NSGA (Agarwal et al., 2006)	**Using numerical differentiation formulas (Matlab library) and DE (Present Study)**	
			Case A	**Case B**
M_n (kg/kmol)	21900[*]	21901	21793	21900
X_M	0.3[*]	0.2971	0.3	0.3
SCB (per 10^3 C atom)	30[Δ]	30.13	29.63	29.91
V_i (per 10^3 C atom)	0.1[§]	0.1	0.099	0.099
V_{id} (per 10^3 C atom)	0.7[Δ]	0.7	0.684	0.695

[*]Data taken from Asteasuain et al. (2001); [§]Data taken from Gupta et al. (1985); [Δ]Data taken from Goto et al. (1981)

Table 5.14 Bounds, reported values and final tuned values (present study) of the parameters

Parameter	Bounds	Value of the parameter			
		Reported (Brandoline et al., 1996)	Using Gears method and NSGA (Agarwal et al., 2006)	Using Numerical differentiation formulas (NDFs) and DE (Present study)	
				Case A	Case B
E_o	125604 < E_o< 138164	135945	132168	133232	134892
E_{d1}	117230 < E_{d1}< 136071	94621-133140	119929	123702	130189
E_{d2}	117230 < E_{d2}< 133977	94621-132721	123117	127803	122373
E_p	14653 < E_p< 18003	17626	17431	18002	17809
E_{trs}	14653 < E_{trs}< 20934	17253	18406	20927	20930
E_{bb}	56521 < E_{bb}< 66988	61964	60537	60832	60591
E_{b1}	71175 < E_{b1}< 87922	79967	84747	79828	79809
E_b	62802 < E_b< 87922	79967	70205	76149	75959
V_{j2}	0.005<V_{j2}<0.007	0.0012	0.00403	0.00690141	0.00673415
V_{j3}	0.005<V_{j3}<0.007	0.0012	0.00394	0.00634553	0.00399092
V_{j4}	0.005<V_{j4}<0.007	0.0012	0.00332	0.00167684	0.00097869
V_{j5}	0.001<V_{j5}<0.005	0.0012	0.00022	0.00125074	0.00278861
a_v	0.009<a_v<0.0185	0.017	0.018	0.0132271	0.01477835

Table 5.15 shows that the maximum temperature attained in the reactor and the length at which it is attained play an important role in deciding the overall quality of the polymer. Polydispersity index (PDI), which is a measure of the distribution of polymer molecular mass in a given polymer sample, depends on these two factors. As per the kinetics, a lower value of jacket temperatures delays the propagation reaction. Fig. 5.47 shows that the maximum attained temperature (T_{MAX}) and its location depend on the temperature of jacket fluid. As the initiator concentration gets depleted, the temperature of the reaction mass increases. Once the maximum temperature in the reactor is attained, the monomer conversion ceases and the properties such as, M_n, ρ, and concentration of [*SCB*], [v*inyl*] & [v*inylidene*] remain constant until the addition of another initiator at a length of 850 m along the length of the reactor (Figs. 5.48 - 5.50). The concentrations of side chains ([*SCB*], [*vinyl*] and [*vinylidene*]) depend on the maximum temperature attained in the reactor. Higher the value of peak temperature attained in the reactor, the higher is the concentration of undesired side chain species. Sr. No. 4 of Table 5.15 corresponds to the lowest value of jacket temperatures (383 K in zones 1, 4, and 5; and 430 K in zones 2 and 3). The low heating rate resulted in lowest value of maximum temperature attained among the 5 different cases considered in Table 5.15. The low value of jacket fluid temperature also resulted in a greater reactor length (Fig. 5.47 and L_a in Table 5.15) to attain the maximum temperature. This operating condition however resulted in low values of unwanted side chain concentration with an enhanced value of polydispersity index. Sooner is the peak temperature achieved in the reactor length, the smaller is the concentration of undesired side chains. The lower bound of jacket temperature (i.e., Sr. No. 4 in Table 5.15) due to low heating rate causes shortest distance of peak temperature, resulting in the lowest value of side chain concentrations per 1000

carbon atoms (i.e., SCB = 26.26, vinyl end group = 0.083846 and vinylidene end group = 11.891). The reaction mixture is cooled in the fourth zone in order to obtain a maximum efficiency of the initiator. It is also interesting to note that maximum temperature attained in the reactor and the concentrations of side chain products are relatively insensitive to the feed temperature over the ranges covered in this study. This result is consistent with those reported by Gupta et al. (1985). However, the changes in the values of jacket temperature show the effect on these parameters as shown in Table 5.15. PDI also depends on the jacket temperature and feed temperature. Smaller the value of jacket temperature and feed temperature (considered in this study), the greater is the value of PDI. Undesired side chain profiles (Figs. 5.48 - 5.50) show that the concentration of SCB, vinyl and vinylidene groups are observed immediately after the initiator injection in zone 3. The concentration of these species remains almost constant until the second initiator is injected in the fifth zone. The change in concentration of unwanted side products in zone 5 is less abrupt as compared to that observed in zone 3. This could be due to the high concentration of already formed polymer in zone 3, 4 and at the beginning of zone 5.

Effect of initiators concentration on the reactor performance

Figs. 5.51 – 5.55 show the effect of change in the injected initiator concentration on the axial variation of various entities along the length of the reactor. Initiator I_1 and I_2 are injected at a length of 160 m and 850 m from the entrance respectively. The effect of initiator injections on temperature profile along the reactor length is shown in Fig. 5.51a.

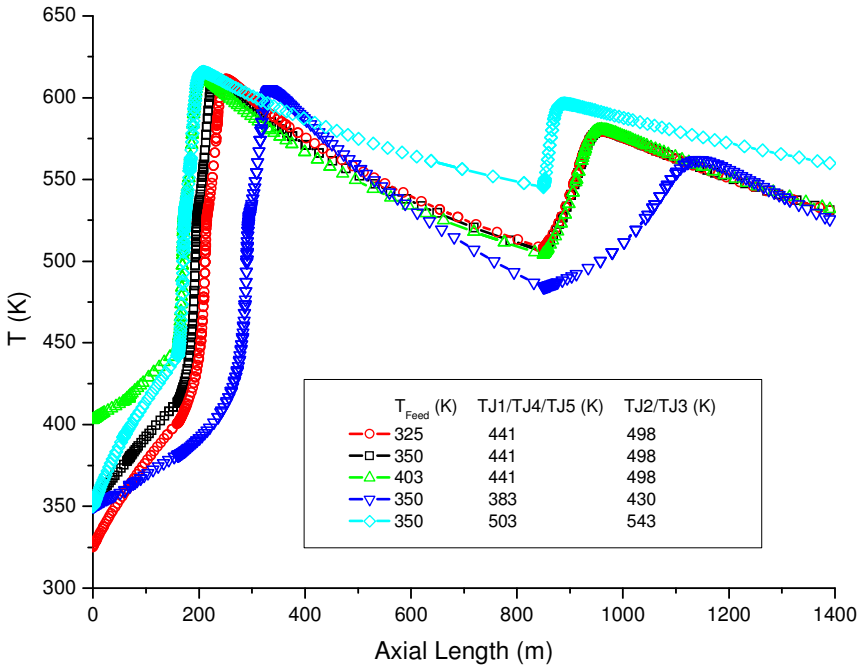

Fig. 5.47 Effect of jacket temperature on the temperature profile along the reactor length

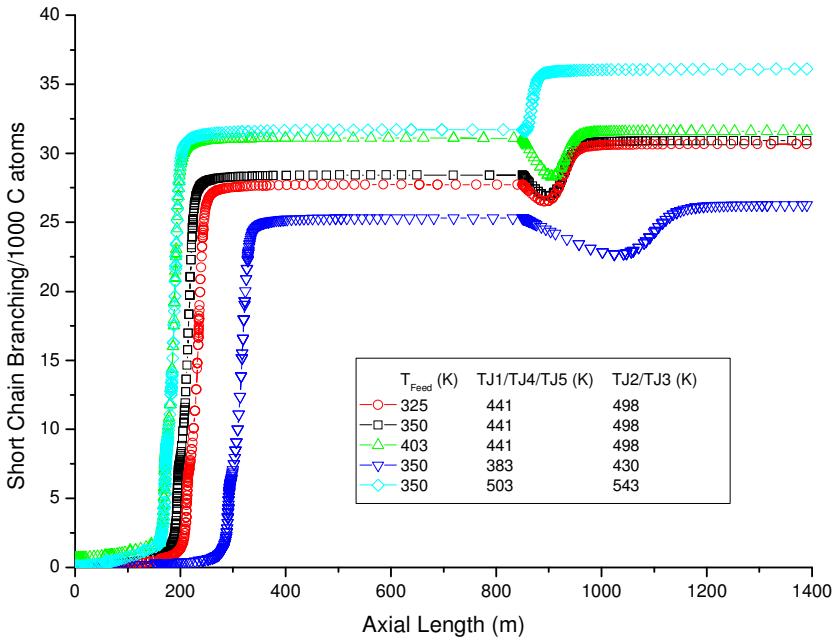

Fig 5.48 Effect of feed and jacket temperature on short chain branching content along the reactor length

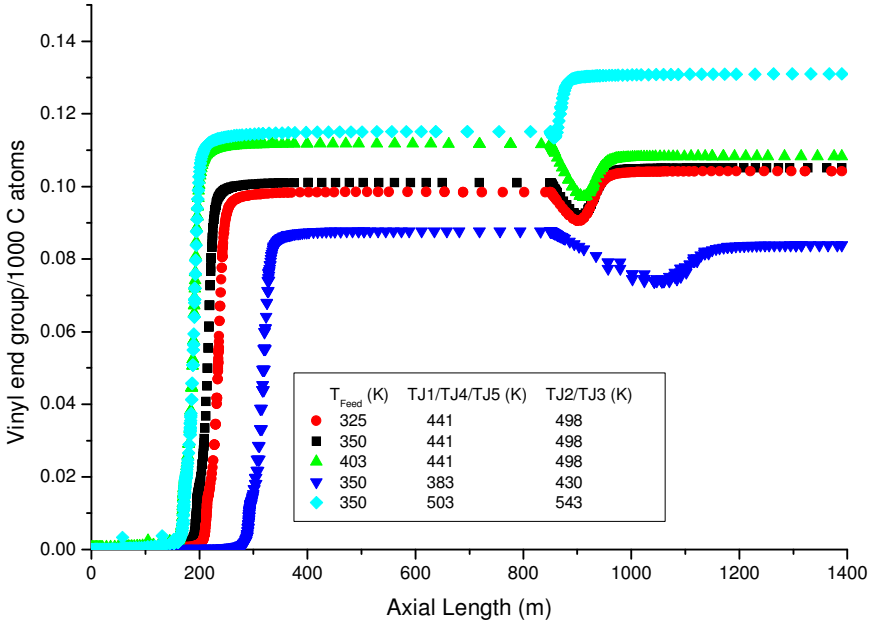

Fig. 5.49 Effect of feed and jacket temperature on vinyl end group profile along the reactor length

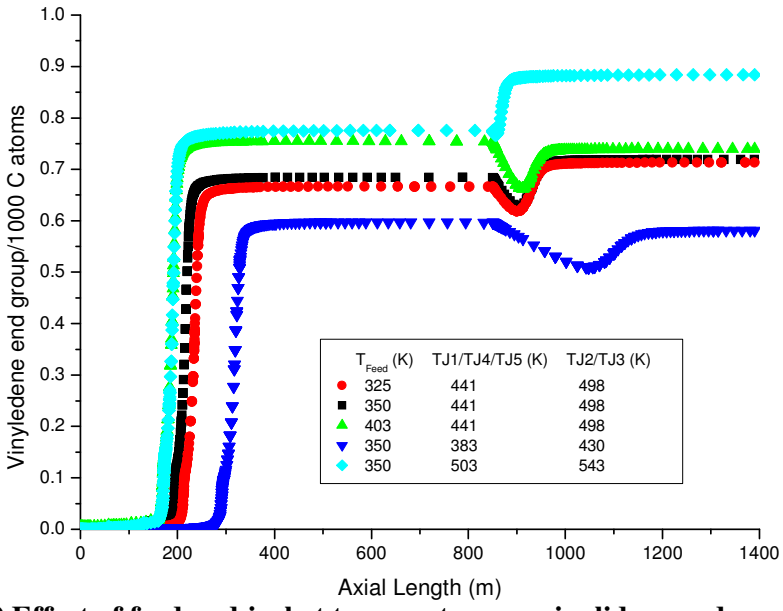

Fig. 5.50 Effect of feed and jacket temperature on vinylidene end group profile along the reactor length

Table 5.15 Various properties and exit concentration of different functional groups at various feed and reactor jacket temperatures

Sr. No.	T_{Feed} (K)	Jacket temperature		Max. temp T_{MAX} (K)	Axial position at Max temp L_a (m)	M_w (kg/kmol)	M_n (kg/kmol)	PDI	X_m (%) (Exit)	Exit side chain concentration/10^3 C atoms			Unconverted ethylene (kmol/m^3)
		T_1 (K)	T_2 (K)							Methyl group (SCB)	Vinyl group	Vinylidene group	
1	325	441	498	611.29	231.8	295175	21004	14.053	0.316	30.66874	0.10419	0.712635	13.61
2	350	441	498	611.29	251.9	242368	20827	11.636	0.310	30.91519	0.105093	0.718724	13.796
3	403	441	498	612.86	204.8	162743	20245	8.0384	0.2932	31.60865	0.108265	0.73925	14.616
4	350	383	430	605.18	334.7	554464	25388	21.8393	0.3922	26.26394	0.083846	0.580967	11.891
5	350	503	543	615.66	207.3	133493	17064	7.8230	0.2444	36.10889	0.130979	0.883567	15.7839

T_1 = Jacket temperature in zones 1, 4, and 5; T_2 = Jacket temperature in zones 2 and 3

For clarity, Fig. 5.51a is magnified in Fig. 5.51b and Fig. 5.51c. Both figures are magnified in such a way that the region of initiator injection (150-300m and 800-1250m) is clearly visible. Lower the concentration of initiator I_1, the greater is the length it acquires for reaching the maximum temperature (see Fig. 5.51a). The peak attained in the temperature marks the depletion of initiator concentration. Thereafter, not much happens in the reactor, except the cooling of reaction mixture. The concentrations of side chains ([*SCB*], [*vinyl*] and [*vinylidene*] end groups) also depend on the peak attained by temperature in the respective regions (Figs. 5.52 - 5.54). The peaks attained in these regions in turn depend on the extent of propagation reaction that occurs in the respective regions in the reactor. Figs. 5.51b-5.51c and Table 5.16 show that the length required attaining the maximum temperature in the reactor, in both the zones, increases with an increase in the concentration of initiators in the respective zones. The studies reported by Gupta et al. (1985), Brandoline et al. (1988), and Shirodkar and Taien, (1986) show a single peak in the profiles of temperature, unwanted side chain concentrations, and the monomer conversion. However, in this study and other studies reported in the literature (Asteasuain et al., 2001; Agarwal et al., 2006), multiple peaks of temperature, side chain concentrations and monomer conversion are observed. The exit monomer conversion remains nearly independent of initiator concentration over the ranges considered in this study (Fig. 5.55). However, the number-average molecular weight decreases with an increase in the values of initiator 1 and initiator 2 over the ranges reported in Table 5.16. The value of Reynolds number gradually decreases along the post peak temperature region (Fig.5.56). The initiator injection marks the start of highly exothermic reaction, thus increasing the values of Reynolds number and temperature.

Effect of reactor diameter, wall heat transfer coefficient and initial solvent concentration

Table 5.17 shows the effect of reactor diameter, the wall heat transfer coefficient, and the initial solvent concentration on the performance of LDPE reactor. With an increase in reactor diameter, the time taken to attain the peak temperature in the reactor increases (Fig. 5.57) and the monomer conversion decrease. Effect of each parameter is studied independently keeping the values of other parameters constant at reference value (as given in Table D1 in Appendix D). Again the peak temperature remains almost constant with a change in values of these variables; however the location of peak temperature changes (Fig. 5.57). Polydispersity index increases with increasing the reactor diameter (Fig. 5.58 and Table 5.17). Polydispersity index is the ratio of weight-average molecular weight to the number-average molecular weight, which is a measure of the distribution of molecular mass in a given polymer sample. PDI also varies slightly with a variation in the wall heat transfer coefficient. The effect of presence of solvent is also tested on PDI. PDI shoots to a value of 37.84 when solvent concentration is neglected. Sr. No. 1 to 3 of Table 5.17 and Fig.5.59 show that the number-average molecular weight decreases marginally with an increase in diameter. But the weight-average molecular weight increases (with relatively high value) with an increase in the reactor diameter, which tends to increase the PDI. The number-average molecular weight increases substantially to a very high value in the first zone in the absence of solvent. The solvent plays an important role in controlling the temperature of the reactor by terminating the chain to the solvent.

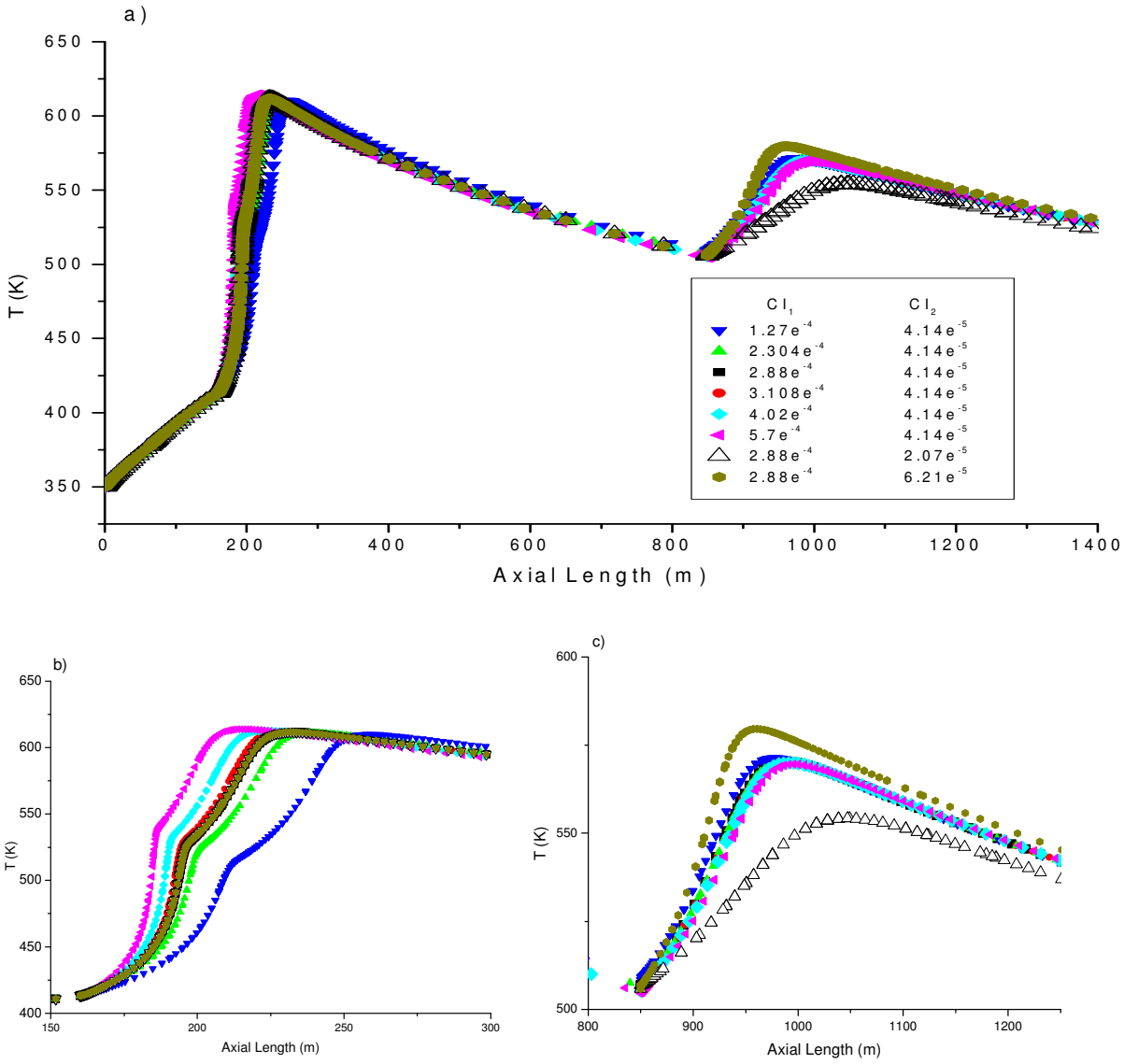

Fig. 5.51 (a) Effect of initiator concentration on the reactor temperature profile; (b) Magnified part of Figure (a) in the range of 150-300 m reactor length (c) Magnified part of Figure (a) in the range of 800-1250 m reactor length

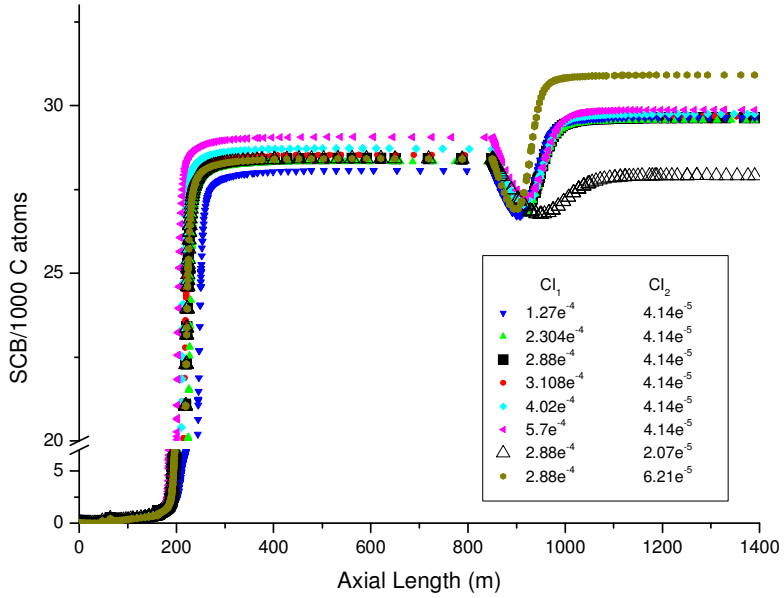

Fig. 5.52 Effect of initiator concentration on short chain branching content profile along the reactor length

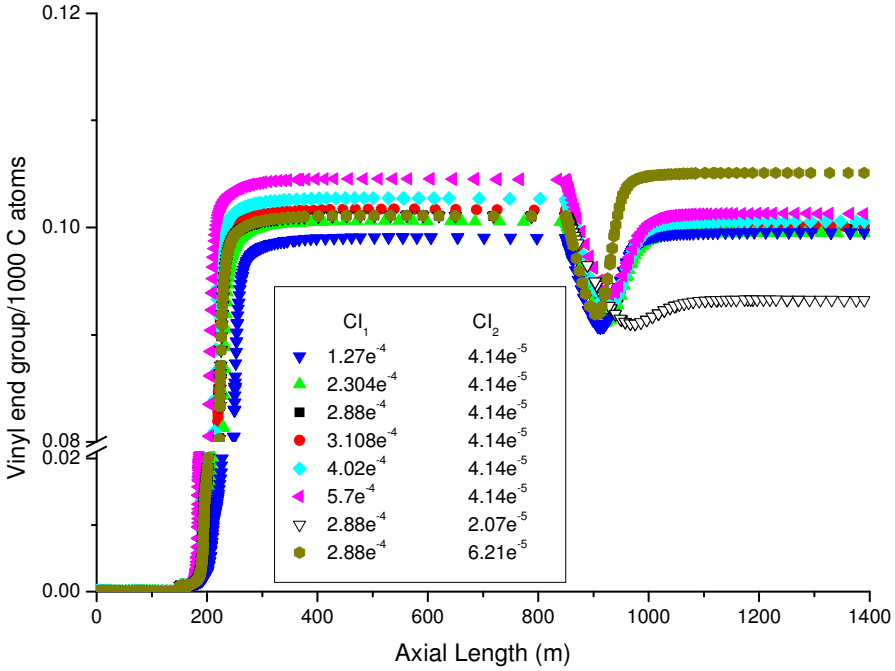

Fig. 5.53 Effect of initiator concentration on vinyl end group per 1000 C atoms profile along the reactor length

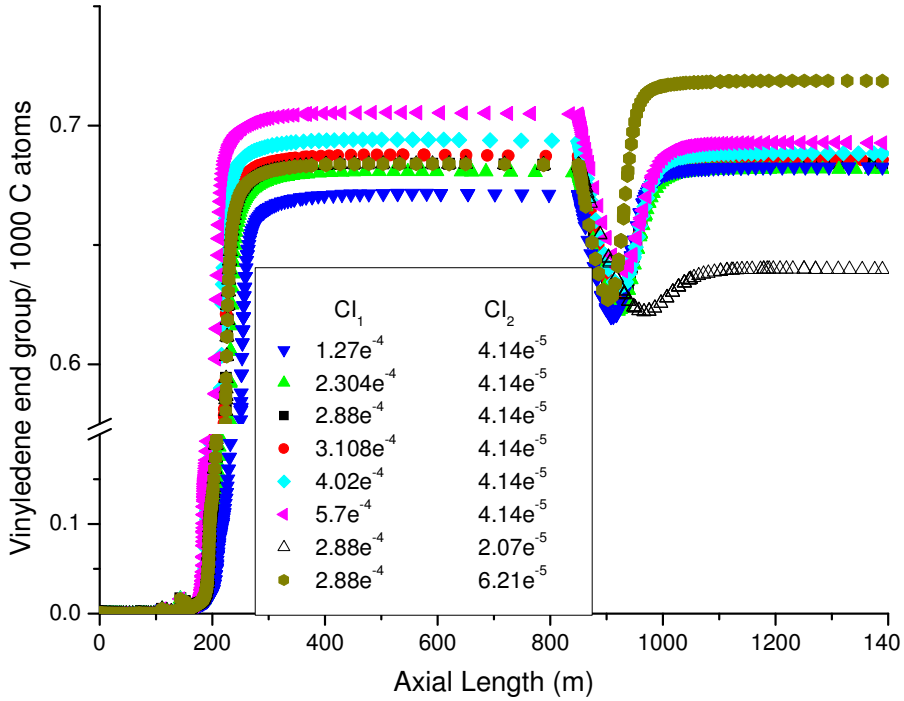

Fig. 5.54 Effect of initiator concentration on vinylidene end group per 1000 C atoms profile along the reactor length

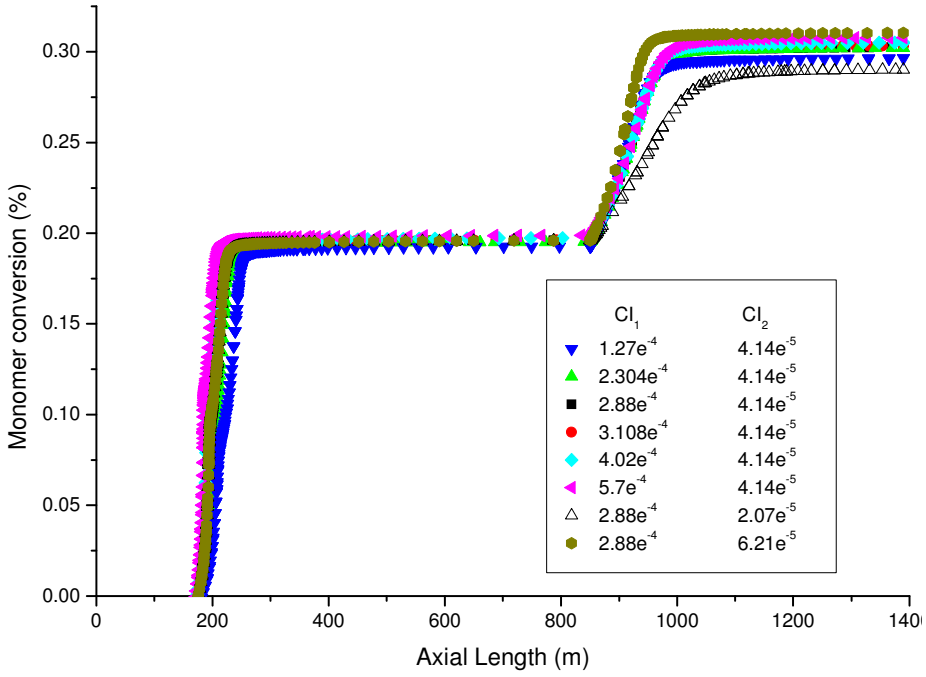

Fig. 5.55 Effect of initiator concentration on monomer conversion along the reactor length

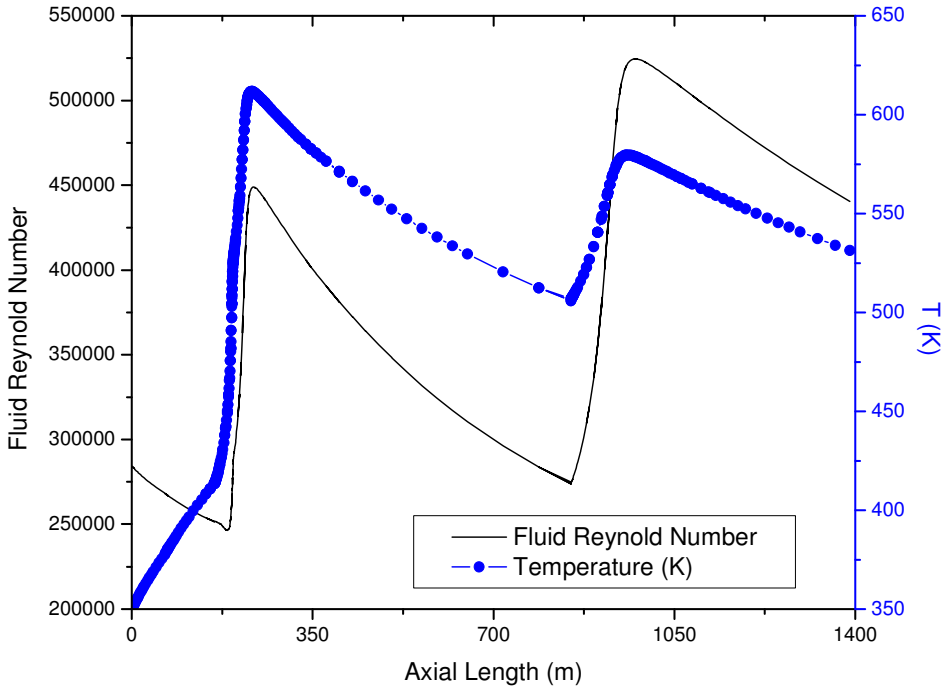

Fig. 5.56 Fluid Reynolds number and temperature profile of tubular LDPE reactor along the reactor length

Table 5.16 Various properties and exit concentrations of various species at different values of initiator concentration

Sr. No	CI_1 (kmole/m^3)	CI_2 (kmole/m^3)	Max temp. T_{MAX} (K)	Axial position at T_{MAX}, L_a (m)	M_w (kg/kmol)	M_n (kg/kmol)	PDI	Xm (%) (Exit)	Side chain concentration/10^3 C atoms			Unconverted ethylene (kmol/m^3)
									Methyl group (SCB)	Vinyl group	Vinylidene group	
1	$1.270e^{-4}$	$4.14e^{-5}$	609.99	258.73	280599	22286	12.59	0.2964	29.64	0.0995	0.6825	14.05
2	$2.304e^{-4}$	$4.14e^{-4}$	611.16	239.25	256053	22020	11.62	0.302	29.57	0.099	0.6817	13.96
3	$2.880e^{-4}$	$4.14e^{-5}$	611.63	231.82	243594	21792	11.17	0.302	29.63	0.09985	0.6807	13.96
4	$3.168e^{-4}$	$4.14e^{-5}$	611.93	229.63	238116	21668	10.98	0.303	29.68	0.100	0.6857	13.94
5	$4.02\ e^{-4}$	$4.14e^{-5}$	612.63	223.17	223829	21371	10.48	0.305	29.75	0.100	0.68838	13.91
6	$5.760e^{-4}$	$4.14e^{-5}$	611.64	214.73	201120	20821	9.659	0.307	29.87	0.1012	0.69276	13.87
7	$2.88e^{-4}$	$2.07e^{-5}$	613.82	231.82	246426	23127	10.66	0.290	27.91	0.0932	0.639	14.21
8	$2.88e^{-4}$	$6.21e^{-5}$	611.63	231.82	242368	20827	11.63	0.310	30.92	0.1050	0.7187	13.80

Table 5.17 Various properties and exit concentration of different species at different reactor diameter, the wall heat transfer coefficient and the initial solvent content

Sr. No	D_i (m)	h_w (W/m^2.^{0}C)	$[S]_0$ (kmol/m^3)	Max temp. T_{MAX} (K)	Axial position at T_{MAX}, L_a (m)	M_w (kg/kmol)	M_n (kg/kmol)	PDI	Xm (%) (Exit)	Side chain concentration/10^3 C atoms			Unconverted ethylene (kmol/m^3)
										Methyl group (SCB)	Vinyl group	Vinylidene group	
1	0.038	1256	0.0641	610.95	218.77	205163	21558	9.5167	0.3188	30.065	0.1009	0.69214	13.79
2	0.05	1256	0.0641	611.63	231.82	242368	20827	11.636	0.3104	30.915	0.1050	0.71872	13.79
3	0.063	1256	0.0641	612.16	245.76	278176	20547	13.538	0.3089	31.213	0.1068	0.72945	13.74
4	0.05	628	0.0641	613.14	274.03	333787	19605	17.025	0.2975	32.297	0.1127	0.76675	13.83
5	0.05	1884	0.0641	610.99	218.01	204120	21386	9.5443	0.3162	30.259	0.1018	0.69818	13.84
6	0.05	1256	0	611.69	231.98	871875	23262	37.480	0.3110	30.951	0.1052	0.71984	13.78

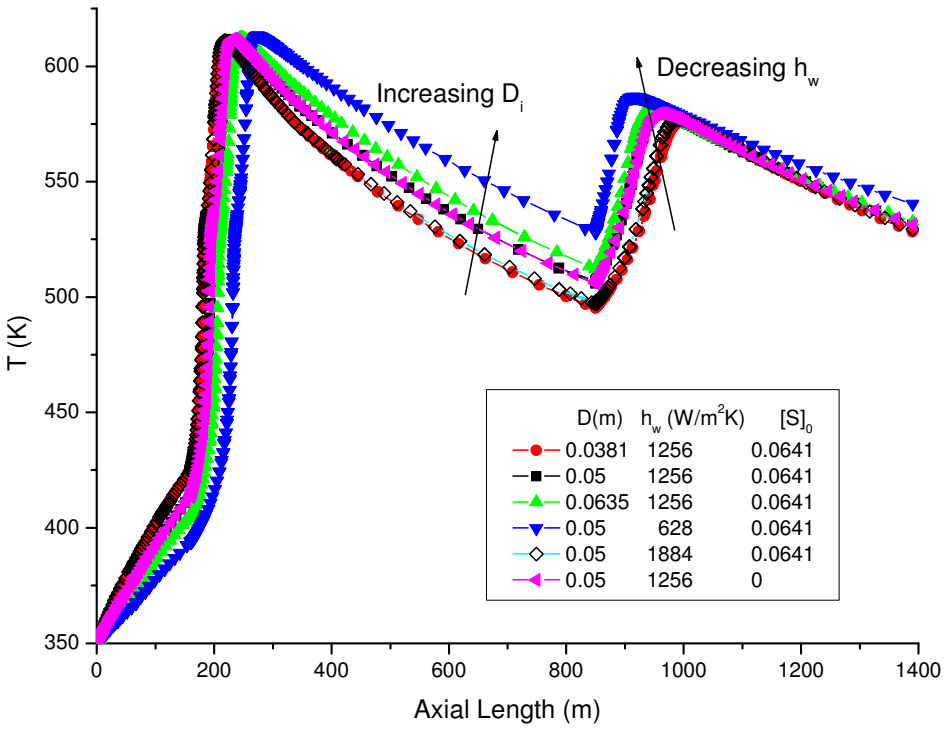

Fig. 5.57 Influence of reactor diameter, wall heat transfer coefficient and initial solvent content on the temperature of the reactor

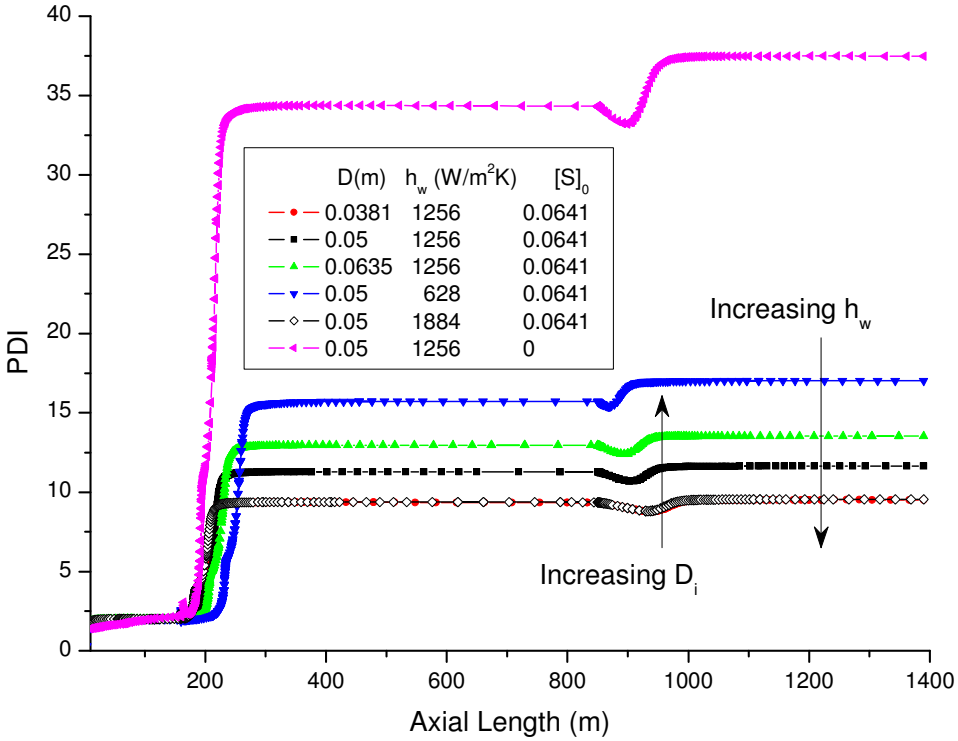

Fig. 5.58 Influence of reactor diameter, wall heat transfer coefficient and initial solvent content on the polydispersity index

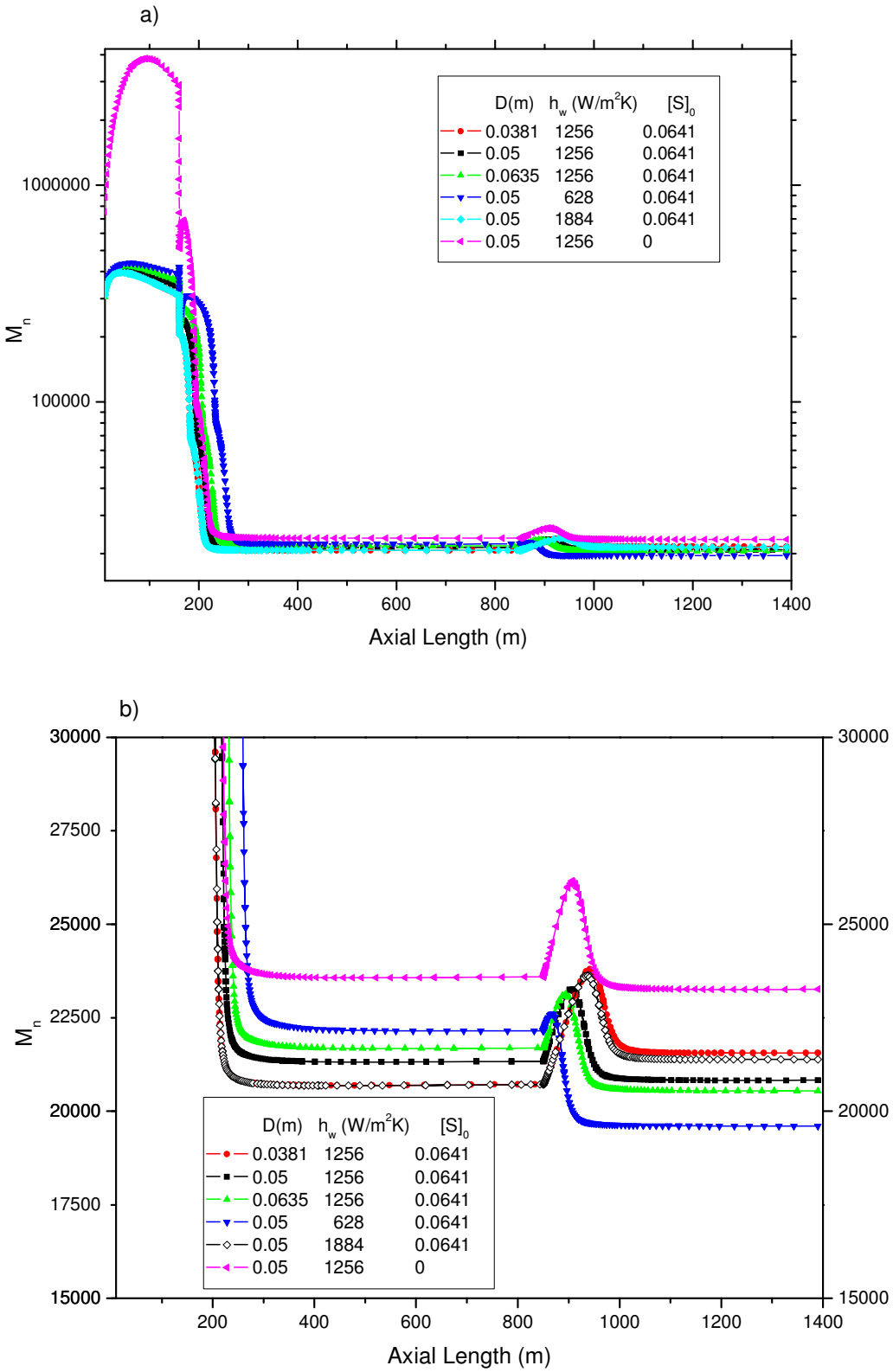

Fig. 5.59 (a) Influence of reactor diameter, wall heat transfer coefficient and initial solvent content on the number-average molecular weight of polymer (b) Magnified part of Fig. (a) in the range of 15000-30000 M_n on y axes

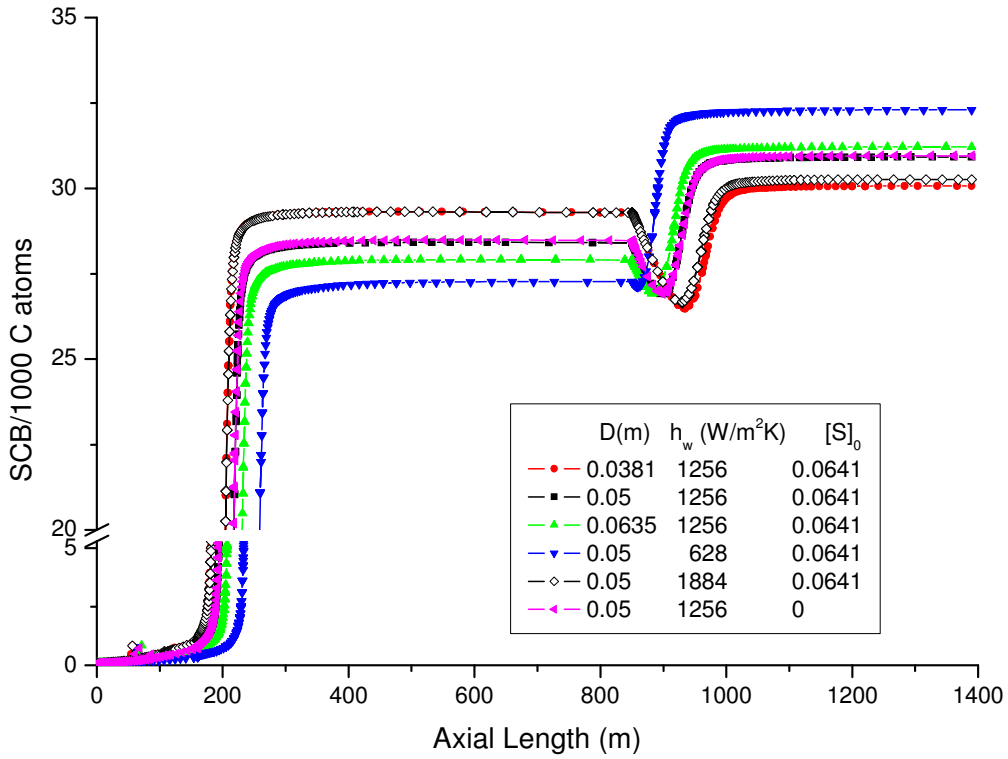

Fig. 5.60 Influence of reactor diameter, wall heat transfer coefficient and initial solvent content on the short chain branching per 1000 C atoms along the reactor length

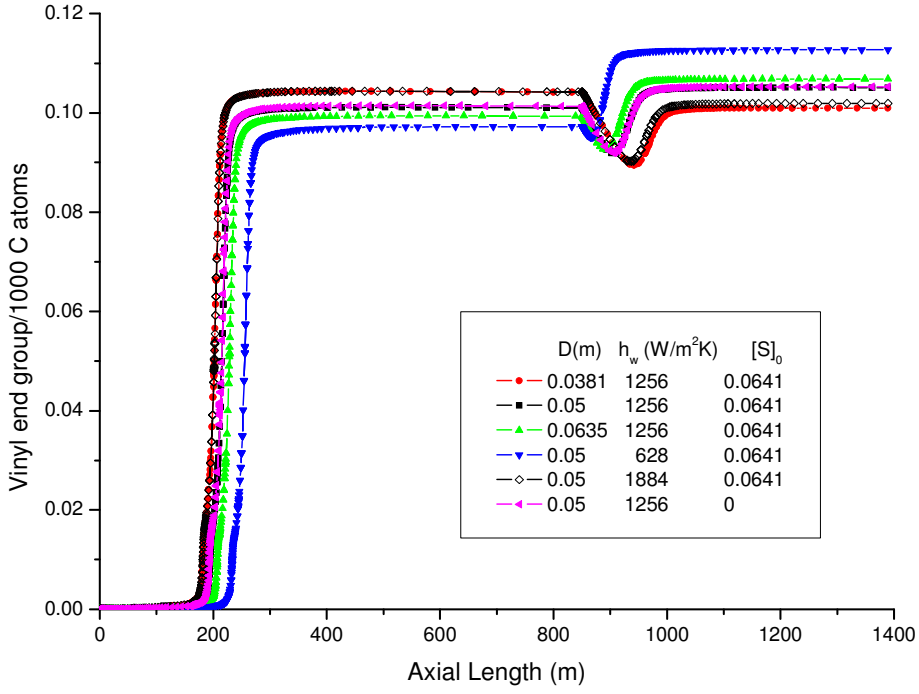

Fig. 5.61 Influence of reactor diameter, wall heat transfer coefficient and initial solvent content on the vinyl end group per 1000 C atoms along the reactor length

An optimum choice of solvent is required in order to avoid the reactor instabilities and formation of side chains. In the absence of solvent, a relatively high value of M_n (=23, 262) is observed at the exit of reactor, which substantiates the above discussion. Figs. 5.60 - 5.61 show that the concentration of the side chain increases with increasing the reactor diameter, while it remains high at a lower value of the wall heat transfer coefficient. The side chain concentration is relatively independent of solvent concentration over the ranges covered in this study.

Effect of initial monomer concentration and initial feed velocity

The effect of initial concentration of monomer and the initial feed velocity on temperature, short chain branching and monomer conversion are shown in Figs. 5.62 – 5.64. With a low value of initial monomer concentration, the location at which the peak temperature is attained in the reactor is delayed (Fig. 5.62). The concentration of SCB and the monomer conversion is raised to a very high value when a relatively low monomer concentration was injected at the inlet of the reactor. With an increase in the initial monomer concentration (in the range considered in this study), the peak temperature increases while the concentration of side chain (SCB) and monomer conversion decrease as shown in Figs. 5.62 and 5.64. With an increase in the feed velocity, the monomer conversion increases while the concentration of SCB decreases. The reduction in SCB at relatively lower feed velocity is due to the lower value of maximum temperature attained in the reactor (see Figs. 5.62 and 5.63). With an increase in the feed velocity, the location of peak temperature is delayed as shown in Fig. 5.63.

In the next subsection, results obtained on MOO of LDPE tubular reactor are discussed.

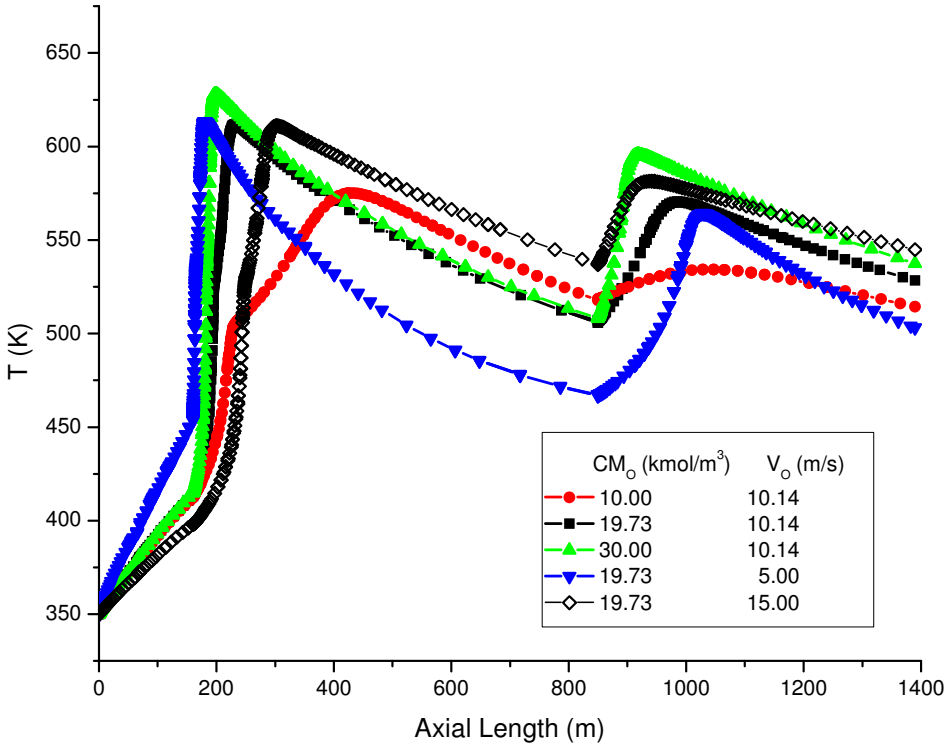

Fig. 5.62 Influence of initial monomer flow rate and feed velocity on the temperature profile along the reactor length

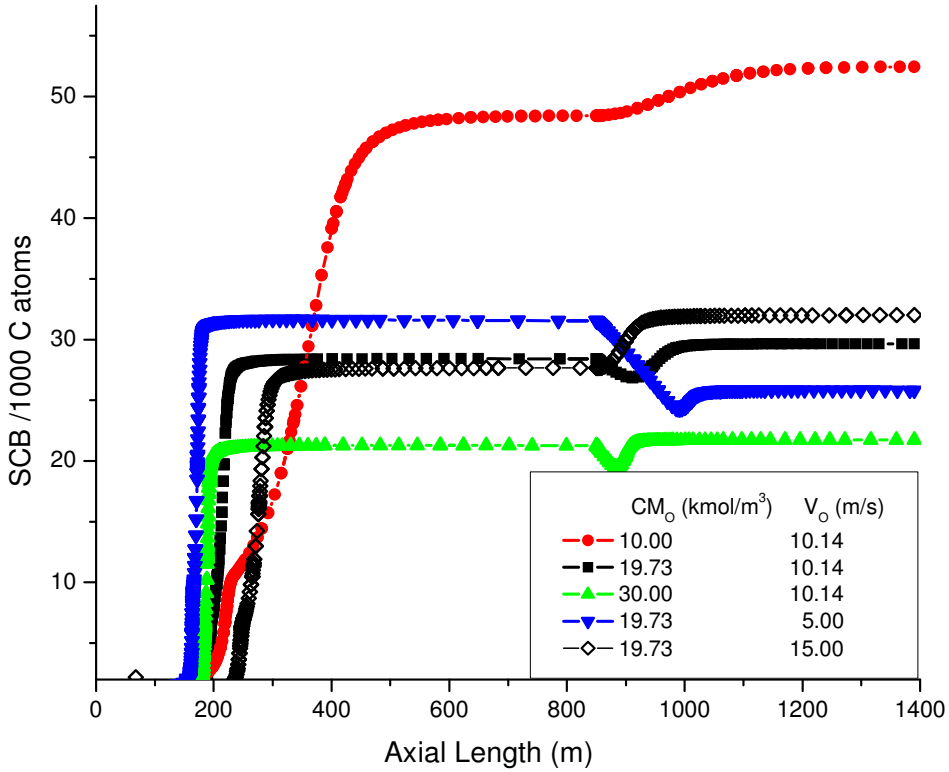

Fig. 5.63 Influence of initial monomer flow rate and feed velocity on the short chain branching profile along the reactor length

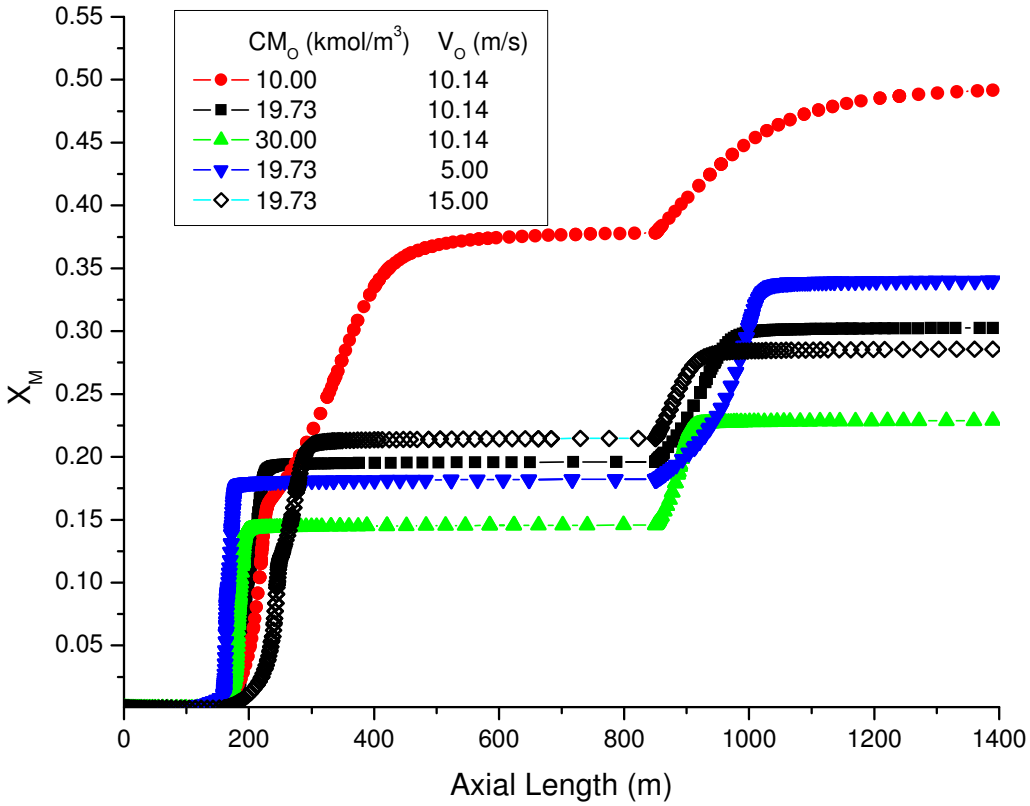

Fig. 5.64 Influence of initial monomer flow rate and feed velocity on the monomer conversion profile along the reactor length

5.2.4.2 Multi-objective optimization of low density polyethylene (LDPE) tubular reactor

ODE15s subroutine of MATLAB (7.0) library, which uses numerical differentiation formulas (NDFs), is used in the present study. The model equations were solved on Pentium-IV, 2.4 GHz core 2 duo processor. The cpu time for MODE III, hybrid MODE, and trigonometric MODE algorithms for 1500 generations is 206041.3, 2317101, and 353610 seconds respectively. Detailed description of simulation and analysis of LDPE tubular reactor is given in section 5.2.4.1. The present study involves MOO of two objectives namely, maximization of conversion and minimization of sum of normalized side products (methyl, vinyl and vinylidene end groups). The problem formulation is given in section 4.2.4. In simulation, the following values of parameters are used for multi-objective optimization: NP = 200, CR = 0.9, F = random (0, 1). The maximum number of generations is fixed at 1500 generations. The penalty function approach is used with normalized form of the constraints. Weights, $w_{1,}$ and w_2 are imposed on violation of constraints, namely, temperature and the number-average molecular weight. The value of both the weights ($w_{1,}$ and w_2) is set to 10^{10} for all the cases. However, to study the effects of weights, w_1=10^2 and w_2=10^5 are also tried and the results are reported. The MOO study is carried out using MODE, MODE III, hybrid MODE and trigonometric MODE algorithms. However, MODE algorithm could not result in any set of feasible solutions.

Case 1: Two-objective optimization study

Multi-objective optimization of two objectives, namely maximization of conversion and minimization of sum of normalized side products is carried out using the algorithms developed in this study. A set of eleven decision variables, which consists of operating variables, namely, inlet temperature (T_{in}), inlet pressure (P_{in}), the feed flow rates of -

oxygen (F_o), -solvent (F_S), -initiators ($F_{I,1}$, $F_{I,2}$), and the five average jacket temperatures ($T_{J,1}$ - $T_{J,5}$), is considered.

The Pareto fronts obtained using MODE III, hybrid MODE and trigonometric MODE algorithms are shown in Fig. 5.65. Three variations are considered in case 1 study (as given in section 4.2.4). The equality constraint on number-average molecular weight is relaxed by ± 2, ± 20, ± 200, and ± 1100 kg/kmol from its original value of 21, 900 kg/kmol. However, the constraint with $M_{N,f}$ = 21,900 ± 200 kg/kmol, is considered as a reference case and the results are discussed with respect to the reference case. Fig. 5.65 shows that the trigonometric MODE algorithm converged to a local Pareto as compared to the Pareto fronts obtained using MODE III and hybrid MODE algorithms. Both hybrid MODE and MODE III algorithms converged to the same front. However, the diversity of solutions obtained using both the algorithms is different. To compare the performance of MODE III and hybrid MODE algorithms, the Pareto fronts obtained using both the algorithms are shown on the same plot (Fig. 5.66). MODE III algorithm covered a range of conversion of 0.335-0.375 on the abscissa. Fig. 5.67 shows the converged Pareto optimal solutions for various end point constraints on the number-average molecular weight (i.e., $M_{N,f}$ = 21, 900 ± 2; $M_{N,f}$ = 21, 900 ± 20; $M_{N,f}$ = 21, 900 ± 200; $M_{N,f}$ = 21, 900 ± 1100) using hybrid MODE algorithm. More relaxed is the constraint, the better is the distribution of solutions (Fig. 5.67). With a strict constraint, i.e., $M_{N,f}$ = 21, 900 ± 2, it is difficult to obtain a smooth Pareto front. Also, with such a strict constraint, the solutions obtained have a typical nature of high value of side chain products and a low conversion value as shown in Fig. 5.67.

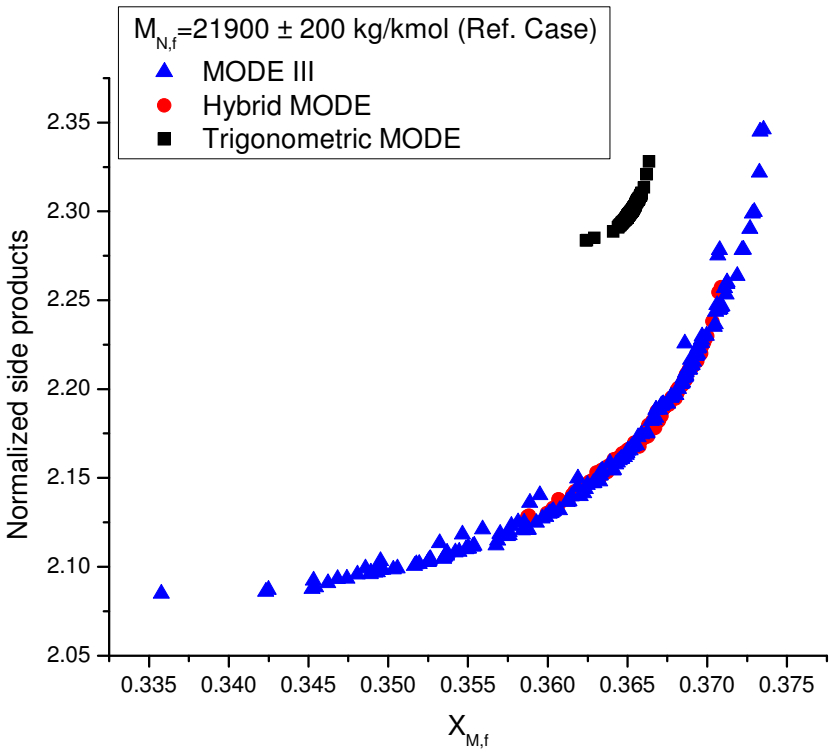

Fig. 5.65 Pareto optimal solutions for case 1 using strategies of MODE for a reference case ($M_{N,f}$ = 21,900 ± 200 kg/kmol)

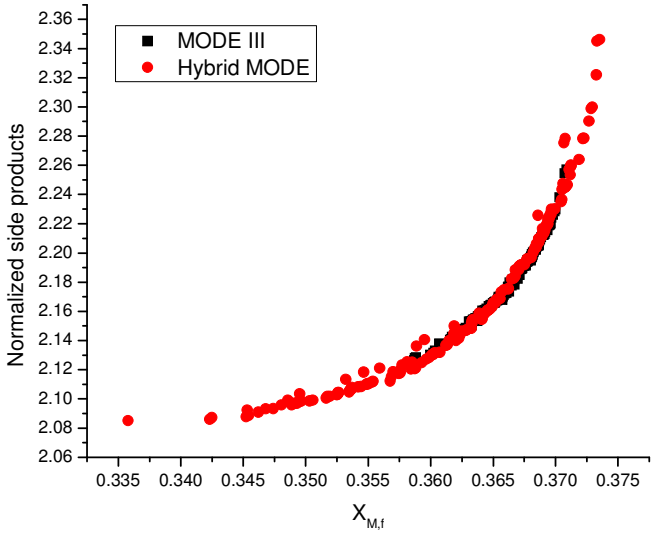

Fig. 5.66 Pareto optimal solutions for case 1 using MODE III and hybrid MODE algorithms for a reference case ($M_{N,f}$ = 21,900 ± 200 kg/kmol)

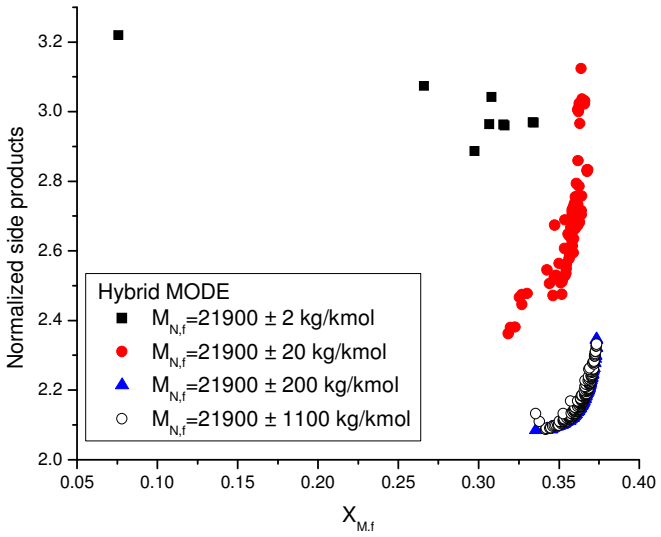

Fig. 5.67 Converged Pareto optimal solutions for various end point constraints on the number-average molecular weight using hybrid MODE algorithm

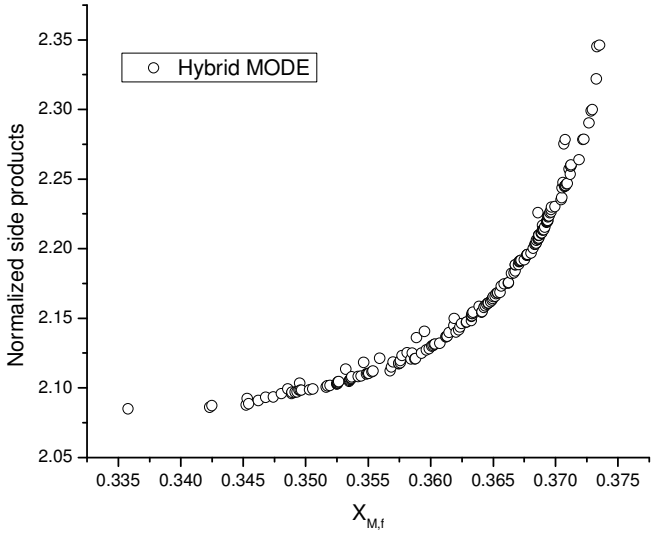

Fig. 5.68 Pareto optimal solutions for case 1 using hybrid MODE algorithm for a reference case ($M_{N,f}$ = 21,900 ± 200 kg/kmol)

The Pareto optimal solutions obtained for case 1, using hybrid MODE algorithm after 1500 generations for a reference case ($M_{N,f}$ = 21,900 ± 200 kg/kmol) is shown in Fig. 5.68. Fig. 5.68 shows that a good distribution of solutions is obtained in the middle portion of Pareto front using hybrid MODE algorithm. However, the distribution is poor at the periphery of the Pareto front. The choice of step size in hybrid MODE algorithm was to be made after several trial and error runs. The step size used in generating a new neighborhood solution, in this problem is same, as that reported in section 5.2.1 for the case of MOO of styrene reactor. For a problem having more number of variables, it is difficult to consider a variation in step size for each individual variable. This drawback of hybrid MODE algorithm is observed during the MOO study of LDPE tubular reactor. For all the remaining test problems and the industrial case studies, the hybrid MODE algorithm performed better than MODE III. This shows that, unless a judicious choice of step size in generating a neighborhood solution is made, hybrid MODE cannot guarantee a well-diversed Pareto front. However, the hybrid MODE algorithm is able to converge to the same Pareto front as that obtained using MODE III algorithm.

Fig. 5.69 shows the converged Pareto optimal solutions for various end point constraints on the number-average molecular weight (i.e., $M_{N,f}$ = 21, 900 ± 2; $M_{N,f}$ = 21, 900 ± 20; $M_{N,f}$ = 21, 900 ± 200; $M_{N,f}$ = 21, 900 ± 1100) for case 1 objectives using trigonometric MODE algorithm. It is difficult to obtain a smooth Pareto front with a strict constraint imposed on the number-average molecular weight.

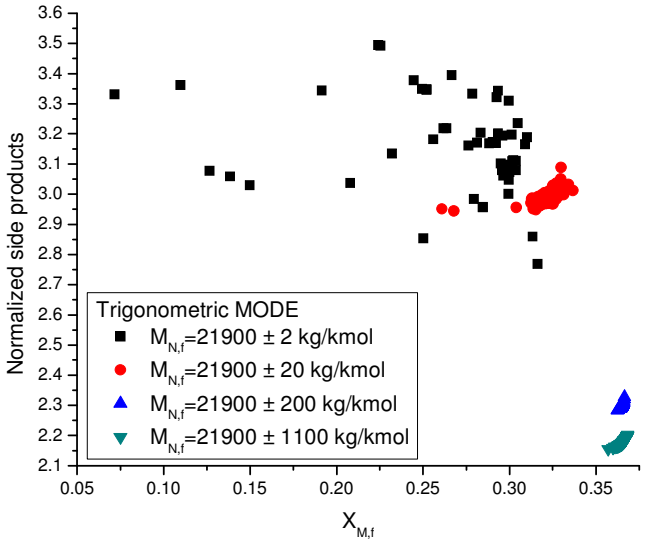

Fig. 5.69 Converged Pareto optimal solutions for various end point constraints on the number-average molecular weight using trigonometric MODE algorithm

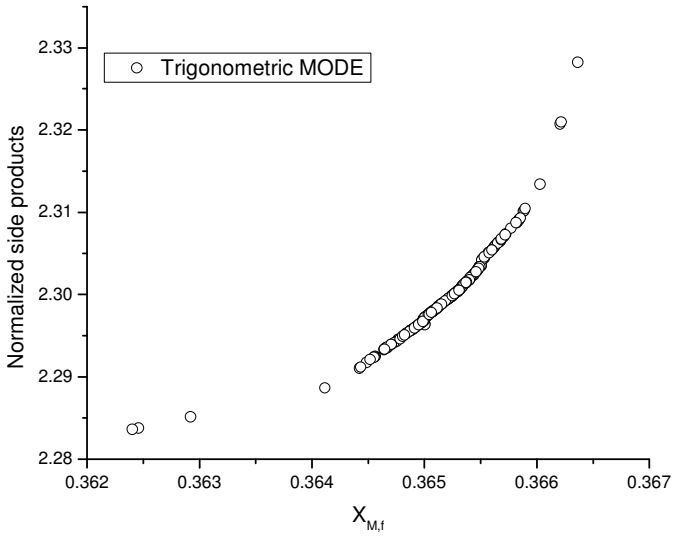

Fig. 5.70 Pareto optimal solutions for case 1 using trigonometric MODE algorithm for a reference case ($M_{N,f}$ = 21,900 ± 200 kg/kmol)

As per the discussions made in section 5.2.4.1, the number-average molecular weight is a strong function of operating variables. Very limited range of optimum variables exists for such a strict constraint and even a slight change in operating variables from its optimum value may make it difficult to satisfy the constraints, and the algorithm may result in an infeasible set of solutions. Thus, it is difficult for any algorithm to converge to a smooth and well-diverse Pareto front. The trigonometric MODE algorithm could not approach the true Pareto front, as it involved a mutation strategy, which is greedy in nature. In the original article on trigonometric MODE algorithm (Fan and Lampinen, 2003), it is referred that the mutation operation used in the trigonometric differential evolution (TDE) algorithm for a single objective optimization problem, may result in a premature convergence, as the strategy of mutation used in TDE is greedy in nature and acquires a fast convergence. Therefore, the trigonometric MODE algorithm needs to be used with lesser value of trigonometric mutation probability, for an industrial problem, where a true Pareto is not known. Fig. 5.70 shows the Pareto front resulted for case 1 using trigonometric MODE algorithm. The quality of solutions from the Pareto front reveals that, the algorithms are not able to generate sufficient number of solutions especially at both ends of the front (extreme solutions). Thus, both the innovations considered in MODE III algorithms have their own benefits (both local and global search for faster convergence in case of hybrid MODE and an improved mutation strategy for trigonometric MDOE algorithm for a faster convergence). But the trigonometric mutation algorithm converged to a local Pareto front, and the hybrid MODE could not produce a well-diverse set of solutions as compared to the solutions obtained using MODE III algorithm.

Fig. 5.71 shows the converged Pareto optimal solutions for various end point constraints on the number-average molecular weight using MODE III algorithm. It is interesting to note that, unlike the results obtained using hybrid MODE and trigonometric MODE algorithm (where different Pareto fronts are obtained by relaxing the constraints bounds), the Pareto fronts obtained using MODE III algorithm for all the end point constraints (except, $M_{N,f} = 21900 \pm 2$) is same. However, the distribution of solutions on the Pareto front varies in each case. Fig. 5.72 shows the converged Pareto optimal solutions for various end point constraints on the number-average molecular weight (i.e., $M_{N,f} = 21, 900 \pm 20$; $M_{N,f} = 21, 900 \pm 200$; $M_{N,f} = 21, 900 \pm 1100$) using MODE III algorithm. The Pareto front obtained with an end point constraint, of $M_{N,f} = 21, 900 \pm 1100$, covers a wide range of solutions as compared to the range of solutions obtained when a strict constraint on $M_{N,f}$ is used (as shown in Figs. 5.72 - 5.73).

The set of decision variables corresponding to the Pareto optimal solutions obtained using MODE III algorithm for case 1 objectives using a reference case of $M_{N,f} = 21900 \pm 200$ is plotted along with one of the objectives and is shown through Figs. 5.74a - 5.74k. PDI and number-average molecular weight for the reference case run using MODE III algorithm are also plotted against one of the objective functions and are shown in Figs. 5.74l - 5.74m. Fig. 5.74a shows that a lower inlet temperature is favored for a higher conversion. This is because; at high temperature the degradation reactions are more favorable, which are responsible to produce more side products, thus reducing the conversion value.

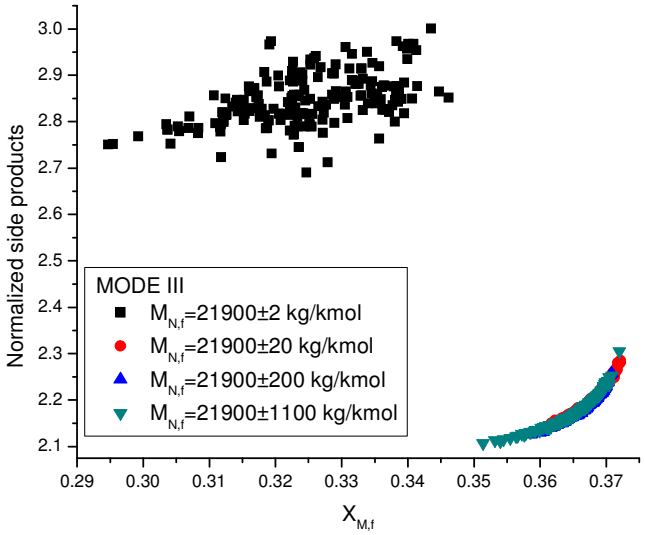

Fig. 5.71 Converged Pareto optimal solutions for various end point constraints on the number-average molecular weight using MODE III algorithm

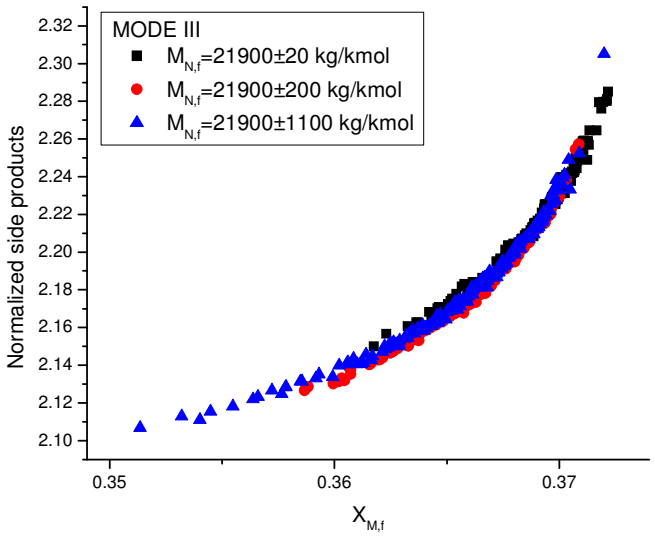

Fig. 5.72 Converged Pareto optimal solutions for various end point constraints on the number-average molecular weight using MODE III algorithm

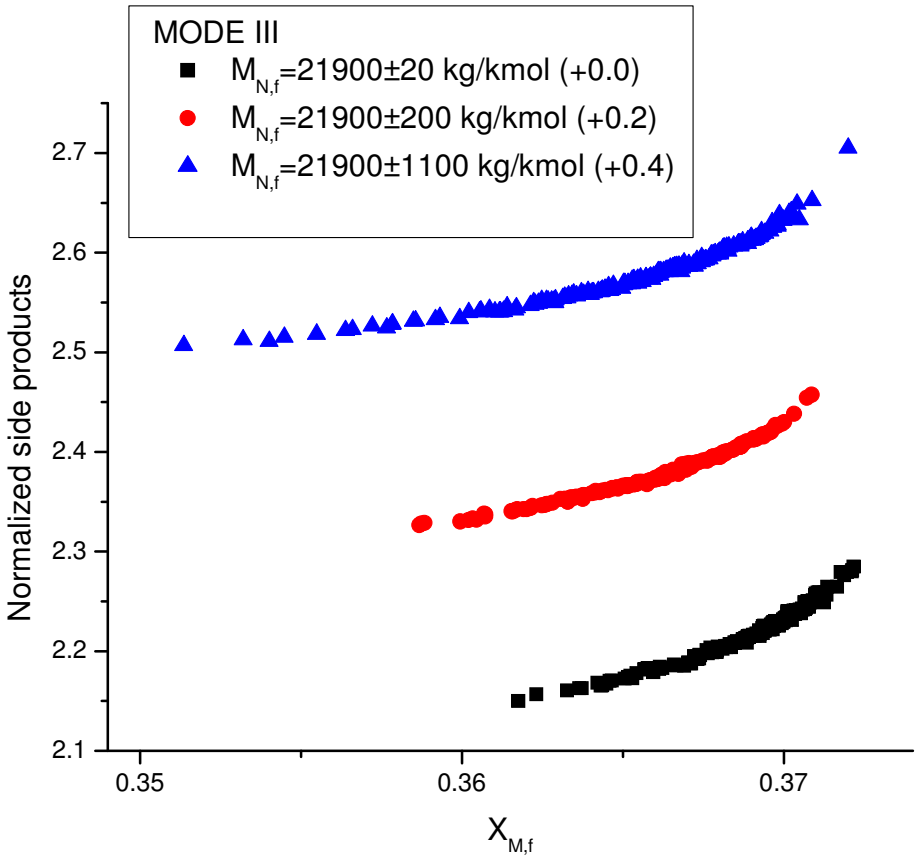

Fig. 5.73 Results of Fig. 5.72 are replotted with vertical shift of 0.2 (i.e., the values of the ordinate for $M_{N,f}$ = 21900 ± 200, $M_{N,f}$ = 21900 ± 1100 and are displaced vertically upwards by 0.2, and 0.4 respectively

A lower pressure is also favored for a higher conversion value as shown in Fig. 5.74b. The bounds on oxygen concentration lie in between 7.55414×10^{-5} - 1.5766×10^{-4} kmol/m^3. Thus, Fig. 5.74c shows that the optimum decision variables, corresponding to the Pareto solutions obtained using MODE III algorithm for case 1, converged towards their lower bounds. However, the solvent concentration varies in between 0.19 – 0.255 kmol/m^3 (Fig. 5.74d). The conversion increases by increasing the flow rates of both the initiators (Figs. 5.74e - 5.74f). However, the initiation reaction, being exothermic in nature, is responsible for generating a sudden high temperature in the reactor. A high temperature affects the number-average molecular weight and also is responsible for producing unwanted side chains as discussed in section 5.2.4.1.

A lower value of inlet temperature to the reactor is favored (from Fig. 5.74a). Thus a lower bound of jacket temperature for zone-1 is established corresponding to the Pareto optimal solutions (Fig 5.74g). The initiator-1 is injected at the inlet of zone-2 of reactor, causing a sharp rise in the temperature of the reactor. To remove the exothermic heat of reaction, a relatively cold utility is preferred in zones 2-5. This is evident from Figs. 5.74h - 5.74k. The PDI increases with an increase in conversion (Fig. 5.74l). The number-average molecular weight varies between the specified bounds, i.e., $M_{N,f}$ =21, 900 ± 200 (Fig. 5.74m). This also ensures that all the solutions lying on the Pareto front belong to the feasible solutions (i.e., no violation of constraints).

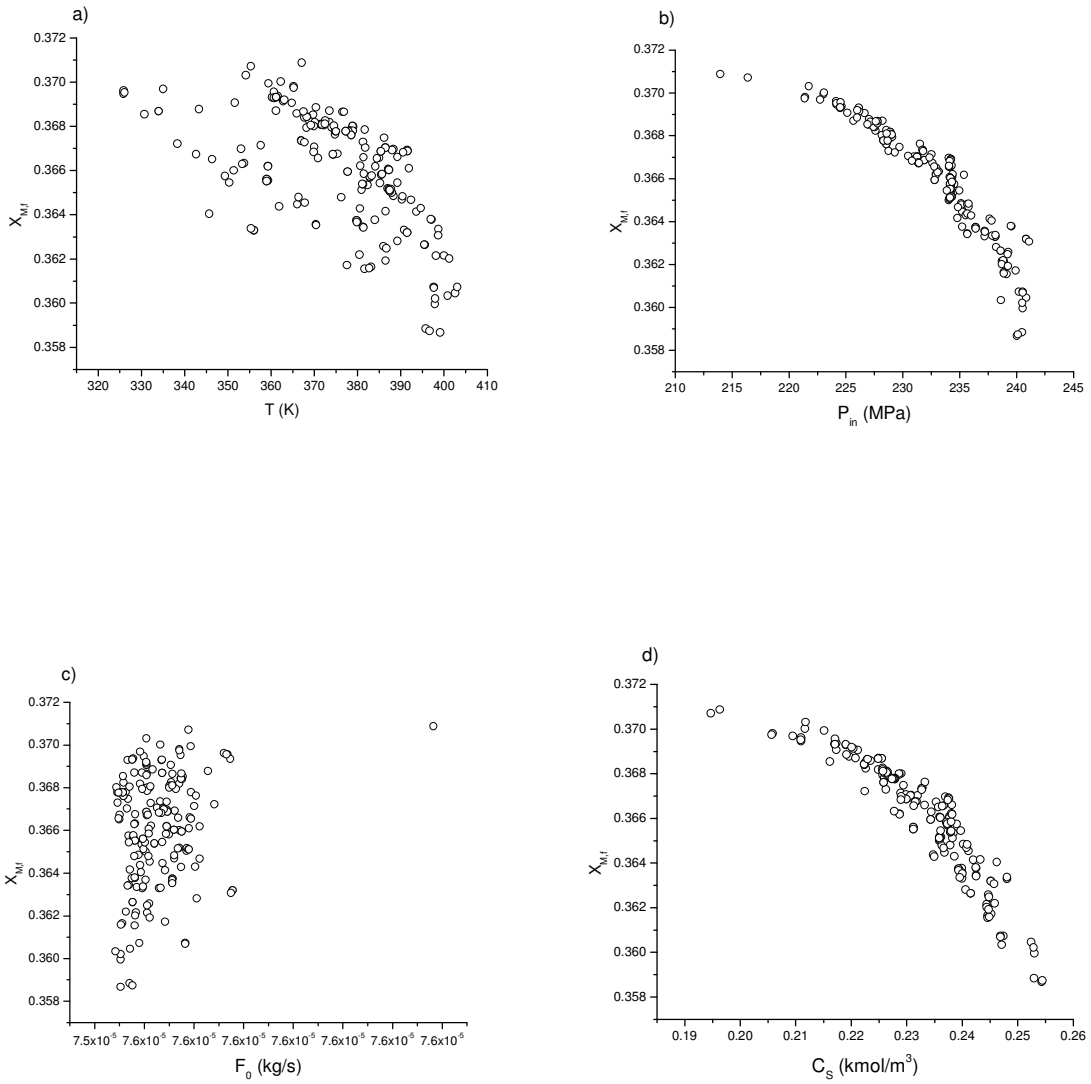

Fig. 5.74 (Contd…..)

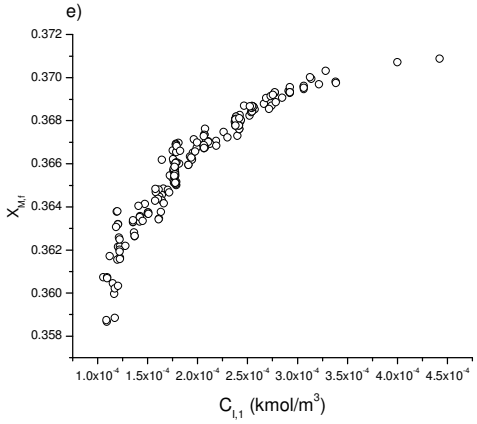

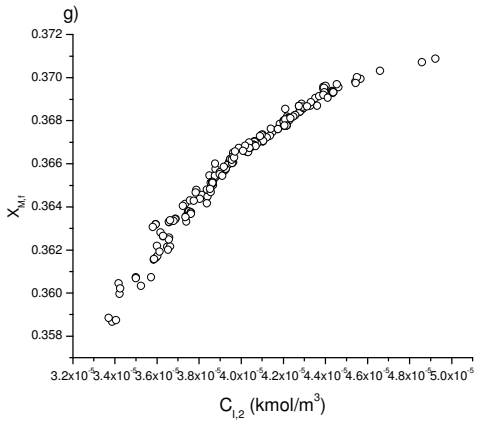

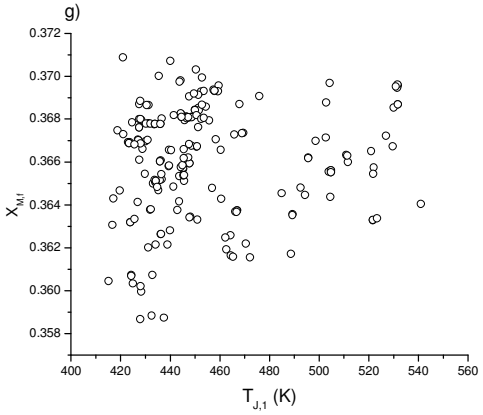

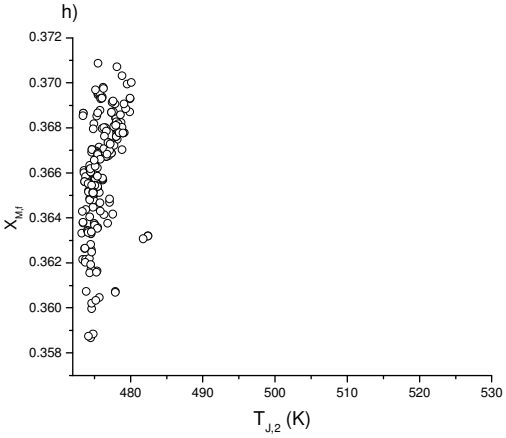

Fig. 5.74 (Contd…..)

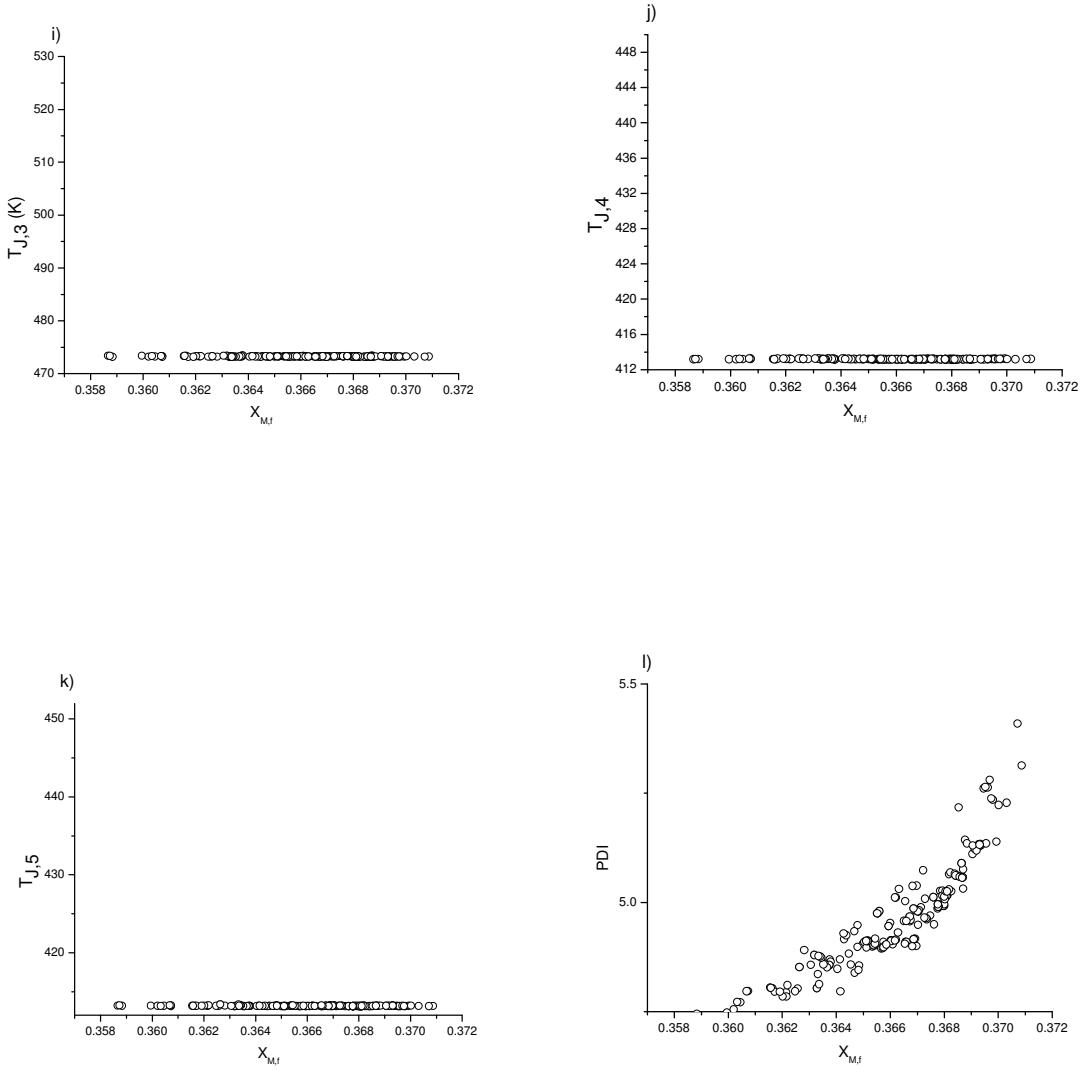

Fig. 5.74 (Contd…..)

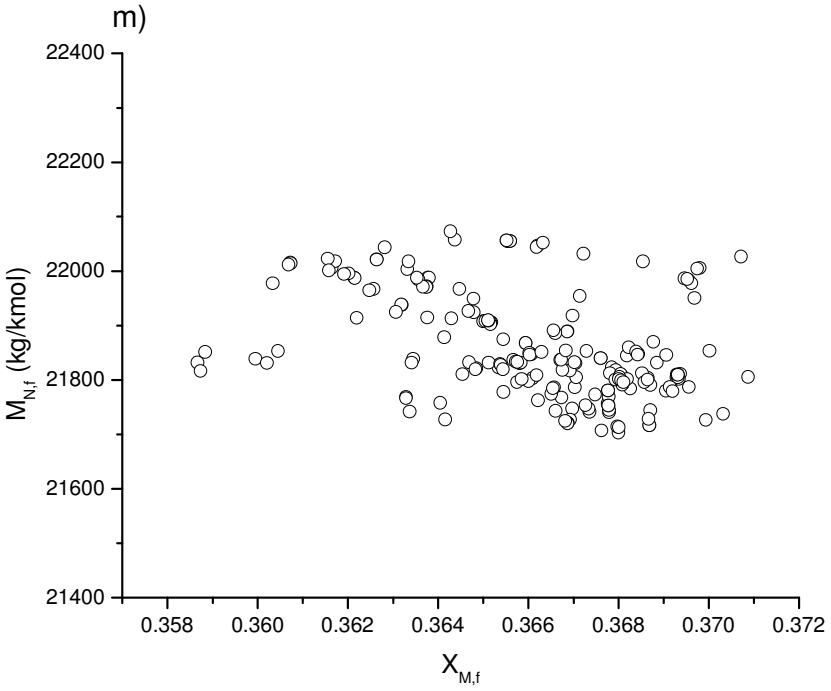

Fig. 5.74 (a-m) Decision variables, $M_{N,f}$ and PDI corresponding to the Pareto optimal solutions obtained using MODE III algorithm for the reference case ($M_{N,f}$ = 21900 ± 200)

Effect of weight of the penalty parameter on the Pareto front

The penalty function method (Deb, 2001) is used to handle the constraints in this study. Sufficiently high weights of penalty weights are used in this study to ensure the feasibility of Pareto optimal solutions. The normalized form of constraints is used. Two different simulation runs on MOO of case 1 are carried out using different sets of Penalty weights. In set 1, the weights of the penalty parameters are set as $w_1=10^2$ and $w_2=10^5$. In the second set of the penalty parameters, both the weights are set to as 10^{10}. Fig. 5.75 shows the Pareto fronts obtained using both the sets of penalty parameter weights. MODE III algorithm is able to converge to the same Pareto front irrespective of the weight of the penalty parameters considered in this study. However, such results can be obtained, only if, a large value of penalty parameter weight (as used in the present study) is used. For a smaller value of Penalty parameter, infeasible solutions may be obtained on the Pareto front.

Effect of the monomer feed rate on the Pareto front

The effect of the monomer (ethylene) feed rate on the Pareto optimal solution is also studied. MOO simulation runs are carried out by varying the monomer feed rate (such as, F_M = 13 kg/s, F_M = 11 kg/s, and F_M = 9 kg/s), using MODE III algorithm, for case 1 objectives using the reference case, i.e., $M_{N,f}$ = 21900 ± 200. As observed in the previous results (as discussed in section 5.2.4.1), monomer conversion reduces by increasing the monomer feed rate (Fig. 5.76). A higher conversion is obtained for a lower value of feed monomer rate.

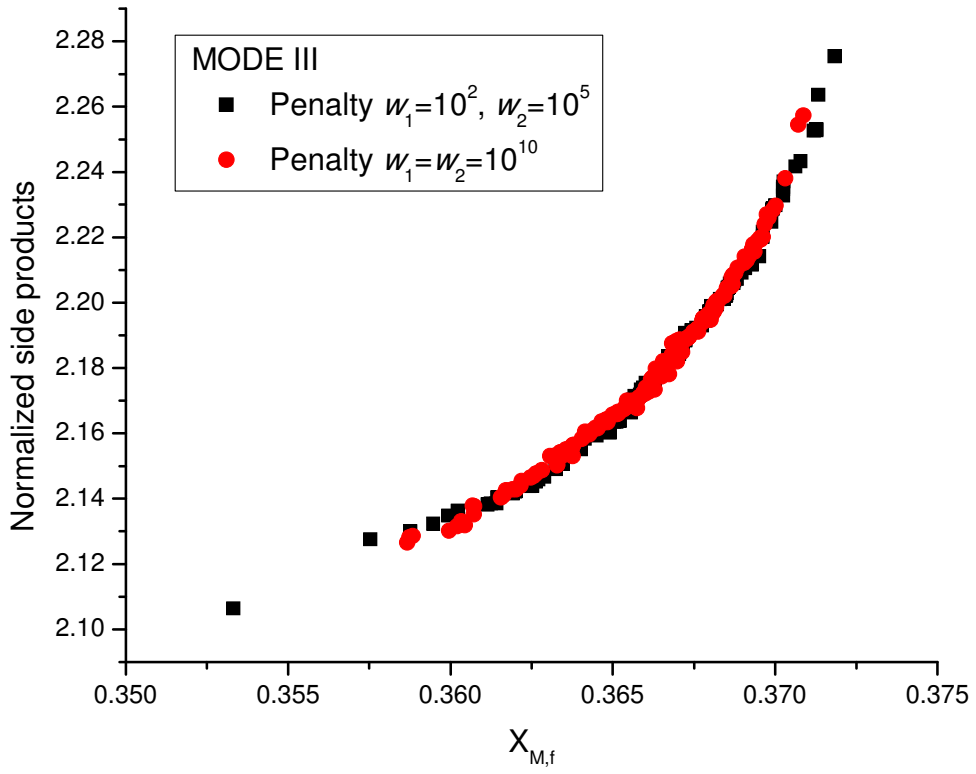

Fig. 5.75 Pareto optimal solutions obtained using different weights of Penalty parameter using MODE III algorithm for the reference case ($M_{N,f}$ = 21900 ± 200)

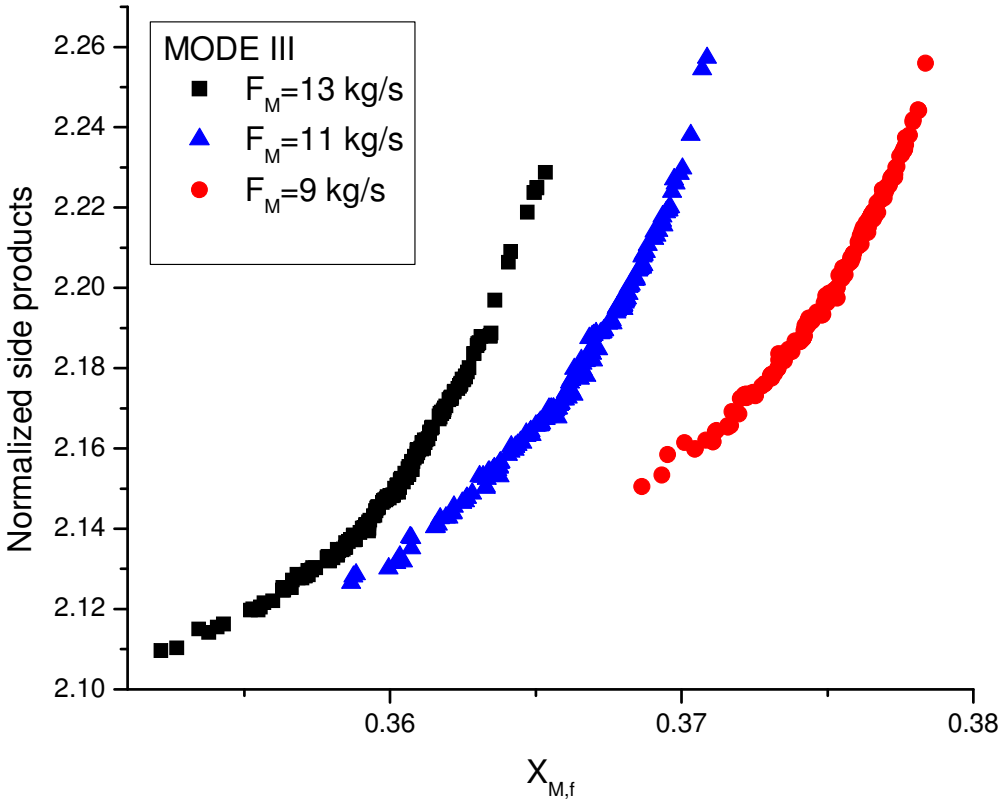

Fig. 5.76 Pareto optimal solutions obtained using different initial monomer feed rates using MODE III algorithm for the reference case ($M_{N,f}$ = 21900 ± 200)

Case 2: Four-objective optimization study

Four-objective optimization problem is considered in which each of the side products is taken as an independent objective function, along the maximization of the conversion. Thus case 2 considers simultaneous minimization of methyl, vinyl and vinylidene side chain content/1000 C atoms and maximization of the monomer conversion.

Fig. 5.77 shows the Pareto fronts obtained after 1500 generations for case 1, and 2500 generations for case 2 problems, using MODE III algorithm, for the reference case of $M_{N,f}$ = 21900 ± 200. As expected, the Pareto front obtained using four-objective optimization study for case 2 objectives, is scattered as compared to the Pareto front obtained using case 1 objectives (two-objective optimization study). While achieving the simultaneous satisfaction of all the objectives (in case of more than two-objectives) it may not be possible to obtain a smooth Pareto front and hence results in a scattered front (as is the case with 4-objective optimization of this study).

The generation-wise progress of non-dominated set of solutions obtained for case 2 problem using MODE III algorithm is shown in Fig. 5.78. The algorithm is able to reach towards the feasible Pareto region in less number of generations (i.e., less than 500 generations). However, at higher generations, the convergence speed reduces as it is relatively difficult to find new and improved solutions than the existing ones. The side chain concentrations (such as methyl, vinyl and vinylidene groups/1000 C atoms) are plotted as a function of population points (in increasing number) named as population index and are shown through Figs. 5.79a - 5.79d respectively.

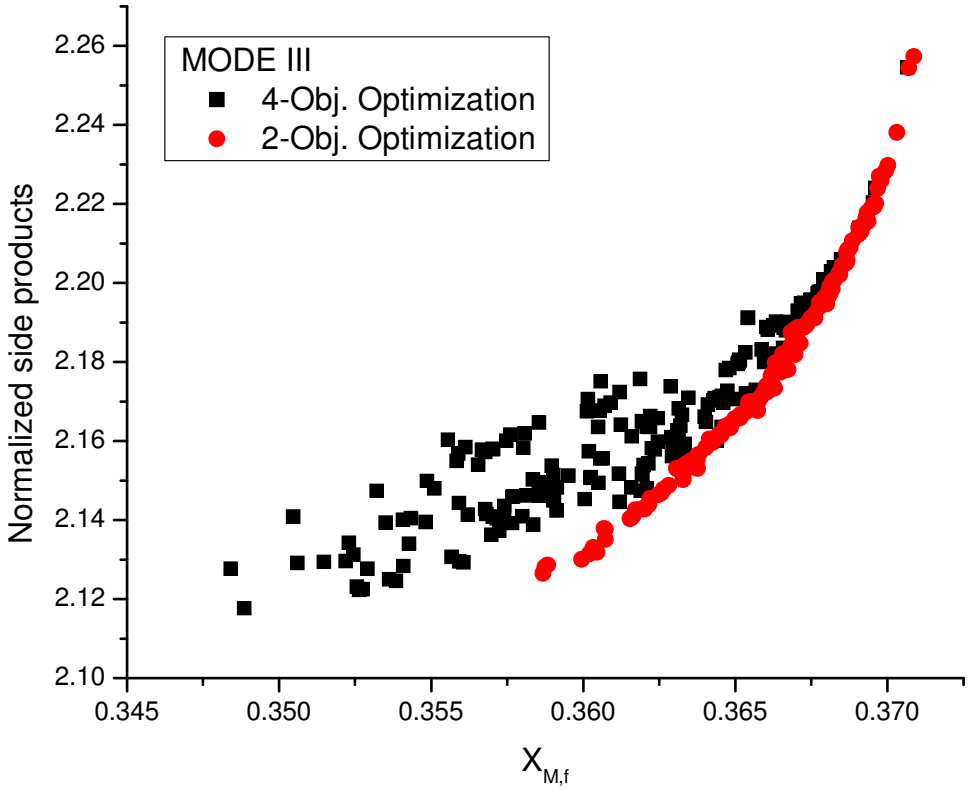

Fig. 5.77 Pareto optimal solutions obtained using four-objective optimization (case 2) and two-objective optimization (case 1) using MODE III algorithm for the reference case ($M_{N,f}$ = 21900 ± 200)

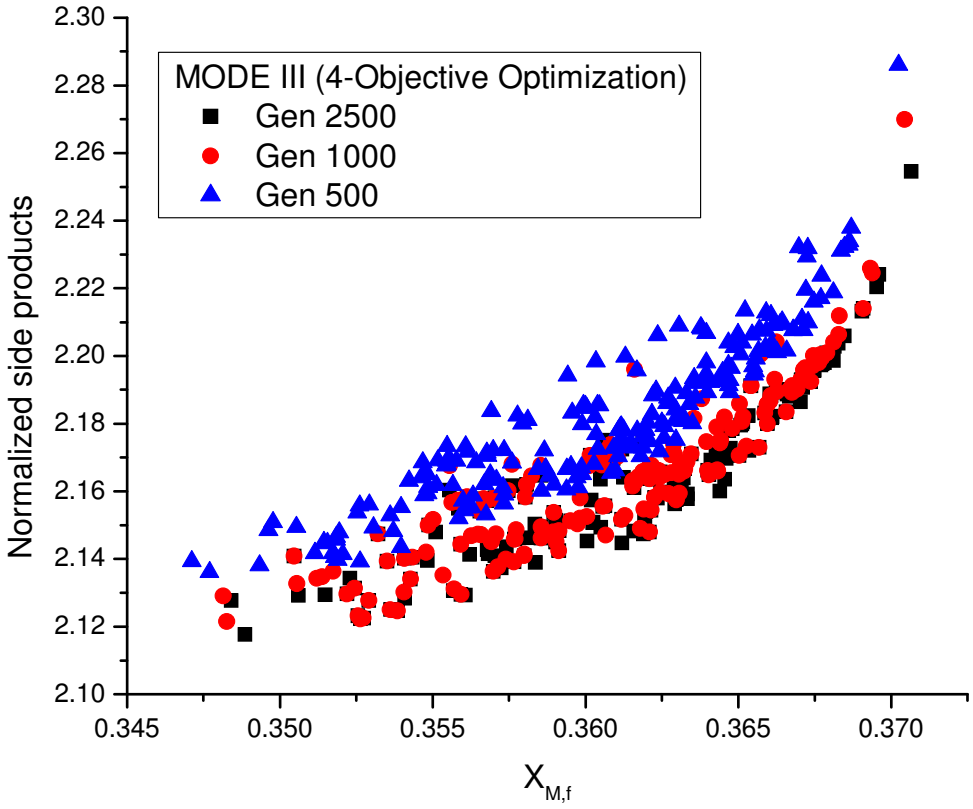

Fig. 5.78 Solutions obtained for case 2 at various generations using MODE III algorithm for the reference case ($M_{N,f}$ = 21900 ± 200)

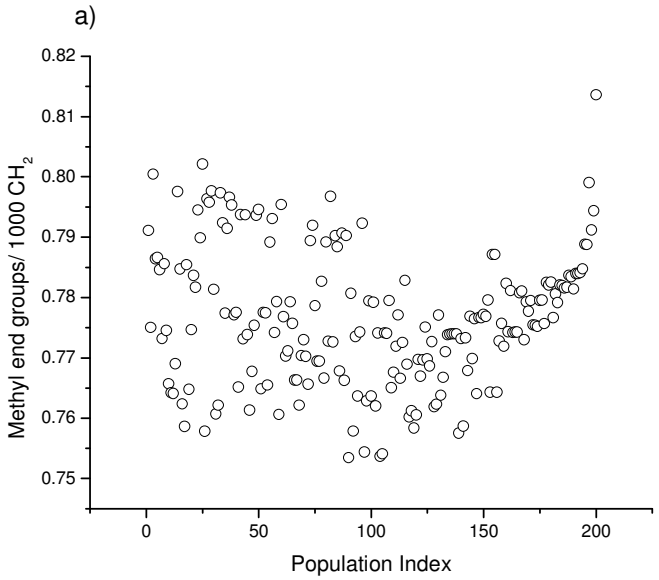

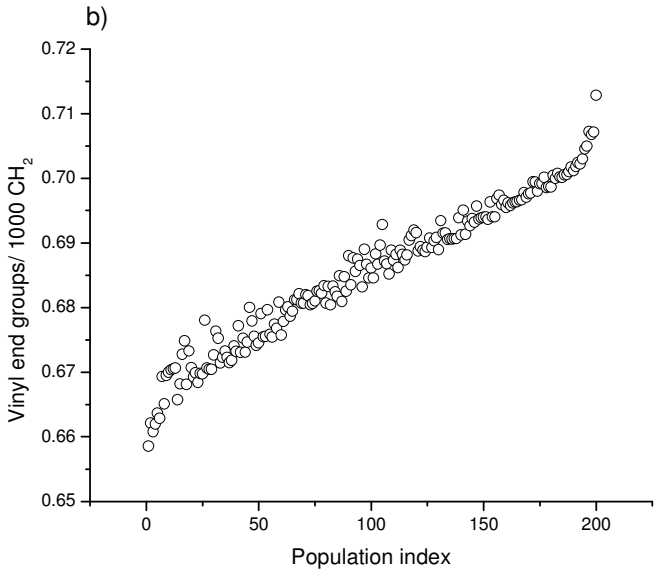

Fig. 5.79 (Contd…)

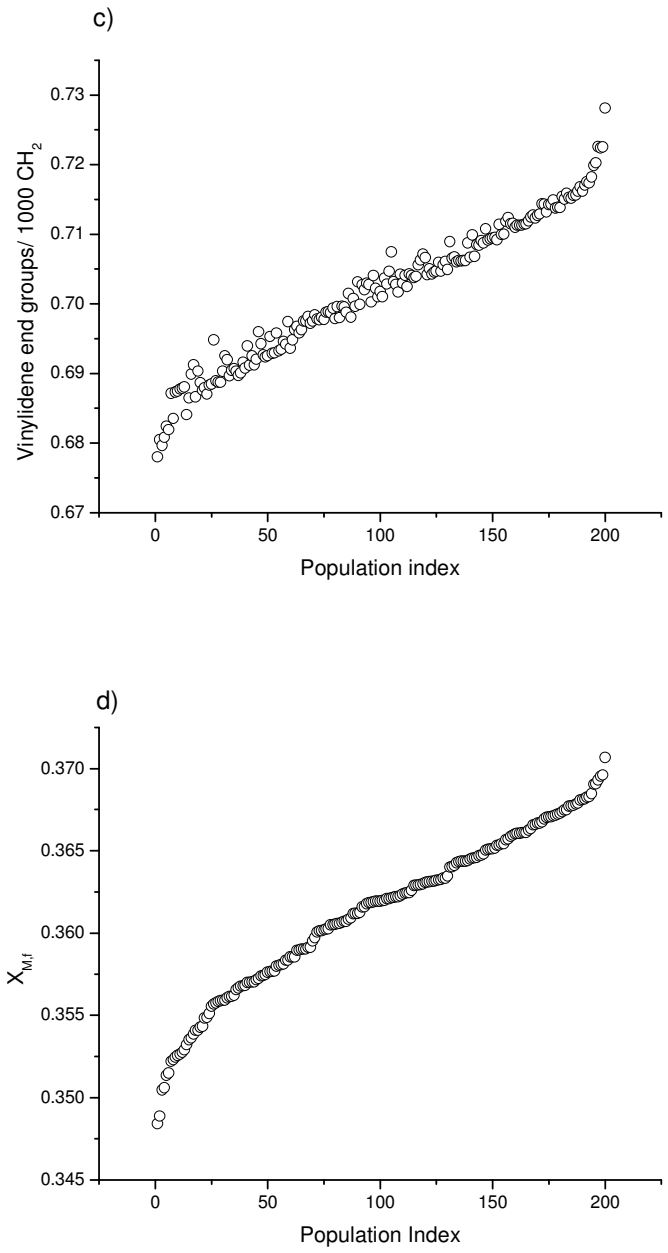

Fig. 5.79 (a-d) Side chain concentrations (methyl, vinyl, and vinylidene) per 1000 C atoms and monomer conversion vs. population index respectively for case 2 using MODE III algorithm for the reference case ($M_{N,f}$ = 21900 ± 200)

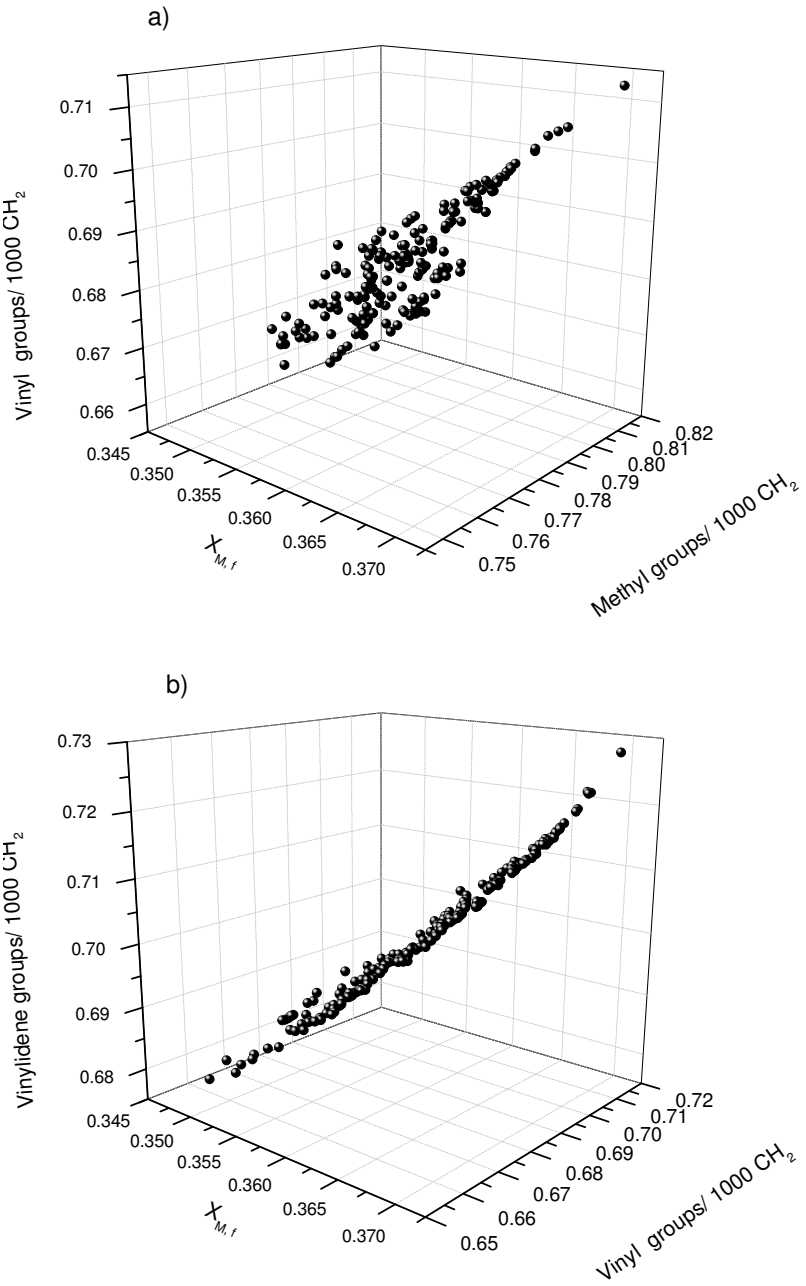

Fig. 5.80 (a-b) Three dimensional plot corresponding to the objectives, namely methyl, vinyl, and vinylidene per 1000 C atoms and monomer conversion for case 2 using MODE III algorithm for the reference case ($M_{N,f}$ = 21900 ± 200)

The population is first sorted in increasing order of conversion. The rest of the values of the objective functions are rearranged in increasing order of conversion and then plotted in Figs. 5.79a - 5.79d. It is observed that a scattered variation of methyl end groups is observed with respect to the monomer conversion. This is also evident from Figs. 5.80a - 5.80b, where three-dimensional Pareto fronts are plotted among the objectives. However, increasing trends are observed for vinyl and vinylidene end groups/ 1000 C atoms when plotted against the monomer conversion (Figs. 5.79b - 5.79c and Fig. 5.80b).

In the next subsection, the results obtained on supply chain and planning problem using multi-objective optimization considered in this study are discussed.

5.2.5 Multi-objective optimization of supply chain and planning

In the present study, so far the attention is given in testing the performance of developed strategies of MODE on test problems (to validate their convergence and divergence issues) and some industrial case studies where major process design decisions are involved. Supply chain and planning is another area which is directly related with the profitability of several organizations. Though the problem of supply chain and planning is not directly related to process design decisions, in this study we made an attempt to test the performance of one of the strategies of multi-objective differential evolution (MODE) algorithm on the problem related to supply chain and planning. The detailed problem formulation (Pinto, 2007) is given in section 4.2.5. In this study, multi-objective differential evolution algorithm is applied successfully to solve multi-objective optimization problem on supply chain and planning. Several simulations runs were carried out using different sets of MODE parameters. Smooth Pareto fronts are obtained from each combination. The obtained results are also compared with those obtained using the evolutionary multi-objective optimization algorithm (NSGA-II).

5.2.5.1 Case 1: Minimization of TOC and ratio of MC to TOC

Figs. 5.81 – 5.83 show the Pareto fronts between total operating cost and the ratio of manufacturing cost to total operating cost obtained using MODE algorithm and NSGA-II (Pinto, 2007). Fig. 5.81 also shows the effect of *NP* on Pareto front after 10 generations and comparison of results of MODE study with NSGA-II, where the results are taken from the literature (Pinto, 2007).

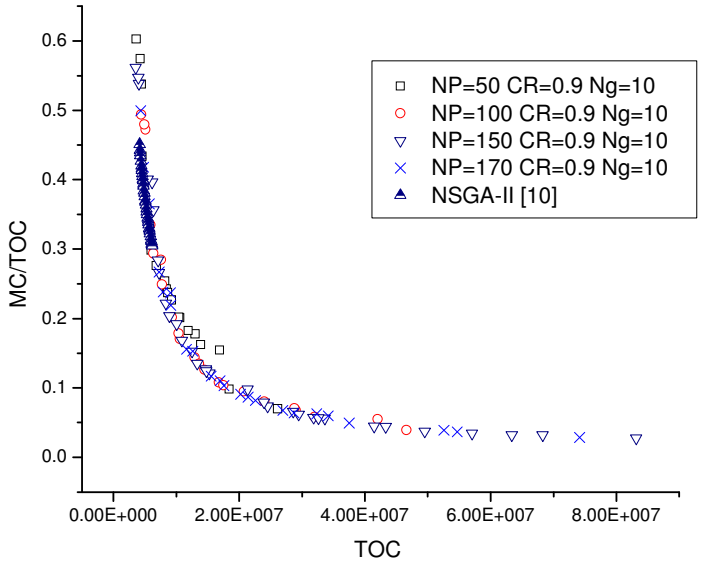

Fig. 5.81 Comparison of Pareto fronts between TOC and MC/TOC using NSGA-II and MODE and effect of *NP* on Pareto front using MODE algorithm

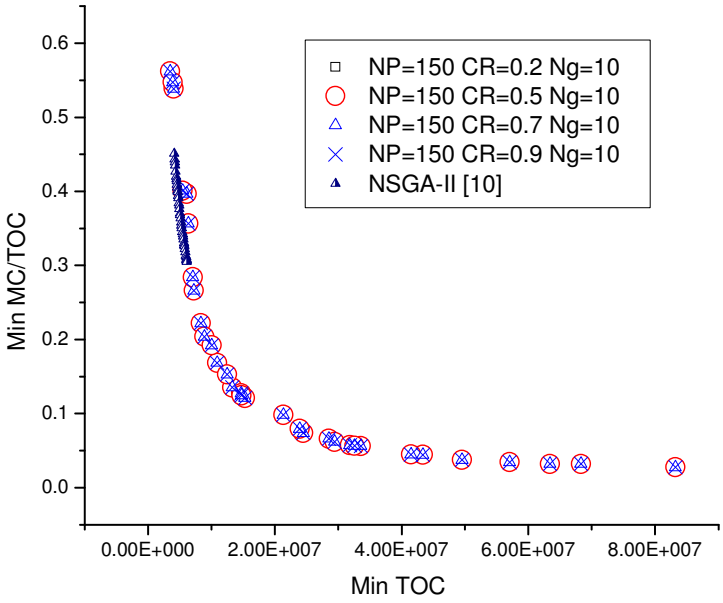

Fig. 5.82 Pareto front between TOC and MC/TOC using MODE (at various values of CR) and NSGA-II

The same problem formulation is considered in this study. It is observed that there is no change in the number of solutions or the Pareto front after 10 generations. The Pareto front obtained is well diverged and smooth for all the reported values of *NP* (Fig. 5.81). However, for *NP* = 50, the number of non-dominated solutions is less (only 19 solutions are obtained). The Pareto front is found to be dragged towards the right in the region of MC/TOC value of 1.5 - 2.0 for this *NP* value. Fig. 5.81 also illustrates that for *NP* value of 100, or greater than 100, although the Pareto front remains the same, the number of non-dominated solutions vary. The number of non-dominated solutions for *NP* value of 50, 100, 150 and 170 are 19, 23, 32 and 23 respectively. Fig. 5.82 shows the effect of CR on Pareto front at a fixed *NP* (= 150) and fixed number of generation (*Ng* = 10). Several simulation runs were carried out using various values of CR, and some of the combinations are shown in Fig. 5.82. MODE algorithm gives a smooth and well-diversified set of non-inferior solutions for all values of CR in the range considered in this study. Population points at first generation (*Ng* = 1) and Pareto front after 10 generations (*Ng* = 10) are shown in Fig. 5.83. After 10 generations, TOC is found to vary between the value of 35,14,335 and 8,31,75,376 while the ratio of MC to TOC varies between the range of 0.027752 and 0.561639. There is a clear trade off in these solutions. Table 5.18 shows the comparative analysis of current study results with results reported in literature (Pinto, 2007). As this is minimize-minimize (min-min) type of multi-objective optimization problem, the extreme left point on the Pareto front would be the point that gives the maximum value of MC/TOC and a minimum value of TOC.

In the study mentioned in literature (Pinto, 2007), the maximum value of objective function (TOC) does not correspond to the minimum value of objective function MC/TOC. In the current study, the maximum value of objective function TOC

in the entire Pareto range is 8,31,75,376, and the corresponding value of MC/TOC is 0.0261639 which is the minimum value of MC/TOC in the entire Pareto set (Table 5.18). If the extreme right point on Pareto front is compared, then MODE algorithm gives better results than NSGA-II, which is shown in Table 5.18, when same problem is considered.

5.2.5.2 Case 2: Maximization of profit and minimization of MC

Fig. 5.84 shows the Pareto front between the objective functions, profit and MC. This set consists of maximize-minimize (max-min) type of objective functions. The values for profit vary between 287 and 94,466 while the values for manufacturing cost varies between 2,03,990 and 2,28,709. Fig. 5.84 also shows the Pareto front between two objectives and objective space after generation 1 and after 10 generations. The objective space is discrete in nature. This could be due to the effect of several complex constraints on objective space. The Pareto front remains the same for all reported values of the number of population points. The number of non-dominated points for *NP* values of 50, 100, 150, and 170 are 6, 6, 8 and 8 respectively. The effect of the control parameter CR on the spread and diversity of Pareto front with *NP* = 150 and after 10 generations is also studied. No change in number of solutions or Pareto front is observed for different CR values in range (0.2 to 1.0).

5.2.5.3 Case 3: Maximization of revenue and minimization of transportation cost

Transportation cost is considered as an important cost in every supply chain problem. The trade-off among the objectives of revenue and transportation cost is shown in Fig. 5.85.

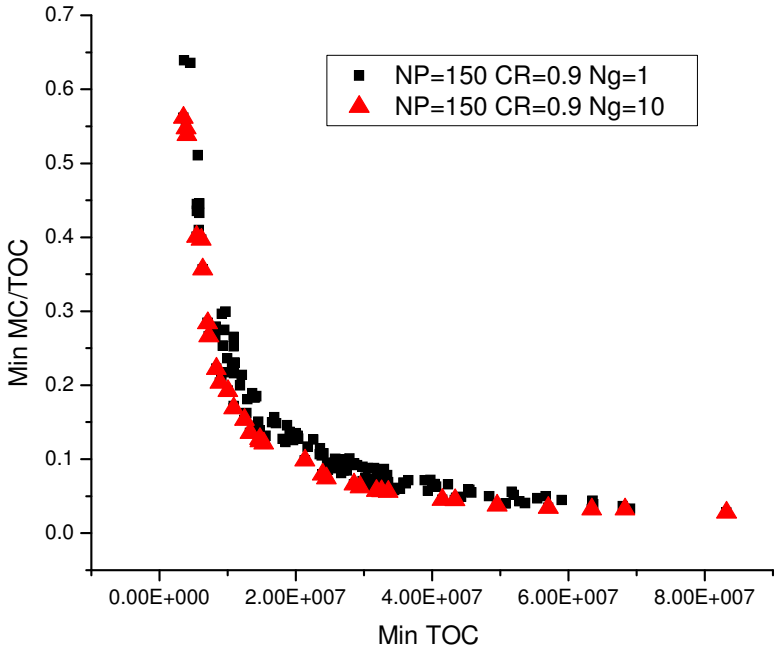

Fig. 5.83 Trade-off between TOC and MC/TOC after 10 generations and population points at generation 1

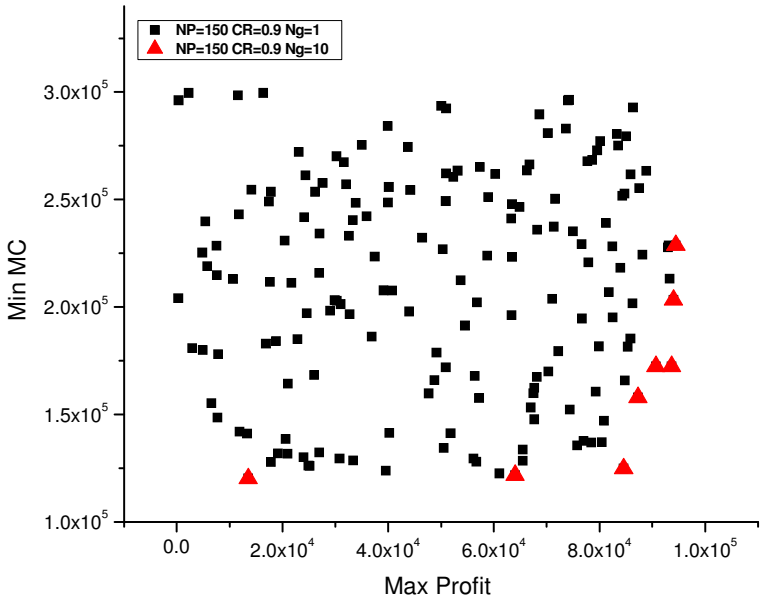

s

Fig. 5.84 Trade-off between Profit and MC after 10 generations and initial population points at generation 1

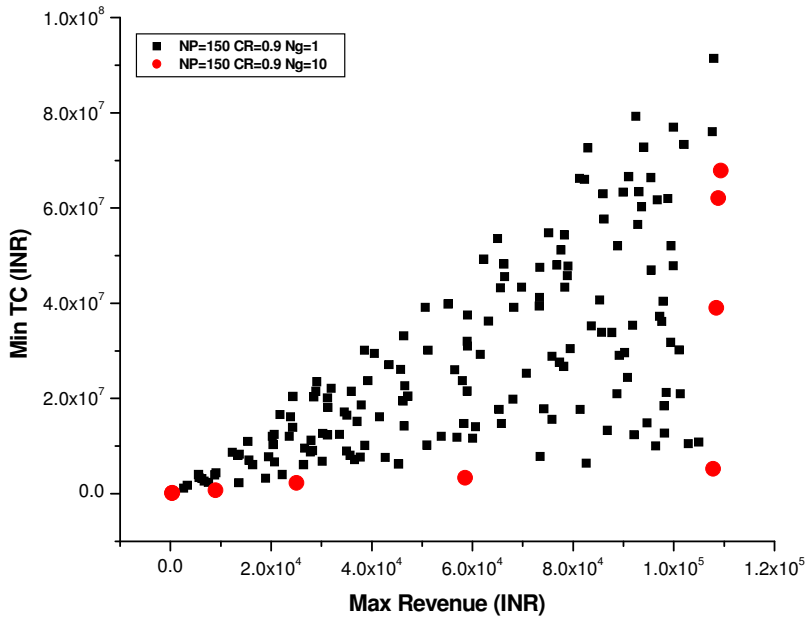

Fig. 5.85 Trade-off between revenue and TC after 10 generations and objective space at generation 1

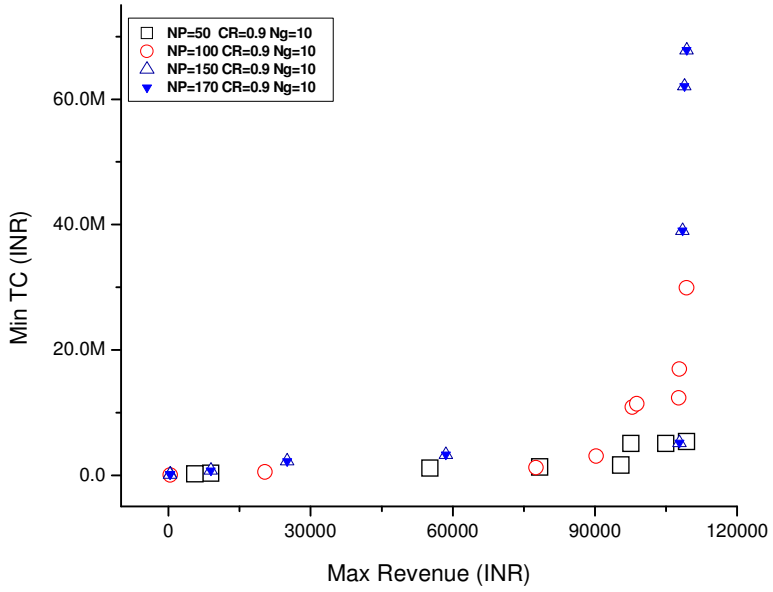

Fig. 5.86 Pareto fronts after 10 generations and effect of *NP* on Pareto front

The Pareto front for CR value of 0.9 and after 10 generations with different *NP* values is shown in Fig. 5.86. It is interesting to note that with 50 number of population points (*NP*), the Pareto front is converged to the local region. But if *NP* is increased subsequently beyond the value of 100, the Pareto set of solutions remains the same in terms of number of solutions and objective function values.

Simulation runs are carried out with *NP* = 150 and *Ng* =10. Pareto fronts are obtained with good spread and diversity. Fig. 5.85 also illustrates the objective space for current supply chain problem. The objective space is discrete and the shape of objective space is nearly triangular with more number of solutions in the dominated region. Also the objective space is constructed in such a way that there are few points in the region of Pareto front. Because of very less number of solutions in the preferred region, the number of non-dominated solutions in the Pareto front is less. Fig. 5.86 shows the comparison of Pareto front obtained using MODE and NSGA-II (Pinto, 2007). NSGA-II has shown good diversity but in the region of higher value of objective function revenue. The Pareto front obtained using MODE is also well spread but in the range of lower value of revenue and higher value of TC.

Table 5.19 shows the comparison of results obtained in present study with those reported in the literature (Pinto, 2007) using revenue and TC as objective functions. The standard deviation and mean values for objective function revenue using MODE algorithm are 58,656.33 and 50487.34 respectively. For objective function TC, the values for mean and standard deviation are 20,08,0159 and 2,87,273,803 respectively.

Table 5.18 Comparison of objective functions TOC vs. MC/TOC

	NSGA-II (Pinto, 2007)		MODE (Present Study)	
	Objective function	**Corresponding value**	**Objective function**	**Corresponding value**
Statistic	TOC	MC/TOC	TOC	MC/TOC
Maximum	1,75,129	0.327840	8,31,75,376	0.027752
Minimum	51,477.0742	0.4800	3,5,14,335	0.561639
Mean	1,07,536.784		2,45,25,698	
Std. Dev.	25,382.0615		2,11,06,445	
	MC/TOC	TOC	MC/TOC	TOC
Maximum	0.494218	1,11,098.08593	0.561639	35,14,335
Minimum	0.168562	87,393.14848	0.027752	83,17,537
Mean	0.356052		0.175072	
Std. Dev.	0.051778		0.161984	

Table 5.19 Comparison of objective functions revenue vs. TC

	NSGA-II (Pinto, 2007)		MODE (Present Study)	
	Objective function	**Corresponding value**	**Objective function**	**Corresponding value**
Statistic	Revenue	TC	Revenue	TC
Maximum	4,97,068.625	80233.382813	1,09,382	67,84,773
Minimum	3,08,609.468	47546.855469	332	1,12,367.4
Mean	4,36,037.487		58,656.33	
Std. Dev.	36,426.0705		50,487.34	
	TC	Revenue	TC	Revenue
Maximum	82,823.6171	493821.8750	67,847,736	1,09,382
Minimum	47,546.8554	308609.45875	1,12,367.4	332
Mean	66,736.9272		2,00,80,159	
Std. Dev.	6,267.46296		28,273,803	

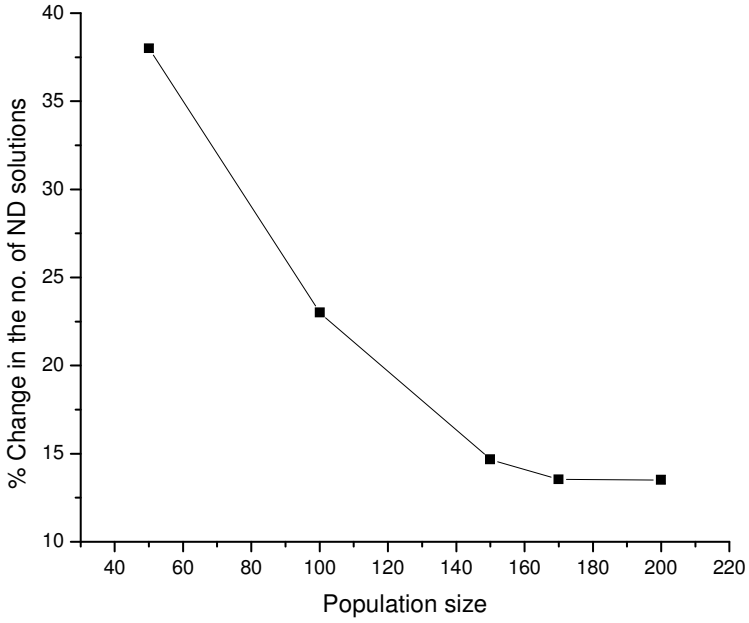

Fig 5.87 Change in number of non-dominated solutions (ND) vs. population size using MODE algorithm

This study also shows that the Pareto front obtained with various values of key parameters is almost same (except for very low value of *NP*). It is observed that the percentage of change in number of non-dominated solutions decreases with an increase in the number of population points. When CR values are changed in between 0.2 and 0.9, the Pareto front obtained is the same. *F* is assigned as a random value which ranges between 0 and 1. The % change in the number of non-dominated solutions decreases if *NP* value exceeds the value of 100 (Fig. 5.87), i.e., more number of non-dominated solutions are obtained when a higher value of NP is used.

The success of MODE largely depends on its strong combined mutation and crossover policy. This combined operation is named as recombination. Usually in genetic algorithm both the mutation and crossover operations are carried out separately. Any multi-objective optimization algorithm needs to include two very important aspects, i.e., convergence and divergence of solutions. In MODE, crossover operator takes care of divergence, which enables it to search for better solution in every step. At the same time the scaling factor takes care of convergence of solutions, thus making the algorithm faster and accurate in a single step.

Summary of the chapter: In this chapter, the results obtained using newly developed strategies of MODE algorithm (namely, MODE, MODE III, hybrid MODE, elitist MODE and trigonometric MODE) are discussed. This chapter is broadly divided into two parts. The first part is related to the analysis of MODE algorithm on the test problems. Effects of various parameters on MODE algorithms using several benchmark test problems are reported. Search space related analysis is carried out using complex test functions using newly developed strategies of MODE. Performance estimation (in terms of convergence and divergence metric) of newly developed strategies of MODE

algorithms is carried out and compared with other well known algorithms [(NSGA-II (both real- and binary- coded variants), SPEA, and PAES]. In part 2, the developed strategies of MODE are used to find the Pareto optimal fronts for several industrial case studies [which include, styrene reactor (both adiabatic and steam injected configuration], PET reactor, oxidation of p-xylene to PTA, LDPE tubular reactor and supply chain and planning).

Next chapter deals with the concluding remarks of results obtained in the present study which includes the summary, conclusions and the major contributions followed by the future scope of research.

CHAPTER – 6

CONCLUDING REMARKS

The present study deals with development of new algorithms on evolutionary multi-objective differential evolution and establishing their performance on several test problems and also on industrial case studies. Multi-objective differential evolution (MODE) algorithm is modified for improving its performance and new strategies of MODE, which include, MODE III, hybrid MODE, elitist MODE and the trigonometric MODE are developed in this study. A detailed literature survey is carried out on various evolutionary multi-objective optimization algorithms and their industrial case applications. The identified industrial case studies for present research which involve multiple process design decisions (which are considered as multiple objectives) include styrene reactor (both adiabatic and steam injected configuration), Polyethylene terephthalate (PET) reactor, oxidation of p-xylene to purified terephthalic acid (PTA), Low density polyethylene (LDPE) tubular reactor and supply chain & planning. This chapter presents a brief summary of the present work followed by conclusions, and future scope for research in this area.

6.1 Summary

6.1.1 Introduction

An optimization problem involving more than one objective to be optimized simultaneously is referred as multi-objective optimization (MOO) problem. The expected outcome of MOO algorithm is a set of solutions which are non-dominated with respect to

each other. Such a set of solutions is called the Pareto optimal front. Unlike single objective optimization problems, MOO problems involve two search spaces, namely the decision variable space and the objective space. Two major goals that need to be achieved in any MOO algorithm are, (1) to converge to the true Pareto front, and (2) to have a diverse set of solutions on the Pareto front. Due to these multiple goals and multiple search spaces, the MOO problems are considered to be more difficult to solve, as compared to the single objective optimization problems.

Industrial problems which involve multiple process design decisions such as maximization of yield of a complex process, maximization of conversion of a reactant, maximization of profit or the productivity of entire process plant or an individual process, maximization of selectivity of a process, minimization of unwanted byproducts, minimization of unwanted side chains in case of free radical reactions, minimization of sum of square of normalized error between the model predicted and the industrial results/data, maximization of heat exchanger area or minimization of heat load in heat exchange processes, maximization of mass transfer or rate of reaction in case of a complex chemical reaction, maximization of distillate in case of mass transfer processes, etc. This clearly indicates that there is a need to make multiple process design decisions in process industries; moreover, there exists a trade-off among many process design decisions. Many decision makers are interested in achieving two or more of the objectives simultaneously. The complexity of the industrial processes (which are unique blends of various aspects associated with reaction engineering, heat transfer, mass transfer, fluid flow phenomena, thermodynamics, separations, etc.), and the interest of decision makers, have attracted the attention of researchers to develop new and improved MOO algorithms. These MOO algorithms not only handle the complex search space of industrial problems efficiently, but also result in a set of non-dominated or non-inferior

solutions, i.e., the Pareto front for the said process. Therefore there is a need towards developing new and efficient algorithms.

6.1.2 Gaps in Literature

The existing literature on evolutionary multi-objective optimization algorithms suggests that great strides have been made in developing new algorithms based on natural phenomena in the last two decades. However, due to the complexity involved in the industrial processes and benchmark test problems, the attainment of global Pareto front with good diverse set of solutions is scarce. Various algorithms such as NSGA, NSGA-II and its improved variants, SOMA, SPEA, PAES are applied successfully to find the Pareto optimal set of solutions. Though these algorithsm have been successfully applied to some problems, they failed to give global Pareto fronts with diverse set of solutions for many other problems. MODE algorithm has been successful even for those problems which the popular EMO algorithms (NSGA) failed to give multiple solutions on Pareto front. Differential evolution which is an improved version of GA is found to give optimal solutions at a faster rate for single objective optimization (Angira, 2005). Therefore there exists a scope to extend DE to solve multi-objective optimization problems. Though MODE algorithm was developed earlier, it has specific problems such as removal of dominated solutions in each generation and non-preservation of solutions. MODE algorithm gave comparable Pareto fronts for few industrial problems. However, there is a great scope and potential to improve the existing MODE algorithm. There is also a need to test the performance and robustness of MODE algorithm with the help of benchmark test problems.

Various industrial applications as discussed in section 2.2 involving multiple objectives to be optimized are studied and gaps have been identified as mentioned against each of process in section 2.2. These problems are solved using different algorithms. But

as true Pareto optimal front for industrial applications is not known, there is a demand to revisit such industrial applications and then apply the newly developed and validated (for their performance) algorithms to find the Pareto optimal fronts and the optimal set of decision variables.

As MODE algorithm is a newly developed algorithm, there exists a need towards developing new strategies of MODE. Hybrid algorithms involve a combination of traditional deterministic methods and the evolutionary algorithms to improve the performance of a standalone evolutionary algorithm. Hybrid algorithms have shown good potential in terms of achieving the optimal solutions at a faster rate in case of single objective optimization (Chiou and Wang, 1999). Hybrid methods have been developed for solving both single- and multi-objective optimization problems. But MODE algorithm or its strategies are not yet been hybridized with the local search methods. Therefore there is a great potential and need to develop a hybrid strategy of MODE algorithm and test its performance on identified processes and benchmark test problems. NSGA-II algorithm involves combination of elite population preservation and a crowding distance approach for solving MOO problems. There is a scope towards developing an elitist strategy of MODE. Along with Elitist and hybrid strategy of MODE, there also exists a need towards improving the performance of MODE by perturbing its mutation strategy using trigonometric mutation approach.

It is necessary to check the performance of newly developed algorithms (especially in terms of Pareto front and convergence & divergence) with other well known algorithms. Many evolutionary algorithms, though give good visual view of the Pareto front, its comparison with true Pareto front using benchmark test function is important. Therefore, there exists a need towards checking the performance metrics of

newly developed strategies of MODE algorithm and compare them with other widely accepted algorithms.

6.1.3 Scope of Work

Industrial applications reported in the literature which involve multiple process design decisions are studied and the gaps of the research have been identified (as mentioned in section 2.2 & 2.3). These processes are simulated using suitable numerical techniques and multi-objective differential evolution algorithm is used to obtain the Pareto optimal set of solutions and the decision variables. The industrial applications include Styrene reactor, PET reactor, LDPE tubular reactor, oxidation of p-xylene to PTA and supply chain & planning. New strategies of MODE namely MODE III, Elitist MODE, hybrid MODE and trigonometric MODE are developed. The Pareto optimal sets of solutions are obtained for benchmark test problems using new strategies of MODE and are compared with the results obtained using NSGA-II. The Pareto optimal set for industrial applications (case studies) is also obtained using strategies of MODE and is compared with Pareto front obtained using other evolutionary algorithms. Important performance metrics such as convergence metric and divergence metrics are computed for newly developed strategies and their performance with other well known algorithms from the literature [such as NSGA-II (both real and binary versions), SPEA, PAES] are compared.

6.1.4 Newly Developed Algorithms

In this study, the existing strategy of MODE algorithm is improved for its performance, keeping in view the objectives of convergence to the true Pareto front and divergence of solutions on the Pareto front. Three major objectives are set to improve the performance of MODE algorithm: 1) To maintain a constant population size (thus giving stability and enough opportunity to all points to converge towards the Pareto front), 2) To improve the

convergence of MODE algorithm, so as to converge to the true Pareto front, 3) To maintain the diversity of solutions on the obtained Pareto front. In the beginning, two new strategies of MODE, i.e., MODE II and MODE III are proposed. MODE II algorithm is developed considering the drawback of removal of solutions from the original MODE algorithm After the non-dominated sorting in MODE algorithm, the dominated solutions are removed and equal number of solutions [randomly generated using the mapping rule (Price and Storn, 1997)], are added to the population. But it is found that this algorithm does not converge to the true Pareto front, because there is a random addition of population in each generation, which disturbs the stable search process. Therefore, the concept of elitism is incorporated in MODE II algorithm along with crowded distance sorting procedure and a new algorithm is proposed as the elitist MODE algorithm. MODE III algorithm is a simple extension of differential evolution algorithm with a modified selection scheme to handle multiple objectives simultaneously. As MODE III algorithm strongly relies on a simple working principle of differential evolution (with improved selection scheme), it converges towards the true Pareto front for majority of the test problems. However, hybridization of MODE III with a local search method is thought of and a new algorithm, namely hybrid MODE, is proposed. Hybrid MODE algorithm involves hybridization of evolutionary MODE III algorithm with a deterministic sequential simplex method. Trigonometric mutation operation is incorporated in the MODE III algorithm and another new algorithm, trigonometric MODE also has been proposed in this study.

6.1.5 Results and discussion

The MOO study is divided into two major parts, i.e., MOO of the test problems and the industrial case studies. In the following sections, the MOO results obtained in the present study are summarized.

6.1.5.1 Test problems

Several benchmark test problems (both constrained and unconstrained) are considered in this study. The results obtained using newly developed strategies of MODE algorithm (namely, MODE, MODE III, hybrid MODE, elitist MODE and trigonometric MODE) are discussed. Test function analysis is divided in three parts. The first part is devoted to the analysis of MODE algorithms with respect to its control parameters. Various control parameters of MODE, which include, Crossover constant (CR), Number of population points (*NP*), Scaling factor (F), Number of generations (*N*g) and Penalty parameter (*R*) are varied to test the performance and robustness of MODE algorithm. The results obtained in this study showed that MODE algorithm requires a high value of initial population size. But with increase in initial population size, the complexity of algorithm increases, thus making the algorithm more complex. MODE algorithm results in the same Pareto front, irrespective of the value of CR. However, a high value of CR is recommended, which is used consistently in the rest of the study. MODE algorithm has a typical drawback of removal of dominated solutions in each-iteration, which disturbs the search process. Focusing on these issues, MODE is improved further and additional strategies of MODE are developed, which caters towards the need of achieving both the convergence and divergence of Pareto solutions in case of MOO study.

The second part of test function analysis includes checking the performance of new developed strategies of MODE algorithm (i.e., MODE III, hybrid MODE, elitist

MODE and the trigonometric MODE). Two widely accepted and important metrics from the point of view of MOO study are considered for evaluating the performance of newly developed strategies of MODE algorithm. These metrics include the convergence metric and the divergence metric. Pareto fronts are obtained using newly developed strategies of MODE and are compared with the Pareto front obtained using another evolutionary multi-objective optimization (EMO) strategy (NSGA-II). The important performance metrics are calculated for the selected test problems (SCH, FON, KUR, ZDT1, ZDT2, ZDT4, and ZDT3 and ZDT4) and the results are compared with other EMOs from the literature [NSGA-II (both real- and –binary coded variants), SPEA and PAES]. It is found that all the developed strategies of MODE converge to the true Pareto front for most of the test problems. However, the strategies of MODE result in slightly lower value of diversity metric as compared to NSGA-II for most of the test problems considered in this study. The elitist MODE and MODE III algorithms achieved a lowest value of convergence metric for KUR (=0.002921) and and ZDT3 (=0.01019) test problems respectively. The value of variance obtained is zero for all the newly developed strategies of MODE algorithm for test problems (SCH, FON and KUR), which indicates that these strategies of MODE algorithm are able to give a consistent set of results. None of the other EMOs from literature (as given above), have a variance value of zero for the test problems (SCH, FON and KUR).

The search space analysis of selected test problems [SCH2 and POL (unconstrained) and Constr-Ex and TNK (constrained) (Table 4.1 and 4.2 respectively)] is carried out using the newly developed strategies of MODE. The discrete search space and a discontinuous Pareto front renders difficulty in the search process. It is difficult to obtain a uniform distribution of solutions on the Pareto front (in case of a discontinuous Pareto front). In case of Constr-Ex test problem the convergence of Pareto front obtained

using MODE III is restricted to a small portion of the front (region X in Fig. 5.19b). However, the hybrid-, trigonometric- and elitist strategy of -MODE algorithms are able to capture the entire region (i.e., regions X and Y in Fig. 5.19b) and thus give a well diverse set of solutions on the Pareto front.

6.1.5.2 Industrial case studies

A. MOO of industrial styrene reactor

Multi-objective optimization of industrial styrene reactor is carried out using newly developed strategies of MODE. Two reactor configurations, namely, adiabatic and steam injected configurations are considered. Three objectives namely, maximization of productivity, yield and selectivity are considered. Four cases consisting of three cases of two-objective and one case of three-objective optimization are studied. For case-1 study (maximization of the F_{ST} and S_{ST}), it is found that MODE III, hybrid MODE, trigonometric MODE and the elitist MODE algorithms achieved 100% convergence to the Pareto front. A comparatively better trend of decision variables is observed in case of hybrid MODE, elitist MODE and trigonometric MODE algorithms, whereas the decision variables are slightly scattered in case of MODE and MODE III algorithms. For a few of the points, MODE algorithm approached lower bound of temperature and upper bound of initial flow rate of ethyl benzene (Figs. 5.24b and 5.24f). This resulted in a lower combined inlet temperature of the steam and the ethyl benzene mixture. Thus MODE algorithm resulted in local Pareto solutions, as due to high value of initial ethyl benzene flow & lower steam temperature. Thus, in order to reach towards the global Pareto solutions, it is necessary to attain a relatively high temperature of the combined stream of mixture of steam and ethyl benzene to the inlet of reactor. The Pareto front is obtained using initial population size of 100 and 200, where the convergence is equally good for

both the cases. The Pareto front is able to cover a wider range (with scattered points) when initial population size is kept at 200. However, with an initial population size of 100 the convergence of algorithm to the Pareto front is good with nearly uniform diversity.

The percentage of initial population points converged to the final Pareto front for step size-1, step size-2 and step size-3 (step size used in obtaining the neighbourhood point) are 86%, 96% and 93% respectively (Fig. 5.26a). The diversity of Pareto front is better when a step size-2 is used. With step size-1, the location of neighborhood solution may be far away from the current solution (as per Eq. 5.3), which may not give a better solution when local search method is used. However, when step size-3 is used, the solutions are crowded on the Pareto front. Therefore, step size-2 is recommended for this study.

The profit function is analyzed using the newly developed strategies of MODE, i.e., MODE III, hybrid MODE, elitist MODE and the trigonometric MODE. The profit function considers the cost of major feed materials (cost of ethyl benzene and steam) and final valued products (such as Styrene, benzene and toluene). However, it does not account for the cost of separation. As the value of F_{ST} increases, the profit values also increase. MODE III algorithm, the maximum profit obtained is 584 ($/h) which is obtained at F_{ST} value of 11.91 kmol/h. Using hybrid MODE, the maximum profit obtained is 728 ($/h). In terms of both the selectivity and yield, nearly the same values are obtained using both the algorithms. However, using MODE III and hybrid MODE algorithms, the values of S_{ST} vary in between 87.14 - 95.5 % and 87.22 - 95.41 % whereas the values of Y_{ST} vary between 21.38 - 42.02 % and 20.41 - 36.90 % respectively. The profit obtained using MODE III and hybrid MODE algorithms ranges in between 344.62 - 584.47 $/h and 383.32 - 728.44 $/h respectively. The profit obtained

using elitist MODE and trigonometric MODE algorithms ranges in between 362.5 - 732.5 \$/h and 344.6 - 701.5 \$/h respectively. The major improvement obtained in profit function value is due to the increased value of F_{ST} obtained using hybrid MODE. The value of F_{ST} ranges from 6.60 - 12.36 kmol/h and from 7.72 - 15.81 kmol/h using MODE III and hybrid MODE algorithms respectively. However, with F_{ST} value of 15.50 kmol/h and 14.48 kmol/h, the trigonometric MODE and elitist MODE resulted in a profit value of 701 \$/h and 738 \$/h. The maximum profit obtained among all the algorithms corresponds to that obtained using elitist MODE.

In case-2 results, when a higher initial ethyl benzene flow rate is obtained (in case of hybrid algorithm), the values of corresponding decision variables, such as *T* and *SOR* are also high. This is because, the higher temperature of mixed stream (steam and initial ethyl benzene) is responsible for a higher productivity. It is important for any efficient algorithm to explore the entire multi-dimensional search space so that a true Pareto front is obtained. MODE III algorithm in this study (see Fig. 5.29), and MODE and NSGA algorithms in earlier studies (Yee et al., 2003; Babu et al., 2005) converged to the lower bound of initial ethyl benzene flow rate, hence resulted in a local Pareto front. The value of S_{ST} decreases while the value of calculated Y_{ST} increases as the value of F_{ST} increases. The range covered by MODE III and hybrid MODE algorithm in terms of calculated value of Y_{ST} is 21.38 - 42.02 % and 20.41 - 37.51 % respectively. The NSGA algorithm resulted in a local Pareto front because *SOR* approached a lower bound.

Unlike the results obtained for case-1 and case-2 (where the decision variable F_{EB}^{0} either approached lower or upper bound), for case-3 the decision variable F_{EB}^{0} is also equally important in producing the Pareto solutions. While maximizing F_{ST} and Y_{ST} simultaneously, the decision variable, *P*, remains practically constant and acquires the

upper bound. The conflicting variables observed in this study (which are responsible for producing the Pareto solutions) are *T, SOR* and F_{EB}^{0}. These results show the ability of existing algorithm to produce more valuable and practical results which are important to the plant engineer. The industrial point lies below the Pareto front and the non-dominated solutions are present on either side of the industrial point, thus offering a wide range and choice to the decision maker. However, in the study of Yee et al.(2003), the industrial point (for maximization of F_{ST} and Y_{ST}) lies at one extreme (left) end of the obtained non-dominated solutions (Pareto front in their work) giving a limited choice for the decision maker.

The profit obtained for S_{ST} vs. Y_{ST} objectives (using MODE III, hybrid MODE and NSGA) is lower than the profit of industrial operating point. The profit strongly depends on the amount of styrene produced. As the productivity of styrene is not one of the objectives in S_{ST} vs. Y_{ST} studies, the obtained best profit is lower than that of the industrial operating point. However, for the remaining cases (case-1, case-3 and case-4) (both two-objective and three-objective optimization studies), the strategies of MODE resulted in higher profit than that obtained with the industrial operating point using MODE III & NSGA algorithms. Unlike hybrid MODE and MODE III algorithms results, NSGA algorithm results show that the profit obtained during a three-objective optimization study is less than the industrial operating profit.

In case of steam injected configuration, an enhanced value of the selectivity (in case-1 and case-2 results), and enhanced values of yield and the productivity (in case-3 results) are obtained using the steam injected reactor configuration as compared to an adiabatic rector configuration. For Case-1, the majority of the variable values (temperature of ethyl benzene) approached an upper bound as compared to adiabatic

configuration decision variables for (T_{EB}).. The major reaction being a reversible endothermic reaction, a high temperature and low pressure value is preferred for forward reaction, which resulted in higher selectivity values for some of the variables of the steam injected reactor configuration. As the productivity is directly related to the feed flow rate, an upper bound on the initial flow rate of ethyl benzene is approached for both the reactor configurations. SOR variable range varies between 9.47 – 15.45 and 12.59 – 19.73 for the adiabatic and the steam injected reactor configurations respectively. These ranges of variables resulted in the productivity values varying between 9.47 & 15.45 kmol/h and 6.26 & 14.413 kmol/h for the adiabatic and the steam injected reactor configuration respectively. The selectivity values vary between 87.8 & 95.5 % and 89.28 & 96.15 % respectively for the adiabatic and the steam injected reactor configurations. Thus an upper bound of selectivity is achieved in case of steam injected configuration, while an upper bound of productivity is achieved in case of adiabatic configuration.

B. MOO of PET reactor

In case-1, the optimization problem of simultaneous minimization of acid and vinyl end groups is solved using four decision variables, namely, temperature, pressure, dimensionless time and dimensionless agitator speed. MODE algorithm resulted in local Pareto fronts as compared to the Pareto fronts obtained using MODE II, hybrid MODE, elitist MODE and the trigonometric MODE. The solutions obtained using MODE III, hybrid MODE, elitist MODE and trigonometric MODE algorithms lie on the same front. However the diversity and range of solutions vary. The Pareto fronts obtained using MODE III, hybrid MODE and elitist MODE algorithms are well spread with uniform diversity which covers a wide range of objective function values against that obtained using trigonometric MODE algorithm. NSGA study resulted in a single optimum point for the same problem, when same set of decision variables and constraints were used. For

case-2, a lower value of T (decision variable) is approached for meeting both the objectives simultaneously. By increasing the temperature (from T = 564 K to 568 K), the decision maker has to sacrifice for both the objectives under consideration. This is because the degradation reactions (Eqs. B2 and B9) are more favourable at high temperatures, and thus tend to increase the concentrations of acid and vinyl end groups. At higher temperatures, the value of the objective function depends upon the speed of agitation.

For case-3, at a high temperature, i.e., T = 568 K, if high pressure value is used, the set of equally good solutions or the Pareto set cannot be obtained. However, if the value of temperature is lowered to T = 564 K (or if the pressure is lowered [at high temperatures (i.e., T = 568) as discussed in case-2 results], the Pareto front is obtained. However, hybrid MODE, elitist MODE and the trigonometric MODE algorithms are able to produce the Pareto set of solutions even when a high value of temperature is selected for case-3 study. For case-4, none of the algorithms resulted in any feasible set of solutions, when T is held constant to a value of 568 K. However, a smooth Pareto front is obtained when T is allowed to reduce to a lower value and kept constant at a value of T = 564 K. When θ^* and N^* are considered constant, there is no Pareto front, but a unique solution is obtained, when MODE algorithm is used. However, a smooth Pareto front is obtained using MODE II, hybrid MODE, elitist MODE and the trigonometric MODE. Also in case of results obtained when MODE algorithm is used, the values of pressure are found to be almost same, i.e., around 0.6 mm Hg and not scattered (Fig 5.38b). However, a uniform variation of pressure against the objectives is observed when, the improved strategies of MODE (developed in this study) are used (Figs. 5.38b - 5.38c). These results show that the effect of pressure is dependent on the speed of rotation of agitator. However, if the agitator speed is kept constant at a reference value, a single optimum

value of pressure is obtained and not a scattered one, when MODE algorithm is used. Thus the effect of pressure on producing Pareto front depends on the agitator speed, and there is no Pareto front produced using MODE algorithm when θ^* and N^* are constant. However, the values of the decision variable, P, corresponding to the solution on the Pareto front (Fig. 5.38a), varied between its range (0.4 – 2.0 mm Hg), when improved strategies of MODE algorithm are used. These results also show that the improvements made in the MODE algorithm resulted in a better set of solutions when industrial problem of MOO of PET reactor is reattempted to solve in this study.

C. Oxidation of p-xylene to PTA

For case-1, the Pareto solutions obtained from all the strategies of MODE algorithms lie on the same Pareto front. Majority of the points lie on the upper bound of the decision variable in case of elitist MODE. However, a scattered set of variables are observed in the results obtained using all the strategies of MODE. In case of trigonometric MODE algorithm, most of the points of decision variable, [*C*o], converged towards the middle portion of the bounds (i.e., 500-600 ppm). For case-2, an additional decision variable, namely, water content, W_{H_2O} is considered. Pareto solutions obtained in this study using MODE, MODE III, hybrid MODE, elitist MODE, trigonometric MODE and NSGA-II algorithms lie on the same Pareto front. As all algorithms converged to the same front, the Pareto front resulted in present study may be termed as a global Pareto front. However, MODE is able to cover a better range than other strategies of MODE and NSGA-II. The elitist MODE algorithm gave a better distribution of solutions compared to the MODE algorithm. Thus an improvement proposed in terms of preserving the elite population members resulted in a better set of solutions with equal distribution on the Pareto front. The catalyst concentration plays an important role in controlling

concentration of 4-CBA at the exit of the reactor, but in the presence of another decision variable, i.e., % of water in the solvent, catalyst concentration becomes almost independent of the 4-CBA concentration.

For case-3, the MODE and elitist MODE captured the entire range of second objective, i.e., concentration of 4-CBA. MODE III, hybrid MODE and the trigonometric MODE converged to a local front and could not cover a complete range of second objective, i.e., concentration of 4-CBA, below a value of 500 ppm. Unlike the results of case-2, in the presence of other decision variables (V_{O_2}, [*C*o], and F_{PX}), the effect of value of W_{H_20} is negligible. The concentration of 4-CBA is almost independent of % water content (unlike the results of case-2). Thus in the presence of oxygen content, the water content does not affect the 4-CBA concentration at the exit of reactor. The concentration of 4-CBA depends more on oxygen content irrespective of the presence of % water content. This consolidates the dominance of vent oxygen content over water content. However, in the absence of vent oxygen content (or when vent oxygen content value is fixed), the W_{H_20} parameter plays an important role in deciding the exit concentration of 4-CBA. The catalyst concentration is found to lie on the upper bound of its range. High catalyst concentration is preferred for the reduction in 4-CBA concentration at the exit of the reactor. From Fig. 5.44f, it is evident that the majority of the points have a value of [*C*o] greater than 720 ppm. Hence, we may conclude at this juncture that it is not a single variable that controls the output (4-CBA concentration) at the exit. But, the output depends on several variables, which is the typical feature of dependence of objective functions on the values of decision variables that are responsible for generating a trade-off in multi-objective optimization problems.

Liquid phase *p*-xylene oxidation is a zero-order reaction with respect to the oxygen content and first-order reaction with respect to *p*-xylene concentration. For case-4, lowest value of the 4-CBA concentration is achieved at the exit of the reactor, if the first oxidation step occurs at a faster rate. This is possible by means of a higher temperature (according to Arrheneous law) or at a higher oxygen concentration. If the first-stage oxidation is restricted, due to lack of oxygen concentration or reduced temperature, then the unconverted *p*-xylene may compete for reaction with the remaining oxidation products. In this way, it is possible to have an unconverted 4-CBA in the final product as an impurity. At lower concentration of vent oxygen, the concentration of 4-CBA in the reactor effluent increases (Fig. 5.44b). Catalyst plays an important role in enhancing the rate of reaction. However, there are a few points on the Pareto front, which lead to high 4-CBA concentration despite having high catalyst concentration. Those points either belong to a low water content or to a low temperature. In the same way, there are a few points which have low catalyst concentration values but also resulted in low value of 4-CBA concentration as they possess high temperature values.

D. LDPE tubular reactor

i) Parametric Study: Simulation of Low density Polyethylene tubular reactor is carried out using ode15s subroutine of MATLAB (7.0). An efficient numerical solution procedure (Numerical differentiation formula) resulted in an improved model output when compared with the results reported in the literature. Differential Evolution, an evolutionary algorithm is applied successfully for finding the optimum rate law parameters and the operating conditions. In terms of monomer conversion, model predictions are exactly matching with industrial data in both the cases (i.e., case A & case B). Case B model predicted the exact value of number-average molecular weight,

whereas case A model predicted the value of M_n with a relative error of 0.48%. Following results are obtained during parametric study of LDPE tubular reactor.

The maximum temperature attained in the reactor and the length at which it is attained play an important role in deciding the overall quality of the polymer. As the initiator concentration gets depleted, the temperature of the reaction mass increases. Once the maximum temperature in the reactor is attained, the monomer conversion ceases and the properties such as, M_n, ρ, and concentrations of [*SCB*], [v*inyl*] & [v*inylidene*] remain constant until the addition of another initiator at a length of 850 m along the length of the reactor. The maximum temperature attained in the reactor and the concentrations of side chain products are relatively insensitive to the feed temperature over the ranges covered in this study. Polydispersity index (PDI) also depends on the jacket temperature and feed temperature. Smaller the value of jacket temperature and feed temperature (considered in this study), the greater is the value of PDI.

Lower the concentration of initiator I_1, the greater is the length it acquires for reaching the maximum temperature. The peak attained in the temperature marks the depletion of initiator concentration. Thereafter, not much happens in the reactor, except the cooling of reaction mixture. The concentrations of side chains ([*SCB*], [*vinyl*] and [*vinylidene*] end groups) also depend on the peak attained by temperature in the respective regions. The number of peaks achieved in a reactor depends on the number of injections.

With an increase in the reactor diameter, the time taken to attain the peak temperature in the reactor increases and the monomer conversion decreases. PDE increases with increasing the reactor diameter. PDI shoots to a value of 37.84 when solvent concentration is neglected. The number-average molecular weight increases substantially to a very high value in the first zone in the absence of solvent. The solvent plays an important role in controlling the temperature of the reactor and for terminating

the chain to the solvent. The concentration of the side chain increases with increasing the reactor diameter, while it remains high at a lower value of the wall heat transfer coefficient. With a low value of initial monomer concentration, the location at which the peak temperature is attained in the reactor is delayed. The reduction in SCB at relatively lower feed velocity is due to the lower value of maximum temperature attained in the reactor. With an increase in the feed velocity, the locations of peak temperature in the reactor are delayed.

ii) Multi-objective optimization study: Two case studies consisting of two-objective optimization and four-objective optimization are considered. In case-1, two objectives, namely, maximization of conversion and minimization of the sum of square of normalized side chain concentrations are considered. A set of eleven decision variables, which consists of operating variables, namely, inlet temperature (T_{in}), inlet pressure (P_{in}), the feed flow rates of -oxygen (F_o), -solvent (F_S), -initiators ($F_{I,1}$, $F_{I,2}$), and the five average jacket temperatures ($T_{J,1}$ - $T_{J,5}$), are considered.

The trigonometric MODE algorithm converged to a local Pareto front as compared to the Pareto fronts obtained using MODE III and hybrid MODE algorithms. Both hybrid MODE and MODE III algorithms converged to the same front. However, the diversity of solutions obtained using both the algorithms is different. A good distribution of solutions is obtained in the middle portion of Pareto front using hybrid MODE algorithm. However, the distribution is poor at the periphery of the Pareto front. Unless a judicious choice of step size in generating a neighborhood solution is made, hybrid MODE cannot guarantee a well-diversed Pareto front. However, the hybrid MODE algorithm is able to converge to the same Pareto front as that obtained using MODE III algorithm. The trigonometric MODE algorithm could not approach the true Pareto front, as it involved a mutation strategy, which is greedy in nature. Unlike the results obtained

using hybrid MODE and trigonometric MODE algorithms (where different Pareto fronts are obtained by relaxing the constraints bounds), the Pareto fronts obtained using MODE III algorithm for all the end point constraints (except, $M_{N,f} = 21900 \pm 2$) are same. The Pareto front obtained with an end point constraint of $M_{N,f} = 21, 900 \pm 1100$, covers a wide range of solutions as compared to the range of solutions obtained when a strict constraint on $M_{N,f}$ is used. A lower inlet temperature is favored for a higher conversion. This is because, at high temperature the degradation reactions are more favorable, which are responsible to produce more side products, thus reducing the conversion value.

MODE III algorithm is able to converge to the same Pareto front irrespective of the weight of the penalty parameters considered in this study. However, such results can be obtained, only if, a large value of penalty parameter weight (as used in the present study) is used. The monomer conversion reduces by increasing the monomer feed rate. A higher conversion is obtained for a lower value of feed monomer rate. The Pareto front obtained using the four-objective optimization study for case-2 objectives, is scattered as compared to the Pareto front obtained using case-1 objectives (two-objective optimization study).

E. Supply Chain and Planning

In this subsection a summary of results obtained on MOO of supply chain and planning (as discussed in section 4.2.5) is given. Multi-objective optimization consisting of two objectives simultaneously of minimization of total operating cost (TOC) and minimization of the ratio of MC to TOC is considered for case-1. There is no change in the number of solutions or the Pareto front after 10 generations. The Pareto front obtained is well diversified and smooth for all the reported values of NP (Fig. 5.81). However, for NP = 50, the number of non-dominated solutions is less (only 19 solutions are obtained). The number of non-dominated solutions for NP value of 50, 100, 150 and 170 are 19, 23,

32 and 23 respectively. MODE algorithm gives a smooth and well-diversified set of non-inferior solutions for all values of CR in the range considered in this study. Case-2 consists of two objectives, namely maximization of profit and minimization of MC. The values for profit vary between 287 and 94,466 while the values for manufacturing cost varies between 2,03,990 and 2,28,709. The Pareto front remains the same for all reported values of the number of population points. The number of non-dominated points for NP values of 50, 100, 150, and 170 are 6, 6, 8 and 8 respectively. No change in number of solutions or Pareto front is observed for different CR values in the chosen range (0.2 to 1.0). Case-3 consists of two objectives, namely maximization of revenue and minimization of transportation cost. With 50 number of population points (NP), the Pareto front is converged to the local region. But if NP is increased subsequently beyond the value of 100, the Pareto set of solutions remains the same in terms of number of solutions and objective function values. The objective space is discrete and the shape of objective space is nearly triangular with more number of solutions in the dominated region. Also the objective space is constructed in such a way that there are very few points in the region of Pareto front. Because of very less number of solutions in the preferred region, the number of non-dominated solutions in the Pareto front is less. The standard deviation and mean values for the objective function (revenue) using MODE algorithm are 58,656.33 and 50487.34 respectively. For objective function TC, the values for mean and standard deviation are 20,08,0159 and 2,87,273,803 respectively.

6.2 Conclusions

Based on the results obtained in the present study, following conclusions are drawn.

1. The outcome of Multi-objective differential evolution algorithm depends on the size of population. A large value of initial population size is recommended.
2. The elitist MODE and MODE III algorithms achieved a lowest value of convergence metric for KUR (= 0.002921) and ZDT3 (= 0.01019) test problems.
3. The value of variance obtained is zero for all the newly developed strategies of MODE algorithm for test problems (SCH, FON and KUR), which indicates that these strategies of MODE algorithm are able to give a consistent set of results. None of the other EMOs from the literature (Table 5.2), has a variance value of zero for the test problems (SCH, FON and KUR).
4. In case of Constr-Ex test problem the convergence of Pareto front obtained using MODE III is restricted to a small portion of the front (region X in Fig. 5.19b). However, the hybrid-, trigonometric- and elitist strategy of -MODE algorithms are able to capture the entire region (i.e., regions X and Y in Fig. 5.19b) and thus give a well diversed Pareto front.
5. Diversity metric values obtained using the strategies of NSGA-II are better as compared to the diversity metric values obtained using other algorithms considered in this study.
6. For case-1 (Maximization of Y_{ST} and S_{ST}) of styrene reactor, all the strategies of MODE algorithm (except MODE) converged to the same front. However the diversity of solutions on the Pareto front varies.
7. For case-1 of styrene reactor, a comparatively better trend of decision variables is observed in case of hybrid MODE, elitist MODE and trigonometric MODE algorithms whereas the decision variables are slightly scattered in case of MODE and MODE III algorithms.

8. For case-1 of styrene reactor, in order to reach towards the global Pareto solutions, it is necessary to attain a relatively high temperature of the combined stream of mixture of steam and ethyl benzene to the inlet of the reactor.
9. For case-1 of styrene reactor, the Pareto front is able to cover a wider range (with scattered points) when initial population size is kept 200. However, with an initial population size of 100, the hybrid MODE algorithm converges to the same Pareto front with nearly uniform diversity.
10. The choice of step size used in generating a new neighborhood point in hybrid MODE algorithm affects the quality of Pareto front, thus the outcome of hybrid MODE algorithm depends on the value of step size used.
11. For case-1 of styrene reactor, The maximum profit obtained among all the algorithms corresponds to that obtained using elitist MODE algorithm.
12. For case-1 of styrene reactor, The higher initial temperature coupled with a higher initial flow rate of ethyl benzene, is responsible for producing higher flow rate of styrene, which in turn is responsible for giving higher profit values. As the value of temperature (decision variable) increases, the values of objective function F_{ST} and the profit also increase.
13. For case-2 (Maximization of F_{ST} and S_{ST}) of styrene reactor, MODE III algorithm in this study, and MODE and NSGA algorithms in earlier studies (Yee et al., 2003; Babu et al., 2005) converged to the lower bound of initial ethyl benzene flow rate, hence resulted in local Pareto front. The NSGA algorithm resulted in a local Pareto front also because *SOR* (decision variable) approached a lower bound, which resulted in lower value of combined stream of steam and reactant.
14. The profit obtained for S_{ST} vs. Y_{ST} objectives (using MODE III, hybrid MODE and NSGA) is lower than the profit of industrial operating point. The profit

strongly depends on the amount of styrene produced. As the productivity of styrene is not one of the objectives in S_{ST} vs. Y_{ST} studies, the obtained best profit is lower than that of the industrial operating point.

15. For Case-1, case-3 (Maximization of F_{ST} and Y_{ST}) and case-4 (both two-objective and three-objective optimization studies), the strategies of MODE resulted in higher profit than that obtained with the industrial operating point and NSGA algorithms.
16. In case of steam injected configuration, an enhanced value of the selectivity (in case-1 and case-2 results), and enhanced values of yield and the productivity (in case-3 results) are obtained compared to an adiabatic rector configuration.
17. For case-1 (With *T, P,* θ^* and N^*as decision variables) of PET reactor, the Pareto fronts obtained using MODE III, hybrid MODE and elitist MODE algorithms are well spread with uniform diversity which covers a wide range of objective function values against that obtained using trigonometric MODE algorithm. NSGA study resulted in a single optimum point for the same problem, when same set of decision variables and constraints were used.
18. For case-2 (With *P,* θ^* and N^*as decision variables) of PET reactor, a lower value of T (decision variable) is approached for meeting both the objectives simultaneously. By increasing the temperature (from T = 564 K to 568 K), the decision maker has to sacrifice for both the objectives under consideration.
19. For case-3 (With θ^* and N^*as decision variables) of PET reactor, at a high temperature, i.e., T = 568 K, if high pressure value is used, the set of equally good solutions or the Pareto front is not obtained. However, if the value of temperature is lowered to T = 564 K (or if the pressure is lowered at high temperatures (i.e., T

= 568)], the Pareto front is obtained. However, hybrid MODE, elitist MODE and the trigonometric MODE algorithms are able to produce the Pareto set of solutions even when a high value of temperature is selected.

20. For case-4 (only P as decision variables) of PET reactor, none of the algorithms resulted in any feasible set of solutions, when T is held constant to a value of 568 K. However, a smooth Pareto front is obtained when T is allowed to reduce to a lower value and kept constant at a value of T = 564 K.
21. For case-1 of PTA oxidation, the Pareto solutions obtained from all the strategies of MODE algorithms lie on the same Pareto front. Majority of the points lie on the upper bound of the decision variable in case of elitist MODE. However, a scattered set of variables is observed in the results obtained using all the strategies of MODE.
22. For case-2 of PTA oxidation, all algorithms converged to the same front. However, MODE is able to cover a better range than the other strategies of MODE and NSGA-II. The elitist MODE algorithm gave a better distribution of solutions compared to MODE algorithm.
23. For case-3 of PTA oxidation, MODE and elitist MODE algorithms captured the entire range of second objective, i.e., concentration of 4-CBA. MODE III, hybrid MODE and the trigonometric MODE converged to a local front and could not cover a complete range of second objective, i.e., concentration of 4-CBA, below a value of 500 ppm.
24. For case-4 of PTA oxidation, at lower concentration of vent oxygen, the concentration of 4-CBA in the reactor effluent increases.
25. In LDPE problem, an efficient numerical solution procedure (numerical differentiation formulas) is used to integrate and simulate the mathematical

model. In terms of monomer conversion, model predictions are exactly matching with industrial data in both the cases (i.e., case A & case B). Case B model predicted the exact value of number-average molecular weight, whereas Case A model predicted the value of M_n with a relative error of 0.48%.

26. Differential evolution, an evolutionary algorithm is applied successfully for finding the optimum rate law parameters and the operating conditions.
27. Detailed simulation based study of LDPE tubular reactor is carried out emphasizing on the effects of feed and jacket temperature, initiators concentrations, reactor diameter, wall heat transfer coefficient, initial solvent concentration, initial monomer concentration and initial feed velocity on the performance of reactor.
28. It is important to control the jacket temperature which affects the location of peak temperature in the reactor. The location of peak temperature affects the important characteristic properties of LDPE such as the concentration of side chain groups, *PDI,* and M_n, etc.
29. Initiator concentration gets depleted at a faster rate soon after the initiator injection with sharp peak in temperature profile. Not much happens in the reactor once the conversion of initiator is completed. It becomes important to control the temperature of reactor at this point in order to avoid the formation of undesired side chain groups and also to have a control on mean molecular weight.
30. The concentration of solvent plays an important role in controlling the number average molecular weight and the PDI; however the side chain concentration is relatively independent of solvent concentration over the ranges covered in this study.

31. For LDPE reactor MOO study, the trigonometric MODE algorithm converged to a local Pareto front as compared to the Pareto fronts obtained using MODE III and hybrid MODE algorithms. Both hybrid MODE and MODE III algorithms converged to the same front. However, the diversity of solutions obtained using both the algorithms is different.
32. Unlike the results obtained using hybrid MODE and trigonometric MODE algorithms (where different Pareto fronts are obtained by relaxing the constraints bounds), the Pareto fronts obtained using MODE III algorithm for all the end point constraints (except, $M_{N,f} = 2190 \pm 2$) are same. The Pareto front obtained with an end point constraint of $M_{N,f} = 21,900 \pm 1100$, covers a wide range of solutions as compared to the range of solutions obtained when a strict constraint on $M_{N,f}$ is used.
33. MODE III algorithm is able to converge to the same Pareto front irrespective of the weight of the penalty parameters considered in this study. However, such results can be obtained, only if, a large value of penalty parameter weight (as used in the present study) is used.
34. The monomer conversion reduces by increasing the monomer feed rate. A higher conversion is obtained for a lower value of feed monomer rate. The Pareto front obtained using the four-objective optimization study for case-2 objectives, is scattered as compared to the Pareto front obtained using case-1 objectives (two-objective optimization study).
35. Multi-objective optimization of supply chain and planning problem is carried out using MODE algorithm and the results are compared for 4 different cases. The MODE algorithm output gives consistent set of results for all the cases even after varying the set of its control parameters (CR, *NP*, and *F*). MODE algorithm also

performed better than NSGA-II, in terms of spread and diversity, when same problem formulation is considered.

6.3 Major Contributions

Major contributions of the present study are

1. The original MODE algorithm is modified and two additional strategies, namely, MODE II and MODE III are developed.
2. Hybridization of evolutionary MODE III algorithm is carried out with deterministic sequential simplex method and hybrid MODE algorithm is proposed.
3. MODE II algorithm is improved further by incorporating the concepts of elitism and the crowding distance approach and another new algorithm, viz., elitist MODE is proposed.
4. The trigonometric mutation operation is included in the evolutionary MODE III algorithm and trigonometric MODE algorithm is proposed.
5. The performance metrics (in terms of convergence and divergence) of developed algorithms are compared with the performance metric values obtained using other evolutionary MOO algorithms from the literature.
6. The Pareto fronts are obtained for the selected test problems using the newly developed strategies of MODE and are compared with those obtained using another evolutionary MOO algorithm (NSGA-II).

7. MOO of selected industrial case studies (styrene reactor, PET reactor, oxidation of *p*-xylene to PTA, LDPE tubular reactor and supply chain & planning) are carried out using the newly developed strategies of MODE. The performance of newly developed strategies of MODE algorithm (with respect to the effect of set of key dominant decision variables on the values of objectives) is compared among themselves and with other EMOs reported in the literature.

6.4 Future Scope of Research

1. An improved constraint handling technique can be included in the existing MOO algorithms.
2. The existing MODE algorithm and its strategies can further be improved by incorporating new recombination and selection schemes.
3. In the present study, all the variables are initialized using the mapping rule. However, more initialization methods may be incorporated and their performance may be compared with the existing algorithms.
4. Various mutation schemes may be tried in the existing strategies of evolutionary MOO algorithms and their performance may be compared with the existing algorithms.
5. More local search methods may be hybridized with the existing strategies of evolutionary MOO algorithms and their performance may be compared with existing standalone evolutionary MOO methods and the hybrid evolutionary methods.
6. The Pareto front for the existing MOO industrial case studies may be obtained using newly developed algorithms.

7. More new industrial problems can be identified and the existing & newly developed strategies of evolutionary MOO algorithms can be used to obtain the Pareto optimal front for the industrial case studies.
8. More complex test problems can be designed so that it resembles with the complexity of industrial problems. Such test problems can be used to test the performance of evolutionary MOO algorithms.

REFERENCES

Abbass, H. A., Sarker, R., Newton, C. (2001). PDE: A Pareto-frontier Differential Evolution Approach for Multi-objective Optimization Problems. In Proceedings of the 2001 Congress on Evolutionary Computation (CEC'2001), 971-978.

Abdalla, B. K., Elnashaie, S. S. E. H., Alkhowaiter, S., Elshishini, S. S. (1994). Intrinsic kinetics and industrial reactors modeling for the dehydrogenation of ethyl benzene to styrene on promoted iron oxide catalysts. Applied Catalysis A: General, 113, 89-102.

Agrawal, N., Rangaiah, G.P., Ray, A.K., Gupta, S.K., (2006). Multi-objective optimization of the operation of an industrial low-density polyethylene tubular reactor using genetic algorithm and its jumping gene adaptations. Industrial and Engineering Chemical Research, 45, 3182–3199.

Agrawal, S., Han, C. D. (1975). Analysis of the high-pressure polyethylene tubular reactor with axial mixing. American Institute of Chemical Engineering Journal. 21, 449-465.

Angira, R. (2005). Evolutionary computation for optimization of selected nonlinear chemical processes. Ph. D. Thesis, Birla Institute of Technology and Science (BITS), Pilani, India.

Angira, R., Alladwar, S. (2007). Optimization of dynamic systems: A trigonometric differential evolution approach, Computers and Chemical Engineering, 31, 1055–1063.

Angira, R., Babu, B. V. (2005). Non-dominated Sorting Differential Evolution (NSDE): An Extension of Differential Evolution for Multi-objective Optimization, In Proceedings of The 2nd Indian International Conference on Artificial Intelligence (IICAI-2005), 1428-1443.

Angira, R., Babu, B. V. (2006a). Optimization of process synthesis and design problems: A modified differential evolution approach. Chemical Engineering Science, 61, 4707-4721.

Angira, R., Babu, B. V. (2006b). Performance of modified differential evolution for optimal design of complex and non-linear chemical processes. Journal of Experimental and Theoretical Artificial Intelligence, 18, 501-512.

Angira, R., Babu, B. V. (2006c). Multi-Objective optimization using modified differential evolution (MDE). International Journal of Mathematical Sciences: Special Issue on Recent Trends in Computational Mathematics and Its Applications, 5, 371-387.

Asteasuain, M. Tonelli, S.M. Brandoline, A., Bandoni, J. A. (2001). Dynamic simulation and optimization of tubular polymerization reactors in gPROMS, Computers and Chemical Engineering, 25, 509-515.

Babu, B. V. Process plant simulation, Oxford Press, New York, 2004.

Babu, B. V., Angira, R. (2005). Optimal design of an auto-thermal ammonia synthesis reactor, Computers and Chemical Engineering. 29, 1041-1045.

Babu, B. V., Angira, R. (2006). Modified differential evolution (MDE) for optimization of non-linear chemical processes. Computers and Chemical Engineering, 30, 989-1002.

Babu, B. V., Chakole, P. G., Mubeen, J. H. S. (2005b). Multi-objective differential evolution (MODE) for optimization of adiabatic styrene reactor. Chemical Engineering Science, 60, 4822-4837.

Babu, B. V., Jehan, M. M. L. (2003) Differential evolution for multi-objective optimization, Proceedings of 2003 Congress on Evolutionary Computation (CEC-2003), Canberra, Australia, 2696-2703.

Babu, B. V., Mubeen, J. H. S., Chakole, P.G. (2007a). Modeling, simulation, and optimization of wiped film poly ethylene terephthalate (PET) reactor using multi-objective differential evolution (MODE). Materials and Manufacturing Processes: Special Issue on Genetic Algorithms in Materials, 22, 541-552.

Babu, B. V., Munawar, S. A. (2007). Differential evolution strategies for optimal design of shell-and-tube heat exchangers. Chemical Engineering Science, 62, 3720.

Babu, B. V., Sastry, K. K. N. (1999). Estimation of heat transfer parameters in a trickle bed reactor using differential evolution and orthogonal collocation. Computers and Chemical Engineering 23, 327–339.

Babu, B. V., Chakole, P. G. and Mubeen, J. H. S. (2007b). Differential evolution strategy for optimal design of gas transmission network, Journal of Multidisciplinary Modeling in Materials and Structures, 1, 315-328.

Babu, B. V., Improved differential evolution for single- and multi-objective optimization: MDE, MODE, NSDE, and MNSDE. Advances in Computational Optimization and its Applications, Edited by Kalyanmoy Deb, Partha Chakroborty, N G R Iyengar, and Santosh K Gupta. Universities Press, Hyderabad, 24-30, 2007.

Back, T. Evolutionary algorithms in theory and practice: Oxford University Press, New York, 1996.

Belegundu, A. D., Chandragupta, T. R. Optimization concepts and applications in engineering, Pearson Education Inc., New Delhi, 1999.

Bhaskar, V., Gupta, S. K., Ray, A. K. (2000). Multi-objective optimization of an industrial wiped film PET reactor. American Institute of Chemical Engineers Journal, 46, 1046-1058.

Bhaskar, V., Gupta, S. K., Ray, A. K. (2001). Multi-objective optimization of an industrial wiped film poly(ethylene terephthalate) reactor: some further insights. Computers and Chemical Engineering, 25, 391–407.

Binh, T. T., Korn, U. (1997). MOBES: A multi objective evolutions strategy for constrained optimization problems, in 'The third International conference on Genetic Algorithms', (Mendel 97), Brno, Czech Republic, 176-182.

Bird, R. B., Stewart, W. E., Lightfoot, E. N. Transport phenomena; John Wiley and Sons (Asia) Pte Ltd.: Singapore, 2005.

Biswas, A., Chakraborti, N., Sen, P. K. (2009a). A genetic algorithms based multi-objective optimization approach applied to a hydrometallurgical circuit for ocean nodules. Mineral Processing and Extractive Metallurgy Review, 30, 163-189.

Biswas, A., Chakraborti, N., Sen, P. K. (2009b). Multiobjective optimization of manganese recovery from sea nodules using genetic algorithms. Materials and Manufacturing Processes, 24, 22-30.

Brandoline, Capiati, N.J., Farber, J.N., Valles, E.M. (1988). Mathematical model for high-pressure tubular reactor for ethylene polymerization. Industrial and Engineering Chemistry Research, 27, 784-790.

Brandoline, Lucanza, M.H., Urgin, P.E., Capiati, N.J. (1996). High-pressure polymerization of ethylene: an improved mathematical model for industrial tubular reactors, Polymer Reaction Engineering, 4, 193-241.

Brandoline, Valles, E. M., Farber, J. N. (1991). High-pressure tubular reactors for ethylene polymerization optimization aspects. Polymer Engineering Science, 31, 381-390.

Cao, G., Pisu, M., Massimo, M. A. (1994a). Lumped kinetic model for liquid phase catalytic oxidation of *p*-xylene to terephthalic acid, Chemical Engineering Science, 49, 5775-5788.

Cao, G., Servida, A., Pisu, M., Massimo, M. (1994b). Kinetics of *p*-xylene liquid phase catalytic oxidation. Americal Institute of Chemical Engineering Journal, 40, 1156-1166.

Chakraborti, N., Kumar, A. (2003). The optimal scheduling of a reversing strip mill: studies using multipopulation genetic algorithms and differential evolution, Materials and Manufacturing Processes, 18, 433-445.

Chankong, V., Haimes, Y. Y. Multiobjective decision making theory and methodology, Dover publications, North-Holland, 1983.

Charnes, A., Cooper, W., Ferguson, R. (1955). Optimal estimation of executive compensation by linear programming. Management science, 1, 138-151.

Chen, C.H., Vermeychuk, J.G., Howell, J. A., Ehrlich, P. (1976). Computer model for tubular high-pressure polyethylene reactors. American Institute of Chemical Engineering Journal, 22, 463-471.

Cheng, Y., Li, X., Wang, L., Wang, Q. (2006). The optimum ratio of Co/Mn in the liquid phase catalytic oxidation of *p*-xylene to terephthalic acid. Industrial and Engineering Chemistry Research, 45, 4156-4162.

Cheng, Y., Li, X., Wang, Q., Wang, L. (2005). Effects of guanidine on the liquid phase catalytic oxidation of *p*-xylene to terephthalic acid. Industrial and Engineering Chemistry Research, 44, 7756-7759.

Chiou, J. P., Wang, F. S. (1999). Hybrid method of evolutionary algorithms for static and dynamic optimization problems with application to a fed-batch fermentation process. Computers and Chemical Engineering, 23, 1277–1291.

Chopra, S., Meindl, P. Supply Chain Management: Strategy, Planning and operation: Pearson Education, Singapore, 2004.

Clough, D. E., Ramirez, W. F. (1976). Mathematical modeling and optimization of the dehydrogenation of ethyl benzene to form styrene. American Institute of Chemical Engineering Journal, 22, 1097–1105.

Coello, C. A. C., Lamont, G. B. Applications of multi-objective evolutionary algorithm: Advances in natural computation – Vol. 1: World Scientific Publishing Co. Pte. Ltd, Singapore, 2004.

Deb, K. Multi-objective optimization using evolutionary algorithms; John Wiley and Sons Limited, New York, 2001.

Deb, K. Optimization for engineering design algorithms and examples, Prentice-Hall of India Pvt. Ltd., 2005.

Deb, K., Pratap, A., Agarwal, S. Meyarian, T. (2002a). A fast and elitist multiobjective genetic algorithm: NSGA-II. IEEE transactions on Evolutionary Computation, 6, 182-197.

Deb, K., Thiele, L., Laumanns, M., Zitzler, Z. (2002b). Scalable multiobjecitve optimization test problems. In proceedings of the 2002 congress in evolutionary computation, 825-830.

Denis, H. J., Castor, W. M. (1992). Styrene In: B. Elvers, S. Hawkin and W. Russey (Eds.), Ullmann's Encyclopedia of Industrial Chemistry, New York: Wiley, vol. A25, 325-335.

Dhib, R. Al-Nidawy, N. (2002). Modeling of free radical polymerization of ethylene using difunctional initiators, Chemical Engineering Science, 57, 2735-2746.

Eiben, A. E., Smith, J. E. Introduction to evolutionary computing: Springer-Verlag Berlin Hiedelberg, 2003.

Elnashaie, S. S. E. H., Abdalla, B. K., Hughes, R. (1993). Simulation of the industrial fixed bed catalytic reactor for the dehydrogenation of ethyl benzene to styrene: heterogeneous dusty gas model. Industrial and Engineering Chemistry Research, 32, 2537–2541.

Elnashaie, S. S. E. H., Elshishini, S. S. Modeling, simulation and optimization of industrial fixed bed catalytic reactors. Gordon and Breach Science Publisher, London, 1994.

Fan, H. Y., Lampinen, J. (2003). A trigonometric mutation operation to differential evolution. Journal of Global Optimization, 27, 105-129.

Ferrio, J., Wassick, J. (2008). Chemical supply chain network optimization. Computers and Chemical Engineering, 32, 2481-2501.

Fonseca, C. M., Fleming, P. J. (1995). An overview of evolutionary algorithms in multi-objective optimization. Evolutionary Computation Journal, 3, 1-16.

Goldberg, D. E. Genetic algorithms in search, optimization and machine learning. Addission-Wesley, Reading, MA, 1989.

Goto, S., Yamamoto, K.S., Furui, S., Sugimoto, M. (1981). Computer model for commercial high-pressure polyethylene reactor based on elementary reaction rates obtained experimentally. Journal of Applied Polymer Science, 36, 21-40.

Gupta, S. K., Kumar, A., Krishnamurthy, M. V. G. (1985). Simulation of tubular low-density polyethylene reactor. Polymer Engineering and Science, 25, 37-47.

Haimes, Y. Y., Lasdon, L. S., Wismer, D. A. (1971). On the bicriterion formulation of the problems of integrated system identification and system optimization, IEEE Transactions on Systems, Man, and Cybernetics, 1, 296-297.

Huang, V. L., Suganthan, P. N., Qin, A. K., Baskar, S. (2005). Multi-objective differential evolution with external archive and harmonic distance-based diversity measure, Technical Report, Nanyang Technological University, Singapore.

ICIS. Home Page of ICIS, (2007). the URL of which is http://www.icispricing.com/il_shared/Chemicals/pta.pdf

ICIS., Home Page of ICIS, (2009a). the URL of which is *http://www.icis.com/v2/chemicals/9076423/polyethylene-terephthalate.html*

ICIS. Home Page of ICIS, (2009b). the URL of which is *http://www.icis.com/v2/chemicals/9076426/polyethylene-terephthalate/uses.html*

Kalyon, D.M., Chiou, Y.N., Kovenklioglu, S., Bouaffar, A. (1994). High pressure polymerization of ethylene and rheological behavior of polyethylene product. Polymer Engineering and Science, 34, 804-814.

Kasat, R. B., Gupta, S. K. (2003). Multi-objective optimization of an industrial fluidized-bed catalytic cracking unit (FCCU) using genetic algorithm (GA) with the jumping genes operator. Computers and Chemical Engineering, 27, 1785-1800.

Katz, S., Saidel, G.M. (1967). Moments of the size distribution in radical polymerization, American Institute of Chemical Engineers Journal. 13, 319-326.

Kim, D. M., Iedema, P. D. (2008). Modeling of branching density and branching distribution in low density polyethylene polymerization. Chemical Engineering Science, 63, 2035-2046.

Kim, I. Y., De Weck, O. L. (2004). Adaptive weighted sum method for multiobjective optimization, in proceedings of 10th AIAA/ISSMO multidisciplinary analysis and optimization conference, Albany, New York.

Kiparissides, C., Verros, G., MacGregor, J. F. (1993). Mathematical modeling, optimization, and quality control of high pressure ethylene polymerization reactors. Polymer Reviews, C33, 437-527.

Knowels, J. D., Corne, D. W. (1999). The Pareto archived evolution strategy: A new baseline algorithm for multi-objective optimization. In: Proceedings of the 1999 congress on evolutionary computation, 98-105.

Knowels, J. D., Corne, D. W. (2000). Approximating the nondominated front using Pareto archived evolutionary strategy. Evolutionary Computation, 8, 149-172.

Knowles, J. D. and Corne, D. W. (2002). On metrics for comparing nondominated sets, In Proceedings of 2002 congress on evolutionary computation (CEC 2002), 711-716.

Kursawe, F. (1990). A variant of evolution strategies for vector optimization. In Proceedings of the 1st Workshop on Parallel Problem Solving From Nature I (PPSN I), 193-197.

Lacunza, M. H., Urdin, P. G., Brandoline, A. Capiati, N.J. (1998). Heat transfer coefficients in a high pressure tubular reactor for ethylene polymerization, Polymer Engineering Science, 38, 992-1013.

Lasschuit, W., Thijssen, N. (2004). Supporting supply chain planning and scheduling decisions in the oil and chemical industry. Computers and Chemical Engineering, 28, 863-870.

Laubriet, C., LeCorre, B., Choi K. Y. (1991). Two-phase model for continuous final stage melt poly-condensation of poly ethylene terephthalate: 1. steady-state analysis. Industrial and Engineering Chemistry Research, 30, 2-12.

Lee, H. J., Yeo, Y. K., Chang J. Y. (2000). Modeling of industrial high pressure autoclave polyethylene reactor including decomposition phenomena, Korean Journal of Chemical Engineering, 17, 223-229.

Lee, M. H., Han, C., Chang, K. S. (1999). Dynamic optimization of a continuous polymer reactor using a modified differential evolution algorithm, Industrial and Engineering Chemistry Research, 38, 4825–4831.

Li, C. H.; Hubbell, O. S. Styrene. In: Mcketta, J.J., Weismantel, G.E. (Eds.), Encyclopedia of chemical processing and design; Wiley: New York, 1982.

Martinez, S. Z., Coello, C. A. C. (2008). Hybridizing an evolutionary algorithm with mathematical programming technique for multi-objective optimization, In proceedings of genetic and evolutionary computation conference, Atlanta, Georgia, USA.

Masini, G., Petracci, N., Bandoni, A. (2009). Supply chain planning optimization in the fruit industry. technical report, Available online at http://cepac.cheme.cmu.edu/pasilectures/bandoni/FOCAPO%202003%20Paper%20Sam-4%20.pdf as on 4th October, 2009.

Melachrinoudis, E., Min, H. (2000). The dynamic relocation and phaseout of a hybrid, two-echelon plant/warehousing facility: A multiple objective approach. European Journal of Operations Research, 123, 1-15.

Miettinen, K. M. Nonlinear multiobjective optimization: Kluwer Academic Publishers, Boston, Massachusetts, 1999.

Milan, H., Cvengrošovà, Z., Ilavskŷ, J. (1985). Kinetics and mechanism of cobalt catalyzed oxidation of *p*-xylene in the presence of water. Industrial and Engineering Chemistry Process Design and Development, 24, 787-794.

Milan, H., Ilavskŷ, J. (1982). Oxidation of polyalkylaromatic hydrocarbons. Technological aspects of *p*-xylene oxidation to terephthalic acid in water. Industrial and Engineering Chemistry Product Research and Development, 21, 455-460.

Mu, S. J. Private email communication with present authors, dated June, 6, 2007.

Mu, S. J., Su, H. Y., Jia, T., Gu, Y., Chu, J. (2004). Scalable multi-objective optimization of industrial purified terephthalic acid (PTA) oxidation process. Computers and Chemical Engineering, 28, 2219-2231.

Mu, S. J., Su, H. Y., Jia, T., Gu, Y., Chu, J. (2004). Scalable multi-objective optimization of industrial purified terephthalic acid (PTA) oxidation process. Computers and Chemical Engineering, 28, 2219-2231.

Nam, D. K. and Park, C.H. (2000). Multiobjective simulated annealing: a comparative study to evolutionary algorithms. International Journal of Fuzzy Systems, 2, 87-97.

Nelder, J. M., Mead, R. (1965). A Simplex method for function minimization. The Computational Journal, 7, 308-313.

Nozick, L. K., Turnquist, M. A. (2001). Inventory, transportation, service quality and the location of distribution centers. European Journal of Operations Research, 129, 362-371.

Onwubolu G. C., Babu, B. V. New optimization techniques in engineering, Springer-Verlag, Heidelberg, Germany, 2004.

Partenheimer, W. (1995). Methodology and scope of metal bromide catalyzed autooxidation of hydrocarbons. Catalysis Toady, 23, 60-69.

PEP, (2007). Process economics program (PEP) report 9E: Terephthalic acid and dimethyl terephthalate. SRI consulting, January (1997). The URL of which is http://www.sriconsulting.com/PEP/Public/Reports/Phase_95/RP009E/ as on June 2007.

Pinto, E. G. (2007). Supply chain optimization using multi-objecitve evolutionary algorithm, technical report, available online at

http://www.engr.psu.edu/ce/Divisions/Hydro/Reed/Education/CE%20563%20Projects/Pinto.pdf, as on 12th June, 2007.

Poloni, C.; Giurgevich A., Onesti, L.; Pediroda, V. (2000). Hybridization of a multi-objective genetic algorithm, a neural network and a classical optimizer for a complex design problem in fluid dynamics. Computational Methods in Applied Mechanical Engineering, 186, 403-420.

Price, K. V., Storn, R. (1997). Differential evolution - a simple evolution strategy for fast optimization. Dr. Dobb's Journal, 22, 18-22.

Purchasing. Purchasing.com. *Available online at http://www.purchasing.com* as on May 23, 2009.

Raghavendrachar, P., Ramachandran, S. (1992). Liquid-phase catalytic oxidation of *p*-xylene. Industrial and Engineering Chemistry Research, 31, 453-462.

Rao, S.S. Optimization theory and applications; Wiley Eastern: New Delhi, 1991.

Ravindranath, K., Mashelkar, R. A. (1982). Modelling of poly(ethylene terephthalate) reactors: A continuous process for final stages of polycondensation. Polymer Engineering Science, 22, 625-632.

Ravindranath, K., Mashelkar, R. A. (1984). Finishing stages of PET synthesis: a comprehensive model. American Institute of Chemical Engineers Journal. 30, 415-423.

Ravindranath, K., Mashelkar, R. A. (1986a). Polyethylene terephthalate-I: Chemistry, thermodynamics and transport properties. Chemical Engineering Science, 41, 2197-2214.

Ravindranath, K., Mashelkar, R. A. (1986b). Polyethylene terephthalate-II: Engineering analysis. Chemical Engineering Science, 41, 2969-2987.

Saint, M. H. C., Choi, K.Y. (1991). Two phase model for continuous final stage melt polycondenstaion poly(ethylene terephthalate): 2. analysis of dynamic behavior. Industrial and Engineering Chemistry Research, 30, 1712-1718.

Savoretti, A. A., Borio, D. O., Bucala, V., Porras, J. A. (1999). Non-adiabatic radial-flow reactor for styrene production. Chemical Engineering Science, 54, 205-213.

Schaffer, J. D. (1985). Some experiments in machine learning using vector evaluated genetic algorithms. Ph. D. Thesis, Nashville, T.N.: Vanderbilt University.

Shah, J. Supply chain management: Pearson Education Inc., New Delhi, 2009.

Shampine, L.F., Reichelt, M. (1997). The matlab ODE suite, SIAM Journal in Scientific Computing, 18, 1-22.

Sheel, J. G. P., Crowe, C. M. (1969). Simulation and optimization of an existing ethyl benzene dehydrogenation reactor, Canadian Journal of Chemical Engineering, 47, 183-187.

Sheppard, C. M., Maier, E. E., Caram, H. S., (1986). Ethyl benzene dehydrogenation reactor model. Industrial and Engineering Chemistry Process Design and Development, 25, 207-210.

Shirodkar, P.P., Taien, G.O. (1986). A mathematical model for the production of low density polyethylene in a tubular reactor. Chemical Engineering Science, 41, 1031-1038.

Silva, C. A., Sousa, J. M. C., Runkler, T. A., Sá da Costa, J. M. G. (2009). Distributed supply chain management using ant colony optimization. European Journal of Operations Research, 199, 349-358.

Silver, E. A., Pyke, D., and Peterson, R. Inventory Management and Production Planning: John Wiley and Sons, New York, 1998.

Simchi-Levi, D., Kaminsky, P., Simchi-Levi, E., Shankar, R. Designing and managing the supply chain: Concepts, strategies and case studies: Tata McGraw Hill, New York, 2008.

Smith, J. M., Vanness, H.C. Introduction to chemical engineering thermodynamics, Third edition, McGraw-Hill, Tokyo, 1975.

Srinivas, N., Deb, K., (1994). Multi-objective optimization using nondominated sorting in genetic algorithms. Journal of Evolutionary Computation, 2, 221-248.

Stumberger, G., Dolinar, D., Pahner, U., Hameyer, K. (2000). Optimization of radial active magnetic bearings using the finite element technique and the differential evolution algorithm, IEEE Transactions on Magnetics 36, 1009-1013.

Styreneforum. Available online at *http://styreneforum.org* as on May, 23, 2009.

Suganthan, P. N. Private email communication with present authors, dated February, 7, 2008.

Suresh, A. K., Sharma M. M., Sridhar, T. (2000). Engineering aspects of industrial liquid-phase air oxidation of hydrocarbons. Industrial and Engineering Chemistry Research, 39, 3958-3997.

Taha, H. A. Operations research: an introduction: Pearson Education Inc., New Delhi, 2007.

Tan, K. C., Khor, E. F., Lee, T. H. Multi-objective evolutionary algorithms and applications: Springer-Verlag, London, 2005.

Tanaka, M. (1995). GA-based decision support system for multi-criterion optimization, In proceedings of the international conference on systems, man and cybernetics, 2, 1556-1561.

Trzaskalik, T., Michnik, J., Multiple objective and goal programming: Recent developments: Springer-Verlag, Heidelberg, 2002.

Wang, E., Li, X., Wang, L., Cheng, Y., Xie, G. (2005a). Effect of water content on the kinetics of the *p*-xylene liquid phase catalytic oxidation to terephthalic acid. Industrial and Engineering Chemistry Research, 44, 4518-4522.

Wang, L, Cheng, Y., Wang, Q., Li, X. (2007). Progress in research and development of *p*-xylene Liquid phase oxidation process. Frontiers of Chemical Engineering in China, 1, 317-326.

Wang, Q., Li, X., Wang, L. (2005b). Kinetics of *p*-xylene liquid phase catalytic oxidation to terephthalic acid. Industrial and Engineering Chemistry Research, 4, 261-266.

Yan, X., Du, W. Qian, F. G. (2004). Development of a kinetic model for industrial oxidation of *p*-xylene by RBF-PLS and CCA. American Institute of Chemical Engineering Journal, 50, 1169-1176.

Yao, F. Z., Lohi, A., Upreti, S. R., Dhib, R. (2004). Modeling, simulation and optimal control of ethylene polymerization in non-isothermal, high-pressure tubular reactors. International Journal of Chemical Reactor Engineering, 2, 1-25.

Yee, A. K. Y., Ray, A. K., Rangiah, G. P. (2003). Multi-objective optimization of industrial styrene reactor. Computers and Chemical Engineering, 27, 111-130.

Zitzler, E., Deb, K., Thiele, L. (2000). Comparison of multi-objective evolutionary algorithms: Empirical results. Evolutionary Computation, 8, 173-195.

Zitzler, E., Laumanns, M., Thiele, L. (2001). SPEA2: Improving the strength Pareto evolutionary algorithm. Technical Report 103, Computer engineering and networks laboratory (TIK), Swiss Federal Institure of Technology (ETH), Zurich, Switzerland.

Zitzler, E., Thiele, L., (1999). Multiobjective evolutionary algorithms: A comparative case study and strength Pareto approach. IEEE Ttransactions on Evolutionary Computation, 3, 257-271.

LIST OF PUBLICATIONS

International Journals

1. Babu, B. V. and Gujarathi, A. M. (2007). Multi-Objective Differential Evolution (MODE) Algorithm for Multi-Objective Optimization: Parametric Study on Benchmark Test Problems. Journal on Future Engineering and Technology, 3, 47-59.
2. Gujarathi, A. M. and Babu, B. V. (2009). Improved Multi-Objective Differential Evolution (MODE) Approach for Purified Terephthalic Acid (PTA) Oxidation Process. Materials and Manufacturing Processes, 24, 303-319.
3. Gujarathi, A. M. and B. V. Babu. Hybrid Multi-objective Differential Evolution (H-MODE) for optimization of Polyethylene Terephthalate (PET) Reactor. International Journal of Bio-inspired Computation. Accepted (In Press).
4. Gujarathi, A. M. and Babu, B. V. (2010). Multi-objective Optimization of Industrial Styrene Reactor: Adiabatic and Pseudo-isothermal Operation. Chemical Engineering Science, 65, 2009-2026.
5. Gujarathi, A. M. and Babu, B. V. (2009). Optimization of Adiabatic Styrene Reactor: A Hybrid Multi-Objective Differential Evolution (H–MODE) Approach. Industrial and Engineering Chemistry Research, 48, 11115–11132.
6. Gujarathi, A. M. and Babu, B. V. Evolutionary Multi-objective Optimization using Hybrid Multi-objective Differential Evolution (H-MODE). To be Communicated.
7. Gujarathi, A. M. and Babu, B. V. Elitist Multi-Objective Differential Evolution Algorithm for Multi-Objective Optimization of Industrial Styrene Reactor. Communicated. Applied Computational Intelligence and Soft Computing.
8. Gujarathi, A. M. and Babu, B. V. Multi-objective optimization of industrial processes using elitist multi-objective differential evolution. To be communicated. Materials and Manufacturing Processes.
9. Gujarathi, A. M. and Babu, B. V. Multi-objective optimization and parametric estimation of low-density polyethylene tubular reactor. To be communicated.

International Conference Proceedings

1. Gujarathi, A. M. and Babu, B. V. Multi-Objective Optimization of Styrene Reactor Using Multi-Objective Differential Evolution (MODE): Adiabatic vs. Steam Injected Operation. Proceedings of International Symposium and 59th Annual Session of IIChE in association with International Partners (CHEMCON-2006), GNFC Complex, Bharuch, December 27-30, 2006.

2. Babu, B. V., Gujarathi, A. M., Katla, P. and Laxmi, V. B. Strategies of Multi-Objective Differential Evolution (MODE) for Optimization of Adiabatic Styrene Reactor. Proceedings of International Conference on 'Emerging Mechanical Technology-Macro to Nano (EMTMN-2007), BITS Pilani, February 16-18, 2007, pp. 243-250, 2007.
3. Babu, B. V. and Gujarathi, A. M. Multi-Objective Differential Evolution (MODE) for Optimization of Supply Chain Planning and Management. Proceedings of IEEE Congress on Evolutionary Computation (CEC-2007), Swissotel The Stamford, Singapore, September 25-28, pp. 2732-2739, 2007.
4. Babu, B. V. and Gujarathi, A. M. Elitist-Multi-Objective Differential Evolution (E-MODE) Algorithm for Multi-objective Optimization. Proceedings of 3rd Indian International Conference on Artificial Intelligence (IICAI-2007), Pune, December 17-19, 2007, pp. 441-456, 2007.
5. Gujarathi, A. M. and Babu, B. V. Modeling and Simulation of Low Density Polyethylene (LDPE) High Pressure Tubular Reactor. Proceedings of International Symposium and 61st Annual Session of IIChE in association with International Partners (CHEMCON-2008), Panjab University, Chandigarh, December 27-30, 2008.
6. Gujarathi, A. M. and Babu, B. V. Improved Strategies of Multi-objective Differential Evolution (MODE) for Multi-objective Optimization. Proceedings of 4th Indian International Conference on Artificial Intelligence (IICAI-09), Tumkur, Bangalore, December 16-18, 2009.
7. Gujarathi, A. M., Sharma D., and Babu, B. V. Multi-Objective Optimization of Polyethylene Terephthalate (PET) Reactor Using Hybrid Multi-objective Differential Evolution. Proceedings of International Symposium and 62nd Annual Session of IIChE in association with International Partners (CHEMCON-2009), December 27-30, 2009.
8. Gujarathi, A. M., Mishra, M., Lohumi, A., Sharma, D., and Babu, B. V. Multi-Objective Optimization Using Trigonometric Mutation Multi-Objective Differential Evolution Algorithm. Proceedings of International Symposium and 62nd Annual Session of IIChE in association with International Partners (CHEMCON-2009), December 27-30, 2009.

Book Chapter

1. Gujarathi A. M., and Babu, B. V. Advances in Optimization and Simulation of Low Density Polyethylene (LDPE) Tubular Reactor. In Advances in Chemistry and Chemical Engineering, Edited by A K Haghi, Nova Science Publishers, USA. Communicated. (2009).

BIOGRAPHIES

Biography of the candidate

Ashish M Gujarathi was born in Akot, Maharashtra, India on October 10, 1977. He received the Masters degree in Chemical Engineering from BITS Pilani in year 2002 and currently pursuing his Ph.D. He is currently working as a Lecturer of chemical engineering at BITS Pilani since July, 2004. He is a nucleus member of Community Welfare & International Relations Unit (CWIRU) at BITS Pilani. He is also a non-resident warden of Ram Bhavan (Hostel) at BITS Pilani for last 4 years. He has guided 3 Professional Practice –I and II students, 2 Thesis students and around 50 project students (first and higher degrees). He has taught courses such as, Reaction Engineering (Higher degree), Bio-Chemical Engineering, Optimization, Thermodynamics, Structure and Properties of Materials and involved in the tutorials of Process Design Decisions, Fluid Flow Operations, Heat Transfer Operations, Mass Transfer Operations, and Kinetics and Reactor design. His current research and consultancy interests include process design and synthesis, process modeling and simulation, reaction engineering, polymers, optimization, evolutionary computation, and concept to commissioning aspects of industrial optical brighteners and dyes.

He has over 9 years of experience in the fields of Industry, Academics, Administration and Consultancy. He was associated at various capacities with industries like, 'Paramount Minerals and Chemicals Limited, Ambarnath', 'Oswal Chemicals and Fertilizers Limited., Paradeep', 'Kenya Vegext (EPZ) Limited, Nairobi, Kenya', 'Fitwell Engineering Company, Thane', and 'Mecon Limited (A Govt. of India Enterprise), Ranchi'. He acted as honorary consultant for 'Ghari Detergents, Kanpur' and currently associated with Parshwanath Dye Chem. Limited, Ahmedabad. He is a review panel member of Mc-Graw-Hill Educations India Pvt. Ltd., Chemical Engineering Journal (Elsevier), Memetic Computing Journal (Springer), the 2nd and 3rd International Multi-Conference on Engineering and Technological Innovation: IMETI 2009 & 2010, U.S.A. He chaired session of 3rd Indian International Conference on Artificial Intelligence, Pune, India. He was local organizing committee member of national conference of environmental conservation, BITS Pilani. He has reviewed 3 books and several journals and conference papers. He is an associate life member of Indian Institute of Chemical Engineers (IIChE) and a life member of International Association of Engineers.

Biography of supervisor

Dr B V Babu is Professor of Chemical Engineering and Dean of Educational Hardware Division (EHD) at Birla Institute of Technology and Science (BITS), Pilani. He did his PhD from IIT-Bombay. His biography is included in 2005, 2006 & 2007 editions of Marquis Who's Who in the World, in Thirty-Third Edition of the Dictionary of International Biography in September 2006, in 2000 Outstanding Intellectuals of the 21st Century in 2006, and in First Edition of Marquis Who's Who in Asia in 2007. He is the Coordinator for PETROTECH Society at BITS-Pilani. He is on various academic and

administrative committees at BITS Pilani. He is the member of project planning & implementation committees of BITS-Pilani Dubai Campus, BITS-Pilani Goa Campus, and BITS-Pilani Hyderabad Campus. He is external expert member of Board of Studies at Banasthali University and MNIT-Jaipur. He is expert peer committee member of National Assessment and Accreditation Council (NAAC), Bangalore, India. He is also member of peer review committee for the Natural Sciences and Engineering Research Council of Canada (NSERC), Canada; and National Research Foundation (NRF), International Research Grants, South Africa.

He has 24 years of Teaching, Research, Consultancy, and Administrative experience. He guided 5 PhD students, 36 ME Dissertation students and 35 Thesis students and around 200 Project students. He is currently guiding 5 PhD candidates and 2 Thesis students. He is on doctoral advisory committee for 10 PhD students. He currently has 4 research and sponsored projects from MHRD, UGC, DST & KK Birla Academy. He is PhD Examiner for 7 candidates and PhD Thesis Reviewer for 6 Candidates.

His research interests include Evolutionary Computation (Population-based search algorithms for optimization of highly complex and non-linear engineering problems), Environmental Engineering, Biomass Gasification, Energy Integration, Artificial Neural Networks, Nano Technology, and Modeling & Simulation.

He is the recipient of National Technology Day (11th May, 2003) Award given by CSIR, obtained in recognition of the research work done in the area of 'A New Concept in Differential Evolution (DE) – Nested DE'. His paper entitled "Convective and Radiative Heat Transfer in Pyrolysis of a Biomass Particle" authored by A S Chaurasia, B V Babu, Amanpreet Kaur, and V Thiruchitrambalam, published in Indian Chemical Engineer Journal, Vol. 47 (No. 2), pp. 75-80, April-June, 2005 earned the Kuloor Memorial Award, 2006 awarded for the Best Technical Paper published in the Institute's Journal "Indian Chemical Engineer" in its issues for 2005.

He is the Life member of Indian Institute of Chemical Engineers (IIChE), Life member of Indian Society for Technical Education (ISTE), Life member of Institution of Engineers (IE), Fellow of International Congress of Chemistry and Environment (ICCE), Life member of Indian Environmental Association (IEA), Life member of Society of Operations Management (SOM), Associate Member of International Society for Structural and Multidisciplinary Optimization (ISSMO), Member of International Institute of Informatics and Systemics (IIIS), Member of International Association of Engineers (IAENG). Nine of his technical papers have been included as successful applications of Differential Evolution (DE: a population based search algorithm for optimization) on their Homepage at http://www.icsi.berkeley.edu/~storn/code.html#appl.

He has around 190 research publications (International & National Journals and Conference Proceedings) to his credit. He completed three consultancy projects successfully and he has been Technical Consultant for Maharashtra Electricity Regulatory Commission (MERC), Mumbai and offering Advisory Services in the "Study relating to Bagasse Based Co-generation". He also has been invited as a consultant by a Bahrain (Middle East) based company for making a complex of chemical factories. He is a Panel Expert for www.chemicalhouse.com the most vibrant and active site for the Chemical Industry on the net which specializes in exchange of Information in a structured way among the chemical world in more than a Hundred Countries and a

Million core chemical manufacturers, traders, scientists, etc. He is Technical Consultant for Sangam (India) Limited Textile Industry at Bhilwara for Removal of Color, BOD, and COD from Effluent Treatment Plant.

He has published five books (1) "Process Plant Simulation", EDD, BITS-Pilani, 2002, (2)"New Optimization Techniques in Engineering", Springer-Verlag, Germany, 2004, and (3)"Process Plant Simulation", Oxford University Press, India, 2004, (4) "Environmental Management Systems", EDD, BITS-Pilani, 2005, (5) "Chemical Engineering Laboratory Manual", EDD, BITS-Pilani, 2006. In addition he has written several chapters and invited articles in various books, lecture notes, and International Journals. He was invited to write an editorial and for cover design on Conservation of Natural Resources, for December 2006 Issue of International Research Journal of Chemistry & Environment.

He was the Invited Chief Guest and delivered the Keynote addresses at seven international conferences and workshops (Desert Technology–7, Jodhpur; Life Cycle Assessment, Kaula Lumpur; Indo-US Workshop, IIT-Kanpur; Indo-French Workshop, TERI-New Delhi; Indo-US Workshop, Kolkata; Research tools Workshop, BITS Pilani-Goa Campus; Process Modeling & Simulation Workshop, UPES-Dehradun) and three national seminars. He organized many Seminars & Conferences at BITS-Pilani. He also chaired 20 Technical Sessions at various International & National Conferences. He delivered 43 invited lectures at various IITs and Universities abroad.

He is Editorial Board Member of five International Journals 'Energy Education Science & Technology', 'Research Journal of Chemistry and Environment', 'International Journal of Computer, Mathematical Sciences and Applications', 'Journal on Future Engineering and Technology', and 'International Journal of Applied Evolutionary Computation'. He is the referee & expert reviewer of 59 International Journals. He is also on the Programme Committees at many (around 100) International Conferences. He reviewed five books of McGraw Hill, John Wiley & Science, Elsevier, Oxford University Press, and Tata McGraw Hill publishers.

He is the Organizing Secretary for "National Conference on Environmental Conservation (NCEC-2006)" held at BITS-Pilani during September 1-3, 2006. He is also the Organizing Committee Member (Publicity Chair), and Session Organizer for the Special Session on "Evolutionary Computation" at The Second International Conference on "Computational Intelligence, Robotics, and Autonomous Systems (CIRAS-2003)", National University of Singapore, Singapore, December 15-17, 2003. He was the Session Chair and organized an Invited Session on "Engineering Applications of Evolutionary Computation Techniques" at "The Eighth World Multi-Conference on Systemics, Cybernetics, and Informatics (SCI-2004)", Orlando, Florida, USA, July 18-21, 2004.

APPENDIX A

The rates of reaction are as follows (Elnashaie and Elshishini, 1994):

$$r_1 = k_1\left(p_{EB} - p_{ST}\ p_{H2} / K_{EB}\right) \tag{A1}$$

$$r_2 = k_2\left(p_{EB}\right) \tag{A2}$$

$$r_3 = k_3\left(p_{EB}\ p_{H2}\right) \tag{A3}$$

$$r_4 = k_4\left(p_{H2O}\ p_{ETH}^{0.5}\right) \tag{A4}$$

$$r_5 = k_5\left(p_{H2O}\ p_{MET}\right) \tag{A5}$$

$$r_6 = k_6\left(p_{H2O}\ p_{CO}\right)\left(P_T / T^3\right) \tag{A6}$$

The rate constants k_i of reaction i are expressed by:

$$k_i = \exp\ \left[A_i - \left(E_i / RT\right)\right] \tag{A7}$$

where A_i and E_i are the apparent frequency factors and activation energy of reaction i.

The Six material balance equations are given by:

$$\frac{d\,x_i}{d\,l} = \frac{\rho_b\,A_t\,r_i}{F_{EB}^0} \qquad i \text{ is for reactions 1, 2 and 3} \tag{A8}$$

x_i - fractional conversion of ethyl benzene in each of the three reactions

$$\frac{d\,x_i}{d\,l} = \frac{\rho_b\,A_t\,r_i}{F_{H2O}^0} \qquad i \text{ is for reactions 4, 5 and 6} \tag{A9}$$

x_i - fractional conversion of steam in each of the remaining three reactions

The Ergun equation (Bird et al., 2005) is used to compute the pressure profiles

$$\left(\frac{\left(p_0 - p_L\right)\rho_G}{D_p}\right)\left(\frac{D_p}{L}\right)\left(\frac{\varepsilon^3}{\left(1-\varepsilon\right)}\right) = 150\left(\frac{1-\varepsilon}{D_p G_0 / \mu_G}\right) + \frac{7}{4}$$

(A10a)

However, as pressure is used in the units of 'bar', following form of Ergun equation was used in this study

$$\frac{\Delta P}{L} = -1\times 10^{-5}\,\frac{(1-\varepsilon)G_0}{D_p\,\varepsilon^3\,\rho_G}\left[\frac{150\;\;(1-\varepsilon)\mu_G}{D_p} + 1.75\;\;G_0\right] \tag{A10b}$$

The energy balance differential equation can be derived from this equation

$$\sum_{i=1}^{10} F_i\,Cp_i\,dT + \sum_{j=1}^{6}\Delta H_j\,A_t\,\rho_b\,r_j\,dl = U\,A_H\;\,dl\,(T-T_e) \tag{A11}$$

As reactor is adiabatic: $U\,A_H\;\,dl\,(T-T_e)=0$ and the energy balance differential equation is given by:

$$dT/dl = \sum_{j=1}^{6}\Delta H_j\,A_t\,\rho_b\,r_j\;\;/\sum_{i=1}^{10} F_i\,Cp_i \tag{A12}$$

The heats of reactions are computed as functions of temperature from the following relation (Sheel and Crowe, 1969):

$$\Delta H_j = a_j + b_j T \tag{A13}$$

The set of values of a_j and b_j in Eq. A13 is taken from Sheel and Crowe (1969) is given in Table A3.

The molar heat capacities (Cp_i and Cp_j) of the components are given by Eqs. A14, A15 as functions of temperature.

$$Cp_i = \alpha_i + \beta_i T + \gamma_i T^2 \qquad \text{(Organic Components)} \tag{A14}$$

$$Cp_j = a_j + b_j T + c_j / T^2 \qquad \text{(Inorganic Components)} \tag{A15}$$

The set of the values of the constants is given in Table A4 for organic components and Table A5 for inorganic components (Smith and Van Ness, 1975).

The additional data for equilibrium constant of ethyl benzene is found from the literature (Elnashaie and Elshishini, 1994), and the values are given in A2. The equations for conversion and molar flow rate are taken from Elnashaie and Elshishini, (1994).

Table A1 Operating conditions and design for the industrial reactor (Elnashaie and Elshishini, 1994)

Quantity	**Numerical value and dimension**
Reactor diameter	1.95 m
Reactor length	1.7 m
Catalyst bulk density	2146 kg/m^3
Catalyst particle diameter	0.0047 m
Bed void fraction	0.445
Catalyst composition	62 % Fe_2O_3, 36 % K_2CO_3, 2 % Cr_2O_3
Inlet pressure	2.4 bar
Inlet temperature	922.59 K
Ethyl benzene in the feed	36.87 kmol/h
Styrene in the feed*	0.67 kmol/h
Benzene in the feed*	0.11 kmol/h
Toluene in feed*	0.88 kmol/h
Steam	453.63 kmol/h
Total molar feed	491.63 kmol/h

*These components are present as impurities in the ethyl benzene feed.

Table A2 Frequency factor and activation energy for the six reactions (Sheel and Crowe, 1969)

Reaction No.	**Frequency factor A_i (dimensionless)**	**Activation energy E_i (kJ/kmol)**
1	-0.0854	90981.40
2	13.2392	207989.23
3	0.2961	91515.26
4	-0.0724	103996.71
5	-2.9344	65723.34
6	21.2402	73628.40

Equilibrium constant $K_{EB} = Exp\left[\frac{-\Delta F_0}{RT}\right]$; $\Delta F_0 = a + bT + cT^2$; (kJ/kmol);

a = 122725 kJ/kmol; b = -126.3 kJ/kmolK; and c = -0.002194 kJ/kmolK^2 (Elnashaie and Elshishini, 1994).

Table A3 Values of the constants a and b for heat of reactions $\Delta H_i = a_i + b_i T$ (Sheel and Crowe, 1969)

Reaction No.	**a_i (kJ/kmol)**	**b_i (kJ/kmol K)**
1	120649.6337	4.56
2	108723.9635	-7.9476
3	-53132.186	-13.176
4	81994.734	8.826
5	211073.068	16.5645
6	-45184.528	10.4574

Table A4 Values of the constants of molar heat capacities Cp_i for organic components (Smith and Vanness, 1975; Elnashaie and Elshishini, 1994)

Components	α_i **(kJ/kmol K)**	β_I **(kJ/kmol K^2)**	$-\gamma_i$ **X 10^5 (kJ/kmol K^3)**
Ethyl benzene	9.3458	0.4604	15.361
Styrene	17.0437	0.417	13.852
Benzene	-1.7126	0.325	11.10
Toluene	2.41	0.392	13.10
Ethylene	11.85	0.120	3.65
Methane	14.16	0.076	1.80

The expression is $Cp_i = \alpha_i + \beta_i T + \gamma_i T^2$

Table A5 Values of the constants of molar heat capacities Cp_i for inorganic components (Smith and Vanness, 1975; Elnashaie and Elshishini, 1994)

Components	α_i **(kJ/kmol K)**	β_I **(kJ/kmol K^2)**	$-\gamma_i$ **X 10^{-5} (kJ/kmol K^{-1})**
Steam	28.849	0.012	1
Hydrogen	27.012	$3.508e^{-3}$	0.690062
Carbon monoxide	28.068	$4.63e^{-3}$	-0.257734
Carbon dioxide	45.369	$8.688e^{-3}$	-9.619

The expression is $C_{pi} = \alpha_i + \beta_i T + \gamma_i T^{-2}$

Table A6 Comparison of simulation runs of present study with industrial data (Sheel and Crowe, 1969; Elnashaie and Elshishini, 1994)

Parameter at the exit of reactor	**Simulation Results (Present Study)**	**Industrial data**
Temperature (K)	850.08	850
Pressure (bar)	2.33	2.32
Conversion of ethyl benzene per pass (%)	46.78	47.25
Styrene flow rate (kmol/h)	15.37	15.57
Flow rate of ethyl benzene (kmol/h)	19.61	19.45
Benzene flow rate (kmol/h)	1.46	1.5
Toluene flow rate (kmol/h)	2.07	2.03

APPENDIX B

The set of reactions in the melt polymerization of PET are:

Ester Interchange Reaction (Main Poly-condensation)

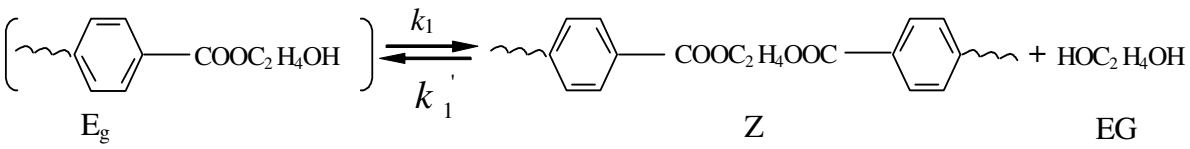

(B1)

Acetaldehyde Formation (a)

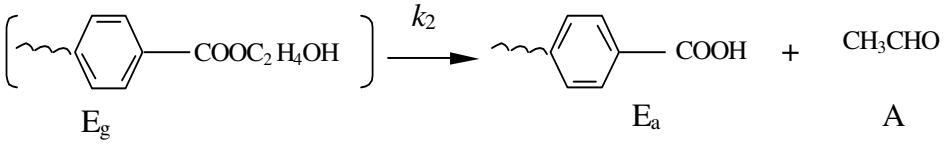

(B2)

Acetaldehyde Formation (b)

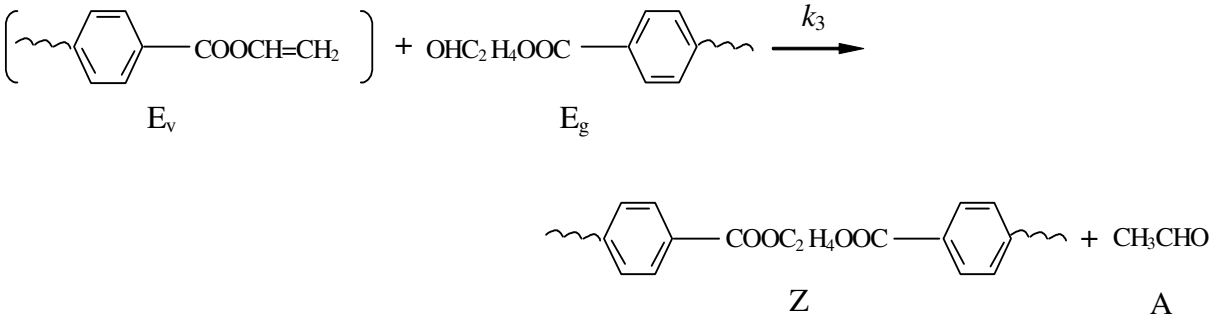

(B3)

Diethylene Glycol Formation (a)

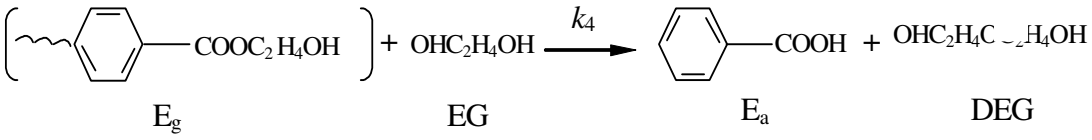

(B4)

Diethylene Glycol Formation (b)

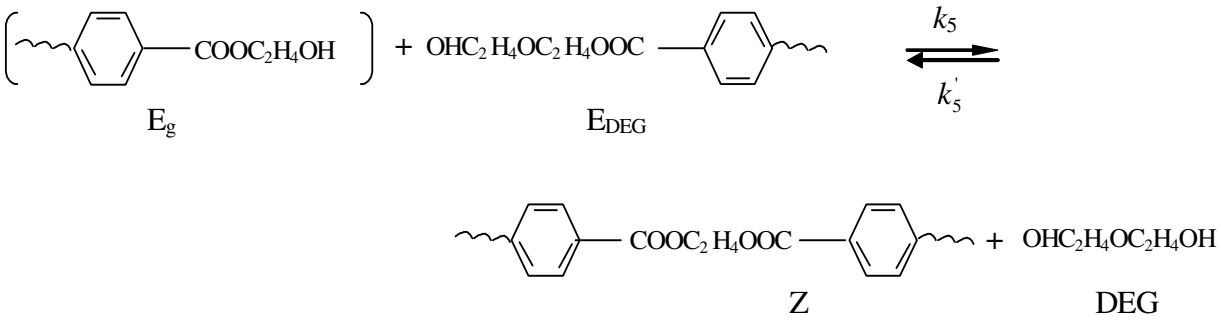

(B5)

Diethylene Glycol Formation (c)

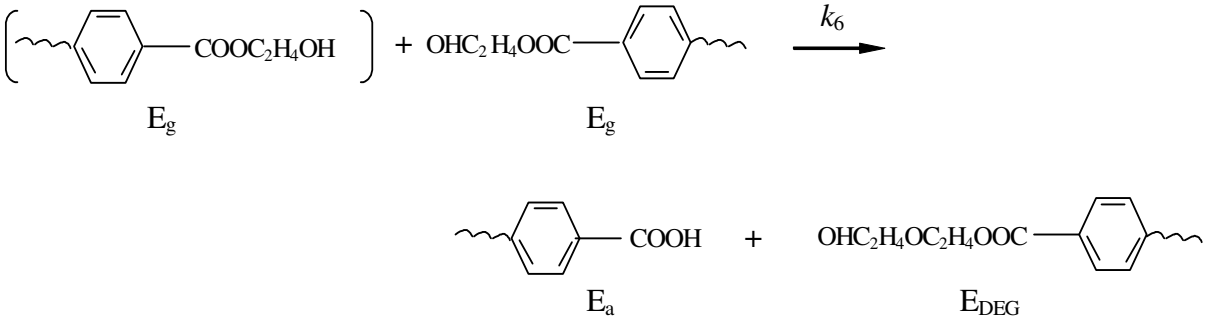

(B6)

Water Formation (a)

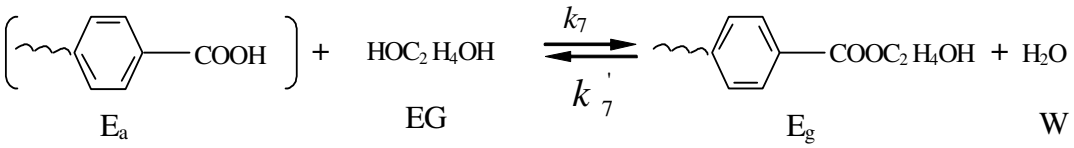

(B7)

Water Formation (b)

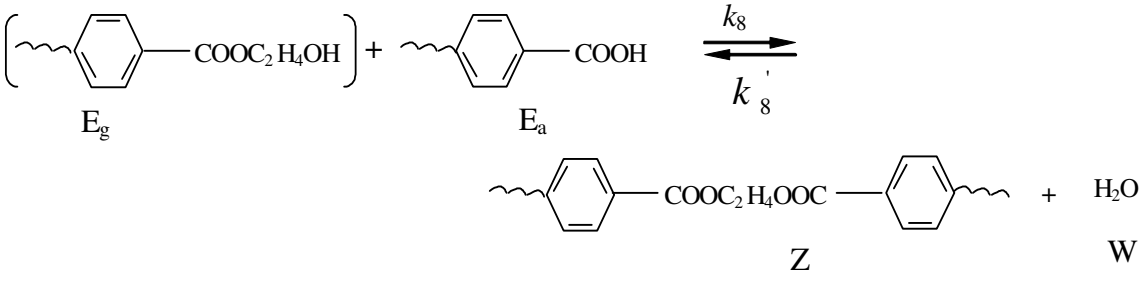

(B8)

Degradation of Diester Group

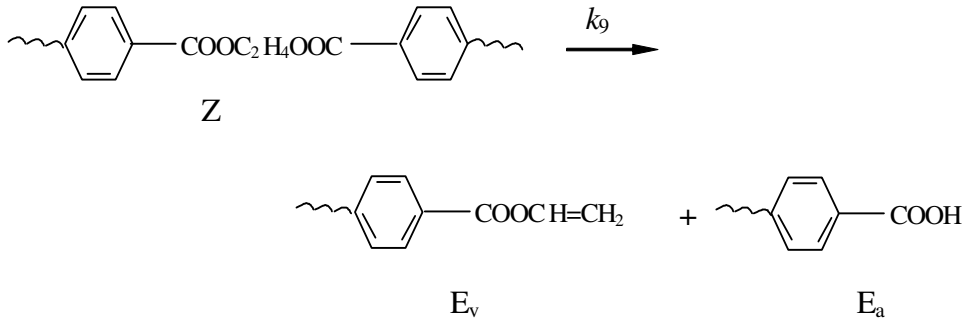

(B9)

The detailed set of model equations used in the present study is same as that reported in the literature (Bhaskar et al, 2001).

Table B1 Feed conditions used for simulation in the present study

Feed Concentrations (kmol/m^3) of Pure Liquid Components	
$[E_g]_f = 4.0 \times 10^{-1}$	$[E_{DEG}]_f = 0.17$
$[E_a]_f = 2.57 \times 10^{-3}$	$[EG]_f = 6.5 \times 10^{-3}$
$[Z]_f = 11.2$	$[W]_f = 4.6 \times 10^{-4}$
$[E_v]_f = 1.17 \times 10^{-3}$	$[DEG]_f = 4.0 \times 10^{-4}$

Table B2 Values of the parameters / properties for the reference case

Parameters	**Values**
$(k_l a)_{ref}$	2.6875
α	2.6647
ao	1.0378
bo	2.1838
ρ_{EG} (kg/m^3)	1108
ρ_{W} (kg/m^3)	1000
ρ_{DEG} (kg/m^3)	1118
P (mmHg)	2.00*, 1.5***
T (K)	566*, 567**

*Set 1; **Set 2;***Set 3

Table B3 Comparison of the simulation results with the reported data (Bhaskar et al., 2001)

Set No	**Product Property**	**Industrial Value**	**Model Predicted Value**
1	*DP* $[E_{DEG}]$ (kmol/m^3) $[E_a]$ (kmol/m^3)	82.00 0.17 1.038×10^{-3}	82.00 0.167 1.028×10^{-3}
2	*DP*	82.60	82.53
3	*DP*	82.70	82.65

APPENDIX C

Material balance equations for series of oxidation reactions are related by following differential equations.

$$\frac{d(C_{PX})}{d\tau} = -k_1 C_{PX} \tag{C1}$$

$$\frac{d(C_{TALD})}{d\tau} = k_1 C_{PX} - k_2 C_{TALD} \tag{C2}$$

$$\frac{d(C_{p-T})}{d\tau} = k_2 C_{TALD} - k_3 C_{p-T} \tag{C3}$$

$$\frac{d(C_{4-CBA})}{d\tau} = k_3 C_{p-T} - k_4 C_{4-CBA} \tag{C4}$$

$$\frac{d(C_{TA})}{d\tau} = k_4 C_{4-CBA} \tag{C5}$$

The kinetic expressions involved in the rate law are given by the following expressions.

$$k_j^o = k_{j,0} \exp\left(\frac{-E_j}{RT}\right) \tag{C6}$$

$$k_1 = \left(\frac{V_{0_2}}{7.65}\right)^{0.44} k_1^0 \tag{C7}$$

$$k_2 = 1.2\left(\frac{V_{0_2}}{7.65}\right)^{0.44} k_2^0 \tag{C8}$$

$$f_1 = 0.4987 - \frac{1}{1 + ([Co]/165.1)^{3.07}} \tag{C9}$$

$$f_2 = 0.5443 - \frac{1}{1 + ([Co]/170)^{1.3}} \tag{C10}$$

$$f_3 = 0.1178 + 8.26 \times 10^{-4}[Co] \tag{C11}$$

$$f_4 = 0.0641 + 5.72 \times 10^{-4}[Co] \tag{C12}$$

Above correlations are only valid for $[Co^{2+}]$, $[Mn^{2+}]$ and $[Br^-]$ ratio fixed to 1.

The rate constant is related to % water in solvent by following expression.

$$k_j = k_{j,0}\left(1 + \alpha_j w_{H_2 0} + \gamma_j W_{H_2O}{}^2\right) \qquad \text{where } j = 1 \text{ to } 4. \tag{C13}$$

$$\tau = \left(\frac{1.0175 \times 10^7}{F_{FEED}}\right) + \left(\frac{3.6731 \times 10^6}{F_{FEED}}\right) \tag{C14}$$

Table C1 Optimal parameters for various water contents used in model equations (Wang et al., 2005a)

Parameter	***j*=1**	***j*=2**	***j*=3**	***j*=4**
α_j	2.19	-1.65	3.51	0.79
γ_j	-23.15	-7.05	-4.60	1.58

Table C2 Parameters and constants used in model equations (Wang et al., 2005b)

Reaction No.	d_j (kgHOAc/mol)	β_j	θ
j=1	1.4247	0	0.0146
j=2	0	0.5254	
j=3	0	0	
j=4	4.8419	0.8111	

Table C3 Specific Reaction rate constants and activation energies (Wang et al., 2005b)

Kinetic Parameter	***j*=1**	***j*=2**	***j*=3**	***j*=4**
$K_{j,0}$ (min^{-1})	4.07 X 10^6	1.08 X 10^6	9.80 X 10^8	1.17 X 10^9
E_j (kJ/mol)	65.5	54.9	92.8	84.9

Table C4 Reference values of various variables

Parameter	**Reference Value**
T (K)	461[a]
$[C_0]$ (ppm)	341.07[b]
F_{PX} (kg/h)	26243.57[b]
F_{FEED} (kg/h)	143008.71[b]
V_{O_2} (%)	4.075[b]
W_{H_20} (%)	6.015[c]

[a]: optimum value obtained from the simulation of present study
[b]: Mu et al. (2004)
[c]: Wang et al. (2005b)

APPENDIX D

Reaction scheme involved in the LDPE reactor

Oxygen Initiation	$O_2 + M \xrightarrow{k_o} 2R_1(O)$	(D1)
Peroxide Initiation	$I_m \xrightarrow{f_m k_{dm}} 2R_1(O)$ (for m = 1,2)	(D2)
Propagation	$R_i(x) + M \xrightarrow{k_p} R_i(x+1)$	(D3)
Termination by combination	$R_i(x) + R_j(y) \xrightarrow{k_{tc}} P_{i+j-1}(x+y)$	(D4)
Termination by Thermal degradation	$R_i(x+1) + M \xrightarrow{k_{tdt}} P_i(x) + R_1(O)$	(D5)
Chain transfer to telogen	$R_i(x) + S \xrightarrow{k_{trs}} P_i(x) + R_1(O)$	(D6)
Chain transfer to polymer	$R_i(x) + P_j(y) \xrightarrow{k_{trp}} P_i(x) + R_{j+1}(y)$	(D7)
Intramolecular chain transfer	$R_i(x) \xrightarrow{k_{bb}} R_i(x)$	(D8)
(short-chain branching)		
β-scission of secondary radical	$R_i(x+1) \xrightarrow{k_{b1}} P_i(x) + R_1(O)$	(D9)
(formation of vinyl group)		
β-scission of territory radical	$R_i(x+1) \xrightarrow{k_b} P_i(x) + R_1(O)$	(D10)
(formation of vinylidene group)		

MODEL EQUATIONS

Continuity equation

$$\frac{dv}{dz} = -\frac{v}{\rho}\left(\frac{d\rho}{dz}\right) \tag{D11}$$

Mass balance Model Equations for components j

$$v\frac{d\left[C_j\right]}{dz}=-\left(r_j+[C_j]\frac{dv}{dz}\right) \tag{D12}$$

Where j=3, 4,..11 for I_1, I_2, O_2, M, S, M_e, V_i, and $V_{id,}$ $R_{i(0)}$ respectively

Reactor temperature: Heating and reaction zones

$$\rho C_p v\frac{dT}{dz}=-\left\{\frac{4U\left(T-T_j\right)}{1000D_i}+k_p C_M \lambda_{00}\left(\Delta H\right)\right\} \tag{D13}$$

Frictional pressure drop

$$\frac{dP}{dz}=-10^{-6}\left\{\frac{2f_r\rho v^2}{D_i}+\rho v\frac{dv}{dz}\right\} \tag{D14}$$

Moment equations related to dead and live polymer

$$v\frac{d\left[\lambda_{np}\right]}{dz}=-\left(r_{\lambda_{np}}+\left[\lambda_{np}\right]\frac{dv}{dz}\right)\quad(\text{for n}=0,1\ldots\text{and p}=0,1,2,\ldots) \tag{D15}$$

Where

$$r_{\lambda_{np}}=-\begin{pmatrix}2k_o C_M C_{O_2}^{1.1}\delta_{p0}+2\sum_{j=1}^{2}f_j k_{d_j}\delta_{p0}+pk_p C_M\lambda_{n,p-1}-k_{tc}\lambda_{00}\lambda_{np}+k_{tdt}\left(\lambda_{00}\delta_{p0}-\lambda_{np}\right)\\+k_{trs}C_S\left(\lambda_{00}\delta_{p0}-\lambda_{np}\right)+k_{trp}\left(\lambda_{00}\sum_{j=0}^{n}\left({}^nC_j\right)\mu_{j,p+1}-\lambda_{np}\mu_{01}\right)\end{pmatrix} \tag{D16}$$

$$v\frac{d\left[\mu_{np}\right]}{dz}=-\left(r_{\mu_{np}}+\left[\mu_{np}\right]\frac{dv}{dz}\right)\quad(\text{for n}=0,1\ldots\text{and p}=0,1,2,\ldots) \tag{D17}$$

Where,

$$r_{\mu_{np}}=-\begin{pmatrix}\frac{ktc}{2}\sum_{j=0}^{n}\sum_{k=0}^{j}\sum_{i=0}^{p}\left({}^nC_j\right)\left({}^jC_k\right)\left({}^pC_i\right)(-1)^{n-j}\lambda_{ki}\lambda_{j-k,p-i}\\+k_{tdt}\lambda_{np}+k_{trs}C_S\lambda_{np}+k_{trp}\left(\lambda_{np}\mu_{01}-\lambda_{00}\mu_{n,p+1}\right)\end{pmatrix} \tag{D18}$$

$$\mu_{03} = \mu_{00}\left(\frac{\mu_{02}}{\mu_{01}}\right)^3 \tag{D19}$$

$$\mu_{13} = \mu_{10}\left(\frac{\mu_{12}}{\mu_{11}}\right)^3 \tag{D20}$$

$$X_M = 1 - \frac{v}{v_{in}}\left(\frac{C_M}{C_{M_{in}}}\right) \tag{D21}$$

$$M_n = 28\left(\frac{\mu_{01} + \lambda_{01}}{\mu_{00} + \lambda_{00}}\right) \tag{D22}$$

$$M_W = 28\left(\frac{\mu_{02} + \lambda_{02}}{\mu_{01} + \lambda_{01}}\right) \tag{D23}$$

$$PDI = \frac{M_W}{M_n} \tag{D24}$$

$$\text{Methyl Group (SCB) per } 10^3 \text{ C atoms} = \frac{500 C_{M_{exit}}}{\mu_{01} + \lambda_{01}} \tag{D25}$$

$$\text{Vinyl Group per } 10^3 \text{ C atoms} = \frac{500 C_{Vi_{exit}}}{\mu_{01} + \lambda_{01}} \tag{D26}$$

$$\text{Vinylidene Group per } 10^3 \text{ C atoms} = \frac{500 C_{Vid_{exit}}}{\mu_{01} + \lambda_{01}} \tag{D27}$$

$$k = A\exp\left(-\frac{E + 10^3 P\Delta V}{RT}\right) \tag{D28}$$

$f = 0.316/(\mathrm{Re})^{1/4}$ from Gupta et al. [7] (Case A) (D29a)

$f = \frac{16}{\mathrm{Re}};$ $\mathrm{Re} < 2100$ from Kiparissides et al. [13] (Case B) (D29b)

$(\mathrm{Re})^{1/2} = 4\log(\mathrm{Re}\, f^{1/2}) - 0.4;$ $2.1\times10^3 < \mathrm{Re} < 5\times10^6$ (Case B) (D29c)

Table D1 Operating conditions used for industrial tubular LDPE reactor in the present study for reference run (Brandoline et al., 1996; Agarwal et al., 2006)

Parameter	**Value**
Feed temperature, T_{in}	349.15 K
Feed pressure P_{in}	227.98 Mpa
Initiator 1 feed flow rate, F_{I1}	1.0×10^{-3} kg/s
Initiator 2 feed flow rate, F_{I2}	1.6×10^{-4} kg/s
Feed flow rate of oxygen, F_{O2}	6.8×10^{-5} kg/s
Feed flow rate of solvent, F_S	7.4×10^{-2} kg/s
Feed flow rate of inert, F_{inrt}	0.22 kg/s
Feed flow rate of jacket fluid, $V_{jm\ (m=2,\ldots5)}$ Feed flow rate of jacket fluid, $V_{jm\ (m=2,\ldots5)}$	$6.90e^{-3}$, $6.34e^{-3}$,$1.67e^{-3}$,$1.25e^{-3}$ m^3/s (Case A)* $6.73e^{-3}$, $3.99e^{-3}$,$0.978e^{-3}$,$2.78e^{-3}$ m^3/s (Case B)*
Wall heat transfer coefficient, h_W	1256 W/m^2C
Feed conditions for live and dead moment, λ_{np} μ_{np} (n=0,1; p=0,1,2)	0.0 $kmol/m^3$
Specific heat of reaction mixture, C_{pm}	2.42834, 2.42834, 3.1401, 3.1401, 4.01933 kJ/kg K
Mean jacket temperature, $T_{j,m}$ (m=1,…,5)	441.15, 498.15, 498.15, 441.15, 441.15 K
Feed velocity v	10.14 m/s
Total reactor length, L_t	1390 m
Inside diameter of reactor, D_t	0.05 m
Thickness of reactor wall, t	0.0254 m
Inner diameter of outer (jacket) wall D_{Ji}	0.2032 m
Axial lengths of reactor zones , L_{zn} (n=1,2,..5)	60, 100,180, 510, 540 m

*Results obtained in present study

APPENDIX E

Multi-objective optimization algorithms developed in this study:

```
%%MATLAB CODE FOR Multi-objective Differential Evolution- (MODE)%%%%
%DEVELOPED BY ASHISH M. GUJARATHI AND B V BABU, BITS PILANI, INDIA – 333031
clc
clear all
t=cputime;
CR =0.8;          %%%Insert Value of Cross over constant here
Np=500;           %%%%%%%Insert Population size here
GMAX=200;         %%%%%%%%Insert Maximum no of generations here
D=1;  %%%%%%%%%%%%%Insert No. of dimensions here
n_obj=2;    %%%%%%%%%%%%Insert number of objectives here
xl=-10;  %%%%%%%%%%Insert lower bound of variables here
xu=10;      %%%%%%%%%%%Insert upper bound of objectives here %SCH Test function
for i=1:Np
   for j=1:D
      pop1(i,j)=xl(j)+(xu(j)-xl(j))*rand(1);
   end
%TYPE OBJECTIVE FUNCTIONS HERE%%%%%%%%%%%%%%%
      f1(i,1)=pop1(i,1)^2;
      f2(i,1)=(pop1(i,1)-2)^2;
      f3(i,1)=0;   %%% Add third objective function here, if present
   end
for gen=1:GMAX
   gen
   nond=ones(1,D);
   nondf=[0 0 0];
   a=1;
   for i=1:Np
      flag=0;
      for j=1:Np
%following code is for min-min type of problems
         if (((f1(i)>=f1(j))&(f2(i)>=f2(j))) & ((f1(i)>f1(j))|(f2(i)>f2(j))))
            flag=1;
            break;
         end
      end
      if(flag~=1)
         nond(a,:)=pop1(i,:);
         nondf(a,1)=f1(i,1);
```

```
        nondf(a,2)=f2(i,1);
        nondf(a,3)=f3(i,1);
        a=a+1;
    end
end
nond;
 tmp=size(nond);
Np=tmp(1,1);
 if(Np<4)
    break;
end

% DE
for i=1:Np
    Xt=nond(i,:);
    n=randperm(D);
    flag=0;
    for(k=1:D)
        c=rand(1);
        if ((c<CR)|(k==D) )
            if(flag==0)
                flag=1;
                r1=ceil(rand(1)*Np);
                while(r1==i)
                    r1=ceil(rand(1)*Np);
                end
                r2=ceil(rand(1)*Np);
                while(r2==i|r2==r1)
                    r2=ceil(rand(1)*Np);
                end
                r3=ceil(rand(1)*Np);
                while(r3==i|r3==r1|r3==r2)
                    r3=ceil(rand(1)*Np);
                end
                Xa=nond(r1,:);
                Xb=nond(r2,:);
                Xc=nond(r3,:);
                Diff=Xa-Xb;
                F=rand(1);
                Wdiff=F.*Diff;
                Xc1=Xc+Wdiff;
            end
            Xtr(:,n(k))=Xc1(:,n(k));
        else
            Xtr(:,n(k))=Xt(:,n(k));
        end
```

```
      end
      for j=1:D
         if(Xtr(1,j)<xl(j) | Xtr(1,j)>xu(j))
            Xtr(1,j)=xl(j) + (xu(j)-xl(j))*rand(1);
         end
      end
      f1Xt=nondf(i,1);
      f2Xt=nondf(i,2);
      f3Xt=nondf(i,3);
%%%Type OBJECTIVE Function here for calculating Trial Variables Cost
      f1Xtr=(Xtr(1,1))^2;
      f2Xtr=(Xtr(1,1)-2)^2;
      f3Xtr=0;
      if (((f1Xtr<=f1Xt)&(f2Xtr<=f2Xt)) & ((f1Xtr<f1Xt)|(f2Xtr<f2Xt)))
         nond(i,:)=Xtr;
         nondf(i,1)=f1Xtr;
         nondf(i,2)=f2Xtr;
         nondf(i,3)=f3Xtr;
      end
   end   %%% end of population loop
================================================
%MATLAB CODE FOR Multi-objective Differential Evolution- III (MODE-III)%%%DEVELOPED BY ASHISH M. GUJARATHI AND B V BABU, BITS PILANI, INDIA – 333031
clc
clear all
t=cputime;
CR =0.8;          %%%%%%%%Insert Value of Cross over constant here
Np=500;           %%%%%%%%Insert Population size here
GMAX=200;         %%%%%%%%Insert Maximum no of generations here
D=1;              %%%%%%%%Insert No. of dimensions here
n_obj=2;          %%%%%%%%Insert number of objectives here
xl=-10;           %%%%%%%%Insert lower bound of variables here
xu=10;            %%%%%%%%Insert upper bound of objectives here %SCH Test function
for i=1:Np
   for j=1:D
      pop1(i,j)=xl(j)+(xu(j)-xl(j))*rand(1);
   end
end
for gen=1:GMAX
   gen
   for i=1:Np
%TYPE OBJECTIVE FUNCTIONS HERE%%%%%%%%%%%%%%%
      f1(i,1)=pop1(i,1)^2;
      f2(i,1)=(pop1(i,1)-2)^2;
      f3(i,1)=0;   %%% Add third objective function here, if present
```

```
   end
%%DO NOT CHANGE BELOW TILL FURTHER INFORMATION%
   for i=1:Np
      %        dei=i
      %        Np
      Xt=pop1(i,:);
      n=randperm(D);
      flag=0;
      for(k=1:D)
         c=rand(1);
         if ((c<CR)|(k==D) )
            if(flag==0)
               flag=1;
               Np
               r1=ceil(rand(1)*Np);
               while(r1==i)
                  gh=i
                  r1=ceil(rand(1)*Np)
               end
               r2=ceil(rand(1)*Np);
               while(r2==i|r2==r1)
                  r2=ceil(rand(1)*Np);
               end
              r3=ceil(rand(1)*Np);
               while(r3==i|r3==r1|r3==r2)
                  r3=ceil(rand(1)*Np);
               end
               Xa=pop1(r1,:);
               Xb=pop1(r2,:);
               Xc=pop1(r3,:);
               Diff=(Xa-Xb);
               F=rand(1);
               F=0.7;
               Wdiff=F.*Diff;
               Xc1=Xc+Wdiff;
            end
            Xtr(:,n(k))=Xc1(:,n(k));
         else
            Xtr(:,n(k))=Xt(:,n(k));
         end
      end
      for j=1:D
         if(Xtr(1,j)<xl(j) | Xtr(1,j)>xu(j))
            Xtr(1,j)=xl(j) + (xu(j)-xl(j))*rand(1);
         end
      end
```

```
        f1Xt(i)=f1(i,1);
        f2Xt(i)=f2(i,1);
        %  f3Xt(i)=f3(i,1);
%%%%Type OBJECTIVE Function here for calculating Trial
        f1Xtr=(Xtr(1,1))^2;
        f2Xtr=(Xtr(1,1)-2)^2;
        f3Xtr=0;  %%%%%Insert third objective function here, if present
        flag=0;
        if (((f1Xt>f1Xtr)|(f2Xt>f2Xtr)))
           pop1(i,:)=Xtr;
           f1(i)=f1Xtr;
           f2(i)=f2Xtr;
           f3(i)=f3Xtr;
           flag=1;
           break;
        end
        if flag==0
           for pp=1:Np
              if (((f1(pp)>f1Xtr)|(f2(pp)>f2Xtr)))
                 pop1(pp,:)=Xtr;
                 f1(pp)=f1Xtr;
                 f2(pp)=f2Xtr;
                 f3(pp)=f3Xtr;
                 flag=1;
                 break;
              end
           end
        end
    end% end of pop loop
end  % end of generation loop
nond=zeros(1,D);
nondf=[0 0 0];
a1=1;
for i=1:Np
    flag=0;
    for j=1:Np
        if (((f2(i)>=f2(j))&(f1(i)>=f1(j))) & ((f2(i)>f2(j))|(f1(i)>f1(j))))
           flag=1;
           break;
        end
    end
    if(flag~=1)
        nond(a1,:)=pop1(i,:);
        nondf(a1,1)=f1(i,1);
        nondf(a1,2)=f2(i,1);
        nondf(a1,3)=f3(i,1);
```

```
        a1=a1+1;
    end
end
nond;
a1
Np=a1-1
clear f1
clear f2
clear f3
for i=1:Np
    f1(i,1)=nondf(i,1);
    f2(i,1)=nondf(i,2);
    f3(i,1)=0;
end
clear pop1
pop1=nond
```

==========

%%%%%%%%%%%%%%%%%%%%MATLAB CODE FOR HYBRID MULI-OBJECTIVE DIFFERENTIAL EVOLUTION %%%%%%%%%%%%%%THIS CODE IS DEVELOPED BY ASHISH M GUJARATHI AND B V BABU

%%%%ENTER YOUR OBJECTIVE FUNCTION in mo_test_file

%%%Enter the number and bounds of variables in fun file

```
clc
clear all
    t=cputime;
    CR=0.9;
    Np=300;
    GMAX=100;
    %step=[1,10,.1,.1];
    %%% VALUES OF CONSTANTS USED IN HYBRID ALGORITHM
    step=.002;
    d=0.5;
    count=0;
    DPD=82;
    C1=0;
    C2=0;
    Beta = 0.5;
    gamma=2;
    p=1;
    [D,n_obj,xl,xu]=fun(p);
    for i=1:Np
        for j=1:D
            pop1(i,j)=xl(j)+(xu(j)-xl(j))*rand(1);
        end
    end
    for gen=1:GMAX
```

```
gen
for i=1:Np
   [f]=mo_test_func(pop1(i,:),D,p);
   f1(i,1)=f(1,1);
   f2(i,1)=f(1,2);
   f3(i,1)=0;
end
%DO NOT CHANGE BELOW TILL FURTHER INFORMATION%
for i=1:Np
   %       dei=i
   %       Np
   Xt=pop1(i,:);
   n=randperm(D);
   flag=0;
   for(k=1:D)
      c=rand(1);
      if ((c<CR)|(k==D) )
         if(flag==0)
            flag=1;
            Np
            r1=ceil(rand(1)*Np);
            while(r1==i)
               gh=i
               r1=ceil(rand(1)*Np)
            end
            r2=ceil(rand(1)*Np);
            while(r2==i|r2==r1)
               r2=ceil(rand(1)*Np);
            end
            r3=ceil(rand(1)*Np);
            while(r3==i|r3==r1|r3==r2)
               r3=ceil(rand(1)*Np);
            end
            Xa=pop1(r1,:);
            Xb=pop1(r2,:);
            Xc=pop1(r3,:);
            Diff=(Xa-Xb);
            F=rand(1);
            F=0.7;
            Wdiff=F.*Diff;
            Xc1=Xc+Wdiff;
         end
         Xtr(:,n(k))=Xc1(:,n(k));
      else
         Xtr(:,n(k))=Xt(:,n(k));
      end
```

```
        end
        for j=1:D
           if(Xtr(1,j)<xl(j) | Xtr(1,j)>xu(j))
              Xtr(1,j)=xl(j) + (xu(j)-xl(j))*rand(1);
           end
        end
        f1Xt(i)=f1(i,1);
        f2Xt(i)=f2(i,1);
        %  f3Xt(i)=f3(i,1);
        sum=0;
        % % % %      [f]=mo_test_func(Xtr(1,:),D,p);
        % % % %      i
        [f]=mo_test_func(Xtr(1,:),D,p);
        f1Xtr=f(1,1);
        f2Xtr=f(1,2);
        f3Xtr=0;
        %%%%%%%%%%%%%%%%%%%%CHANGE THE SIGN DEPENDING
UPOM MAX-MIN PROBLEM%%
        if (((f1Xt>f1Xtr)|(f2Xt>f2Xtr)))
           pop1(i,:)=Xtr;
           f1Xt(i)=f1Xtr;
           f2Xt(i)=f2Xtr;
        else
           pop1(i,:)=Xt;
        end
        %hybrid starts
        for u=1:D
           ls(1,u)=pop1(i,u);
           for m=2:D+1
              ls(m,u)=500000000;
              while (ls(m,u)<=xl(u) | ls(m,u)>=xu(u))
                 DDzii1=i
                 if (rand<.5)
                    ls(m,u)=pop1(i,u) - (step*rand);
                 else
                    ls(m,u)=pop1(i,u) + (step*rand);
                 end
              end
           end
           %% neighbourhood point
        end
        for kk=1:(D+1)
           % %     [f]=mo_test_func(ls(kk,:),D,p);
           [f]=mo_test_func(ls(kk,:),D,p);
           ls_f1(kk)=f(1,1);
           ls_f2(kk)=f(1,2);
```

```
    ls_f3(kk)=0;
  end
  %%SELECT ANY ONE OF THE FLOOWING DESIRABILITY EQNS DEPENDING UPON THE
  %%TYPE OF PROBLE, COMMENT THE REMAINING LINES%%%%
  %if min-min
  for kk = 1:(D+1)
    f_avg(kk) = (abs(1/((d*ls_f1(kk))+((1-d)*ls_f2(kk)))))^0.5;
  end
  [Bf,I1]=max(f_avg);              %% finding out best element
  B(1,:)=ls(I1,:);              %% assigning the decision varibles
  costBf1=ls_f1(I1);
  costBf2=ls_f2(I1);              %%assinging the idividual cost
  costBf3=ls_f3(I1);
  [Wf,I2]=min(f_avg);
  W(1,:)=ls(I2,:);
  costWf1=ls_f1(I2);
  costWf2=ls_f2(I2);
  costWf3=ls_f3(I2);
  %%%start of sequential simplex method
  %for o=1:5
  Q=10;
  while(Q >.01)   % for tolerance check
    for u=1:D
      s(1,u)=0;
    end
    for kk = 1:D+1
      s(1,:)= s(1,:)+ls(kk,:);
    end
    P(1,:)=(s(1,:)-W(1,:))/D;% centroid of existing point except worst
    %           P(1,:)=(N(1,:)+B(1,:))/2;
    R(1,:)=P(1,:)+(P(1,:)-W(1,:));  % Reflection point
     for m=1:D
      while(R(1,m)<xl(m) | R(1,m)>xu(m))
        %                 DDrrr=i
        if ((R(1,m)<=xl(m) | R(1,m)>=xu(m)))
          if rand<0.5
            R(1,m)= pop1(i,m)+step*rand;    %making R in Range
          else
            R(1,m)= pop1(i,m)-step*rand;
          end
        end
      end          %%end of while
    end   %end of for
    [f]=mo_test_func(R(1,:),D,p);
     Rf1=f(1,1);
```

```
Rf2=f(1,2);            %%assinging the cost to R
Rf3=0;
Rf = (abs(1/((d*Rf1)+((1-d)*Rf2))))^0.5;  % cost of R=reflection
[f]=mo_test_func(P(1,:),D,p);
Pf1=f(1,1);
Pf2=f(1,2);            %%assinging the cost to P
Pf3=0;
Pf = (abs(1/((d*Pf1)+((1-d)*Pf2))))^0.5;
          if(Rf> Bf)
   E=P+gamma*(R-P);%%% expansion coefficient calculated
   for m=1:D
      while(E(1,m)<xl(m) | E(1,m)>xu(m))
         %                  DDEEr=i
         if ((E(1,m)<=xl(m) | E(1,m)>=xu(m)))
            if rand<0.5
               E(1,m)= pop1(i,m)+step*rand;    %making E in range
            else
               E(1,m)= pop1(i,m)-step*rand;
            end
         end
      end          %%end of while
   end   %end of for
   % %     [f]=mo_test_func(E(1,:),D,p);
   [f]=mo_test_func(E(1,:),D,p);
   Ef1=f(1,1);
   Ef2=f(1,2);            %%assinging the cost to E
   Ef3=0;
    Ef = (abs(1/((d*Ef1)+((1-d)*Ef2))))^0.5;
    if(Ef>Bf)
      ls(I2,:)=E(1,:);
      ls_f1(I2)=Ef1;
      ls_f2(I2)=Ef2;
      ls_f3(I2)=Ef3;
      f_avg(I2)=Ef;
   else
      ls(I2,:)=R(1,:);
      ls_f1(I2)=Rf1;
      ls_f2(I2)=Rf2;
      ls_f3(I2)=Rf3;
      f_avg(I2)=Rf;
   end
else
   if (Rf>Wf)
       ls(I2,:)=R(1,:);
      ls_f1(I2)=Rf1;
      ls_f2(I2)=Rf2;
```

```
            ls_f3(I2)=Rf3;
            f_avg(I2)=Rf;
        else
            C= P+Beta*(W-P);  % contraction coefficent
            for m=1:D
                while(C(1,m)<xl(m) | C(1,m)>xu(m))
                    %                   DDCCr=i
                    if ((C(1,m)<=xl(m) | C(1,m)>=xu(m)))
                        if rand<0.5
                            C(1,m)= pop1(i,m)+step*rand;    %making C in Cange
                        else
                            C(1,m)= pop1(i,m)-step*rand;
                        end
                    end
                end          %%end of while
            end   %end of for
            % %     [f]=mo_test_func(C(1,:),D,p);
            [f]=mo_test_func(C(1,:),D,p);
            Cf1=f(1,1);
            Cf2=f(1,2);           %%assinging the cost to P
            Cf3=0;
            Cf = (abs(1/((d*Cf1)+((1-d)*Cf2))))^0.5;
            if(Cf>Bf)
                ls(I2,:)=C(1,:);
                ls_f1(I2)=Cf1;
                ls_f2(I2)=Cf2;
                ls_f3(I2)=Cf3;
                f_avg(I2)=Cf;
            else
                for kk =1:D+1
                    ls(kk,:)=(ls(kk,:)+B(1,:))/2;
                end
            end
        end
    end
    sum =0;
    for kk=1:D+1
        sum = sum+(f_avg(kk)-Pf)^2
    end
    Q = (sum/(D+1))^0.5
end     %% end of while loop or o loop
[Bf,I1]=max(f_avg);               %% finding out best element
B(1,:)=ls(I1,:);              %% assigning the decision varibles
costBf1=ls_f1(I1);
costBf2=ls_f2(I1);              %%assinging the idividual cost
costBf3=ls_f3(I1);
```

```
            for (pp=1:Np)
               if (f1(pp,1)>costBf1 & f2(pp,1)>costBf2)
                   %  if (f1Xt>costBf1 | f2Xt>costBf2)
                  pop1(pp,:)=B(1,:);
                  f1(pp,1)=costBf1;
                  f2(pp,1)=costBf2;
                  f3(pp,1)=costBf3;
                 count=count+1;
                  break;
               end
            end
            pop1;
            %hybrid ends
            Ttime=cputime-t;
            % count
         end    % end of pop loop
          Ttime=cputime-t;
         % count
      end  % end of generation loop
      nond=zeros(1,D);
      nondf=[0 0 0];
      a=1;
      for i=1:Np
         flag=0;
         for j=1:Np
            if (((f2(i)>=f2(j))&(f1(i)>=f1(j))) & ((f2(i)>f2(j))|(f1(i)>f1(j))))
               flag=1;
               break;
            end
         end
         if(flag~=1)
            nond(a,:)=pop1(i,:);
            nondf(a,1)=f1(i,1);
            nondf(a,2)=f2(i,1);
            nondf(a,3)=f3(i,1);
            a=a+1;
         end
      end
      nond;
      a
      Np=length(nond);
   Np=a-1
       for i=1:Np
         [f]=mo_test_func(nond(i,:),D,p);
         f1(i,1)=f(1,1);
         f2(i,1)=f(1,2);
```

```
    f3(i,1)=0;
    %           g(i,1)=g;
end
for i=1:(a-1)
    f1(i,1)=nondf(i,1);
    f2(i,1)=nondf(i,2);
    f3(i,1)=0;
end
obj1 = nondf(:,1);
obj2 = nondf(:,2);
obj3 =nondf(:,3);
figure(1);
plot(obj1 , obj2 ,'*')
```

```
%%%%%%%%%%%%%%%%%%%%MATLAB CODE FOR ELITIST MULI-OBJECTIVE DIFFERENTIAL EVOLUTION
%%%%%%%%%%%%%%%THIS CODE IS DEVELOPED BY ASHISH M GUJARATHI AND B V BABU
%%%%ENTER YOUR OBJECTIVE FUNCTION in mo_test_file
%%%Enter the number and bounds of variables in fun file
clc
clear all
nond=1;
pop1=0;
Xtr=0;
gen=1
t=cputime;
CR=0.85;
Np=100;
GMAX=60;
R=10000;
t=cputime;
t1=cputime;
CR=0.85;
Np=100;
GMAX=100;
p=1;  %%problem 1 for SCH
[D,n_obj,xl,xu]=fun(p);
for i=1:Np
    for j=1:D
        pop1(i,j)=xl(j)+(xu(j)-xl(j))*rand(1);
    end
    [f]=mo_test_func(pop1(i,:),D,p);
    f1(i,1)=f(1,1);
    f2(i,1)=f(1,2);
    f3(i,1)=0;
```

```
   Ttime=cputime-t
end
for gen=1:GMAX
   pole=0;
   count=0;
   a1=1;
   Q=0;
   i=1;j=1;
   for i=1:Np
      flag=0;
      for j=1:Np
         if (((f2(i)>=f2(j))&(f1(i)>=f1(j))) & ((f2(i)>f2(j))|(f1(i)>f1(j))))
            flag=1;
            break;
         end
      end
      if(flag==0)
         for j=1:D
            nond(a1,j)=pop1(i,j);  %%%% population points
         end
         nondf(a1,1)=f1(i,1);  %%% function
         nondf(a1,2)=f2(i,1);
         nondf(a1,3)=f3(i,1);
         a1=a1+1;
      end
   end
   nond;
   nondf(:,1);
   nondf(:,2) ;
   nondf(:,3);
   Q=a1-1;
   for i=1:Np
      Xt=pop1(i,:);
      n=randperm(D);
      flag=0;
      for(k=1:D)
         c=rand(1);
         if ((c<CR)|(k==D) )
            if(flag==0)
               flag=1;
               r1=ceil(rand(1)*Np);
               while(r1==i)
                  r1=ceil(rand(1)*Np);
               end
               r2=ceil(rand(1)*Np);
               while(r2==i|r2==r1)
```

```
            r2=ceil(rand(1)*Np);
          end
          r3=ceil(rand(1)*Np);
          while(r3==i|r3==r1|r3==r2)
            r3=ceil(rand(1)*Np);
          end
          Xa=pop1(r1,:); Xb=pop1(r2,:);Xc=pop1(r3,:);
          Diff=(Xa-Xb);F=rand(1);
          Wdiff=F.*Diff;Xc1=Xc+Wdiff;
        end
        Xtr(:,n(k))=Xc1(:,n(k));  %% tral vextr
      else
        Xtr(:,n(k))=Xt(:,n(k));
      end
    end
    for j=1:D
      if(Xtr(1,j)<xl(j) | Xtr(1,j)>xu(j))
        Xtr(1,j)=xl(j) + (xu(j)-xl(j))*rand(1);
      end
    end
    sum=0;
    [f]=mo_test_func(Xtr(1,:),D,p);
    f1Xtr=f(1,1);
    f2Xtr=f(1,2);
    f3Xtr=0;
CHANGE THE SIGN DEPENDING UPOM MAX-MIN PROBLEM%%
    flag=0;
    flag1=0;
    if (((f1(i)>=f1Xtr)&(f2(i)>=f2Xtr)) & ((f1(i)>f1Xtr)|(f2(i)>f2Xtr)))
      %          if (((f1(i)>f1Xtr)&(f2(i)>f2Xtr)))
      if flag1==0
        pop1(i,:)=Xtr;
        f1(i)=f1Xtr;
        f2(i)=f2Xtr;
        f3(i)=f3Xtr;
        flag1=1;
      end
    end
    if flag1==0
      for pp=1:Np
        if flag1==0
          if (((f1(pp)>=f1Xtr)&(f2(pp)>=f2Xtr)) & ((f1(pp)>f1Xtr)|(f2(pp)>f2Xtr)))
            %                 if (((f1(pp)>f1Xtr)&(f2(pp)>=f2Xtr)))
            pop1(pp,:)=Xtr;
            f1(pp)=f1Xtr;
            f2(pp)=f2Xtr;
```

```
                f3(pp)=f3Xtr;
                flag1=1;
                break;
            end
        end
    end
end
end    % end of pop loop
Ttime=cputime-t;
mixedpop=pop1;
mixedf1=f1;
mixedf2=f2;
mixedf3=f3;
for i=1:Q
    for j=1:D
        mixedpop(Np+i,j)=nond(i,j);
    end
    mixedf1(Np+i,1)=nondf(i,1);
    mixedf2(Np+i,1)=nondf(i,2);
    mixedf3(Np+i,1)=nondf(i,3);
end
Npt=Np+Q;
count=Npt;
% % now ND sorting on mixed pop
nextpop=0;
for kk=1:Npt
    for j=1:D
        mixedback(kk,j)=mixedpop(kk,j);
    end
end
mixedbackf1=mixedf1;
mixedbackf2=mixedf2;
mixedbackf3=mixedf3;
a2=0;a3=0; a4=1;
pole=0; ccount=1;
while(pole<Np)
    a2=0;  a3=0;
    clear front;
    clear frontf1;
    clear frontf2;
    clear frontf3;
    clear copyf1;
    clear copyf2;
    clear copyf3;
    clear copy;
    clear posn;
```

```
copyf1=mixedbackf1;
copyf2=mixedbackf2;
copyf3=mixedbackf3;
copy = mixedback;
posn(count) = 0; k=0;
for i=1:count
   flag=0;
   for j=1:count
      if (((mixedbackf1(i)>=mixedbackf1(j))&(mixedbackf2(i)>=mixedbackf2(j))) &
((mixedbackf1(i)>mixedbackf1(j))|(mixedbackf2(i)>mixedbackf2(j))))
         flag=1;
         posn(i)=i;
         break;
      end
      if(flag == 0)
         posn(i) = 0;
      end
   end
end  %% end of for count
clear mixedbackf1;
clear mixedbackf2;
clear mixedbackf3;
clear mixedback;
%        posn
for i = 1:count
   if(posn(i)==0)
      a2=a2+1;
      for j=1:D
         front(a2,j)=copy(i,j);  %%%% population points
      end
      frontf1(a2,1)=copyf1(i,1);  %%% function
      frontf2(a2,1)=copyf2(i,1);
      frontf3(a2,1)=copyf3(i,1);          %front(a1,3)=0; here when p=8
   elseif (i==posn(i))
      a3=a3+1;
      for j=1:D
         mixedback(a3,j)=copy(i,j);
      end
      mixedbackf1(a3,1)=copyf1(i,1);
      mixedbackf2(a3,1)=copyf2(i,1);
      mixedbackf3(a3,1)=copyf3(i,1);
   end
end
count = a3;
frontpop=a2;
```

```
    if ((frontpop+pole)<=Np)
        for j=1:frontpop
            for kk=1:D
                nextpoplist(pole+j,kk)=front(j,kk);
            end
            nextpoplistf1(pole+j,1)=frontf1(j,1);
            nextpoplistf2(pole+j,1)=frontf2(j,1);
            nextpoplistf3(pole+j,1)=frontf3(j,1);
        end
        pole=pole+frontpop;
        poleflag=0;
    else
        poleflag=1;
        break;
    end
end %end of while loop
a=1; b=1;
clear dist;
if (((frontpop+pole)>Np) & (poleflag==0))
    for b=1:frontpop
        for a=1:frontpop-1
            if(frontf1(a,1)<frontf1(a+1,1))        %%%%%%% sorting of variables wrt f1
                temp=frontf2(a+1,1);
                frontf1(a+1,1)=frontf1(a,1);
                frontf1(a,1)=temp;

                temp=frontf2(a+1,1);
                frontf2(a+1,1)=frontf2(a,1);
                frontf2(a,1)=temp;

                temp=frontf3(a+1,1);
                frontf3(a+1,1)=frontf3(a,1);
                frontf3(a,1)=temp;
                for pp=1:D
                    temp=front(a+1,pp);
                    front(a+1,pp)=front(a,pp);
                    front(a,pp)=temp;
                end
            end
        end
    end
    [f1min,i1]=min(frontf1);
    [f1max,i2]=max(frontf1);
    [f2min,i3]=min(frontf2);
    [f2max,i4]=max(frontf2);
    [f3min,i5]=min(frontf3);
```

```
[f3max,i6]=max(frontf3);
rangef1=f1max-f1min;
rangef2=f2max-f2min;
rangef3=f3max-f3min;
for ptr=1:frontpop
   dist(ptr,1)=0;   %%%%%initializing all distances to zero
end
dist(1,1)=100;
dist(frontpop,1)=100;
dist;
for ptr=2:(frontpop-1)

   dist(ptr,1)=dist(ptr,1)+ (abs(frontf1(ptr-1,1)-frontf1(ptr+1,1))/rangef1);
end
dist;
for b=1:frontpop
   for a=1:frontpop-1
      if(frontf2(a,1)<frontf2(a+1,1))
         temp=frontf1(a+1,1);
         frontf1(a+1,1)=frontf1(a,1);
         frontf1(a,1)=temp;

         temp=frontf2(a+1,1);frontf2(a+1,1)=frontf2(a,1);
         frontf2(a,1)=temp;temp=frontf3(a+1,1);
         frontf3(a+1,1)=frontf3(a,1);
         frontf3(a,1)=temp;
         for pp=1:D
            temp=front(a+1,pp);
            front(a+1,pp)=front(a,pp);
            front(a,pp)=temp;
         end
      end
   end
end
ptr=0;
for ptr=1:frontpop
   dist(ptr,2)=0;   %%%%%initialising all distances to zero
end
dist(1,2)=100;
dist(frontpop,2)=100;

for ptr=2:frontpop-1
   dist(ptr,2)=dist(ptr,1)+  (abs(frontf2(ptr-1,1)-frontf2(ptr+1,1))/rangef2);
end
ptr=0;
for b=1:frontpop
```

```
        for a=1:frontpop-1
            if(dist((a),2)<dist((a+1),2))
                temp=dist(a+1,2); dist(a+1,2)=dist(a,2);
                dist((a),2)=temp;
               temp=frontf1(a+1,1);
                frontf1(a+1,1)=frontf1((a),1);
                frontf1((a),1)=temp;temp=frontf2(a+1,1);
                frontf2(a+1,1)=frontf2((a),1);
                frontf2((a),1)=temp;temp=frontf3(a+1,1);
                frontf3(a+1,1)=frontf3((a),1);
                frontf3((a),1)=temp;
                for pp=1:D
                    temp=front(a+1,pp);
                    front(a+1,pp)=front(a,pp);
                    front(a,pp)=temp;
                end
            end
        end
    end
    for chk=1:frontpop
        if (pole+chk<=Np)
            nextpoplist(pole+chk,:)=front(chk,:);
            nextpoplistf1(pole+chk,1)=frontf1(chk,1);
            nextpoplistf2(pole+chk,1)=frontf2(chk,1);
            nextpoplistf3(pole+chk,1)=frontf3(chk,1);
        else
            break
        end
    end
    size(nextpoplist);
end %end of  if nextpop>Np crowded loop
if poleflag==1
    nextpoplist=pop1;nextpoplistf1=f1;
    nextpoplistf2=f2;nextpoplistf3=f3;
end
size(pop1);
clear pop1,f1,f2;   clear f3
pop1=nextpoplist;
f1=nextpoplistf1;
size(f1);
f2=nextpoplistf2;
size(f2);
f3=nextpoplistf3;
size(f3);
plot(f1,f2,'*');
pole=0;
```

```
    clear a1;
    clear Q;
    clear mixedpop
    clear mixedpopf1
    clear mixedpopf2
    clear mixedpopf3
    clear nextpoplist
    clear nextpoplistf1
    clear nextpoplistf2
    clear nextpoplistf3
    clear crowdpopdist
    clear nextpoplist
    clear nextpoplistf1
    clear nextpoplistf2
    clear nextpoplistf3
    Ttime=cputime-t;
    t2=cputime-t;
    plot(f1,f2,'*');
end% end of generation loop
nond=zeros(1,D);
nondf=[0 0 0];
a=1;
for i=1:Np
    flag=0;
    for j=1:Np
        if (((f2(i)>=f2(j))&(f1(i)>=f1(j))) & ((f2(i)>f2(j))|(f1(i)>f1(j))))
            flag=1;
            break;
        end
    end
    if(flag~=1)
        nond(a,:)=pop1(i,:);
        nondf(a,1)=f1(i,1);
        nondf(a,2)=f2(i,1);
        nondf(a,3)=f3(i,1);
        a=a+1;
    end
end
Np=length(nond);
Np=a-1
for i=1:Np
    [f]=mo_test_func(nond(i,:),D,p);
    f1Xtr=f(1,1);
    f2Xtr=f(1,2);
    f3Xtr=0;
    nondf1(i,1) = f(1,1);
```

```
   nondf2(i,1) = f(1,2);
   nondf3(i,1) = f(1,3);
end
for i=1:(a-1)
   f1(i,1)=nondf1(i,1);
   f2(i,1)=nondf2(i,1);
   f3(i,1)=nondf3(i,1);
end
plot(f1,f2,'*');
```

%MATLAB CODE FOR TRIGONOMETRIC MUTATION MULI-OBJECTIVE DIFFERENTIAL EVOLUTION ALGORITHM THIS CODE IS DEVELOPED BY ASHISH M GUJARATHI AND B V BABU %ENTER YOUR OBJECTIVE FUNCTION in mo_test_file %%%Enter the number and bounds of variables in fun file

```
clc
clear all
nond=1;
pop1=0;
Xtr=0
mt=0.05;
t=cputime;
t1=cputime;
CR=0.85;
Np=100;
GMAX=300;
p=1;  %%problem number 1 SCH
[D,n_obj,xl,xu]=fun(p);
for i=1:Np
   for j=1:D
      pop1(i,j)=xl(j)+(xu(j)-xl(j))*rand(1);
   end
end
for gen=1:GMAX
   gen
    for i=1:Np
         [f]=mo_test_func(pop1(i,:),D,p);
      f1(i,1)=f(1,1);
      f2(i,1)=f(1,2);
      f3(i,1)=0;
   end
%%DO NOT CHANGE BELOW TILL FURTHER INFORMATION%
   for i=1:Np
     Xt=pop1(i,:);
      n=randperm(D);
      flag=0;
      for(k=1:D)
```

```
c=rand(1);
if ((c<CR)|(k==D) )
   if(flag==0)
      flag=1;
      r1=ceil(rand(1)*Np);
      while(r1==i)
         r1=ceil(rand(1)*Np)
      end
      r2=ceil(rand(1)*Np);
      while(r2==i|r2==r1)
         r2=ceil(rand(1)*Np);
      end
      r3=ceil(rand(1)*Np);
      while(r3==i|r3==r1|r3==r2)
         r3=ceil(rand(1)*Np);
      end
      r4=ceil(rand(1)*Np);
      while(r4==i|r4==r1|r4==r2|r4==r3)
         r4=ceil(rand(1)*Np);
      end
      Xa=pop1(r1,:);
      Xb=pop1(r2,:);
      Xc=pop1(r3,:);
      Xd=pop1(r4,:);
         if(rand>mt)
         tempp1 =mo_test_func(Xa(1,:),D,p) ;
         tempp2 = mo_test_func(Xb(1,:),D,p);
         tempp3= mo_test_func(Xc(1,:),D,p);
         sum= tempp1+tempp2+tempp3  ;
         p1= tempp1/ sum ;
         p2= tempp2/sum ;
         p3=  tempp3/sum ;
         for j=1:D
Xtr(1,j)  =  (Xa(1,j)+Xb(1,j)+Xc(1,j))/3   +(p2-p1)*(Xa(1,j)-Xb(1,j))+(p3-p2)*(Xb(1,j)-
Xc(1,j))+(p1-p3)*(Xc(1,j)-Xa(1,j));
            if Xtr(1,j)<xl(j) | Xtr(1,j)>xu(j)
               Xtr(1,j)=xl(j) + (xu(j)-xl(j))*rand(1);
            end
         end
        else
         Diff1=((Xa-Xb));
         Diff2=((Xc-Xd));
         F=rand(1);
         F1=rand(1);
         Wdiff=F1.*Diff1 + F.*Diff2;
         W1diff=F1.*Diff1 ;
```

```
            for ii=1:Np
               flag=0;
               for jj=1:Np
                  if (((f2(ii)>=f2(jj))&(f1(ii)>=f1(jj))) & ((f2(ii)>f2(jj))|(f1(ii)>f1(jj))))
                     flag=1;
                     break;
                  end
               end
               if(flag~=1)
                  Xbestpop = pop1(ii,:);
                  break;
               end
            end
            %                    Xc1=Xbestpop + Wdiff;
            Xc1=Xc+ W1diff;
            Xtr(:,n(k))=Xc1(:,n(k));  %% tral vextr
            end              end
   else
      Xtr(:,n(k))=Xt(:,n(k));
   end
end
for j=1:D
   if(Xtr(1,j)<xl(j) | Xtr(1,j)>xu(j))
      Xtr(1,j)=xl(j) + (xu(j)-xl(j))*rand(1);
   end
end
sum=0;
[f]=mo_test_func(Xtr(1,:),D,p);
f1Xtr=f(1,1);
f2Xtr=f(1,2);
f3Xtr=0;
%CHANGE THE SIGN DEPENDING UPOM MAX-MIN PROBLEM%%
flag=0;
if (((f1(i)>=f1Xtr)&(f2(i)>=f2Xtr)) & ((f1(i)>f1Xtr)|(f2(i)>f2Xtr)))
   if flag==0
      pop1(i,:)=Xtr;
      f1(i)=f1Xtr;
      f2(i)=f2Xtr;
      f3(i)=f3Xtr;
      flag=1;
   end
end
if flag==0
   for(pp=1:Np)
      if (((f1(pp)>=f1Xtr)&(f2(pp)>=f2Xtr)) & ((f1(pp)>f1Xtr)|(f2(pp)>f2Xtr)))
         pop1(pp,:)=Xtr;
```

```
                f1(pp)=f1Xtr;
                f2(pp)=f2Xtr;
                f3(pp)=f3Xtr;
                flag = 1
                break;
            end
        end
    end
    pop1;
    % count
end    % end of pop loop
midnond(:,1)=f1(:,1);
midnond(:,2)=f2(:,1);
midnond(:,3)=f3(:,1);
t2= cputime - t1;
nond=zeros(1,D);
a1=1;
for i=1:Np
    flag=0;
    for j=1:Np
        if (((f2(i)>=f2(j))&(f1(i)>=f1(j))) & ((f2(i)>f2(j))|(f1(i)>f1(j))))
            flag=1;
            break;
        end
    end
    if(flag~=1)
        nond(a1,:)=pop1(i,:);  %%%% population points
        nondf(a1,1)=f1(i,1);  %%% function
        nondf(a1,2)=f2(i,1);
        nondf(a1,3)=f3(i,1);
        a1=a1+1;
    end
end
obj1=nondf(:,1);
obj2=nondf(:,2)
plot(obj1,obj2,'*');
end  % end of generation loop
t1=cputime-t  %% CPU TIME in seconds
obj1 =f1;
obj2 = f2;
obj3 =f3;
figure(1);
plot(obj1 , obj2 ,'*')
```